Synthesis and luminescence of iridium and rhodium complexes incorporating NCN-coordinating terdentate ligands

Victoria Louise Whittle

Synthesis and Luminescence of Iridium and Rhodium Complexes Incorporating NCN-Coordinating Terdentate Ligands

Victoria Louise Whittle

Department of Chemistry

University of Durham

A thesis submitted in part-fulfilment for the degree of

Doctor of Philosophy

15th December 2008

Abstract

Synthesis and Luminescence of Iridium and Rhodium Complexes Incorporating NCN-Coordinating Terdentate Ligands

Victoria Louise Whittle

The luminescent properties of transition metal complexes containing polypyridyl and cyclometalating ligands make them potential candidates for a range of applications; for example, as triplet-harvesting agents in organic light-emitting devices (OLEDs), owing to the potentially high quantum yields of triplet emission; in solar cells, converting light to electrical energy; and as sensors and probes in biological systems.

The synthesis of a series of $[M(NCN)(X^X^X)]^{n+}$ and $[M(NCN)(X^X)Cl]^{n+}$ coordinated complexes (where M = Ir or Rh; X = heterocyclic N or cyclometalated aryl C; and n = 0–2) bearing pyridyl and pyrazolyl-based NCN-coordinating ligands (cyclometalating through the central phenyl ring) is reported, alongside their photophysical and electrochemical properties. Whilst luminescence was generally observed from the pyridyl-based iridium(III) complexes at ambient temperature, the charge-neutral Rh(III) complex [Rh(NCN)(NC)Cl] was the only complex amongst those containing a rhodium centre to be emissive under these conditions. Similarly, the pyrazolyl Ir(III) complexes exhibit lower luminescence intensities than their pyridyl analogues, owing to the poorer π-accepting ability of the pyrazole rings which results in a blue-shift in the emission profile and more ligand-based character.

In addition to the synthesis of these complexes, a sequential cross-coupling – bromination – cross-coupling strategy has been developed for the linear stepwise expansion of an $[Ir(NCN)(NNC)]^+$ coordinated complex, incorporating a pendant bromophenyl group on the central pyridyl ring of the NNC ligand, *via in situ* palladium-catalysed Suzuki cross-coupling reactions with aryl boronic acids. This strategy has been further extended to the controlled synthesis of linear multimetallic assemblies using boronic acid appended Ir(III) and Ru(II) complexes. A heterometallic trinuclear $[Ir–\phi–Ir–\phi_2–Ru]^{4+}$ assembly was prepared, where the phenylene bridges between the metal centres do not contribute to the excited state of the trimetallic system, and efficient energy-transfer occurs to the lower energy ruthenium terminus. The emissive and energy-channelling properties of such multimetallic assemblies can be tailored by the careful choice of the constituent "building blocks".

Declaration

The work described herein was carried out in the Department of Chemistry at the University of Durham between October 2004 and December 2007. This thesis is the work of the author, unless otherwise stated, and no part of it has been submitted for a degree at this or any other university.

Statement of Copyright

Acknowledgements

First and foremost, I would like to express my most sincere thanks to my supervisor Dr. J.A. Gareth Williams for all his help and advice throughout this PhD.

I must also acknowledge the Department of Chemistry, University of Durham and the EPSRC for the financial support to undertake this research.

My gratitude also goes to the following people:-

Dr. Alan Kenwright, Catherine Heffernan and Ian McKaeg for NMR spectroscopy; Dr. Mike Jones and Lara Turner for electrospray mass spectrometry; Drs. Dave Parker and Jackie Mosely for MALDI mass spectrometry; Jarika Dorstal and Judith Magee for elemental analysis.

The staff in the chemistry department who have made it an enjoyable place to work, including everybody in stores, the glass blowers, those in the workshops and the lab technicians.

Fellow members of the Williams group, especially Kathryn and Dave for all their help and support from the start and Will for his endless patience whilst helping me to run the DFT calculations. Also Stéphanie, Pierpaolo, Lisa, Louise and the fourth year project students particularly Octavia and Rosemary.

The past and present members of CG1: Aileen, John, John Mina, Jonathon, Kathryn, Lisa, Marie, Marvis, Matt, Michal, Nick, Pete and Tom.

My 'Cake Day Monday' friends: Emma, Helen, Jamie, Matt and Sara-Jane.

All my friends from within the department, especially Joe, Jules, Lucas, Ricky, Seb and Shelley.

..... but, most of all to my Mum and 'the Kirkham family' for their continued support and encouragement throughout.

Table of Contents

Abbreviations

bibH	1,3-bis(benzimidazol-2-yl)benzene
biq	2,2'-biquinoline
bpy	2,2'-bipyridine
bmpqpyH	2,6-bis(7'-methyl-4'-phenyl-2'-quinolyl)pyridine
Brbpy	4-bromo-2,2'-bipyridine
BSA	bovine serum albumin
CFSE	crystal field stabilisation energy
Cltpy	4'-chloro-2,2':6',2''-terpyridine
COD	cyclooctadiene
COSY	correlation spectroscopy
CS	charge-separated
DCM	dichloromethane
DFT	density functional theory
dinpy	2,6-di(2'-indolyl)pyridine
dpzdmbH-Me_2	1,5-dimethyl-2,4-bis(3-methylpyrazolyl)benzene
DME	1,2-dimethoxyethane
DMF	dimethylformamide
DMSO	dimethylsulfoxide
DNA	deoxyribonucleic acid
dpp	2,3-bis(2-pyridyl)pyrazine
dppyH_2	2,6-diphenylpyridine
dpybH	1,3-di(2-pyridyl)benzene
dpydmbH	1,3-di(2-pyridyl)-4,6-dimethylbenzene
dpydmbH-Br	1-bromo-3,5-di(2-pyridyl)-2,6-dimethylbenzene
dpzbH-Me_2	1,3-bis(3-methylpyrazolyl)benzene
dpzbH	1,3-di(1-pyrazolyl)benzene
dpzbH-Br	1,3-di(1-pyrazolyl)-5-bromobenzene
dpzdFbH-Me_2	1,5-difluoro-2,4-bis(3-methylpyrazolyl)benzene
dpzdmbH	1,3-di(1-pyrazolyl)-4,6-dimethylbenzene
dpzmbH	1,3-di(1-pyrazolyl)-5-methylbenzene
DSC	dye-sensitised solar cells
$E_{1/2}^{ox}$	half wave oxidation potential

$E_{1/2}^{red}$	half wave reduction potential
ECP	effective core potential
EI	electron ionisation
EPA	diethyl ether-isopentane-ethanol
ES^-	negative ion electrospray ionisation
ES^+	positive ion electrospray ionisation
F_2dppyH_2	1,3-bis(3-fluorophenyl)pyridine
F_6dppyH_2	1,3-bis(2,3,4-trifluorophenyl)pyridine
GC-MS	gas chromatography-mass spectrometry
HF	Hartree-Fock
HPLC	high-performance liquid chromatography
HSA	human serum albumin
HSQC	heteronuclear single quantum correlation
IC	internal conversion
ILCT	intraligand charge transfer
ISC	intersystem crossing
ISC'	back intersystem crossing
iso-tpy	2,2':6',4"-terpyridine
ITO	indium tin oxide
$k_Q^{O_2}$	bimolecular rate constant for quenching by oxygen
k_r	radiative rate constant
LC	ligand-centred
LLCT	ligand-to-ligand charge transfer
MALDI	matrix assisted laser desorption ionisation
MC	metal-centred
MebibH	1,3-bis-(1-methylbenzimidazol-2-yl)benzene
Mebip	1,3-bis-(1-methylbenzimidazol-2-yl)pyridine
MLCT	metal-to-ligand charge transfer
MO	molecular orbital
mp	melting point
MS	mass spectrometry
mtbpyH-ϕ-Bneo	4'-(*p*-neopentylglycolatoboron)-phenyl-6'-(*m*-tolyl)- bipyridine
mtbpyH-ϕ-Br	4'-(*p*-bromophenyl)-6'-(*m*-tolyl)-bipyridine
mtbpyH-ϕ_2-NMe_2	4'-(*p*-dimethylamino)biphenyl-6'-(*m*-tolyl)-bipyridine

mtbpyH-ϕ-ph	4'-(*p*-biphenyl)-6'-(*m*-tolyl)-bipyridine
NMR	nuclear magnetic resonance
NOESY	nuclear Overhauser effect spectroscopy
pbaH	4-(2-pyridyl)benzaldehyde
phbpyH	6-phenyl-2,2'-bipyridine
phen	1,10-phenanthroline
PMT	photomultiplier tube
ppyH	2-phenylpyridine
FppyH	2-(4-fluorophenyl)pyridine
F_2ppyH	2-(4,6-difluorophenyl)pyridine
PVK	poly(vinylcarbazole)
pydmbH-Br_2	1,3-dibromo-5-(2-pyridyl)-2,4-dimethylbenzene
pzbH	1-phenylpyrazole
pzbH-Br_2	1-pyrazolyl-3,5-dibromobenzene
pzdmbH-I	1-iodo-3-pyrazolyl-4,6-dimethylbenzene
qtpy	4'-(4'''-pyridyl)-2,2':6',2''-terpyridine
RNA	ribonucleic acid
S_0	ground singlet state
SBLCT	sigma-bond-to-ligand charge transfer
SCE	standard calomel electrode
S_n	n^{th} excited singlet state
τ	lifetime
TCSPC	time-correlated single-photon counting
tdppyH_2	2,6-diphenyl-4'-(*p*-tolyl)pyridine
thpy	2-thienylpyridine
TLC	thin layer chromatography
tlpyH	2-(*p*-tolyl)pyridine
T_n	n^{th} excited triplet state
ToF	time of flight
tphbpyH	4'-tolyl-6-phenyl-2,2'-bipyridine
tppicH_2	4-*p*-tolyl-6-phenylpicolinic acid
tpy	2,2':6',2''-terpyridine
tpybH	1,3,5-tri(2-pyridyl)benzene
tpydmbH	1,3,5-tri(2-pyridyl)-2,4-dimethylbenzene

tpyO	2,6-bis(2-pyridyl)-4-pyridone
tpy-ϕ-Br	4'-(*p*-bromophenyl)-2,2':6',2''-terpyridine
tpzbH	1,3,5-tri(1-pyrazolyl)benzene
ttpy	4'-(*p*-tolyl)-2,2':6',2''-terpyridine
ΔE^{ox}	peak to peak separation of the oxidation process
ΔE^{red}	peak to peak separation of the reduction process
Φ_{em}	emission quantum yield
λ_{max}^{em}	maximum emission wavelength
λ_{ex}	excitation wavelength
Σk_{nr}	sum of non-radiative rate constants
τ	emission lifetime

CHAPTER 1

INTRODUCTION

1 Introduction

For the past 50 years there has been considerable research interest into metal complexes containing polypyridyl and cyclometalating ligands, owing to their luminescent properties. Following excitation, such complexes can undergo intense phosphorescence, making them potentially appropriate candidates for use in organic light-emitting devices, OLEDs, as photosensitisers and as probes and sensors in biological systems.[1, 2]

The first example of a luminescent transition metal complex was that of the d^6 ruthenium(II) complex $[Ru(bpy)_3]^{2+}$, bpy = 2,2'-bipyridine. This was initially isolated by Burstal in 1930,[3] with the luminescent properties being investigated in 1959 by Paris and Brandt.[4] Since then complexes of Ru(II) containing polypyridyl and cyclometalating ligands have undergone a vast number of studies. Related iridium(III) and especially rhodium(III) complexes have, however, been studied to a much lesser extent, owing to the synthetic challenges associated with the higher charge of the metal ions and increased kinetic inertness making ligand substitution more difficult. Following on from some studies in the late 1980's and 1990's, complexes of iridium(III) became of intense interest at the beginning of this decade, with most of the studies to date having focused upon tris-bidentate, rather than bis-terdentate, complexes.

1.1 An introduction to luminescence

Most molecules exist in a singlet electronic ground state (S_0), where all the electrons are paired. Upon absorption of a photon of light of suitable wavelength, an electron is promoted to a higher energy orbital, producing a singlet excited electronic state (S_n). This process, termed excitation, is denoted by the orbital that the electron originated from, and to which it is promoted, *e.g.* π–π^*. In a singlet excited state (S_n), the orientation of the spin of the excited electron is anti-parallel to that of the ground state electron. According to Kasha's rule the excited molecule undergoes rapid relaxation *via* a non-radiative pathway to the lowest singlet excited state (S_1), owing to this being much faster than the competing radiative process.[5] This is followed by relaxation to the ground state (S_0), in a process termed fluorescence.

Although the transition to a triplet excited state, $T_n \leftarrow S_0$, is formally forbidden, the T_n state may be populated indirectly. A molecule in the excited singlet state (S_n) undergoes intersystem crossing (ISC) to the excited triplet state (T_n), from which it relaxes non-radiatively to the lowest triplet excited state (T_1). This is followed by radiative decay to the singlet ground state (S_0) *via* a process termed phosphorescence. Being formally forbidden, the rate of phosphorescence is very low under ambient conditions. These competing processes are displayed on the Jablonski diagram in Figure 1.1. It should be noted that triplet excited states are always lower in energy than singlet excited states, thus making phosphorescent emission lower in energy than the corresponding fluorescent emission.

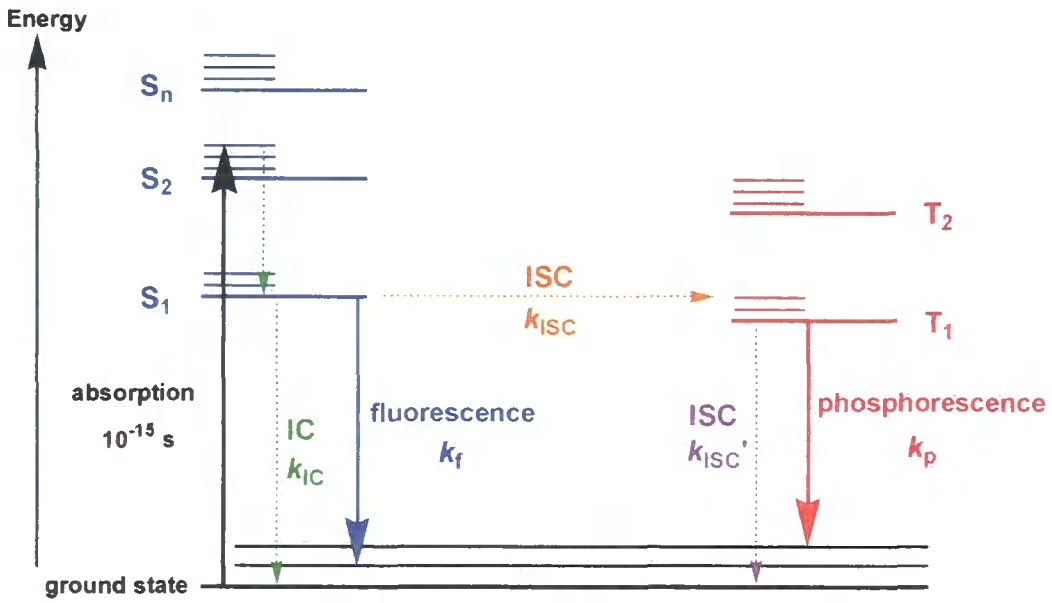

Figure 1.1: Jablonski Diagram.

According to the Frank-Condon principle, the electronic transitions that occur in the formation of the excited state do so at a faster rate than the geometrical changes taking place within the molecule.[6] The molecule undergoes molecular reorganisation to reach the lowest vibrational state, of the lowest excited state, prior to emission *via* fluorescent or phosphorescent pathways. As a result of the losses in energy that occur during the non-radiative processes, the energy of emission is lower, red-shifted, with respect to that of absorption. This phenomenon is known as Stokes' shift and its extent is dependent upon the degree of geometric distortion and electronic redistribution between the excited and ground states of the molecule.[6]

Since fluorescence, *i.e.* emission, from a state with the same multiplicity as the ground state is a spin allowed process; decay *via* this pathway is rapid with emission lifetimes (τ) typically on a nanosecond timescale. Fluorescence is the usual decay pathway for organic fluorophores *e.g.* fluorescein and other aromatic molecules. Phosphorescence, *i.e.* emission from a state of different multiplicity to the final state, however, is formally forbidden thus resulting in the corresponding natural emission lifetimes being much longer, on a millisecond-to-second timescale. In fact, the rate constant for triplet radiative decay is normally so slow that it is unable to compete with other faster non-radiative processes and hence phosphorescence is rarely observed under ambient conditions. However, the presence of heavy atoms within molecules, including those of second or third row transition metals, results in this process being partially allowed due to significant spin-orbit coupling. This leads to electric dipole transitions occurring with $\Delta S \neq 0$. The spin quantum number thus becomes an insufficient description of the system, and the promotion of the triplet-to-singlet radiative pathway increases the rate constant of phosphorescence to such an extent that it becomes competitive with the other processes.[6, 7]

Transition metal complexes have complicated electronic structures due to the combination of ligand and metal d orbitals, thus a wide range of excited states are available to them. Molecular orbitals, MOs, comprise of several atomic orbitals and can be described as being of predominantly metal or ligand character depending upon which atomic orbitals have the most similar energy to the MO. When radiation is absorbed, an electronic transition between two molecular orbitals occurs and the resulting excited state can be characterised approximately by the molecular orbitals involved.[8] The main transitions that will be focused upon here are metal-centred (MC), ligand-centred (LC), metal-to-ligand charge transfer (MLCT) and ligand-to-ligand charge transfer (LLCT). A MC excited state is formed when an electron in a d orbital is promoted to a higher d-orbital whilst a LC excited state is formed when the excitation is from a π to a π^* orbital on the same ligand. MLCT excited states occur when an electron from a metal d-orbital is promoted to a π^* orbital of a ligand bound to the metal centre, and LLCT excited states are formed when an electron in one ligand's π orbital is promoted to another ligand's π^* orbital.

1.2 Ruthenium complexes

1.2.1 Ruthenium tris-2,2'-bipyridine complexes

The d^6 octahedral ruthenium(II) complex $[Ru(bpy)_3]^{2+}$ (Figure 1.2) is one of the most well studied of all metal complexes, beginning in 1959 when Paris and Brandt reported its emission as being fluorescence from a singlet ^{1}MLCT, d→π*, excited state.[4, 9] This was subsequently disproved, following the assignment of the bands in the absorption spectra. The band at 285 nm was assigned to LC transitions and those at 240 and 450 nm to ^{1}MLCT transitions.[10] At low temperature, 77 K, in an ethanol-methanol glass, a shoulder is observed at 550 nm which corresponds to the lowest ^{3}MLCT excited state.[11] Alongside reports of rapid deactivation of the upper excited states *via* non-radiative decay, and long luminescence lifetimes, this led to emission being assigned as spin-forbidden phosphorescence from a triplet ^{3}MLCT, d→π*, excited state.[12, 13]

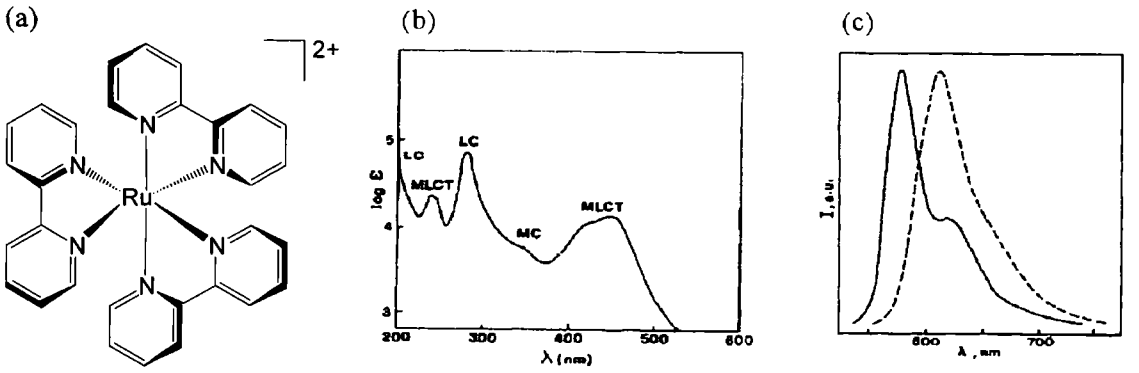

Figure 1.2: (a) structure of $[Ru(bpy)_3]^{2+}$, (b) absorption spectrum[9] and (c) emission spectra[9] at 77 K (solid line) and at room temperature (dashed line). Images (b) and (c) are reprinted from A. Juris *et al.*, *Coord Chem. Rev.*, 1988, 84, 85, Copyright 1988, with permission from Elsevier.

In 1979 the ground state structure of the hexafluorophosphate salt of $[Ru(bpy)_3]^{2+}$ was deduced by X-ray crystallography. The complex was reported to have D_3 symmetry with short (205.6 pm) Ru–N bond lengths, indicating significant π backbonding between the Ru(II) and π* orbitals of bpy.[14] This allows the 2,2'-bipyridine ligand to act as a π-acceptor for the excited electron in MLCT transitions. The photophysical properties of the complex can be tailored by modification of the geometric and electronic structure of the acceptor.

The effect of sterically bulky substituents was illustrated in 1997 by Damrauer *et al.* (Figure 1.3). Their study revealed that as the steric bulk of the derivatised ligand

increases, the ability of the peripheral phenyl rings to lie coplanar with the 2,2'-bipyridine moiety becomes progressively more hindered. A combination of spectroscopic, computational and crystallography studies of complexes containing such ligands showed that the ligands bearing phenyl pendants were non-planar in the ground state, with very little electron delocalisation evident; whilst in the excited state the ligands were planar with significant intraligand electron delocalisation. The extent of the increase in delocalisation, which occurs upon excitation, is enhanced as the steric bulk of the substituents increases and thus the MLCT π^* acceptor levels become more stabilised. This in turn leads to an increase in the non-radiative decay constant, Σk_{nr}, alongside a reduction of the radiative decay constant, k_r, and hence a decrease in observed luminescence lifetimes.[15]

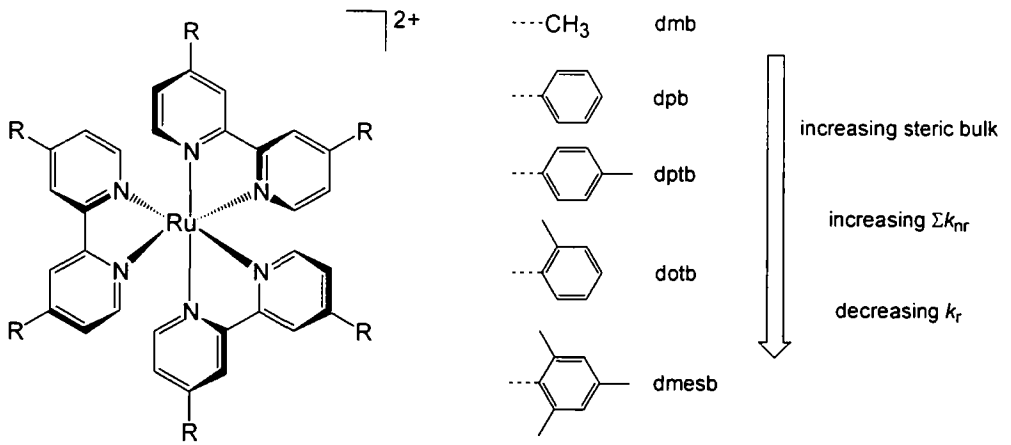

Figure 1.3: Ruthenium complexes with bipyridine ligands bearing sterically bulky groups.

Complexes belonging to the $[Ru(bpy)_3]^{2+}$ family offer the potential for a wide variety of applications: as luminescent photosensitisers, photocatalysts and electron transfer reagents converting light to chemical energy.[9, 16] Whilst intermolecular photochemical processes have been well studied and used, the energy of the photons are better utilised by photoinduced processes in well designed covalently-linked multicomponent systems.[17] Such systems are achieved by the assembly of suitable monometallic "building blocks". Complexes based upon $[Ru(bpy)_3]^{2+}$ have been used, but are not geometrically ideal due to their existence as a racemic mixture of Λ and Δ isomers. Thus when two or more such complexes are linked together, stereoisomers are formed which are difficult to separate on a preparative scale and may exhibit subtly different photophysical properties. The successful purification of the geometrical isomers of

monometallic ruthenium complexes, incorporating mono-functionalised bipyridine ligands, *via* preparative plate chromatography has recently been reported by Fletcher *et al.*[18, 19] The isolation of such isomerically pure building blocks opens up the possibility for the stereoselective synthesis of multicomponent systems.

1.2.2 Ruthenium bis-2,2':6,2''-terpyridine complexes

Bis-terdentate complexes offer a structural advantage, being achiral, and allow the formation of linear assemblies *via* substitution at the central 4' position of the terdentate ligand. Ruthenium complexes containing the terdentate ligand 2,2':6',2''-terpyridine, tpy, and its derivatives, coordinating to the central metal atom *via* three nitrogen atoms, have been well studied.

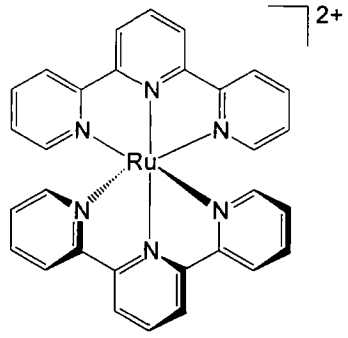

Figure 1.4: $[Ru(tpy)_2]^{2+}$

Whilst $[Ru(tpy)_2]^{2+}$ (Figure 1.4) has been found to be highly emissive in a rigid matrix at 77 K, due to long-lived phosphorescence from the ^{3}MLCT excited state,[20] it is virtually non-emissive in solution at room temperature with a lifetime of only 250 ps.[21] Over the years several explanations have been linked to this weak emission at room temperature, with respect to that observed in most ruthenium(II) polypyridyl complexes.[22-25] The most recent explanation is attributed to the poor bite angle of the terpyridyl ligand to the central ruthenium(II) atom, resulting in weak ligand field splitting. Consequentially the ^{3}MC excited state is lowered in energy, resulting in its thermal accessibility from the ^{3}MLCT state and fast deactivation by non-radiative processes.[24, 25]

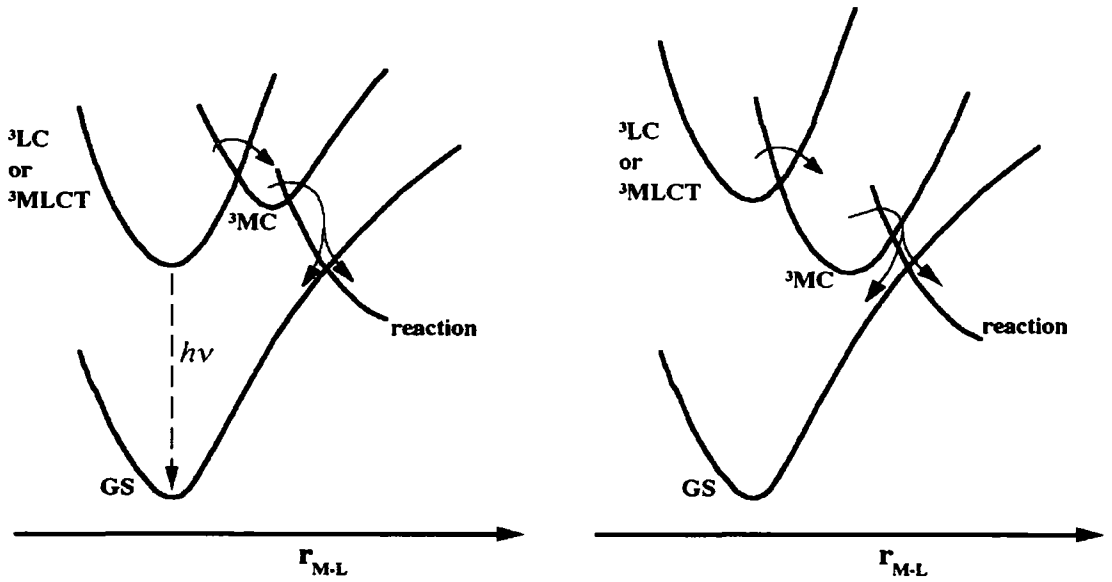

Figure 1.5: Radiative versus non-radiative decay.[9] Reprinted from A. Juris *et al.*, *Coord. Chem. Rev.*, 1988, 84, 85, Copyright 1988, with permission from Elsevier.

Excited ^{3}MLCT and ^{3}LC states have a similar geometry to that of the ground state; consequently if a ^{3}MLCT or ^{3}LC state is sufficiently low in energy, compared to the neighbouring ^{3}MC state, radiative decay occurs from this excited state and luminescence is observed (Figure 1.5). However, if the ^{3}MC state is lowest in energy, or the energy gap between it and the lowest excited state is small, then decay will occur *via* a non-radiative pathway (from the ^{3}MC state) and luminescence will not be observed. This results from the ^{3}MC state having a different geometry to the ground state, due to longer metal-ligand bonds. The ^{3}MC state is thus reported to effectively quench the emission from the neighbouring ^{3}MLCT or ^{3}LC states.[9, 26] For this reason, research in recent years has examined how to limit this decay by increasing the energy gap, ΔE, between the ^{3}MLCT and ^{3}MC excited states.[27] Such strategies have included the use of electron-withdrawing groups at the 4' position,[17] extended tpy-type ligands,[28] and also cyclometalating ligands (Section 1.2.3).[29]

The photochemical and photophysical properties of ruthenium(II) complexes bearing tpy ligands with aryl substituents have been well studied.[30-32] In the early 90's, Sauvage *et al.* investigated the series of ruthenium complexes, $[Ru(ttpy)_2]^{2+}$ (Figure 1.6a), $[Ru(4,4'\text{-dptpy})_2]^{2+}$ (Figure 1.6b) and $[Ru(tptpy)_2]^{2+}$ (Figure 1.6c).[30] $[Ru(ttpy)_2]^{2+}$ was found to be virtually non-emissive in solution at room temperature, like $[Ru(tpy)_2]^{2+}$, whilst $[Ru(4,4'\text{-dptpy})_2]^{2+}$ and $[Ru(tptpy)_2]^{2+}$ were both emissive. As the number of phenyl groups bound to the ligand increases, the ligand's π-acceptor ability is enhanced

and the ligand field splitting energy increases. The increase in the MC excited state and decrease in the MLCT state work synergistically to increase ΔE, enhancing luminescence.[30] The decrease in the energy of the MLCT band, upon increasing the number of phenyl groups, is observed as a red-shift of the MLCT absorption band from 490 to 495 and subsequently to 500 nm.[31]

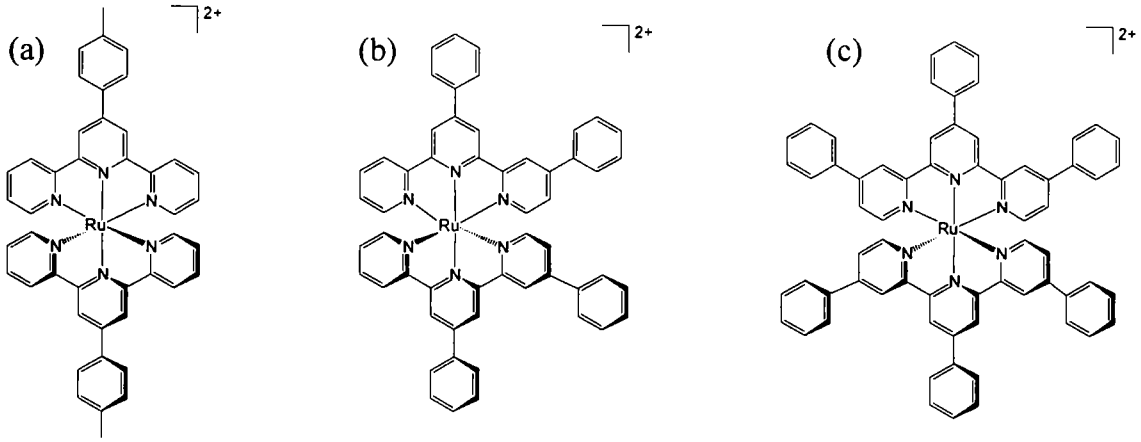

Figure 1.6: Structure of (a) $[Ru(ttpy)_2]^{2+}$, (b) $[Ru(4,4'\text{-}dtpy)_2]^{2+}$ and (c) $[Ru(tptpy)_2]^{2+}$.

No such increase in emission was observed when phenyl groups were bound to the 6- and 6"-positions of the terminal pyridyl rings in $[Ru(6,6''\text{-}dptpy)_2]^{2+}$ (Figure 1.7). This is the result of the steric interactions between the two 6,6"-dptpy ligands leading to a reduction in the ligand field strength, and thus the destabilisation of the MLCT state. Consequently ΔE between the MLCT and MC states is reduced, quenching luminescence.[32]

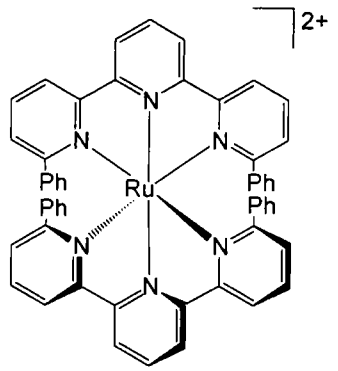

Figure 1.7: $[Ru(6,6''\text{-}dptpy)_2]^{2+}$

A range of 4'-substituents incorporated into the complex $[Ru(Xtpy)_2]^{2+}$, X = $MeSO_4$, OH and NMe_2, were investigated by Constable *et al.*[25] Whilst electron-withdrawing substituents are reported to increase the luminescence lifetime, as mentioned above, electron-donating substituents destabilise the LUMO, π^*, orbital of the ligand and the d, t_{2g}, orbital of the metal. Consequently the energy barrier between the MLCT and MC states is still low, with non-radiative decay from the MC state remaining the most efficient pathway.[25]

1.2.3 Cyclometalating ruthenium(II) complexes

In recent years interest has shifted towards complexes containing cyclometalating ligands, which coordinate to the central metal atom *via* at least one M-C bond. Anionic carbon atoms are stronger σ-donors than nitrogen atoms, thus cyclometalating ligands induce a strong ligand field, and increased electron density upon the metal centre. As a result the crystal field splitting energy of the d orbitals is increased, and the energy of the MC state raised, therefore favouring MLCT transitions and increasing luminescence.[27]

A range of tris-bidentate ruthenium(II) complexes containing the cyclometalating ligand 2-phenylpyridine (ppyH) have been synthesised. $[Ru(bpy)_2(ppy)]^+$ (Figure 1.8a) was synthesised by Constable *et al.* from $[Ru(bpy)_2Cl_2]$ and ppyH in the presence of silver(I).[33] The absorption spectra maxima were reported to be red-shifted with respect to $[Ru(bpy)_3]^{2+}$ due to an anionic carbon being bound to the metal centre.

Constable *et al.* synthesised the ligand phbpyH = 6-phenyl-2,2'-bipyridine in 1990 and reported its potential use as a cyclometalating analogue of tpy, binding in a CNN manner to rhodium, palladium, platinum, gold and mercury.[34] $[Ru(ttpy)(phbpy)]^{2+}$ (Figure 1.8b), however, remained elusive until Collin *et al.* reported its synthesis and luminescence the following year.[35] Unlike $[Ru(ttpy)_2]^{2+}$ (Figure 1.6a), which is non-emissive at room temperature, $[Ru(ttpy)(phbpy)]^+$ emits from a ^{3}MLCT excited state with a lifetime of 60 ns. This results from the increased ΔE between the ^{3}MLCT and ^{3}MC excited states imparted by the anionic cyclometalating carbon.

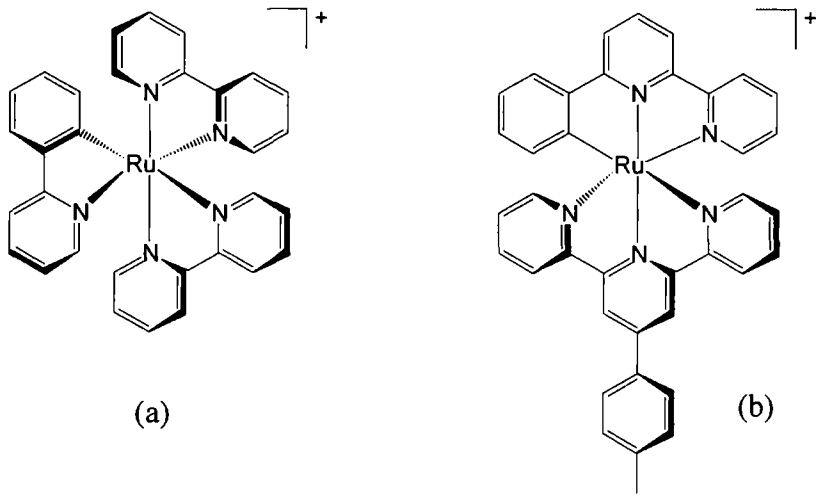

Figure 1.8: Structure of (a) $[Ru(bpy)_2(ppy)]^+$ and (b) $[Ru(ttpy)(phbpy)]^+$.

In 1995 Constable *et al.* reported the use of 2,2':6',4''-terpyridine (*iso*-tpy) as both a cyclometalating and non-cyclometalating ligand with ruthenium(II), in a solvent dependent study.[36] They attempted to synthesise the cyclometalated complex $[Ru(tpy)(iso\text{-}tpyH)][PF_6]_2$ (Figure 1.9) and its derivatives bearing the ligand *iso*-tpyH protonated on the non-coordinating nitrogen atom, binding *via* CNN. When the reactions were carried out in ethane-1,2-diol, the desired cyclometalated complexes were obtained. However, when the reaction was carried out in glacial acetic acid, the non-cyclometalated complexes of $[Ru(tpy)(iso\text{-}tpyH)Cl][PF_6]$, $[Ru(ttpy)(iso\text{-}tpyH)Cl][PF_6]$, and $[Ru(phtpy)(iso\text{-}tpyH)Cl][PF_6]$ were formed as the major products.

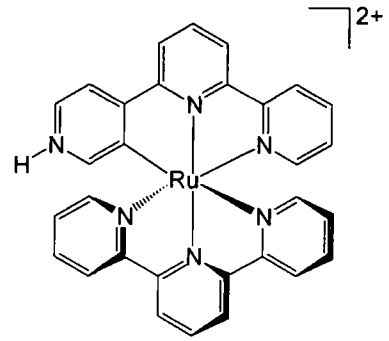

Figure 1.9: $[Ru(tpy)(iso\text{-}tpyH)]^{2+}$

Upon studying the absorption spectra of the non-cyclometalated complexes it was noticed that the lowest energy MLCT bands were at longer wavelength, lower energy, than in $[Ru(tpy)_2][PF_6]_2$. This feature is due to the increased σ-donation from the anionic chloride ligands to the central metal atom. The increase in energy of the MC

excited state favours MLCT based emission. Whilst the protonated cyclometalated complexes were seen to be only very weakly emissive at room temperature in degassed acetonitrile, the deprotonated analogues were emissive indicating that protonation effectively quenches emission.[36]

In another study, Barigelletti *et al.* investigated a series of Ru(II) complexes containing sterically hindered cyclometalated and non-cyclometalated ligands synthesised in acetic acid in the presence of N-ethylmorpholine. Whilst cyclometalation is known to enhance non-radiative decay from the MLCT excited state, the presence of bulky rigid ligands bound to the metal centre further enhances it. This results from the rigid ligands undergoing π–π interligand interactions and thus imparting greater electron delocalisation upon the MLCT state.[37] Such complexes, *e.g.* $[Ru(mappy)(dtp)]^+$ (Figure 1.10a), are luminescent at room temperature in degassed acetonitrile, with lifetimes of between 70 and 110 ns and quantum yields of 2.8×10^{-4} to 2.0×10^{-2}. $[Ru(ttpy)(dtp)]^+$ (Figure 1.10b), however, was found to be non-luminescent despite cyclometalation, due to the lack of these interligand interactions.

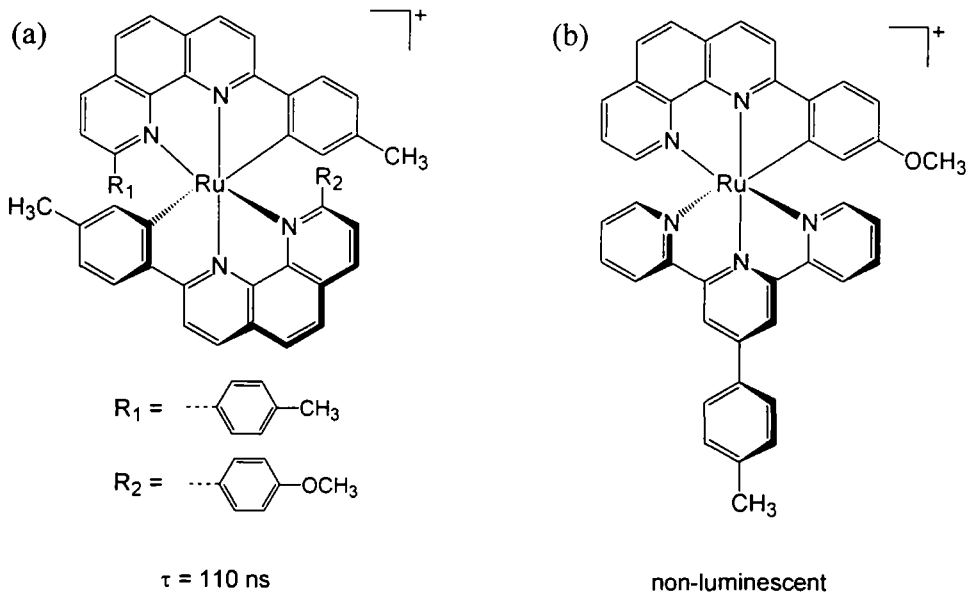

Figure 1.10: Ruthenium(II) cyclometalated complexes bearing sterically hindered and non-sterically hindered ligands, (a) $[Ru(mappy)(dtp)]^+$ and (b) $[Ru(ttpy)(dtp)]^+$.

1.3 Iridium complexes

Iridium is a third row transition metal with a ground state electronic configuration of $5d^76s^2$. It has accessible oxidation states from –3 to +6, but the high crystal field stabilisation energy, CFSE, that results from the low spin t_{2g}^6 octahedral state makes +3 the most common oxidation state. Iridium(III) is isoelectronic with ruthenium(II) lying diagonally related to it in the periodic table. As a third row transition metal, its coordination sphere is highly inert with harsh reaction conditions required to substitute the classical chloride ligands of the typical iridium salts, $IrCl_3$, used as starting materials.[38]

In recent years, research has taken place into d^6 iridium(III) complexes, with most studies focusing upon tris-bidentate complexes, especially $[Ir(ppy)_3]$, the archetypal complex used in OLED studies. Bis-terdentate iridium complexes have been studied to a much lesser extent by only a limited number of research groups, ours included.

1.3.1 Iridium(III) polypyridyl complexes

The synthesis of $[Ir(bpy)_3]^{3+}$ (Figure 1.11a) was first reported by Martin *et al.* in 1958, by heating K_3IrCl_6 in bpy at 272°C for 20 minutes.[39] In 1974, the synthetic route was adapted by Demas *et al.* now involving the conversion of $K_3IrCl_6.3H_2O$ into its sulfate salt by treatment with $K_2S_2O_8$ and $KHSO_4$ in boiling water, followed by evaporation and fusion in the air at > 250°C for 30 minutes. Subsequently the sulfate was reacted with bpy at 230°C for 6 hours under a CO_2 atmosphere. A laborious work-up and purification followed to give $[Ir(bpy)_3]^{3+}$ in 50% yield.[40] More recently the use of a microwave reaction was reported, involving the irradiation of $[IrCl_6][NH_4]_3.H_2O$ and bpy in ethylene glycol for 15 minutes, followed by precipitation into saturated aqueous KPF_6 solution and recrystallisation to give $[Ir(bpy)_3][PF_6]_3$ in 84% yield.[41]

At 77K, $[Ir(bpy)_3]^{3+}$ has highly structured ligand-centred emission with λ_{max}^{em} at 440 nm and a lifetime of 80 μs.[40] In degassed acetonitrile at 293 K, however, the lifetime is much shorter, 1.2 μs, with a quantum yield of 0.025. This is indicative of an emissive state that is primarily ligand centred with a relatively small element of MLCT character, unlike $[Ru(bpy)_3]^{2+}$ (Figure 1.2) which exhibits emission from an MLCT excited state. Cyclic voltammetry studies revealed metal-based oxidation of $[Ir(bpy)_3]^{3+}$

at a high potential, +2.17 V, and six one-electron reductions corresponding to the six pyridyl rings, with the first occurring at –0.76 V.[42]

In 1937, Morgan and Burstall reported the first synthesis of $[Ir(tpy)Cl_3]$, involving the reaction of Na_3IrCl_6 with tpy in water.[43] It was not until 1990, however, that the first account of the synthesis and photophysical properties of $[Ir(tpy)_2]^{3+}$ (Figure 1.11b) was published by Demas *et al.*[44, 45] This was based upon the fusion method they had previously used for $[Ir(bpy)_3]^{3+}$ resulting in typical isolated yields of 10–25%.[40] The difficult laborious preparation and purification resulted in little attention being directed towards such complexes for almost a decade.

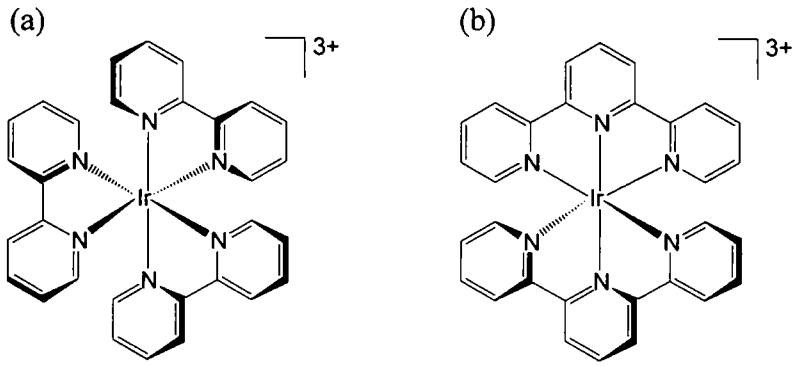

Figure 1.11: Structure of (a) $[Ir(bpy)_3]^{3+}$ and (b) $[Ir(tpy)_2]^{3+}$.

A two-step synthetic approach to the formation of iridium(III) bis-terpyridine complexes was devised by Sauvage *et al.* in 1999. This involved the introduction of the first ligand by reacting it with $[IrCl_3.3H_2O]$ in refluxing ethanol or ethylene glycol, depending upon the ligand solubility, to form the precursor $[Ir(tpy)Cl_3]$. This was subsequently reacted with the second ligand in degassed ethylene glycol at various temperatures between 140°C and reflux, 196°C, under an inert atmosphere, to displace the chloride ligands.[46] Purification of these tri-cationic complexes usually involves conversion to the hexafluorophosphate salts, which are soluble in polar organic solvents, allowing column chromatography to be utilised.

Heteroleptic complexes may be synthesised by this method, but short reaction times must be employed to try to minimise ligand scrambling, which can result in a mixture of heteroleptic and homoleptic complexes alongside several side products. The potential emissive properties of the undesired complexes can lead to interference in their photo-

spectroscopic analysis even when they are present in trace amounts, too low to be detected by ^{1}H-NMR or elemental analysis. The use of this milder, stepwise methodology has led to new interest in $[Ir(tpy)_2]^{3+}$ type complexes.

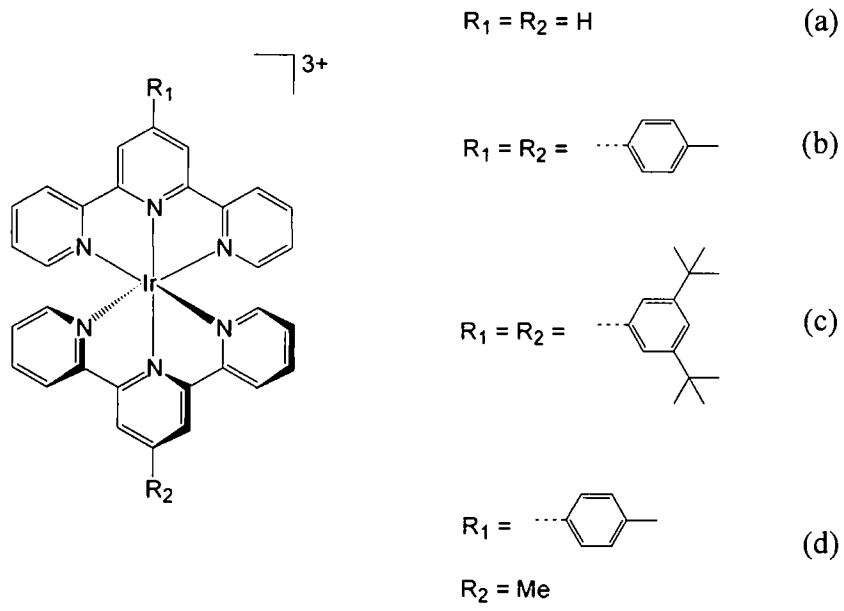

Figure 1.12: 4'-substituted iridium(III) bis-terpyridyl complexes.

Studies of the absorption spectra of this series of $[Ir(tpy)_2]^{3+}$ type complexes (Figure 1.12) revealed that the excited states are mainly ligand-centred, as previously reported for similar systems.[40, 44] It was observed that the intensities of emission from these complexes varied, with $[Ir(tpy)_2]^{3+}$ being ligand-centred in character and having the lowest intensity. The presence of 4'-substituents on the central ring results in greater electron delocalisation of the LC excited state, leading to longer-lived luminescence, a red-shift, and the broadening of the emission spectrum (Figure 1.13). The solution-state emission spectra of the complexes shown in Figure 1.12 were reported in both degassed and aerated acetonitrile; the emission lifetimes remained relatively unchanged under the two conditions indicating inefficient quenching by oxygen. The poorly overlapping emission spectra of the donor and absorption spectra of the acceptor alongside the unfavourable driving force for electron transfer from the complex to the dioxygen molecule, could account for this inefficiency. Cyclic voltammetry studies of these complexes revealed two one-electron reductions, one relating to each ligand, but no metal-based oxidation of Ir(III) to Ir(IV) within the range accessible.[46]

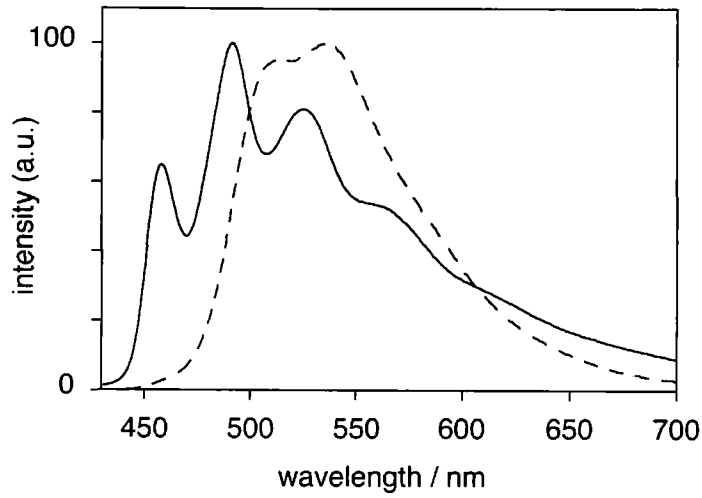

Figure 1.13: Room temperature emission spectra of $[It(tpy)_2]^{3+}$ (solid line) and $[Ir(ttpy)_2]^{3+}$ (broken line) in degassed acetonitrile solution.[47]

Owing to their long-lived luminescence lifetimes, iridium(III) bis-terpyridine complexes have been investigated as potential sensors. Williams *et al.* reported the synthesis of a series of such complexes bearing protonatable pyridyl, and deprotonatable phenolic groups (Figure 1.14) in 1999.[48] Upon protonation and deprotonation of the respective complexes, *via* a change in pH, their emission lifetimes and intensities varied, thus outlining the potential use of such complexes as pH sensors.

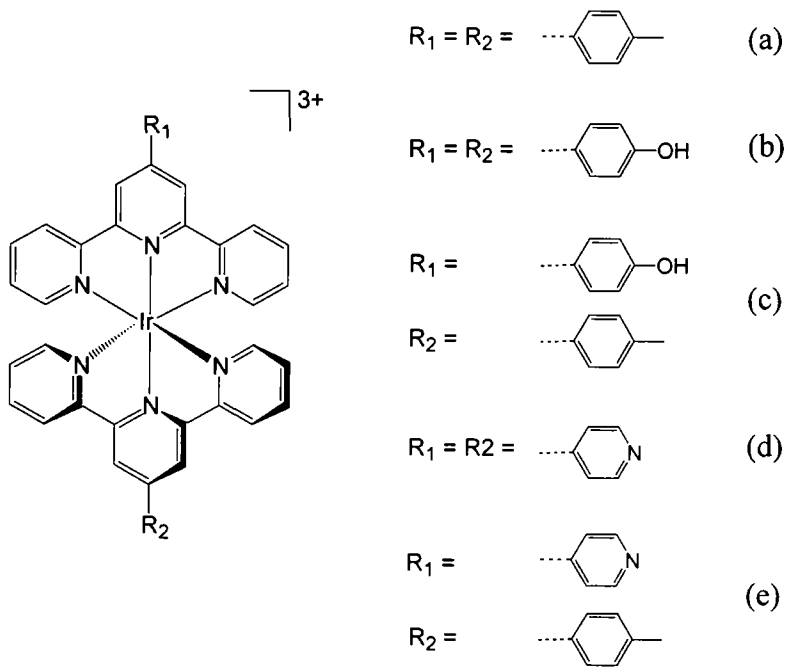

Figure 1.14: Potential pH sensors; (a) $[Ir(ttpy)_2]^{3+}$, (b) $[Ir(tpy\text{-}OH)_2]^{3+}$, (c) $[Ir(tpy\text{-}OH)(qtpy)]^{3+}$, (d) $[Ir(qtpy)_2]^{3+}$ and (e) $[Ir(qtpy)(ttpy)]^{3+}$.

The greatest effect on the luminescence lifetimes was observed for $[Ir(qtpy)(ttpy)]^{3+}$ (Figure 1.14e) where an eight-fold decrease in emission intensity and a reduction in lifetime from 4.7 to 0.5 μs, was seen upon protonation, lowering the pH from 7 to 2. This complex constitutes a particularly useful pH sensor owing to the significant change in luminescence with pH variation. At higher pH the excited state is predominantly ligand-centred. A reduction of pH, upon protonation of the appended pyridyl group, is accompanied by the lowering of the energy of the ^{3}MLCT state resulting in the mixing of CT character into the LC state, shortening the lifetime. It was also noted that the introduction of pyridyl substituents at the 4'-postion, $[Ir(qtpy)_2]^{3+}$ (Figure 1.14d), has little effect on the emission spectra at ambient pH. This results from the poorer conjugation of the pyridyl substituents with the tpy moiety of the ligand compared to aryl substituents. Lifetimes in degassed acetonitrile thus remain of the order of 1 μs as for $[Ir(tpy)_2]^{3+}$. In complexes containing one aryl and one pyridyl substituents, $[Ir(qtpy)(ttpy)]^{3+}$ (Figure 1.14e), however, the emission spectrum was reported to be much broader and red-shifted resembling that of $[Ir(ttpy)_2]^{3+}$ (Figure 1.14a) with the corresponding lifetimes being much longer, ~ 6 μs. This supports Kasha's rule, that emission occurs from the lowest excited state, here localised on the ttpy ligand.[48, 49]

In 2000 Williams *et al.* reported the potential use of iridium(III) bis-terpyridine complexes as sensors for chloride ions at physiological concentrations. One of the complexes (Figure 1.15) experiences a six-fold decrease in luminescence lifetime upon going from the presence of zero to 0.1 M chloride ions.[50]

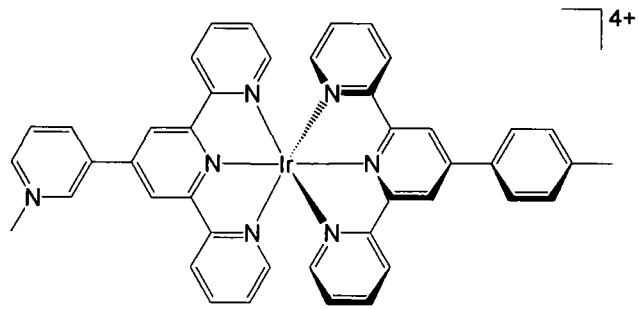

Figure 1.15: Potential chloride ion sensor.

The harsh conditions required for the synthesis of aryl appended iridium(III) bis-terpyridine complexes pose a potential problem if sensitive functional groups are to be incorporated. To overcome this problem, Williams *et al.* have been investigating the

possibility of "chemistry on the complex" involving *in situ* palladium catalysed cross-coupling reactions (Figure 1.16). This approach can be used for the introduction of sensitive functional groups to monometallic complexes, which would otherwise not be able to withstand the severe reaction conditions used in conventional synthesis,[51] alongside the controlled synthesis of linear multimetallic assemblies from appropriately functionalised monometallic building blocks.[52]

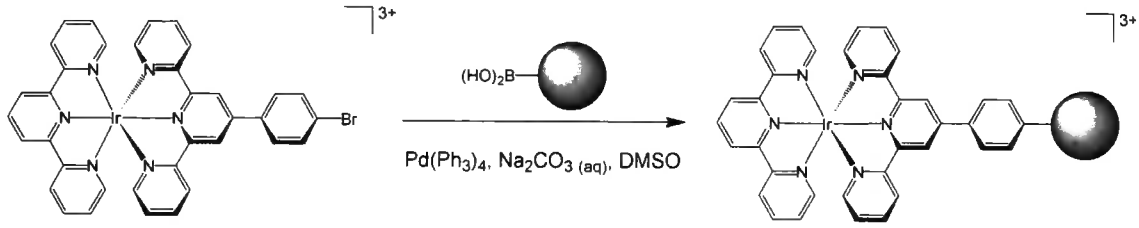

Figure 1.16: Cross-coupling reaction of $[Ir(tpy)(tpy\text{-}\phi\text{-}Br)]^{3+}$ with aryl boronic acids or boronic acid appended monometallic complexes.

The common starting material for this strategy is the bromo-appended complex $[Ir(tpy)(tpy\text{-}\phi\text{-}Br)]^{3+}$, tpy-ϕ-Br = 4'-(*p*-bromophenyl)-2,2':6',2''-terpyridine, which is synthesised in adequate yield from the reaction of the precursor $[Ir(tpy)Cl_3]$ with tpy-ϕ-Br in refluxing degassed ethylene glycol. The bromo-appended complex is subsequently reacted with an aryl boronic acid, or a metal complex incorporating a boronic acid group in one of its ligands, in dimethylsulfoxide in the presence of base, $Na_2CO_{3\,(aq)}$, and palladium catalyst, $Pd(PPh_3)_4$. The reaction times for these *in situ* complexations (Figure 1.16) are significantly shorter than those required for the free ligand,[53] due to either increased labilisation of the C-Br bond resulting from its *para* orientation to the charged metal centre, or the removal of competitive complexation of the palladium catalyst to the terpyridine.

Complexes synthesised in this manner incorporating terpyridyl ligands containing a biaryl pendant, *e.g.* $[Ir(tpy)(tpy\text{-}\phi\text{-}ph)]^{3+}$ exhibit a significant red-shift in emission, λ_{max}^{em} = 560 nm,[54] compared to $[Ir(tpy)_2]^{3+}$, λ_{max}^{em} = 458 nm in acetonitrile. This is much larger than the corresponding shift seen for $[Ir(ttpy)_2]^{3+}$, λ_{max}^{em} = 506 nm,[46] resulting from the increased conjugation of the terpyridyl ligand with each additional phenyl group. Such biaryl appended iridium(III) bis-terpyridyl complexes are reported to have remarkably long luminescence lifetimes, > 100 μs in aqueous solution, indicative of their predominantly LC emissive excited states. With a thirty-fold

reduction in the luminescence lifetime of $[Ir(tpy)(tpy\text{-}\phi\text{-}ph)]^{3+}$ observed upon saturation of the degassed aqueous solution with oxygen,[54] it is also an extremely efficient singlet oxygen sensor, $\Phi(O_2\text{–}^1\Delta_g) = 0.95$.

1.3.2 Iridium(III) cyclometalated complexes

1.3.2.1 Tris-bidentate complexes

In 1977 Watts *et al.* reported the synthesis of a cyclometalated iridium complex, formed by reacting 2,2'-bipyridine, bpy, with iridium(III) trichloride in ethylene glycol at 180°C.[55] There has been some debate over the years about the actual structure of this complex; it was at first mistakenly identified as $[Ir(bpy\text{-}NN')_2(bpy\text{-}N)(H_2O)]^{3+}$ (Figure 1.17a) with a monodentately bound bipyridine ligand and a water molecule occupying the sixth coordination site.[55] This later evolved into a theory where a molecule of water added to the bipyridine ligand itself, before it bound to the iridium(III) centre (Figure 1.17b).[56] The actual structure of the complex was finally determined in 1981 by X-ray crystallography,[57] where it was shown that the bipyridine ligand bound *via* one nitrogen atom and one cyclometalating carbon, at the 3-position, giving the structure $[Ir(bpy\text{-}NN')_2(Hbpy\text{-}C^3N')]^{3+}$ (Figure 1.17c).[57-59]

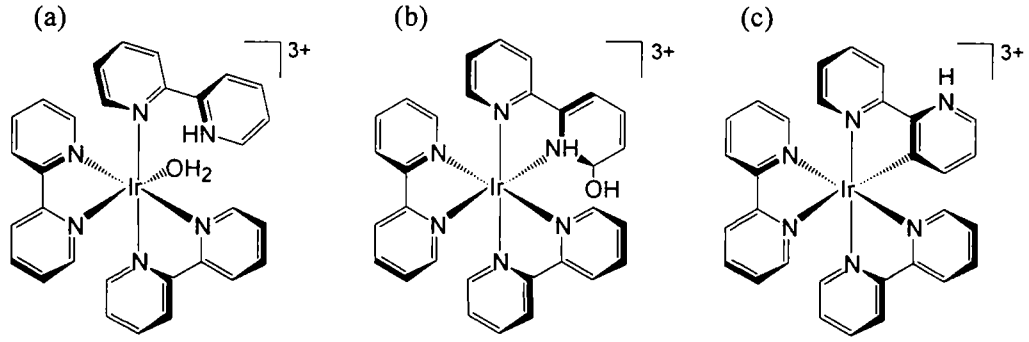

Figure 1.17: Proposed binding modes for $[Ir(bpy\text{-}NN')_2(Hbpy\text{-}C^3N')]^{3+}$.

Whilst 2,2'-bipyridine and its derivatives rarely cyclometalate, ligands containing one benzene ring and a functional group with a coordinating atom do *e.g.* 2-phenylpyridine (ppyH). The preparation of the dichloro-bridged di-iridium complex $[Ir(ppy)_2(\mu\text{-}Cl)]_2$ (Figure 1.18), was first reported in 1985 from the reaction of ppyH with iridium(III) trichloride.[60, 61]

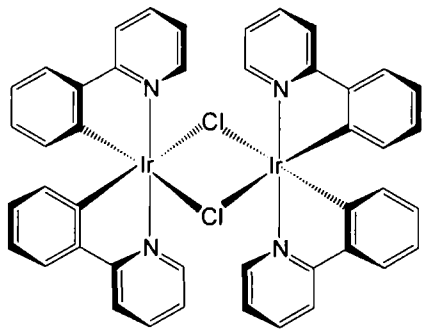

Figure 1.18: $[Ir(ppy)_2(\mu\text{-}Cl)]_2$

This dimeric species can be used as an intermediate in the synthesis of the prototypical cyclometalated charge neutral complex $[Ir(ppy)_3]$, with *fac*-$[Ir(ppy)_3]$ (Figure 1.19a) itself having been identified as a side product in the synthesis of $[Ir(ppy)_2(\mu\text{-}Cl)]_2$.[61] To date, most of the synthetic routes for $[Ir(ppy)_3]$ have resulted in the thermodynamically favourable facial isomer (Figure 1.19a).[61-64] This is due to the *trans*-directing effect of cyclometalating ligands directing the nitrogen of the pyridyl ring on a neighbouring ppyH ligand into the *trans* position. In 2000 the first report of the application of *fac*-$[Ir(ppy)_3]$ to OLEDs was published.[65]

In 2003, Thompson *et al.* reported the first preparation of the kinetically stable meridional isomer (Figure 1.19b).[66] This was formed by the reaction of the $[Ir(ppy)_2(\mu\text{-}Cl)]_2$ intermediate with ppyH at 140°C, in the presence of potassium carbonate. Higher reaction temperatures, typically over 200°C, lead to the formation of the facial isomer. Likewise the synthesis of facial and meridional isomers of iridium(III) complexes containing 2-(*p*-tolyl)pyridine, tlpyH, and 1-phenylpyrazole, pzbH, were reported.[66]

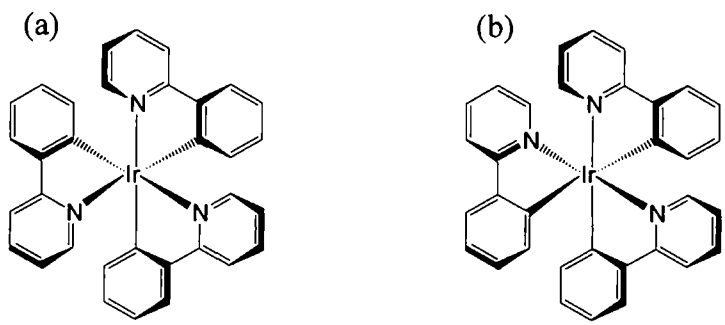

Figure 1.19: Structure of (a) *fac*-$[Ir(ppy)_3]$ and (b) *mer*-$[Ir(ppy)_3]$.

X-ray crystallographic studies of *fac*- and *mer*-[Ir(tlpy)$_3$] reveal that the two isomers have distinctly different molecular structures. In the facial isomer, all of the Ir–C (2.025 Å) and Ir–N (2.133 Å) bonds are of equivalent length, as Ir–C bonds are always *trans* to Ir–N bonds.[67] In the meridional isomer, however, the lengths of the Ir–C and Ir–N bonds vary. Whilst the Ir–C bonds (2.021 Å) *trans* to Ir–N (2.152 Å) are comparable to those in the facial isomer, the mutually *trans* Ir–N bonds are considerably shorter (~ 2.055 Å), due to the weaker *trans*-influence of the pyridyl group. The stronger *trans*-influence of the cyclometalating phenyl group, similarly, lengthens the mutually *trans* Ir–C bonds (~ 2.081 Å).[66]

Room temperature emission, from the facial and meridional isomers of [Ir(ppy)$_3$] and its derivatives was reported to be broad and structureless, characteristic of a predominantly ^{3}MLCT excited state, induced by the presence of the three cyclometalating ligands. Meridional isomers being easier to oxidise were reported to exhibit broader, red-shifted emission. This broader character signifies the larger geometric distortion of the excited state, believed to lead to an increase in the length of the long *trans* Ir–C bonds, its cleavage and the consequent formation of the facial isomer. With the radiative decay constants of the two isomers being comparable, the smaller luminescence quantum yield of the meridional isomer is attributed to the large non-radiative decay constants linked with photoisomerisation.[66]

Whilst the trends between *fac*- and *mer*-[Ir(pzb)$_3$] are the same as for ppy, the spectroscopic properties of the phenylpyrazolyl-based complexes vary significantly with respect to those containing the phenylpyridyl ligand.[66] This owes to the fact that pyrazole is a poorer π-acceptor than pyridine, thus affecting the distribution of electron density within the complex. The facial isomer of [Ir(pzb)$_3$] was reported to be only weakly emissive at room temperature in solution, unlike [Ir(ppy)$_3$], whilst highly emissive at 77 K. The emission bands were significantly blue-shifted, with respect to complexes containing phenyl-based ligands, and the observed lifetimes much longer; indicative of an excited state with considerable ligand-centred character.[62, 63, 66]

The synthesis and photophysical properties of [Ir(ppy)$_2$(bpy)]$^+$, (Figure 1.20a) containing both cyclometalating and polypyridyl ligands, has been described by Watts *et al.*[68] This was formed in good yield by the reaction of the [Ir(ppy)$_2$(μ-Cl)]$_2$

intermediate with bpy in dichloromethane at ambient temperature. Theoretically there are two possible isomers that could have been formed, however, the cisoid relationship of the Ir–C bonds in the dimeric intermediate was retained and only one isomer formed.[67, 68] Whilst $[Ir(bpy)_3]^{3+}$ is an excellent photo-oxidant with LC emission characteristics and $[Ir(ppy)_3]$ a superb photo-reductant with MLCT emission characteristics, this complex lies in between, thus exhibiting electrochemical properties of an intermediate nature. Watts *et al.* reported that oxidation at the iridium(III) centre occurs much more readily in $[Ir(ppy)_2(bpy)]^+$ (1.26 V *vs.* SCE) than in $[Ir(bpy)_3]^{3+}$, whilst the reduction is more difficult owing to a +1 complex being harder to reduce than a +3 complex.[69] Broad structureless emission is observed at 77 K, with two components, λ_{max}^{em} = 520 nm and 550 nm, which may be resolved by selective excitation.[68, 70] These two transitions arise due to unequilibrated MLCT states with very similar lifetimes, the lower energy component involving the electron transfer to the π^* orbital of the bpy ligand and the higher energy component to the ppy ligand.[68] These conclusions were supported by excited state absorption measurements[71] and the solvent dependence of emission.[72] It was reported that at room temperature, emission was predominantly from the lowest energy bpy-based MLCT transition.[70]

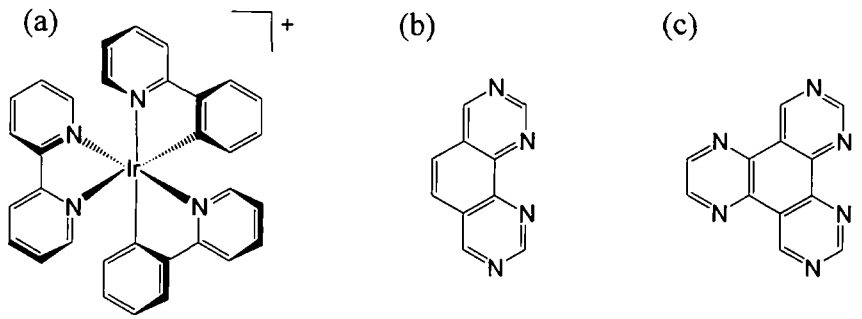

Figure 1.20: Structure of (a) *fac*-$[Ir(ppy)_2(bpy)]^+$ (b) 1,4,5,8-tetraazaphenanthrene (TAP) and (c) 1,4,5,8,9,12-hexaazatriphenylene (HAT).

A similar reaction involving the cleavage of the dichloro-bridged di-iridium species was reported with 1,4,5,8-tetraazaphenanthrene, TAP, (Figure 1.20b) and the potentially bridging ligand 1,4,5,8,9,12-hexaazatriphenylene, HAT, (Figure 1.20c),[73] thus allowing the synthesis of dinuclear mixed metal assemblies.[74] It was reported that, at room temperature, $[Ir(ppy)_2(HAT)]^+$ emitted from an MLCT excited state with $\lambda_{max}^{em} > 770$ nm and $\tau < 10$ ns. Whilst at 77 K, dual emission was observed, with the

two components being assigned to an MLCT, $\tau = \sim 1.5$ μs, and a sigma-bond-to-ligand charge transfer (SBLCT) excited state, $\tau = \sim 3$ μs.[73]

1.3.2.2 Complexes incorporating terdentate ligands

Iridium(III) complexes bearing terdentately bound cyclometalating ligands are still relatively unstudied with only a limited number of groups researching them worldwide. In 1997, Mamo *et al.* reported the first synthesis of such a complex, bearing the potentially cyclometalating ligand 2,6-bis(7'-methyl-4'-phenyl-2'-quinolyl)pyridine, bmpqpyH (Figure 1.21). This can bind either through three nitrogen atoms, NNN (Figure 1.21a), or through two nitrogen atoms and a cyclometalating carbon, NNC (Figure 1.21b). Refluxing the ligand with [$IrCl_3.3H_2O$] in glycerol for 24 hours resulted in the formation of two complexes: [Ir(bmpqpyH-*NNN*)(bmpqpy-*NNC*)]$^{2+}$, and [Ir(bmpqpy-*NNC*)$_2$]$^+$ containing two mutually *cis* cyclometalating carbons. Attractive face-to-face stacking interactions were reported between the 4'-phenyl pendant on the NNC-coordinated ligands and the electron-deficient central pyridine of the second ligand. This interaction was indicated by the unusually low chemical shifts of the *ortho* and *meta* protons of the pendant group in the ^{1}H-NMR spectra, resulting from the mutual diamagnetic shielding of the aromatic rings by the ring facing it.

Emission from both these complexes was reported to be of predominantly ^{3}MLCT character owing to the introduction of a cyclometalating carbon into the coordination sphere of the iridium centre. The heteroleptic, mono-cyclometalated complex [Ir(bmpqpyH-*NNN*)(bmpqpy-*NNC*)]$^{2+}$, however, was reported to display surprisingly weak luminescence ($\Phi = 5 \times 10^{-3}$, $\tau = 325$ ns) in degassed acetonitrile at room temperature.[75] A probable explanation for this was given by Williams *et al.* following the synthesis of mono-cyclometalated [Ir(NCN)(NNN)]$^{2+}$ complexes (Figure 1.24). They suggested that it was associated with the higher degree of ligand-to-ligand charge transfer character and low metal contribution of the excited state.[76] Mamo *et al.* reported the luminescence quantum yield ($\Phi = 6.6 \times 10^{-2}$, $\tau = 2.3$ μs) of the homoleptic complex [Ir(bmpqpyH-*NNC*)$_2$]$^+$ to be one order of magnitude higher than that of the heteroleptic [Ir(bmpqpyH-*NNN*)(bmpqpy-*NNC*)]$^{2+}$, resulting from the introduction of the second cyclometalating carbon and the consequential increase in MLCT character of the excited state.[75]

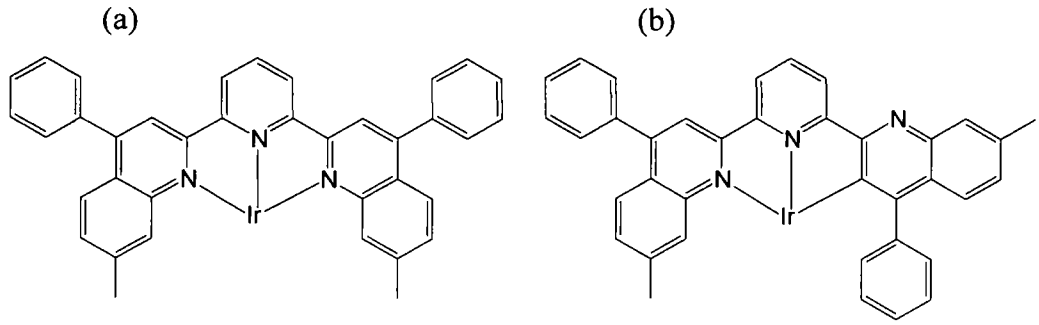

Figure 1.21: The (a) non-cyclometalating and (b) cyclometalating binding of bmpqpyH.

This explanation is supported by electrochemical studies which revealed that the heteroleptic, mono-cyclometalated complex showed no oxidation of the metal up to +2.0 V *vs.* SCE, whilst oxidation of the metal in the homoleptic bis-cyclometalated complex occurred at +1.40 V *vs.* SCE. This was explained due to a decrease in oxidation potential occurring upon an increase in the number of cyclometalating carbons in the coordination sphere of the metal.[75]

6-Phenylbipyridine, phbpyH, is known to bind in a terdentate cyclometalating, NNC manner, having been investigated with Ru(II), Rh(III) and Pt(II).[34] When attempts were made by Williams *et al.* to react this with $[Ir(tpy)Cl_3]$, however, the complex isolated was $[Ir(tpy)(phbpyH\text{-}NN)Cl]^{2+}$ (Figure 1.22a).[77] This structure was determined by ^{1}H-NMR spectroscopy, which revealed that the two-fold symmetry of the phenyl moiety of phbpyH was maintained upon binding to Ir(III) indicating that cyclometalation had not occurred. The unusually low chemical shifts of the *ortho* and *meta* protons, as seen in Mamo's complexes (Figure 1.21), indicated that the pendant phenyl ring lay above the plane of the terpyridyl ligand. Emission from $[Ir(tpy)(phbpyH\text{-}NN)Cl]^{2+}$ was reported to be less structured and red-shifted compared to that from $[Ir(tpy)_2]^{3+}$. This was attributed to the significant contribution of the 6'-phenylbipyridine ligand to the HOMO and/or LUMO, alongside an increase the charge-transfer character of the excited state brought about by the presence of the anionic chloride ligand.[77]

A different binding problem was observed in the reaction of $[Ir(tpy)Cl_3]$ with 4'-tolyl-6-phenyl-2,2'-bipyridine, tphbpyH. Here the presence of the 4'-tolyl group favours the bidentate, NC, binding of the ligand *via* the nitrogen of the terminal pyridine ring and the $C^{3'}$-cyclometalating position of the central pyridine ring. The terminal phenyl ring

was thus not able to cyclometalate and was directed away from the metal with a chloride occupying the sixth coordination site, being orientated *trans* to the cyclometalating carbon giving $[Ir(tphbpy\text{-}NC)(tpy)Cl]^+$ (Figure 1.22b). ^{1}H-NMR studies confirmed this surprising cyclometalation of the central pyridine and the positioning of the tolyl group above the plane of the tpy ligand. $[Ir(tphbpy\text{-}NC)(tpy)Cl]^+$ was reported to exhibit lower energy bands in the absorption spectrum than $[Ir(tpy)(phbpyH\text{-}NN)Cl]^{2+}$ alongside stronger emission, $\Phi = 16 \times 10^{-2}$ compared to 0.7×10^{-2}. This was attributed to the introduction of the cyclometalating carbon in the coordination sphere of the former.[77]

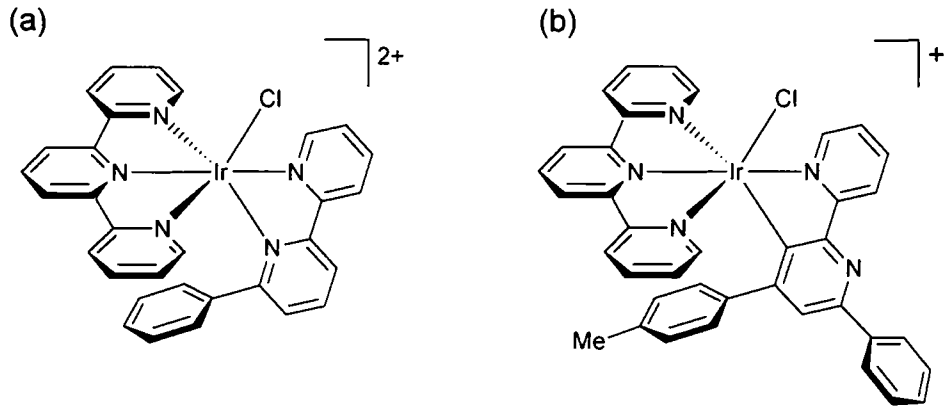

Figure 1.22: Structure of (a) $[Ir(phbpyH\text{-}NN)(tpy)Cl]^{2+}$ and (b) $[Ir(tphbpy\text{-}NC)(tpy)Cl]^+$.

Previous work within the Williams group investigated the introduction of 1,3-di(2-pyridyl)benzene, dpybH, into the coordination sphere of Ir(III) (Figure 1.23a).[78] Whilst dpybH had been seen to coordinate to Ru(II),[29, 79] Os(II)[29, 79] and Pt(II)[80, 81] in a terdentate NCN manner, the main product isolated with Ir(III), following reaction with $[IrCl_3.3H_2O]$ in 2-ethoxyethanol/water (3:1) at 130°C for 6 hours, was that involving the bidentate binding of dpybH (Figure 1.23b). It appeared that cyclometalation of the phenyl ring with Ir(III) was kinetically favoured at the $C^{4'}$-position over the more hindered $C^{2'}$-position. To overcome the problem of this alternative bidentate binding, the $C^{4'}$- and $C^{6'}$-cyclometalating sites were blocked by the introduction of methyl substituents. The new ligand, 1,3-di(2-pyridyl)-4,6-dimethylbenzene, dpydmbH, was prepared by the palladium catalysed Stille cross-coupling of 1,3-dibromo-4,6-dimethylbenzene with 2-tri-*n*-butylstannyl-pyridine. The subsequent reaction of dpydmbH with $[IrCl_3.3H_2O]$, at 80°C, gave the dichloro-bridged dimer $[Ir(dpydmb)Cl(\mu\text{-}Cl)]_2$ (Figure 1.23c). Whilst the dimeric species is insoluble in most

common solvents, heating it with d_6-DMSO affords the solvated structure [Ir(dpydmb)(d_6-DMSO)Cl_2]. The ^{1}H-NMR spectra of this complex reveals the loss of the signal corresponding to $H^{2'}$, thus indicating cyclometalation at $C^{2'}$ and the desired NCN terdentate binding. X-ray crystallography confirmed the solvated structure as being [Ir(dpydmb)(d_6-DMSO)Cl_2].[76, 78]

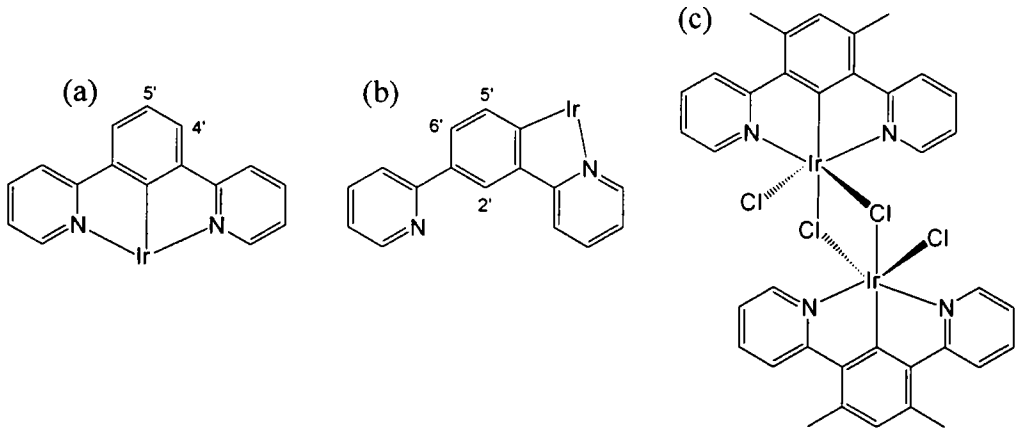

Figure 1.23: The (a) NCN and (b) NC binding modes of 2,6-di(2-phenyl)benzene alongside (c) the dichloro-bridged dimer [Ir(dpydmb)Cl(μ-Cl)]$_2$.

Reaction of the dimer with 2,2':6',2''-terpyridine, tpy, and 4'-(*p*-tolyl)-2,2':6',2''-terpyridine, ttpy, in refluxing ethylene glycol for 1 hour, gave $[Ir(dpydmb)(tpy)]^{2+}$ (Figure 1.24a) and $[Ir(dpydmb)(ttpy)]^{2+}$ (Figure 1.24b) respectively, in high yield. The absorption spectra of these complexes displayed relatively weak bands extending into the visible region, beyond 400 nm, not present in $[Ir(tpy)_2]^{3+}$ type complexes. These complexes were reported to be scarcely emissive with structured profiles, at both room temperature ($\Phi < 10^{-3}$ in degassed acetonitrile) and 77 K. Density functional theory, DFT, calculations revealed that the lowest-energy excited state has a significant amount of ligand-to-ligand charge transfer character; with the HOMO being localised on the NCN ligand, with very little contribution from the metal, and the LUMO being localised on the tpy-based ligand. Owing to the lack of metal character in the excited state, the oscillator strength and hence radiative rate constant, k_r, are very small, accounting for the weak bands beyond 400 nm in the absorption spectra and for the weak emission.[76]

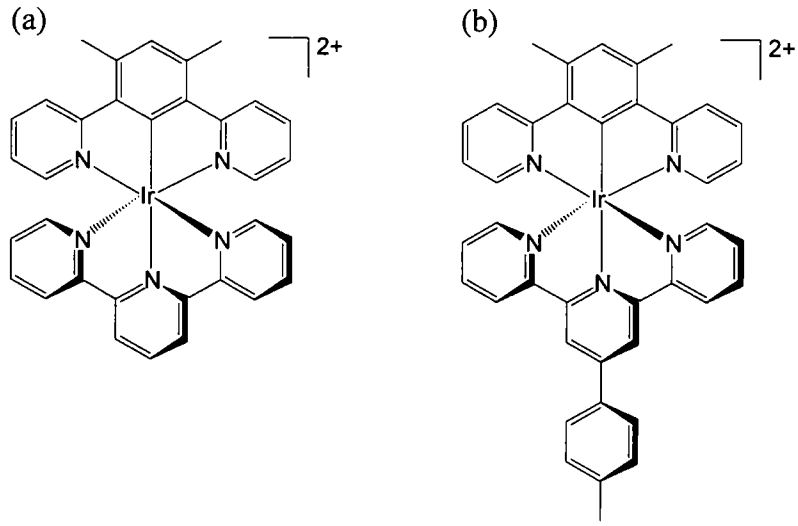

Figure 1.24: Structure of (a) $[Ir(dpydmb)(tpy)]^{2+}$ and (b) $[Ir(dpydmb)(ttpy)]^{2+}$.

$[Ir(NCN)(NNN)]^{2+}$ complexes have also been reported by Haga *et al.*; they incorporated bis-benzimidazole ligands into the coordination sphere of Ir(III). Synthesis involved the reaction of $[Ir(Mebip)Cl_3]$, Mebip = 1,3-bis-(1-methylbenzimidazol-2-yl)pyridine, with 1,3-bis-(1-methylbenzimidazol-2-yl)benzene, MebibH, in refluxing ethylene glycol to afford $[Ir(Mebip)(Mebib)]^{2+}$ (Figure 1.25).[82] Whilst this complex displays weak, low energy bands in the absorption spectrum like Williams' $[Ir(NCN)(NNN)]^{2+}$ complexes, it was found to be much more emissive, with $\Phi = 0.10$ in degassed acetonitrile.[82] This increased emission was attributed to the larger metal contribution in the HOMO, and the stronger σ-donating ability of MebibH than dpydmbH; this led to greater ^{3}MLCT character in the excited state, and a higher radiative rate constant, k_r.

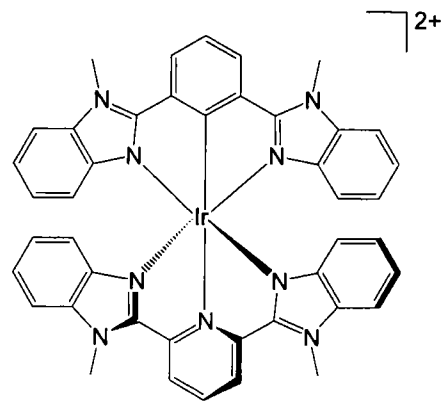

Figure 1.25: Haga's $[Ir(Mebip)(Mebib)]^{2+}$ complex.

In 2004 Scandola *et al.* reported the successful cyclometalation of a series of 4'-aryl-substituted-2,6-diphenylpyridine ligands with Ir(III); *e.g.* $[Ir(tdppy)(tpy\text{-}\phi\text{-}Br)]^+$ (Figure 1.26), following the reaction of the ligand 2,6-diphenyl-4'-(*p*-tolyl)pyridine, $tdppyH_2$, with $[Ir(tpy\text{-}\phi\text{-}Br)Cl_3]$ in degassed ethylene glycol at 190°C.[83, 84] $[Ir(tdppy)(tpy\text{-}\phi\text{-}Br)]^+$ was reported to exhibit Ir–N bonds between the metal and the terpyridine fragment, equivalent in length to those seen in $[Ir(tpy)_2]^{3+}$ type complexes. On the other hand the Ir–N bonds between the metal and the CNC fragment were reported to be relatively short (2.023 Å) and the Ir–C bonds relatively long (2.095 and 2.123 Å). As in $[Ir(ppy)_3]$, these longer bonds were attributed to the *trans*-influence of the cyclometalating phenyl ring.[83]

These *trans* disposed bis-cyclometalated complexes exhibit broad structureless emission deep into the red region; *e.g.* $[Ir(tdppy)(tpy\text{-}\phi\text{-}Br)]^+$ with λ_{max}^{em} = 690 nm. The emission was reported to be weak, Φ = 0.032, with a relatively long lifetime, τ = 1.7 μs, indicative of a low radiative rate constant, $k_r = 1.9 \times 10^{-4}\ s^{-1}$.[83] DFT studies attributed these findings to the predominantly tdppyH based HOMO and tpy-ϕ-Br localised LUMO, resulting in emission from an excited state with substantial ligand-to-ligand (tdppy→tpy-ϕ-Br), LLCT, character.[83, 84] Cyclic voltammetry studies of $[Ir(tdppy)(tpy\text{-}\phi\text{-}Br)]^+$ revealed a reversible one-electron oxidation at +1.08 V *vs.* SCE.[83] This is lower than the oxidation potential observed for *cis*-disposed bis-cyclometalated complexes,[75] but comparable to those where the Ir–C bonds have a *trans* geometry.[66] A one-electron reduction of the tpy-ϕ-Br was reported at –1.27 V *vs.* SCE, ~ 0.5 V lower than that observed for the analogous iridium bis-terpyridyl complexes.[83]

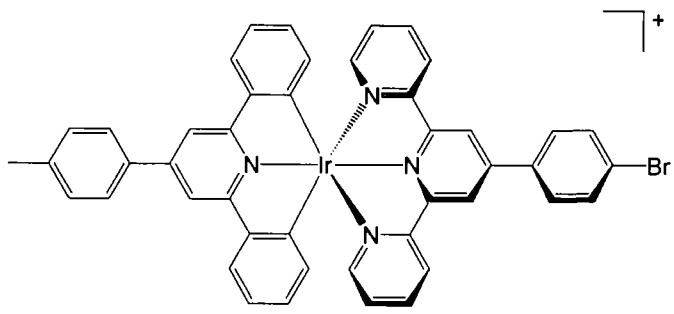

Figure 1.26: $[Ir(tdppy)(tpy\text{-}\phi\text{-}Br)]^+$

Comparing this to Mamo's *cis*-disposed bis-cyclometalated complex $[Ir(bmpqpyH\text{-}NNC)_2]^+$ (Figure 1.21b) it becomes apparent that the emission properties are dependent upon the orientation of the two carbon atoms. The predominantly LLCT excited state reported for the *trans*-orientated bis-cyclometalated complex accounts for the low radiative rate constant, k_r, and low energy emission maxima.[84] The HOMO and HOMO-1 of the *cis*-disposed bis-cyclometalated complex, however, displays a more equal contribution from the two cyclometalating rings and the iridium centre. Hence it exhibits higher energy emission and a radiative rate constant significantly higher than that seen in the *trans*-complex. The luminescence quantum yield, however, remains relatively unchanged due to a comparable decrease in the non-radiative rate constant.[47, 75]

With the charge-neutral tris-bidentate complex *fac*-$[Ir(ppy)_3]$ being of great interest as a triplet harvesting agent in OLEDs,[65] and bis-terdentate complexes offering structural advantages over their tris-bidentate analogues, the Williams group investigated the synthesis of a series of charge neutral bis-terdentate complexes.[76, 78] Initial attempts to synthesise the bis-terdentate analogue of *fac*-$[Ir(ppy)_3]$ containing two cyclometalating ligands, one binding *via* NCN and the other CNC, were reported to have failed under the usual solution-based forcing conditions required for bis-terpyridyl complexes. The main product isolated from the reaction of the dichloro-bridged di-iridium NCN complex (Figure 1.23c) with 2,6-diphenylpyridine, $dppyH_2$, under these conditions was found to contain dppyH bound in a bidentate, NC, manner with the second phenyl ring left unbound and the sixth coordination site occupied by a labile solvent molecule. The development of a solvent-free method involving the heating of $[Ir(dpydmb)Cl(\mu\text{-}Cl)]_2$ with silver(I) trifluoromethanesulfonate in molten $dppyH_2$, at 110°C, followed by rapid purification by column chromatography was reported to afford the desired charge-neutral complex [Ir(dpydmb)(dppy)] (Figure 1.27a).

The absorption spectra of [Ir(dpydmb)(dppy)] exhibited strong bands in the visible region (458, 481 and 510 nm), which were assigned to MLCT transitions and occurred at significantly lower energy than the equivalent bands for $[Ir(ppy)_3]$. This was rationalised as being the result of increased delocalisation across the three aromatic rings of the NCN, dpydmb, ligand lowering the energy of the π^* orbitals of the acceptor ligand.[78] [Ir(dpydmb)(dppy)] was observed to be strongly luminescent in degassed

acetonitrile, Φ = 0.21, displaying a single, broad, structureless emission band, λ_{max}^{em} = 585 nm, significantly red-shifted compared to *fac*-[Ir(ppy)$_3$]. DFT studies revealed the LUMO to be localised on the NCN-coordinating ligand and the HOMO to have contributions from both ligands and the iridium centre. This is indicative of emission from a mixed MLCT/LLCT/LC, d(Ir)/π(dpydmb)/π(dppy)$\rightarrow\pi^*$(dpydmb), excited state. The significant ligand-centred character is thought to account for the lifetime, τ = 3.8 μs, being longer than those observed from purely MLCT excited states. The tetrafluorinated derivative [Ir(dpydmb)(F$_4$dppy)] (Figure 1.27b) was synthesised under similar conditions, with emission being observed at higher energy than the non-fluorinated complex owing to the stabilisation of the HOMO, resulting from the electron-withdrawing nature of the fluorine substituents.[76]

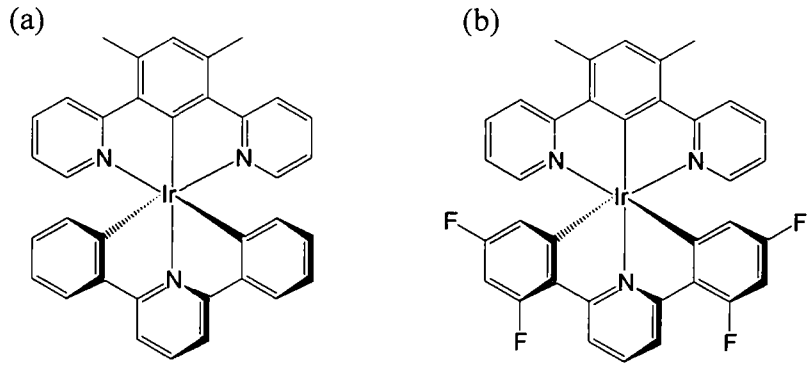

Figure 1.27: Structure of (a) [Ir(dpydmb)(dppy)] and (b) [Ir(dpydmb)(F$_4$dppy)].

As reported in Section 1.3.2.1 the luminescence efficiency of the meridional isomer of [Ir(ppy)$_3$] was found to be significantly lower than that of the facial isomer. This results from *mer*-to-*fac* photoisomerisation, owing to the lability of two mutually *trans* Ir–C bonds in the former. Whilst [Ir(dpydmb)(dppy)] is the bis-terdentate analogue of *mer*-[Ir(ppy)$_3$], its non-radiative rate constant, Σk_{nr} is comparable to that of the facial isomer. Following a photodissociation study of the complex in acetonitrile, irradiated with a xenon lamp, ^{1}H-NMR spectroscopy identified [Ir(dpydmb)(dppyH-*CN*)L]$^+$ as the major product, indicating the cleavage of one of the mutually *trans* Ir–C bonds.[78] This is believed to be the first step in the photoisomerisation of *mer*-[Ir(ppy)$_3$] to *fac*-[Ir(ppy)$_3$]. The terdentate ligand, however, cannot isomerise and thus results in the bidentate coordination of dppyH in the partially dissociated complex [Ir(dpydmb)(dppyH-*CN*)L]$^+$. This photodissociation is sufficiently slow to not significantly affect the luminescence

quantum yield of the complex, but could be the reasoning behind the failed solution-based synthesis.[47]

Other charge-neutral complexes reported in Williams' study included [Ir(dpydmb)(tppic)] (Figure 1.28a) incorporating the ligand 4-*p*-tolyl-6-phenylpicolinic acid, tppicH_2, coordinating *via* CNO, and [Ir(dpydmb)(ppy)Cl] (Figure 1.28b). Emission from [Ir(dpydmb)(ttpic)] was similar to that of [Ir(dpydmb)(dppy)], indicative of a mixed MLCT/LLCT/LC excited state. The quantum yield and observed lifetime, however, were reported to be significantly lower than in [Ir(dpydmb)(dppy)] due to the weaker nature of the Ir–O bond compared to the Ir–C bond, resulting in an increased rate of photochemical cleavage. [Ir(NCN)(NC)X] complexes (where X is an anionic ligand) *e.g.* [Ir(dpydmb)(ppy)Cl] with $\Phi = 0.76$, are reported to be the brightest emitters of all iridium complexes bearing terdentate ligands.[76] This bodes well for the future use of such complexes in light-emitting devices.[47] The emission from [Ir(dpydmb)(ppy)Cl] was reported to be significantly blue-shifted compared to that from [Ir(dpydmb)(dppy)], consistent with the lowering of the HOMO energy upon the substitution of a cyclometalating carbon with a weaker ligand-field chloride.

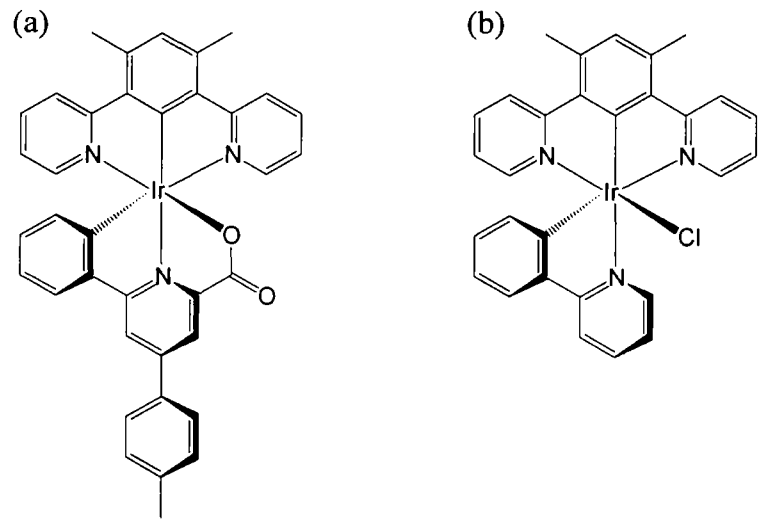

Figure 1.28: Structure of (a) [Ir(dpydmb)(tppic)] and (b) [Ir(dpydmb)(ppy)Cl].

1.4 Rhodium complexes

To date studies into luminescent inorganic complexes have lain mainly with ruthenium(II), with much less time having been spent on the isoelectronic complexes of iridium(III) and rhodium(III).[85] The significant gap in research at present lies with the fact that these tri-cationic metal ions are far less reactive than ruthenium(II), often resulting in a large amount of unreacted precursors following synthesis, making purification difficult.[86]

1.4.1 Rhodium(III) polypyridyl complexes

Rhodium complexes bearing polypyridyl ligands are of great interest as target specific sites to DNA and RNA in biological sensors and probes,[87] as well as boasting interesting photophysical and electrochemical properties, providing a potential use in electronic and photomolecular devices.[88]

Synthesis of the archetypal tris-bidentate complex of $[Rh(bpy)_3]^{3+}$ (Figure 1.29a) was reported by the same method employed for $[Ir(bpy)_3]^{3+}$ by Demas *et al.* in 1974.[40] Photophysical studies revealed it to be much less emissive at room temperature in degassed acetonitrile than $[Ru(bpy)_3]^{2+}$ or $[Ir(bpy)_3]^{3+}$, with a very short lifetime, $\tau < 15$ ns.[89] At 77 K, however, it was seen to possess long-lived, $\tau = 2.2$ ms, structured emission. This low temperature emission was subsequently assigned to an excited state with π–π^*, ligand-centred character.[90, 91] This temperature dependence can be explained by the decay of the LC state, at 298 K, by a thermally activated process involving a higher metal centred state.[92]

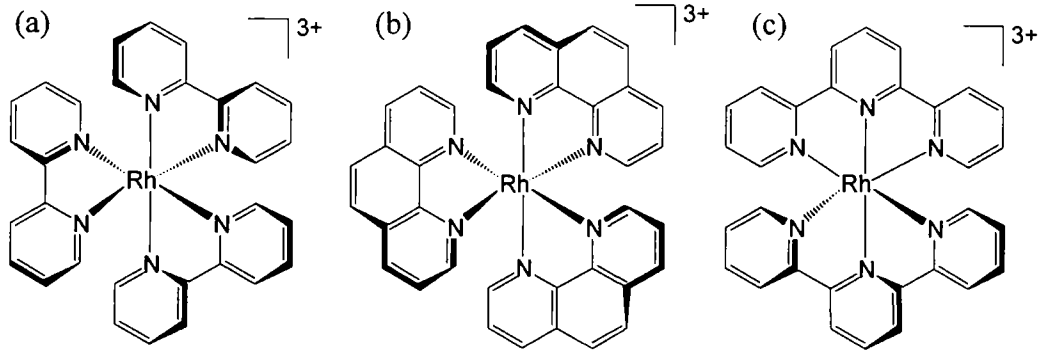

Figure 1.29: Structure of (a) $[Rh(bpy)_3]^{3+}$, (b) $[Rh(phen)_3]^{3+}$ and (c) $[Rh(tpy)_2]^{3+}$.

Likewise the tris-bidentate complex $[Rh(phen)_3]^{3+}$ (Figure 1.29b) incorporating the ligand 1,10-phenanthroline, phen, was synthesised by the same method. This exhibited similar photophysical properties at 77 K with intense, $\Phi \sim 1$, long-lived, $\tau = 50$ ms, structured emission,[91, 93, 94] again assigned as ligand-centred phosphorescence.[95, 96] Mixed-ligand complexes *i.e.* $[Rh(bpy)_2(phen)]^{3+}$ and $[Rh(phen)_2(bpy)]^{3+}$, however, exhibit dual emission, one localised to the bipyridine and the other to the phenanthroline ligand.[97]

The bis(2,2':6',2"-terpyridine) rhodium complex, $[Rh(tpy)_2]^{3+}$, (Figure 1.29c) is known to have a more unfavourable bite angle, due to the two terpyridine ligands providing a lower ligand field strength than three bipyridine or phenanthroline ligands.[24] Thus $[Rh(tpy)_2]^{3+}$ and related compounds only exhibit emission at 77 K, this being less intense, $\Phi = 0.09$, broad and structureless from a MC excited state.[98]

Quite recently Paul *et al.* reported the synthesis of a series of 4'-aryl substituted rhodium(III) terpyridyl complexes as potential DNA binding agents, owing to their inertness and stability under physiological conditions.[99] These complexes (Figure 1.30) contain the extended terpyridines, 4'-(4'"-pyridyl)-2,2':6',2"-terpyridine, qtpy, and 4'-phenyl-2,2':6',2"-terpyridine, phtpy. Synthesis of the $[Rh(tpy)L]^{3+}$ type complexes (Figure 1.30a and c) was achieved under mild conditions, involving the reaction of the ligand with $[Rh(tpy)Cl_3]$ in refluxing ethanol:water, 1:1, for 5 hours under an inert atmosphere. Reaction with phtpy first requires the pre-treatment of $[Rh(tpy)Cl_3]$ with three equivalents of silver(I). The $[RhL_2]^{3+}$ complexes (Figure 1.30b and d) were, however, obtained by reacting the ligand directly with $[RhCl_3.3H_2O]$ under the same reaction conditions.[99]

X-ray crystallographic studies of the hexafluorophosphate salts revealed that these complexes had distorted octahedral geometries just like $[Rh(tpy)_3]^{3+}$, with the central Rh–N bond being the shortest. The bite angles involving N-donors on the same ligand were found to be $\sim 80^{\circ}$, whilst the equivalent angles involving nitrogens on different ligands were more obtuse, $\sim 100^{\circ}$. An almost planar arrangement was observed for the three coordinating pyridines, with non-coordinating pyridyl rings being twisted away from the plane.[99]

The absorption spectra of these complexes revealed low-energy bands which were assigned to MLCT transitions, and correspond to the lowest-energy excited state. The higher energy absorption bands were of LC character. Cyclic voltammetry studies revealed no oxidation processes,[99] typical for rhodium(III) complexes, but chemically irreversible reductions at ~ –0.5 V which based upon previous studies were assigned to the two-electron reduction of Rh(III) to Rh(I).[100] The more cathodic reductions observed were thought to be the result of one-electron ligand-based reductions.[99]

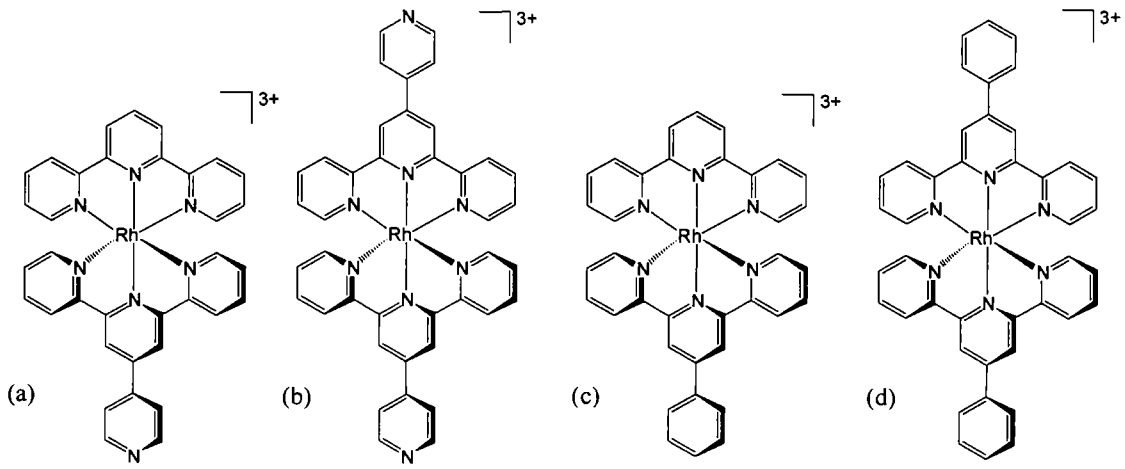

Figure 1.30: Structure of (a) $[Rh(tpy)(qtpy)]^{3+}$, (b) $[Rh(qtpy)_2]^{3+}$, (c) $[Rh(tpy)(phtpy)]^{3+}$ and (d) $[Rh(phtpy)_2]^{3+}$.

1.4.2 Rhodium(III) cyclometalated complexes

Tris-cyclometalated rhodium(III) complexes, containing phosphine ligands, were reported as far back as 1972, but owing to the π-backbonding character of the phosphine ligands, the excited ^{3}MLCT state was high in energy and the emission lifetimes short.[101] It was not until some 20 years later when *fac*- and *mer*-$[Rh(ppy)_3]$ were synthesised successfully that interest into cyclometalated rhodium(III) complexes really took off again. The same temperature dependent synthetic strategy was reported for $[Rh(ppy)_3]$ as employed for $[Ir(ppy)_3]$. However, emission was much weaker than that of the iridium analogue, being barely observable for *fac*-$[Rh(ppy)_3]$ (Figure 1.31a) in degassed acetonitrile at 298 K.[63]

The most commonly studied of all cyclometalated rhodium complexes are the bis-cyclometalated tris-bidentate complexes, bearing *cis*-disposed carbons, *e.g.* $[Rh(ppy)_2(bpy)]^+$ (Figure 1.31b) and its derivatives.[102] The same synthetic strategy,

going *via* a $[M(ppy)_2(\mu\text{-}Cl)_2]_2$ intermediate, was employed for such complexes as for their iridium analogues. Structured, long-lived (τ = 170 μs) emission was observed from $[Rh(ppy)_2(bpy)]^+$ at low temperature. This emission was reported to arise from a predominantly ppy-based π–π^*, LC, excited state, with which there is believed to be a small amount of mixing with the MLCT state associated with the ppy ligands. This differs significantly from the iridium analogue, from which dual emission of purely MLCT origin was observed.[103, 104] DFT studies supported the assignment of the emission, revealing the HOMO to be of mixed character, being delocalised over the central rhodium ion and the cyclometalating ligands.[85] At room temperature, however, only very weak, short-lived emission was observed resulting from the deactivation of the LC excited state by the low lying MLCT state.[103]

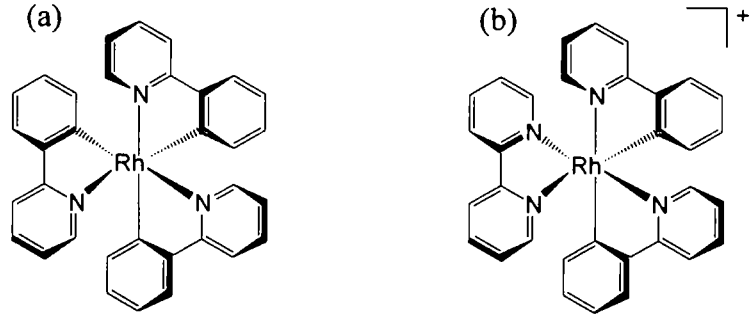

Figure 1.31: Structure of (a) *fac*-$[Rh(ppy)_3]$ and (b) $[Rh(ppy)_2(bpy)]^+$.

The photophysical properties of $[Rh(NC)_2(NN)]^+$ complexes can be tailored by varying or functionalising the NC and/or NN-coordinating ligands. The substitution of ppy for 2-thienylpyridine, thpy (Figure 1.32a), results in the enrichment of the solution-based emission intensity and lifetime at room temperature.[103, 105, 106] This is attributed to the lower energy of emission and consequential lower efficiency of the thermal deactivation of the emissive state by the higher lying MC states.[106, 107] Upon substitution of the bpy ligand with 1,10-phenanthroline, phen (Figure 1.32b) or 2,2'-biquinoline, biq (Figure 1.32c), the emissive state was still reported to be of predominately LC character. Like $[Rh(ppy)_2(bpy)]^+$, the lowest excited state of the phen complex was localised on the cyclometalating ppy ligands, whilst for the biq complex it involved the biq ligand itself.[108] When a more π-deficient NN-coordinating ligand was involved *e.g.* 1,4,5,8-tetraazaphenanthrene, TAP, (Figure 1.20b) or 1,4,5,8,9,12-hexaazatriphenylene, HAT, (Figure 1.20c), single, broad, structureless emission was observed at 77 K indicative of a charge transfer state. This differs from the analogous iridium complexes from which

dual emission was reported. DFT calculations revealed that electron density in the HOMO is localised on the metal and cyclometalating ligands carbon bonds, whilst the LUMO is localised on the non-cyclometalating ligand. This indicated that in these complexes emission is best described as being from a mixed LLCT/MLCT excited state.[85]

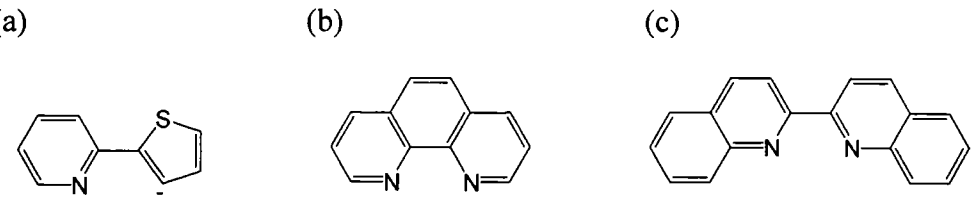

Figure 1.32: The NC-coordinating ligand (a) thpy and NN-coordinating ligands (b) phen and (c) biq.

Accounts of studies involving rhodium(III) complexes incorporating cyclometalating terdentate ligands are virtually non-existent. In 1999 Gowda *et al.* reported the synthesis of a series of such complexes with the NCN-coordinating ligand 1,3-bis(benzimidazol-2-yl)benzene, bibH, and its methyl derivative 1,3-bis-(1-methylbenzimidazol-2-yl)benzene, MebibH. The intermediate chloro-bridged dimer, $[Rh(Rbib)Cl(\mu\text{-}Cl)]_2$, (Figure 1.33a) was synthesised by reacting rhodium(III) trichloride with bibH or MebibH in refluxing methanol for 5 hours. ^{1}H-NMR studies of the dimer and the free ligand showed the loss of the $H^{2'}$-proton of the central benzene ring in the former, indicating cyclometalation; whilst molecular modelling studies revealed that the *cis* isomer was favoured on steric grounds. The cleavage of the dimer was described using a range of monodentate coordinating ligands (Figure 1.33). Upon reaction with monodentate $AsPh_3$ in refluxing methanol, the mononuclear complex $[RhCl_2(Rbib)(AsPh_3)]$ (Figure 1.33b) was formed. Reaction with the bidentate ligand 2,2'-bipyridine or 10-phenanthroline in the presence of excess sodium perchlorate was reported to result in their monodentate binding and thus $[RhCl(Rbib)(NN)(OClO_3)]$ complexes (Figure 1.33c). Bridging bidentate ligands *e.g.* pyrazine or 4,4'-bipyridine were, however, reported to yield binuclear complexes of the type $[RhCl_2(Rbib)]_2(\mu\text{-}NN)$ (Figure 1.33d).[109]

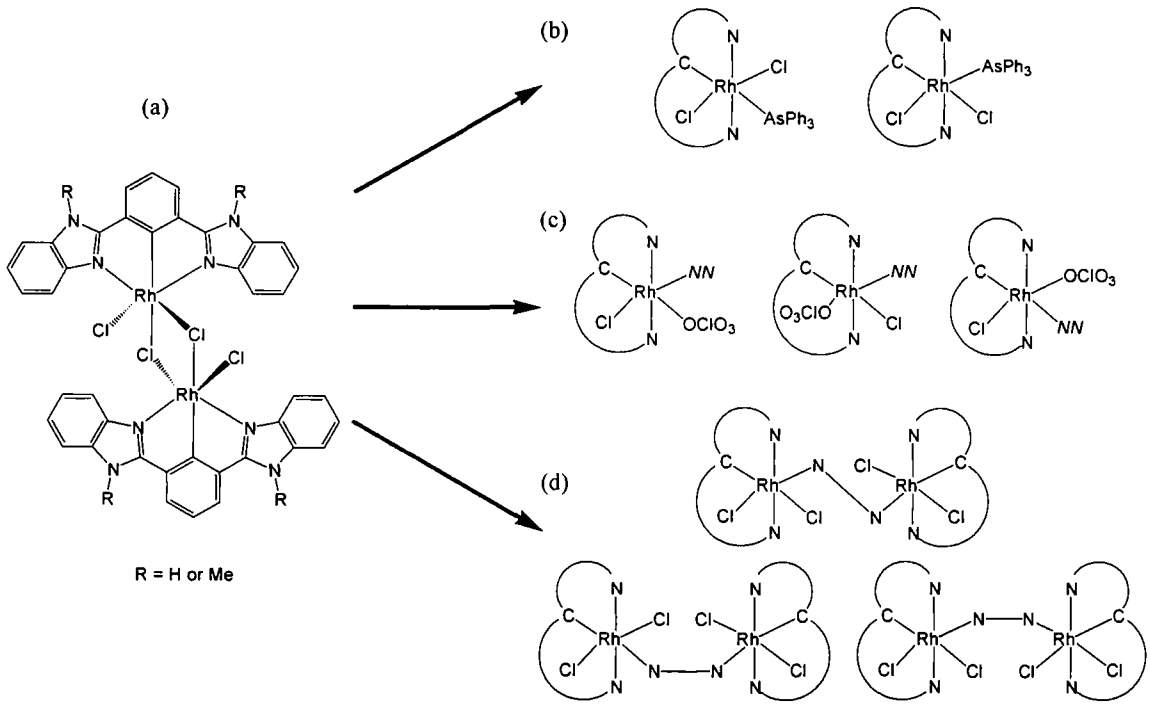

Figure 1.33: Structure of (a) [Rh(Rbib)Cl(μ-Cl)]$_2$, (b) [RhCl$_2$(Rbib)(AsPh$_3$)], (c) [RhCl(Rbib)(*NN*)(OClO$_3$)] and (d) [RhCl$_2$(Rbib)]$_2$(μ-*NN*).

1.5 Multimetallic complexes

The linking of metal complexes to generate multimetallic assemblies has attracted considerable attention in the field of coordination chemistry. These systems can display properties related to each monometallic metal unit, as well as to the whole assembly. Thus careful consideration during design can allow the directional control of energy and electron transfer processes within these systems, with potential applications including triplet harvesting agents in photochemical molecular devices, solar energy conversion, electroluminescence and information storage.[8]

1.5.1 'Complexes as metals, complexes as ligands' strategy

The usual approach applied to the synthesis of homo- and heteronuclear multimetallic assemblies is that of 'complexes as metal, complexes as ligands'.[110] This involves the use of complexes with easily replaceable ligands as 'complex metals' and complexes containing ligands with free chelating sites as 'complex ligands'.[8] Using this strategy to synthesise dinuclear homometallic complexes is particularly easy with the metal complex and the spacer ligand being reacted in a stoichiometric ratio (Figure 1.34a). A two step synthesis, however, is the usual requirement for dinuclear heterometallic

complexes (Figure 1.34b) with the first step involving the preparation of a mononuclear 'complex ligand' by reacting the metal with an excess of spacer ligand. In the second step the 'complex ligand' is reacted with the second metal in stoichiometric quantities.

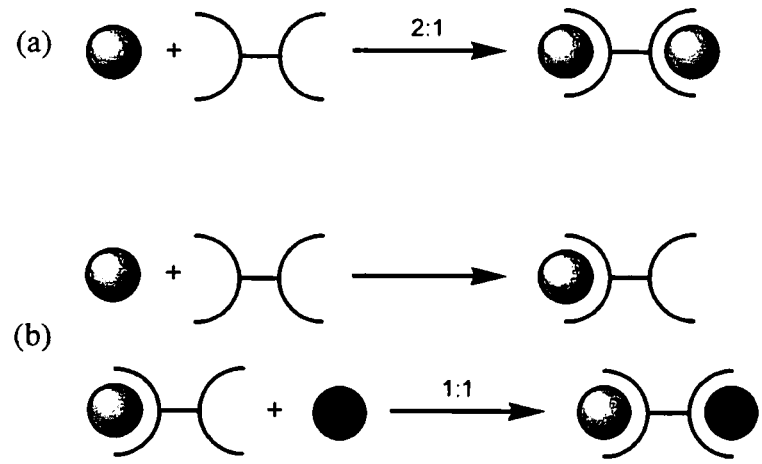

Figure 1.34: Schematic representation of the synthesis of (a) homodinuclear and (b) heterodinuclear complexes.

Considerable attention has been directed towards the use of this strategy in the synthesis of polynuclear systems, with most examples to date involving ruthenium(II) homo- and heterometallic complexes. A limited number of homometallic polynuclear iridium(III) complexes have been reported with organic bridges, including bpy-ph$_3$-bpy (Figure 1.35a),[111] bpy-ph$_4$-bpy (Figure 1.35a),[112] bpt (Figure 1.35b)[113] and bpb (Figure 1.35c).[114] These relatively simple complexes were formed upon reaction of the Ir(ppy)$_2$-based 'complex metal' with the bridging ligand, as portrayed in Figure 1.34a. In all of these systems, luminescence was reported to originate from a ^{3}MLCT excited state involving the bridging ligand.[26]

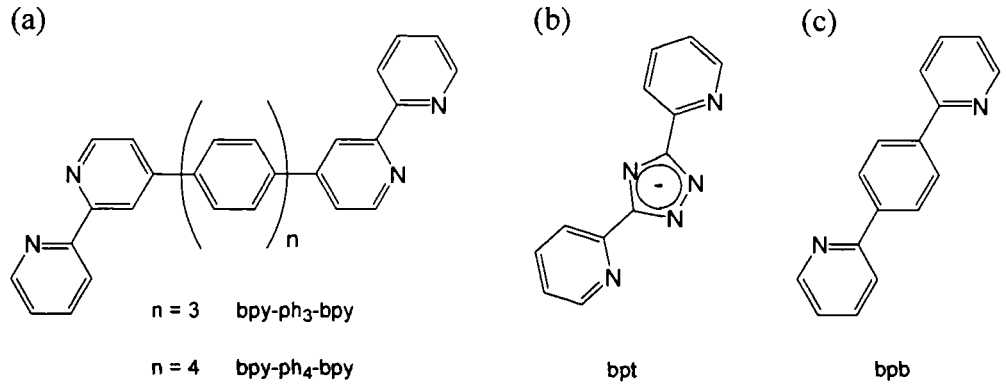

Figure 1.35: Bridging ligands used in homometallic di-iridium complexes.

Polynuclear complexes containing ruthenium(II) or osmium(II) units linked to iridium(III) centres by a variety of bridging ligands, have been reported to display photoinduced energy transfer processes that are characterised by the components involved.[26] Kirsch-De Mesmaeker *et al.* reported the synthesis of the dinuclear assembly $[(bpy)_2Ru\text{-}\mu\text{-}(HAT)Ir(ppy)_2]^{3+}$ (Figure 1.36a) by reacting the 'complex ligand' $[Ru(bpy)_2(HAT)]^+$, containing the bridging HAT ligand (Figure 1.20c), with the dimeric complex metal $[Ir(ppy)_2Cl]_2$ in refluxing CH_2Cl_2/MeOH for 6 hours.[74] The emission (λ_{max}^{em} = 760 nm, τ = 10 ns) from this dinuclear complex was identified as being iridium-centred and of SBLCT (sigma-bond-to-ligand charge transfer) character, as reported for one of the low temperature emission bands from the mononuclear $[Ir(ppy)_2(HAT)]^+$ complex (Section 1.3.2.1). This was consistent with Ru→Ir energy transfer.

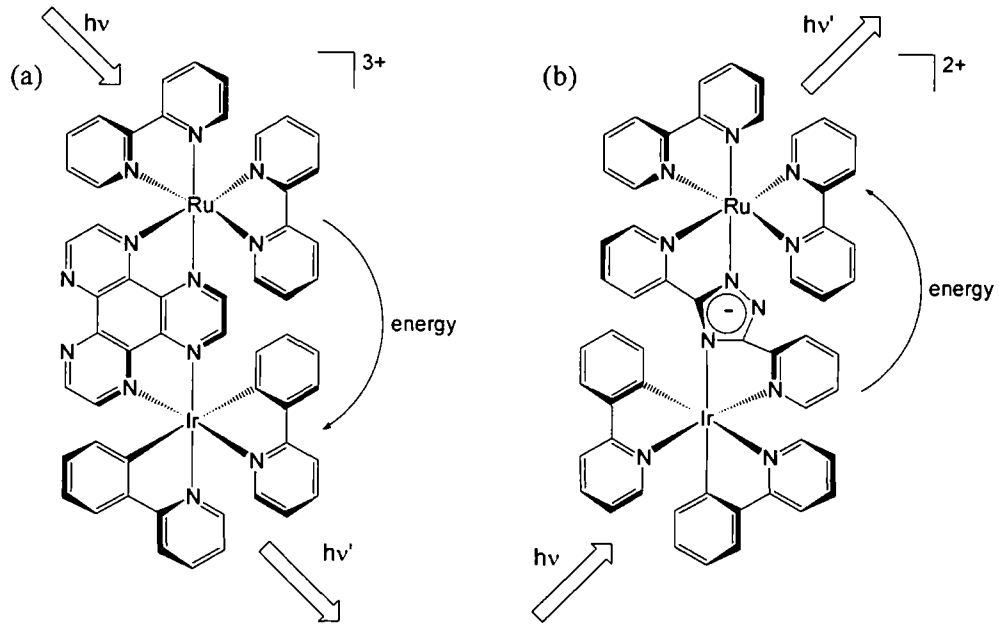

Figure 1.36: Dinuclear assemblies incorporating iridium(III) and ruthenium(II) centres; (a) $[(bpy)_2Ru\text{-}\mu\text{-}(HAT)Ir(ppy)_2]^{3+}$ and (b) $[(bpy)_2Ru(bpt)Ir(ppy)_2]^{2+}$.

Another dinuclear complex, $[(bpy)_2Ru\text{-}\mu\text{-}(bpt)Ir(ppy)_2]^{2+}$ (Figure 1.36b) was synthesised by Reedijk *et al.*,[113] the two metal centres being linked *via* a bpt bridging ligand (Figure 1.35c) containing a monoanionic triazole unit. Synthesis was achieved by reacting $[Ru(bpy)_2(bpt)]^+$ and $[Ir(ppy)_2Cl]_2$ in refluxing 2-methoxyethanol for 2 days. The anionic nature of the bridging ligand was reported to result in the MLCT states being localised on the two metal complexes and the peripheral ligands. Emission from

this assembly is characteristic of the ruthenium-based unit, indicating efficient Ir→Ru energy transfer, *i.e.* opposite to that observed for $[(bpy)_2Ru\text{-}\mu\text{-}(HAT)Ir(ppy)_2]^{3+}$.

In the early 1990's Brewer *et al.* reported the synthesis of $[Ir(tpp)Cl_3]$, where tpp is a bridging ligand capable of coordinating in an NNN manner twice, by reacting $[IrCl_3.3H_2O]$ with tpp in ethylene glycol for 25 minutes.[115] In the same study they also reported a dinuclear complex incorporating iridium(III) and ruthenium(II) units bridged by the tpp ligand. Reacting $[Ir(tpp)Cl_3]$ as the 'complex ligand' with $[Ru(tpy)Cl_3]$ in refluxing DMF/EtOH for 4 hours afforded $[(tpy)Ru\text{-}\mu\text{-}(tpp)IrCl_3]^{2+}$ (Figure 1.37) in 62% yield. Irrespective of the excitation wavelength and thus which ligand is excited, the emission (λ_{max}^{em} = 810 nm, τ = 22 ns) was reported to be ruthenium-based with MLCT character involving the bridging ligands.

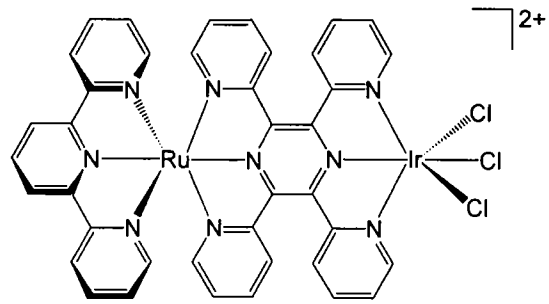

Figure 1.37: The dinuclear Ru(II)-Ir(III) complex $[(tpy)Ru\text{-}\mu\text{-}(tpp)IrCl_3]^{2+}$.

Alongside the aforementioned dinuclear complexes incorporating organic bridges Campagna *et al.* have reported several examples of tetranuclear bimetallic complexes formed upon reaction of $[Ir(ppy)_2Cl]_2$ with either a $[Ru(dpp)_3]^{2+}$ or $[Os(dpp)_3]^{2+}$ unit in refluxing dichloromethane for 2½ hours. 2,3-Bis(2-pyridyl)pyrazine, dpp (Figure 1.38a), acts as a bridging spacer ligand coordinating *via* two NN sites. The unit that is excited within these tetranuclear complexes is dependent upon the metal centres employed. The absorption of light by the $[Ru(dpp)_3]^{2+}$ unit in $[Ru\{(dpp)Ir(ppy)_2\}_3]^{5+}$ (Figure 1.38b) results in the transfer of excitation energy with unit efficiency to one of the peripheral $[(dpp)Ir(ppy)_2]^{+}$ fragments, which subsequently emits. In the $[Os\{(dpp)Ir(ppy)_2\}_3]^{5+}$ assembly (Figure 1.38c), however, absorption is localised on one of the peripheral iridium(III) fragments. This is followed by peripheral moiety-to-central unit excitation energy-transfer, with the resulting emission being $[Os(dpp)_3]^{2+}$

based. These results were reported to agree with the ordering of the triplet state energy levels; $[Ru(dpp)_3]^{2+} > [(dpp)Ir(ppy)_2]^{+} > [Os(dpp)_3]^{2+}$.[26, 38, 116]

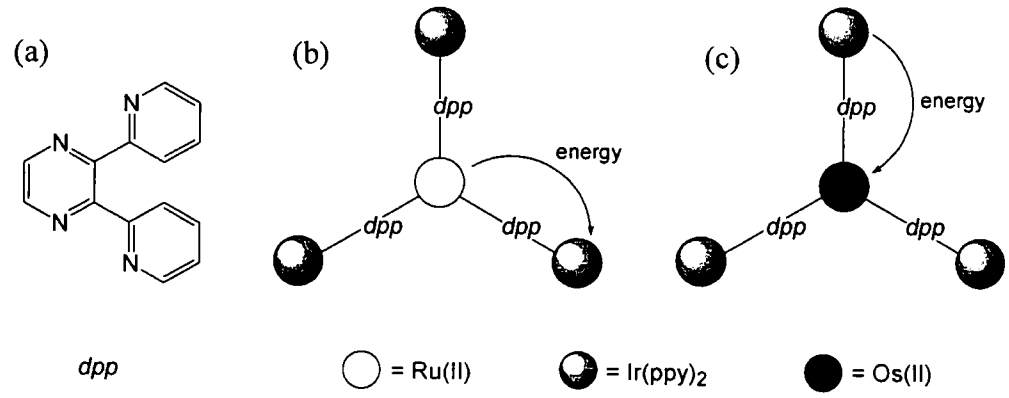

Figure 1.38: Structure of (a) the dpp ligand, and the photoinduced energy transfer processes in the (b) Ru(II)- and (c) Os(II)-centred tetranuclear $[M\{(dpp)Ir(ppy)_2\}_3]^{5+}$ complexes.

Recently a tetranuclear system, $[(tpy)Ir(\mu\text{–}X)Ru(\mu\text{–}X)Ru(\mu\text{–}X)Ir(tpy)]^{10+}$ (Figure 1.39), incorporating iridium(III) and ruthenium(II) subunits joined together by the bridging ligand X containing two terpyridine groups linked by a relatively rigid polyphenyl spacer was reported.[117] At room temperature dual emission was observed, with one band corresponding to the iridium(III) centres, $\lambda_{max}^{em} = 572$ nm and $\tau = 2.9$ μs, and the other to the ruthenium(II) centres, $\lambda_{max}^{em} = 681$ nm and $\tau = 82$ ns. At 77 K, however, a single ruthenium-based emission band was observed owing to efficient Ir→Ru energy transfer.

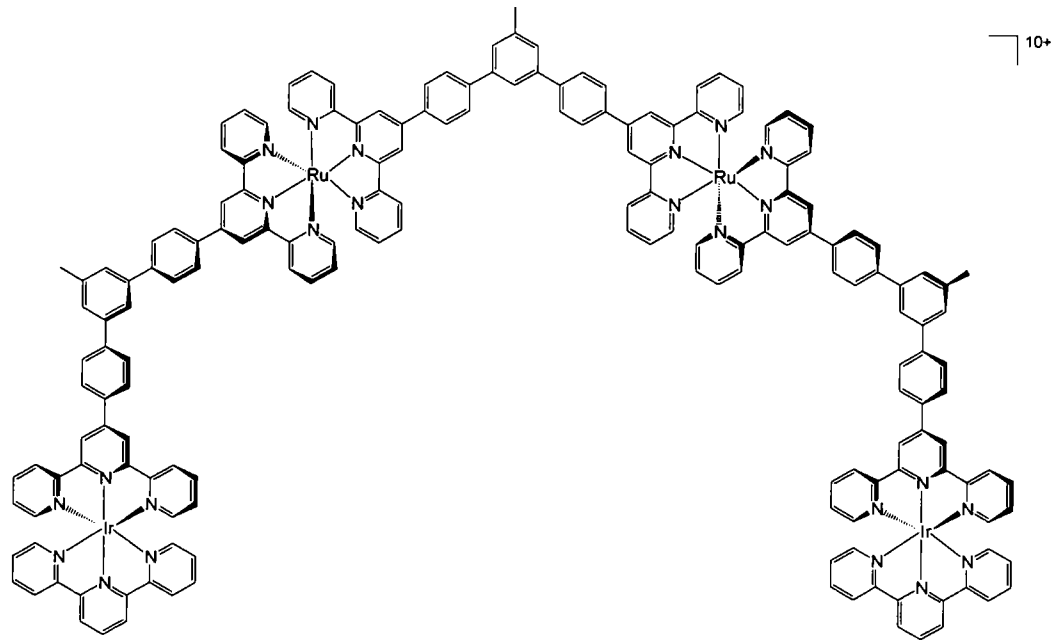

Figure 1.39: Tetranuclear $[(tpy)Ir(\mu\text{-}X)Ru(\mu\text{-}X)Ru(\mu\text{-}X)Ir(tpy)]^{10+}$.

1.5.2 *'In situ' elaboration of complexes*

Whilst the 'complexes as metals, complexes as ligands' approach to the synthesis of multimetallic assemblies has been widely used, the compact and rigid structure of the bridging ligands makes the synthesis of large multimetallic systems difficult due to steric congestion.[118] Further potential problems associated with this method include the reduced luminescence lifetimes of the multimetallics compared to the mononuclear complexes, due to the electronic properties of the bridging ligands.[9]

The 'chemistry on the complex' approach overcomes the aforementioned problems. Here the complex is converted into a 'complex ligand' by carrying out elaboration reactions on the ligand *in situ* to form new sites capable of coordinating to the metal centre. Such an approach was reported by Constable *et al.*, who took the ruthenium complexes $[Ru(tpy)(Cltpy)]^{2+}$ and $[Ru(Cltpy)_2]^{2+}$ containing 4'-chloro-2,2':6',2''-terpyridine, Cltpy, ligands and reacted them with 2,6-bis(2-pyridyl)-4-pyridone, tpyO. 'Complex ligands' were formed containing at least one vacant terpyridine coordination site which were in turn reacted with $[Ru(tpy)Cl_3]$ (Figure 1.40).[119]

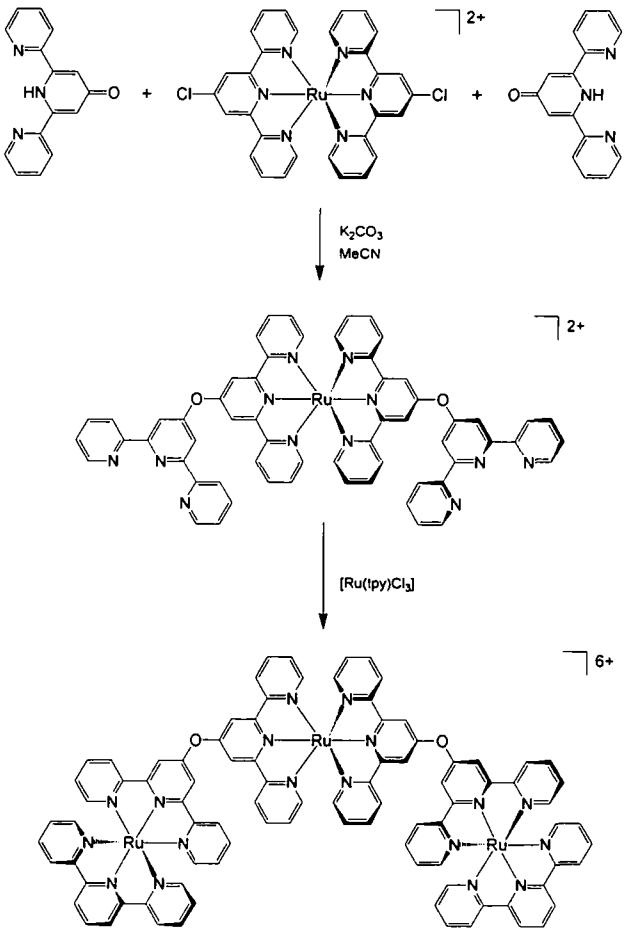

Figure 1.40: ***In situ*** **elaboration of complexes.**

1.5.3 Multimetallic complexes via cross-coupling reactions

There are reports of metal catalysed cross-coupling reactions having been employed in the *in situ* generation of new binding sites. Hanan *et al.* demonstrated the use of cross-coupling methodology to synthesise a bidentate NN-coordinating site by the reaction of a ruthenium(II) complex containing a bromo-substituted bipyridine ligand and 2-pyridylzinc bromide. This NN appended complex was subsequently reacted with an osmium 'complex metal' to form a dinuclear assembly.[120, 121]

As an alternative to the 'complexes as metals, complexes as ligands' strategy, metal catalysed cross-coupling reactions have been used to link together metal complexes in high yielding single-step syntheses.[122] Tor *et al.* reported the use of a Pd(0) catalysed cross-coupling reaction to link together $[Ru(bpy)_2(RPhenR)]^{2+}$ units, where RPhenR is the mono- or dibromo-appended 1,10-phenanthroline ligand.[123] The bromo-substituted complexes were joined together by reacting them with acetylenes in the presence of the palladium(0) catalyst, $Pd(PPh_3)_2Cl_2$, and CuI to form multinuclear arrays in high yields.[124] Subsequently they reported the synthesis of mixed metal systems containing Ru(II) and Os(II) units linked together by –C≡C– bonds, achieved by the direct reaction of bromo and ethynyl-substituted complexes (Figure 1.41).[123, 125]

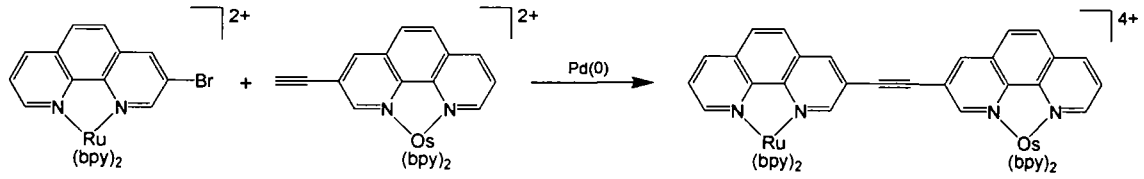

Figure 1.41: Pd(0) catalysed cross-coupling reaction between functionalised Ru(II) and Os(II) "building blocks".

The Suzuki-Miyaura cross-coupling reaction has also been successfully applied to the synthesis of multimetallic complexes. To date most of the literature reports the formation of homo-dinuclear species upon reaction of two mononuclear metal complexes, one containing a bromo-substituted ligand and the other a diboronate-appended aryl linker, in the presence of a palladium(II) catalyst and a base.[111, 126-128] Figure 1.42 illustrates the use of this method by De Cola *et al.* to synthesise the di-iridium complex $[(ppy)_2Ir\text{-}\mu\text{-}(bpy\text{-}\phi\text{-}bpy)Ir(ppy)_2]^{2+}$ by reacting $[Ir(ppy)_2(bpy\text{-}\phi\text{-}Br)]^{+}$ with phenyl-diboronic acid in the presence of $Pd(PPh_3)_4$ and $K_2CO_{3\,(aq)}$.[111]

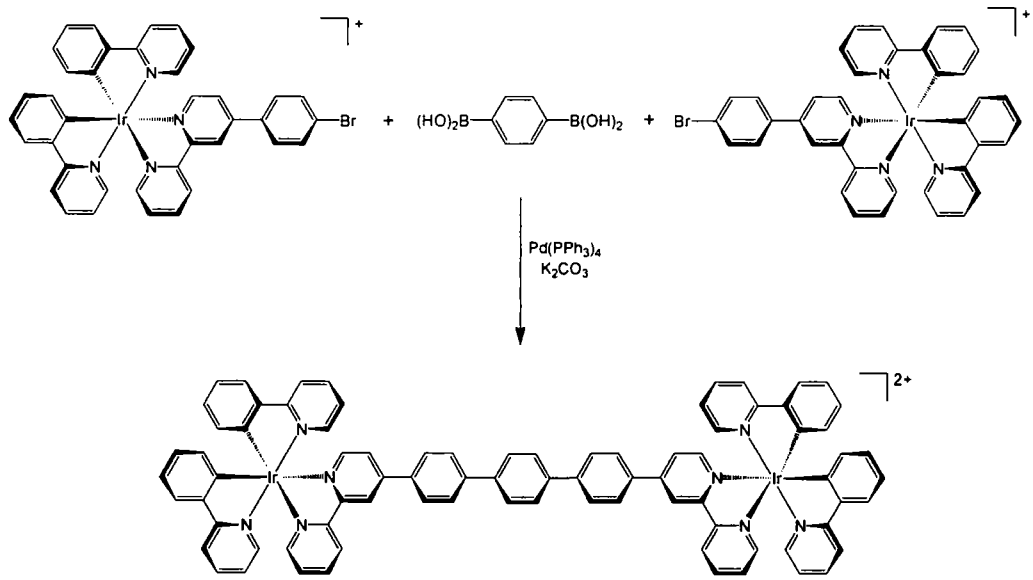

Figure 1.42: Synthesis of a di-iridium complex *via* a Suzuki-Miyaura cross-coupling reaction.

All of the heterometallic complexes described so far have contained conjugated bridging ligands *e.g.* dpp, or ethynylene linkages. The properties of these bridges can seriously perturb the photochemical and photophysical properties of the complexes and govern the direction of the energy transfer. By promoting non-radiative decay pathways they can reduce the luminescence intensity and lifetimes to below that of the related monometallic complexes. Insulating phenylene bridges like those used for the homometallic di-iridium complex in Figure 1.42, however, perturb the excited state properties of the individual units to a much lesser extent.[129]

This research laboratory recently reported the first complexes incorporating a boronic acid group into one of the ligands. Synthesis involved a Pd-catalysed Miyaura cross-coupling reaction between the bromo-substituted complex and a diboron ester of the form $(RO)_2$-B-B-$(OR)_2$ *e.g.* bis-neopentylglycolato diboron.[51] Following successful incorporation of the diboronic acid functionality, the direct reaction of boronic acid appended and bromo-substituted metal complexes in a palladium catalysed cross-coupling reaction was reported to yield heterometallic assemblies with phenylene bridges between the metal centres.[51, 129] This "building block" approach to multimetallics is exemplified in Figure 1.43. This shows the cross-coupling of $[Ir(tpy)(tpy\text{-}\phi\text{-}Br)]^{3+}$ with the boronic acid appended ruthenium tris-bipyridine derivative $[Ru(bpy)_2\{bpy\text{-}\phi\text{-}B(OH)_2\}]^{2+}$ carried out in DMSO in the presence of

$Pd(PPh_3)_4$ and Na_2CO_3 $_{(aq)}$ under an inert atmosphere, forming $[(tpy)Ir(tpy\text{-}\phi_2\text{-}bpy)Ru(bpy)_2]^{5+}$.[130]

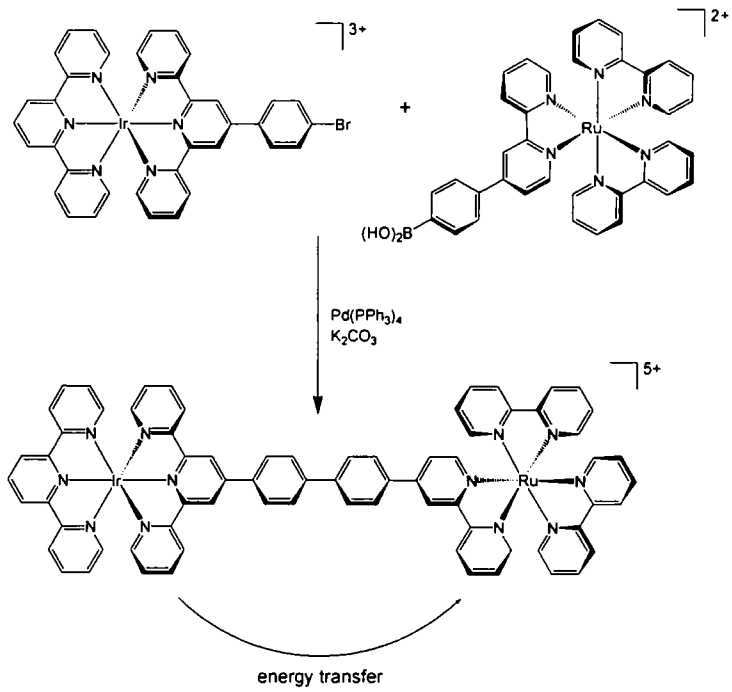

Figure 1.43: "Building block" approach to a heterometallic iridium-ruthenium dimer incorporating a tpy-ϕ_2-bpy bridging ligand [130]

The absorption spectrum was reported to resemble the sum of the individual mononuclear components, whilst the emission spectrum, consisted of a single emission band characteristic of the mononuclear complex $[Ru(bpy)_2(bpy\text{-}\phi\text{-}Ph)]^{2+}$. This was attributed to the rapid energy transfer from the higher energy iridium end to the lower energy ruthenium end.[130] The phenylene bridge shows no evidence of perturbing the excited state energies of the monometallic "building blocks" and the *in situ* approach to the formation of the tpy-ϕ-bpy bridging ligand prevented the selectivity issues that would have arisen from a pre-formed ligand owing to the similarity of bipyridine and terpyridine units in complexation with Ru(II) and Ir(III).[47, 129, 130]

1.6 Applications

1.6.1 Organic light-emitting devices

Organic light-emitting devices (or organic electroluminescent devices), OLEDs, were first reported in the 1980's,[131] and have received considerable attention since their

conception.[132-134] Their development has been driven by their potential application in flat-panel-displays which possess the ability to replace current liquid-crystal displays, LCDs, used in computer and television screens and mobile devices such as laptop computers and mobile telephones. Inorganic light-emitting devices, LEDs, were reported much earlier than OLEDs, being commercialised in the 1960's with devices containing GaAsP.[135] Whilst inorganic devices offer superior lifetimes, OLEDs have many advantages including lower initiator voltages, requiring less power and simpler, less expensive fabrication and manufacturing methods allowing thinner more flexible displays.[136, 137] Their emission intensity, colour and lifetime can be tuned by simple structural modifications of the organic molecules.[136, 137]

In simple electroluminescent devices, an organic emissive semiconductor is sandwiched between two electrodes. Under an applied electric potential the organic layer at the anode is oxidised injecting holes into the HOMO, and the cathode is simultaneously reduced injecting electrons into the LUMO. The electron and hole-carriers migrate *via* a hopping mechanism towards the opposite electrode under the applied field. The two carriers may recombine *en route* forming an excited state, known as an exciton, giving rise to the emission of light, termed electroluminescence. Unlike photoluminescence which arises from the absorption of a photon of light, the combination of charge carriers in electroluminescent devices results in the formation of both singlet and triplet excitons in 1:3 ratio. Phosphorecence from triplet excited states is spin-forbidden, being rarely observed from organic molecules at room temperature; emission from this state thus generates unwanted heat in the electroluminescent devices which have a limited device efficiency of 25%.[138-140]

Organic light-emitting devices are very thin and consist of several layers of material deposited upon a substrate of either glass, or a polymeric frame in flexible displays (Figure 1.44). On top of this substrate is the anode which must be transparent making indium tin oxide, ITO, the material of choice. Sandwiched between the anode and the cathode is the organic substrate. The outer cathode layer comprises of a metal such as Al, Mg, In or an alloy *e.g.* Mg:Ag, which must be protected from the atmosphere to prevent its oxidation.[138, 139, 141]

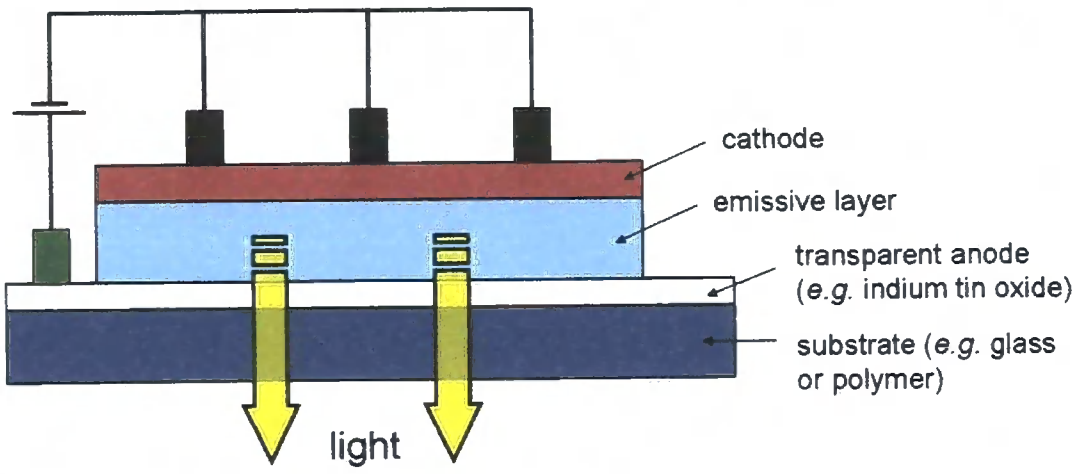

Figure 1.44: Design of an electroluminescent device.

Device efficiency of purely fluorescent electroluminescent devices is limited by the percentage formation of singlet excitons. The incorporation of phosphorescent compounds *e.g.* heavy metal complexes into the emissive organic layer, however, allows emission from both singlet and triplet excitons, significantly improving the internal efficiency up to a potential 100%.[140, 142, 143] In such doped systems the excited state generated upon electron-hole recombination is trapped on the complex; termed triplet state harvesting. As a result of strong spin-orbit coupling, singlet-triplet mixing occurs and hence phosphorescent emission is observed at room temperature. Important characteristics for the metal complexes used as dopants include high electron mobility and phosphorescent quantum yields alongside relatively short phosphorescent lifetimes, giving high device efficiency and brightness. To be of commercial value, however, true blue, red and green emitters are required to allow a full colour range to be available to the device.[138, 144]

The first electroluminescent devices incorporated platinum complexes as the triplet state harvesters, but their long triplet lifetimes often, > 10 μs, resulted in triplet-triplet annihilation at high currents, thus limiting device efficiency.[143, 145, 146] Iridium(III) complexes display much shorter luminescence lifetimes, $\tau \sim 1$ μs, making them more favourable as phosphorescent dopants. In 2000, Thompson *et al.* reported the first example of a device incorporating such a complex. The *fac*-[Ir(ppy)$_3$] (Figure 1.19a) doped OLED had an observed external electroluminescent quantum efficiency of 15%, and an internal efficiency of 80%.[65]

Polymeric hosts can be used instead of the organic substrate. The covalent linkage of the complex and the polymer in such polymer blends prevents the aggregation and self-quenching of the complex.[147] In 2000, a single layer device was reported incorporating a poly(vinycarbazole), PVK, emitting layer doped with *fac*-[Ir(ppy)$_3$], with an external electroluminescent quantum efficiency of 1.9%.[148] Two years later a multilayered polymeric device was designed with an increased efficiency of 8.5%.[149] Studies have been carried out into the use of iridium(III) dopants with modified ligands incorporating bulky groups, allowing higher dopant concentrations to be used without self-quenching occurring.[150] Studies of related fluorinated complexes with blue-shifted emission revealed a reduction in radiationless decay and self-quenching, alongside enhanced electron mobility thus resulting in higher device efficiencies.[151-153] In 2004 Williams *et al.* reported the synthesis of the charge neutral bis-terdentate complex [Ir(dpydmb)(dppy)] (Figure 1.27a). The intense room temperature emission and charge neutrality of this complex was reported to make it a suitable candidate for use in solid state OLEDs; the lability of the Ir–C bonds in solution is described in Section 1.3.2.2.[78]

Whilst charge neutral dopant molecules have received the most attention, charged transition metal complexes have also been investigated for applications in OLEDs. The first example reported the use of a substituted phenanthroline ruthenium(II) complex,[154] and subsequently considerable attention has been directed towards [Ru(bpy)$_3$]$^{2+}$ type complexes.[155] More recently cationic iridium(III) complexes based upon [Ir(ppy)$_2$(bpy)]$^+$ have been reported in single-layer electroluminescent devices; the neat complex was sandwiched as a homogeneous film between an air-stable indium tin oxide anode and a gold cathode. Since the counter ions of such complexes are mobile, an applied potential initiates charge injection at the electrodes.[156] Whilst such single-layer devices show relatively high efficiencies, their long turn-on times and poor stability hamper their commercial application.[157]

1.6.2 Luminescent sensors

Luminescent sensors contain an analyte binding site and a light emitting, signalling group. Upon binding to specific analytes, a change is brought about in their emission, which could be observed as a shift in emission wavelength, luminescence lifetime or intensity. The extent of the observed change is often related to the concentration of the analyte. A wide variety of analytes can be detected from H^+, oxygen, and ions *e.g.* Cl^-

and K^+ to more complex biological materials such as DNA, biotin (vitamin H) and insulin.[1, 158-161] Transition metal and lanthanide complexes have received considerable attention in this field owing to their long-lived phosphorescent emission, which is easily distinguishable from the shorter-lived background fluorescence often observed from biological samples. Time-resolved detection procedures are usually employed, by setting a delay between the excitation pulse and the measurement of emission, during which the background fluorescence decays to a negligible level (Figure 1.45).[162]

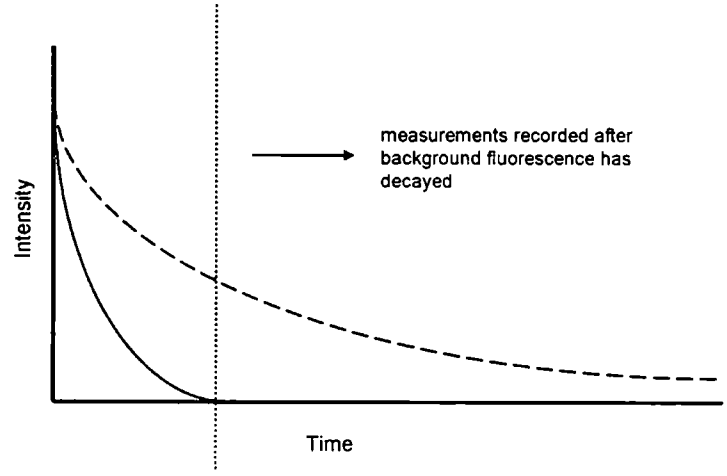

Figure 1.45: Time-resolved measurement of phosphorescent emission.

Complexes of $[Ir(R\text{-}tpy)_2]^{3+}$ show particular promise in such applications owing to their long luminescence lifetimes, > 1 μs, even in air-equilibrated aqueous solution at room temperature.[47] Such complexes bearing pyridyl substituents have been investigated as pH sensors by this laboratory and are discussed in Section 1.3.1. They were reported to exhibit a reduction in intensity and lifetime upon acidification in aqueous solution.[48] A change in lifetime is probably the best response to probe, as unlike intensity it is free from errors arising from fluctuations in light detection efficiency.[163] Alongside the pH sensors described in Section 1.3.1 the *meta* $[Ir(ttpy)(tpy\text{-}Mepy)]^{3+}$ complex (Figure 1.15) was reported as a chloride sensor. Unlike the *ortho* and *para* isomers, emission from the *meta* isomer is not quenched upon methylation with a lifetime of 5.8 μs making it suitable for such applications. Upon addition of chloride ions (0.045 M) in aqueous solution the emission is quenched, with a six-fold decrease in intensity observed, accompanied by a 2.5-fold decrease in luminescence lifetime. The Stern-Volmer plot at 295 K was reported to be approximately linear at low concentrations, below 0.2 mM, with a calculated quenching constant, K_{sv}, of 0.034 M.[50] Thus this

complex is potentially suitable for the biomedical analysis of chloride, owing to its sensitivity within the physiological concentrations of 0.005–0.075 M.[47]

Luminescent transition metal complexes, including those of iridium(III), exhibit long-lived triplet excited states that can efficiently transfer energy to the triplet ground state of molecular oxygen, quenching emission and forming singlet oxygen.[164] This allows such complexes with high quantum yields to be used as oxygen probes in medical, chemical and environmental applications owing to their distinctive change in luminescent properties in the presence of oxygen.[161] The further development and commercialisation of such solid state sensors has been held back by the self-quenching of neighbouring molecules. Potential solutions to this problem have included embedding the complexes in oxygen permeable polymer matrices. This has, however, been hindered by the requirement of low loading concentrations to prevent aggregation leading to low sensitivity.[161] Investigations are being carried out into the reduction in size of the luminescent molecules to overcome this problem.[157]

Recently the use of luminescent rhenium(I),[165-167] ruthenium(II),[168-172] osmium(II),[168, 170] iridium(III)[162, 173, 174] and rhodium(III)[175, 176] complexes have been reported in the detection of biological molecules. The first example of iridium(III) complexes as labels for biological molecules was reported in 2001. The complexes were based on $[Ir(ppy)_2(R\text{-phen})]^+$, containing 1,10-phenanthroline ligands bearing isothiocyanate and iodoacetamide substituents (Figure 1.46) which were coupled to human serum albumin, HSA, *via* reaction with primary amine and sulfonyl groups respectively.[160]

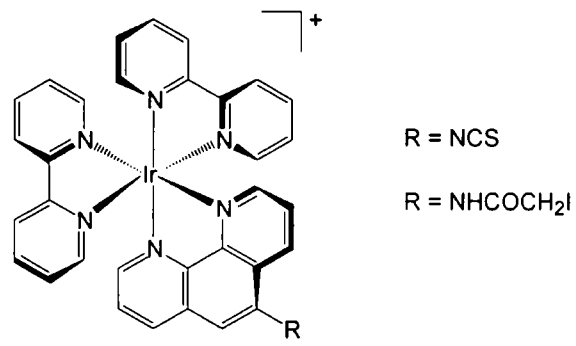

Figure 1.46: Isothiocyanate and iodoacetamide substituted $[Ir(ppy)_2(Rphen)]^+$ complexes.

Perhaps the most widely studied of all biological systems is that of avidin-biotin. Avidin is a glycoprotein that naturally forms strong protein ligand interactions with

biotin, vitamin H.[177] Due to the strong specific interactions, avidin molecules labelled with organic fluorophores have been widely used in detecting biotinylated biomolecules.[178] Biotin-fluorophore complexes, however, are usually quenched upon binding to avidin rendering them unsuitable as avidin probes.[179-181] It has recently been discovered that biotin molecules labelled with luminescent transition metal complexes of ruthenium(II) and iridium(III) experience an increase in emission lifetimes and intensity upon binding to avidin, giving rise to a new class of probes for this protein.[178] $[Ir(ppy)_2(dpqB)]^+$ (Figure 1.47a) and $[Ir(ppy)_2(dppzB)]^+$ (Figure 1.47b) labelled biotin complexes were reported to be non-emissive in aqueous buffer; but emissive upon addition of avidin. A new emission band emerged at 490 nm with a shoulder at 520 nm, increasing the emission intensity of the former complex 31-fold and the latter eight-fold, efficiently probing avidin.[177]

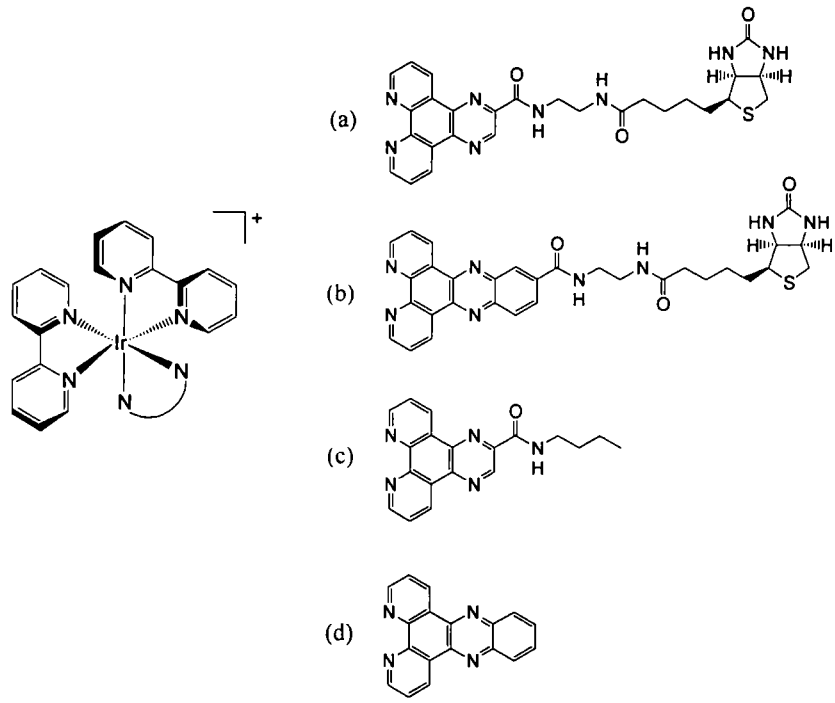

Figure 1.47: Biotinylated complexes of (a) $[Ir(ppy)_2(dpqB)]^+$ and (b) $[Ir(ppy)_2(dppzB)]^+$ as probes for avidin, and the non-biotinylated complexes (c) $[Ir(ppy)_2(dpqa)]^+$ and (d) $[Ir(ppy)_2(dppz)]^+$.

The non-biotinylated complexes $[Ir(ppy)_2(dpqa)]^+$ (Figure 1.47c) and $[Ir(ppy)_2(dppz)]^+$ (Figure 1.47d) were also reported to be non-emissive in aqueous buffer solution, but in the presence of double stranded calf thymus DNA they exhibited new emission bands at around 600 nm, with respective emission intensities of 40 and 12 times that of the background in the absence of DNA. The complexes were described as intercalating to the base-pairs of the double stranded DNA. The biotinylated complexes were reported

not to show any change in emission upon the addition of DNA, attributed to the sterically bulky biotin moiety inhibiting intercalation.[174, 177, 182, 183] Most studies of iridium(III) complexes as labels and probes for biological molecules have focused upon tris-bidentate complexes. Lo *et al.* have, however, reported the synthesis of iridium(III) terpyridyl complexes with isothiocyanate functional groups and their use as labels for HSA and bovine serum albumin, BSA.[184]

Studies of rhodium(III) complexes as biological probes have included the investigation of $[Rh(pba)_2(NN)]^+$ complexes where pba is 4-(2-pyridyl)benzaldehye and NN is 2,2'-bipyridine or 1,10-phenanthroline.[176] Such complexes were reported to exhibit long-lived emission between 4 and 9 μs at room temperature owing to the electron withdrawing aldehyde groups, but low intensities. They have been successfully used to label BSA, displaying similar emission properties to the free complex. However, the poor emission quantum yields of the rhodium complexes compared to their iridium analogues makes them less favourable luminescent labels.

1.6.3 Directional energy and electron transfer in multimetallic assemblies

The development of syntheses for multimetallic assemblies has been described in detail in Section 1.5 along with the advantages of using achiral bis-terdentate complexes. Directional energy transfer can be observed from the higher energy to lower energy end in such multinuclear systems. This was reported by Williams *et al.* for $[(tpy)Ir\text{-}\mu\text{-}(tpy\text{-}\phi_2\text{-}bpy)Ru(bpy)_2]^{5+}$ (Figure 1.43) with emission exclusively from the low energy $[Ru(bpy)_3]^{2+}$ centre.[130] De Cola *et al.* also reported such energy transfer processes in a self-assembled non-covalent assembly. In their system, energy was transferred from $[Ir(tpy)(tpy\text{-}\phi\text{-}ph)]^{3+}$ to a $[Ru(bpy)_3]^{2+}$ derivative with one *β*-cyclodextrin receptor appended to each bpy molecule. In aqueous solution the biphenyl tail of the iridium(III) complex was reported to bind to the *β*-cyclodextrin receptor, resulting in fast energy transfer to the ruthenium centre now in close proximity.[185]

Triad systems consisting of a central transition metal complex appended with electron donor and acceptor units facilitate multi-step electron transfer leading to charge separation, an important process in light-to-chemical energy conversion.[186]

Sauvage *et al.* reported such a system containing a central $[Ir(tpy)_2]^{3+}$ unit instead of $[Ru(tpy)_2]^{2+}$ as used in previous studies.[186] This was appended with a zinc tetra-aryl-porphyrin donor and a gold tetra-aryl porphyrin acceptor (Figure 1.48). The use of a high energy iridium(III) centre was favourable over the ruthenium(II) centres, where undesirable competitive energy transfer occurred to the low-lying MLCT states of the metal centre and there was a consequential depletion of the excited state of the porphyrin photosensitiser. The $[Ir(tpy)_2]^{3+}$ complex also displays a less negative reduction potential, thus favouring electron transfer processes.[26, 187, 188]

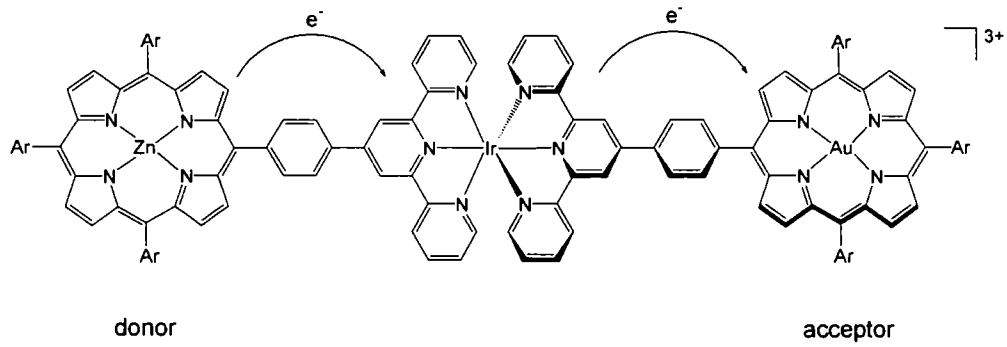

Figure 1.48: Iridium-terpyridine donor-acceptor assembly.

Upon excitation of the zinc porphyrin donor, rapid electron-transfer ($\tau < 20$ ps) occurs from the porphyrin excited state to the iridium(III) centre. This is followed by a further electron-transfer to the gold porphorin accepter forming a charge separated, CS, excited state assembly, PZn^{+}-Ir-PAu^{-}, with a lifetime of 450 ns.[187, 188] This charge separation occurs with 100% efficiency in toluene, whilst in dichloromethane electron-transfer from the iridium(III) centre to the gold porphorin acceptor is thermodynamically unfavourable and PZn^{+}-Ir^{-}-PAu decays to the ground state directly.[189-191]

1.6.4 Dye-sensitised solar cells

Dye-sensitised solar cells, DSC, have the ability to directly convert sunlight into electrical energy and are of great interest as sources of renewable energy. These solid state devices consist of a sensitiser, here a luminescent metal complex, bound to the surface of a semiconductor *via* anchoring ligands. TiO_2 is often the semiconductor of choice due to its non-toxicity, low cost and high availability. Upon excitation by light, the sensitiser is oxidised injecting electrons into the conduction band of the semiconductor. The surrounding electrolyte subsequently donates the electrons back to

the sensitiser returning it to its original form. The migration of the electron to the counter electrode through the external circuit allows its regeneration in a process catalysed by the deposition of a small amount of catalyst on the anode.[192-195]

Polypyridyl d^6 metal complexes are good sensitizers owing to intense MLCT bands in the visible region of their absorption spectra, and their ability to inject charge into the conduction band of the devices. Ruthenium(II) polypyridyl complexes have shown the greatest potential as sensitisers to date due to their ideal redox, spectroscopic and excited state properties, alongside a well matched energy to the TiO_2 semiconductor.[195] The first example of such a system was reported in 1991.[196] Two of the best sensitisers to date have been the N3 dye[197] (Figure 1.49a) and the 'black dye'[198] (Figure 1.49b). The carboxylic acid functional groups provide them with an easy point of attachment to the surface of the semiconductor. The N3 dye was reported to have MLCT character, with the transfer of an electron from the metal to the bpy ligand, attached to the TiO_2 surface, and device efficiency for the conversion of light-to-chemical energy of 8.6%.[197, 199] This was later superseded by the 'black dye' with an improved efficiency of 10.4%.[198]

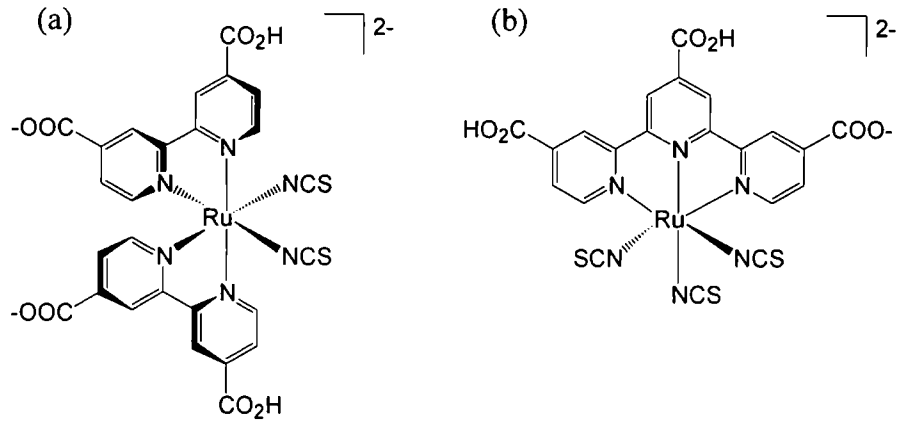

Figure 1.49: Ruthenium(II) sensitisers used in dye-sensitised solar cells; (a) N3 dye and (b)'black dye'.

Heteroleptic iridium(III) complexes, with their tunable photophysical properties and favourable characteristics for sensitisers in such systems, offer a promising potential area for future research. Recently Lowry *et al.* reported an iridium(III) complex as a photosensitiser for photoinduced hydrogen production in fuel cells.[200] Solar energy was channelled through a catalytic cycle, splitting water into hydrogen and oxygen *via* oxidation and reduction respectively. The high energy density and clean combustion of

hydrogen make it an attractive fuel source. The use of an iridium(III) photosensitiser instead of ruthenium(II) was reported to result in increased hydrogen production owing to iridium(III) being a stronger reducing agent than ruthenium(II),[157] and thus is likely to fuel future research into dye-sensitising solar cells incorporating iridium(III) complexes.

1.7 Concluding remarks

Herein an overview has been given of the development of luminescent transition metal complexes, from the early work on ruthenium(II) to later studies including isoelectronic iridium(III) and rhodium(III). Both tris-bidentate and bis-terdentate complexes have been described along with the advantages of the latter, owing to their achiral nature and their ability to be linearly expanded. A whole host of excited-state energies and photoluminescent properties have been observed in these complexes by varying the central metal ion or the coordinating ligands. This ability to design luminescent transition metal complexes with specific excited-state properties makes them suitable for a wide range of applications. Their use as efficient triplet harvesting agents in OLEDs, as oxygen sensors, pH sensors, luminescent labels and probes in biological systems, in light-to-chemical energy conversion in solar cells, and in electron and energy transfer systems has been studied by various research groups and an account of this has been given in Section 1.6. The future of research into the photochemistry of transition metal complexes looks bright. There is considerable interest into pushing the emission boundaries of these complexes further into the blue and improving quantum yields and lifetimes, with their potential commercial applications continually driving the research forward.

1.8 Aims and objectives

1. To investigate the synthesis of a series of monometallic iridium(III) and rhodium(III) d^6 octahedral complexes, incorporating NCN-coordinating terdentate ligands. Chapter 2 discusses the preparation of several NCN, NNC and CNC-coordinating terdentate ligands, dimeric complexes of the NCN ligands of the form $[M(NCN)Cl(\mu\text{-}Cl)]_2$, and the use of the latter in conjugation with other ligands in the synthesis of a range of monometallic complexes.

2. To investigate the linear stepwise expansion of the monometallic complexes. Chapter 3 describes the introduction of appropriate functionalities into the ligands, allowing their *in situ* elaboration with complementary organic groups to form extended complexes.

3. To investigate the use of Suzuki-Miyaura cross-coupling reactions for the controlled synthesis of linear multimetallic arrays *via* the direct coupling of appropriately functionalised monometallic building blocks (Chapter 5).

4. To investigate the luminescent and electrochemical properties of the monometallic complexes and multimetallic assemblies (Chapters 4 and 5 respectively).

CHAPTER 2

SYNTHESIS OF MONOMETALLIC IRIDIUM AND RHODIUM COMPLEXES

2 Synthesis of Monometallic Iridium(III) and Rhodium(III) Complexes

2.1 Ligand synthesis

A range of terdentate ligands have been used in this work that can potentially coordinate as NNC NCN, CNC and CNO ligands. Here, N normally represents the nitrogen atom of a pyridyl ring, C a cyclometalated carbon atom of a phenyl ring, and O a carboxylate oxygen atom. In the case of the NCN ligands, a second class incorporating 1-linked pyrazoles in place of pyridines have also been prepared. This section discusses the methods employed in the synthesis of these ligands, which involve either classical condensation reactions, in which a central pyridine ring is generated in the reaction (NNC and CNO systems), or metal-catalysed cross-coupling reactions (used for the other systems).

2.1.1 Ring-closing synthesis of pyridines

The synthesis of pyridine rings *via* ring-closing methodologies can be achieved using the classical Hantzsch synthesis. Dating back over a century for substituted pyridines, it was applied in the 1950s by Case and Kasper to the preparation of a number of aryl-substituted bipyridine and terpyridine derivatives.[201] This multi-step synthesis (Figure 2.1) involves the condensation of two ketones with an aldehyde in the presence of ammonia, which is the source of the nitrogen atom in the pyridyl ring generated.

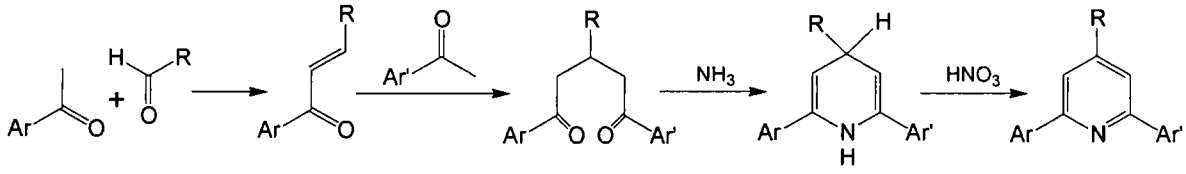

Figure 2.1: The Hantzsch synthesis of pyridines.

The Kröhnke synthesis (Figure 2.2), first reported in 1962, is an adaptation of this Hantzsch methodology.[202] This approach is ideally suited for the synthesis of cyclometalating terdentate ligands that contain a central pyridyl ring. A significant advantage over the Hantzsch synthesis is the exclusion of the need for any dehydrogenation step. The use of carboxylate appended ketones (*e.g.* pyruvic acid) in

place of the aryl ketone allows its application to the synthesis of 2,4-disubstituted as opposed to 2,4,6-trisubstituted pyridine rings, since thermal decarboxylation can be carried out following ring closure. This provides a convenient route to 4-aryl substituted bipyridines.[202, 203]

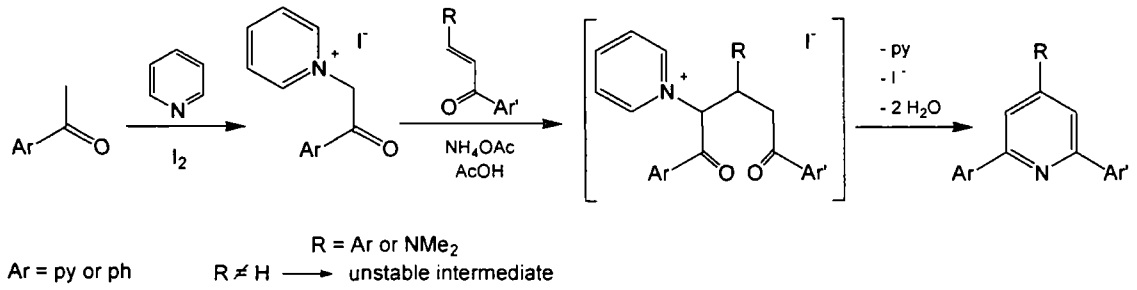

Figure 2.2: The Kröhnke synthesis of pyridines.

2.1.1.1 6-Phenyl-bipyridines: NNC-coordinating ligands

Whilst the classical Kröhnke synthesis (Figure 2.2) necessitates an aryl-group in the 4'-position, the use of a Mannich base does away with this requirement. This was first reported in 1991 by Jameson and Guise for the synthesis of 2,2':6',2"-terpyridine (tpy).[204] In the present study, a modified Kröhnke approach was employed for the preparation of the NNC-coordinating ligand 6-phenyl-2,2'-bipyridine (phbpyH) **1**.[77, 205] Following a Mannich reaction (Figure 2.3) the Mannich base **2** was formed in 50% yield. This readily loses Me_2NH to form an α,β-unsaturated carbonyl compound and was subsequently reacted with the pyridinium iodide salt **3**,[203] and ammonium acetate to yield phbpyH in 43% yield (Figure 2.3).

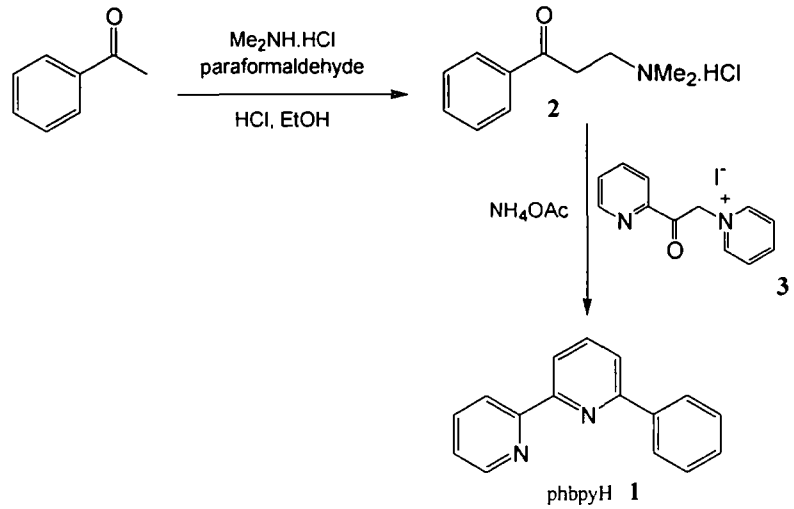

Figure 2.3: Synthesis of phbpyH *via* a Mannich base reaction.

The ligand mtbpyH–ϕ–Br was formed in a similar manner from *p*-bromobenzaldehyde (Figure 2.4). It incorporates a *p*-bromoaryl pendant which would hopefully allow its elaboration pre- or post-complexation.

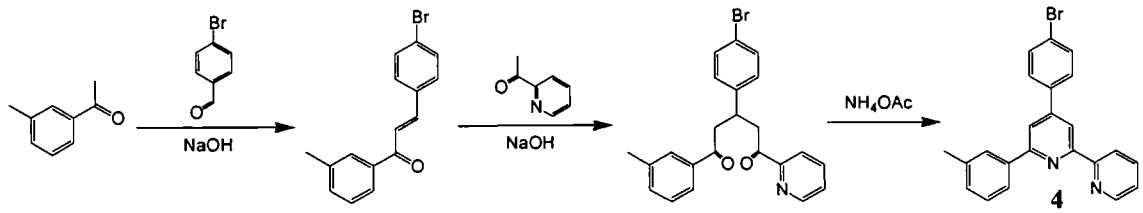

Figure 2.4: Modified Kröhnke synthesis of mtbpyH-ϕ-Br 4.

2.1.1.2 CNO-coordinating ligands

As previously reported by this research group, the CNO-coordinating ligand 4'-*p*-tolyl-6-phenylpicolinic acid ($tppicH_2$) **5** can be synthesised *via* a modified ring-closing Kröhnke approach.[76] The 2-oxo-4'-*p*-tolyl-but-3-enoic acid starting material can be prepared in good yield from the reaction of the aryl aldehyde and sodium pyruvate.[76, 206] Heating this to reflux in water with 1-(2-oxo-2-phenylethyl)pyridinium iodide **6** (formed in 50% yield *via* an established methodology)[203] and ammonium acetate resulted in the desired product in 82% yield (Figure 2.5).

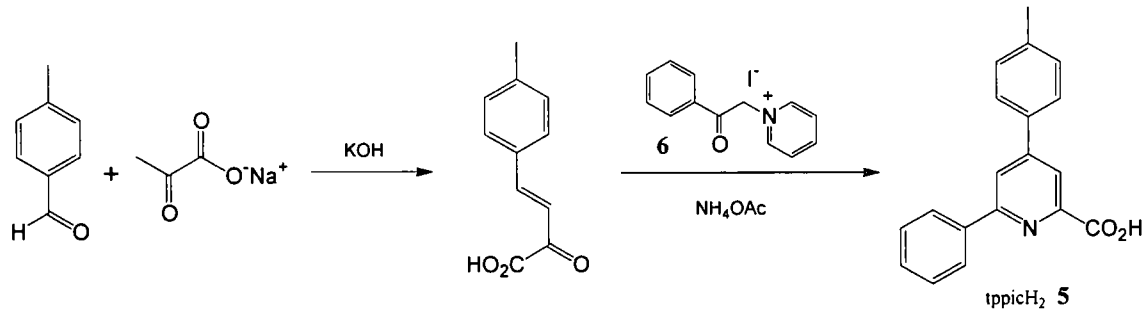

Figure 2.5: Synthesis of $tppicH_2$ 5 *via* a modified Kröhnke methodology.

2.1.2 The use of cross-couplings reactions

Since ring-closing reactions, *e.g.* Kröhnke syntheses, are generally unsuitable for the closure of phenyl rings, an alternative methodology was required for the NCN-coordinating ligands. Palladium and copper-catalysed cross-coupling reactions have been used for the pyridyl and pyrazolyl ligands respectively.

2.1.2.1 NCN-coordinating ligands

The archetypal NCN-coordinating ligand used within this study is 1,3-di(2-pyridyl)-4,6-dimethylbenzene (dpydmbH). To date, two methodologies have been reported in the literature for the synthesis of the parent, unsubstituted, ligand 1,3-di(2-pyridyl)benzene (dpybH). The early studies involved a cobalt-catalysed cyclotrimerisation reaction between 1,3-dicyano-benzene and acetylene at high pressure (Figure 2.6). Although this route was high yielding (90%), it is extremely hazardous due to the use of explosive, high pressure, acetylene making it far from ideal.[207-209]

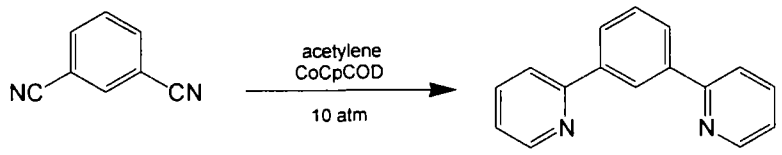

Figure 2.6: Formation of lateral pyridyl rings *via* a cyclisation reaction.

More recently, Stille,[81] Suzuki[210] and Negishi[211] cross-couplings (Figure 2.7) have been used, involving the reaction of 1,3-dibromobenzene with organometallic pyridine reagents, py–M (M = SnR_3, $B(OH)_2$ and ZnR respectively). Despite the Suzuki cross-coupling reaction being reported as a route to dpybH,[210] the preparation and use of pyridine-2-boronic acids is known to be troublesome; the method requiring stabilisation of the boronate with N-phenyldiethanolamine and the coupling being accompanied by undesirable aryl exchange scrambling with the phosphine catalyst. For this reason Negishi and Stille cross-couplings have been favoured. The zinc-based Negishi cross-coupling reaction[212] was reported for the synthesis of 5-methyl-1,3-di(2-pyridyl)benzene (dpymbH), in an attempt to avoid the need for the highly toxic tin reagents required by Stille reactions.[211] Whilst good (86%) yields have been reported by one group for dpymbH,[211] previous attempts within this laboratory to synthesise dpydmbH 7 by this method were unsuccessful, with low yields and predominantly the mono-substituted product being reported.[206]

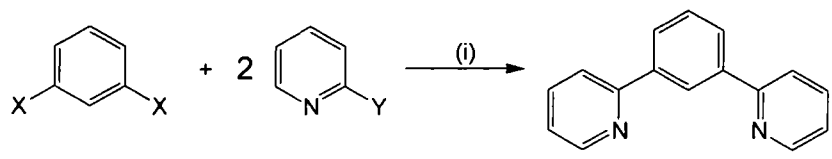

X = Br	Y = $SnBu_3$	(i) = $PdCl_2(PPh_3)_2$, LiCl	Stille
	= ZnCl	(i) = $Pd(PPh_3)_4$	Negishi
	= $B(OH)_2$	(i) = $Pd(PPh_3)_4$, K_2CO_3 (aq)	Suzuki
X = $B(OH)_2$	Y = Br	(i) = $Pd(PPh_3)_4$, K_2CO_3 (aq)	Suzuki

Figure 2.7: Synthesis of dpybH using cross-coupling reactions.

Cárdenas *et al.* were the first to demonstrate the preparation of dpybH *via* a Stille cross-coupling reaction (Figure 2.7) in 1999.[81] Similarly in this study, a Stille reaction was employed to synthesise the 4,6-dimethyl derivative dpydmbH **7**, with the availability and stability of the stannane reagent and good synthetic yields outweighing the issue of high toxicity. The precursor, namely 1,3-dibromo-4,6-dimethylbenzene (Figure 2.8) can be formed in high yield upon reaction of *meta*-xylene with bromine in the presence of a catalytic amount of iodine. Subsequent reaction of this with 2-tri-*n*-butyl-stannylpyridine, under an inert atmosphere, afforded dpydmbH **7** in 77% yield (Figure 2.8).

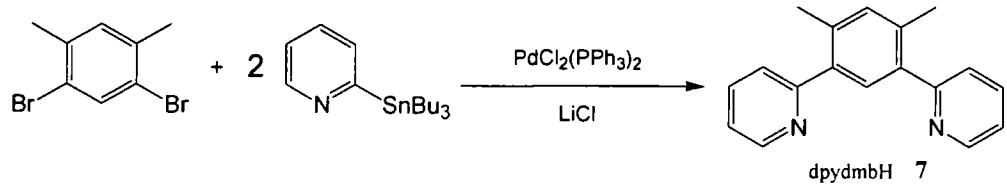

Figure 2.8: Synthesis of dpydmbH 7 *via* a Stille cross-coupling reaction.

As discussed in Sections 1.5 and 1.6.3 multinuclear metal complexes are of great interest in molecular electronics owing to their potential ability to transfer charge or energy through the assembly from one metal centre to the next.[130, 185] In this study, considerable attention was paid to the attempted synthesis of ligands bearing bromo and boronic acid functionalities (Chapter 3) which, when incorporated into the coordination sphere of the metal complex, would allow them to be used as "building blocks" in Suzuki cross-coupling reactions to synthesise multinuclear assemblies (Chapter 5). Several attempts were made to synthesise 1-bromo-3,5-di(2-pyridyl)-2,6-

dimethylbenzene, (dpydmbH-Br) **8**, the brominated derivative of the archetypal NCN ligand dpydmbH **7**, under a range of subtly different Stille conditions.

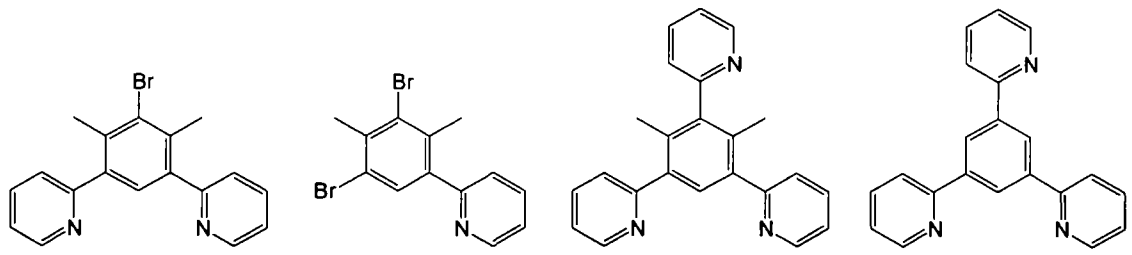

dpydmbH-Br **8** pydmbH-Br_2 **10** tpydmbH **11** tpybH **22**

The required precursor for dpydmbH-Br **8**, namely 1,3,5-tribromo-4,6-dimethylbenzene **9**, was prepared in 64% yield by bromination of 3,5-dimethylaniline, followed by deamination *via* the diazonium salt (Figure 2.9).

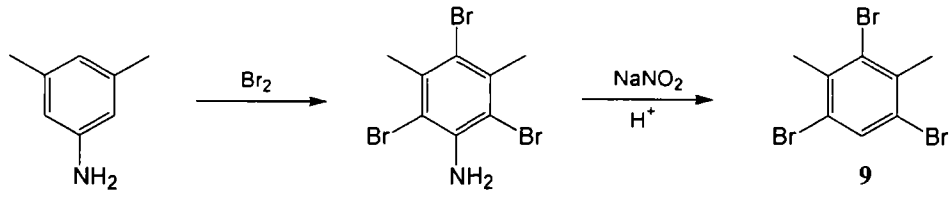

Figure 2.9: Synthesis of 1,3,5-tribromo-4,6-dimethylbenzene 9.

Whilst dpydmbH-Br **8** was one of the products of the Stille reaction of **9** with py-$SnBu_3$, it was formed in low yield with the mono-substituted side-product, pydmbH-Br_2 **10**, being isolated as the major product. Attempts to react this with a further equivalent of 2-tri-*n*-butylstannylpyridine also failed, with dpydmbH-Br **8** remaining elusive and 1,3,5-tri(2-pyridyl)-2,4-dimethylbenzene (tpydmbH) **11** identified as the predominating product. It was thus concluded that selective coupling at the less hindered C^3- and C^5-positions could not be achieved by Stille cross-coupling reactions.

2.1.2.2 CNC-coordinating ligands

The di-fluorinated CNC ligand, 1,3-bis(3-fluorophenyl)pyridine (F_2dppyH_2) **12**, was prepared in 97% yield *via* the Suzuki cross-coupling of 2,6-dibromopyridine and 3-fluorophenyl boronic acid (Figure 2.10), an analogous approach to that previously employed by this laboratory for the tetra-fluorinated derivative 2,6-bis(2,4-difluoro-phenyl)pyridine (F_4dppyH_2).[76, 213]

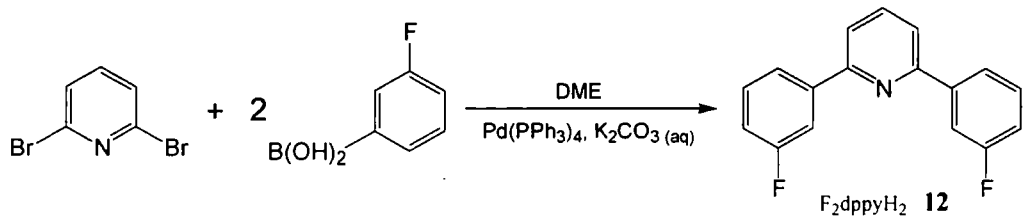

Figure 2.10: Synthesis of F_2dppyH_2 12 *via* a Suzuki cross-coupling.

2.1.2.3 Copper(I) catalysed synthesis of pyrazole-based NCN ligands

A series of NCN-coordinating pyrazole-based ligands were synthesised analogous to the pyridyl ligands described in Section 2.1.2.1. The initial synthetic strategy attempted was based upon that reported by Lexy and Kauffmann for 1,3,5-tri(1-pyrazolyl)benzene (tpzbH) in 1980,[214-216] involving the preparation of sodium pyrazolate, which was subsequently reacted with 1,3,5-tribromobenzene under an inert atmosphere (Figure 2.11). In our hands, following purification by column chromatography, the sought-after product tpzbH **13** was obtained in only 2% yield, with the main products isolated being the mono-substituted 1-pyrazolyl-3,5-dibromobenzene (pzbH-Br_2) **14** in 49% yield and the di-substituted 1,3-di(1-pyrazolyl)-5-bromobenzene (dpzbH-Br) **15** in 34% yield.

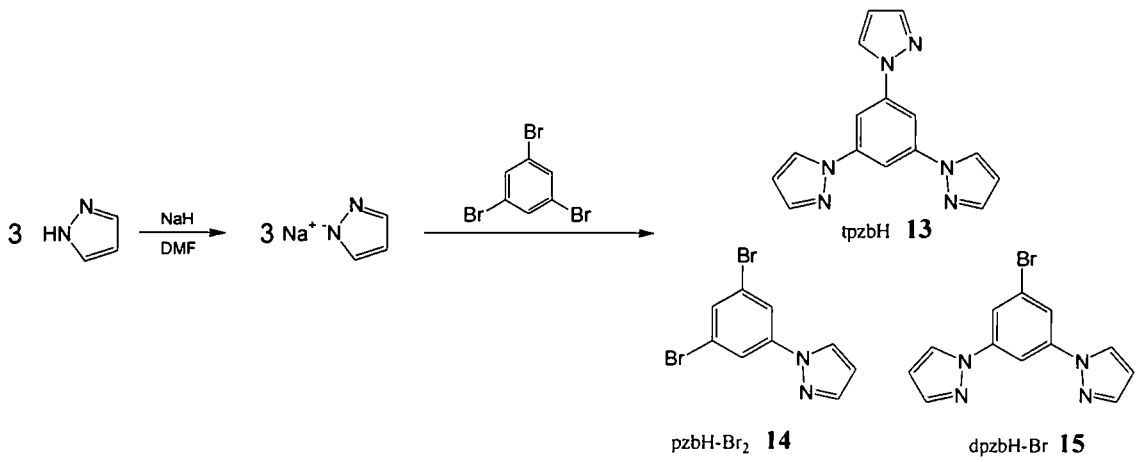

Figure 2.11: Synthesis of tpzbH 13, pzbH-Br_2 14 and dpzbH-Br 15.

Numerous modifications were made to try to optimise the yield of tpzbH **13** including increasing the number of equivalents of sodium hydride used to compensate for the presence of any residual water in the DMF, using a larger excess of sodium pyrazolate, and increasing the reaction time and temperature. Unfortunately none of these had a significant effect on the outcome of the reaction. Attempts were also made to drive the reaction to completion by the introduction of an additional synthetic step, where the

mono-substituted side-product **14** was reacted with a large excess of sodium pyrazolate. These also failed to yield significant quantities of tpzbH **13**, making it apparent that upon substituting the first pyrazolyl ring into the central benzene, the rate of subsequent reaction with sodium pyrazolate is severely retarded. This theory being further supported by poor results in the attempted synthesis of 1,3-di(1-pyrazolyl)benzene (dpzbH) **16** by this method, where the mono-substituted species was the predominating product.

Whilst the formation of aryl-aryl bonds by palladium-catalysed cross-coupling reactions (Section 2.1.2) has been well studied since the 1960s, the use of cross-coupling reactions to generate aryl-N bonds was relatively unstudied until recently. The copper(I) catalysed Ullmann coupling first reported in 1901,[217] can be used to from aryl-N bonds upon reaction of an aryl halide with an appropriate nucleophile, but the harsh reaction conditions and erratic yields obtained make it far from ideal. Upon the addition of supplementary catalytic reagents, Buchwald *et al.* reported a much milder copper(I) catalysed aryl amination strategy in 2001,[218] since which these reactions have been the subject of intense interest. Following the failure of the attempted synthesis of 1,3-di(1-pyrazolyl)benzene (dpzbH) **16** *via* sodium pyrazolate by the aforementioned method, a copper(I) catalysed reaction based upon Buchwald's work was employed.[218] The reaction of 1,3-di-iodobenzene with pyrazole in degassed 1,4-dioxane (Figure 2.12) afforded dpzbH **16** in 64% yield.

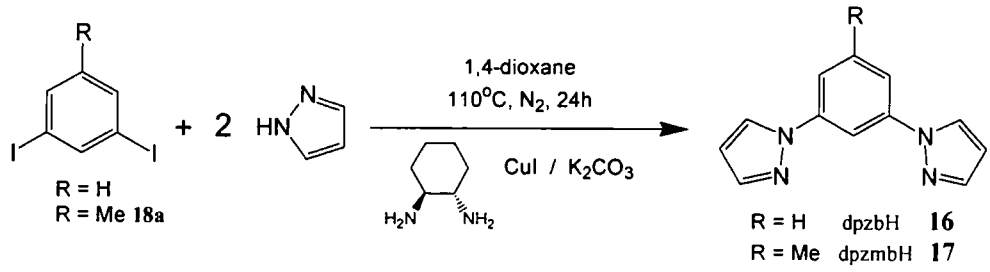

Figure 2.12: Synthesis of dpzbH 16 and dpzmbH 17 *via* Buchwald's copper(I) catalysed method.

The same methodology (Figure 2.12) was also employed for the mono-methyl derivative, 1,3-di(1-pyrazolyl)-5-methylbenzene (dpzmbH) **17**, formed in 75% yield from 1,3-di-iodo-5-methylbenzene **18a**. Unlike 1,3-di-iodobenzene, this precursor is not commercially available. It was obtained by a copper-catalysed halide exchange from the di-bromo analogue (Figure 2.13) as reported by Buchwald *et al.* in a separate

study, in which N,N-dimethylethylenediamine, as the ligand for Cu(I), was found to give the highest conversions.[219]

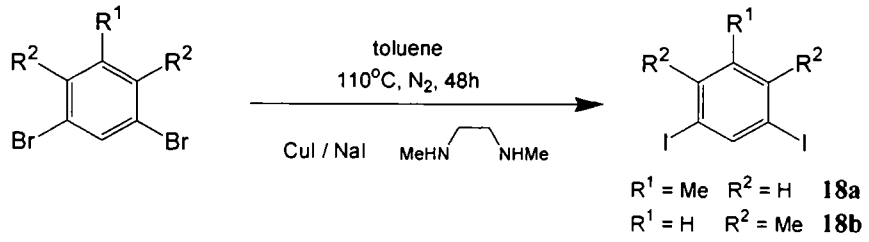

Figure 2.13: Copper-catalysed halide exchange of 1,3-dibromobenzene derivatives.

The synthesis of 1,3-di(1-pyrazolyl)-4,6-dimethylbenzene (dpzdmbH) **19** proved unsuccessful *via* both the sodium pyrazolate and Buchwald's copper(I) catalysed methodologies, presumably owing to hindrance of the C^1- and C^3-positions by the neighbouring methyl groups. Instead a related copper(I) catalysed reaction (Figure 2.14) based upon work by Cristau and Taillefer was employed, which makes use of a different ligand, N,N-bis(pyridyl)-1,2-cyclo-hexanediamine **20**, in conjunction with Cu_2O as the copper source.[220] The ligand was prepared upon reaction of *trans*-1,2-diaminocyclohexane with 2-pyridine carboxaldehyde (Figure 2.14), as reported by Belokon *et al.*[221] The desired compound dpzdmbH **19** was isolated in 18% yield following column chromatography, alongside the mono-substituted side-product 1-iodo-3-pyrazolyl-4,6-dimethylbenzene (pzdmbH-I) **21** obtained in 44% yield. PzdmbH-I **21** was successfully reacted with a further equivalent of pyrazole to yield additional dpzdmbH **19**, whilst also providing the potential for the formation of asymmetrical ligands.

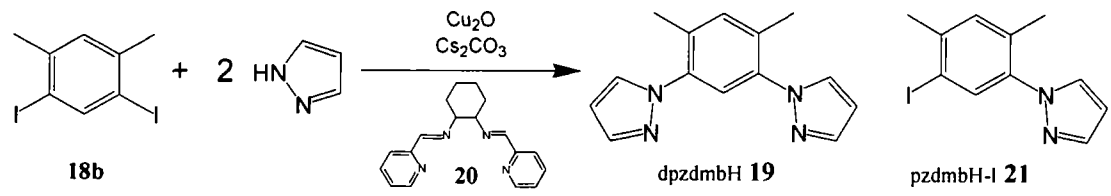

Figure 2.14: Copper-catalysed synthesis of dpzdmbH 19.

2.2 Pyridyl-NCN-based complexes of iridium and rhodium

A two-step complexation strategy was employed for the synthesis of the heteroleptic bis-terdentate iridium(III) and rhodium(III) complexes in this study.[76, 78, 206] Step 1 involved the preparation of a dimer comprising of two M(NCN)Cl units joined by two chloro-bridges, as discussed in Sections 2.2.1 and 2.3.1, and step 2 the reaction of the dimer with two equivalents of a second ligand, cleaving the chloro-bridges and forming a d^6 octahedral complex, as discussed in Sections 2.2.2 and 2.3.2.

2.2.1 Step 1: Synthesis of chloro-bridged Ir(III) and Rh(III) dimers

The chloro-bridged dimers were formed upon reaction of the NCN-coordinating ligand with $MCl_3.xH_2O$ (M = Ir(III) or Rh(III)) in a 7:3 mixture of 2-ethoxyethanol and water at 80°C (Figure 2.16). As reported in the preceding work by Wilkinson, the flanking methyl groups prevent competitive cyclometalation at the $C^{4'}$- and $C^{6'}$-position (Figure 2.15).[76, 206]

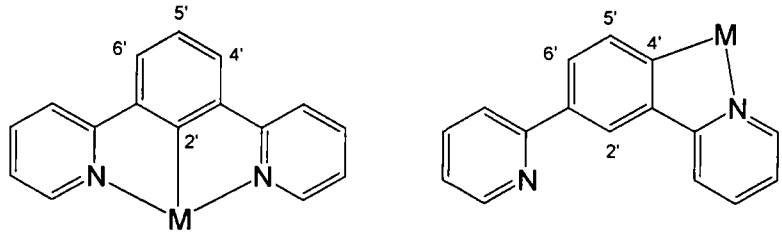

Figure 2.15: Two potential binding modes of dpyb.

In the present study, the use of the C_3-symmetric ligand 1,3,5-tri-(2-pyridyl)benzene (tpybH) **22** [222] was investigated as an alternative solution to this binding problem. TpybH incorporates a third pyridyl ring, resulting in all three potential cyclometalating positions being equivalent, effectively eliminating the bidentate binding (binding mode II: Figure 2.15) to the metal centre. The dimeric iridium intermediate $[Ir(tpyb)Cl(\mu\text{-}Cl)]_2$ **23** (Figure 2.16) was synthesised as an orange solid in 68% yield following reaction of tpybH **22** with $IrCl_3.3H_2O$.

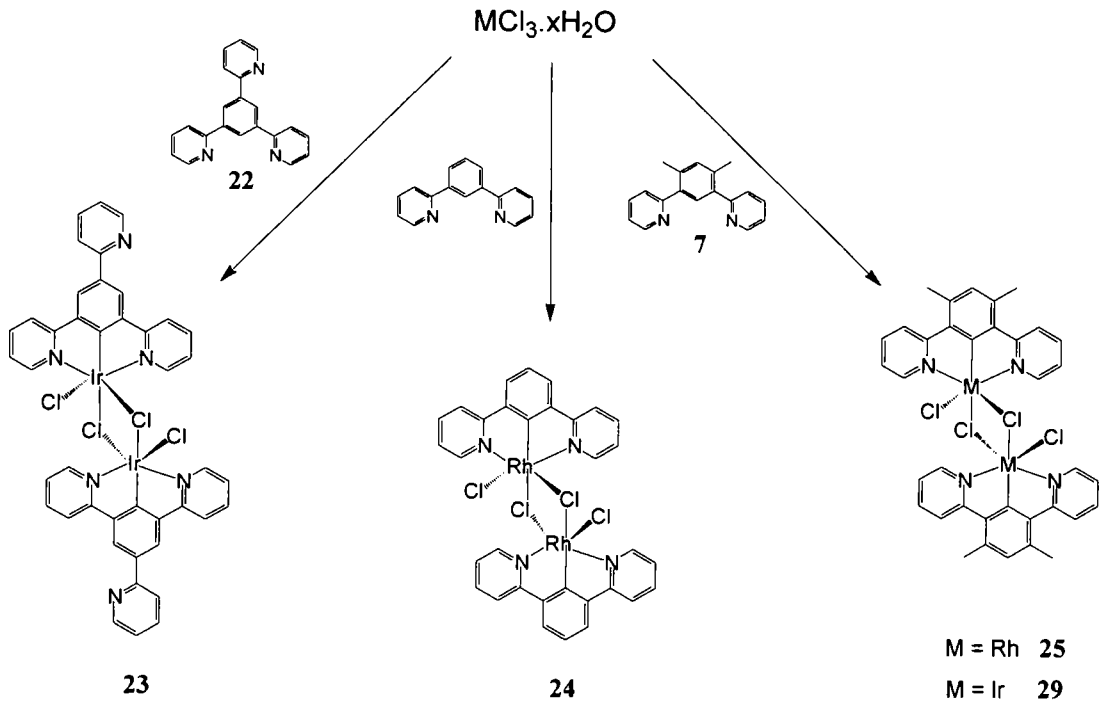

Figure 2.16: Synthesis of the pyridyl-based dimers.

Dimeric rhodium complexes [Rh(dpyb)Cl(μ-Cl)]$_2$ **24** and [Rh(dpydmb)Cl(μ-Cl)]$_2$ **25** (Figure 2.16) were also prepared in this study, by reaction of rhodium trichloride monohydrate with dpybH and dpydmbH **7** respectively. A Rh(NCN) unit has never been investigated for 1,3-di(2-pyridyl)benzene (dpyb) and its derivatives; thus these mark the first examples of complexes containing such moieties. As with iridium, dpyb exhibited a mixture of binding modes to the Rh(III) centre (Figure 2.15), however, ^{1}H-NMR spectroscopy indicated that the terdentately bound [Rh(dpyb)Cl(μ-Cl)]$_2$ **24** was the predominant species formed with Rh(III) (*i.e.* binding mode I: Figure 2.15). Owing to poor solubility in all common solvents, purification at this intermediate stage was not feasible, thus this dimeric species, along with the others reported herein, was reacted on in its crude form with rigorous purification being undertaken following the introduction of the second ligand. The introduction of methyl groups at the alternative $C^{4'}$- and $C^{6'}$-cyclometalating positions was again seen to eliminate the binding problem observed with dpyb: [Rh(dpydmb)Cl(μ-Cl)]$_2$ **25** was formed as a yellow/orange solid in 72% (Figure 2.16).

Although insoluble in most common solvents, heating [Rh(dpydmb)Cl(μ-Cl)]$_2$ **25** in d_6-DMSO results in the cleavage of the chloro-bridges, affording a solution of sufficient concentration for analysis by ^{1}H-NMR spectroscopy. The ^{1}H-NMR spectrum revealed

the absence of a singlet peak when compared to the free ligand, due to the loss of the $H^{2'}$-phenylene proton between the two pyridine rings upon cyclometalation. As expected for cyclometalation at this position, an upfield shift was observed in the peak corresponding to the proton *para* to this carbon. The structure of the solvated complex was deduced as [Rh(dpydmb)(d_6-DMSO)Cl_2] based upon this observation and by analogy to the X-ray crystallographic study of the iridium analogue, which indicated that the d_6-DMSO molecule was bound through the sulfur *trans* to the cyclometalated carbon.[78]

2.2.2 Step 2: Cleaving the dimer

Upon the successful preparation of a range of dimeric [M(NCN)Cl(μ-Cl)]$_2$ precursors, a series of mononuclear d^6 octahedral complexes were synthesised. This involved the cleavage of the chloro-bridges of the dimeric intermediate upon reaction with a second bidentate or terdentate ligand (Figure 2.17), usually for a short time at high temperature in ethylene glycol.

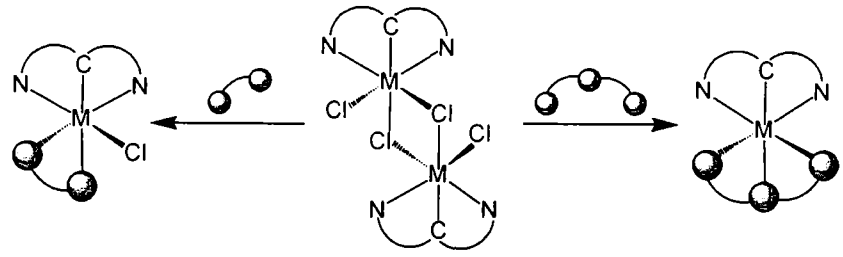

Figure 2.17: Cleaving the chloro-bridged dimeric intermediate.

2.2.2.1 Synthesis of [Rh(NCN)(NNN)]$^{2+}$ complexes

The first complex synthesised here was [Rh(dpyb)(tpy)]$^{2+}$ **26**, formed in 7% yield upon reaction of [Rh(dpyb)Cl(μ-Cl)]$_2$ **24** and 2,2':6',2"-terpyridine (tpy) in refluxing ethylene glycol (196°C) for one hour, precipitation as the PF_6^- salt, and isolation following chromatographic separation. This is the first example of a [Rh(NCN)(NNN)]$^{2+}$ complex containing both polypyridyl and cyclometalating ligands bound to a central rhodium(III) ion. The only other Rh(NCN) unit reported in the literature incorporates the terdentate ligand 1,3-bis(benzimidazol-2-yl)benzene,[109] but there are no reports of this Rh(NCN) unit with multidentate polypyridyl ligands (see Section 1.4.2). Analogous reactions of [Rh(dpydmb)Cl(μ-Cl)]$_2$ **25** with tpy and with 4-(4-bromo)phenyl-2,2':6',2"-terpyridine

(tpy-ϕ-Br) were also carried out giving $[Rh(dpydmb)(tpy)]^{2+}$ **27** in 58% yield, and $[Rh(dpydmb)(tpy\text{-}\phi\text{-}Br)]^{2+}$ **28** in 46% yield respectively.

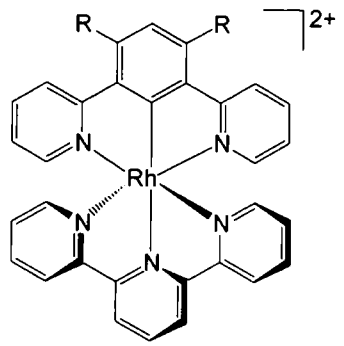

R = H **26**
R = Me **27**

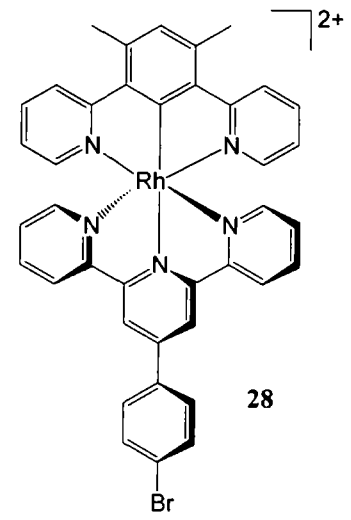

28

2.2.2.2 Synthesis of $[M(NCN)(NN)Cl]^+$ and $[M(NCN)(NNC)]^+$ complexes

The introduction of a second cyclometalating carbon or an anionic ligand, *e.g.* a chloride ion, into the coordination sphere of the central metal ion is known to have a profound impact upon the photophysical properties of the complex. In this study, such a series of $[M(NCN)(NN)Cl]^+$ and $[M(NCN)(NNC)]^+$ coordinated complexes with *cis*-disposed anionic groups were prepared.

Iridium and rhodium complexes with $[M(NCN)(NN)Cl]^+$ coordination were synthesised upon reaction of the dimeric intermediates $[M(dpydmb)Cl(\mu\text{-}Cl)]_2$ (M = Ir(III) **29** and M = Rh(III) **25**) with 2,2'-bipyridine (bpy) in refluxing ethylene glycol. The resulting complexes $[Ir(dpydmb)(bpy)Cl]^+$ **30** and $[Rh(dpydmb)(bpy)Cl]^+$ **31** were isolated as their PF_6^- salts in ≥ 95% yield. Similarly, $[Ir(tpyb)(bpy)Cl]^+$ **32** was prepared in 84% yield in the analogous reaction of $[Ir(tpyb)Cl(\mu\text{-}Cl)]_2$ **23** with bpy.

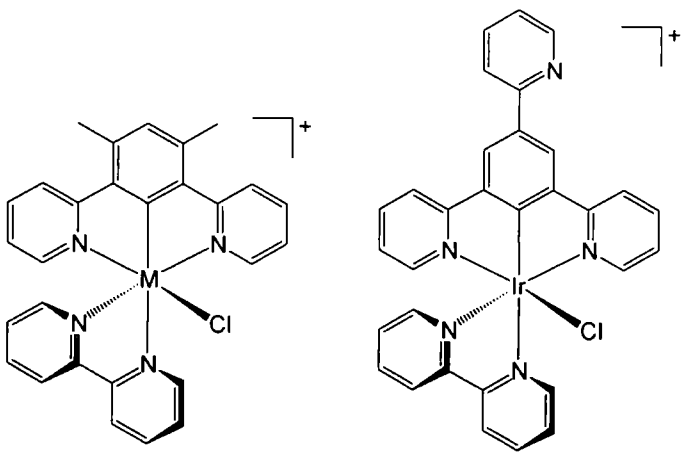

M = Ir **30**
M = Rh **31**

32

Iridium and rhodium complexes with $[M(NCN)(NNC)]^+$ coordination were synthesised upon reaction of phbpyH **1** with the appropriate $[M(dpydmb)Cl(\mu\text{-}Cl)]_2$ intermediate (M = Ir(III) **29** and M = Rh(III) **25**) as seen in Figure 2.18. $[Ir(dpydmb)(phbpy)]^+$ **33** was isolated as a yellow/orange solid in 78% yield,[205] and $[Rh(dpydmb)(phbpy)]^+$ **34** as a yellow solid in 43% yield following chromatographic separation.

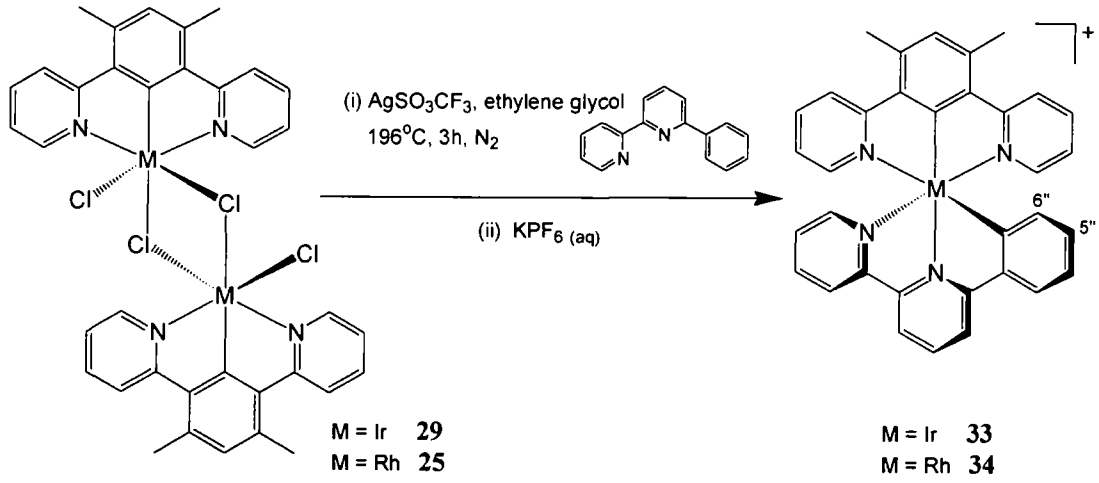

Figure 2.18: Synthesis of $[M(NCN)(NNC)]^+$ coordinated complexes.

The introduction of the terdentate NNC-coordinating ligand 6-phenyl-2,2'-bipyridine (phbpyH) **1** into the coordination sphere of the M(dpydmb) units dictates a mutually *cis* arrangement of the cyclometalated carbons in the resulting complexes, **33** and **34** (Figure 2.18), making them bis-terdentate analogues of the $[M(ppy)_2(bpy)]^+$ series of complexes (Figure 2.19a). The $[Ir(ppy)_2(bpy)]^+$ based complexes are known to display excited state properties similar to those of the archetypal luminescent d^6 transition metal complex $[Ru(bpy)_3]^{2+}$ and are thus of considerable interest.[26, 38] To date the most

closely related bis-terdentate complex of iridium(III) has been Scandola's recently reported $[Ir(CNC)(NNN)]^+$ complex (Figure 2.19b) with *trans*-disposed cyclometalating carbons,[83, 84] whilst no bis-terdentate bis-cyclometalated rhodium(III) complexes have ever been reported.

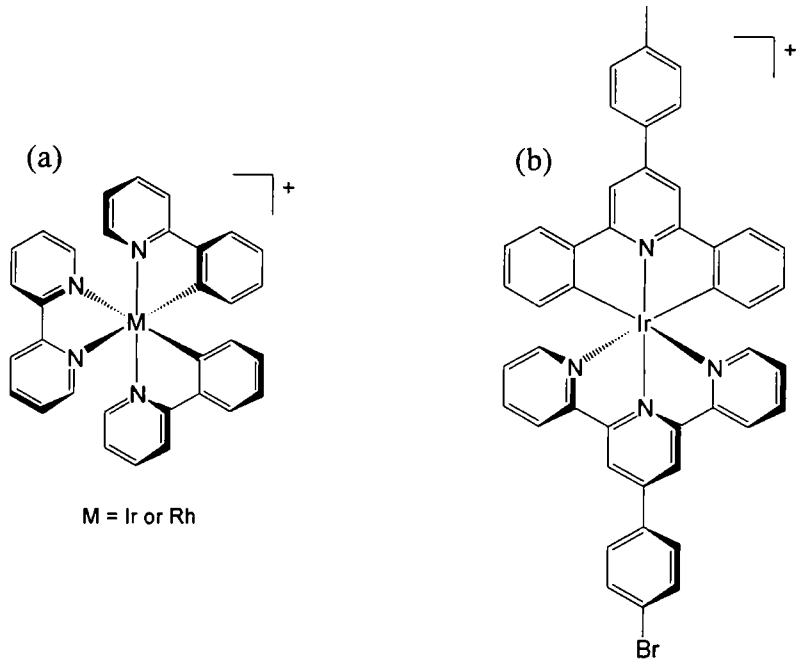

Figure 2.19: (a) $[M(ppy)_2(bpy)]^+$ and (b) Scandola's $[Ir(CNC)(NNN)]^+$ complex. [83, 84]

The cyclometalation of phbpy in the $[M(dpydmb)(phdpy)]^+$ complexes was confirmed by the presence of a low-frequency doublet of integral one in their ^{1}H-NMR spectra corresponding to $H^{6''}$-NNC (at 5.94 (Ir) and 6.19 (Rh) ppm), coupled to a low-frequency triplet with single integration corresponding to $H^{5''}$-NNC (at 6.62 (Ir) and 6.67 (Rh) ppm), alongside the loss of the 2-fold symmetry of the phenyl ring. These low frequency / high field shifts are characteristic of the protons adjacent to the site of cyclometalation in complexes containing cyclometalated aryl-pyridine ligands. In **33** and **34** the shift is further enhanced by the positioning of these protons above the plane of the central phenyl ring of the dpydmb ligand, which induces a diamagnetic ring current. The relevant section of the ^{1}H-NMR spectra of complex **33** is shown in Figure 2.20.

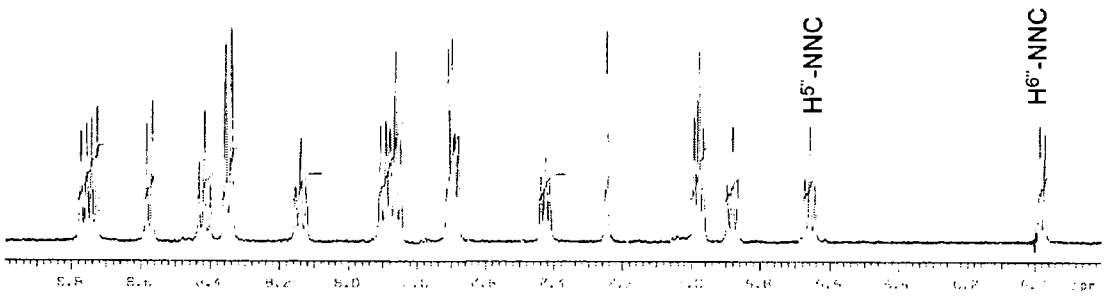

Figure 2.20: ^{1}H-NMR spectrum of [Ir(dpydmb)(phbpy)]$^+$.

The NNC-coordination of phbpy observed in complexes **33** and **34**, contrasts with that previously seen upon reaction of phbpyH with [Ir(tpy)Cl_3] under similar conditions (see Section 1.3.2.2), where phbpy displayed bidentate NN-coordination in the product [Ir(tpy)(phbpyH-*NN*)Cl]$^{2+}$.[77]

2.2.2.3 Synthesis of [M(NCN)(CNC)] complexes

In the preceding work, Wilkinson reported a solvent-free approach to the synthesis of the [Ir(NCN)(CNC)] coordinated complex [Ir(dpydmb)(dppy)]. This charge neutral bis-terdentate analogue of the archetypal tris-bidentate complex [Ir(ppy)$_3$] is discussed in Section 1.3.2.2.[76, 78, 206]

In this study, attempts were made to synthesise the equivalent charge-neutral rhodium complex [Rh(dpydmb)(dppy)] *via* a series of solvent-free and solution-based techniques. Reaction of [Rh(dpydmb)Cl(μ-Cl)]$_2$ **29** with dppyH (Figure 2.21) under the solvent-free conditions used by Wilkinson,[78] afforded [Rh(dpydmb)(dppy-*CN*)L]$^+$ **35** as the main product. Solution-based attempts similarly failed to show any evidence of the formation of the [Rh(NCN)(CNC)] coordinated complex, with only trace amounts of the cationic side-product **35**.

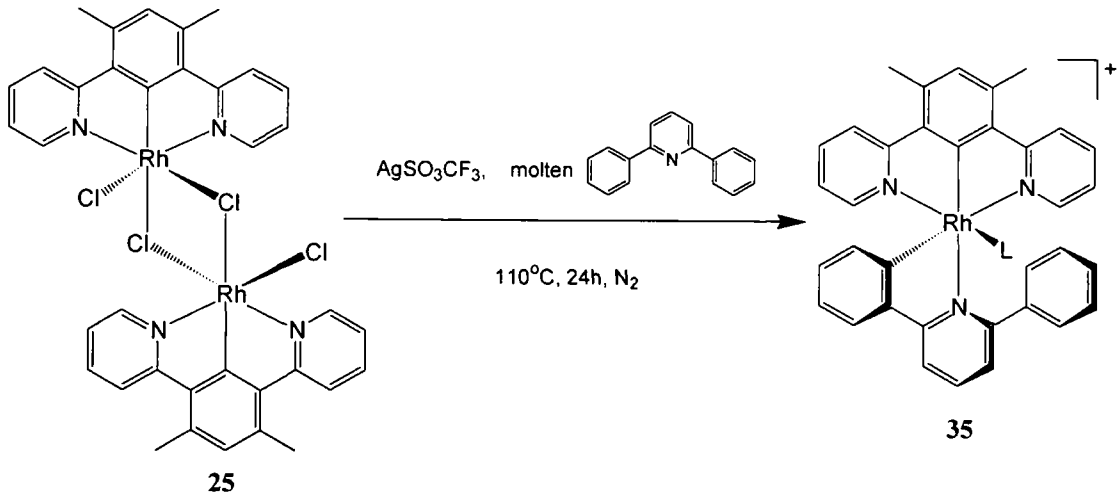

Figure 2.21: The attempted solvent-free synthesis of [Rh(dpydmb)(dppy)]

It is the poor photostability of [M(NCN)(CNC)] coordinated complexes in solution that severely hinders their isolation and results in the decomposed $[M(NCN)(NC)L]^+$ product often being the main or only product isolated. This instability is thought to be the result of "transphobia" *i.e.* the presence of mutually *trans*-cyclometalating carbons.[223] With the strong *trans*-effect of the cyclometalating carbon donor atom weakening the bond to the ligand opposite and the *trans*-influence increasing the ground state bond length. Unlike in *mer*-$[Ir(ppy)_3]$ which also contains *trans* M–C bonds, the steric constraints of the bis-terdentate complexes prevents their isomerisation into the *facial* thermodynamic product resulting in the cleavage of the M–C bond being irreversible (Figure 2.22).

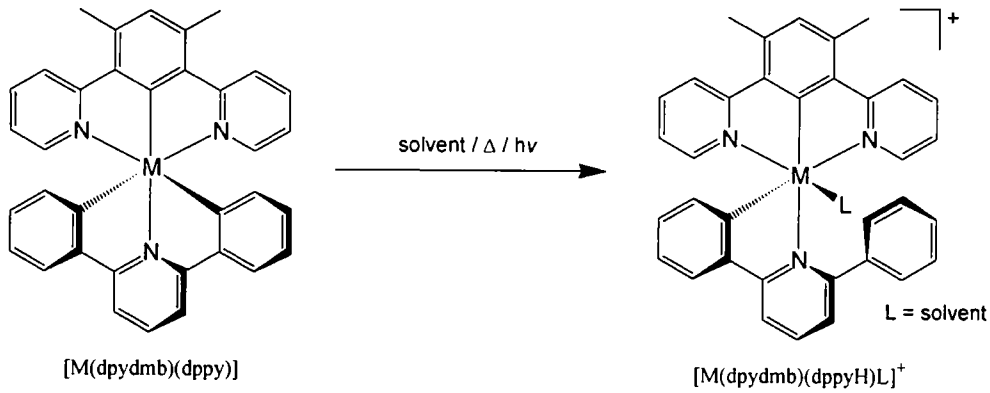

Figure 2.22: Decomposition of [M(dpydmb)(dppy)] to $[M(dpydmb)(dppyH)L]^+$.

The introduction of electron-withdrawing fluorine substituents into the CNC-coordinated ligand was considered as a method to stabilise the [M(NCN)(CNC)] complex with respect to the dissociation of the Ir–C bond. It was hoped that these substituents would stabilise the negative charge at the carbon end of the $Ir^+–C^-$ bond and

reduce its lability, perhaps assisted by a synergistic $Ir^{\delta+}$------$F^{\delta-}$ interaction. Stabilisation over the non-fluorinated complexes had previously been observed in Wilkinson's [Ir(dpydmb)(F_4dppy)][76] and Thompson's *mer*-[Ir(F_2ppy)$_3$][66] complexes (Figure 2.23).

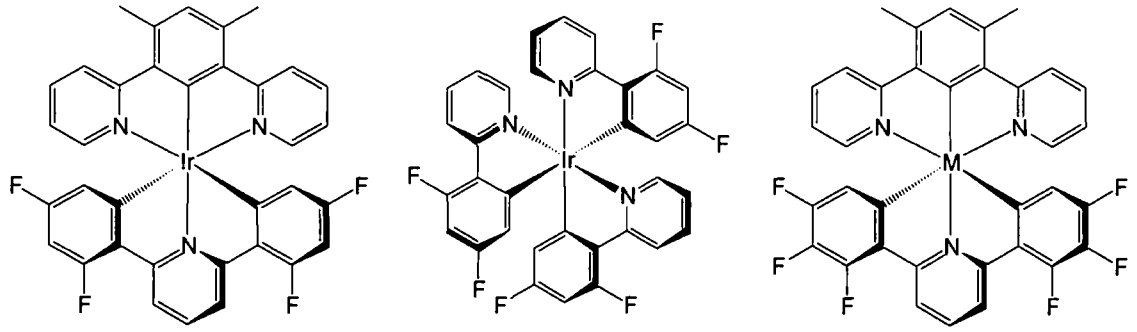

[Ir(dpydmb)(F_4dppy)] *mer*-[Ir(F_2ppy)$_3$] [M(dpydmb)(F_6dppy)]

Figure 2.23: Fluorinated tris-cyclometalated complexes.

In this study, attempts to synthesise the rhodium and iridium [M(dpydmb)(F_6dppy)] complexes (Figure 2.23) incorporating the ligand 1,3-bis(2,3,4-trifluorophenyl)pyridine (F_6dppyH_2) *via* a range of solvent-free and solution-based methodologies proved fruitless. However, an [Ir(NCN)(CNC)] complex, [Ir(dpydmb)(F_2dppy)] **36**, was synthesised by reacting [Ir(dpydmb)Cl(μ-Cl)]$_2$ **29** with 1,3-bis-(3-fluorophenyl)pyridine (F_2dppyH_2) **12** in a solution-based technique (Figure 2.24). ES^+ mass spectrometry confirmed the identity of the product, which was isolated as a yellow solid in 17% yield. Unfortunately, prior to full ^{1}H-NMR and HRMS characterisation being carried out, this decomposed in solution forming a complicated mixture of products. A pure sample of [Ir(dpydmb)(F_2dppy)] **36** could not be obtained when the synthesis was repeated.

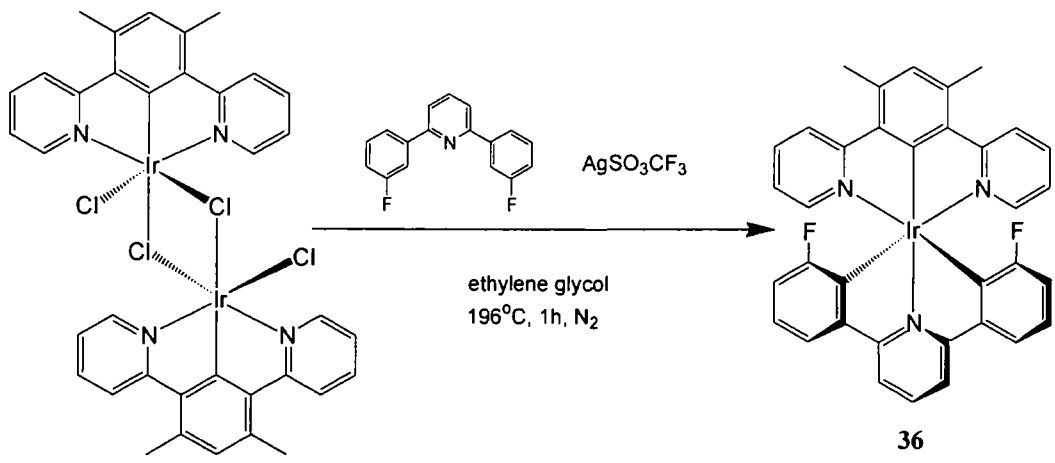

29 **36**

Figure 2.24: Synthesis of [Ir(dpydmb)(F_2dppy)].

2.2.2.4 Synthesis of [M(NCN)(NNN)] complexes

The terdentate ligand 2,6-di(2'-indolyl)pyridine (dinpyH_2), containing two five-membered indolyl rings, is capable of binding to a central metal *via* three nitrogen atoms following deprotonation of the NH groups ($^-$NNN$^-$-coordination) or *via* cyclometalating carbons (CNC-coordination). Reaction of dinpyH_2 with [Rh(dpydmb)Cl(μ-Cl)]$_2$ **25** in ethylene glycol in the presence of K_2CO_3 afforded the charge-neutral complex [Rh(dpydmb)(dinpy-*NNN*)] **37** in 10% yield following chromatographic separation.

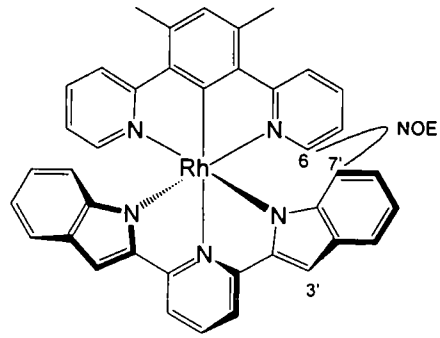

37

This NNN-coordination of dinpy was confirmed by the ^{1}H-NMR spectrum, which when compared to that of the free ligand revealed the retention of the singlet corresponding to $H^{3'}$-dinpy, alongside the absence of the broad NH peak. Further support was offered by the ^{1}H-^{1}H NOESY NMR spectrum displaying weak coupling between H^6-dpydmb and $H^{7'}$-dinpy. The favouring of this NNN-coordination of dinpy can be attributed to it being hard to accommodate mutually *trans* carbons in the coordination sphere around a metal centre, as discussed in Section 1.3.2.2.

This binding appears to differ from that reported by Wilkinson with Ir(III), where [Ir(dpydmb)(dinpy-*CNC*)] was formed and isolated under the same reaction conditions and the coordination mode was perceived to be solvent dependent (Figure 2.25).[206] However, it should be noted that the particularly low yields in which the two iridium complexes were obtained, means that the formation of the other isomer under both solvent conditions cannot be definitely ruled out.

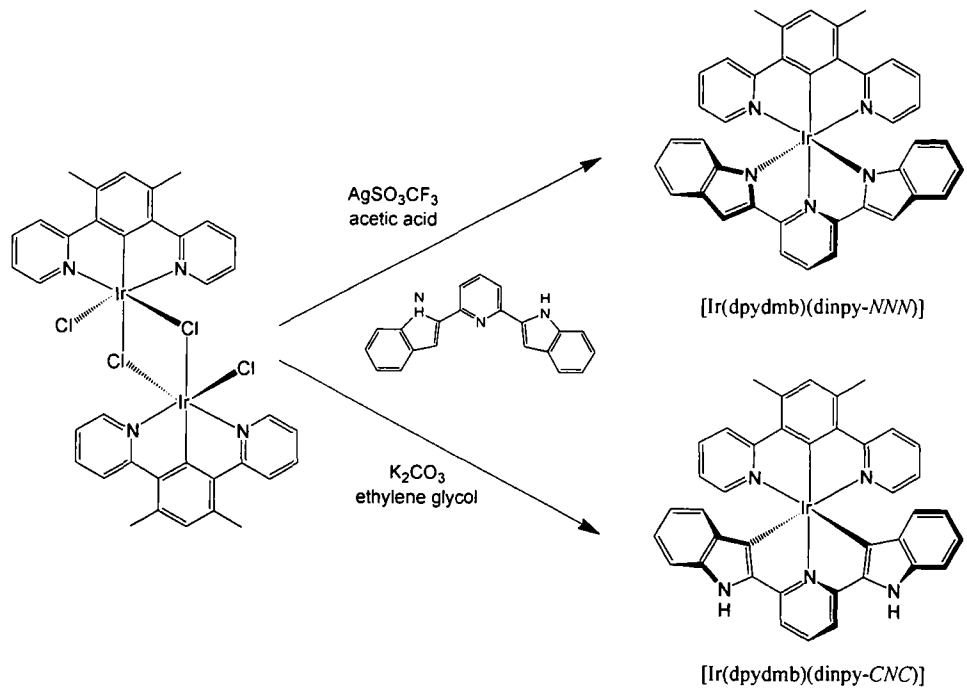

Figure 2.25: Wilkinson's [Ir(dpydmb)(dinpy-*NNN*)] and [Ir(dpydmb)(dinpy-*CNC*)].

Unlike with Ir(III), the attempted reaction of the Rh(III) dimer **25** with dinpyH_2 in acetic acid showed no evidence of the formation of either product, with the reasoning behind the different binding of dinpy with Rh(III) and Ir(III) not being fully understood.

2.2.2.5 Synthesis of [M(NCN)(CNO)] complexes

Alongside the preparation of the charge-neutral [Ir(NCN)(CNC)] and [Ir(NCN)(NNN)] coordinated complexes, Wilkinson reported the synthesis of [Ir(dpydmb)(ttpic)] bearing [Ir(CNC)(CNO)] coordination.[76] In this study, attempts were made to prepare the rhodium analogue [Rh(dpydmb)(ttpic)] from the Rh(III) dimer **25** and 4'-*p*-tolyl-6-phenylpicolinic acid (ttpicH_2) **5**, using the same methodology (Figure 2.26). The only identifiable complex isolated from the reaction was that of [Rh(dpydmb)(ttpicH-*NO*)L]$^+$ **38**. Its structure deduced by ^{1}H-NMR spectroscopy, from the absence of low frequency peaks that would have been characteristic of the proton adjacent to the point of cyclometalation and from the 2-fold symmetry observed in the phenyl ring of ttpicH, indicating that it remained unbound. Mass spectrometry showed that the sixth coordination site was occupied by a water molecule; however, this could easily have arisen upon exchange with another solvent molecule inside the aqueous conditions of the mass spectrometer and could not be relied upon.

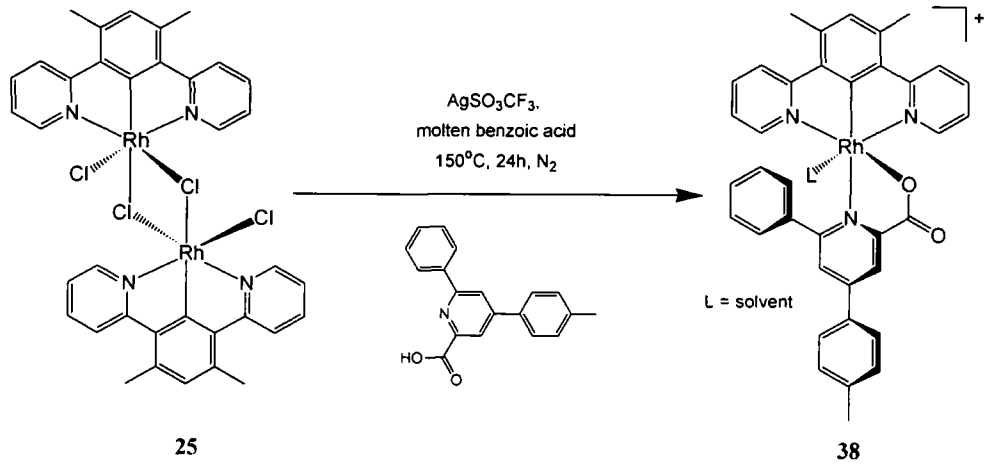

25 38

Figure 2.26: Attempted synthesis of [Rh(dpydmb)(ttpic)].

Solution-based techniques carried out in ethylene glycol in the presence of silver triflate also failed to yield [Rh(dpydmb)(ttpic)] following chromatographic separation, despite the ^{1}H-NMR spectrum of the crude reaction mixture indicating low resonance peaks, characteristic of cyclometalation.

2.2.2.6 Synthesis of [M(NCN)(NC)Cl] complexes

Charge-neutral [M(NCN)(NC)Cl] complexes can be prepared by cleavage of the NCN-coordinated dimer with a cyclometalating bidentate ligand, as previously reported by Wilkinson in the single example of [Ir(dpydmb)(ppy)Cl].[47, 76] In this study two approaches were attempted to synthesise a charge-neutral rhodium complex bearing the same coordination (Figure 2.27).

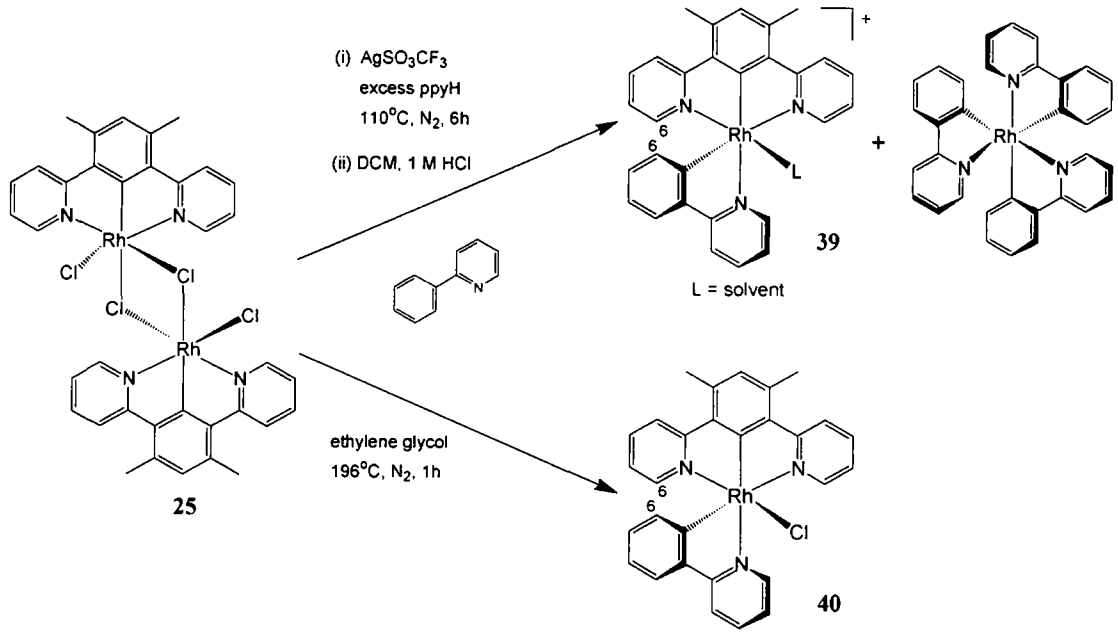

25 39 40

Figure 2.27: Two synthetic approaches towards [Rh(dpydmb)(ppy)Cl].

The first approach was based upon that used by Wilkinson for iridium and involved heating the intermediate **25** in an excess of neat 2-phenylpyridine (ppyH). This afforded [Rh(dpydmb)(ppy)L] **39** in 16% yield alongside the significant side-product [$Rh(ppy)_3$] (Figure 2.27). ^1H-^1H NOESY NMR analysis of **39** revealed a cross-peak between H^6-dpydmb and H^6-ppy, confirming the expected thermodynamic product with *cis*-disposed cyclometalating carbons. Mass spectrometry further confirmed the structure of **39**, revealing a vacant sixth coordination site indicative of the loss of a labile solvent molecule and formation of a singly charged species. The formation of the side-product [$M(ppy)_3$] with Rh(III), but not Ir(III)[47, 76] suggests that the bonds between dpydmb and second row rhodium are weaker than those to third row iridium, allowing them to be easily broken and two additional ppy molecules to bind and form [$Rh(ppy)_3$].

The second attempt was solution-based, involving the reaction of the intermediate **25** with stoichiometric amounts of ppyH (Figure 2.27). This afforded *mer*-[Rh(dpydmb)(ppy)Cl] **40** in 75% yield, with structural determination being carried out by NMR spectroscopy and mass spectrometry. Once again the ^1H-^1H NOESY NMR spectrum showed a cross-peak between H^6-dpydmb and H^6-ppy, confirming that the product was exclusively the *mer*-isomer, with *cis*-disposed M–C bonds. Mass spectrometry carried out immediately on a sample of **40** in acetonitrile confirmed the presence of an anionic chloride in the sixth coordination site. Analysis of the same sample after several days, however, revealed a vacant sixth site. A similar loss of an anionic chloride, upon displacement by a CH_3CN molecule, had previously been reported in [Ir(Mebib)(ppy)Cl] by Haga *et al.* (Figure 2.28).[224]

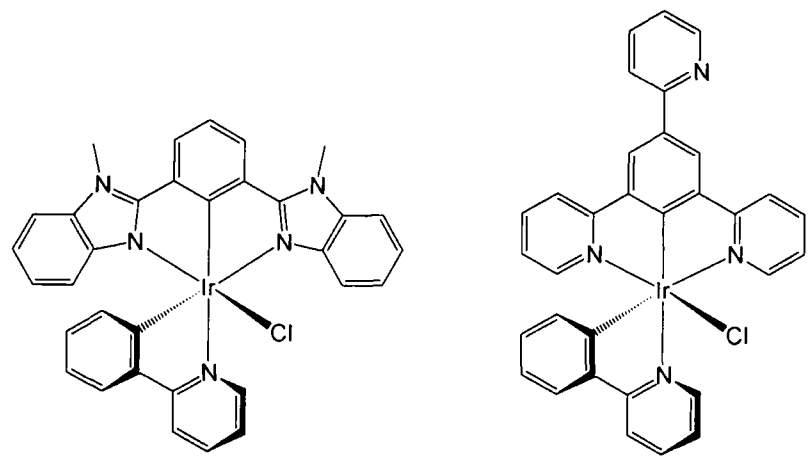

[Ir(Mebib)(ppy)Cl] **41**

Figure 2.28: Charge neutral [Ir(NCN)(NC)Cl] complexes.

A similarly coordinated iridium complex [Ir(tpyb)(ppy)Cl] **41** (Figure 2.28) was prepared as an orange solid in 50% yield *via* the same solution-based methodology.

A series of charge-neutral [Ir(NCN)(NC)Cl] coordinated complexes were also synthesised bearing NC-coordinated pyrazolyl analogues of ppy. Solution-based reactions between [Ir(dpydmb)Cl(μ-Cl)]$_2$ **29** and the NC-coordinating ligands 1-phenylpyrazole (pzbH) and 1-pyrazolyl-3,5-dibromobenzene (pzbH-Br$_2$) **14** afforded [Ir(dpydmb)(pzb)Cl] **42** and [Ir(dpydmb)(pzb-Br$_2$)Cl] **43** in 54% and 45% yield respectively.

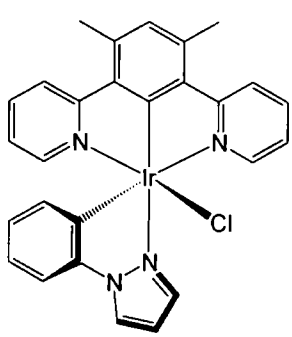

42

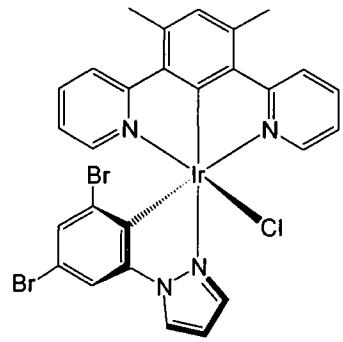

43

As expected, ^{1}H-^{1}H NOESY NMR revealed both products to be exclusively the *mer*-isomer with *cis*-disposed Ir–C bonds. Whilst ES$^+$ mass spectrometry failed to show definitive evidence of a bound chloride ion in both **42** and **43**, with the sixth coordination site being occupied by a labile CH_3CN solvent molecule, the low polarity of solvent required upon column chromatography suggested that the products obtained were charge-neutral. The presence of the chloride in the sixth coordination site was subsequently confirmed by C, H and N analysis.

2.3 Pyrazolyl-NCN-based complexes of iridium(III)

Complexes containing pyrazolyl NCN ligands are of particular photophysical interest owing to pyrazole being a poorer π-accepter than pyridine, with a resultant blue-shift in the emission wavelength of these complexes being anticipated.

2.3.1 Step 1: Synthesis of chloro-bridged iridium dimers

The synthesis of the dimeric complex $[Ir(dpzb)Cl(\mu\text{-}Cl)]_2$ **44** (Figure 2.30) was attempted by reacting the unsubstituted ligand 1,3-di(1-pyrazolyl)benzene (dpzbH) **16** with $IrCl_3.3H_2O$; a yellow/green precipitate was obtained which, like its pyridyl analogue (Section 2.2.1), was seen to contain a mixture of cyclometalated products (Figure 2.29) upon characterisation by ^{1}H-NMR spectroscopy. The determination of the predominating binding mode of dpzb with iridium, however, was only achieved following complexation of the dimer with a second ligand (Section 2.3.2).

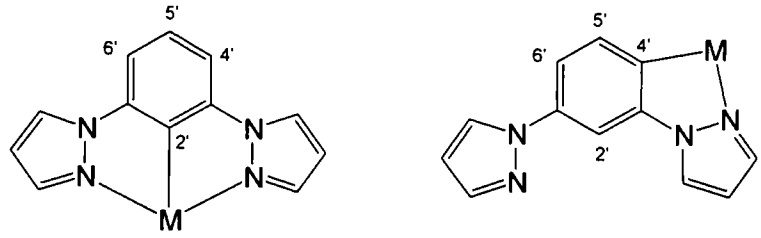

I II

Figure 2.29: Two potential binding modes of dpzb 16.

The introduction of methyl and bromo-substituents at the 5'-position of the central phenyl ring was seen to alleviate the aforementioned binding problem (Figure 2.29), with $[Ir(dpzmb)Cl(\mu\text{-}Cl)]_2$ **45** and $[Ir(dpzb\text{-}Br)Cl(\mu\text{-}Cl)]_2$ **46** (Figure 2.30) being the predominating species formed upon reaction of $Ir_3Cl_3.3H_2O$ with 1,3-di(1-pyrazolyl)-5-methylbenzene (dpzmbH) **17** and 1,3-di(1-pyrazolyl)-5-bromobenzene (dpzbH-Br) **15** respectively. Complete prevention of binding at the alternative $C^{4'}$ and $C^{6'}$-cyclometalating positions (binding mode II: Figure 2.29) was once again achieved upon the introduction of methyl-substituents at these sites, where reaction with 1,3-di(1-pyrazolyl)-4,6-dimethylbenzene (dpzdmbH) **19** afforded $[Ir(dpzdmb)Cl(\mu\text{-}Cl)]_2$ **47** (Figure 2.30) in 66% yield.

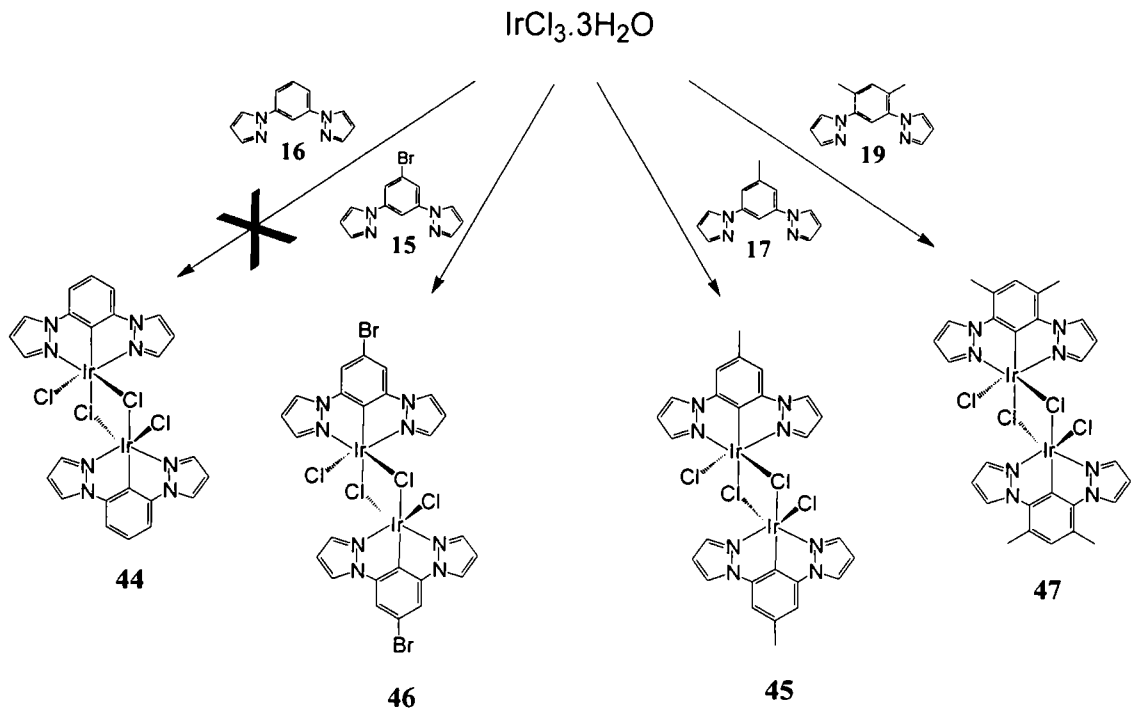

Figure 2.30: Synthesis of pyrazole-based dimers.

2.3.2 Step 2: Cleaving the dimer

Reaction of the iridium dimer [Ir(dpzb)Cl(μ-Cl)]$_2$ **44** with 2,2'-bipyridine (Figure 2.31) afforded the tris-bidentate complex [Ir(dpzb-*NC*$^{4'}$)$_2$(bpy)]$^+$ **48** as a yellow solid in low yield. The undesired bidentate (NC) binding in the product (**48**) originating from the dimeric precursor **44**, is indicative of the preference of dpzb to cyclometalate at the less hindered C$^{4'}$- and C$^{6'}$-positions (binding mode II: Figure 2.29). This binding problem mirrors that seen with the unsubstituted pyridyl-based ligand dpyb (Figure 2.15), and in one of the products formed upon reaction of dpzbH with Pt(II), recently reported by Connick *et al.*, where the second pyrazole unit bridges to a second Pt(II) centre resulting in a *trans*-arrangement of the Pt–N bonds.[225]

The reaction of **44** with 2,2':6',2''-terpyridine was also attempted, but failed to form any products in quantities sufficient for structural determination.

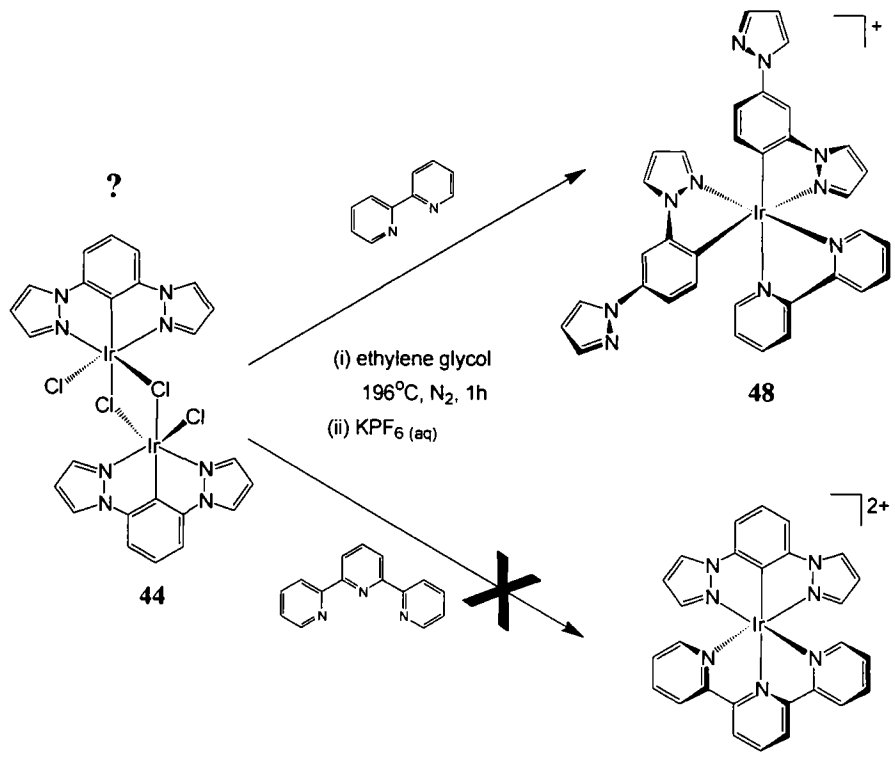

Figure 2.31: Reaction of $[Ir(dpzb)Cl(\mu\text{-}Cl)]_2$ with bpy and tpy.

Analogous solution-based reactions between the methyl-substituted intermediate $[Ir(dpzmb)Cl(\mu\text{-}Cl)]_2$ **45** and bpy and tpy gave $[Ir(dpzmb)(bpy)Cl]^+$ **49** as a yellow solid and $[Ir(dpzmb)(tpy)]^{2+}$ **50** as an orange solid in 16% and 23% yield respectively. The structure of **49** was supported by ES^+ mass spectrometry which confirmed the presence of a chloride ion in the sixth coordination site, as expected for mono-cyclometalated complexes.

Whilst the yields of **49** and **50** were relatively low, no products were isolated bearing the alternative bidentate *NC*$^{4'}$ coordination: the methyl substituent at the $C^{5'}$-position appears to hinder cyclometalation at the alternative $C^{4'}$- and $C^{6'}$-positions.

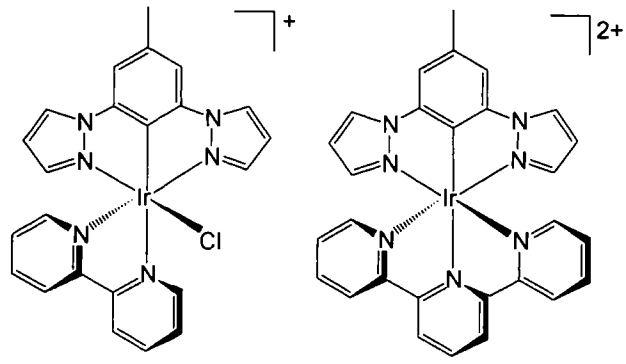

49 **50**

Reaction of the 5'-bromo-substituted dimer $[Ir(dpzb\text{-}Br)Cl(\mu\text{-}Cl)]_2$ **46** with bpy under the same conditions in refluxing ethylene glycol, gave a mixture of products following chromatographic purification which displayed the two binding modes (Figure 2.29): namely $[Ir(dpzb\text{-}Br)(bpy)Cl]^+$ **51** and $[Ir(dpzb\text{-}Br\text{-}NC^{4'})_2(bpy)]^+$ **52** in 19% and 11% yield respectively.

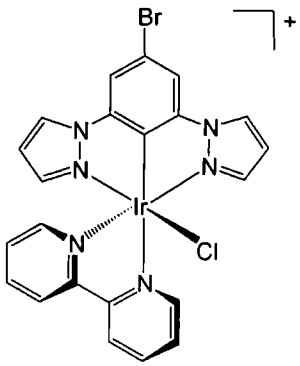

51

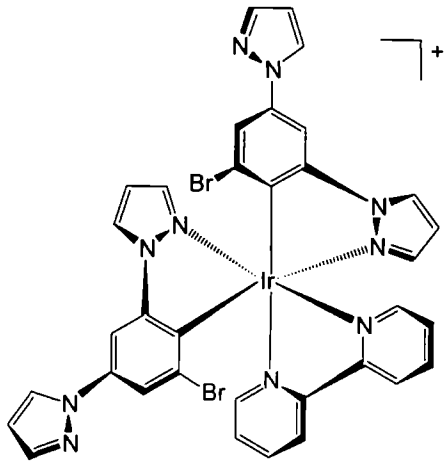

52

The analogous reaction of **46** with tpy, gave $[Ir(dpzb\text{-}Br\text{-}NC^{4'})(tpy)Cl]^+$ **53** in 20% yield and upon addition of silver triflate to the reaction mixture $[Ir(dpzb\text{-}Br)(tpy)]^{2+}$ **54** in 27% yield.

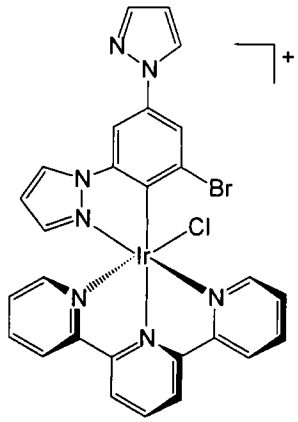

53

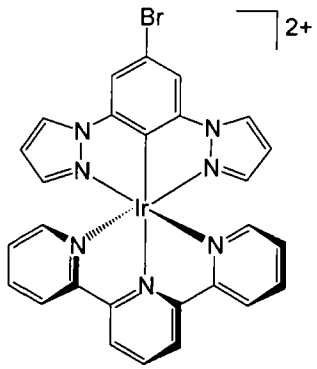

54

The presence of both bidentately and terdentately bound dpzb-Br in the monometallic complexes (**51**–**54**) indicates that the introduction of the bromo-substituent at the 5'-position in 1,3-di(1-pyrazolyl)-5-bromobenzene (dpzb-Br) **15** only partially alleviates the binding problem (binding mode II: Figure 2.29).

A series of complexes bearing the Ir(dpzdmb) unit were synthesised (Figure 2.32) upon reaction of the dimethyl-substituted dimer $[Ir(dpzdmb)Cl(\mu\text{-}Cl)]_2$ **47** with a second ligand. Reaction with bpy gave the desired product $[Ir(dpzdmb)(bpy)Cl]^+$ **55**, obtained in 49% yield, whilst the identity of the product formed upon reaction with tpy was dependent upon the presence of silver triflate. In its absence, tpy bound to the Ir(III) centre *via* two nitrogens only to give $[Ir(dpzdmb)(tpy\text{-}NN)Cl]^+$ **56** in 41% yield, whilst in its presence the bis-terdentate complex $[Ir(dpzdmb)(tpy)]^{2+}$ **57** was obtained as a yellow solid in 62% yield. Akin to the pyridyl ligand, dpydmbH **7**, the presence of methyl groups at the alternative $C^{4'}$ and $C^{6'}$-cyclometalating positions in the pyrazolyl analogue, dpzdmbH **19**, prevents bidentate binding to the Ir(III) centre (binding mode II: Figure 2.29).

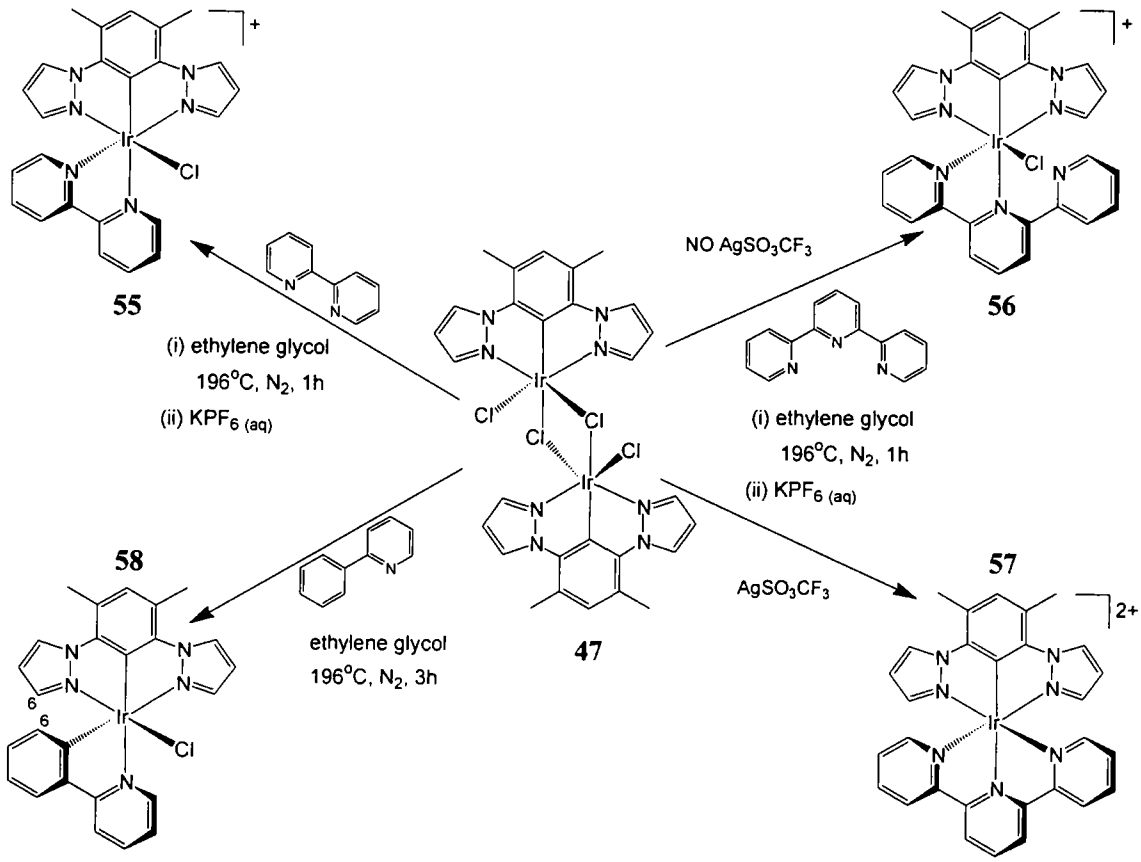

Figure 2.32: Synthesis of d^6 octahedral complexes incorporating the Ir(dpzdmb) unit.

Alongside the cationic complexes described above, the charge-neutral [Ir(NCN)(NC)Cl] coordinated pyrazolyl complex [Ir(dpzdmb)(ppy)Cl] **58** was synthesised upon reaction of the dimethyl-substituted dimer **47** with ppyH (Figure 2.32) and obtained as a yellow solid in 28% yield. Formation of the expected *mer*-isomer with *cis*-disposed

cyclometalating carbons was supported by ^{1}H-^{1}H NOESY NMR spectroscopy, which revealed a cross peak between H^6-ppy and H^6-dpzdmb. ES^+ mass spectrometry indicated that complex **58** contained a vacant sixth coordination site. However, the low solvent polarity required to isolate the product by column chromatography suggests that complex **58** was actually formed with a chloride ion bound, and like its pyridyl analogue [Ir(dpydmb)(ppy)Cl], the chloride is easily replaced by a labile solvent molecule when left in solution for an extended period of time.

When this research was carried out, there were no reports in the literature of complexes incorporating an NCN-coordinating pyrazolyl ligand bound to an iridium(III) centre. However, it should be noted that during the compilation of this thesis, Haga *et al.* published the synthesis of a series of charge-neutral [Ir(NCN)(NC)Cl] coordinated complexes, [Ir(R_2-dpzb-Me_2)(ppy)Cl] (Figure 2.33), containing the NCN ligand 1,3-bis(3-methylpyrazolyl)benzene (dpzb-Me_2) and the di-fluoro (dpzdFb-Me_2) and di-methyl (dpzdmb-Me_2) substituted derivatives.[226]

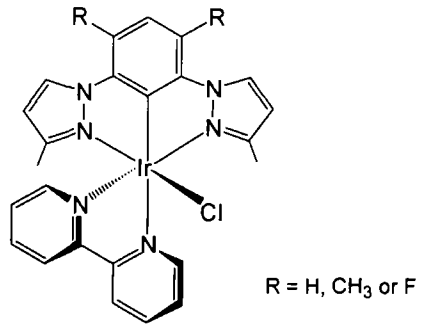

Figure 2.33: Haga's recently reported [Ir(R-dpzb)(ppy)Cl] complexes.[226]

These complexes were synthesised *via* microwave reactions involving ppy and the appropriate [Ir(R_2-dpzb-Me_2)Cl(μ-Cl)]$_2$ dimer in glycerol, followed by precipitation with NaCl and recrystallisation. [226] A binding problem reminiscent of that seen by Wilkinson for dpyb (Figure 2.15),[78] and herein for dpzb **19** (Figure 2.29) was reported for their unsubstituted ligand dpzb-Me_2.[226]

2.4 Concluding remarks

In this chapter the synthesis of a series of NCN, NNC and CNC-coordinating terdentate ligands *via* ring-closing and palladium-catalysed cross-coupling reactions has been discussed (Section 2.1), alongside several dimeric complexes of the type $[M(NCN)Cl(\mu\text{-}Cl)]_2$, containing two M(NCN)Cl units incorporating pyridyl (Section 2.2.1) or pyrazolyl-based (Section 2.3.1) ligands and joined by two chloro-bridges. Following the preparation of these dimers, the synthesis of a range of cyclometalated d^6-octahedral complexes of iridium(III) and rhodium(III) containing an M(NCN)Cl unit are reported upon cleavage of the chloro-bridges by a second terdentate or bidentate ligand (Sections 2.2.2 and 2.3.2).

The rhodium(III) complexes reported herein mark the first examples of complexes with this metal centre incorporating the NCN-coordinating ligand 1,3-di(2-pyridyl)benzene and its derivatives. Similarly, at the time of their synthesis there were no known examples of complexes incorporating such binding between an iridium(III) centre and NCN-coordinating pyrazolyl ligands.

CHAPTER 3

CHEMISTRY ON THE COMPLEX

3 Chemistry on the Complex

The synthesis of an array of iridium(III) and rhodium(III) monometallic complexes was described in Chapter 2. However, when complexes incorporating ligands that bear sensitive functional groups are desired, the forcing conditions required for complexation often prove too harsh. In such cases, carrying out "chemistry on the complex" can be advantageous. The general concept of post-complexation functionalisation, with numerous examples, has recently been reviewed by Ren.[227]

3.1 Synthesis of brominated complexes

Bromo-functionalised bis-terdentate complexes are of particular interest in this study owing to their ability to undergo elaboration *via* Suzuki cross-coupling reactions with arylboronic acids or boronic acid appended complexes (Figure 3.1). By positioning the bromo-group *para* to the point of metalation on the central ring, this will take place in a linear manner along the principal axis.

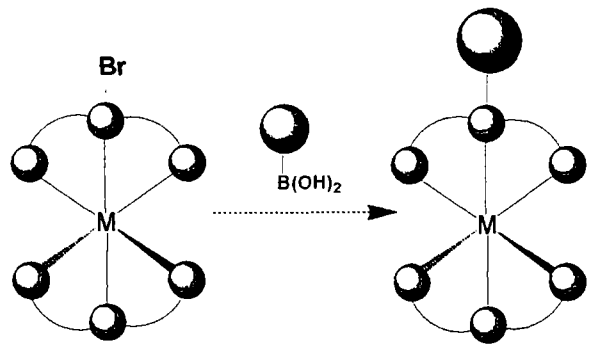

Figure 3.1: Elaboration *via* a Suzuki cross-coupling.

3.1.1 In situ bromination of monometallic complexes

Following the failed synthesis of the "free" bromo-substituted NCN ligand dpydmbH-Br **8** (Section 1.1.2.1), the *in situ* bromination of a monometallic complex incorporating dpydmb was attempted (Figure 3.2) to investigate whether bromination could indeed be achieved between the two flanking methyl groups. The technique used was based upon that reported by Coudret *et al.*[228] for the regiospecific bromination of $[Ru(bpy)_2(ppy)]^+$ with N-bromosuccinimide (NBS) and previously used by this group[52, 130] for the $[Ir(ppy)_2(bpy)]^+$ series of complexes. The susceptibility of such

complexes to facile electrophilic bromination of the cyclometalating ligand, *para* to the point of metalation, is attributed to the increase in electron density of the phenyl ring that accompanies cyclometalation.

Reaction of $[Ir(dpydmb)(ttpy)]^{2+}$ with NBS successfully formed $[Ir(dpydmb\text{-}Br)(ttpy)]^{2+}$ **59**, with bromination of dpydmb at the $C^{4'}$-position being confirmed by ^{1}H-NMR spectroscopy from the disappearance of the singlet resonance at 7.43 ppm (in d_6-acetone) corresponding to $H^{4'}$-dpydmb, and from a shift in the 6H methyl singlet from 3.02 to 3.23 ppm.

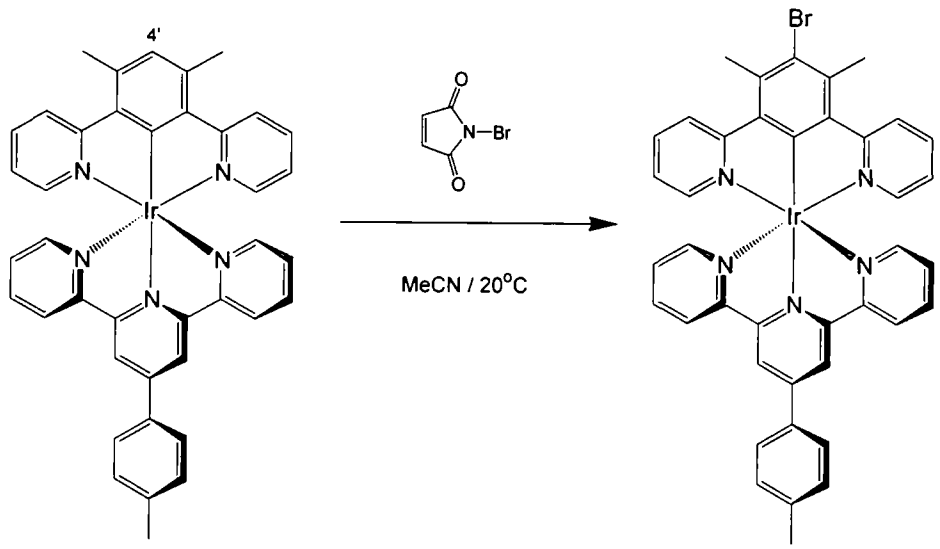

59

Figure 3.2: *In situ* bromination of $[Ir(dpydmb)(ttpy)]^{2+}$.

Following this successful *in situ* bromination of dpydmb, attempts were made to selectively brominate the bis-cyclometalated complex $[Ir(dpydmb)(phbpy)]^+$ **33** at this position under the same conditions. The reaction was followed by ^{1}H-NMR spectroscopy, which showed the disappearance of both the singlet resonance at 7.21 ppm (in d_6-acetone) corresponding to $H^{4'}$-dpydmb and the two degenerate methyl singlets at 2.97 ppm, alongside the appearance of a new methyl singlet at 3.19 ppm, consistent with the bromination of dpydmb at the $C^{4'}$-position. However, significant changes were also observed in the resonances of the phbpy protons, indicative of the simultaneous bromination of phbpy at the $C^{4''}$-position. Whilst the rate of bromination of the dpydmb ligand was seen to be faster than that of phbpy, the relative rates were too similar to allow selective bromination, with the addition of a second equivalent of NBS affording $[Ir(dpydmb\text{-}Br)(phbpy\text{-}Br)]^+$ **60** in approximately quantitative yield.

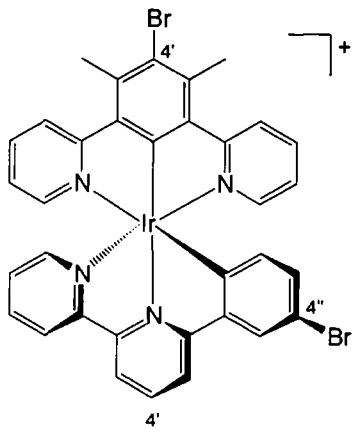

60

3.1.2 *Modification of the [Ir(NCN)(NNC)]$^+$ coordinated complex*

To limit the bromination of the $[Ir(NCN)(NNC)]^+$ complex to the NCN ligand, the competitive $C^{4''}$-bromination site of the NNC ligand must be blocked. To achieve this, a new NNC-coordinating ligand was targeted, 4'-(*p*-bromophenyl)-6'-(*m*-tolyl)bipyridine (mtbpyH-ϕ-Br) **4**, which was synthesised as described in Chapter 2.

The modified $[Ir(NCN)(NNC)]^+$ complex, $[Ir(dpydmb)(mtbpy\text{-}\phi\text{-}Br)]^+$ **61**, was successfully formed upon reaction of mtbpyH-ϕ-Br **4** with $[Ir(dpydmb)Cl(\mu\text{-}Cl)]_2$ **29**, being isolated as an orange solid in 84% yield following chromatographic separation (Figure 3.3). ^{1}H-NMR spectroscopy confirmed that there was no evidence of the formation of the alternative isomer with metalation *ortho* to the methyl group. This alternative binding is presumably both sterically and electronically disfavoured.[205]

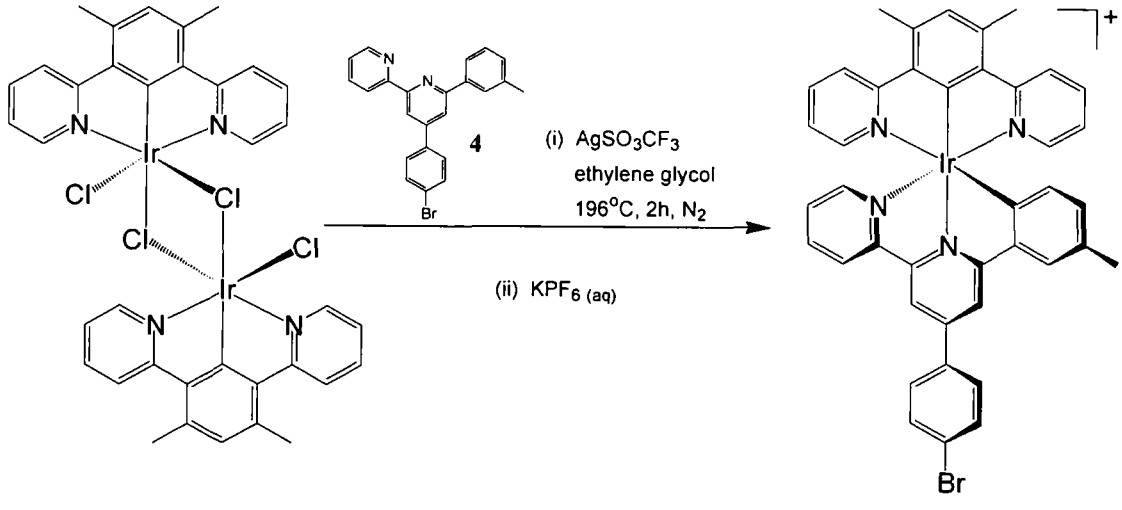

29 61

Figure 3.3: Synthesis of $[Ir(dpydmb)(mtbpy\text{-}\phi\text{-}Br)]^+$.

3.2 In situ linear elaboration

3.2.1 Cross-coupling – bromination – cross-coupling strategy

Previous work within this research group, showed that *in situ* Pd-catalysed Suzuki cross-coupling reactions can be successfully used to couple bromo-substituted bis(terpyridyl)-ruthenium(II) and iridium(III) complexes with arylboronic acids to form more elaborate complexes.[51, 54, 130] In this study, we investigated the possibility of carrying out such elaboration on bis-terdentate bis-cyclometalating complexes. By combining *in situ* bromination and cross-coupling reactions, it was hoped that a stepwise cross-coupling – bromination – cross-coupling strategy could be developed for the purpose of their linear elaboration (Figure 3.4).

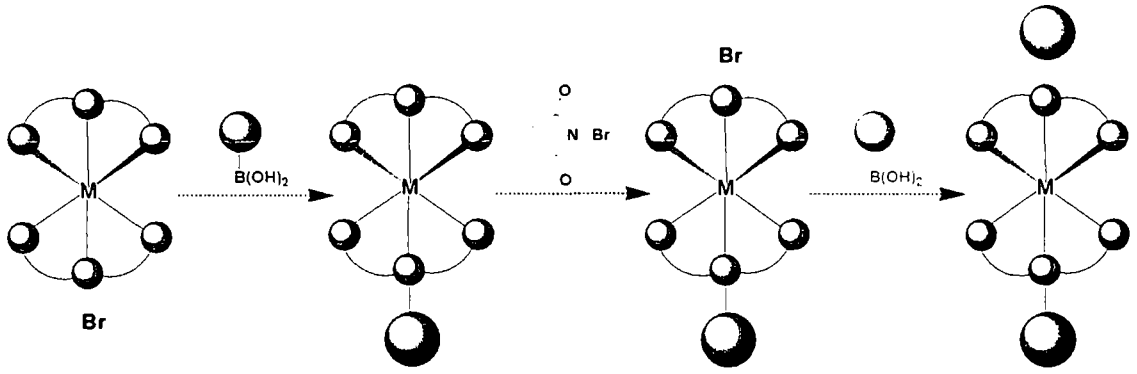

Figure 3.4: Cross-coupling – bromination – cross-coupling strategy.

3.2.2 Cross-coupling reactions between flanking methyl groups

An investigative cross-coupling reaction was carried out on the NCN ligand of $[Ir(dpydmb\text{-}Br)(ttpy)]^{2+}$ **59** to see if the steric hindrance of the two methyl groups flanking the C–Br bond would significantly hamper the reaction at this position, or necessitate the use of a stronger base as sometimes required for sterically hindered organic systems.[229] Reaction of $[Ir(dpydmb\text{-}Br)(ttpy)]^{2+}$ **59** with 4-dimethylamino-phenylboronic acid (Figure 3.5) under an inert atmosphere afforded $[Ir(dpydmb\text{-}\phi\text{-}NMe_2)(ttpy)]^{2+}$ **62** as an orange solid in 65% yield. The successful incorporation of the -ϕ-NMe_2 group was confirmed by ^{1}H-NMR spectroscopy, which showed the introduction of a pair of doublets at 7.24 and 7.01 ppm (in d_6-acetone) corresponding to H^b-NCN and H^a-NCN respectively, alongside a methyl singlet at 2.72 ppm integrating to 6H.

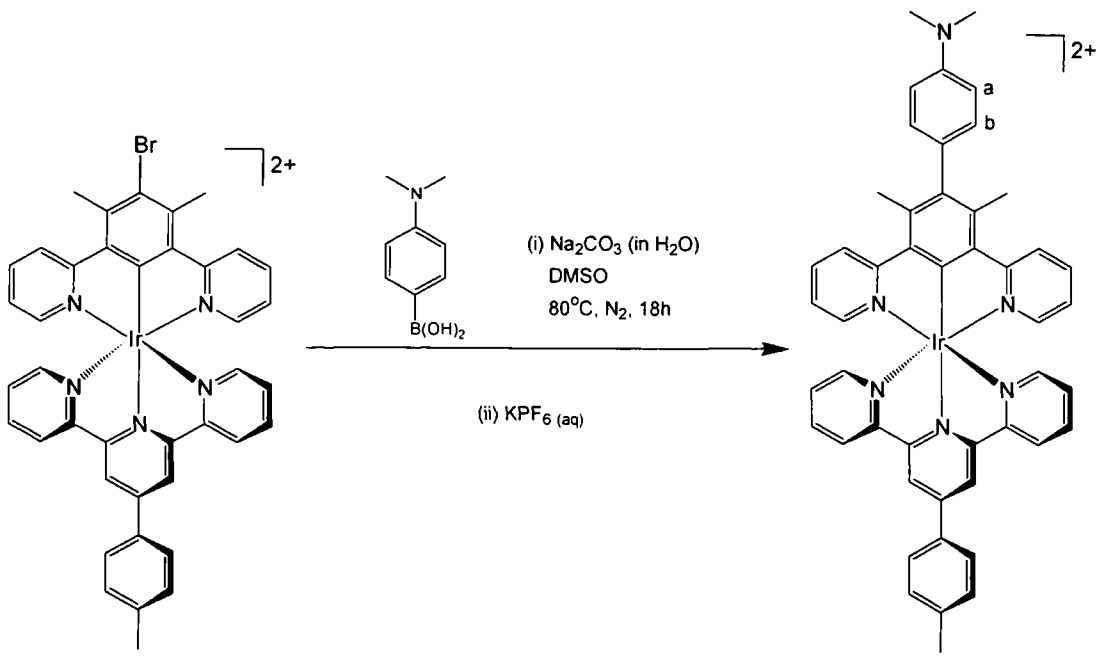

59 62

Figure 3.5: Cross-coupling of $[Ir(dpydmb)(ttpy)]^{2+}$ 59 between flanking methyls.

3.2.3 Linear elaboration of the modified $[Ir(NCN)(NNC)]^{+}$ complex

Following confirmation that the flanking methyl groups did not hinder the cross-coupling on the NCN ligand of the dicationic complex **59**, attempts were made to linearly elaborate the modified $[Ir(NCN)(NNC)]^{+}$ complex on both sides *via* the cross-coupling – bromination – cross-coupling strategy (Figure 3.6).[205]

Cross-coupling

Initial attempts at the first cross-coupling step on the bromo-substituted NNC ligand were carried out by reacting $[Ir(dpydmb)(mtbpy\text{-}\phi\text{-}Br)]^{+}$ **61** with 4-dimethylamino-phenylboronic acid, under the same conditions as above (Figure 3.5), and gave $[Ir(dpydmb)(mtbpy\text{-}\phi_2\text{-}NMe_2)]^{+}$ **63** as an orange solid in 84% yield. The successful incorporation of the $\text{-}\phi\text{-}NMe_2$ group into the mtbpy-ϕ-Br ligand was confirmed by ^{1}H-NMR spectroscopy from the introduction of a pair of doublets at 7.73 and 6.92 ppm (in d_6-acetone) corresponding to the $H^{b'}$-NNC and $H^{a'}$-NNC protons respectively, alongside a methyl singlet at 3.05 ppm.

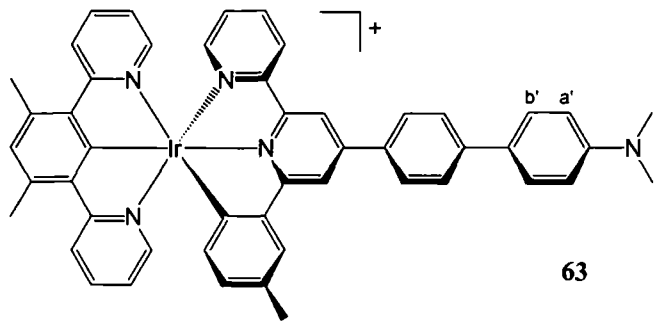

63

Unfortunately, upon storage in air for several days, complex **63** appeared to degrade. This was indicated by ES^+ and MALDI mass spectrometry, where a loss of one and two $-CH_2$ units was observed, thought possibly to be the result of the loss of a methyl from the $-NMe_2$ group accompanied by protonation. Upon this degradation, the ^{1}H-NMR spectrum of the complex became complicated due to the formation of multiple products.

Rather than take the unstable complex **63** through the latter stages of elaboration, phenylboronic acid was applied to the first cross-coupling step (Figure 3.6), to form $[Ir(dpydmb)(mtbpy\text{-}\phi\text{-}ph)]^+$ **64** as an orange solid in 79% yield alongside a small amount of debrominated starting material, which could be separated chromatographically.

Bromination

Following cross-coupling, the air stable complex **64** was selectively brominated at the $C^{4'}$-position of the NCN ligand upon treatment with NBS, in solution in acetonitrile at room temperature, to form $[Ir(dpydmb\text{-}Br)(mtbpy\text{-}\phi\text{-}ph)]^+$ **65** in stoichiometric yield (Figure 3.6). Successful bromination was confirmed by ^{1}H-NMR spectroscopy (in d_6-acetonitrile) which revealed the disappearance of the $H^{4'}$-NCN resonance peak, accompanied by a shift in the singlet methyl-NCN peak from 2.98 to 3.22 ppm.

Cross-coupling

The bromo-appended complex **65** was suitably functionalised for the elaboration of the NCN-coordinated ligand with another organic group in the second cross-coupling step, where the same reaction conditions were employed. Here a different boronic acid was used, namely 3,5-dimethylphenyl boronic acid, which upon reaction with **65** gave $[Ir(dpydmb\text{-}C_6H_3Me_2)(mtbpy\text{-}\phi\text{-}ph)]^+$ **66** as an orange solid in 53% yield (Figure 3.6).

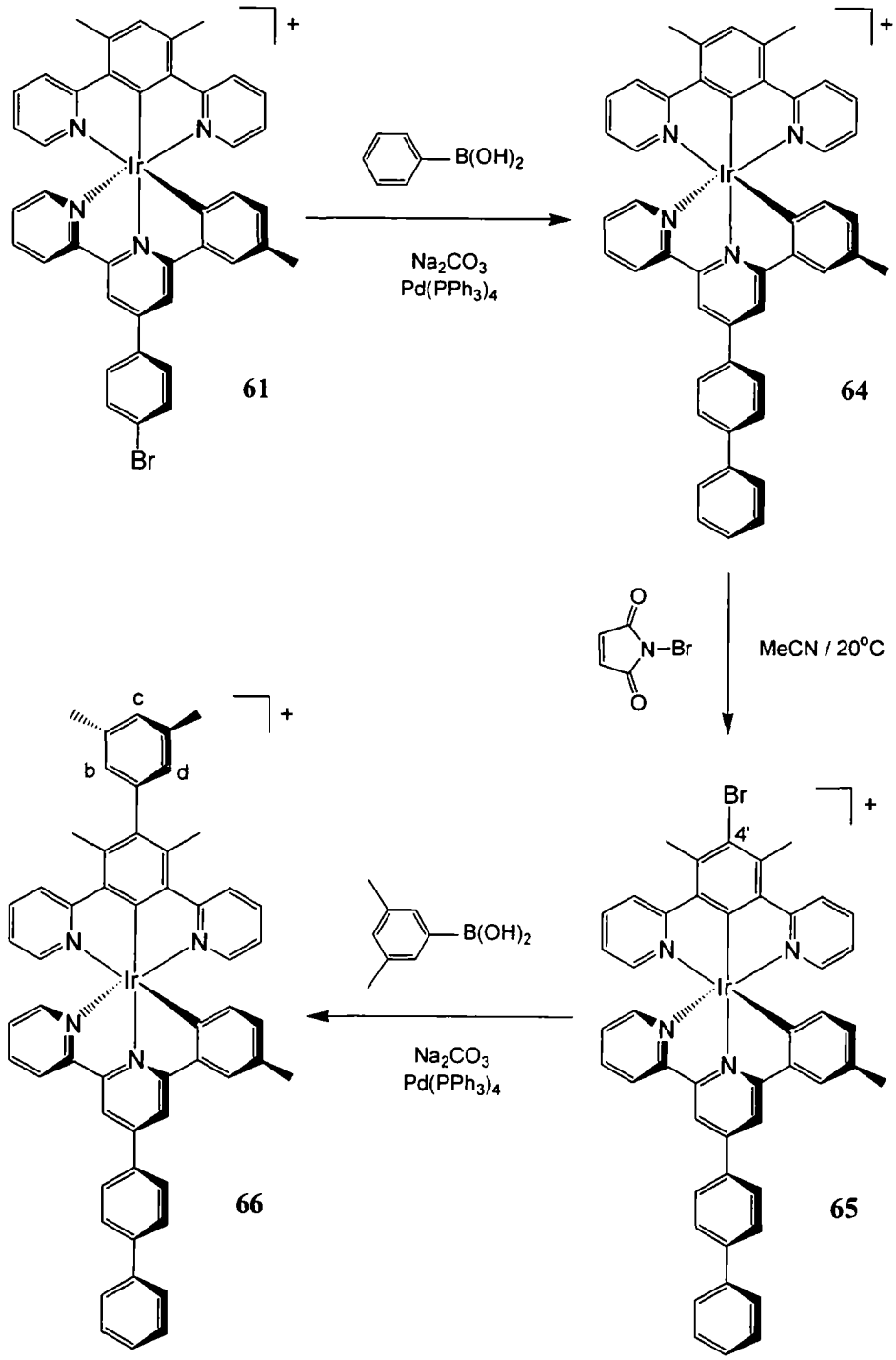

Figure 3.6: Sequential cross-coupling – bromination – cross-coupling of the modified $[Ir(NCN)(NNC)]^+$ complex.

^{1}H-NMR spectroscopy of **66** confirmed the successful incorporation of the 3,5-dimethylphenyl group into the complex, from the appearance of three new singlets at 7.16, 7.07 and 7.02 ppm (in d_6-acetone) corresponding to the three protons *para* (H^c-NCN) and *ortho* (H^b-NCN and H^d-NCN) to the newly formed aryl–aryl bond. The inequivalence of the two *ortho* protons arises from a lack of rotation about the aryl–aryl bond, due to the flanking methyl groups on the dpydmb NCN ligand. This pendant ring

thus lies orthogonal to dpydmb, *i.e.* in the plane of mtbpy-ϕ-ph, with H^b-NCN closest to the pyridyl ring of mtbpy-ϕ-ph and H^d-NCN to the phenyl ring.

Variable temperature ^{1}H-NMR experiments of complex **66** in d_6-DMSO showed no evidence of rotation around the aryl–aryl bond up to 363 K. With the barrier to rotation in 2,6-dimethylbiphenyl having previously been estimated to be > 100 kJ mol^{-1},[230] and an increase from room temperature to 393 K being equivalent to only 3 kJ mol^{-1}, it is not surprising that such variable temperature studies failed to induce rotation.

3.3 Boronic acid appended complexes

Whilst bromo-functionalised bis-terdentate complexes are capable of undergoing elaboration with boronic acid appended organic groups (Section 3.2), the incorporation of boronic acid functionality into one of the ligands in a metal complex would hopefully provide an attractive route to linear multimetallic complexes *via* the cross-coupling of these "building blocks" (Chapter 5).

Previously, this laboratory demonstrated the synthesis of boronic acid appended tris-bidentate and bis-terpyridyl complexes *via* Pd-catalysed Suzuki-Miyaura cross-coupling reactions with diboron esters, $(RO)_2B–B(OR)_2$, *e.g.* bis(neopentylglycolato) diboron (B_2neo_2) or bis(pinacolato)diboron.[51, 52] In this study, attempts were made to carry out such a reaction on a bis-terdentate bis-cyclometalated complex.

The modified $[Ir(NCN)(NNC)]^+$ complex **61**, incorporating a bromo-phenyl pendant, was reacted with an excess of B_2neo_2 in DMSO under an inert atmosphere (Figure 3.7). Unfortunately no boronated complex was isolated, with the main product being identified as debrominated starting material by ^{1}H-NMR spectroscopy and mass spectrometry. Further synthetic attempts involving the use of additional quantities of B_2neo_2 and longer reaction times also proved fruitless, as did attempts to boronate the NCN-coordinating ligand of $[Ir(dpydmb\text{-}Br)(mtbpy\text{-}\phi\text{-}ph)]^+$ **65** at the $C^{4'}$-position, which gave a mixture of unreacted **65** and debrominated starting material **64**.

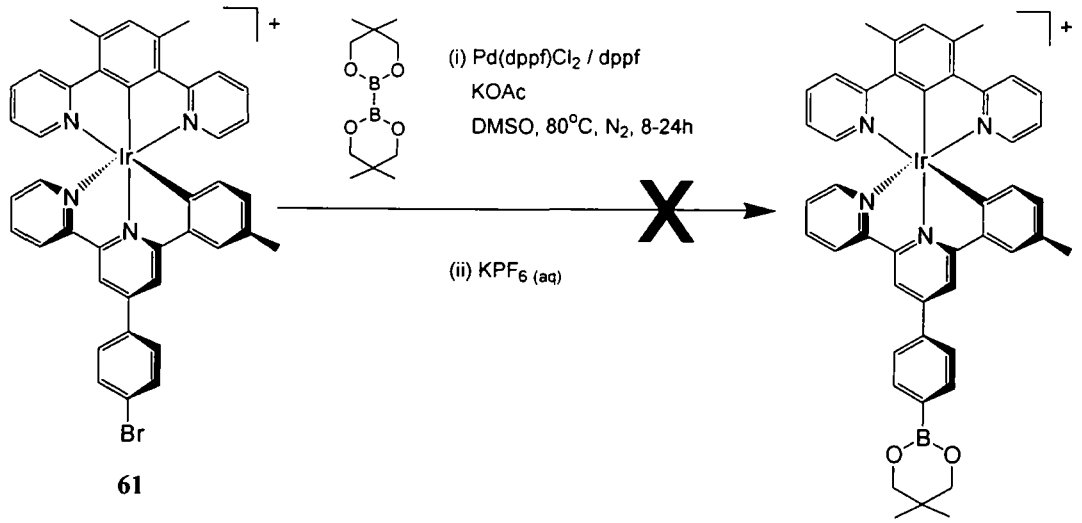

Figure 3.7: Attempted *in situ* boronation of the modified $[Ir(NCN)(NNC)]^+$ complex.

Following the failed attempts to boronate $[Ir(NCN)(NNC)]^+$ coordinated complexes *via in situ* Suzuki-Miyaura reactions, attention was directed towards the boronation of the "free" NNC ligand **4** prior to complexation, an approach previously employed by this group for the elaboration of terpyridyl ligands at the $C^{4'}$-position.[51] Reaction of mtbpyH-ϕ-Br **4** with B_2neo_2 in DMSO under an inert atmosphere successfully afforded mtbpyH-ϕ-Bneo **67** (Figure 3.8). Confirmation was provided by ^{1}H-NMR spectroscopy which, upon comparison to the bromo-substituted starting material, revealed the introduction of two singlet peaks, one at 3.79 ppm (in $CDCl_3$) corresponding to the CH_2 group and the other at 1.03 ppm corresponding to the two methyls of the Bneo-appendage.

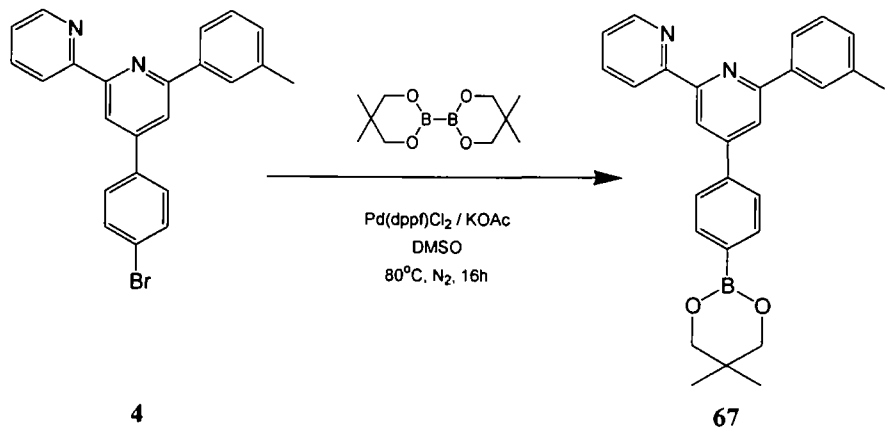

Figure 3.8: Boronation of the modified NNC ligand mtbpyH-ϕ-Br 4 *via* a Suzuki-Miyaura cross-coupling reaction.

The boronated ligand mtbpyH-ϕ-Bneo **67** could not be complexed to iridium(III) under the usual high temperature conditions owing to the sensitive nature of the Bneo group,

thus a lower temperature of 140°C was used with a longer reaction time, 3h, (Figure 3.9). The boronated complex, [Ir(dpydmb){mtbpy-ϕ-B(OH)(OMe)}]$^+$ **68**, was successfully obtained as an orange solid in 89% yield following chromatographic purification, during which the Bneo appendage was converted to B(OH)(OMe). Complex **68** can subsequently be reacted with complementary bromo-substituted complexes *via* Suzuki cross-couplings to form multimetallic assemblies, as discussed in Section 5.

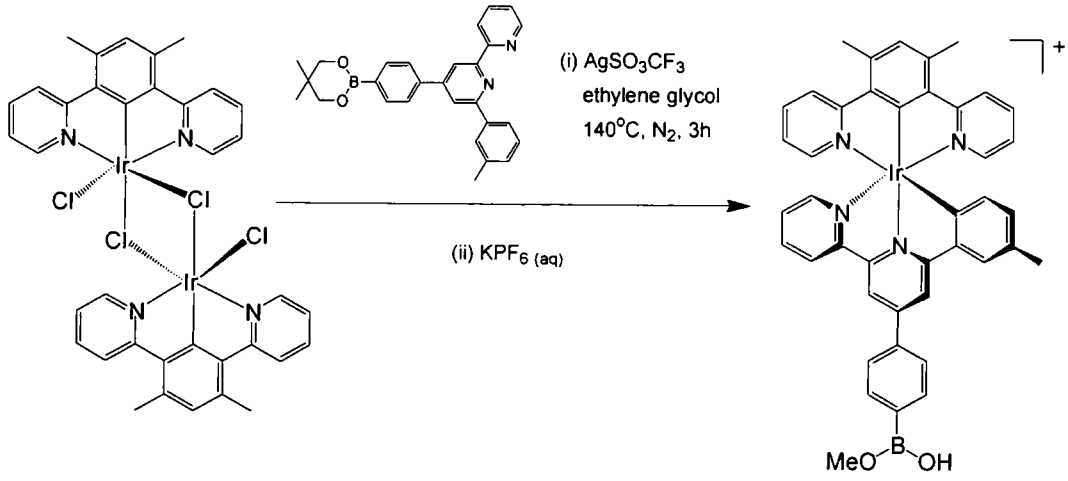

29 68

Figure 3.9: Synthesis of a boronated [Ir(NCN)(NNC)]$^+$ complex.

3.4 Concluding remarks

This chapter has discussed the modification of the [Ir(NCN)(NNC)]$^+$ coordinated complex to incorporate a pendant bromo-phenyl group on the central pyridyl ring of the NNC ligand, alongside the development of a sequential cross-coupling – bromination – cross-coupling strategy for its stepwise linear elaboration along the principal axis with boronic acid appended aryl groups.

The achiral nature of bis-terdentate systems avoids the problems associated with diastereoisomer formation, observed with tris-bidentate complexes, upon joining such complexes together and makes them ideal candidates for the formation of extended systems. The preparation of [Ir(NCN)(NNC)]$^+$ coordinated complexes containing bromo and boronic acid substituents have been reported in this chapter, and will be used to investigate the application of this stepwise linear elaboration technique to the generation of multimetallic arrays in Chapter 5.

CHAPTER 4

PHOTOPHYSICAL AND ELECTROCHEMICAL STUDIES OF MONOMETALLIC COMPLEXES

4 Photophysical and Electrochemical Studies of Monometallic Complexes

4.1 Complexes bearing pyridine-based NCN ligands

4.1.1 Photophysical properties of $[M(NNN)_2]^{3+}$ complexes

Prior to discussing the electrochemical and photophysical properties of the mononuclear Ir(III) and Rh(III) complexes (bearing pyridine-based NCN ligands) prepared in this study (Chapters 2 and 3), the relevant photophysical properties (Table 1) of the bis-terpyridyl complexes will first be overviewed.

Complex [a]	$[Ir(tpy)_2]^{3+}$ [44, 46]	$[Ir(ttpy)_2]^{3+}$ [46]	$[Rh(tpy)_2]^{3+}$ [98, e]
Absorption maxima / nm (ε / M^{-1} cm^{-1})	374 (1300) 352 (5800) 336 (8500) 325 (11800) 313 (11400) 277 (22200) 251 (27600)	373 (2900) 347 (36800) 321 (43000) 305 (46200) 278 (45900) 251 (62300)	355 (34000) 338 (15000) 324 (9300) 268 (28000) 244 (34000)
Emission maxima / nm	458, 491, 525	506, 528 sh	–
Emission maxima at 77 K / nm	458, 491, 525	494, 517	–
Φ_{em} x 10^2 [b]	3.0	11.5	9.0 [f]
Lifetime [c] / μs degassed (aerated)	1.2 (1.0)	9.5 (2.4)	–
Lifetime at 77 K [c] / μs	26 [g]	39 [g]	8.0 [f]
k_r [d] / 10^4 s^{-1}	2.5	1.2	–
Σk_{nr} [d] / 10^5 s^{-1}	8.1	0.93	–

(a) Complexes as their hexafluorophosphate salts in degassed CH_3CN at 298 K, except where stated otherwise. (b) Luminescence quantum yield measured at 298 K using $[Ru(bpy)_3]Cl_2$ as a standard. (c) Lifetime registered at the emission maximum following excitation at 374 nm. (d) Radiative and non-radiative rate constants calculated from τ and Φ values at 298 K. (e) ClO_4^- salt in 10^{-3} M $HClO_{4\,(aq)}$. (f) ClO_4^- salt in an EtOH/MeOH glass at 77 K. (g) In a butyronitrile glass at 77 K.

Table 1: The photophysical properties of the $[MN_6]^{3+}$ complexes.

The $[IrN_6]^{3+}$ coordinated complex $[Ir(tpy)_2]^{3+}$ has been well studied and exhibits an absorption spectrum predominated by intense LC bands < 350 nm, alongside an absorption tail to lower-energy which is assigned to an MLCT transition.[46] Upon excitation in the near-UV, $[Ir(tpy)_2]^{3+}$ displays highly structured green-blue emission under ambient conditions.[44, 46] The vibrational spacing of ~1400 cm^{-1} is indicative of emission from a primarily ligand-centred (LC, π–π^*) excited state, which is further delocalised upon the addition of 4'-substituents resulting in longer-lived, red-shifted

emission.[46] Unlike $[Ir(tpy)_2]^{3+}$, $[Rh(tpy)_2]^{3+}$ is non-emissive under ambient conditions, with only weak structureless emission observed at 77 K, thought to originate from a MC excited state.[98]

4.1.2 $[M(NCN)(NNN)]^{2+}$ complexes

4.1.2.1 Electrochemical studies

A series of mono-cyclometalated, $[Rh(NCN)(NNN)]^{2+}$ coordinated complexes have been prepared (Section 2.2.2.1), and electrochemical studies carried out on $[Rh(dpydmb)(tpy)]^{2+}$ **27** in the presence of 0.1 M Bu_4NBF_4 (in acetonitrile) as the supporting electrolyte between –2.5 and +2.0 V. No oxidation processes were observed within this range, in line with the tris-bidentate analogue $[Rh(bpy)_2(ppy)]^{2+}$ reported by Constable *et al.*[102] However, a reversible reduction process was observed at –1.04 V *vs.* SCE, which was assigned to the terpyridyl ligand upon comparison to Scandola's mono-cationic $[Ir(CNC)(NNN)]^+$ complex, $[Ir(tddpy)(tpy\text{-}\phi\text{-}Br)]^+$, which was reported to display a tpy-based reduction process at –1.27 V.[83] The more facile reduction process in **27** results from the higher charge of this 2+ complex. Whilst the bis-terdentate complex $[Rh(bpy)_2(ppy)]^{2+}$ is similarly reported to display a reduction process within the solvent window,[102] this bpy-based reduction occurs at a more negative potential (–1.27 V) than the tpy-based reduction in complex **27** due to less delocalisation of the electron density over the two rings of bpy than the three of tpy.

4.1.2.2 Computational studies

Computational studies can be used in conjunction with photophysical measurements to provide an insight into the structural and spectroscopic properties of transition metal complexes. Whilst empirical molecular mechanics[231] and semiempirical methods[232] can be used, their requirement for suitable parameterisation limits their use. *Ab initio* techniques, in particular Hartree-Fock (HF), are more common providing reasonable results for second and third row transition metals,[233] but they become increasingly impractical as the number of atoms rises. Density Functional Theory (DFT) calculations are therefore favoured, owing to their comparable accuracy to HF methods at a reduced computational cost alongside their inclusion of electron correlation effects.[233, 234]

DFT calculations were carried out on iridium(III) and rhodium(III) $[M(NCN)(NNN)]^{2+}$ coordinated complexes. The B3LYP density functional[66, 235] was used throughout, with

the 6-31G basis set being employed for all ligand atoms and LANL2DZ[236] for the iridium and rhodium atoms. An effective core potential (ECP) was used to replace the chemically inert inner core electrons *i.e.* those below the outer core $(5s)^2(5p)^6$ and valence $(5d)^6$ electrons in Ir(III) and $(4s)^2(4p)^6$ and $(4d)^6$ in Rh(III). These electrons are not involved in bonding, so very little loss in accuracy occurs whilst there is substantial decrease in calculation time. The calculated orbital characteristics for the three highest energy molecular orbitals (HOMO, HOMO–1 and HOMO–2) and the three lowest energy unoccupied molecular orbitals (LUMO, LUMO+1 and LUMO+2) are summarised in Table 2.

Complex	HOMO–2	HOMO–1	HOMO	LUMO	LUMO+1	LUMO+2
62 $[Ir(dpydmb\text{-}\phi\text{-}NMe_2)(ttpy)]^{2+}$	Ir (20%) NCN moiety (62%) $\phi\text{-}NMe_2$ pendant (11%)	$\phi\text{-}NMe_2$ pendant (99%)	$\phi\text{-}NMe_2$ pendant (91%)	NNN (90%)	NNN (97%)	NCN moiety (72%) NNN (22%)
27 $[Rh(dpydmb)(tpy)]^{2+}$	Rh (47%) NCN (15%) NNN (38%)	NCN (97%)	Rh (20%) NCN (75%)	NNN (93%)	NNN (98%)	Rh (53%) NCN (15%) NNN (32%)

Table 2: Calculated molecular orbital characteristics of the $[M(NCN)(NNN)]^{2+}$ complexes according to DFT calculations. The percentages in parentheses denote the proportion of the total electron density localised at that site.

DFT calculations carried out on $[Rh(dpydmb)(tpy)]^{2+}$ **27**, like those previously reported for $[Ir(dpydmb)(tpy)]^{2+}$,[206] revealed that the HOMO is primarily localised on the phenyl ring of the dpydmb ligand with a small contribution from the rhodium centre, and the LUMO is delocalised across the three pyridyl rings of the tpy ligand (Table 2 and Figure 4.1). This is consistent with a predominantly LLCT lowest energy excited state, with which there is a small amount of mixing with MLCT character.

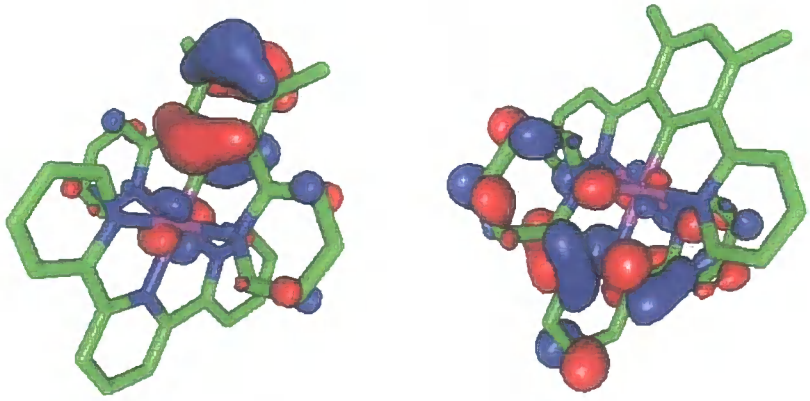

HOMO **LUMO**

Figure 4.1: Contour plots of the HOMO and LUMO of $[Rh(dpydmb)(tpy)]^{2+}$ 27.

Likewise, calculations of the Ir(III) complex $[Ir(dpydmb\text{-}\phi\text{-}NMe_2)(ttpy)]^{2+}$ **62** indicate that the lowest energy excited state is generated primarily from a LLCT transition (Table 2 and Figure 4.2). The electron rich nature of the dimethylamino group in complex **62**, however, results in the localisation of electron density in the HOMO differing significantly from that in the parent complex, $[Ir(dpydmb)(tpy)]^{2+}$, being localised specifically on the dimethylamino-phenyl pendant of the NCN ligand with no contribution from the cyclometalating phenyl ring and the metal centre. Whilst the LUMO and LUMO+1 are both localised on the tpy-moiety of the ttpy ligand, as in the parent complex, the LUMO+2 is primarily based on the "core" NCN portion of the dpydmb-ϕ-NMe_2 ligand. This is indicative of a predominantly LLCT ($NCN_{(pendant)} \rightarrow NNN_{(tpy\text{-}moiety)}$) lowest energy excited state with some ILCT ($NCN_{(pendant)} \rightarrow NCN_{(core)}$) character.

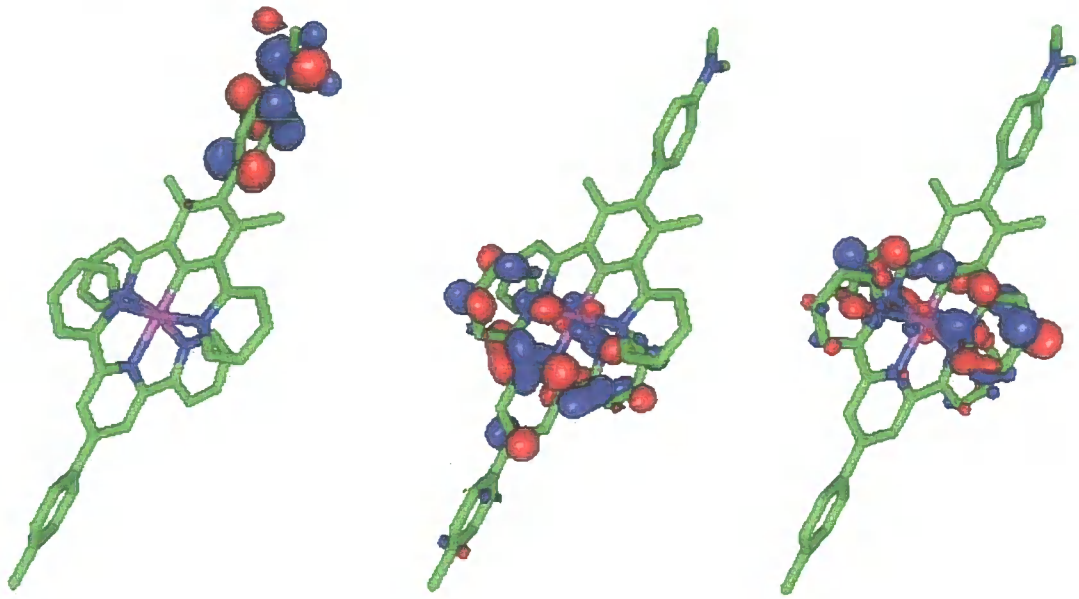

HOMO **LUMO** **LUMO+2**

Figure 4.2: Contour plots of the HOMO, LUMO and LUMO+2 of $[Ir(dpydmb\text{-}\phi\text{-}NMe_2)(ttpy)]^{2+}$ 62.

4.1.2.3 Photophysical studies

The introduction of a cyclometalating carbon, into the coordination sphere of the transition metal centre in d^6-coordinated complexes can have a profound effect upon their photophysical properties.[47] For example, Wilkinson's bis-terdentate $[Ir(dpydmb)(tpy)]^{2+}$ complex (Table 3), incorporating such an Ir–C bond, exhibits only very weak emission at 77 K, whilst displaying weak absorption bands at lower energy (430–470 nm) than those in $[Ir(tpy)_2]^{3+}$ (Table 1).[76, 78] This feeble emission is attributed

to a predominantly ligand-to-ligand charge-transfer (LLCT) excited state, based upon DFT calculations which revealed a dpydmb-based HOMO with little metal contribution and a tpy-based LUMO. It is this low metal contribution in the lowest energy excited state that results in both the oscillator strength and k_r being small and thus in particularly weak low-energy absorption bands and a low emission intensity respectively.

Complex [a]	$[Ir(dpydmb)(tpy)]^{2+}$ [76, 78]	**62** $[Ir(dpydmb\text{-}\phi\text{-}NMe_2)(ttpy)]^{2+}$	$[Ir(ttpy)(bpy)Cl]^{2+}$ [20]
Absorption maxima / nm (ε / M^{-1} cm^{-1})	465 (500) 435 (700) 377 (10100) 335 sh (13100) 311 (25400) 270 (35300) 261 (38500) 244 (33700)	463 (1140) 435 (1650) 359 (20800) 301 (60300) 266 (73700) 227 (72600)	440 sh (1000) 380 sh (6100) 350 sh (14500) 315 (35300) 271 (31900)
Emission maxima / nm	–	550	509, 541
Emission maxima at 77 K / nm	502 [e]	503, 536, 570 sh [e]	–
Φ_{em} x 10^2 [b] degassed (aerated)	< 0.1	1.1 (0.53)	4.3
Lifetime [c] / μs	–	–	1.2
Lifetime at 77 K [c] / μs	–	3.5, 9.5 [e, f]	–
k_r [d] / 10^4 s^{-1}	–	–	3.6
Σk_{nr} [d] / 10^5 s^{-1}	–	–	8.0

(a) Complexes as their hexafluorophosphate salts in degassed CH_3CN at 298 K, except where stated otherwise. (b) Luminescence quantum yield measured at 298 K using $[Ru(bpy)_3]Cl_2$ as a standard. (c) Lifetime registered at the emission maximum following excitation at 374 nm. (d) Radiative and non-radiative rate constants calculated from τ and Φ values at 298 K. (e) In an EPA glass at 77 K. (f) Values estimated by fitting separately the short and long components of the decay.

Table 3: Photophysical properties of the $[IrN_5X]^{2+}$ complexes (X = C or Cl).

The photophysical properties of the mono-cyclometalated complex $[Ir(dpydmb\text{-}\phi\text{-}NMe_2)(ttpy)]^{2+}$ **62** prepared in this study are summarised in Table 3. Like the parent complex, $[Ir(dpydmb)(tpy)]^{2+}$, the absorption spectrum shows a series of intense bands at high energy assigned to LC transitions and several lower energy CT bands above 350 nm. For complex **62**, the latter comprise of a band at 359 nm and a series of very weak features at > 400 nm, only resolvable in concentrated solutions, which based upon DFT studies (Section 4.1.2.2) are assigned to ILCT and LLCT transitions respectively.

Unlike the parent complex, a structureless emission band centred at 550 nm is observed from complex **62** at ambient temperature. DFT studies (Section 4.1.2.2) reveal that this is primarily from a LLCT excited state ($NCN_{(pendant)} \rightarrow NNN_{(tpy\text{-}moiety)}$) with some ILCT character ($NCN_{(pendant)} \rightarrow NCN_{(core)}$). The increased emission intensity from **62** can be attributed to the introduction of the electron rich -ϕ-NMe_2 pendant into the complex, on which the HOMO is based, and thus the incorporation of ILCT character into the excited state. Upon acidification, the CT bands in the absorption spectrum disappear and the emission is quenched. This is a reversible effect that is attributed to the protonation of the amine group which greatly raises the energy of the mixed LLCT/(ILCT) excited state.

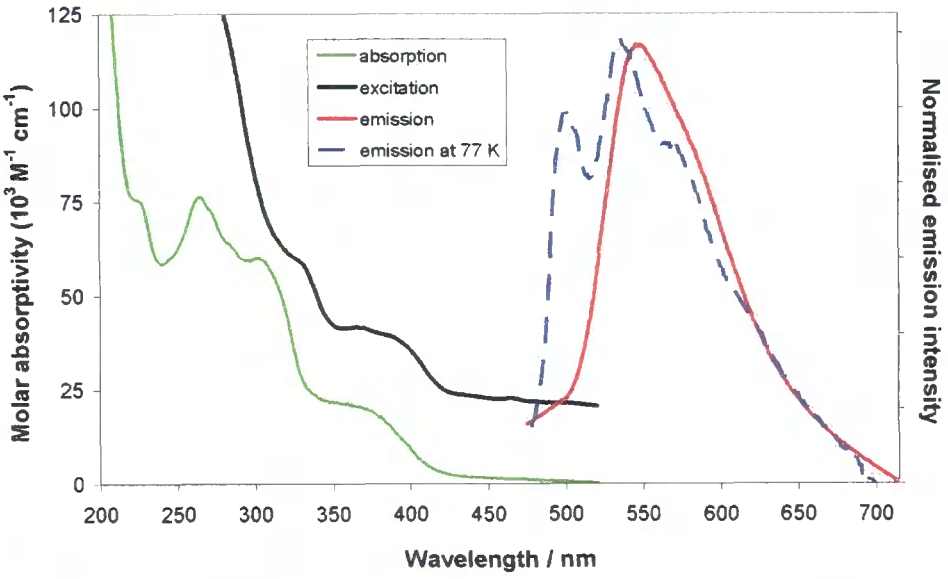

Figure 4.3: Absorption and normalised emission spectra (λ_{ex} = 370 nm) of [Ir(dpydmb-ϕ-NMe_2)(ttpy)]$^{2+}$ 62 with overlaid excitation spectrum (λ_{em} = 540 nm) offset for clarity. All spectra are recorded in MeCN at 298K, except for that of the emission at 77 K which is in EPA (λ_{ex} = 374 nm).

At 77 K the emission profile observed from complex **62** in an EPA glass is structured, like that previously reported for the parent complex.[76, 78] The emission profile is blue-shifted compared to that at 298 K consistent with CT transitions in which a considerable degree of molecular reorganisation accompanies the formation of the excited state.

Contary to the incorporation of a cyclometalating carbon into the coordination sphere of the metal centre, the introduction of an anionic chloride brings about an enhancement in the emission observed. For example, [Ir(ttpy)(bpy)Cl]$^{2+}$ (Table 3) was reported to display considerably red-shifted emission and a three-fold increase in k_r compared to [Ir(ttpy)]$^{3+}$ (Table 1).[46, 82] This arises from an increase in the metal-to-ligand charge-

transfer (MLCT) character of the emissive state, brought about by the anionic chloride significantly raising the metal-contribution in the HOMO.[47]

The photochemical properties of a range of $[M(NCN)(NNN)]^{2+}$ coordinated rhodium(III) complexes, prepared in this work for the first time, are outlined in Table 4.

Complex [a]	**26** $[Rh(dpy)(tpy)]^{2+}$	**27** $[Rh(dpydmb)(tpy)]^{2+}$	**28** $[Rh(dpydmb)(tpy\text{-}\phi\text{-}Br)]^{2+}$
Absorption maxima / nm (ε / M^{-1} cm^{-1})	360 (7470) 305 (16200) 280 (29900) 240 (31700)	359 (7710) 297 (23600) 281 (29600) 252 (34800)	360 (16600) 336 (29400) 295 (68600) 255 (54900)

(a) Complexes as their hexafluorophosphate salts in CH_3CN at 298 K

Table 4: Photochemical properties of the $[Rh(NCN)(NNN)]^{2+}$ complexes.

The absorption spectra (Figure 4.4) of $[Rh(dpyb)(tpy)]^{2+}$ **26**, $[Rh(dpydmb)(tpy)]^{2+}$ **27** and $[Rh(dpydmb)(tpy\text{-}\phi\text{-}Br)]^{2+}$ **28**, like those of the related iridium complexes,[76, 78] are all dominated by high-energy bands typical of LC transitions alongside a series of lower intensity spin-allowed CT transition bands between 330 and 400 nm. However, the CT bands in the rhodium complexes do not extend to as low energy as in their iridium analogues.

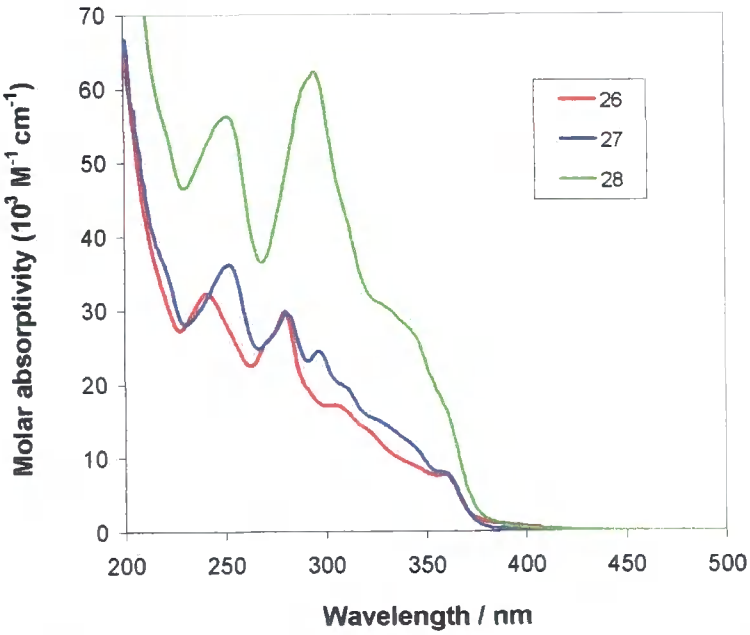

Figure 4.4: Ground-state absorption spectra of the $[Rh(NCN)(NNN)]^{2+}$ coordinated complexes 26, 27 and 28 in acetonitrile solution at 298 K.

Upon excitation at a variety of wavelengths, complexes **26**, **27** and **28** were all seen to be non-emissive, even at 77 K (Table 4), unlike the related iridium complexes $[Ir(dpydmb)(tpy)]^{2+}$ and $[Ir(dpydmb)(ttpy)]^{2+}$ which were found to be weakly emissive at 77 K.[76, 78] It is noteworthy that there are also no reports in the literature of emission from the only other known $[RhN_5C]^{2+}$ complex, $[Rh(bpy)_2(ppy)]^{2+}$.[88, 102]

4.1.3 [M(NCN)(NN)Cl]⁺ complexes

4.1.3.1 Electrochemical studies

The synthesis of the $[M(NCN)(NN)Cl]^+$ coordinated complexes $[Ir(dpydmb)(bpy)Cl]^+$ **30**, $[Rh(dpydmb)(bpy)Cl]^+$ **31** and $[Ir(tpyb)(bpy)Cl]^+$ **32**, bearing cis-disposed anionic groups was described in Section 2.2.2.2. The electrochemical studies of these complexes were carried out at 298 K in Bu_4NBF_4 (1.0 M in MeCN) as the supporting electrolyte within the range of –2.5 to +2.0 V and the results summarised in Table 5.

Complex [a]	$E_{1/2}^{ox}$ / V	ΔE^{ox} / mV [b]	$E_{1/2}^{red}$ / V	ΔE^{red} / mV [b]
30 $[Ir(dpydmb)(bpy)Cl]^+$	1.28 1.43	80 90	– 1.52 – 2.37	110 160
32 $[Ir(tpyb)(bpy)Cl]^+$	0.95	100	– 1.50 – 2.21	130 160
31 $[Rh(dpydmb)(bpy)Cl]^+$	1.43	120	– 1.73 – 2.05	80 110

(a) Complexes as their PF_6^- salts in Bu_4NBF_4 (0.1 M in MeCN) as the supporting electrolyte. (b) ΔE^{ox} and ΔE^{red} are the peak to peak separation of the reversible oxidation and reduction processes respectively. These values were measured at a scan rate of 300 mV s^{-1} and are reported relative to SCE, measured using ferrocene as the standard ($E_{1/2}^{ox}$ = 0.42 V *vs.* SCE).

Table 5: Oxidation and reduction potentials of the $[M(NCN)(NN)Cl]^+$ coordinated complexes obtained by cyclic voltammetry.

$[Ir(dpydmb)(bpy)Cl]^+$ **30** was seen to exhibit two close-lying reversible oxidation processes at ~ 1.35 V *vs.* SCE (Figure 4.5). This agrees well with the mono-cationic tris-bidentate complex $[Ir(ppy)_2(bpy)]^+$, containing two cyclometalating carbons, where a similarly reversible oxidation process was reported at 1.28 V.[69] The oxidation processes cannot be fully assigned to the metal-centre owing to the strong covalent character of the Ir–C bonds in cyclometalated complexes.[38] However, based upon DFT calculations which reveal that the electron density in the HOMO is localised over the

metal centre and the cyclometalating ring of the dpydmb (NCN) ligand (Section 4.1.3.2), they can be attributed to the removal of an electron from an orbital that spans both the metal centre and the cyclometalating ring of the dpydmb ligand.

Complex **30** also exhibits two reversible reduction processes, the first of which occurs at a potential of –1.52 V *vs.* SCE and is assigned to a reduction based on the bpy ligand (Figure 4.5). This compares to a potential of –1.35 V for the equivalent bpy-based reduction in $[Ir(ppy)_2(bpy)]^+$.[69]

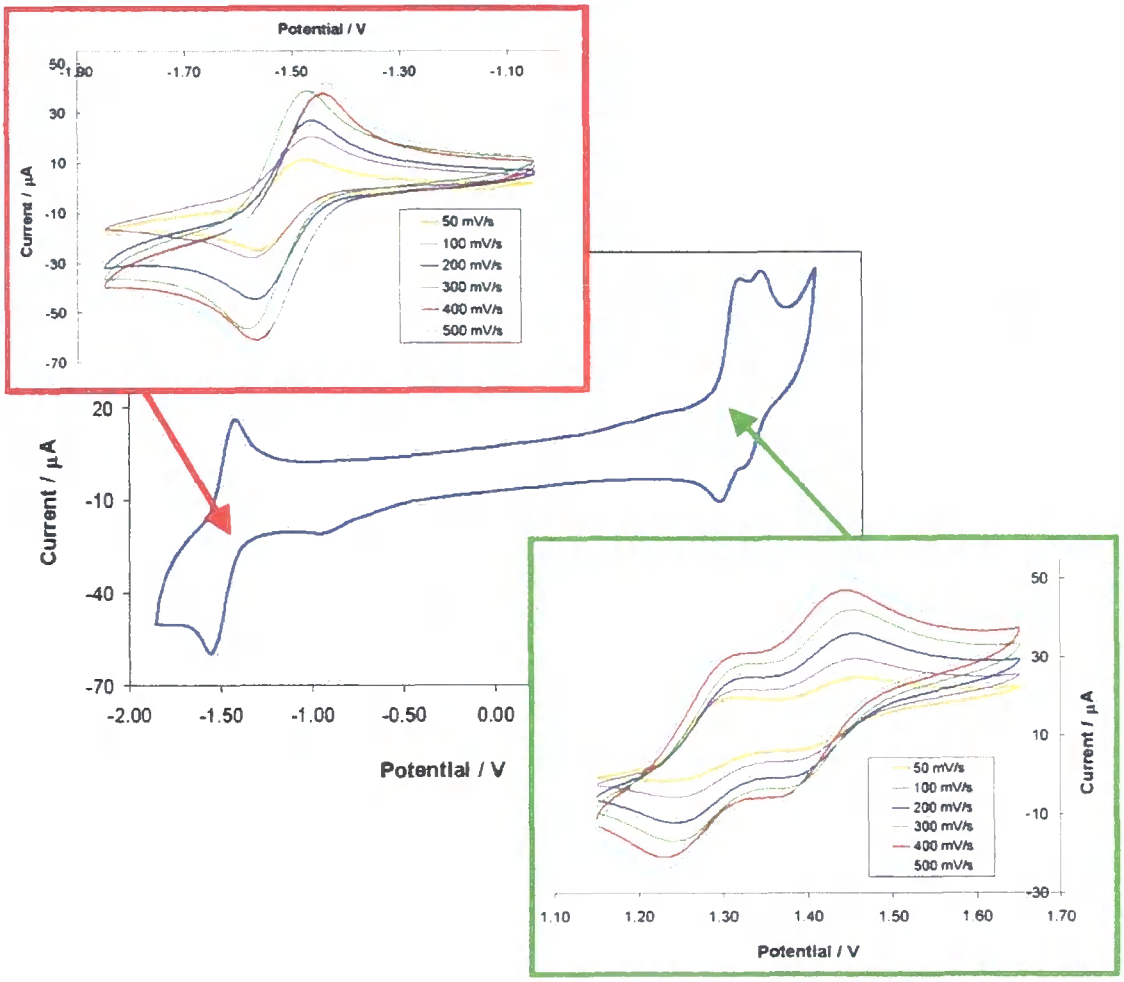

Figure 4.5: Cyclic voltammogram of $[Ir(dpydmb)(bpy)Cl]^+$ 30 at 298 K in Bu_4NBF_4 (0.1 M in acetonitrile) as the supporting electrolyte, at a scan rate of 200 mV s^{-1}. The highlighted regions show the oxidations and first reduction at a series of scan rates (50, 100, 200, 300, 400 and 500 mV s^{-1}); the current varies linearly with the square root of the scan rate.

A single reversible oxidation process was observed for $[Ir(tpyb)(bpy)Cl]^+$ **32** at 0.95 V *vs.* SCE which, as in complex **30**, was assigned to the removal of an electron from an orbital that spans both the metal centre and the cyclometalating ring of the NCN ligand.

Upon comparison with complex **30** (1.28 V), the introduction of the pyridyl-pendant into the NCN ligand of complex **32** appears to facilitate this oxidation. This is thought to arise due to the π-donating nature of pyridyl-pendant increasing the electron density of the cyclometalating ring in the NCN ligand, which contributes to the orbital upon which the oxidation is based. Two reversible reductions were also observed for complex **32**, the first of which occurs at –1.50 V and is assigned to the reduction of the bipyridine ligand. This agree well with the first reduction in **30** (–1.52 V), owing to the bpy-based LUMO being unaffected by the pyridyl-pendant.

Electrochemical analysis of $[Rh(dpydmb)(bpy)Cl]^+$ **31**, the Rh(III) analogue of **30**, revealed a reversible oxidation process at 1.43 V *vs.* SCE. Based upon DFT calculations (Section 4.1.3.2) and akin to **30**, this was assigned to the removal of an electron from an orbital that spans both the metal centre and the cyclometalating ring of the dpydmb (NCN) ligand. A reversible oxidation at a potential of 1.62 V was similarly reported for the closest related mono-cationic rhodium complex in the literature, namely $[Rh(ppy)_2(bpy)]^+$.[69] Complex **31** also displays several reduction processes within the solvent window. The first is a chemically reversible reduction at –1.73 V *vs.* SCE which, like the iridium complexes **30** (–1.52 V) and **32** (–1.50 V), was assigned to the bpy ligand. This compares to a potential of –1.42 V reported for the analogous reduction in $[Rh(ppy)_2(bpy)]^+$.[69]

Upon comparison of the oxidation potentials of both $[Rh(dpydmb)(bpy)Cl]^+$ **31** (1.43 V) and $[Ir(dpydmb)(bpy)Cl]^+$ **30** (1.28 V), and the literature complexes $[Rh(ppy)_2(bpy)]^+$ (1.62 V) and $[Ir(ppy)_2(bpy)]^+$ (1.28 V),[69] it becomes evident that it is harder to oxidise a rhodium(III) metal centre than an iridium(III) metal centre in such complexes. Similarly, the potentials of the bpy-based reductions in the rhodium complexes **31** (–1.73 V) and $[Rh(ppy)_2(bpy)]^+$ (–1.42 V)[69] occur at more negative potentials than those in their respective iridium analogues, **30** (–1.52 V) and $[Ir(ppy)_2(bpy)]^+$ (–1.35 V),[69] indicating that it is also more difficult to reduce ligands bound to a Rh(III) centre.

4.1.3.2 Computational studies

DFT calculations were carried out on both $[Ir(dpydmb)(bpy)Cl]^+$ **30** (Figure 4.6) and $[Rh(dpydmb)(bpy)Cl]^+$ **31** (Figure 4.7). The calculated orbital characteristics for the

three highest energy molecular orbitals and the three lowest energy unoccupied molecular orbitals are summarised in Table 6.

Complex	HOMO–2	HOMO–1	HOMO	LUMO	LUMO+1	LUMO+2
30 $[Ir(dpydmb)(bpy)Cl]^+$	Ir (11%) NCN (61%) Cl (27%)	Ir (39%) NCN (29%) Cl (28%)	Ir (40%) NCN (42%) Cl (13%)	NN (92%)	NN (94%)	NCN (96%)
31 $[Rh(dpydmb)(bpy)Cl]^+$	NCN (49%) Cl (43%)	Rh (25%) NCN (39%) Cl (35%)	Rh (35%) NCN (47%) Cl (15%)	NN (95%)	NCN (12%) NN (86%)	NCN (86%) NN (12%)

Table 6: Calculated molecular orbital characteristics of the $[M(NCN)(NN)Cl]^+$ complexes according to DFT calculations. The percentages in parentheses denote the proportion of the total electron density localised at that site.

The studies on both complexes **30** and **31** reveal that the electron density in the HOMO is primarily localised on the phenyl ring of the dpydmb ligand, with significant contributions from the metal centre and the anionic chloride (Table 6, Figure 4.6 and Figure 4.7), whilst the LUMO is delocalised across the two pyridyl rings of the bpy ligand. This is consistent with the mixed orbital oxidations and bpy-based reductions reported in Section 4.1.3.1 and is indicative that emission will be from a mixed LLCT/MLCT excited state.

Only slight differences are seen in the distribution of electron density in the rhodium (**31**) and iridium (**30**) complexes (Table 6), the most significant being slightly less metal contribution in the HOMO of **31** which may account for the more difficult oxidation of the Rh(III) complex (Section 4.1.3.1).

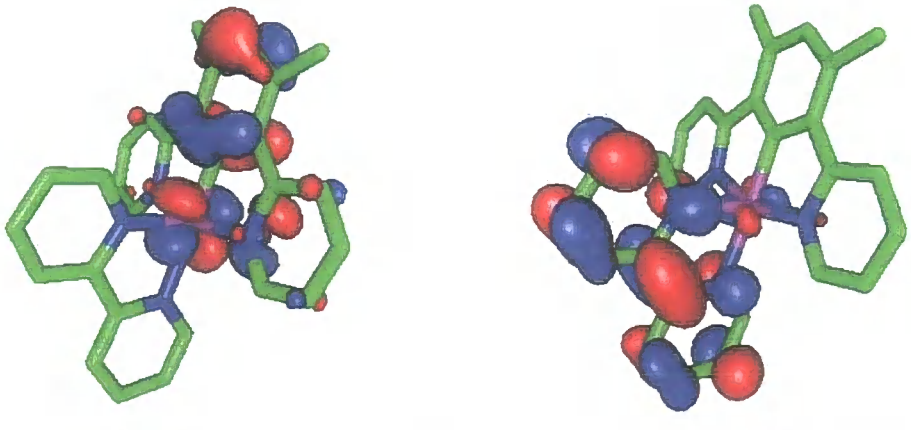

HOMO **LUMO**

Figure 4.6: Contour plots of the HOMO and LUMO of $[Ir(dpydmb)(bpy)Cl]^+$ 30.

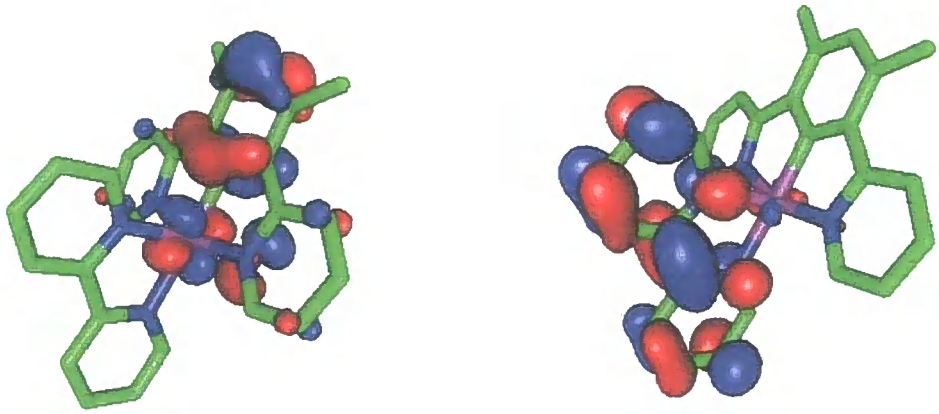

HOMO LUMO

Figure 4.7: Contour plots of the HOMO and LUMO of [Rh(dpydmb)(bpy)Cl]$^+$ 31.

4.1.3.3 Photophysical studies

The photophysical properties of the mono-cationic [M(NCN)(NN)Cl]$^+$ complexes incorporating one cyclometalating carbon and one anionic chloride were investigated and are summarised in Table 7.

Complex [a]	**30** [Ir(dpydmb)(bpy)Cl]$^+$	**32** [Ir(tpyb)(bpy)Cl]$^+$	**31** [Rh(dpydmb)(bpy)Cl]$^+$
Absorption maxima / nm (ε / M^{-1} cm^{-1})	469 (680) 439 (1390) 387 (10100) 275 (27900) 247 (34900)	474 (1260) 445 (2630) 404 (12500) 290 (102000) 252 (73600)	367 (6380) 354 (5560) 312 sh (15500) 295 (20400) 262 (25900)
Emission maxima / nm	502, 535	509, 543 sh	492, 522
Emission maxima at 77 K / nm	488, 527 [f]	478, 514 [f]	–
Φ_{em} x 10^2 [b] degassed (aerated)	11 (0.46)	1.9 (< 0.1)	–
Lifetime [c] / μs degassed (aerated)	1.5 (0.038)	1.7 (0.049)	–
Lifetime at 77 K [c] / μs	3.7 [f]	3.5 [f]	–
k_r [d] / 10^4 s^{-1}	8.1	1.1	–
Σk_{nr} [d] / 10^5 s^{-1}	5.9	5.8	–
$k_Q^{O_2}$ [e] / 10^{10} M^{-1} s^{-1}	1.3	1.1	–

(a) Complexes as their hexafluorophosphate salts in degassed CH_3CN at 298 K, except where stated otherwise. (b) Luminescence quantum yield measured at 298 K using $[Ru(bpy)_3]Cl_2$ as a standard. (c) Lifetime registered at the emission maximum following excitation at 374 nm. (d) Radiative and non-radiative rate constants calculated from τ and Φ values at 298 K. (e) Bimolecular rate constant for quenching by O_2, estimated from τ in degassed and aerated solutions. (f) In an EPA glass at 77 K.

Table 7: Photophysical properties of the [M(NCN)(NN)Cl]$^+$ (M = Ir or Rh) coordinated complexes.

The absorption spectra of $[Ir(dpydmb)(bpy)Cl]^+$ **30** and $[Ir(tpyb)(bpy)Cl]^+$ **32** contain high-energy LC bands (< 300 nm) alongside a series of lower energy bands indicative of CT transitions (Table 7). Based upon DFT studies (Section 4.1.3.2), the CT absorption bands observed at 387 and 404 nm respectively for complexes **30** and **32** are assigned to MLCT transitions, and those at lower energies to LLCT transitions.

Complexes **30** and **32** display structured emission, with a maximum between 500 and 510 nm, in acetonitrile solution at ambient temperature (Figure 4.8). This is assigned as being from a mixed LLCT/MLCT excited state, which is consistent with the predictions made from the DFT calculations carried out on complex **30** (Sections 4.1.3.2). Compared to the di-cationic complex $[Ir(dpydmb)(tpy)]^{2+}$ (Table 3), complexes **30** and **32** (Table 7) display significantly longer luminescence lifetimes and raised emission intensities, indicative of there being increased MLCT contribution in the lowest energy excited states of these mono-cationic complexes. This is the result of increased electron density at the metal centre brought about by the introduction of a second anionic group into its coordination sphere, which is confirmed by DFT calculations (Sections 4.1.2.2 and 4.1.3.2 respectively) which reveal an approximately two-fold increase in the metal-based contribution to the HOMO upon the introduction of the chloride.

Comparison of the two $[Ir(NCN)(NN)Cl]^+$ complexes, however, reveals that the emission intensity observed from $[Ir(tpyb)(bpy)Cl]^+$ **32** is considerably lower than that of the parent complex $[Ir(dpydmb)(bpy)Cl]^+$ **30** (Table 7). This can be attributed to the introduction of a σ-withdrawing (and π-donating) pyridyl-pendant into the NCN ligand of complex **32**, which reduces the electron density at the metal centre and thus the extent of the MLCT character in the emissive state. This is more clearly apparent from the k_r values, that of **30** being almost an order of magnitude smaller than that of **32**, indicative of lower participation of the metal in the excited state.

Upon cooling to 77 K in an EPA glass, the emission profile of both complexes **30** and **32** become more structured and undergo a significant blue-shift. This is typical of a CT transition in which considerable molecular reorganisation accompanies the formation of the excited state. The shift is larger for **32**, evidently associated with the freezing out of the torsional rearrangement of the pendant that can stabilise the excited state in fluid solution. This is the result of the pyridyl pendant in **32** being inductively withdrawing

(irrespective of the torsional angle), lowering the energy of the HOMO at 77 K even when twisted, whilst also being electron donating *via* the π-system when the pendant is coplanar with the ligand backbone. The latter π-donating effect outweighs the former σ-withdrawing effect when torsional rearrangement can occur in fluid solution at 298 K, however, at 77 K the geometry is locked and the σ-withdrawing effect dominates. Alongside the changes in the emission profile, the luminescence lifetimes of both complexes **30** and **32** are lengthened significantly upon cooling.

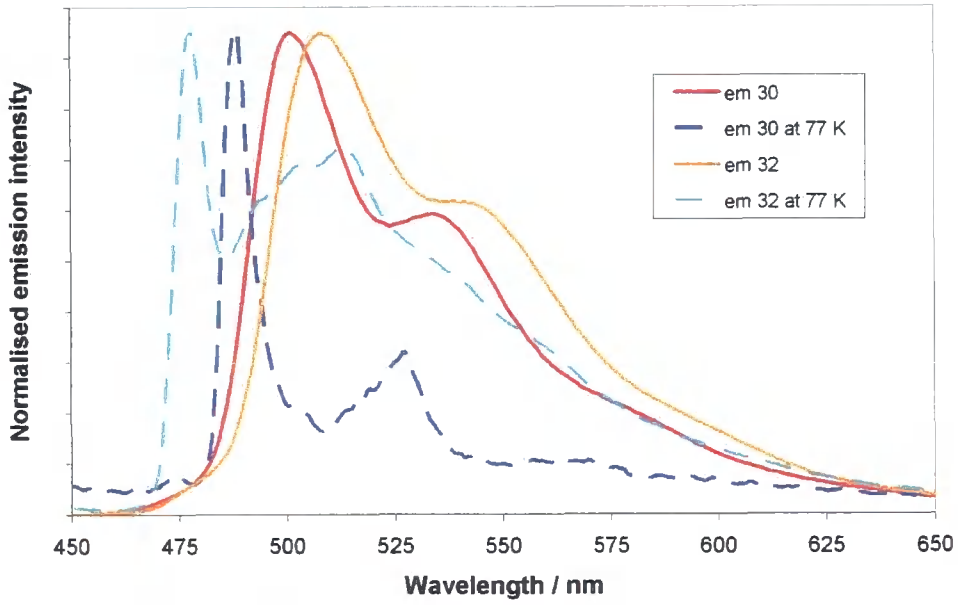

Figure 4.8: Normalised emission spectra of [Ir(dpydmb)(bpy)Cl]$^+$ 30 (λ_{ex} = 387 and 425 nm), and [Ir(tpyb)(bpy)Cl]$^+$ 32 (λ_{ex} = 405 and 400 nm) at 298 K in degassed MeCN and at 77 K in an EPA glass.

The photophysical properties of the rhodium(III) complex [Rh(dpydmb)(bpy)Cl]$^+$ **31** were investigated (Table 7). The absorption spectrum of **31** (Figure 4.9) is dominated by a series of high intensity bands in the range 260–320 nm which are assigned to LC transitions. In addition to these, two absorption bands are observed at 354 and 367 nm, which are attributed to MLCT transitions based upon the assignment of the band at 366 nm reported in the literature for the related mono-cationic complex [Rh(ppy)$_2$(bpy)]$^+$.[69, 103] It should also be noted that the CT bands in both **31** and [Rh(ppy)$_2$(bpy)]$^+$ do not extend to as low-energy as in their analogously coordinated iridium complexes.

Upon excitation at a range of wavelengths between 325 and 450 nm, complex **31** was found to be non-emissive at ambient temperature, whilst very weakly emissive at 77 K.

However, upon analysis of this emission it was unfortunately found to be too weak and erratic for anything meaningful to be concluded. The related tris-bidentate literature complex $[Rh(ppy)_2(bpy)]^+$ was similarly reported to be non-emissive at 298 K, whilst at 77 K it exhibited long-lived (170 μs) structured emission reported to be from a predominantly ppy-based LC emissive state with some MLCT character.[69, 103]

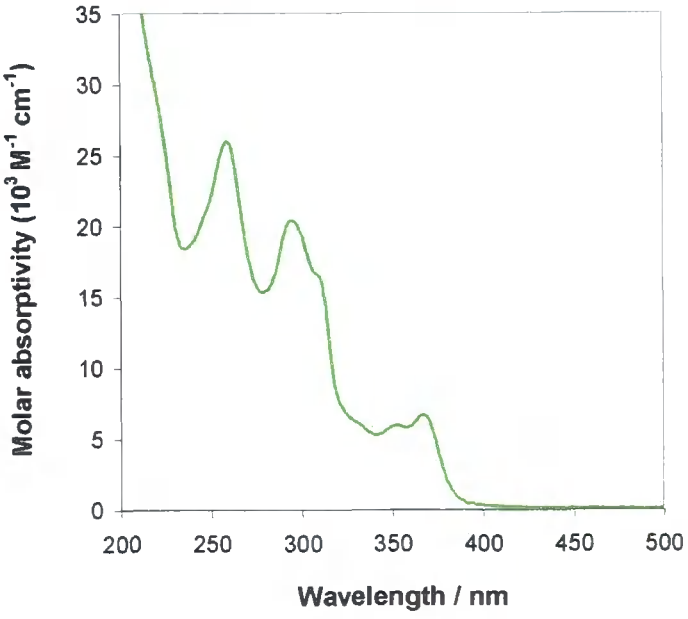

Figure 4.9: Ground-state absorption spectra of $[Rh(dpydmb)(bpy)Cl]^+$ 31 in MeCN at 298 K.

4.1.4 Bis-cyclometalated $[M(NCN)(NNC)]^+$ and $[Ir(CNC)(NNN)]^+$ complexes

Bis-terdentate complexes containing two cyclometalating carbons can possess either a mutually *cis* or *trans* arrangement of the Ir–C bonds. In this section the photophysical (Table 11) and electrochemical properties of a series of $[M(NCN)(NNC)]^+$ complexes with *cis*-disposed Ir–C bonds synthesised in this study (Section 2.2.2.2) are discussed alongside the photophysical properties of the related *trans* $[Ir(CNC)(NNN)]^+$ complexes recently reported by Scandola *et al.* (Section 1.3.2.2 and Table 10).[83, 84]

4.1.4.1 Electrochemical studies of the $[M(NCN)(NNC)]^+$ complexes

The electrochemical properties of the $[Ir(NCN)(NNC)]^+$ coordinated complexes $[Ir(dpydmb)(phbpy)]^+$ **33** (Figure 4.10) and $[Ir(dpydmb)(mtbpy\text{-}\phi\text{-}Br)]^+$ **61** were studied at 298 K in Bu_4NBF_4 (0.1 M in acetonitrile) as the supporting electrolyte, alongside the elaborated complexes $[Ir(dpydmb)(mtbpy\text{-}\phi\text{-}ph)]^+$ **64**, $[Ir(dpydmb\text{-}Br)(mtbpy\text{-}\phi\text{-}ph)]^+$ **65** and $[Ir(dpydmb\text{-}C_6H_3Me_2)(mtbpy\text{-}\phi\text{-}ph)]^+$ **66** and the analogously coordinated

rhodium(III) complex $[Rh(dpydmb)(phbpy)]^+$ **34** (Table 8). All the complexes displayed at least two reversible electrochemical processes within the range of –2.5 to +2.0 V.

Complex [a]	$E_{1/2}^{ox}$ / V	ΔE^{ox} / mV [b]	$E_{1/2}^{red}$ / V	ΔE^{red} / mV [b]
33 $[Ir(dpydmb)(phbpy)]^+$	1.12	80	– 1.39 – 2.12	90 80
61 $[Ir(dpydmb)(mtbpy\text{-}\phi\text{-}Br)]^+$	1.22	80	– 1.15	100
64 $[Ir(dpydmb)(mtbpy\text{-}\phi\text{-}ph)]^+$	0.96	90	– 1.56 – 2.25	90 90
65 $[Ir(dpydmb\text{-}Br)(mtbpy\text{-}\phi\text{-}ph)]^+$	0.94	100	– 1.82	100
66 $[Ir(dpydmb\text{-}C_6H_3Me_2)(mtbpy\text{-}\phi\text{-}ph)]^+$	0.89	90	– 1.66	90
34 $[Rh(dpydmb)(phbpy)]^+$	1.28 1.44	160 140	– 1.64 – 2.32	200 170

(a) Complexes as their PF_6^- salts in Bu_4NBF_4 (0.1 M in MeCN) as the supporting electrolyte. (b) ΔE^{ox} and ΔE^{red} are the peak to peak separation of the reversible oxidation and reduction processes respectively. These values were measured at a scan rate of 300 mV s^{-1} and are reported relative to SCE, measured using ferrocene as the standard ($E_{1/2}^{ox}$ = 0.42 V *vs.* SCE).

Table 8: Oxidation and reduction potentials of the $[M(NCN)(NNC)]^+$ (M = Ir or Rh) coordinated complexes obtained by cyclic voltammetry.

The cyclic voltammogram of $[Ir(dpydmb)(phbpy)]^+$ **33**, shown in Figure 4.10 is representative of all the iridium complexes. It shows a reversible oxidation process at 1.21 V *vs.* SCE, which corresponds well with that of 1.28 V known for the tris-bidentate analogue $[Ir(ppy)_2(bpy)]^+$, with *cis*-disposed Ir–C bonds. As previously reported, this oxidation process cannot be fully assigned to a metal-centred oxidation owing to the strong covalent character of the Ir–C bonds in the cyclometalated complexes.[38] DFT calculations (Section 4.1.4.2) confirm that the HOMO is indeed delocalised over the metal and the cyclometalating ring of the dpydmb (NCN) ligand and thus the oxidation assigned to the removal of an electron from an orbital spanning both the metal centre and this cyclometalating ring. The oxidation potentials of the *cis*-cyclometalated $[Ir(NCN)(NNC)]^+$ iridium complexes are considerably higher than those reported for Scandola's $[Ir(CNC)(NNN)]^+$ coordinated complexes with *trans*-disposed carbon atoms.[83, 84] This agrees well with studies of the *fac*- and *mer*- isomers of $[Ir(ppy)_3]$, which reveal that the *mer*-isomer containing two *trans*-disposed carbons, are more easily oxidised (by ~0.1 V) than the *fac*-isomers.[235]

The first reduction process occurs at –1.39 V for complex **33** and is assigned to the reduction of the bpy-moiety of the phbpy (NNC) ligand, owing to it being close to the reduction potential of –1.35 V observed for $[Ir(ppy)_2(bpy)]^+$ where the reduction is centred on the bipyridine ligand.[38] This reduction is displaced to more negative potentials compared to that of Scandola's $[Ir(CNC)(NNN)]^+$ coordinated complexes (~ –1.27 V *vs.* SCE) where the reduction is localised on the terpyridine ligand. This is due to stabilisation of the LUMO occurring upon going from bipyridine to terpyridine where delocalisation occurs across three rings rather than two. DFT calculations (Section 4.1.4.2) confirm that the LUMO is indeed delocalised over the bpy-moiety of the NNC ligand.

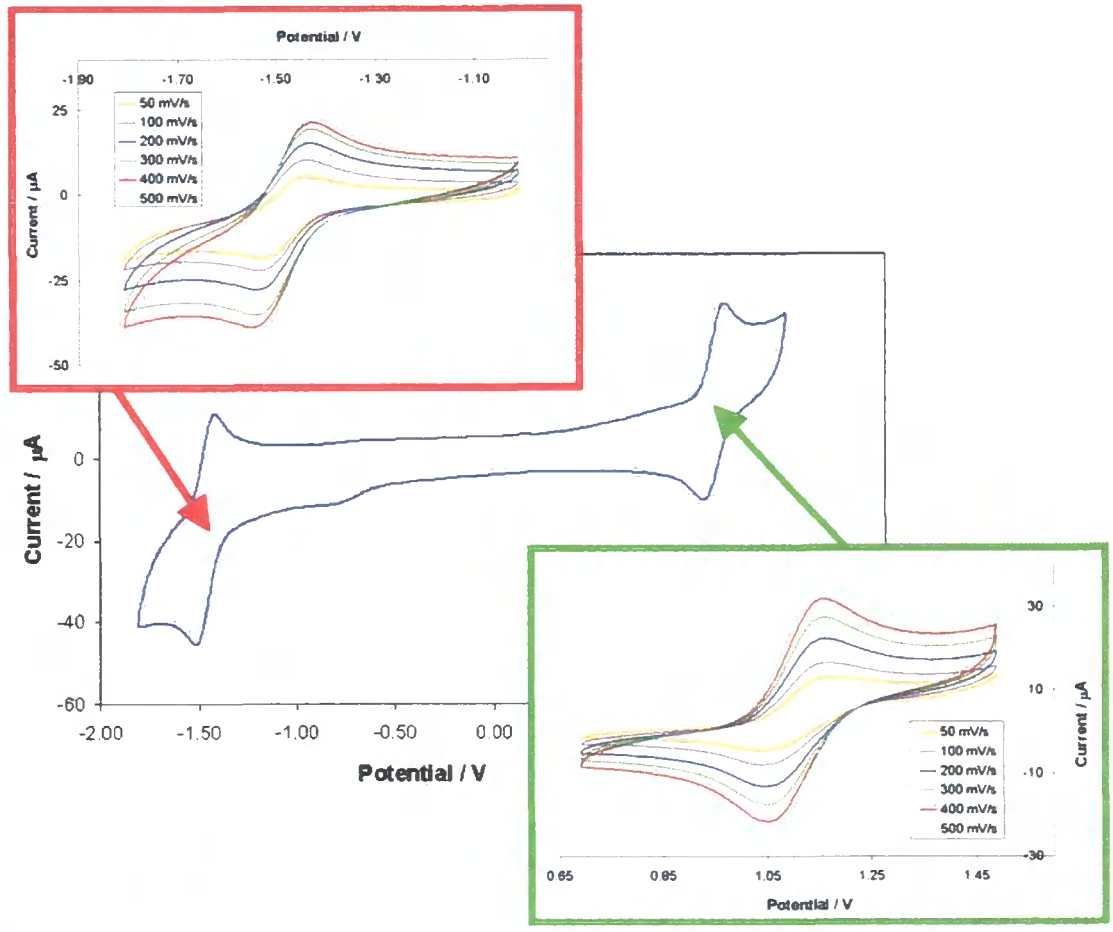

Figure 4.10: Cyclic voltammogram of $[Ir(dpydmb)(phbpy)]^+$ 33 at 298 K in Bu_4NBF_4 (0.1 M in acetonitrile) as the supporting electrolyte, at a scan rate of 200 mV s^{-1}. The highlighted regions show the first oxidation and first reduction at a series of scan rates (50, 100, 200, 300, 400 and 500 mV s^{-1}); the current varies linearly with the square root of the scan rate.

Upon the introduction of a bromophenyl pendant into the NNC ligand (**61**) the reduction is shifted by +0.24 V owing to the net electron-withdrawing effect of the pendant and to more extended conjugation introduced into the NNC ligand, upon which the LUMO is

localised. Further extension to a biphenyl pendant (**64**), however, results in the shift of the reduction process to more negative potentials and the oxidation to more positive potentials, which must result from electron-donation through the π-bonding framework. Meanwhile, the introduction of substituents on the NCN ligand (**65** and **66**) slightly stabilises the oxidation and destabilises the reduction.

Electrochemical analysis of the Rh(III) complex $[Rh(dpydmb)(phbpy)]^+$ **34** reveals two close-lying reversible oxidation processes at ~1.35 V *vs.* SCE which, akin to the analogous Ir(III) complex **33**, are assigned to the removal of an electron from an orbital that spans both the metal centre and the cyclometalating ring of the dpydmb (NCN) ligand. Likewise, a reversible oxidation at a potential of 1.62 V has been reported for the similarly coordinated tris-bidentate complex $[Rh(ppy)_2(bpy)]^+$ with *cis*-disposed cyclometalating carbons.[69] Two reversible reduction potentials are also observed within the solvent window, the first of which occurs at –1.64 V and by analogy with the Ir(III) complex (reduction at –1.39 V) is assigned to the bpy-moiety of the NNC ligand. This compares to a potential of –1.42 V for the analogous reduction in $[Rh(ppy)_2(bpy)]^+$.[69] Upon comparison of the oxidation and reduction potentials of the Rh(III) complex **34** and the Ir(III) complex **33**, it is apparent that it is both harder to oxidise and to reduce the Rh(III) complex **34**. This is in line with the observations made for the $[M(dpydmb)(bpy)Cl]^+$ (M = Ir or Rh) coordinated complexes reported herein (Section 4.1.3.1) and the literature complexes $[M(ppy)_2(bpy)]^+$.[69]

4.1.4.2 Computational studies of the [M(NCN)(NNC)]⁺ complexes

DFT calculations were carried out on the series of $[Ir(NCN)(NNC)]^+$ coordinated complexes **33** (Figure 4.11), **61**, **64**, **65** and **66** (Figure 4.12). The calculated orbital characteristics for the three highest energy molecular orbitals and the three lowest energy unoccupied molecular orbitals are summarised in Table 9.

The studies carried out on $[Ir(dpydmb)(phbpy)]^+$ **33** (Table 9 and Figure 4.11) reveal that electron density in the HOMO is localised primarily on the phenyl ring of the dpydmb (NCN) ligand and the iridium centre, over which the orbital involved in the oxidation of this complex spans, whilst the HOMO–1 is localised on the phenyl ring of the phbpy (NNC) ligand and on the iridium centre. The LUMO is shown to be delocalised across the bpy-moiety of the phbpy ligand, which agrees with the

electrochemical assignment of the first reduction process to this bpy-moiety (Section 4.1.4.1). Upon consideration of the localisation of electron density in the HOMO–1, HOMO and LUMO of this complex, it can be concluded that emission will occur from a mixed MLCT/LLCT excited state.

Complex	HOMO–2	HOMO–1	HOMO	LUMO	LUMO+1	LUMO+2
33 [Ir(dpydmb)(phbpy)]$^+$	NCN (83%) NNC (15%)	Ir (41%) NCN (16%) NNC (43%)	Ir (39%) NCN (48%) NNC (13%)	NNC (93%)	NCN (16%) NNC (82%)	NCN (84%) NNC (13%)
61 [Ir(dpydmb) (mtbpy-ϕ-Br)]$^+$	Ir (39%) NCN (17%) NNC (44%)	Ir (38%) NCN (11%) NNC (51%)	Ir (40%) NCN (46%) NNC (14%)	NNC (92%)	NNC (93%)	NCN (93%)
64 [Ir(dpydmb) (mtbpy-ϕ-ph)]$^+$	NNC (89%)	Ir (38%) NCN (10%) NNC (52%)	Ir (41%) NCN (46%) NNC (13%)	NNC (92%)	NCN (14%) NNC (84%)	NCN (83%) NNC (13%)
66 [Ir(dpydmb-$C_6H_3Me_2$) (mtbpy-ϕ-ph)]$^+$	NNC (88%)	Ir (38%) NCN (12%) NNC (50%)	Ir (38%) NCN (50%) NNC (12%)	NNC (92%)	NNC (93%)	NCN (93%)

Table 9: Calculated molecular orbital characteristics of the [Ir(NCN)(NNC)]$^+$ coordinated complexes according to DFT calculations. The percentages in parentheses denote the proportion of the total electron density localised at that site.

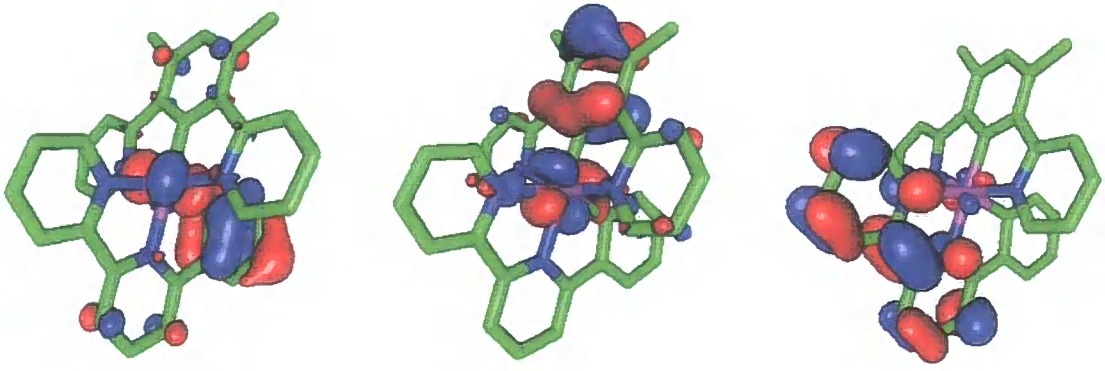

HOMO–1 **HOMO** **LUMO**

Figure 4.11: Contour plots of the HOMO–1, HOMO and LUMO of [Ir(dpydmb)(phbpy)]$^+$ 33.

The introduction of the bromophenyl pendant and methyl blocking unit into the NNC ligand of complex **61** (Table 9) has very little effect on the electron distribution in the HOMO which is localised on the NCN ligand and the LUMO which is localised on the bpy-moiety of the NNC ligand. Likewise, the extension of the bromophenyl pendant to a biphenyl (**64**) and the introduction of substituents into the NCN coordinating ligand (**65** and **66**) have little effect, with the molecular orbitals remaining localised on the "core" of these ligands. The contour plots of the HOMO–1, HOMO and LUMO of

complex **66**, bearing 4'-aryl-substituents on the NCN and NNC coordinating ligands, are shown in Figure 4.12 for comparison with the unsubstituted complex **33** (Figure 4.11).

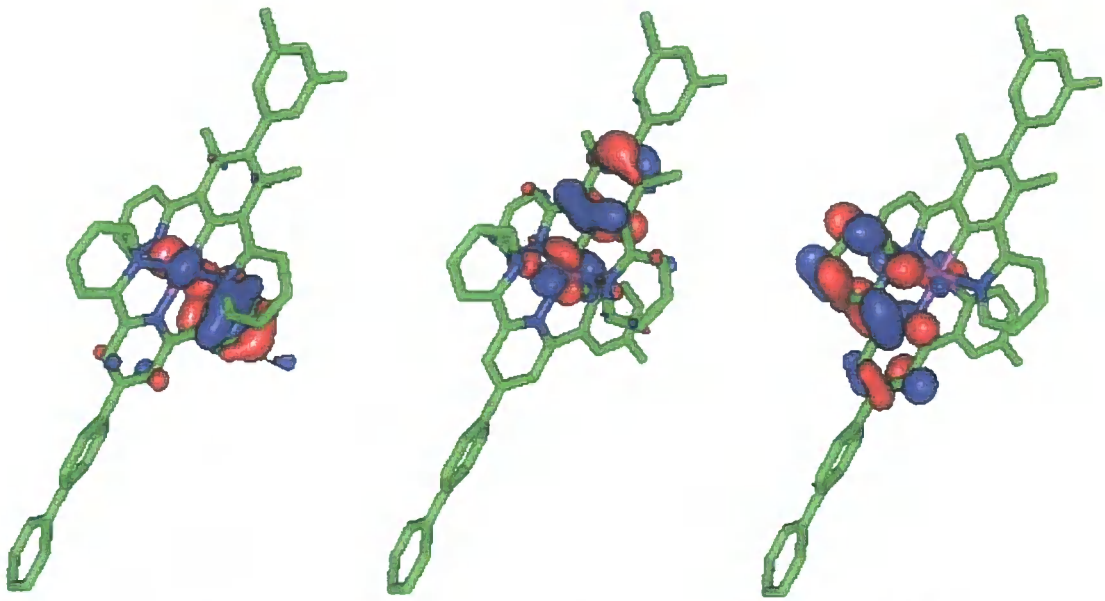

Figure 4.12: Contour plots of the HOMO–1, HOMO and LUMO of [Ir(dpydmb-ϕ-$C_6H_3Me_2$)(mtbpy-ϕ-Br)]$^+$ 66.

4.1.4.3 Photophysical background: Scandola's [Ir(CNC)(NNN)]$^+$ complexes

The [Ir(CNC)(NNN)]$^+$ coordinated complexes with *trans*-disposed carbons, *e.g.* [Ir(tdppy)(tpy-ϕ-Br)]$^+$ recently prepared by Scandola *et al.* are reported to emit deep into the red at ~700 nm, and have small radiative rate constants of the order of 10^4 s^{-1} (Table 10). Their emission is reported to be from a predominantly LLCT excited state, based upon DFT studies revealing a CNC-localised HOMO and tpy-localised LUMO. These LLCT transitions are believed to give rise to the unusually low-energy CT bands (~500 nm) in the absorption spectra.[83, 84]

Complex [a]	λ_{max}^{abs} / nm (ε / M^{-1} cm^{-1})	λ_{max}^{em} / nm	Φ_{em} x 10^2 [b]	τ [c] / μs	k_r / 10^4 s^{-1}	Σk_{nr} / 10^5 s^{-1}
[Ir(tdppy)(tpy-ϕ-Br)]$^+$	514 (9200) 482 (10900) 437 (15000) 323 (53700) 282 (86300)	690	3.5	1.7	1.9	5.7

(a) As its nitrate salt in degassed CH_3CN at 293 K. (b) Luminescence quantum yield measured at 293 K using $[Ru(bpy)_3]Cl_2$ as a standard. (c) Lifetime registered at the emission maximum.

Table 10: Photophysical properties of [Ir(tdppy)(tpy-ϕ-Br)]$^+$.

4.1.4.4 Photophysical studies of the $[M(NCN)(NNC)]^+$ complexes

The photophysical properties of a series of $[Ir(NCN)(NNC)]^+$ coordinated complexes, prepared in this study, bearing two mono-cyclometalating ligands are summarised in Table 11. These complexes contain *cis*-disposed carbons and are found to exhibit very different behaviour to the *trans*-disposed $[Ir(CNC)(NNN)]^+$ complexes (Section 4.1.4.3 and Table 10) reported by Scandola *et al.*[83, 84]

The absorption spectrum of the iridium(III) complex $[Ir(dpydmb)(phbpy)]^+$ **33** in an acetonitrile solution at ambient temperature shows very intense broad bands between 220 and 330 nm (Figure 4.13 and Table 11). Upon comparison with the literature data for the bis-cyclometalated tris-bidentate analogue, $[Ir(ppy)_2(bpy)]^+$,[69] these are assigned to spin-allowed $^1\pi - \pi^*$ transitions of the ligands. Complex **33** also displays a series of bands in the region 330–450 nm which are attributable to spin allowed CT transitions, and a weak low-energy band at approximately 480 nm which is thought to be due to the direct absorption to the lowest-energy triplet state facilitated by the high spin-orbit coupling constant of the iridium centre.

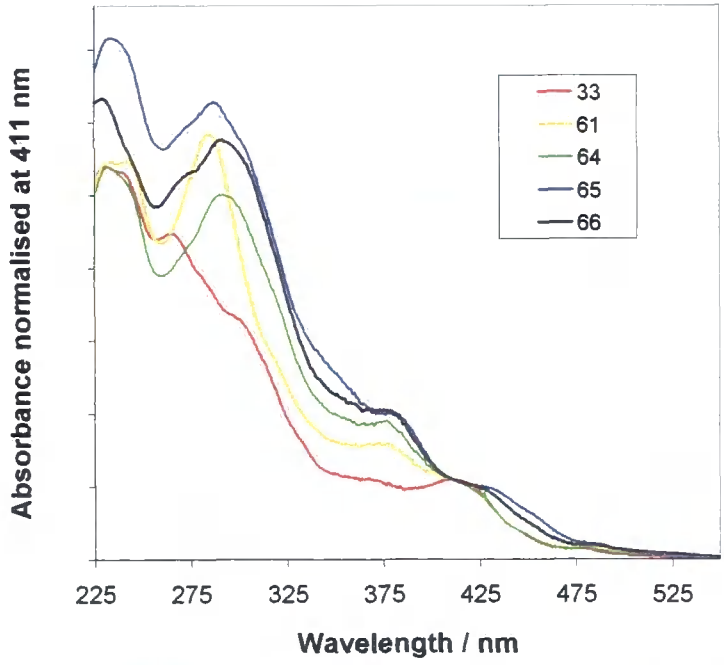

Figure 4.13: Ground-state absorption spectra of the $[Ir(NCN)(NNC)]^+$ series of complexes 33, 61, 64, 65 and 66 in an acetonitrile solution at 298 K, normalised at 411 nm to aid comparison.

Complex [a]	$[Ir(ppy)_2(bpy)]^+$ [68, 235]	**33** $[Ir(dpydmb)(phbpy)]^+$	**61** $[Ir(dpydmb)(mtbpy\text{-}\phi\text{-}Br)]^+$	**64** $[Ir(dpydmb)(mtbpy\text{-}\phi\text{-}ph)]^+$	**65** $[Ir(dpydmb\text{-}Br)(mtbpy\text{-}\phi\text{-}ph)]^+$	**66** $[Ir(dpydmb\text{-}C_6H_3Me_2)(mtbpy\text{-}\phi\text{-}ph)]^+$
Absorption maxima / nm (ε / M^{-1} cm^{-1})	465 (724) 405 (3710) 370 (6160) 334 (9210) 303 (22400) 265 (44100) 256 (45800)	479 (640) 411 (5490) 367 (5360) 294 sh (16600) 265 (22100) 240 (24500)	479 (1800) 411 sh (12100) 372 (17900) 284 (65200) 242 (61600) 232 (61700)	479 (1940) 412 sh (13200) 375 (23200) 293 (60900) 232 (65300)	483 (1600) 425 (8160) 376 (16300) 286 (50700) 235 (58000)	481 (4160) 420 (23400) 375 (47500) 293 (136000) 273 sh (122000) 229 (149000)
Emission maximum / nm	610	632	639	636	625	644
Emission maxima at 77 K / nm	520	544, 576 [f]	556, 592 [f]	553, 590 [f]	544, 582 [f]	556, 593 [f]
Φ_{em} x 10^{2} [b] degassed (aerated)	9.7 (1.8)	2.3 (0.81)	2.8 (1.1)	6.3 (2.5)	4.8 (1.6)	2.9 (1.2)
Lifetime [c] / µs degassed (aerated)	0.37 (0.066)	0.12 (0.049)	0.13 (0.053)	0.15 (0.057)	0.12 (0.063)	0.1 (0.047)
Lifetime at 77 K [c] / µs	–	3.6 [f]	3.9 [f]	4.0 [f]	4.3 [f]	3.5 [f]
k_r [d] / 10^4 s^{-1}	–	19	22	42	25	29
Σk_{nr} [d] / 10^5 s^{-1}	–	81	75	63	50	97
$k_Q^{O_2}$ [e] / 10^{10} M^{-1} s^{-1}	–	0.64	0.59	0.57	0.56	0.59

(a) Complexes as their hexafluorophosphate salts in degassed CH_3CN at 298 K, except where stated otherwise. (b) Luminescence quantum yield measured at 298 K using $[Ru(bpy)_3]Cl_2$ as a standard. (c) Lifetime registered at the emission maximum following excitation at 374 nm. (d) Radiative and non-radiative rate constants calculated from τ and Φ values at 298 K. (e) Bimolecular rate constant for quenching by O_2, estimated from τ in degassed and aerated solutions. (f) In an EPA glass at 77 K.

Table 11: Photophysical properties of the $[Ir(NCN)(NNC)]^+$ coordinated complexes.

The absorption spectra of the other $[Ir(NCN)(NNC)]^+$ coordinated complexes are all very similar to that of the parent complex, **33**, with only a few notable differences being observed (Figure 4.13). The introduction of a bromophenyl pendant into the NNC ligand of the modified complex, $[Ir(dpydmb)(mtbpy\text{-}\phi\text{-}Br)]^+$ **61** (Table 11), results in the appearance of a relatively sharp and well-defined LC transition centred at 285 nm. This feature persists in the elaborated complexes, $[Ir(dpydmb)(mtbpy\text{-}\phi\text{-}ph)]^+$ **64**, $[Ir(dpydmb\text{-}Br)(mtbpy\text{-}\phi\text{-}ph)]^+$ **65** and $[Ir(dpydmb\text{-}\phi\text{-}C_6H_3Me_2)(mtbpy\text{-}\phi\text{-}ph)]^+$ **66** (Table 11). Similarly, a band at 280 nm was previously reported by this group for $[Ir(tpy)_2]^{3+}$ based complexes bearing biphenyl pendants.[54] The well-resolved CT transition band observed at 411 nm in the parent complex **33** becomes less prominent in complexes **61** and **64–66** due to their increased absorption around 375 nm. Complexes **65** and **66** also display a slight red-shift in the two lowest-energy absorption bands at approximately 411 nm and 480 nm, indicating that their energy is affected by the NCN ligand substitution.

Whilst the position of the bands in the absorption spectra are similar to those seen in the analogous *cis*-cyclometalated tris-bidentate complex $[Ir(ppy)_2(bpy)]^+$, the spectra are significantly different to those of the *trans*-cyclometalated complexes *e.g.* $[Ir(tdppy)(tpy\text{-}\phi\text{-}Br)]^+$ (Table 10) which displays intense bands at much lower energies.[83, 84] DFT calculations can be used to help rationalise these differences. In the case of Scandola's *trans*-disposed $[Ir(CNC)(NNN)]^+$ complexes,[83, 84] DFT calculations revealed a HOMO comprising of both metal and dppy character, and a tpy-localised LUMO as in the $[Ir(NCN)(NNC)]^+$ complexes (Section 4.1.4.2), where the LUMO is based on the bpy-moiety of the NNC ligand. The lower-energy absorption bands in the $[Ir(CNC)(NNN)]^+$ coordinated complex $[Ir(tdppy)(tpy\text{-}\phi\text{-}Br)]^+$ are attributed to the increased delocalisation across the three pyridyl rings of tpy compared to the two rings of the bpy-moiety of the NNC ligand. This leads to the lowering in energy of the ligand π^* acceptor orbitals and the destabilisation of the HOMO in these *trans*-disposed complexes.

The series of $[Ir(NCN)(NNC)]^+$ coordinated complexes (**33**, **61**, **64**, **65** and **66**) all display single, structureless emission bands with $\lambda_{max} \sim 630$ nm in degassed acetonitrile solution at 298 K (Figure 4.15 and Table 11), characteristic of emission from a charge-transfer excited state. Based upon DFT calculations (Section 4.1.4.2) this emission is

assigned as being phosphorescence from an excited state with mixed ^{3}d(Ir)/π(NCN)→π*(NNC) character (MLCT/LLCT). The excitation and emission spectra (at 298 and 77 K) of the parent complex, [Ir(dpydmb)(phbpy)]$^+$ **33**, are shown in Figure 4.14.

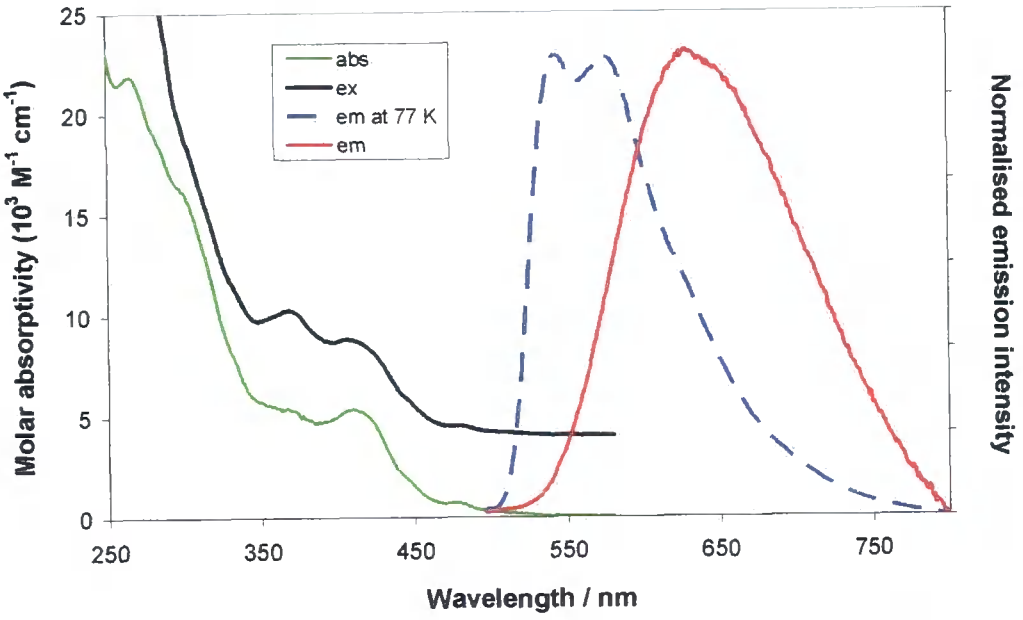

Figure 4.14: Absorption and normalised emission spectra (λ_{ex} = 410 nm) for [Ir(dpydmb)(phbpy)]$^+$ 33 in MeCN at 298 K with an overlaid excitation spectrum (λ_{em} = 600 nm) offset for clarity. The emission spectrum at 77 K in an EPA glass (λ_{ex} = 410 nm) is also shown.

A large blue-shift in the emission maximum is observed upon cooling to 77 K in a rigid glass, typical of CT transitions in which extensive molecular reorganisation accompanies the formation of the excited state. Like the absorption, the emission of the parent complex, **33**, is similar to that observed from the tris-bidentate analogue [Ir(ppy)$_2$(bpy)]$^+$, which also displays a large hypsochromic-shift upon cooling to 77 K.[238] Mirroring the observations made for the absorption spectra, the emission differs significantly from that of Scandola's *trans*-cyclometalated complex [Ir(tdppy)(tpy-ϕ-Br)]$^+$, where λ_{max} = 690 nm.[83]

The introduction of aryl substituents in complexes **61**, **64**, **65** and **66** was found to only have a small influence on the emission maximum (Figure 4.15), with a variation of just 470 cm^{-1} across the whole series.

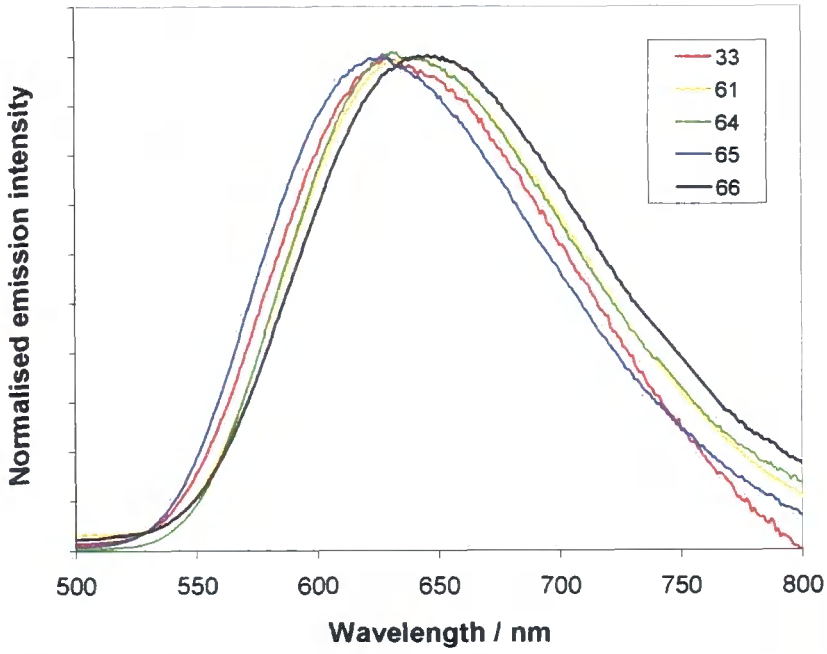

Figure 4.15: Normalised emission spectra of the $[Ir(NCN)(NNC)]^+$ series of complexes 33, 61, 64, 65 and 66 in a degassed acetonitrile solution at 298 K (λ_{ex} = 410 nm).

The luminescence lifetimes of the iridium complexes **33**, **61**, and **64–66** (Table 11) are of the order of 100–200 ns, ~100 times shorter than those observed for Scandola's $[Ir(CNC)(NNN)]^+$ coordinated complexes,[83, 84] and are reduced by a factor of 2–3 in air-equilibrated solution. The luminescence quantum yield of the unsubstituted complex **33** (0.023) is found to be comparable to that calculated for the well-known tris-bidentate analogue $[Ir(ppy)_2(bpy)]^+$ (0.018).[238] It increases upon the introduction of the bromophenyl pendant into the NNC ligand in **61** and further still for the biphenyl appended complex **64**, brought about primarily by an increase in the radiative rate constant (Table 11). In contrast, the introduction of a bromo (**65**) and subsequent aryl-substituent (**66**) into the NCN ligand results in a small decrease in their quantum yields owing to a small decrease in k_r and an increase in Σk_{nr}.

The radiative rate constants of these *cis*-cyclometalated complexes (Table 11) were found to be one order of magnitude greater than the values found for Scandola's *trans*-cyclometalated $[Ir(CNC)(NNN)]^+$ complexes (Table 10),[83, 84] probably due to less LLCT character and a larger contribution of the metal in the HOMO. However, owing to a comparable ratio of the radiative and non-radiative rate constants in these *trans*-cyclometalated complexes, the luminescence quantum yields are of a similar magnitude to the $[Ir(NCN)(NNC)]^+$ complexes reported herein.

In addition to the $[Ir(NCN)(NNC)]^+$ series of complexes described above the photophysical properties of the Rh(III) complex $[Rh(dpydmb)(phbpy)]^+$ **34** were investigated and are summarised in Table 12 alongside the well-known tris-bidentate analogue $[Rh(ppy)_2(bpy)]^+$.[69, 103]

Complex [a]	$[Rh(ppy)_2(bpy)]^+$ [103]	**34** $[Rh(dpydmb)(phbpy)]^+$
Absorption maxima / nm (ε / M^{-1} cm^{-1})	367 (800) 297 (36000) 257 (55000) 239 (53000)	393 (7860) 299 (25600) 261 (33500) 230 (39900)
Emission maxima at 77 K / nm	520 [b]	468, 506, 546, 583 [e]
Lifetime at 77 K / μs	170	57, 166 [e, f]

(a) Complexes as their hexafluorophosphate salts in degassed CH_3CN at 298 K, except where stated otherwise. (b) In a EtOH:MeOH (5:1) glass at 77 K. (e) In an EPA glass at 77 K. (f) τ obtained using a xenon lamp at λ_{ex} = 393 nm.

Table 12: Photophysical properties of $[Rh(dpydmb)(phbpy)]^+$ 34.

Like the $[Ir(NCN)(NNC)]^+$ complexes, the absorption spectrum of **34** (Figure 4.16) is dominated by a series of high intensity bands in the range 220–330 nm which are assigned to LC transitions. In addition to these, a well defined band is observed at 393 nm, which is assigned to an MLCT transition based upon the assignment of the band at 366 nm reported for the tris-bidentate complex $[Rh(ppy)_2(bpy)]^+$.[69, 103] The equivalent band in $[Ir(dpydmb)(phbpy)]^+$ occurs at slightly lower energy (411 nm). In agreement with the $[M(dpydmb)(bpy)Cl]^+$ complexes (M = Ir **30** and Rh **31**) reported herein and the tris-bidentate $[M(ppy)_2(bpy)]^+$ complexes in the literature,[69] the CT bands in **34** do not extend to as low-energy as in the analogous iridium complex **33**.

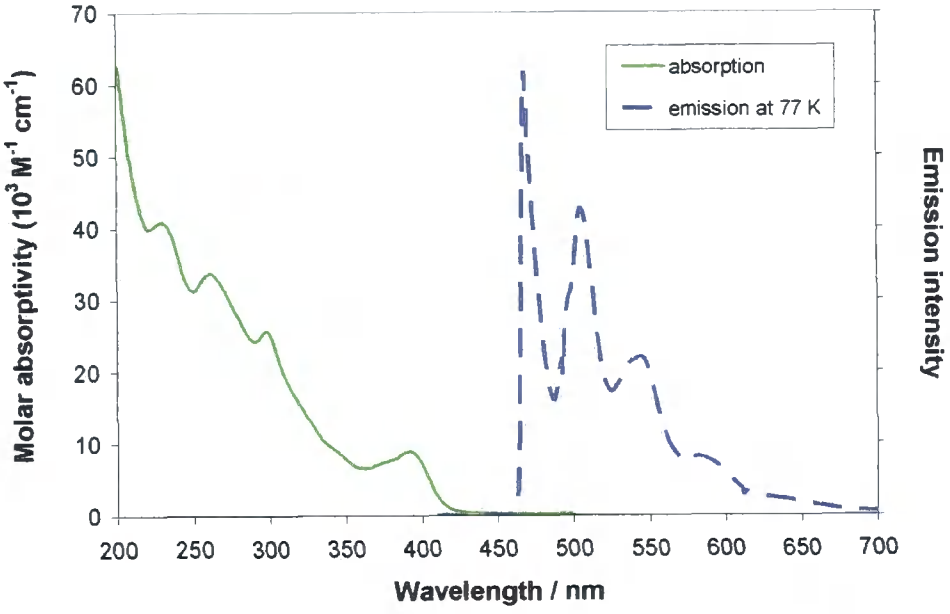

Figure 4.16: The absorption spectrum of $[Rh(dpydmb)(phbpy)]^+$ 34 in MeCN at 298 K and the emission spectrum at 77 K in an EPA glass (λ_{ex} = 393 nm).

Upon excitation at a range of wavelengths between 350 and 450 nm, $[Rh(dpydmb)(phbpy)]^+$ **34** was found to be non-emissive in acetonitrile solution at 298 K. However, cooling to 77 K in a rigid EPA glass results in highly structured emission centred at around 520 nm (Figure 4.16 and Table 12). Similarly, $[Rh(ppy)_2(bpy)]^+$ was reported to be non-emissive at temperatures above 222 K and yet displays structured emission (λ_{max} = 520 nm) with a long luminescence lifetime (170 μs) at 77 K (Table 12) from a predominantly LC (ppy-based) excited state with some MLCT character.[103] The emission from complex **34** at 77 K was found to decay in a biexponential fashion with lifetimes of 57 μs and 166 μs, suggesting that it may originate from two excited states which are poorly coupled. However, heterogeneity in frozen glass samples can sometimes give rise to apparent biexponential decays.

4.1.5 Charge-neutral [M(NCN)(NC)Cl] and [Ir(NCN)(CNC)] complexes

It was hoped that the introduction of a third anionic group (*e.g.* a chloride ion or cyclometalating carbon) into the coordination sphere of the metal centre would result in complexes with high luminescence quantum yields. The synthesis of range of charge-neutral [M(NCN)(NC)Cl] (M = Ir or Rh) coordinated complexes has been discussed in Section 2.2.2.6, and their electrochemical and photophysical properties reported in Sections 4.1.5.1 and 4.1.5.3 respectively. Unfortunately in this study a stable, pure

sample of the charge-neutral [Ir(NCN)(CNC)] coordinated complex [Ir(dpydmb)(F_2dppy)] **36** suitable for photochemical analysis was unobtainable (Section 2.2.2.3). However, the photophysical properties (Table 12) of the related non-fluorinated and tetra-fluorinated complexes, [Ir(dpydmb)(dppy)] and [Ir(dpydmb)(F_4dppy)], have previously been reported by this research group and are discussed in detail in Section 1.3.2.2.[76, 78]

4.1.5.1 Electrochemical studies of the [M(NCN)(NC)Cl] complexes

The electrochemical properties of the charge-neutral complexes [Ir(tpyb)(ppy)Cl] **41** and [Rh(dpydmb)(ppy)Cl] **40** were studied at 298 K within the range of –2.5 to +2.0 V in the presence of 0.1 M Bu_4NBF_4 (in acetonitrile) as the supporting electrolyte. The results are summarised in Table 13 which also includes the complex [Ir(dpydmb)(ppy)Cl] previously prepared by this laboratory.

Complex [a]	$E_{1/2}^{ox}$ / V	ΔE^{ox} / mV [b]	$E_{1/2}^{red}$ / V	ΔE^{red} / mV [b]
41 [Ir(tpyb)(ppy)Cl]	0.90	80	– 1.85 – 2.02	80 90
40 [Rh(dpydmb)(ppy)Cl]	1.07	100	– 1.63	180
[Ir(dpydmb)(ppy)Cl] [239]	0.96	100	–	–

(a) Complexes as their PF_6^- salts in Bu_4NBF_4 (0.1 M in MeCN) as the supporting electrolyte. (b) ΔE^{ox} and ΔE^{red} are the peak to peak separation of the reversible oxidation and reduction processes respectively. These values were measured at a scan rate of 300 mV s^{-1} and are reported relative to SCE, measured using ferrocene as the standard ($E_{1/2}^{ox}$ = 0.42 V *vs.* SCE).

Table 13: Oxidation and reduction potentials of the [M(NCN)(NC)Cl] (M = Ir or Rh) coordinated complexes obtained by cyclic voltammetry.

[Ir(tpyb)(ppy)Cl] **41** revealed a single reversible oxidation process at 0.90 V *vs.* SCE (Figure 4.5) which, in line with the other cyclometalated complexes in this study, is thought to arise from the removal of an electron spanning the metal centre and the two cyclometalating phenyl rings. This compares to a potential of 0.96 V for the related complex [Ir(dpydmb)(ppy)Cl],[239] and 0.70 V for the well-studied tris-bidentate complex *fac*-[Ir(ppy)$_3$] where delocalisation over a third cyclometalating ring facilitates oxidation.[61] As expected, the oxidation potential of complex **41** is lower than that of the

related cationic complex $[Ir(tpyb)(bpy)Cl]^+$ **32** (0.95 V). This is due to the increased stability and facilitation of oxidation that accompanies the reduction of the positive charge on the complex. Further comparison of complexes **41** and **32** with their respective parent complexes, [Ir(dpydmb)(ppy)Cl] and $[Ir(dpydmb)(bpy)Cl]^+$ **33** (1.28 V), reveals a smaller difference in oxidation between the substituted and parent charge-neutral complex. This is the result of the increased delocalisation of the HOMO and thus oxidation in the charge-neutral complexes and subsequently reduced influence of the π-donating pyridyl-pendant.

Two reversible reductions were also observed for complex **41**, which are based upon the two isolated pyridyl rings. The first occurs at –1.85 V *vs.* SCE, and compares to a potential of –1.80 V in *fac*-$[Ir(ppy)_3]$ where the reduction must also be based upon an isolated pyridyl ring.[61] The first reduction process in complex **41** occurs at a significantly more negative potential than that of $[Ir(tpyb)(bpy)Cl]^+$ **32** (–1.04 V), due to the reduction being based on an isolated pyridyl ring of the NCN ligand rather than the bpy ligand where electron density is delocalised over the two pyridyl rings. Surprisingly no reduction processes were observed for the analogously coordinated complex [Ir(dpydmb)(ppy)Cl].[239]

Electrochemical analysis of [Rh(dpydmb)(ppy)Cl] **40** revealed a reversible oxidation process at 1.07 V *vs.* SCE. Based upon DFT calculations (Section 4.1.5.2) and akin to complex **41**, this was assigned to the removal of an electron from an orbital that spans both the metal centre and the two cyclometalating phenyl rings. A reversible oxidation process at a potential of 0.96 V was similarly observed for [Ir(dpydmb)(ppy)Cl],[239] which in line with the other complexes reported herein indicated that Rh(III) complexes are harder to oxidise than those with Ir(III) centres. Complex **40** also displays a reversible reduction process at –1.63 V *vs.* SCE which like complex **32** was assigned to an isolated pyridyl ring on the NCN ligand.

4.1.5.2 Computational studies of the [M(NCN)(NC)Cl] complexes

DFT calculations were carried out on [Rh(dpydmb)(ppy)Cl] **40**. The calculated orbital characteristics for the three highest energy molecular orbitals and the three lowest energy unoccupied molecular orbitals are summarised in Table 14.

Complex	HOMO–2	HOMO–1	HOMO	LUMO	LUMO+1	LUMO+2
40 [Rh(dpydmb)(ppy)Cl]	NCN (30%) NC (11%) Cl (56%)	Rh (37%) NCN (18%) Cl (39%)	Rh (31%) NC (11%) Cl (54%)	NCN (96%)	NC (92%)	NCN (90%)

Table 14: Calculated molecular orbital characteristics of [Rh(dpydmb)(ppy)Cl] according to DFT calculations. The percentages in parentheses denote the proportion of the total electron density localised at that site.

These studies reveal that electron density in the HOMO is delocalised over the phenyl ring of the ppy ligand, the rhodium centre and the chloride, whilst the HOMO–1 is localised on the phenyl ring of the dpydmb (NCN) ligand, the chloride and the rhodium centre and the LUMO delocalised across the three rings of the dpydmb ligand (Table 14 and Figure 4.17). This is indicative of emission from a mixed MLCT(M→NCN)/ LC(NCN π-π*) excited state.

Whilst the calculations are suggestive of there being a contribution from the chloride, photophysically this is not expected. However, if the chloride were to be replaced by another ligand, then a significant influence on the oxidation potential and photophysical properties of the complex might be anticipated.

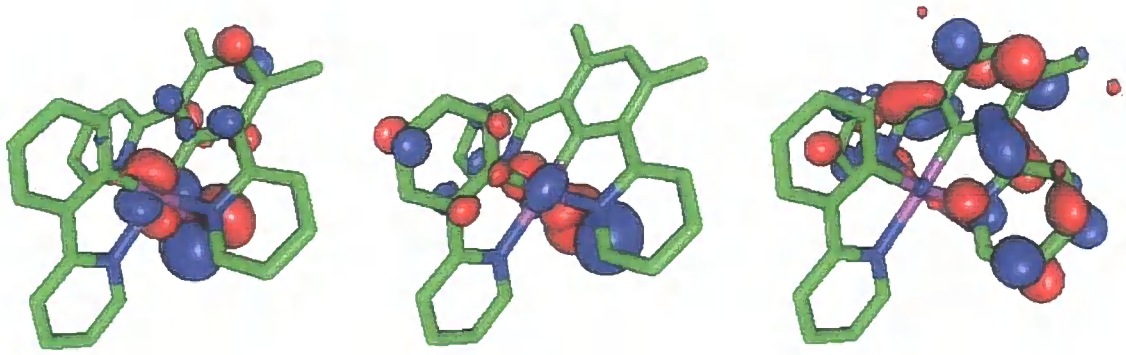

Figure 4.17: Contour plots of the HOMO–1, HOMO and LUMO of [Rh(dpydmb)(ppy)Cl] 40.

4.1.5.3 Photophysical studies

The photophysical properties of the charge neutral [M(NCN)(NC)Cl] coordinated complexes [Ir(tpyb)(ppy)Cl] **41,** [Ir(dpydmb)(pzb)Cl] **42** and [Rh(dpydmb)(ppy)Cl] **40** were investigated and are summarised in Table 15.

Complex [a]	**41** [Ir(tpyb)(ppy)Cl]	**42** [Ir(dpydmb)(pzb)Cl]	**40** [Rh(dpydmb)(ppy)Cl]	[Ir(dpydmb)(ppy)Cl][75]	[Ir(dpydmb)(dppy)]$^{+}$ [77]
Absorption maxima / nm (ε / M^{-1} cm^{-1})	497 (1420) 462 (2830) 415 (6500) 319 (17900) 283 (35500) 225 (29000)	490 (755) 417 (5700) 370 (3520) 290 (17600) 243 (27600) 222 (25800)	381 (4140) 294 (11200) 268 (12900) 222 (15100)	492 (1300) 455 (3600) 417 (11300) 399 (10000) 369 (7800) 353 (6200) 285 (37000) 258 (39700) 239 (44700)	510 (7300) 481 (6800) 458 (5500) 406 (6500) 378 (6900) 349 (7700) 269 (46900)
Emission maxima / nm	516, 550	505, 537	508, 537	508, 540	585
Emission maxima at 77 K / nm	502, 541 [f]	490, 529, 567 [f]	469, 485 sh, 499, 505, 542, 582 [f]	–	–
Φ_{em} x 10^{2} [b] degassed (aerated)	18 (0.52)	74 (0.81)	1.1 (< 0.1)	76	21
Lifetime [c] / μs degassed (aerated)	1.9 (0.044)	1.7 (0.29)	44 [g] (0.63)	1.6	3.8
Lifetime at 77 K [c] / μs	21 [f, h]	11, 120 [f, h]	45, 120 [f, i]	–	–
k_r [d] / 10^4 s^{-1}	9.3	44	0.025	48	5.5
Σk_{nr} [d] / 10^5 s^{-1}	4.3	1.5	0.22	1.5	2.1
$k_Q^{O_2}$ [e] / 10^{10} M^{-1} s^{-1}	1.2	0.15	0.082	–	–

(a) Complexes as their hexafluorophosphate salts in degassed CH_3CN at 298 K, except where stated otherwise. (b) Luminescence quantum yield measured at 298 K using $[Ru(bpy)_3]Cl_2$ as a standard. (c) Lifetime registered at the emission maximum following excitation at 374 nm. (d) Radiative and non-radiative rate constants calculated from τ and Φ values at 298 K. (e) Bimolecular rate constant for quenching by O_2, estimated from τ in degassed and aerated solutions. (f) In an EPA glass at 77 K. (g) τ obtained using a xenon lamp with λ_{ex} = 385 nm. (h) τ obtained using a xenon lamp with λ_{ex} = 415 nm. (i) τ obtained using a xenon lamp with λ_{ex} = 370 nm

Table 15: Photophysical properties of the charge-neutral [M(NCN)(NC)Cl] (M = Ir or Rh) and [Ir(NCN)(CNC)] coordinated complexes.

The ground-state absorption spectra of the iridium complexes [Ir(tpyb)(ppy)Cl] **41** and [Ir(dpydmb)(pzb)Cl] **42** show a number of intense bands below 300 nm corresponding to $^1\pi$–π^* transitions in the ligands, alongside a weaker band at around 415 nm which is assigned to MLCT transitions, similar to the analogously coordinated complex [Ir(dpydmb)(ppy)Cl] (Table 15).[76] These MLCT bands are blue-shifted with respect to those previously reported at around 500 nm for the tris-cyclometalated [Ir(NCN)(CNC)] coordinated complex [Ir(dpydmb)(dppy)] (Table 15).[78] This shift is due to the lowering of the HOMO upon substitution of a cyclometalating carbon atom with a weaker field chloride. A series of weak bands extending to low energies (at approximately 460 and 490 nm) are also observed in complexes **41** and **42**, similar to those observed in the $[Ir(NCN)(NNC)]^+$ complexes. These are assigned to the direct absorption to the lowest-energy triplet state ($^1S \rightarrow {}^1T$), which is facilitated by the high spin-orbit coupling constant of the iridium centre.

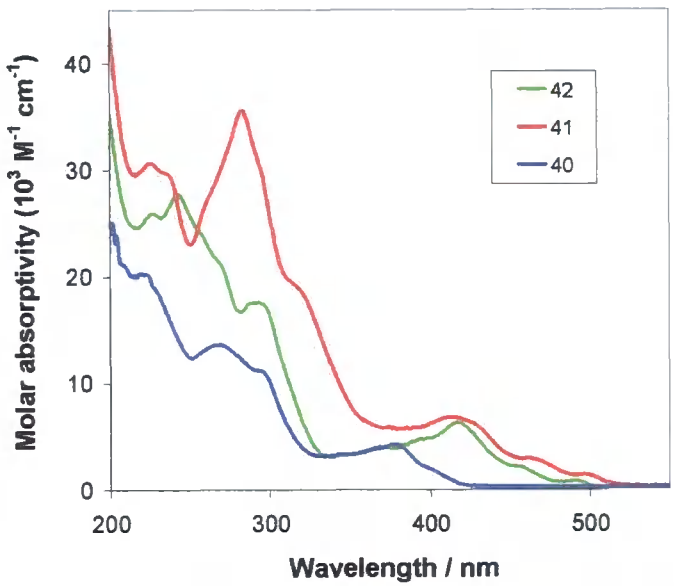

Figure 4.18: Ground-state absorption spectra of the [M(NCN)(NC)Cl] (M = Ir or Rh) complexes 40, 41 and 42 in an acetonitrile solution at 298 K.

Complexes **41** and **42** exhibit structured luminescence at ambient temperature (Figure 4.19 and Table 15), with a maximum at around 500 nm, similar to that observed for the analogously coordinated complex [Ir(dpydmb)(ppy)Cl] (Table 15).[76] This differs significantly from the broad, structureless emission (λ_{max}^{em} = 585 nm) observed from the tris-cyclometalated complex [Ir(dpydmb)(dppy)] (Table 15) which was reported to of mixed MLCT/LLCT/LC character based upon DFT calculations.[78] The increased

structure and blue-shifted emission profile of the [Ir(NCN)(NC)Cl] complexes compared to [Ir(dpydmb)(dppy)] is indicative of more LC character in the excited state of the former, owing to the lowering of the HOMO relative to the NCN-based LUMO, upon substitution of a strong field cyclometalating carbon with a chloride. In line with [Ir(dpydmb)(ppy)Cl],[76] the emission from complexes **41** and **42** is assigned as being from a mixed MLCT(Ir→NCN)/LC(NCN π–π^*) excited state, owing to the HOMO having a comparable energy to the NCN ligand's π-orbital. The blue-shift in the emission maximum on cooling to 77 K in a rigid EPA glass is typical of CT transitions, in which extensive molecular reorganisation accompanies the formation of the excited state.

Comparison of the [Ir(NCN)(NC)Cl] coordinated complexes reveals that the introduction of a σ-withdrawing pyridyl-substituent into the NCN ligand of complex **41** brings about a slight red-shift in the emission profile compared to that of [Ir(dpydmb)(ppy)Cl] (Table 15),[76] whilst the replacement of the NC-coordinating ppy ligand with its pyrazolyl analogue, pzb, in complex **42** has no noticeable effect (Figure 4.19 and Table 15).

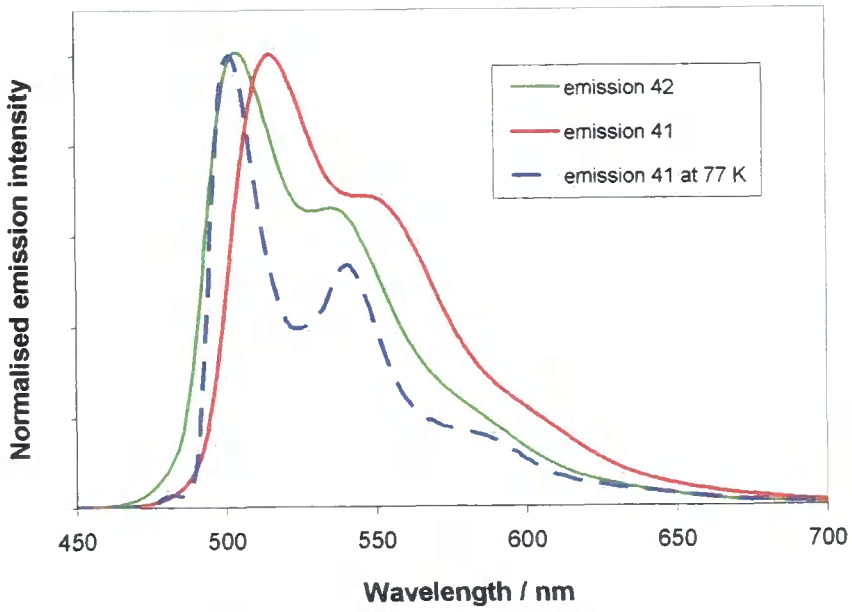

Figure 4.19: Normalised emission spectra of the [Ir(NCN)(NC)Cl] coordinated complexes [Ir(tpyb)(ppy)Cl] 41 (λ_{ex} = 415 nm) and [Ir(dpydmb)(pzb)Cl] 42 (λ_{ex} = 370 nm) in degassed MeCN at 298 K alongside 41 in an EPA glass at 77 K.

The luminescence quantum yield (0.74) and lifetime (1.7 μs) of [Ir(dpydmb)(pzb)Cl] **42** (Table 15) in degassed acetonitrile solution are almost identical to those reported for [Ir(dpydmb)(ppy)Cl] (Table 15),[76] indicating that the substitution of the ppy ligand with pzb, containing a pyrazolyl ring instead of a pyridyl ring, has little effect on the luminescent properties of the complex. These quantum yields are approximately a four-fold improvement upon that reported by Wilkinson for the tris-cyclometalated complex, [Ir(dpydmb)(dppy)] (Table 15).[78] This increased luminescence arises from the blue-shift in the emission maximum, where the energy-gap law predicts a decrease in the non-radiative rate constant, upon substitution of a strong field cyclometalating carbon with a chloride.[6] The presence of the electron-withdrawing pyridyl-pendant in complex **41** compared to [Ir(dpydmb)(ppy)Cl][76] brings about a reduction in emission intensity, owing to an approximately five-fold decrease in the k_r accompanied by a three-fold increase in Σk_{nr}, which results from a reduction in the electron density at the metal centre decreasing the extent of MLCT character in the emissive state. The emission from both complexes **41** and **42** is strongly quenched by oxygen, analogous to the charge-neutral complexes [Ir(dpydmb)(ppy)Cl][76] and [Ir(dpydmb)(dppy)][78] previously reported by Wilkinson.

In addition to the [Ir(NCN)(NC)Cl] coordinated complexes described above the photophysical properties of the Rh(III) complex [Rh(dpydmb)(ppy)Cl] **40** were investigated and are summarised in Table 15. The absorption spectrum of **40** (Figure 4.18), like those of the Ir(III) complexes, is dominated by a series of intense bands below 300 nm corresponding to $^1\pi$–π^* transitions in the ligands and a single band at 381 nm corresponding to an MLCT transition. The band at 381 nm is considerably blue-shifted compared to the equivalent band (~ 415 nm) in the Ir(III) complexes. The weak low-energy $S_0 \rightarrow T_1$ transition bands (460 and 490 nm) observed in the iridium complexes are not seen in complex **40**, due to poorer ISC in the rhodium complex.

Structured emission was observed from [Rh(dpydmb)(ppy)Cl] **40** at ambient temperature, following excitation 385 nm (Table 15 and Figure 4.20). Upon comparison with the related iridium complexes [Ir(dpydmb)(ppy)Cl],[76] [Ir(tpyb)(ppy)Cl] **41** and [Ir(dpydmb)(pzb)Cl] **42**, it was found that following excitation at wavelengths lying within the MLCT bands of their absorption spectra (~ 380 and ~ 415 nm respectively) the emission profiles were very similar. The emission from

complex **40** was assigned as being from a mixed MLCT(M→NCN)/LC(NCN π-π*) excited state, based upon DFT calculations (Section 4.1.5.2) and the emission from the analogous iridium complex, [Ir(dpydmb)(ppy)Cl].

Complex **40** is the only Rh(III) complex prepared within this study to emit at 298 K and is one of only a handful of related complexes from the literature to emit in fluid solution: namely $[Rh(pba)_2(NN)]^+$ (pba = 4-(2-pyridyl)benzaldehyde and NN = bpy, phen *etc.*),[240] $[Rh(bpy)_3]^{3+}$ (barely emissive above 268 K)[89] and $[Rh(ppy)_2(bpy)]^+$ (only emissive up to 222 K).[103] Upon comparison of the luminescence quantum yields of complex **40** (Φ = 1.1) to the equivalent Ir(III) complex [Ir(dpydmb)(ppy)Cl] (Φ = 0.76), however, the former is found to be approximately 70 times less emissive. This low emission intensity results from the very small value of k_r, which is in part expected since second row rhodium will not facilitate the spin-forbidden-transition as well as third row iridium. This is in agreement with the $[M(NCN)(NNN)]^{2+}$ (M = Rh or Ir), $[M(NCN)(NN)Cl]^+$, $[M(NCN)(NNC)]^+$ coordinated complexes reported within this study and $[M(tpy)_2]^{3+}$,[46, 98] $[M(bpy)_3]^{3+}$,[40, 89] $[M(ppy)_2(bpy)]^+$,[69, 103] and $[M(pba)_2(NN)]^+$ [240] from the literature, where the iridium complexes are significantly more emissive than those of rhodium which, with the exception of $[Rh(pba)_2(NN)]^+$, are all non-emissive at ambient temperature.

A luminescence lifetime of 44 μs is observed for [Rh(dpydmb)(ppy)Cl] **40** in degassed acetonitrile solution at 298 K, which compares to only 1.6 μs for [Ir(dpydmb)(ppy)Cl].[76] The significantly longer lifetime of the rhodium complex is in agreement with that observed for the $[M(dpydmb)(phbpy)]^+$ (M = Rh or Ir) complexes at 77 K in Section 4.1.4.4 and for the $[M(pba)_2(NN)]^+$,[240] and $[M(ppy)_2(bpy)]^+$ [69, 103] complexes in the literature.

Upon cooling to 77 K in a rigid EPA glass, the emission profile of complex **40** becomes blue-shifted and more structured (Figure 4.20), consistent with CT transitions in which extensive molecular reorganisation accompanies the formation of the excited state.

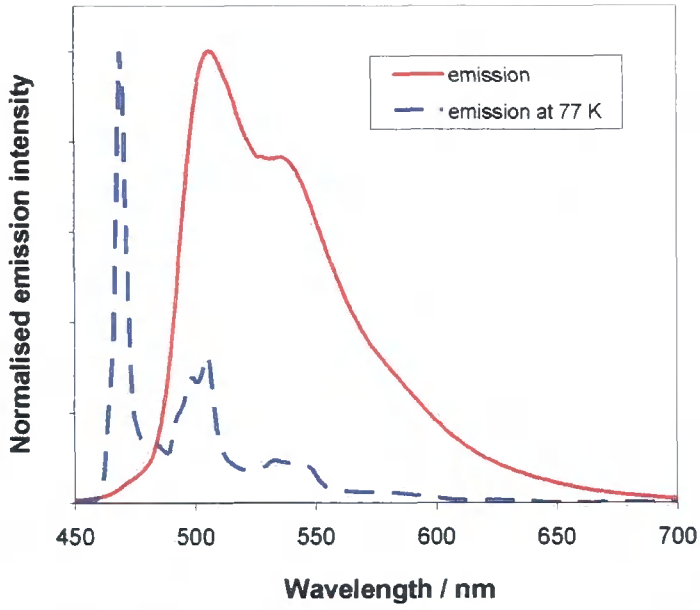

Figure 4.20: Normalised emission spectra of [Rh(dpydmb)(ppy)Cl] 40 in degassed MeCN at 298 K (λ_{ex} = 385 nm) and in an EPA glass at 77 K (λ_{ex} = 468 nm).

4.1.6 The influence of cyclometalation on the excited states of iridium bis-terdentate complexes

In this chapter the luminescence properties of a series of isostructural bis-terdentate iridium(III) complexes containing terpyridyl, dipyridylbenzene and diphenylpyridine ligands have been discussed, differing only in their relative number of pyridyl and cyclometalating phenyl rings. With the exception of Scandola's [Ir(CNC)(NNN)] complexes,[83, 84] the complexes were all prepared either in this study or in the preceding work by Wilkinson.[206] This has allowed the influence of cyclometalation on the luminescence properties of the complexes to be evaluated.

A trend is identified, going from the ligand-centred (LC) luminescence of the bis-terpyridyl $[IrN_6]^{3+}$ complexes through to the charge-neutral tris-cyclometalated $[IrN_3C_3]$ complexes with predominantly metal-to-ligand charge transfer (MLCT) states. Lying in between the two extremes are the mono-cyclometalated $[IrN_5C]^{2+}$ complexes, displaying predominantly ligand-to-ligand charge-transfer (LLCT) character, alongside the bis-cyclometalated complexes $[IrN_4C_2]^{+}$ whose emission is determined by whether the two cyclometalated carbons are *trans*-orientated in the same ligand (predominant LLCT character) or *cis*-orientated in different ligands (mixed LLCT/MLCT character).

This trend can be explained upon consideration of the likely effect of cyclometalation upon the metal and ligand-based orbitals (Figure 4.21). In the $[Ir(tpy)_2]^{3+}$ complexes, the metal d-orbitals are low enough in energy and the ligand π–π^* energy gap sufficiently large to result in a LC emissive state. Upon the introduction of an electron-rich pendant, the HOMO becomes localised on a different part of the ligand and an $n \rightarrow \pi^*$ or $\pi \rightarrow \pi^*$ intra-ligand charge transfer (ILCT) excited state arises.

The replacement of one of the pyridyl rings with a cyclometalating phenyl ring brings about the destabilisation of the metal d-orbitals and a simultaneous rise in the relevant ligands π and π^*-orbitals. Since the molecular orbitals of the NNN ligand are barely affected by the substitution, a switch in the relative ordering of the HOMO and LUMO ligand localisation may occur. This leads to an LLCT emissive state (cyclometalated ligand→NNN ligand), where the lack of metal character results in a low radiative rate constant and thus in weak emission.

The introduction of a second cyclometalating ring into the same ligand, *i.e.* $[Ir(CNC)(NNN)]^+$, results in a further equivalent shift in the energy levels, thus bringing the metal d-orbitals to a comparable energy to the CNC ligand's π-orbital. This results in an MLCT/LLCT emissive state, where the rise in metal character promotes k_r resulting in increased emission intensity. When the two cyclometalating carbons are *cis*-orientated in different ligands, as in the $[Ir(NCN)(NNC)]^+$ coordinated complexes a comparable shift occurs in the metal d-orbitals; however, owing to there only being one Ir–C bond in each ligand neither is destabilised to the extent that the CNC ligand was. Thus the HOMO has a higher metal contribution and the excited state greater MLCT character, resulting in an increased k_r and emission intensity.

The introduction of a third and final cyclometalating carbon atom raises the energy of the metal-based orbitals further, resulting in a predominantly MLCT excited state, much greater k_r and increased emission intensity. The replacement of one of the cyclometalating phenyl rings in a [Ir(NCN)(CNC)] coordinated complex with an anionic chloride, to give [Ir(NCN)(NC)Cl], is seen to bring about an increase in the metal contribution to the HOMO, resulting in exceptionally bright emission from the latter complex.

The electronic transitions are often labelled as being MLCT-based *etc.*; however, they are rarely pure and refer only to the predominating character of the emissive state. Emission from most complexes incorporates a mixture of these transitions, with the proportion of each being dependent upon any structural modifications.

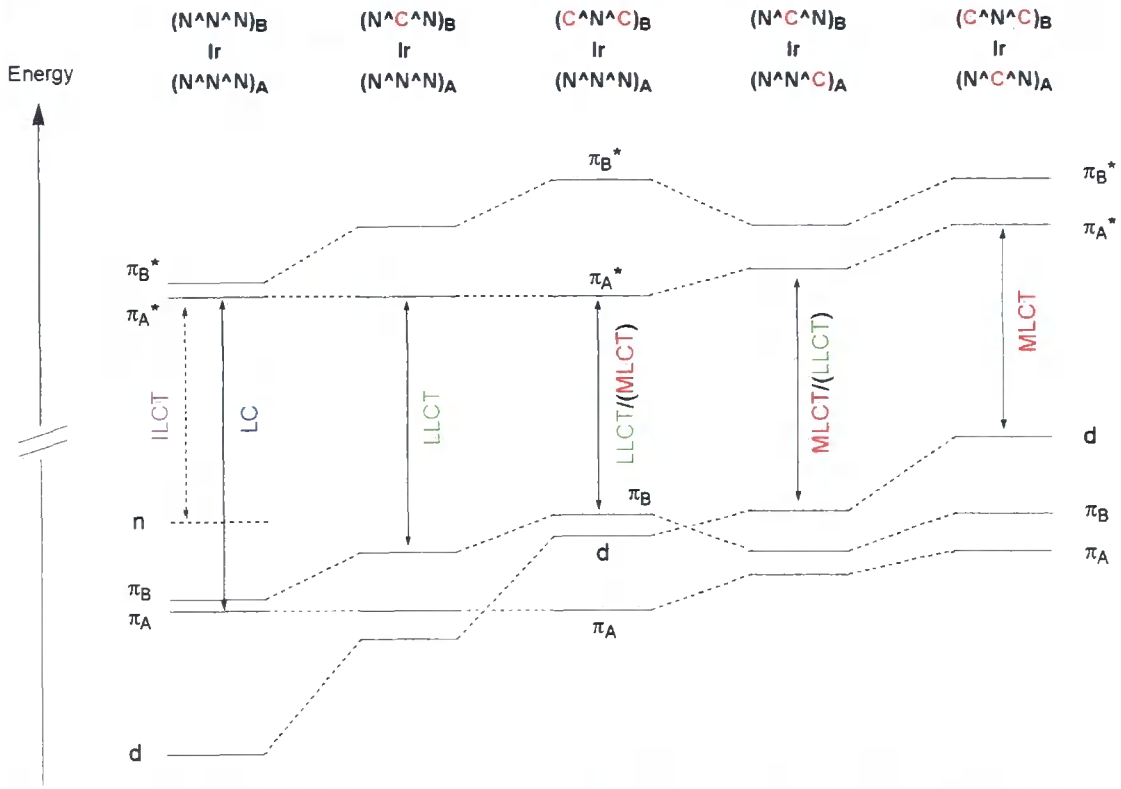

Figure 4.21: The influence of cyclometalation on the frontier orbitals in bis-cyclometalated iridium complexes, and the resulting character of the excited states. The 'n' orbital denoted by a broken line represents an electron-rich n or π orbital localised on a pendant group.[47]

4.1.7 A brief overview of the emission from the rhodium complexes

Unlike complexes of second row iridium, those of third row rhodium are only scarcely emissive. The bis-terdentate polypyridyl complex $[Rh(tpy)_2]^{3+}$ is reported in the literature to display weak structureless emission from a MC excited state at 77 K,[98] whilst the iridium(III) complex displays LC emission at both ambient temperature and 77 K.[46]

The introduction of a cyclometalating carbon into the coordination sphere of the rhodium(III) centre results in $[Rh(NCN)(NNN)]^{2+}$ coordinated complexes that are non-emissive even at 77 K. Whilst introducing a second Rh–C bond, on the opposite ligand,

as in $[Rh(NCN)(NNC)]^+$, resulted in weak biexponential emission being observed at 77 K from two excited states that are poorly coupled.

The introduction of a third anionic group, namely a chloride, into the coordination sphere of the Rh(III) centre in the charge-neutral complex [Rh(NCN)(NC)Cl], results in emission from a mixed MLCT/LC excited state at 298 K. This excited state arises from a HOMO that is delocalised over the metal centre and the central phenyl ring of the NCN ligand and a LUMO localised on the two isolated pyridyl rings of the NCN ligand. This complex, [Rh(dpydmb)(ppy)Cl], marks the only Rh(III) complex prepared within this study that is emissive at 298 K.

4.2 Complexes bearing pyrazole-based NCN ligands

In Section 4.1 the photophysical and electrochemical properties of a range of iridium(III) complexes containing an NCN coordinated 1,3-di(2-pyridyl)benzene based ligand have been discussed. Upon altering the N-heterocyclic rings in the ligand to pyrazole, it was hoped that the emission maximum of the complexes could be blue-shifted, owing to pyrazole having a higher π^*-orbital energy than pyridine, thus making it a poorer π-acceptor. Here we report the photophysical and electrochemical properties of a series of analogously coordinated iridium complexes, containing the NCN-coordinated ligand 1,3-di(1-pyrazolyl)-4,6-dimethylbenzene **19**, whose syntheses were described in Section 2.3.2.

4.2.1 Electrochemical studies

Electrochemical studies were carried out on $[Ir(dpzdmb)(tpy)]^{2+}$ **57**, $[Ir(dpzdmb)(bpy)Cl]^+$ **55** and [Ir(dpzdmb)(ppy)Cl] **58** at 298 K in the presence of Bu_4NBF_4 (0.1M in MeCN) as the supporting electrolyte, within the range of –3.0 to +2.0 V (Table 16).

A chemically reversible oxidation process was observed for $[Ir(dpzdmb)(tpy)]^{2+}$ **57** at 1.30 V *vs.* SCE, which is assigned partially to the oxidation of the cyclometalating ring of the dpzdmb (NCN) ligand and partially to metal-centred oxidation. DFT studies (Section 4.2.2: Table 17 and Figure 4.22) confirm this assignment, with the HOMO indeed being delocalised over the cyclometalating ring of the dpzdmb ligand and the

iridium centre. Similarly, the first oxidation process of $[Ir(dpzdmb)(bpy)Cl]^+$ **55** is reversible and occurs at a potential of 1.19 V. In agreement with the DFT studies (Table 17), this is once again assigned to the removal of an electron from an orbital spanning the metal centre and the cyclometalating ring of dpzdmb. With further reference to the computational studies, the less positive oxidation potential in **55**, compared to **57**, is attributed to the increased electron density at the metal centre of the HOMO in **55** owing to the presence of an electron rich chloride. The electrochemical studies carried out on the charge-neutral complex [Ir(dpzdmb)(ppy)Cl] **58** also reveal a reversible oxidation process, but at the much lower potential of 0.71 V *vs.* SCE. Based upon DFT calculations (Section 4.2.2) this is assigned to an orbital spanning the metal centre and both the cyclometalating ring of the dpzdmb and the ppy ligand, where the delocalisation of electron density in the HOMO of **58** over the three anionic centres (Table 17) facilitates the oxidation. Surprisingly the oxidation potential of [Ir(dpzdmb)(ppy)Cl] **58** (0.71 V *vs.* SCE) is significantly less positive than that of [Ir(dpzdmb-Me_2)(ppy)Cl] (0.94 V *vs.* SCE) recently reported by Haga *et al.*,[226] during the preparation of this thesis, where it was expected that the additional methyl groups on the pyrazolyl rings in the latter would further facilitate the oxidation.

Complex [a]	$E_{1/2}^{ox}$ / V	ΔE^{ox} / mV [b]	$E_{1/2}^{red}$ / V	ΔE^{red} / mV [b]
57 $[Ir(dpzdmb)(tpy)]^{2+}$	1.30	120	– 1.29	170
55 $[Ir(dpzdmb)(bpy)Cl]^+$	1.19 1.33	140 110	– 1.88	140
58 [Ir(dpzdmb)(ppy)Cl]	0.71	120	– 2.72	120

(a) Complexes as their PF_6^- salts in Bu_4NBF_4 (0.1 M in MeCN) as the supporting electrolyte. (b) ΔE^{ox} and ΔE^{red} are the peak to peak separation of the reversible oxidation and reduction processes respectively. These values were measured at a scan rate of 300 mV s^{-1} and are reported relative to SCE, measured using ferrocene as the standard ($E_{1/2}^{ox}$ = 0.42 V *vs.* SCE).

Table 16: Oxidation and reduction potentials of $[Ir(dpzdmb)(tpy)]^{2+}$ 55, $[Ir(dpzdmb)(bpy)Cl]^+$ 57 and [Ir(dpzdmb)(ppy)Cl] 58 obtained by cyclic voltammetry.

At negative potentials, a reversible reduction process was observed for $[Ir(dpzdmb)(tpy)]^{2+}$ **57** at –1.29 V *vs.* SCE which, in agreement with DFT calculations revealing a tpy-based LUMO (Table 17), is assigned to the tpy ligand. $[Ir(dpzdmb)(bpy)Cl]^+$ **55** similarly displays a reversible reduction process at a more negative potential (–1.88 V) than **57**, being assigned to the bpy ligand. The more

negative potential results from there being less delocalisation across the two rings of the bpy ligand in the LUMO of **55** than the three rings of tpy in **57**. Likewise the reduction of [Ir(dpzdmb)(ppy)Cl] **58** occurs at an even more negative potential (–2.72 V), being assigned predominantly to the pyridyl ring of the ppy ligand. This agrees well with Haga's [Ir(dpzdmb-Me_2)(ppy)Cl] complex, where the reduction band at –2.24 V *vs.* SCE was assigned primarily to the pyridyl ring of the ppy ligand.[226]

Upon comparison of $[Ir(dpzdmb)(bpy)Cl]^+$ **55** (Table 16) with the analogously coordinated pyridyl-complex $[Ir(dpydmb)(bpy)Cl]^+$ **30** (Table 5), it becomes apparent that pyrazolyl-complexes are more easily oxidised (1.19 V *vs.* SCE) than pyridyl-complexes (1.28 V). This results from the pyrazolyl ligands being better σ-donors than the analogous pyridyl ligands. At the same time, the replacement of the terminal pyridine rings with poorer π-accepting pyrazole rings leads to more difficult reduction (–1.88 V for **55** and –1.52 V for **30**) owing to the higher energy of the π*-orbitals in the pyrazole complexes.

4.2.2 Computational studies

DFT calculations were carried out on $[Ir(dpzdmb)(tpy)]^{2+}$ **57**, $[Ir(dpzdmb)(bpy)Cl]^+$ **55** and [Ir(dpzdmb)(ppy)Cl] **58**. The calculated orbital characteristics for the three highest energy molecular orbitals (HOMO, HOMO–1 and HOMO–2) and the three lowest energy unoccupied molecular orbitals (LUMO, LUMO+1 and LUMO+2) are summarised in Table 17.

Complex	HOMO–2	HOMO–1	HOMO	LUMO	LUMO+1	LUMO+2
57 $[Ir(dpzdmb)(tpy)]^{2+}$	Ir (49%) NCN (42%)	NCN (94%)	Ir (27%) NCN (66%)	NNN (90%)	NNN (98%)	NNN (97%)
55 $[Ir(dpzdmb)(bpy)Cl]^+$	NCN (80%) Cl (13%)	Ir (41%) NCN (25%) Cl (30%)	Ir (40%) NCN (41%) Cl (14%)	NN (93%)	NN (96%)	NN (97%)
58 [Ir(dpzdmb)(ppy)Cl]	NCN (25%) Cl (64%)	Ir (45%) NCN (26%) Cl (22%)	Ir (47%) NCN (10%) NC (18%) Cl (25%)	NC (93%)	NCN (95%)	NC (96%)

Table 17: Calculated molecular orbital characteristics of the iridium(III) pyrazolyl-complexes, according to DFT calculations. The percentages in parentheses denote the proportion of the total electron density localised at that site.

Studies on $[Ir(dpzdmb)(tpy)]^{2+}$ **57** reveal that the electron density in the HOMO is localised primarily on the phenyl ring of the dpzdmb (NCN) ligand with a small contribution from the metal centre, whilst the LUMO is delocalised across the three pyridyl rings of the tpy ligand (Table 17 and Figure 4.22). This is consistent with a predominantly LLCT lowest energy excited state, with which there is some mixing with the MLCT state.

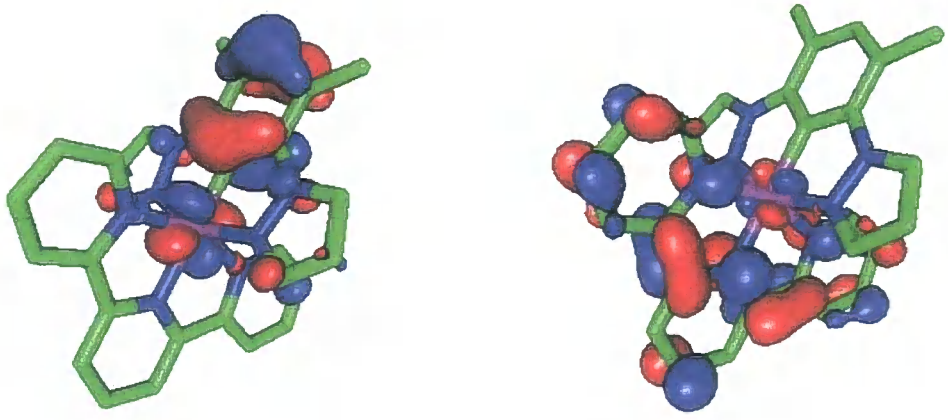

HOMO **LUMO**

Figure 4.22: Contour plots of the HOMO and LUMO of $[Ir(dpzdmb)(tpy)]^{2+}$ 57.

Studies on $[Ir(dpzdmb)(bpy)Cl]^{+}$ **55** reveal that the electron density in the HOMO is localised primarily on the phenyl ring of the dpzdmb ligand and on the iridium centre with a significant contribution also from the anionic chloride, whilst the LUMO is delocalised across the two pyridyl rings of the bpy ligand (Table 17 and Figure 4.23). This is consistent with the studies carried out on the analogously coordinated pyridyl-complex $[Ir(dpydmb)(bpy)Cl]^{+}$ **30**, and suggests that a mixed LLCT/MLCT excited state would be anticipated.

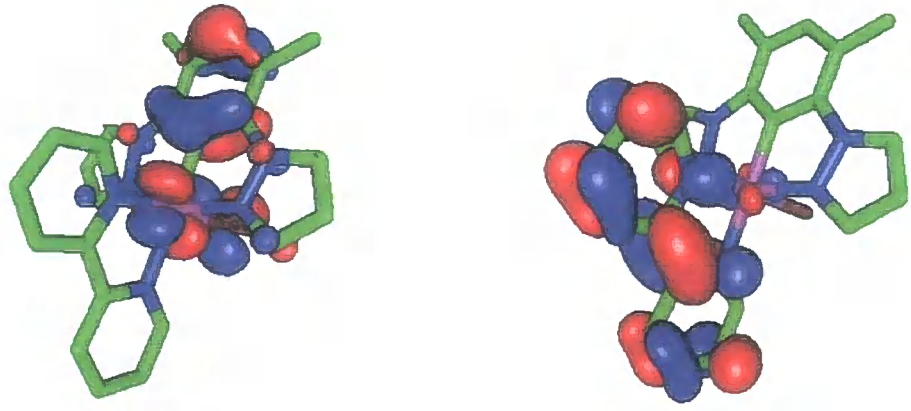

HOMO **LUMO**

Figure 4.23: Contour plots of the HOMO and LUMO of $[Ir(dpzdmb)(bpy)Cl]^{+}$ 55.

Upon carrying out DFT studies on [Ir(dpzdmb)(ppy)Cl] **58** it was revealed that the electron density in the HOMO is delocalised over the iridium centre, the chloride and the phenyl ring of the ppy (NC) ligand with approximately no contribution from the NCN ligand. The HOMO–1, however, is localised on the phenyl ring of the dpzdmb (NCN) ligand, the chloride and the iridium centre and the LUMO on the ppy ligand, with the electron density primarily localised on the pyridyl ring (Table 17 and Figure 4.24). The HOMO and LUMO thus suggest that emission will be from a mixed (MLCT/LLCT/LC) lowest excited state. The predominant localisation of both the HOMO and the LUMO on the ppy ligand is in agreement with the ppy-based reduction reported for complex **58** in Section 4.2.1 and also of an excited state based primarily on the ppy-ligand as reported by Haga *et al.* for the related compound [Ir(dpzdmb-Me_2)(ppy)Cl].[226]

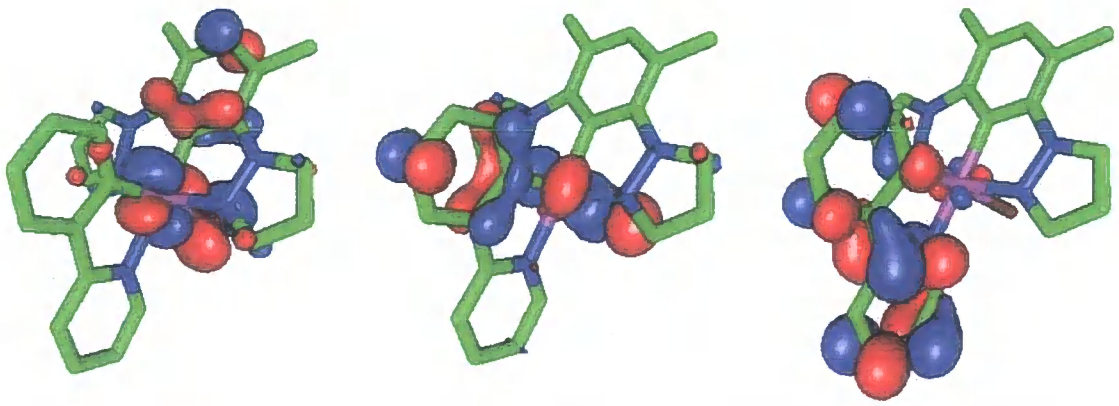

HOMO–1 **HOMO** **LUMO**

Figure 4.24: Contour plots of the HOMO–1, HOMO and LUMO of [Ir(dpzdmb)(ppy)Cl] 58.

4.2.3 Photophysical studies

The photophysical properties of $[Ir(dpzdmb)(tpy)]^{2+}$ **57**, $[Ir(dpzdmb)(bpy)Cl]^{+}$ **55** and [Ir(dpzdmb)(ppy)Cl] **58** are summarised in Table 18.

The absorption spectra of $[Ir(dpzdmb)(tpy)]^{2+}$ **57**, $[Ir(dpzdmb)(bpy)Cl]^{+}$ **55** and [Ir(dpzdmb)(ppy)Cl] **58** (Table 18) all displayed intense broad bands between 200 and 330 nm, assigned to spin-allowed $^{1}\pi$–π^* ligand-based transitions, alongside several very weak absorption bands at lower energy assigned to MLCT transitions. This assignment is in agreement with the DFT calculations carried out on these complexes (Section 4.2.2) and the photophysical studies of the pyridyl analogues (Section 4.1). Upon comparison of the absorption spectra of $[Ir(dpzdmb)(bpy)Cl]^{+}$ **55** and

$[Ir(dpydmb)(bpy)Cl]^+$ **30** (Figure 4.25) it is observed that MLCT transition bands lying above 350 nm are less well defined and of much lower intensity in the pyrazolyl complex. It is thus anticipated that the emission from complex **55** will be of lower intensity than that observed from complex **30** owing to less MLCT character.

Complex [a]	**57** $[Ir(dpzdmb)(tpy)]^{2+}$	**55** $[Ir(dpzdmb)(bpy)Cl]^+$	**58** [Ir(dpzdmb)(ppy)Cl]
Absorption maxima / nm (ε / M^{-1} cm^{-1})	412 (624) 325 (23800) 313 (28400) 281 (48900) 265 (49700) 229 (51500)	427 (1000) 369 (2140) 302 (19100) 258 (42100) 235 (39300)	453 (73) 398 (846) 345 (3640) 260 (6240) 198 (3130)
Emission maxima / nm	–	471, 504, 534 sh	494
Emission maxima at 77 K / nm	–	484, 518, 554, 596 sh [f]	461, 496, 523 [f]
Φ_{em} x 10^2 [b] degassed (aerated)	–	0.70 (0.11)	0.17 (< 0.1)
Lifetime [c] / μs degassed (aerated)	–	2.7 (0.24)	2.2 (0.13)
Lifetime at 77 K [c] / μs	–	6.4 [f]	5.8 [f]
k_r [d] / 10^4 s^{-1}	–	0.26	0.077
Σk_{nr} [d] / 10^5 s^{-1}	–	3.7	4.5
$k_Q^{O_2}$ [e] / 10^{10} M^{-1} s^{-1}	–	0.20	0.38

(a) Complexes as their hexafluorophosphate salts in degassed CH_3CN at 298 K, except where stated otherwise. (b) Luminescence quantum yield measured at 298 K using $[Ru(bpy)_3]Cl_2$ as a standard. (c) Lifetime registered at the emission maximum following excitation at 374 nm. (d) Radiative and non-radiative rate constants calculated from τ and Φ values at 298 K. (e) Bimolecular rate constant for quenching by O_2, estimated from τ in degassed and aerated solutions. (f) In an EPA glass at 77 K.

Table 18: Photophysical properties of the iridium(III) pyrazolyl complexes $[Ir(dpzdmb)(tpy)][PF_6]_2$ 57, $[Ir(dpzdmb)(bpy)Cl][PF_6]$ 55 and [Ir(dpzdmb)(ppy)Cl] 58.

Studies into the emission properties of the $[Ir(NCN)(NNN)]^{2+}$ coordinated complexes $[Ir(dpzdmb)(tpy)]^{2+}$ **57**, $[Ir(dpzmb)(tpy)]^{2+}$ **50** and $[Ir(dpzb\text{-}Br)(tpy)]^{2+}$ **54** revealed emission that was too erratic for anything meaningful to be concluded from. However, upon comparison of the absorption and excitation spectra of these complexes, it became

evident that the absorption bringing about the emission was predominantly occurring at long wavelength (>350 nm) where the $[Ir(NCN)(NNN)]^+$ complexes either did not absorb or did so only very weakly. This alongside the knowledge that the pyridyl analogue $[Ir(dpydmb)(tpy)]^{2+}$ was virtually non-emissive under these conditions, formulated the conclusion that the erratic emission was probably originating from trace impurities of emissive species, perhaps $[Ir(NCN)(tpy\text{-}NN)Cl]^+$.

Like the pyridyl series of complexes reported in Section 4.1.3, the introduction of an anionic chloride into the coordination sphere of the metal centre has a profound effect on the photochemical properties of the complex, with structured emission (Φ = 0.0070) being observed from $[Ir(dpzdmb)(bpy)Cl]^+$ **55** (Figure 4.25 and Table 18) at ambient temperature. The emission profile is indicative of emission from a primarily LC excited state with little or no MLCT character, differing significantly from the mixed LLCT/MLCT excited state predicted from the DFT studies (Section 4.2.2). The emission profile observed from complex **55** (Figure 4.25 and Table 18) is also very different from that of the analogous pyridyl complex $[Ir(dpydmb)(bpy)Cl]^+$ **30** (Figure 4.25 and Table 7), with the former displaying more structured, blue-shifted emission. The blue-shift results from pyrazole being a poorer π-acceptor than pyridine and the structure from an emissive state with less MLCT character. The emission from complex **55** decays with a luminescence lifetime of 2.7 μs in degassed MeCN, which is significantly longer than that of complex **30** (1.5 μs) and consistent with ligand-centred emission, whilst the luminescence quantum yield, Φ = 0.0070, for **55** is significantly lower than that for **30** (Φ = 0.019) which is in line with there being less metal character in the emissive state of the former. Upon cooling to 77 K the emission observed from $[Ir(dpzdmb)(bpy)Cl]^+$ **55** (Figure 4.25) becomes more structured and the luminescence lifetime significantly longer, 6.4 μs. Unlike the pyridyl complex **30**, the emission profile of **55** is not blue-shifted upon cooling to 77 K, which is consistent with a LC emissive state rather than one with CT character.

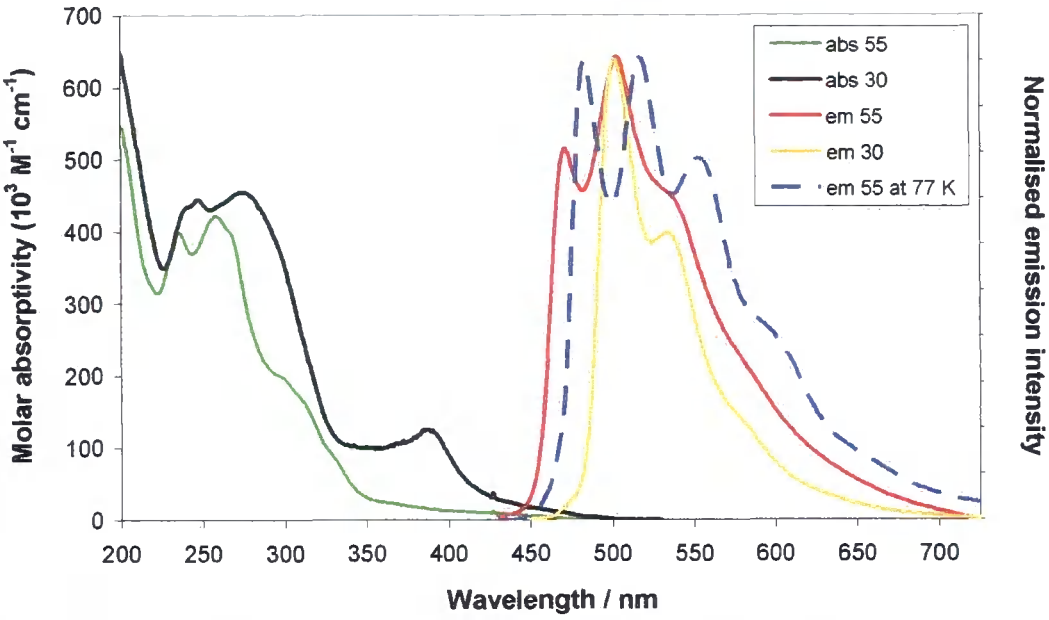

Figure 4.25: Absorption and normalised emission spectra for [Ir(dpydmb)(bpy)Cl]$^+$ 30 (λ_{ex} = 387 nm) and [Ir(dpzdmb)(bpy)Cl]$^+$ 55 (λ_{ex} = 370 nm) in MeCN at 298 K and 55 in EPA at 77 K.

Photochemical studies of [Ir(dpzdmb)(ppy)Cl] **58** (Table 18 and Figure 4.26) in degassed acetonitrile at 298 K revealed a slightly structured emission profile centred around 500 nm with a luminescence lifetime of 2.2 μs, which in agreement with DFT calculations (Section 4.2.2: Figure 4.24) is assigned as being from a mixed MLCT/LLCT/LC excited state. Upon comparison with [Ir(dpzdmb)(bpy)Cl]$^+$ **55**, the emission profile of **58** is found to be less structured and red-shifted, indicative of a more mixed emissive state with increased MLCT character. Surprisingly though, a reduction in emission intensity is observed upon going from [Ir(dpzdmb)(bpy)Cl]$^+$ **55** (Φ = 0.0070) to [Ir(dpzdmb)(ppy)Cl] **58** (Φ = 0.0017) owing to both a reduction in k_r and an increase in Σk_{nr}. The low quantum yield of **58** at 298 K, however, agrees well with that recently reported by Haga *et al.* for the related complex [Ir(dpzdmb-Me_2)(ppy)Cl] (Φ < 0.001).[226]

Upon cooling complex **58** to 77 K, the emission spectrum becomes highly structured and blue-shifted and is assigned to a LC excited state. The emission profile and lifetime (5.8 μs) observed for **58** agrees well with that recently reported by Haga *et al.* for [Ir(dpzdmb-Me_2)(ppy)Cl] (3.9 μs) in a CH_2Cl_2:toluene glass, where the emission was also reported to be from a LC excited state.[226] Haga's study investigated the effect that varying the substituents (R = H, Me or F) at the 4' and 6'-positions of the NCN ligand

has on the emissive properties of the complexes. It was reported that the effect was actually small due to the NCN ligand having a less significant role in the excited state than the ppy ligand, where electrochemical studies revealed the excited state electron to reside.[226]

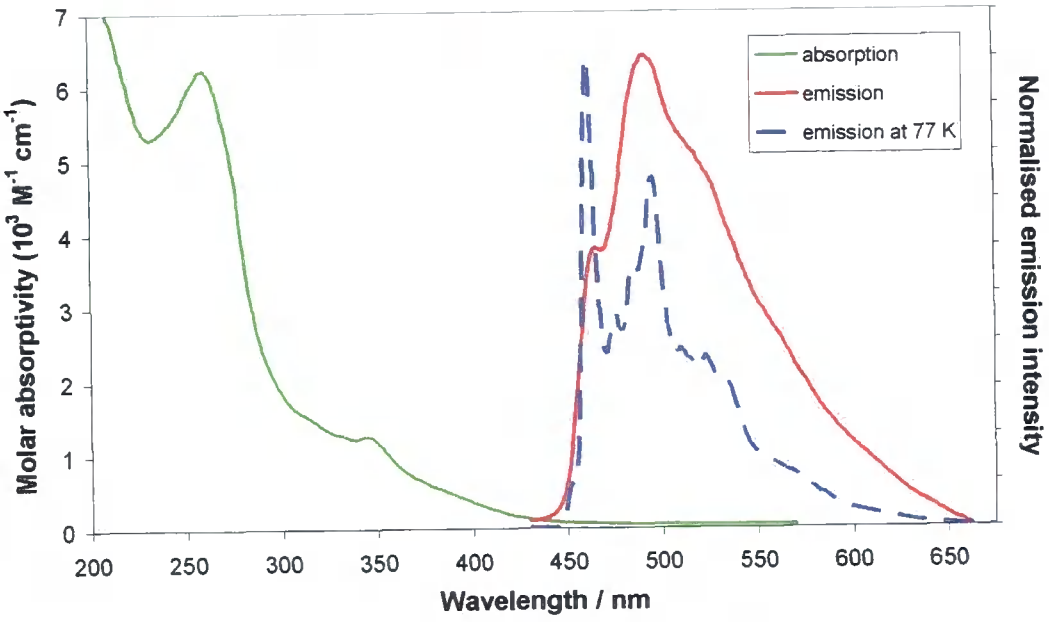

Figure 4.26: Absorption, and normalised emission spectra for [Ir(dpzdmb)(ppy)Cl] 58 (λ_{ex} = 350 nm) in MeCN at 298 K and in an EPA glass at 77 K.

4.3 Concluding remarks

In this chapter, the photophysical and electrochemical properties of a range of monometallic iridium(III) and rhodium(III) complexes with $[M(NCN)(NNN)]^{2+}$, $[M(NCN)(NN)Cl]^{+}$, $[M(NCN)(NNC)]^{+}$, [M(NCN)(NC)Cl] and [Ir(NCN)(CNC)] coordination have been reported alongside their DFT studies.

In conjunction with related complexes previously reported by this research group,[76, 78] the influence of cyclometalation on the photophysical properties of the bis-terdentate complexes of iridium(III) has been investigated. A trend is identified going from the LC luminescence of the $[Ir(NNN)_2]^{3+}$ complexes to the MLCT dominated states of the charge-neutral [Ir(NCN)(CNC)] complexes. Between the two extremes lie the mono-cyclometalated $[Ir(NCN)(NNN)]^{2+}$ complexes with predominantly LLCT character, and the bis-cyclometalated complexes of $[Ir(CNC)(NNN)]^{+}$,[83, 84] and $[Ir(NCN)(NNC)]^{+}$,

where the excited states are dependent upon whether the two cyclometalated carbons are in the same or different ligands.

The complexes of rhodium(III) reported herein were found to be far less emissive than those of iridium(III). [Rh(dpydmb)(ppy)Cl] is the only complex prepared in this study that is emissive at ambient temperature, being itself approximately 70 times less emissive than [Ir(dpydmb)(ppy)Cl].

The properties of a series of iridium(III) $[Ir(NCN)(NNN)]^{2+}$, $[Ir(NCN)(NN)Cl]^{+}$ and [Ir(NCN)(NC)Cl] coordinated complexes bearing the pyrazolyl NCN ligand, 1,3-di(1-pyridyl)-4,6-dimethylbenzene, are also reported. The poorer π-accepting ability of the pyrazole rings in these complexes brings about a blue-shifted, lower intensity emission profile with more ligand-based character compared to their pyridyl analogues.

CHAPTER 5

SYNTHESIS AND LUMINESCENCE OF MULTIMETALLIC COMPLEXES

5 Synthesis and Luminescence of Multimetallic Complexes

The use of "chemistry on the complex" techniques to successfully elaborate $[Ir(NCN)(NNC)]^+$ coordinated complexes in a linear stepwise manner was described in Chapter 3. In the current chapter we discuss the application of this technique to the synthesis of a series of linear homo- and heterometallic multinuclear assemblies.

The preparation of di-, tri, tetra- and octametallic assemblies by the direct coupling of brominated and boronic acid appended tris-bidentate complexes of Ir(III), Rh(III) and Ru(II) has previously been reported by this research group,[49, 52, 237] alongside a ruthenium-iridium dimetallic species incorporating an iridium(III) bis-terpyridyl unit (Section 1.5.3).[130] There are, however, no examples of the use of such couplings in the synthesis of multimetallic assemblies containing cyclometalating bis-terdentate complexes of iridium(III). Bis-terdentate complexes offer a significant advantage over tris-bidentate complexes in the synthesis of multimetallic assemblies, due to the latter being intrinsically chiral and existing as a mixture of Λ and Δ isomers (Figure 5.1a).

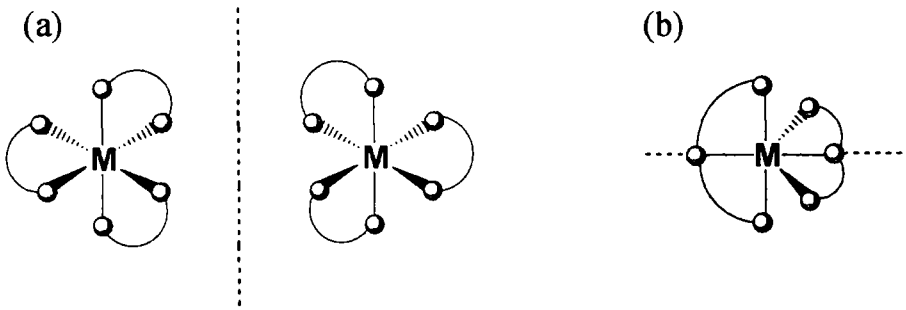

Figure 5.1: (a) Λ and Δ isomers of bis-terdentate complexes and (b) the proposed linear expansion of a tris-bidentate complex.

Thus, when two or more tris-bidentate complexes are linked together, stereoisomers are formed which are often difficult to separate and yet may exhibit subtly different photophysical properties. Bis-terdentate complexes on the other hand, are achiral and form a single species upon being linked together. As demonstrated with organic groups in Chapter 3, substitution at the central position of the terdentate ligands should provide an ideal route to linear multimetallic assemblies (Figure 5.1b) where the two peripheral metal complexes lie at 180° to one another, co-axial with the metal centre.

5.1 Homometallic dinuclear complexes

5.1.1 Aryl diboronic acids in the coupling of bromo-functionalised monometallic complexes to give symmetric dimers

In this study attempts were made to synthesise a series of homometallic dinuclear complexes upon cross-coupling two molecules of the $[Ir(NCN)(NNC)]^+$ coordinated complex $[Ir(dpydmb)(mtbpy\phi\text{-}Br)]^+$ **61** with aryl-diboronic acids. Like the elaboration reactions on **61** in Chapter 3, reaction of this complex with 1,4-benzenediboronic acid was carried out *via* a Suzuki cross-coupling reaction in degassed DMSO in the presence of the $Ph(PPh_3)_4$ catalyst and aqueous sodium carbonate base (Figure 5.2).

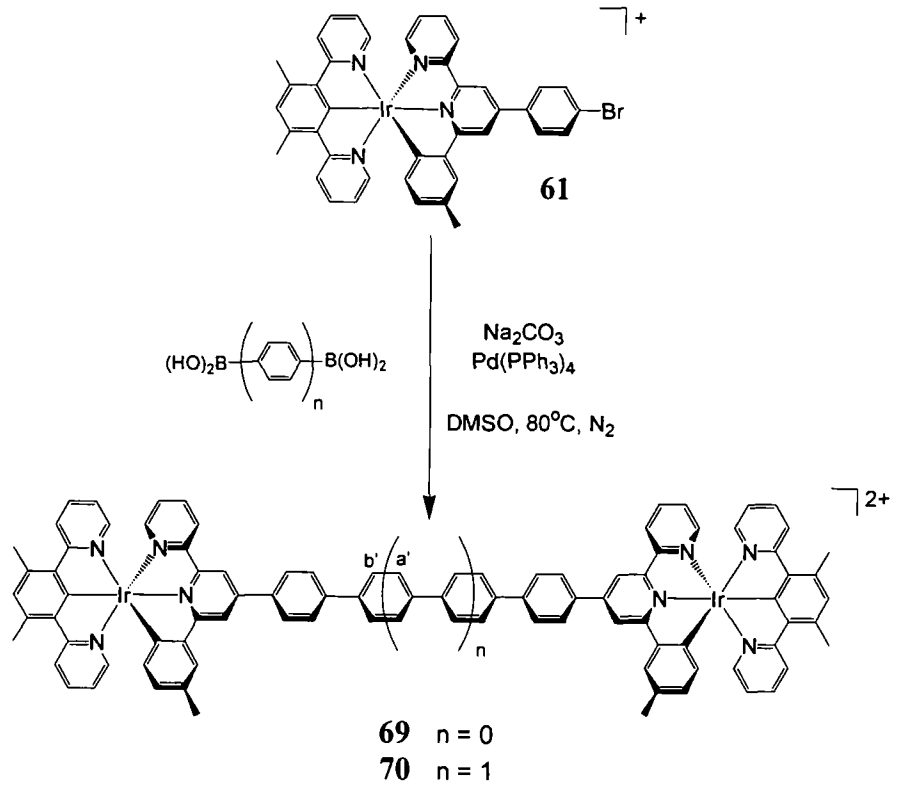

Figure 5.2: Synthesis of the dinuclear complexes 69 and 70 by cross-coupling $[Ir(dpydmb)(mtbpy\text{-}\phi\text{-}Br)]^+$ 61 with aryl-diboronic acids.[205]

Following chromatographic purification, $[\{Ir(dpydmb)\}_2\mu\text{-}(mtbpy\text{-}\phi_3\text{-}mtbpy)][PF_6]_2$ **69** was afforded as an orange solid in 30% yield, in which the constituent iridium complexes are effectively connected by a tri-phenylene bridge.[205] The singly reacted monometallic compound $[Ir(dpydmb)\{mtbpy\text{-}\phi_2\text{-}B(OH)_2\}]^+$ **71**, incorporating a pendant boronic acid, was isolated as an orange side-product in 19% yield.

Similarly, upon reaction of **61** with 4,4'-biphenyldiboronic acid, the corresponding dimetallic assembly $[\{Ir(dpydmb)\}_2\mu\text{-}(mtbpy\text{-}\phi_4\text{-}mtbpy)][PF_6]_2$ **70**, containing a four-ring bridge, was formed as an orange solid in 35% yield.[205] The incorporation of the bridging unit into complexes **69** and **70** was confirmed by the introduction of additional peaks into the ^{1}H-NMR spectrum corresponding to protons ($H^{a'}$) and $H^{b'}$, whilst the 1:2 ratio of the protons on the bridging and coordinated rings confirmed the successful linking of two iridium complexes.

Somewhat related linear homometallic dimers of the form $[\{Ir(dpydmb)\}_2\mu\text{-}(tpy\text{-}\phi\text{-}tpy)]^{4+}$ (n = 0–3) have recently been reported by Collin *et al.*, prepared using preformed polyphenyl bridging ligands.[241]

5.1.2 *Suzuki couplings between brominated and boronic acid appended monometallic "building blocks"*

Whilst boronic acid appended aryl linkers (Section 5.1.1) can be used efficiently to join together two equivalent bromo-substituted metal complexes to give symmetric dimers, they are largely unsuccessful for the controlled and regioselective preparation of multimetallic assemblies containing inequivalent monometallic complexes. The "building block" approach involving the cross-coupling of pre-formed bromo and boronic acid appended complexes can be used to overcome this problem, allowing access to heterometallic complexes as well as asymmetrical homometallic complexes where the metals are in different environments.

Attempts were made within this study to synthesise such an asymmetrical assembly by the direct coupling of two bis-terdentate complexes, the boronic acid appended $[Ir(NCN)(NNC)]^+$ coordinated complex $[Ir(dpydmb)\{mtbpy\text{-}\phi\text{-}B(OH)(OMe)\}]^+$ **68** (Chapter 3) and the bromo-substituted $[IrN_6]^{3+}$ complex $[Ir(tpy)(tpy\text{-}\phi\text{-}Br)]^{3+}$ **72**. The bromo-substituted "building block" **72** was first prepared (Figure 5.3) as an orange solid in 37% yield using the route previously employed by this research group for its synthesis,[54] proceeding *via* the intermediate $[Ir(tpy)Cl_3]$ **73**.[46]

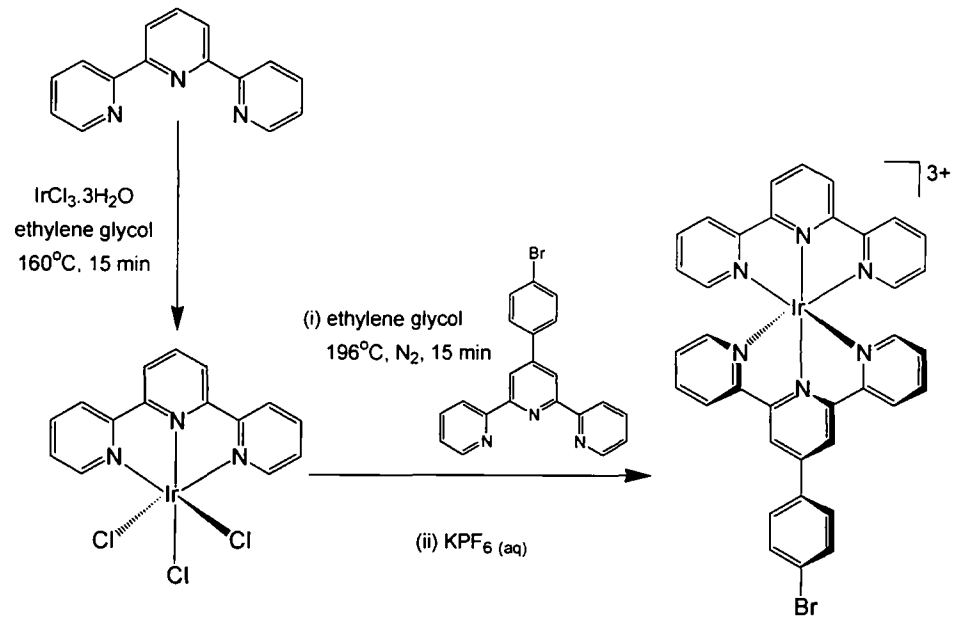

73 72

Figure 5.3: Synthesis of $[Ir(tpy)(tpy\text{-}\phi\text{-}Br)]^{3+}$ 72 *via* $[Ir(tpy)Cl_3]$ 73.

The Suzuki cross-coupling of $[Ir(dpydmb)\{mtbpy\text{-}\phi\text{-}B(OH)(OMe)\}]^{+}$ **68** with $[Ir(tpy)(tpy\text{-}\phi\text{-}Br)]^{3+}$ **72**, was subsequently carried out under the same reaction conditions used for systems **69** and **70**, successfully affording the desired product $[(dpydmb)Ir\text{-}\mu\text{-}(mtbpy\text{-}\phi_2\text{-}tpy)Ir(tpy)]^{4+}$ **74** as an orange solid in 16% yield following chromatographic purification (Figure 5.4).

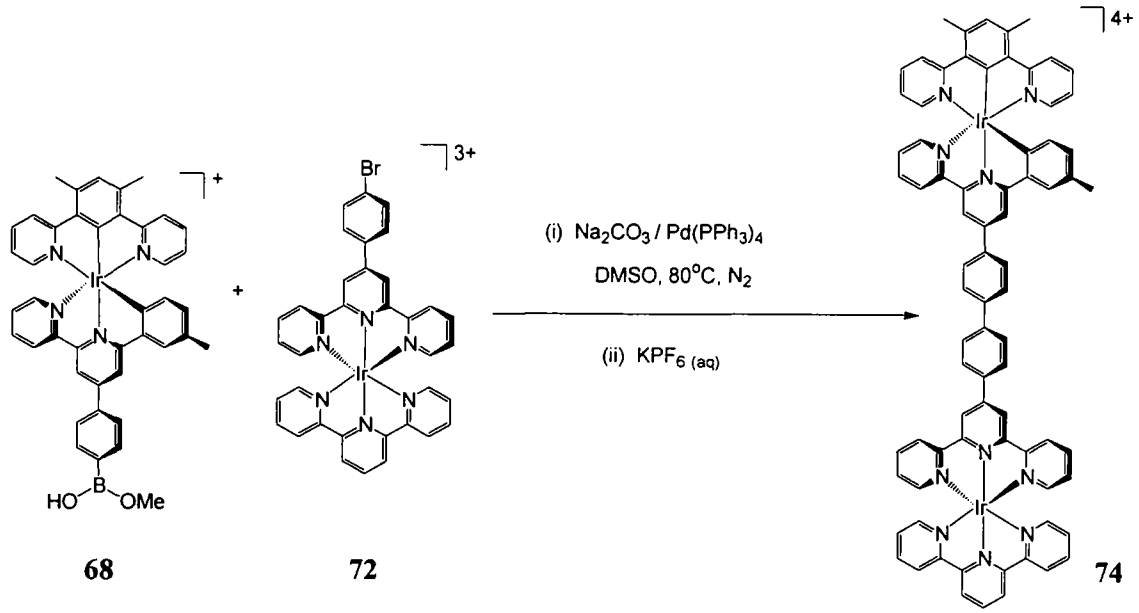

68 72 74

Figure 5.4: Synthesis of $[(dpydmb)Ir\text{-}\mu\text{-}(mtbpy\text{-}\phi_2\text{-}tpy)Ir(tpy)]^{4+}$ 74 *via* a Suzuki cross-coupling reaction employing a boronic acid appended complex as one of the reagents.

The syntheses of **69**, **70** and **74** have all involved elaboration on the central pyridyl-ring of the NNC ligand of an $[Ir(NCN)(NNC)]^+$ complex. Following the related elaboration of such complexes, with organic groups, at the central phenyl-ring of the NCN ligand in Section 3.2, attempts were made to carry out a Suzuki cross-coupling reaction at this position on $Ir(dpydmb\text{-}Br)(mtbpy\text{-}\phi\text{-}ph)]^+$ **65** with a boronic acid appended tris-bidentate iridium(III) complex (Figure 5.5). The synthesis of complex **65** containing a 4'-bromo substituent on the NCN ligand is described in Section 3.2.3, where it was shown that the flanking methyl groups do not hinder coupling at this position.

The Ir(III) tris-bidentate complex $[Ir(Fppy)_2\{bpy\text{-}\phi\text{-}B(OH)_2\}]^+$ used in this coupling was previously prepared within the Williams' group.[237] Unfortunately, the time constraints towards the end of this project had prevented the synthesis of a series of boronic acid appended bis-terdentate complexes, therefore several pre-prepared tris-bidentate complexes were used to demonstrate the conceptual synthetic strategy towards linear multimetallic assemblies.

The reaction of $[Ir(dpydmb\text{-}Br)(mtbpy\text{-}\phi\text{-}ph)]^+$ **65** with $[Ir(Fppy)_2\{bpy\text{-}\phi\text{-}B(OH)_2\}]$ *via* a Suzuki cross-coupling (Figure 5.5) afforded $[(Fppy)_2Ir\text{-}\mu\text{-}(bpy\text{-}\phi\text{-}dpydmb)Ir(mtbpy\text{-}\phi\text{-}ph)]^{2+}$ **75** as a yellow solid in 35% yield following chromatographic separation.

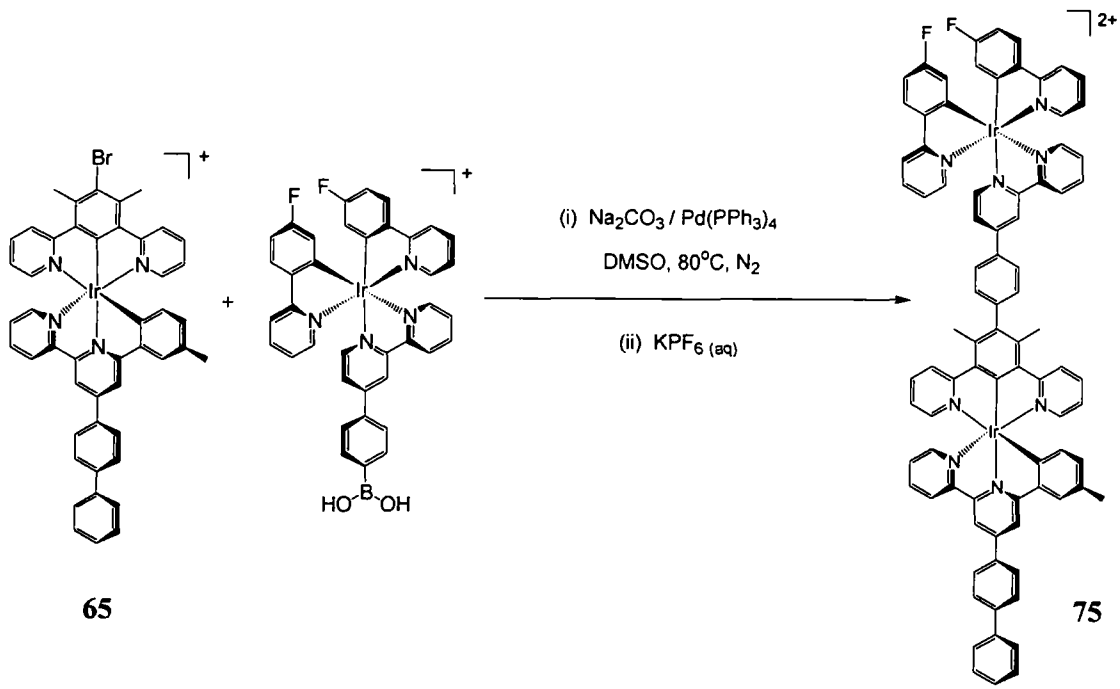

65 **75**

Figure 5.5: Synthesis of $[(Fppy)_2Ir\text{-}\mu\text{-}(bpy\text{-}\phi\text{-}dpydmb)Ir(mtbpy\text{-}\phi\text{-}ph)]^{2+}$ 75 *via* a Suzuki cross-coupling reaction employing a boronic acid appended tris-bidentate complex.

5.2 Heterometallic dinuclear complexes

The preparation of heterometallic dinuclear complexes *via* the direct Suzuki cross-coupling of appropriately functionalised "building blocks" can be anticipated following the successful synthesis of the asymmetrical homometallic complexes **74** and **75**.

The initial synthesis of a heterometallic species was attempted by coupling the bromo-functionalised $[Ir(NCN)(NNC)]^+$ coordinated complex $[Ir(dpydmb)(mtbpy\text{-}\phi\text{-}Br)]^+$ **61**, with the boronated ruthenium(II) tris-bidentate complex $[Ru(bpy)_2(bpy\text{-}\phi\text{-}Bneo)]^{2+}$,[237] under standard Suzuki conditions (Figure 5.6). Following chromatographic separation of the crude product, $[(dpydmb)Ir\text{-}\mu\text{-}(mtbpy\text{-}\phi_2\text{-}bpy)Ru(bpy)_2]^{3+}$ **76** was successfully isolated as an orange solid in 43% yield.

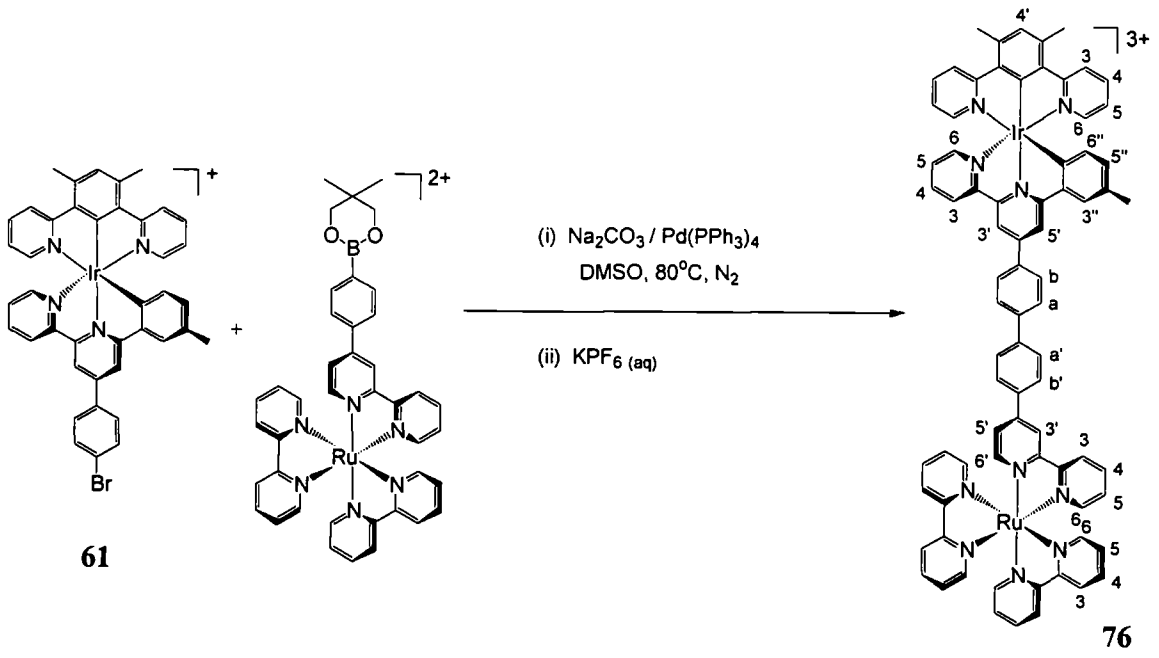

Figure 5.6: Synthesis of $[(dpydmb)Ir\text{-}\mu\text{-}(mtbpy\text{-}\phi_2\text{-}bpy)Ru(bpy)_2]^{3+}$ 76 *via* a Suzuki cross-coupling reaction employing a boronic acid appended ruthenium complex.

The synthesis of $[(dpydmb)Ir\text{-}\mu\text{-}(mtbpy\text{-}\phi_2\text{-}bpy)Ru(bpy)_2]^{3+}$ **76** was supported by ^{1}H-NMR spectroscopy, where the spectrum displayed peaks corresponding to both monometallic "building blocks" in a 1:1 ratio. The complete assignment of the ^{1}H-NMR spectrum of such multimetallic species can be achieved with the aid of the relevant monometallic complexes in the same deuterated solvent alongside ^{1}H-^{1}H COSY and ^{1}H-^{1}H NOESY spectra. The assigned ^{1}H-NMR spectrum of $[(dpydmb)Ir\text{-}\mu\text{-}(mtbpy\text{-}\phi_2\text{-}bpy)Ru(bpy)_2]^{3+}$ **76** is shown in Figure 5.7.

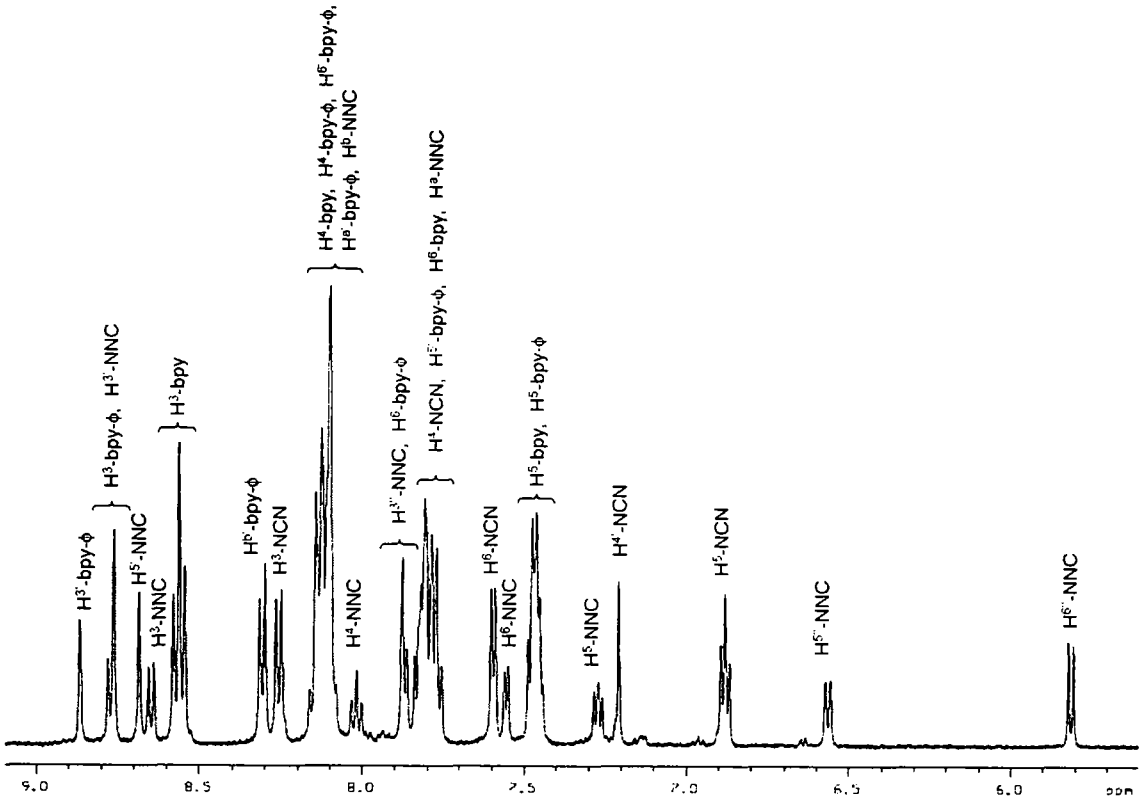

Figure 5.7: Assigned ^{1}H-NMR spectrum of $[(dpydmb)Ir\text{-}\mu\text{-}(mtbpy\text{-}\phi_2\text{-}bpy)Ru(bpy)_2]^{3+}$ 76.

5.3 Synthesis of trimetallic assemblies via in situ Suzuki couplings on multimetallic complexes

In this study, the use of Suzuki cross-coupling reactions in the synthesis of multimetallics assemblies has so far been limited to the controlled coupling of monometallic "building blocks" to form dimetallic species. However, it is hoped that by employing a stepwise linear expansion technique similar to the cross-coupling – bromination – cross-coupling procedure in Section 3.2 for the elaboration of $[Ir(NCN)(NNC)]^+$ type complexes with boronic acid appended aryl groups, suitable trimetallic assemblies can be formed. This laboratory has previously demonstrated the use of such *in situ* Suzuki reactions in the controlled elaboration of large multimetallic systems, but this was limited to non-linear assemblies comprising of tris-bidentate "building blocks".[130]

5.3.1 Choosing the "building blocks"

Multimetallic systems capable of transferring energy to a specific part of the assembly are of particular interest. In order to create this channelling effect the relative excited state energies of the individual "building blocks" involved must be carefully considered.

To extend the heterometallic dinuclear complex [(dpydmb)Ir-μ-(mtbpy-ϕ_2-bpy)Ru(bpy)$_2$]$^{3+}$ **76** (15900 cm^{-1}) to a trimetallic system possessing energy-channelling ability, a boronic acid appended complex providing a "building block" of higher energy than the units already incorporated is required. [Ir(F_2ppy)$_2${bpy-ϕ-B(OH)$_2$}]$^+$ was selected as a suitable candidate to fulfil this role based upon the emission energy of the related [Ir(F_2ppy)$_2$(bpy-ϕ-ph)]$^+$ unit (18600 cm^{-1}). This alongside the energies of the other model monometallic units [Ir(dpydmb-$C_6H_3Me_2$)(mtbpy-ϕ-ph)]$^+$ (16000 cm^{-1}) and [Ru(bpy)(bpy-ϕ)]$^{2+}$ (15900 cm^{-1}), can be used to predict the energy transfer in the [^{F_4}Ir–ϕ–Ir–ϕ_2–Ru]$^{4+}$ trimetallic assembly. Provided that the bridging ligands do not greatly affect the excited state properties of the system, energy transfer is expected to occur rapidly from the high energy fluorinated end to the low energy ruthenium end as portrayed in Figure 5.8.

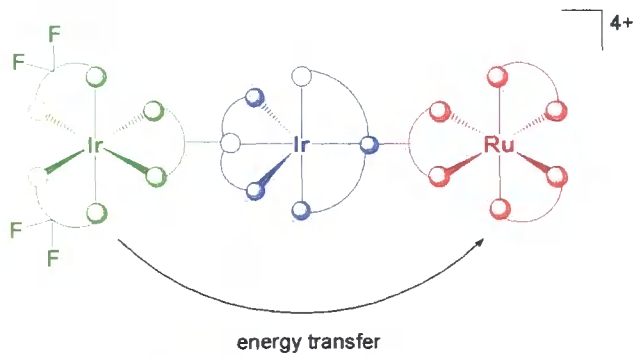

Figure 5.8: Predicted direction of energy transfer in the [^{F_4}Ir–ϕ–Ir–ϕ_2–Ru]$^{4+}$ trimetallic species.

5.3.2 Bromination of the dimeric species

In Chapter 3 the regiospecific *in situ* bromination of [Ir(NCN)(NNC)]$^+$ coordinated monometallic complexes at the site *para* to the cyclometalating carbon was discussed. Here it was anticipated that the application of this technique to a dimetallic species containing an equivalent [Ir(NCN)(NNC)]$^+$ moiety would allow the formation of a brominated species as part of a cross-coupling – bromination – cross-coupling approach to trimetallic systems (Figure 5.9).

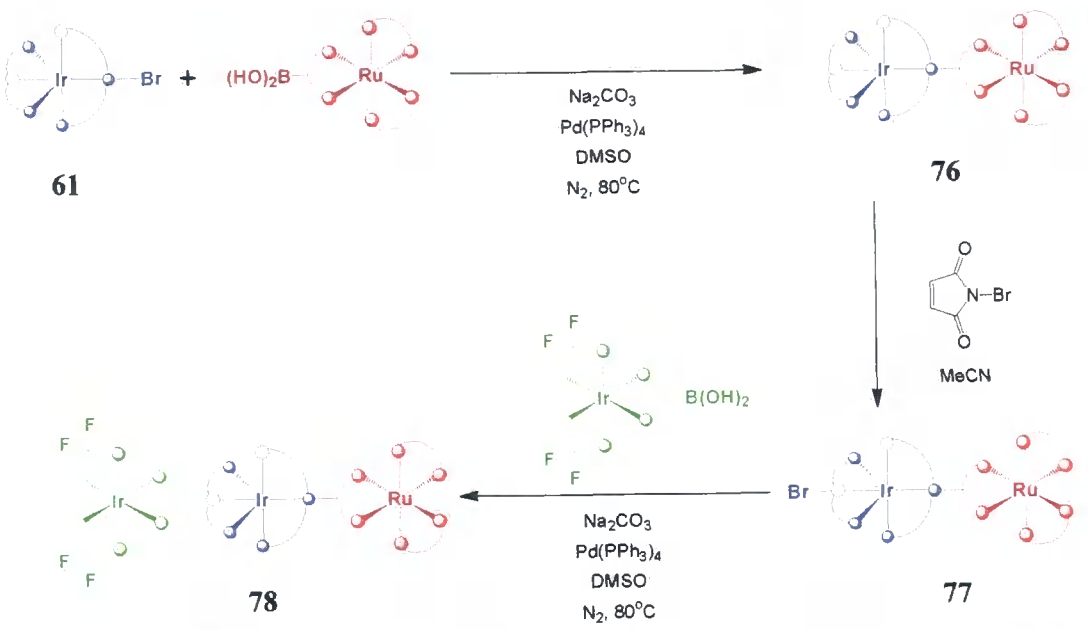

Figure 5.9: The proposed coupling – bromination – coupling procedure to multimetallic systems.

Reaction of the dimetallic complex $[(dpydmb)Ir\text{-}\mu\text{-}(mtbpy\text{-}\phi_2\text{-}bpy)Ru(bpy)_2]^{3+}$ **76** with N-bromosuccinimide (NBS) in acetonitrile solution at room temperature formed $[(dpydmb\text{-}Br)Ir\text{-}\mu\text{-}(mtbpy\text{-}\phi_2\text{-}bpy)Ru(bpy)_2]^{3+}$ **77**, brominated at the site opposite the position of cyclometalation on the NCN ligand (Figure 5.9). The product was isolated as a red solid in quantitative yield following ion exchange to the hexafluorophosphate salt, and was used without further purification.

5.3.3 Suzuki cross-coupling to generate the trimetallic species

The Suzuki cross-coupling of $[(dpydmb\text{-}Br)Ir\text{-}\mu\text{-}(mtbpy\text{-}\phi_2\text{-}bpy)Ru(bpy)_2]^{3+}$ **77** with the boronic acid appended complex $[Ir(F_2ppy)_2\{bpy\text{-}\phi\text{-}B(OH)_2\}]^+$ (Figure 5.9), in the second cross-coupling step, successfully afforded the desired trimetallic product $[(F_2ppy)_2Ir\text{-}\mu\text{-}(bpy\text{-}\phi\text{-}dpydmb)Ir\text{-}\mu\text{-}(mtbpy\text{-}\phi_2\text{-}bpy)Ru(bpy)_2]^{4+}$ **78** (Figure 5.10). Complex **78** was isolated as an orange/red solid in 62% yield following chromatographic purification and ion exchange to the PF_6^- salt.

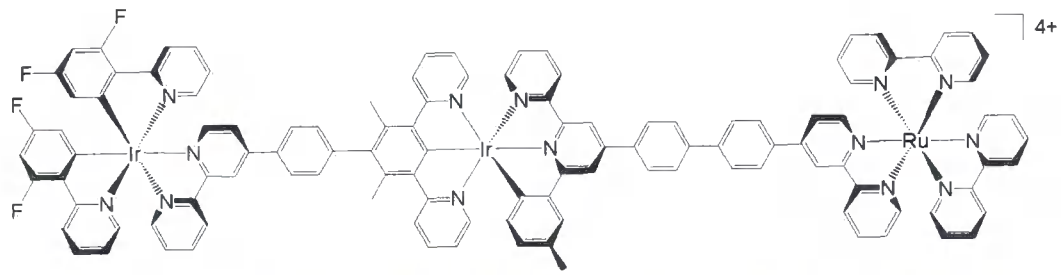

Figure 5.10: $[(F_2ppy)_2Ir\text{-}\mu\text{-}(bpy\text{-}\phi\text{-}dpydmb)Ir\text{-}\mu\text{-}(mtbpy\text{-}\phi_2\text{-}bpy)Ru(bpy)_2]^{4+}$ 78.

The incorporation of a third metal centre makes the ^{1}H-NMR spectrum of **78** very complicated due to the presence of a total of 80 protons. The complete assignment of the ^{1}H-NMR spectrum was, however, achieved with assistance from the spectra of the relevant monometallic and bimetallic complexes in the same deuterated solvent and ^{1}H-^{1}H COSY and ^{1}H-^{1}H NOESY spectra.

The large positive charge associated with the trimetallic complex **78**, like the bimetallic complexes reported herein, makes it ideal for characterisation by ES^+ mass spectrometry, where several peaks are seen for combinations of the complex with various numbers of PF_6^- counter ions. High resolution electrospray mass spectrometry shows excellent correlation between the measured and theoretical masses; however, their large size means several molecular formulae containing only the atoms in the desired complex often closely match the measured mass. The combination of this comparison of masses with isotope peak matching can be used to confirm the identity of the complex. The isotope peak matching for the trimetallic complex **78** is shown in Figure 5.11.

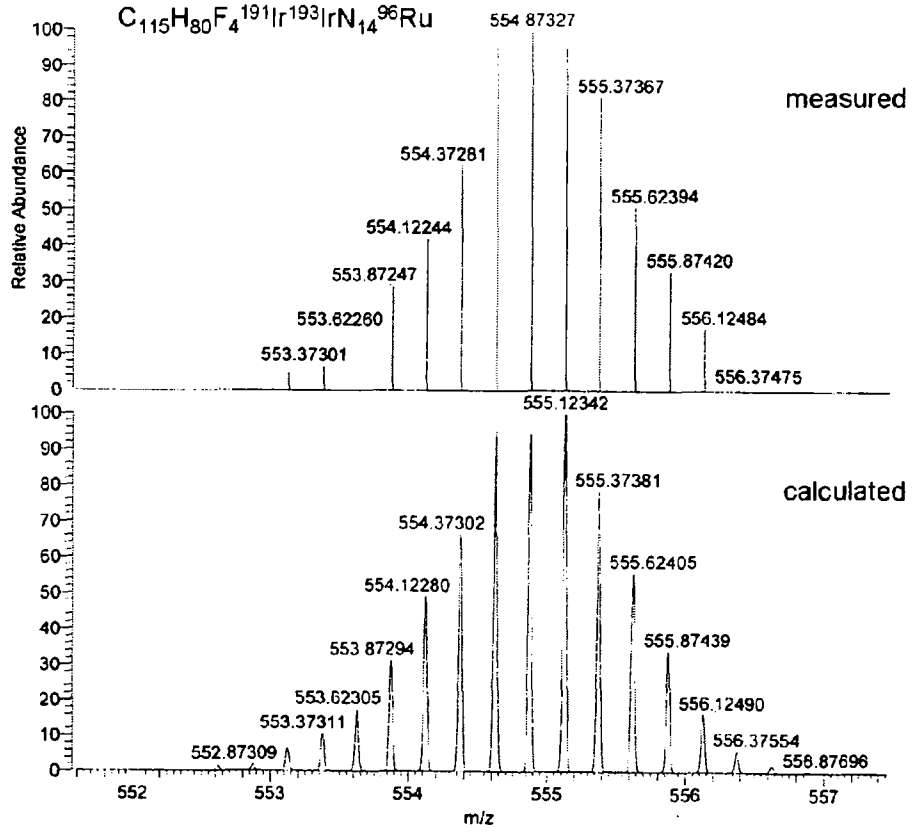

Figure 5.11: Isotope peak matching for the trimetallic complex $[(F_2ppy)_2Ir$-μ-(bpy-ϕ-dpydmb)Ir-μ-(mtbpy-ϕ_2-bpy)Ru(bpy)$_2]^{4+}$ 78.

5.4 Electrochemical studies

Electrochemical studies were carried out within the range of –3.0 to 2.0 V on the di- and trinuclear complexes in the presence of Bu_4NBF_4 (0.1 M in MeCN) as the supporting electrolyte at 298 K and the results summarised in Table 19, Table 20 and Table 21.

5.4.1 Homometallic dinuclear complexes of iridium(III)

The homometallic dyads $[\{Ir(dpydmb)\}_2\mu\text{-}(mtbpy\text{-}\phi_n\text{-}mtbpy)]^{2+}$ **69** (n = 3) and **70** (n = 4) each show a single reversible oxidation process, occurring at 0.84 V *vs.* SCE and 1.01 V respectively (Table 19), corresponding to the oxidation of the two metal centres. The weak electronic communication between the two metal centres in the dyads and the identical nature of the two monometallic units results in the oxidations occurring at the same potential. This is in agreement with the iridium(III) bis-terpyridyl based dyads recently reported by Barigelletti,[241] and those of ruthenium(II) reported by Harriman.[242] The potential of the oxidations in both **69** and **70** is similar to that observed for the related monometallic complex $[Ir(dpydmb)(mtbpy\text{-}\phi\text{-}ph)]^+$ **64** (0.96 V) containing a biphenyl pendant.

Complex [a]	$E_{1/2}^{ox}$ / V	ΔE^{ox} / mV [b]	$E_{1/2}^{red}$ / V	ΔE^{red} / mV [b]
69 * $[Ir\text{–}\phi_3\text{–}Ir]^{2+}$	0.84	100	– 1.84	100
70 * $[Ir\text{–}\phi_4\text{–}Ir]^{2+}$	1.01	140	– 1.72	130
74 $[^{A}Ir\text{–}\phi_2\text{–}^{B}Ir]^{4+}$	1.08 1.67	120 100	– 1.21 – 2.01	150 110
75 $[^{F_2}Ir\text{–}\phi\text{–}Ir]^{2+}$	0.82 1.09	100 80	– 1.66 – 1.72	80 60
64 $[Ir(dpydmb)(mtbpy\text{-}\phi\text{-}ph)]^+$	0.96	90	– 1.56 – 2.25	90 90
$[Ir(tpy)_2]^{3+}$ [46]	–	–	– 0.77	–
$[Ir(ppy)_2(bpy)]^+$ [238]	1.28	–	– 1.35	–

(a) Complexes as their PF_6^- salts in Bu_4NBF_4 (0.1 M in MeCN) as the supporting electrolyte, except those marked * which were in a 0.02 M solution. (b) ΔE^{ox} and ΔE^{red} are the peak to peak separation of the reversible oxidation and reduction processes respectively. These values were measured at a scan rate of 300 mV s^{-1} and are reported relative to SCE (except for those complexes marked * which were measured at 50 mV s^{-1}), using ferrocene as the standard ($E_{1/2}^{ox}$ = 0.42 V *vs.* SCE).

Table 19: Oxidation and reduction potentials of the dinuclear homometallic iridium complexes 69, 70, 74 and 75 alongside the related monometallic complexes 64, $[Ir(tpy)_2]^{3+}$ and $[Ir(ppy)_2(bpy)]^+$ obtained by cyclic voltammetry.

At negative potentials a reversible reduction process occurs in each dyad, –1.84 V for **69** and –1.72 V for **70** (Table 19), assigned to the reduction of the bpy moiety of the NNC ligand, based upon the related monometallic complexes discussed in Section 4.1.4.1. The oxidation and reduction potentials of these dyads support the description of the assemblies in supramolecular terms, where the properties of the individual components are retained.

In contrast, the homometallic complexes [(dpydmb)Ir-μ-(mtbpy-ϕ_2-tpy)Ir(tpy)]$^{4+}$ **74** and [(Fppy)$_2$Ir-μ-(bpy-ϕ-dpydmb)Ir(mtbpy-ϕ-ph)]$^{2+}$ **75**, both contain two iridium complexes of differing environment. Electrochemical studies carried out on these asymmetrical systems reveal two reversible oxidation processes for each dinuclear complex (Table 19). Whilst there are no examples in the literature of electrochemical studies carried out on such asymmetrical homometallic assemblies, several heterometallic systems have been studied where a single oxidation process is observed for each of the unequivalent metal centres.[113, 118, 243] Based upon these heterometallic studies, it is concluded that in both **74** and **75** one oxidation process occurs on each metal centre. In complex **74** it is postulated that the [Ir(NCN)(NNC)]$^+$ coordinated complex is oxidised at the less positive potential (1.08 V *vs.* SCE) and the higher energy bis-terpyridyl complex is oxidised at 1.67 V. This is based upon comparison with the related monometallic complexes [Ir(dpydmb)(mtbpy-ϕ-ph)]$^+$ **64**, displaying a single oxidation process at 0.96 V *vs.* SCE, and [Ir(tpy)$_2$]$^{3+}$ (> 2.4 V *vs.* SCE).[46] It should, however, be noted that the assignment of the oxidation process at 1.67 V to a second oxidation of the Ir(NCN)(NNC) centre, going from +2 to +3, cannot definitely be ruled out.

Similarly in complex **75**, the lower energy [Ir(NCN)(NNC)]$^+$ terminus is believed to be more easily oxidised (0.82 V) than the [Ir(Fppy)$_2$(bpy)]$^+$ unit (1.09 V), following comparison with the monometallic model complexes [Ir(dpydmb)(mtbpy-ϕ-ph)]$^+$ **64** (0.96 V) and [Ir(ppy)$_2$(bpy)]$^+$ (1.28 V).[238] As reported by Juris *et al.* in a review of polynuclear complexes,[8] the fact that the oxidation potentials in these two assemblies do not vary greatly on passing from the mononuclear to the dinuclear species indicates that there is little or no interaction between the two metal centres arising due to poor communication through the phenylene bridge.

At negative potentials two chemically-reversible ligand-based reduction processes were observed for both complexes **74** and **75**. In complex **74** the reduction at –2.01 V *vs.* SCE was assigned to the bpy-moiety on the mtbpy-based ligand and that at –1.21 V to the tpy ligand, following comparison with the monometallic complexes $[Ir(dpydmb)(mtbpy–\phi–ph)]^+$ **64** (–1.54 V) and $[Ir(tpy)_2]^{3+}$ (–0.77 V). In complex **75**, however, the two ligand-based reduction bands are close lying (–1.66 and –1.72 V) making their assignment less clear cut. The close proximity of these two bands is thought to arise due to one being based upon bpy itself and the other on the bpy-moiety of the NNC ligand, both of which are linked to the phenylene bridge.

5.4.2 Heterometallic dinuclear Ir–Ru complexes

Electrochemical studies carried out on the heterometallic dinuclear complex $[(dpydmb)Ir\text{-}\mu\text{-}(mtbpy\text{-}\phi_2\text{-}bpy)Ru(bpy)_2]^{3+}$ **76** reveal two metal-based reversible oxidation processes at 0.81 and 0.98 V *vs.* SCE (Table 20). With oxidation in the corresponding constituent monometallic complexes $[Ir(dpydmb)(mtbpy–\phi–ph)]^+$ **64** and $[Ru(bpy)_3]^{2+}$ [244] occurring at 0.96 V and 1.27 V respectively, the less positive oxidation is concluded to be based upon the iridium unit and the more positive oxidation on the ruthenium centre. In a somewhat related study of linear dinuclear Ir–Ru tris-bidentate systems, De Cola *et al.*[245] reported a small variation in the oxidation potentials upon going from the mononuclear to the dinuclear species. This was attributed to a weak interaction between the two centres, which was found to be too weak to be detected spectroscopically.[243, 245]

Complex [a]	$E_{1/2}^{ox}$ / V	ΔE^{ox} / mV [b]	$E_{1/2}^{red}$ / V	ΔE^{red} / mV [b]
76 $[Ir–\phi_2–Ru]^{3+}$	0.81 0.98	140 160	– 1.67 – 2.42	170 70
$[Ru(bpy)_3]^{2+}$ [244]	1.27	–	– 1.34	–

(a) Complexes as their PF_6^- salts in Bu_4NBF_4 (0.1 M in MeCN) as the supporting electrolyte. (b) ΔE^{ox} and ΔE^{red} are the peak to peak separation of the reversible oxidation and reduction processes respectively. These values were measured at a scan rate of 300 mV s^{-1} and are reported relative to SCE, measured using ferrocene as the standard ($E_{1/2}^{ox}$ = 0.42 V *vs.* SCE).

Table 20: Oxidation and reduction potentials of the heterometallic $[Ir–\phi_2–Ru]^{3+}$ complex 76 and the model monometallic complex $[Ru(bpy)_3]^{2+}$ obtained by cyclic voltammetry.

At negative potentials two ligand-based reduction processes were observed for complex **76** at –1.67 and –2.42 V. These compare to reduction potentials in the contributing constituent monometallic complexes of –1.34 V for $[Ru(bpy)_3]^{2+}$,[244] and –1.54 V for $[Ir(dpydmb)(mtbpy–\phi–ph)]^+$ **64**. Based upon De Cola's findings for the dinuclear $Ir^+–Ru^{2+}$ systems,[245] the first reduction in **76** is thought to occur on the phenylene-substituted bpy ligand of the Ru(II) centre and the phenylene-substituted bpy moiety of the Ir(III) centre, whilst the second reduction is related to the exterior bpy ligands of the ruthenium terminus.

5.4.3 Trinuclear Ir–Ir–Ru complexes

Electrochemical studies of $[(F_2ppy)_2Ir$-μ-(bpy-ϕ-dpydmb)Ir-μ-(mtbpy-ϕ_2-bpy)Ru $(bpy)_2]^{4+}$ **78** (Table 21) reveal two metal-based oxidation processes, one at a potential of 1.16 V *vs.* SCE and the other at 1.31 V. Upon comparison of the oxidation processes in **78** with those observed in the three contributing monometallic complexes $[Ir(dpydmb)(mtbpy–\phi–ph)]^+$ **64** (0.96 V), $[Ru(bpy)_3]^{2+}$ (1.31 V)[245] and $[Ir(F_2ppy)_2(bpy)]^+$ (1.65 V)[245] it is deduced that the oxidation process that occurs at 1.16 V corresponds to the bis-terdentate iridium centre and that at 1.31 V to the ruthenium unit. It is concluded that the oxidation of the tris-bidentate fluorinated iridium centre must lie beyond the limits of the solvent window investigated, in agreement with De Cola's dinuclear $[(F_2ppy)_2Ir$-μ-(bpy-ϕ_n-bpy)$Ru(bpy)_2]^{3+}$ (n = 2-5) species which were reported to exhibit only a ruthenium based oxidation.[245]

Complex [a]	$E_{1/2}^{ox}$ / V	ΔE^{ox} / mV [b]	$E_{1/2}^{red}$ / V	ΔE^{red} / mV [b]
78 $[^{F_4}Ir–\phi–Ir–\phi_2–Ru]^{4+}$	1.16 1.31	140 120	– 1.54 – 2.07	60 120
$[Ir(F_2ppy)(bpy)]^+$ [245]	1.65	–	– 1.29 – 1.97	– –

(a) Complexes as their PF_6^- salts in Bu_4NBF_4 (0.1 M in MeCN) as the supporting electrolyte. (b) ΔE^{ox} and ΔE^{red} are the peak to peak separation of the reversible oxidation and reduction processes respectively. These values were measured at a scan rate of 300 mV s^{-1} and are reported relative to SCE, measured using ferrocene as the standard ($E_{1/2}^{ox}$ = 0.42 V *vs.* SCE).

Table 21: Oxidation and reduction potentials of the trinuclear complex $[^{F_4}Ir–\phi–Ir–\phi_2–Ru]^{4+}$ 78 and the contributing monometallic complex $[Ir(F_2ppy)(bpy)]^+$ obtained by cyclic voltammetry.

At negative potentials two ligand-based reduction processes were observed for complex **78** at –1.54 and –2.07 V. Upon comparison with the reduction processes observed in

the related dimetallic complex **76** (–1.67 and –2.42 V) and monometallic complex $[Ir(F_2ppy)_2(bpy)]^+$ (–1.65 V),[245] it is deduced that the reduction process at –1.65 V most likely corresponds to the reduction of the phenylene-substitued bpy ligands and the bpy-moiety of the NNC ligand. It is therefore thought that the less negative reduction at –2.07 V *vs.* SCE must once again correspond to the reduction of the exterior bpy ligands on the ruthenium terminus, in line with De Cola's work on dinuclear Ir^+–Ru^{2+} systems,[245] and our assignment for complex **76**.

5.5 Photophysical studies

The photophysical properties of the multimetallic complexes prepared by cross-coupling reactions are discussed and compared to the contributing monometallic "building blocks" to help rationalise the observations.

5.5.1 Iridium(III) dyads

The absorption spectra of the dinuclear complexes $[\{Ir(dpydmb)\}_2\mu\text{-}(mtbpy\text{-}\phi_n\text{-}mtbpy)]^{2+}$ (n = 3) **69** and (n = 4) **70** exhibit a series of very intense broad bands between 220 and 400 nm alongside a series of weaker bands extending to lower energy (Table 22 and Figure 5.12).

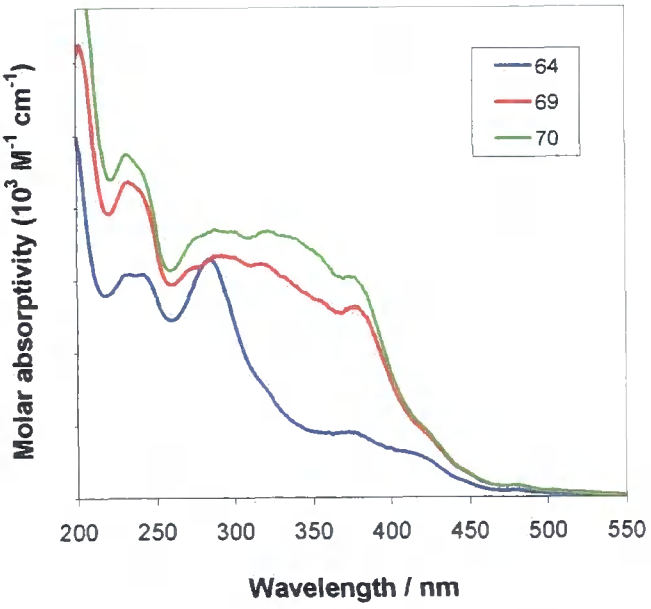

Figure 5.12: Absorption spectra of the $[\{Ir(dpydmb)\}_2\mu\text{-}(mtbpy\text{-}\phi_n\text{-}mtbpy)]^{2+}$ complexes 69 (n = 3) and 70 (n = 4) and the related monometallic complex $[Ir(dpydmb)(mtbpy\text{-}\phi\text{-}ph)]^+$ 64, measured in acetonitrile at 298 K.

The bands between 200 and 330 nm are similar to those observed in the mononuclear complex $[Ir(dpydmb)(mtbpy\text{-}\phi\text{-}ph)]^+$ **64** (Table 22 and Figure 5.12), discussed in Section 4.1.4.4, and are assigned to spin-allowed $^1\pi\text{–}\pi^*$ transitions of the ligands. However, compared to the monometallic complex **64**, the dyads exhibit greatly enhanced absorption in the region of 330 to 400 nm where CT transitions are expected, swamping the previously well-resolved band at around 411 nm. This enhanced absorption is no doubt the result of the intense spin-allowed $^1\pi\text{–}\pi^*$ transitions associated with the oligo(phenylene) bridge that are anticipated in this region.[246]

Complex [a]	**69** $[Ir\text{–}\phi_3\text{–}Ir]^{2+}$	**70** $[Ir\text{–}\phi_4\text{–}Ir]^{2+}$	**64** $[Ir(dpydmb)(mtbpy\text{-}\phi\text{-}ph)]^+$
Absorption maxima / nm (ε / M^{-1} cm^{-1})	479 (32500) 379 (51800) 320 (64600) 292 (67400) 275 (63500) 233 (86300)	479 (33380) 377 (61000) 320 (77000) 287 (74100) 232 (71100)	479 (1940) 412 sh (13200) 375 (23200) 293 (60900) 232 (65300)
Emission maxima / nm	632	633	636 621 [h]
Emission maximum at 77 K / nm	556, 596 [f]	556, 592 [f]	553, 590 [f]
Φ_{em} x 10^2 [b] degassed (aerated)	2.7 (0.75)	2.7 (1.1)	6.3 (2.5) 10 (6.7) [h]
Lifetime [c] / μs degassed (aerated)	0.14 (0.058)	0.14 (0.058)	0.15 (0.057) 11 [h, i] (0.23) [h, i]
Lifetime at 77 K [c] / μs	3.1, 68 [f, g]	2.9, 72 [f, g]	4.0 [f]
k_r [d] / 10^4 s^{-1}	19	19	42 0.91 [h]
Σk_{nr} [d] / 10^5 s^{-1}	70	68	63 0.82 [h]
$k_Q^{O_2}$ [e] / 10^{10} M^{-1} s^{-1}	0.53	0.54	0.57 0.22 [h]

(a) Complexes as their hexafluorophosphate salts in degassed CH_3CN at 298 K, except where stated otherwise. (b) Luminescence quantum yield measured at 298 K using $[Ru(bpy)_3]Cl_2$ as a standard. (c) Lifetime registered at the emission maximum following excitation at 374 nm. (d) Radiative and non-radiative rate constants calculated from τ and Φ values at 298 K. (e) Bimolecular rate constant for quenching by O_2, estimated from τ in degassed and aerated solutions. (f) In an EPA glass at 77 K. (g) Values estimated by fitting separately the short and long components of the decay. (h) In H_2O at 298 K. (i) τ obtained using a xenon lamp with λ_{em} = 420 nm.

Table 22: Photophysical properties of the symmetric homometallic iridium(III) dyads 69 and 70 and the related monometallic "building block" 64.

In degassed acetonitrile at 298 K, the dinuclear complexes $[\{Ir(dpydmb)\}_2\mu\text{-}(mtbpy\text{-}\phi_n\text{-}mtbpy)]^{2+}$ (n = 3) **69** and (n = 4) **70** display single structureless emission bands ($\lambda_{max}^{em} \sim 630$ nm) with lifetimes of 140 ns, typical of phosphorescence from an excited state of predominantly charge-transfer character (Table 22 and Figure 5.13). The emission profile and lifetime of these dyads are in close agreement with those observed for the phenyl-substituted monometallic complex $[Ir(dpydmb)(mtbpy\text{-}\phi\text{-}ph)]^+$ **64** (Table 22 and Figure 5.13), discussed in detail in Section 4.1.4.4. The dinuclear complexes **69** and **70** have luminescence quantum yields of 0.027, roughly half that observed for the phenyl-substituted complex **64** (0.063) and approximately equivalent to the bromo-functionalised starting material $[Ir(dpydmb)(mtbpy\text{-}\phi\text{-}Br)]^+$ **61** (0.023). This variation in quantum yield between the dyads and **64** is thought to arise due to the extended conjugation in **64**, resulting from the phenyl-substituent, whilst the bridging unit of the dyads has little effect on the excited state of the dimetallic complexes. In air equilibrated solution the lifetimes and quantum yields of all three complexes undergo an approximately three-fold reduction, indicative of the partial quenching of the emission by oxygen.

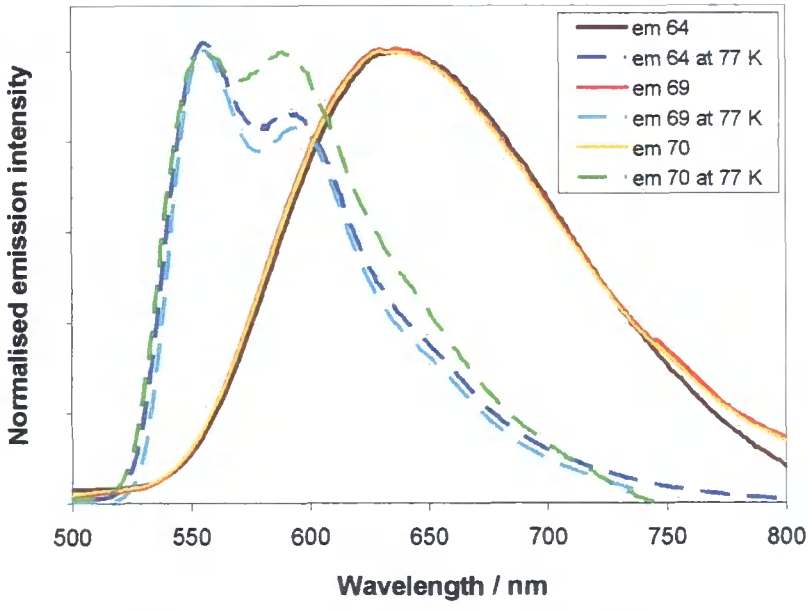

Figure 5.13: Normalised emission spectra of the $[\{Ir(dpydmb)\}_2\mu\text{-}(mtbpy\text{-}\phi_n\text{-}mtbpy)]^{2+}$ complexes (n = 3) 69 and (n = 4) 70 (λ_{ex} = 380 nm) and the related monometallic complex $[Ir(dpydmb)(mtbpy\text{-}\phi\text{-}ph)]^+$ 64 (λ_{ex} = 410 nm at 298 K and 374 nm at 77 K) measured in degassed acetonitrile at 298 K and in an EPA glass at 77 K.

At 77 K, the emission profiles of the dyads, **69** and **70**, and the monometallic complex **64** become structured (λ_{max}^{em} ~ 555 and 590 nm) and are displaced to lower energy (Figure 5.13). The emission decay becomes biexponential for the dinuclear complexes (Table 22), with the shorter component having a lifetime of around 3 μs similar to that observed from the monometallic complex **64** (4.0 μs). This is attributed to emission from an excited state with a similar amount of charge transfer character to the monometallic complex. The longer component (~ 70 μs), however, is far longer than that expected for an excited state with significant metal character and is believed to arise from the triplet π–π* excited state associated with the bridging ligand. In a rigid glass at 77 K the CT states are destabilised, so it is reasonable to assume that the CT and π–π* states have similar energy leading to two decay components being observed at 77 K, even though at 298 K the CT state is far lower in energy resulting in mono-exponential decay being observed. Similarly, De Cola *et al.* reported biexponential decay at 77 K for the somewhat related iridium dinuclear $[\{Ir(F_2ppy)_2\}_2\mu\text{-}(bpy\text{-}\phi_n\text{-}bpy)]^{2+}$ complexes (n = 3 and 4).[128] However, the higher energy of the CT state in the $[Ir(F_2ppy)_2(bpy)]^+$ complex resulted in biexponential decay also being reported at 298 K.

5.5.2 *Asymmetric homometallic dinuclear complexes of iridium(III)*

Unlike the iridium(III) dyads **69** and **70**, the homometallic complexes $[(dpydmb)Ir\text{-}\mu\text{-}(mtbpy\text{-}\phi_2\text{-}tpy)Ir(tpy)]^{4+}$ **74** and $[(Fppy)_2Ir\text{-}\mu\text{-}(bpy\text{-}\phi\text{-}dpydmb)Ir(mtbpy\text{-}\phi\text{-}ph)]^{2+}$ **75** both contain two unequivalent iridium(III) complexes linked by an unsymmetrical bridging ligand. Their photophysical properties are outlined in Table 23. Upon combining two or more unequivalent monometallic "building blocks", the photophysical properties of the resulting multimetallic complexes can be predicted from those of the individual monometallic complexes provided that the bridging units have little or no effect on the excited state energy of the overall complex.[52, 118, 243]

The absorption spectrum of the dimetallic complex $[(Fppy)_2Ir\text{-}\mu\text{-}(bpy\text{-}\phi\text{-}dpydmb)$ $Ir(mtbpy\text{-}\phi\text{-}ph)]^{2+}$ **75** displays peaks characteristic of the two model monometallic iridium complexes: $[Ir(dpydmb)(mtbpy\text{-}\phi\text{-}ph)]^+$ **64** and $[Ir(Fppy)_2(bpy\text{-}\phi)]^+$. The overall shape is similar to that resulting from the sum of the spectra of the two "building blocks" (Figure 5.14) indicating that there is little or no interaction between the two

metal centres. This is in agreement with the electrochemical studies carried out on **75** (Section 5.4.1) which revealed only small changes in the oxidation potentials on passing from the mononuclear "building blocks" to the dinuclear species.

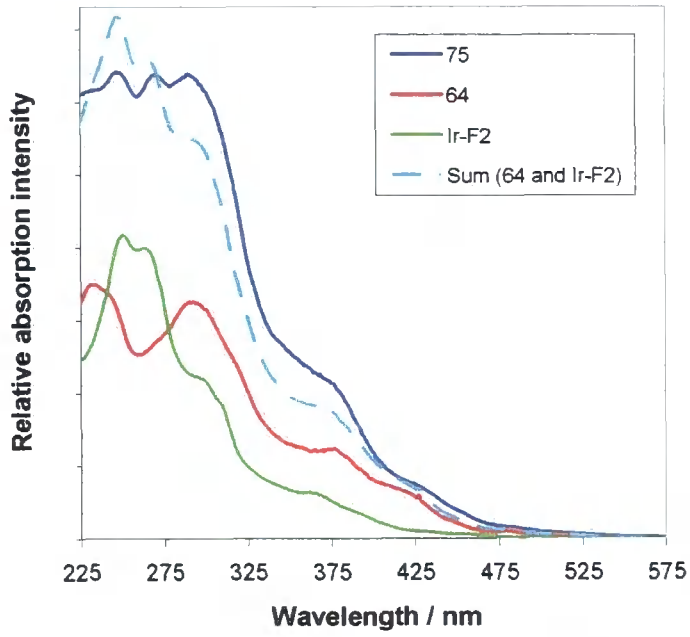

Figure 5.14: Absorption spectra of $[(Fppy)_2Ir$-μ-(bpy-ϕ-dpydmb)$Ir(mtbpy$-ϕ-ph$)]^{2+}$ 75 and the monometallic "building blocks" $[Ir(dpydmb)(mtbpy$-ϕ-ph$)]^+$ 64 and $[Ir(Fppy)_2(bpy$-ϕ$)]^+$, measured in acetonitrile at 298 K.

Excitation of the dinuclear complex $[^{F_2}Ir–ϕ–Ir]^{4+}$ **75** in an acetonitrile solution at wavelengths between 300 and 500 nm, results in a single structureless emission band centred around 616 nm (Table 23 and Figure 5.15). The emission profile lies between that of the model monometallic complexes $[Ir(dpydmb)(mtbpy$-ϕ-ph$)]^+$ **64** (λ_{max}^{em} = 636 nm, Table 22) and $[Ir(Fppy)_2(bpy$-ϕ$)]^+$ (λ_{max}^{em} = 572 nm, Table 23), but is closer lying and more akin to that of the former. Similarly, the luminescence quantum yield observed for **75** (Φ = 0.046) is much more consistent with that observed from **64** (Φ = 0.063) than the higher energy "building block" $[Ir(Fppy)_2(bpy$-ϕ$)]^+$ (Φ = 0.38).

In line with the predictions made from the absorption spectrum and from electrochemical studies it can thus be concluded that there is little or no communication between the two metal centres in $[^{F_2}Ir–ϕ–Ir]^{4+}$ **75**, with the emission emanating from an excited state predominantly localised on the lower energy bis-terdentate centre (**64**). However, the slight blue shift that occurs in the emission maximum of the dinuclear complex $[^{F_2}Ir–ϕ–Ir]^{4+}$ **75** (616 nm) compared to that of $[Ir(dpydmb)(mtbpy$-ϕ-ph$)]^+$ **64**

(636 nm) suggests that the emission observed from this iridium bis-terdentate centre is slightly perturbed by the close proximity to the higher energy ^{F_2}Ir(III) centre, from which there is a separation of only one phenyl ring.

The observed luminescence lifetime for the dinuclear complex **75** (2.5 μs) in degassed acetonitrile solution at ambient temperature is significantly longer than that observed from either iridium component (τ = 150 ns for **64** and τ = 1.0 μs for $[Ir(Fppy)_2(bpy\text{-}\phi)]^+$). This is consistent with there being a contribution from the short phenylene bridge to the emissive excited state.

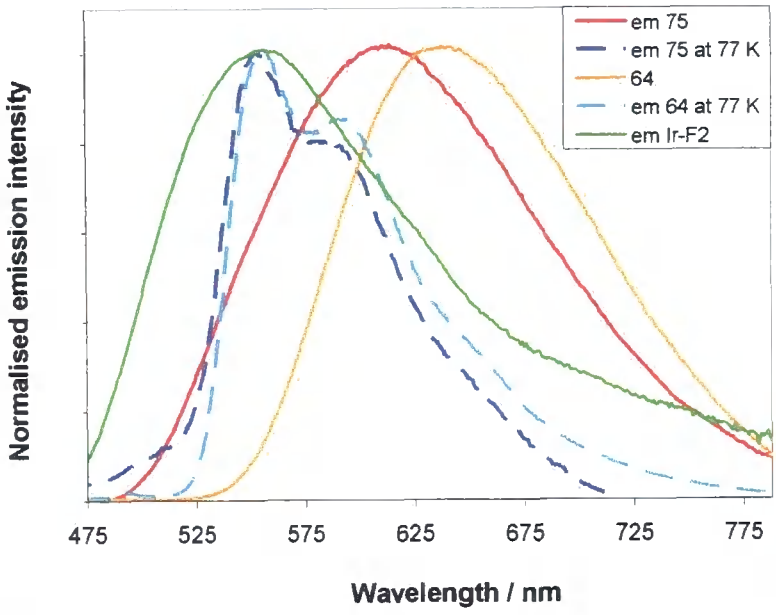

Figure 5.15: The normalised emission spectra of $[(Fppy)_2Ir\text{-}\mu\text{-}(bpy\text{-}\phi\text{-}dpydmb)Ir(mtbpy\text{-}\phi\text{-}ph)]^{2+}$ 75 (λ_{ex} = 365 nm) and the monometallic "building blocks" $[Ir(dpydmb)(mtbpy\text{-}\phi\text{-}ph)]^+$ 64 (λ_{ex} = 410 nm) and $[Ir(Fppy)_2(bpy\text{-}\phi)]^+$ (λ_{ex} = 400 nm) in degassed acetonitrile at 298 K, alongside the emission spectra of 75 and 64 (λ_{ex} = 374 nm) in EPA at 77 K.

A large blue-shift in the emission maximum and the introduction of structure (λ_{max}^{em} = 553 and 586 nm) occurs upon cooling $[^{F_2}Ir\text{–}\phi\text{–}Ir]^{2+}$ **75** to 77 K in a rigid EPA glass (Table 23 and Figure 5.15). Under these conditions, the emission profile and luminescence lifetime (3.2 μs) both closely match those of the monometallic complex **64** (Table 22), indicating that the excited state must be localised on the lower energy $[Ir(NCN)(NNC)]^+$ terminus of **75** and that there is no longer a contribution from the bridging ligand.

Complex [a]	**74** $[^{A}Ir–\phi_2–^{B}Ir]^{4+}$	**75** $[^{F_2}Ir–\phi–Ir]^{2+}$	$[Ir(tpy)_2]^{3+}$ [44, 46]	$[Ir(Fppy)_2(bpy\text{-}\phi)]^{+}$ [237]
Absorption maxima / nm (ε / M^{-1} cm^{-1})	382 (62000) 308 (96800) 280 (109000) 249 (116000)	489 (470) 422 (2890) 366 (8710) 293 (26700) 271 (27000) 248 (27200)	374 (1300) 352 (5800) 336 (8500) 325 (11800) 313 (11400) 277 (22200) 251 (27600)	455 (807) 425 (1370) 338 (12300) 309 (25300) 268 (56700) 254 (54200)
Emission maxima / nm degassed (aerated)	610 (620) 576 [f]	616	458, 491, 525	572
Emission maxima at 77 K / nm	570, 597 [g]	553, 586 [g]	–	–
Φ_{em} x 10^2 [b] degassed (aerated)	0.26 (< 0.1) 1.4 (0.39) [f]	4.6 (2.0)	3.0	38 (3.8)
Lifetime [c] / μs degassed (aerated)	3.2 (0.17) 73 (1.0) [f]	2.5 (0.36)	1.2	1.0 (0.1)
Lifetime at 77 K [c] / μs	3.5, 160 [g, h, i]	3.2 [g]	–	–
k_r [d] / 10^4 s^{-1}	0.017 0.02 [f]	1.8	2.5	38
Σk_{nr} [d] / 10^5 s^{-1}	0.66 0.14 [f]	3.8	8.1	6.2
$k_Q^{O_2}$ [e] / 10^{10} M^{-1} s^{-1}	0.31 0.052 [f]	0.13	–	0.47

(a) Complexes as their hexafluorophosphate salts in degassed CH_3CN at 298 K, except where stated otherwise. (b) Luminescence quantum yield measured at 298 K using $[Ru(bpy)_3]Cl_2$ as a standard. (c) Lifetime registered at the emission maximum following excitation at 374 nm. (d) Radiative and non-radiative rate constants calculated from τ and Φ values at 298 K. (e) Bimolecular rate constant for quenching by O_2, estimated from τ in degassed and aerated solutions. (f) In H_2O at 298 K. (g) In an EPA glass at 77 K. (h) τ obtained using a xenon lamp with λ_{em} = 383 nm. (i) Values estimated by fitting separately the short and long components of the decay.

Table 23: Photophysical properties of the asymmetric homometallic dinuclear complexes 74 and 75 and the related monometallic complexes $[Ir(tpy)_2]^{3+}$ and $[Ir(ppy)_2(bpy)]^{+}$.

Unlike $[^{F_2}Ir–\phi–Ir]^{2+}$ **75**, the absorption spectrum of the asymmetrical dinuclear complex [(dpydmb)Ir-μ-(mtbpy-ϕ_2-tpy)Ir(tpy)]$^{4+}$ **74** (Figure 5.16) appears to be different to that of the sum of the two model monometallic units [Ir(dpydmb)(mtbpy-ϕ-ph)]$^{+}$ **64** and $[Ir(tpy)_2]^{3+}$. Enhanced absorption is observed in the region of 350 to 450 nm for **74**, which as in the homometallic dyads **69** and **70** is thought to result from the strong spin-allowed $^1\pi–\pi^*$ transitions associated with the oligo(phenylene)bridge.[246]

The excitation of $[^{A}Ir–\phi_2–^{B}Ir]^{4+}$ **74**, in acetonitrile solution at 298 K, at wavelengths between 300 and 450 nm results in an emission band centred at 610 nm (Table 23 and Figure 5.16) showing some structure at 517 and 559 nm. The emission profile lies between that observed from the $[Ir(NCN)(NNC)]^{+}$ centre, $\lambda_{max}^{em} = 636$ nm (Table 22), and the $[Ir(tpy)(ttpy)]^{3+}$ unit ($\lambda_{max}^{em} = 515$ and 539 nm), but is closer lying and more characteristic of the former. The luminescence lifetime of 3.2 μs observed from complex **74**, is significantly longer that observed from either of the related monometallic complexes and is consistent with long-lived emission from the π–π* excited state of the biphenyl bridge. In conjunction with the absorption spectrum (Table 23) it can thus be concluded that this emission originates from an excited state localised predominantly on the biphenyl bridge and the $[Ir(dpydmb)(mtbpy\text{-}\phi\text{-}ph)]^{+}$ **64** terminus.

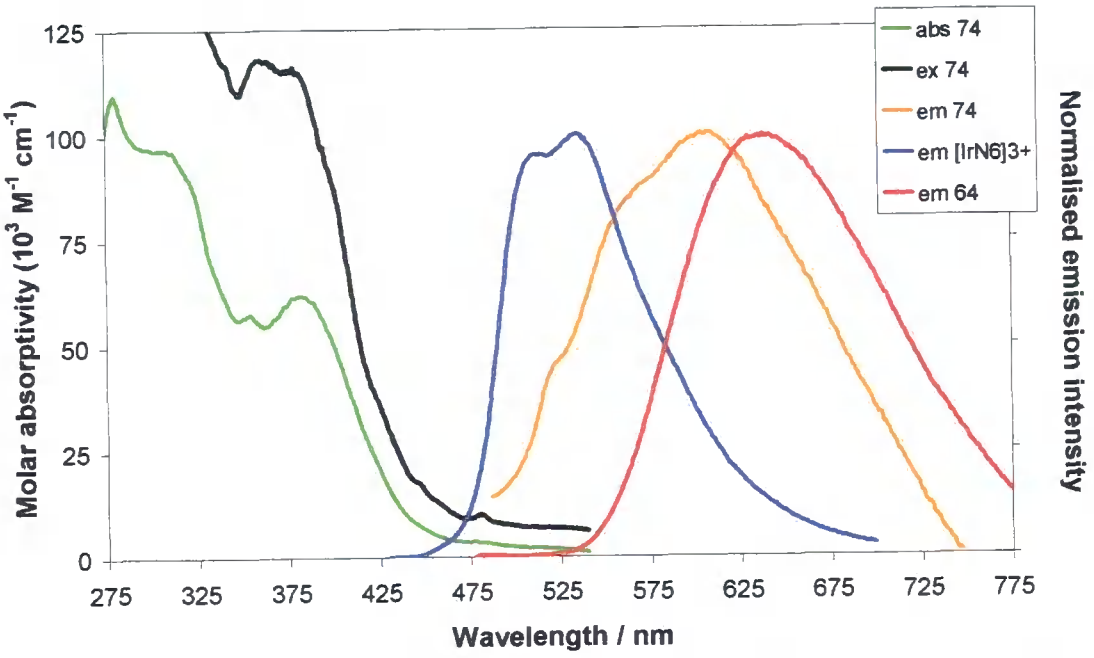

Figure 5.16: Absorption and normalised emission spectra of [(dpydmb)Ir-μ-(mtbpy-ϕ_2-tpy)Ir(tpy)]$^{4+}$ 74 (λ_{ex} = 425 nm) alongside the emission spectra of the monometallic "building blocks" [Ir(dpydmb)(mtbpy-ϕ-ph)]$^{+}$ 64 (λ_{ex} = 410 nm) and [Ir(tpy)(ttpy)]$^{3+}$, with the overlaid excitation spectrum (λ_{em} = 610 nm) offset for clarity. All spectra are recorded in acetonitrile solution at 298 K.

This assignment is further confirmed by emission studies carried out on **74** in degassed aqueous solution at 298 K, where a broad emission band with a long long luminescence lifetime of 73 μs was observed (Table 23). This compares to a luminescence lifetime of 11 μs (Table 22) for the monometallic complex $[Ir(dpydmb)(mtbpy\text{-}\phi\text{-}ph)]^{+}$ **64**. In

aqueous solution, lifetimes of this length are charcteristic of complexes bearing a biphenyl tail contributing considerably to the emissive excited state, as recently reported by Williams *et al.* for a series of biphenyl appended $[Ir(tpy)(tpy\text{-}R)]^{3+}$ complexes.[54]

In air equilibrated acetonitrile solution, the structure in the emission profile is no longer observed, the emission maximum is red-shifted (λ_{max}^{em} = 620 nm) and the luminescence lifetime much shorter (170 ns), comparable to that of the monometallic "building block" $[Ir(dpydmb)(mtbpy\text{-}\phi\text{-}ph)]^{+}$ **64**. Overall, these observations suggest that, under degassed conditions, the emission emanates from an excited state with considerable π–π^* nature associated primarily with the biphenyl bridge, but its long luminescence lifetime leads to severe quenching by oxygen.

Upon cooling $[^{A}Ir\text{–}\phi_2\text{–}^{B}Ir]^{2+}$ **74** to 77 K in a rigid EPA glass, the emission is blue-shifted and significant structure is introduced (λ_{max}^{em} = 570 and 597 nm, Table 23). The emission profile, resembles that of the monometallic complex **64** (λ_{max}^{em} = 553 and 590 nm, Table 22) and the emission decay becomes biexponential with the shorter component having a lifetime of 3.5 μs similar to that observed for **64** (4.0 μs). This is attributed to an excited state with a similar amount of charge transfer charcter to the monometallic complex itself. The longer component (~ 160 μs) is far longer than that expected for an excited state with significant metal character and is believed to arise from the triplet π-π^* excited state associated with the bridging ligand. Akin to the homometallic $[\{Ir(dpydmb)\}_2\mu\text{-}(mtbpy\text{-}\phi_n\text{-}mtbpy)]^{2+}$ complexes (n = 3) **69** and (n = 4) **70**, the CT and π-π^* states are of comparable energy at 77 K leading to the two decay components being observed.

5.5.3 Heterometallic dinuclear Ir–Ru complexes

The photophysical properties of the heterometallic dinuclear complex, $[(dpydmb)Ir\text{-}\mu\text{-}(mtbpy\text{-}\phi_2\text{-}bpy)Ru(bpy)_2]^{3+}$ **76** are outlined in Table 24. The absorption spectrum of this $[Ir\text{–}\phi_2\text{–}Ru]^{3+}$ complex display peaks characteristic of the monometallic complexes $[Ir(dpydmb)(mtbpy\text{-}\phi\text{-}ph)]^{+}$ **64** and $[Ru(bpy)_2(bpy\text{–}\phi)]^{2+}$, with the overall shape being similar to that resulting from the addition of the spectra of the two "building blocks" (Figure 5.17). This suggests that the two components retain the properties they exhibited when isolated and the phenylene bridge has little effect upon the dimetallic

complex. This is in agreement with the somewhat related [(tpy)Ir-μ-(tpy–ϕ_2–bpy)Ru(bpy)$_2$]$^{5+}$ assembly reported by this laboratory,[130] and the [(F$_2$ppy)$_2$Ir-μ-(bpy–ϕ_n–bpy)Ru(bpy)$_2$]$^{3+}$ systems reported De Cola *et al.*,[245] where the absorption spectra are reported to match that of the sum of the monometallic components.

Complex [a]	**76** $[Ir–\phi_2–Ru]^{3+}$	$[Ru(bpy)_2(bpy–\phi)]^{2+}$ [237]
Absorption maxima / nm (ε / M^{-1} cm^{-1})	451 (13800) 426 (15300) 373 (23800) 327 (35900) 288 (46200) 239 (68300)	454 (16900) 430 (14000) 399 (7030) 288 (84100) 253 (35000) 246 (36300)
Emission maximum / nm	630	627
Emission maxima at 77 K / nm	604, 644 [f]	–
Φ_{em} x 10^2 [b] degassed (aerated)	12 (2.2)	9.0 (1.5)
Lifetime [c] / μs degassed (aerated)	1.2 (0.26)	1.3 (0.20)
Lifetime at 77 K [c] / μs	4.9 [f]	–
k_r [d] / 10^4 s^{-1}	10	6.9
Σk_{nr} [d] / 10^5 s^{-1}	7.3	7.0
$k_Q^{O_2}$ [e] / 10^{10} M^{-1} s^{-1}	0.16	0.22

(a) Complexes as their hexafluorophosphate salts in degassed CH_3CN at 298 K, except where stated otherwise. (b) Luminescence quantum yield measured at 298 K using $[Ru(bpy)_3]Cl_2$ as a standard. (c) Lifetime registered at the emission maximum following excitation at 374 nm. (d) Radiative and non-radiative rate constants calculated from τ and Φ values at 298 K. (e) Bimolecular rate constant for quenching by O_2, estimated from τ in degassed and aerated solutions. (f) In an EPA glass at 77 K.

Table 24: Photophysical properties of the heteromometallic dinuclear complex $[Ir–\phi_2–Ru]^{3+}$ 76 and the monometallic "building block" $[Ru(bpy)_2(bpy–\phi)]^{2+}$.

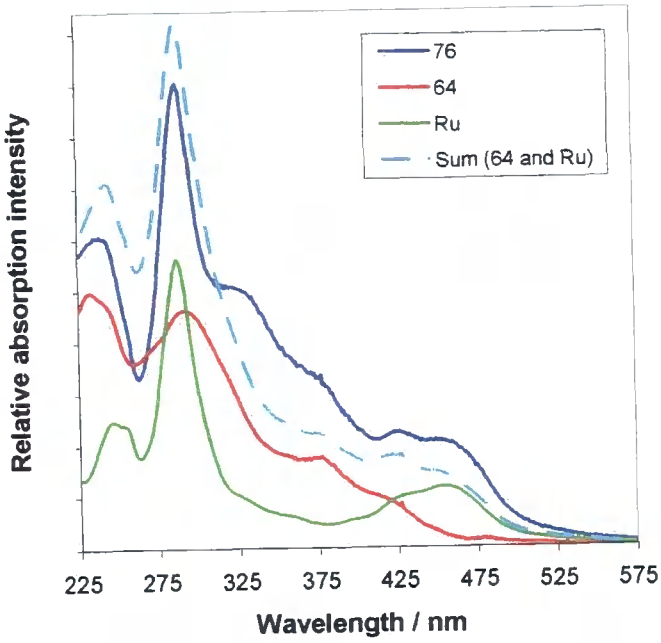

Figure 5.17: Absorption spectra of $[(dpydmb)Ir\text{-}\mu\text{-}(mtbpy\text{-}\phi_2\text{-}bpy)Ru(bpy)_2]^{3+}$ 76 and the monometallic "building blocks" $[Ir(dpydmb)(mtbpy\text{-}\phi\text{-}ph)]^{+}$ 64 and $[Ru(bpy)_2(bpy\text{-}\phi)]^{2+}$, measured in acetonitrile at 298 K.

Upon excitation of the $[Ir\text{–}\phi_2\text{–}Ru]^{3+}$ complex **76** in degassed acetonitrile at wavelengths between 300 and 500 nm, a single structureless emission band centred at 630 nm was observed with a long luminescence lifetime (1.2 μs) and a quantum yield of 0.12 (Table 24 and Figure 5.18). Comparison of the emission profile of **76** with those of the monometallic "building blocks" **64** (Table 22) and $[Ru(bpy)_2(bpy\text{–}\phi)]^{2+}$ (Table 24), displaying broad structureless emission centred at 636 nm and 627 nm respectively, revealed that the emission more closely resembles that observed from the latter component (Figure 5.18). Similarly, the luminescence lifetime (1.2 μs) and quantum yield (0.12) are consistent with the assignment of the excited state to the ruthenium terminus (τ = 1.3 μs and Φ = 0.09) rather than the iridium centre **64** (τ = 150 ns and Φ = 0.063).

Emission from the marginally higher energy ruthenium terminus (15900 cm^{-1}) in this $[Ir\text{–}\phi_2\text{–}Ru]^{3+}$ assembly arises due to the irdium centre (15700 cm^{-1}) being sufficiently high in energy to allow energy transfer to the ruthenium terminus and the population of the ruthenium-based excited state. Emission from the related heterometallic $[(tpy)Ir\text{-}\mu\text{-}(tpy\text{–}\phi_2\text{–}bpy)Ru(bpy)_2]^{5+}$ system, previously reported by this laboratory, occurs exclusively from the ruthenium centre which is of significantly lower energy.[130] The

quenching of the emission from the iridium centre in this $[Ir–\phi_2–Ru]^{5+}$ system is attributed to rapid energy transfer from the higher energy iridium terminus to the lower energy ruthenium centre.[130]

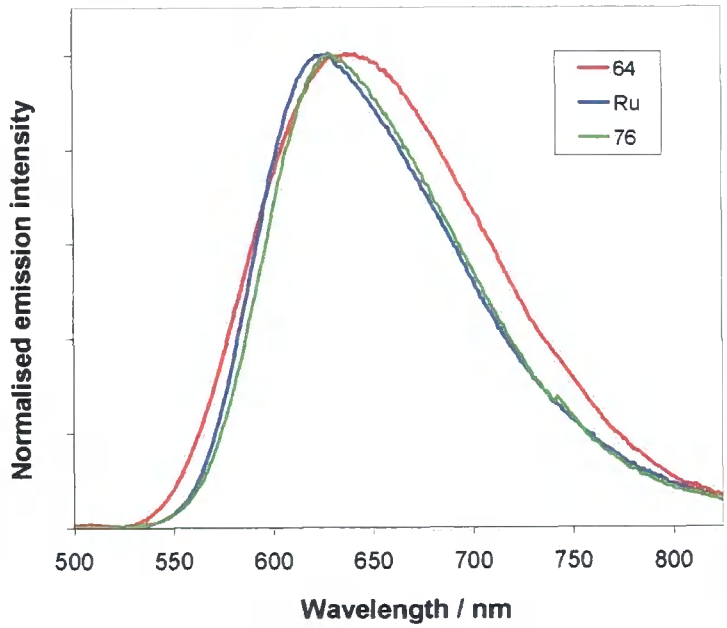

Figure 5.18: The normalised emission spectra of $[(dpydmb)Ir-\mu-(mtbpy-\phi_2-bpy)Ru(bpy)_2]^{3+}$ 76 (λ_{ex} = 374 nm) and the monometallic "building blocks" $[Ir(dpydmb)(mtbpy-\phi-ph)]^{+}$ 64 (λ_{ex} = 410 nm) and $[Ru(bpy)_2(bpy-\phi)]^{+}$ (λ_{ex} = 455 nm) in degassed acetonitrile at 298 K.

Upon cooling to 77 K in a rigid EPA glass, the emission spectrum of **76** becomes structured (λ_{max}^{em} = 604 and 644 nm) and blue-shifted, with a lifetime of 4.9 μs (Table 24), consistent with there being significant CT character in the excited state.

DFT calculations were carried out on this heterometallic dinuclear assembly, $[Ir–\phi_2–Ru]^{3+}$ **76** (Figure 5.19), and the calculated orbital characteristics of the three highest energy occupied molecular orbitals and three lowest energy unoccupied molecular orbitals summarised in Table 25.

Complex	HOMO–2	HOMO–1	HOMO	LUMO	LUMO+1	LUMO+2
76 $[Ir–\phi_2–Ru]^{3+}$	Ir (3%) NCN (82%) NNC (15%)	Ir (42%) NCN (14%) NNC (44%)	Ir (39%) NCN (48%) NNC (13%)	Ru (1%) NN-ϕ (28%) NN (71%)	Ru (8%) NN-ϕ (33%) NN (59%)	Ru (9%) NN-ϕ (32%) NN (59%)

Table 25: Calculated molecular orbital characteristics of $[(dpydmb)Ir-\mu-(mtbpy-\phi_2-bpy)Ru(bpy)_2]^{3+}$ 76 according to DFT calculations. The percentages in parentheses denote the proportion of the total electron density localised at that site.

These calculations revealed that the overall electron density in the HOMO and HOMO–1 of **76** are centred on the iridium moiety, the HOMO being localised primarily on the iridium centre and the phenyl ring of the dpydmb (NCN) ligand and the HOMO–1 on the iridium centre and the phenyl ring of the phbpy (NNC) ligand, whilst the LUMO is delocalised across the three bpy ligands of the ruthenium moiety (Figure 5.19). This is suggestive of emission from an excited state that is localised primarily on the ruthenium terminus of the heterometallic system and is in strong agreement with the assignment made from the photophysical studies (Table 24 and Figure 5.20).

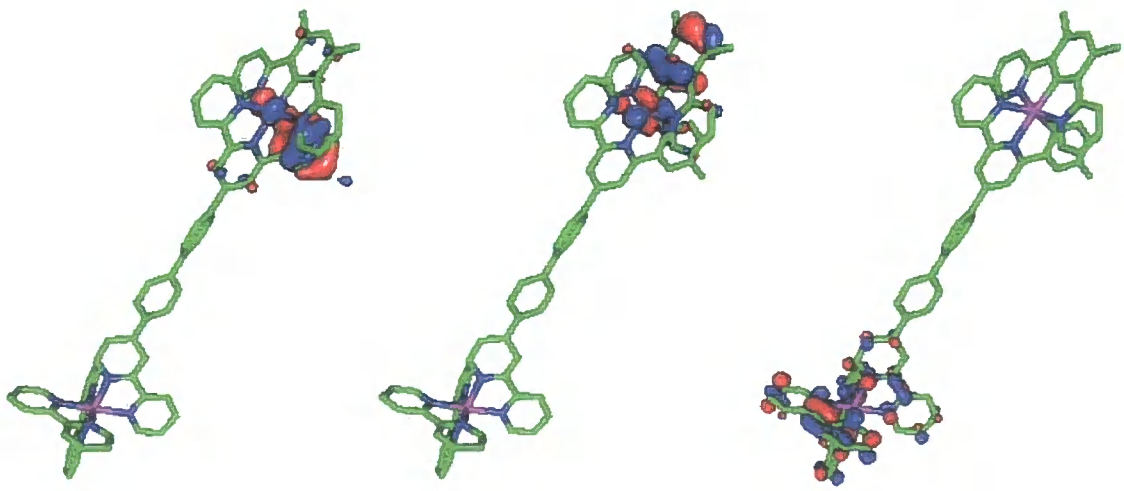

Figure 5.19: Contour plots of the HOMO–1, HOMO and LUMO of $[Ir–\phi_2–Ru]^{3+}$ 76.

5.5.4 Trinuclear Ir–Ir–Ru complexes

The photophysical properties of the trimetallic complex $[(F_2ppy)_2Ir\text{-}\mu\text{-}(bpy\text{-}\phi\text{-}dpydmb)Ir\text{-}\mu\text{-}(mtbpy\text{-}\phi_2\text{-}bpy)Ru(bpy)_2]^{4+}$ **78** are summarised in Table 26, where the "building blocks" can be considered as the monometallic complex $[Ir(F_2ppy)_2(bpy\text{-}\phi)]^+$ (Table 26) and the heterometallic dinuclear assembly $[(dpydmb)Ir\text{-}\mu\text{-}(mtbpy\text{-}\phi_2\text{-}bpy)Ru(bpy)_2]^{3+}$ **76** (Table 24).

Complex [a]	**78** $[^{F_4}Ir–\phi–Ir–\phi_2–Ru]^{4+}$	$[Ir(F_2ppy)_2(bpy–\phi)]^+$ [237]
Absorption maxima / nm (ε / M^{-1} cm^{-1})	453 (8950) 426 (9940) 379 (16700) 288 (99400) 244 (72500)	446 (598) 417 (1300) 359 (7860) 333 (12100) 313 (23500) 300 (28100) 262 (49100) 250 (49200)
Emission maximum / nm	632	539
Emission maxima at 77 K / nm	614, 664 [f]	–
Φ_{em} x 10^2 [b] degassed (aerated)	7.7 (1.4)	66 (5.8)
Lifetime [c] / μs degassed (aerated)	1.2 (0.22)	1.4 (0.14)
Lifetime at 77 K [c] / μs	5.1 [f]	–
k_r [d] / 10^4 s^{-1}	6.4	47
Σk_{nr} [d] / 10^5 s^{-1}	7.7	2.4
$k_Q^{O_2}$ [e] / 10^{10} M^{-1} s^{-1}	0.20	0.34

(a) Complexes as their hexafluorophosphate salts in degassed CH_3CN at 298 K, except where stated otherwise. (b) Luminescence quantum yield measured at 298 K using $[Ru(bpy)_3]Cl_2$ as a standard. (c) Lifetime registered at the emission maximum following excitation at 374 nm. (d) Radiative and non-radiative rate constants calculated from τ and Φ values at 298 K. (e) Bimolecular rate constant for quenching by O_2, estimated from τ in degassed and aerated solutions. (f) In an EPA glass at 77 K.

Table 26: Photophysical properties of the trimetallic $[^{F_4}Ir–\phi–Ir–\phi_2–Ru]^{4+}$ complex 78 and the monometallic "building block" $[Ir(F_2ppy)_2(bpy–\phi)]^+$.

The absorption, excitation and emission spectra obtained for complex **78** are shown in Figure 5.20, alongside the emission spectra for the relevant monometallic and dimetallic "building blocks". The absorption spectrum of **78** is similar to that of the weighted sum of the "building blocks" ($[Ir–\phi_2–Ru]^{3+}$ **76** and $[Ir(F_2ppy)_2(bpy\text{-}\phi)]^+$), suggesting that the phenylene bridge between the two iridium centres does not contribute to the trimetallic species and the properties exhibited by the "building blocks" are retained.

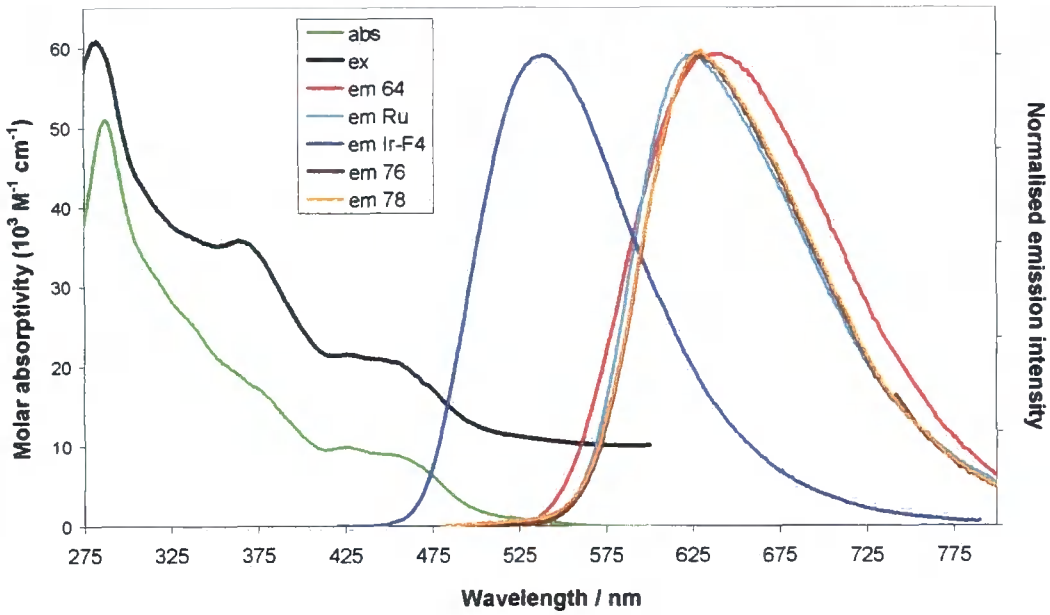

Figure 5.20: The absorption and normalised emission spectra of the trimetallic $[^{F_4}Ir–\phi–Ir–\phi_2–Ru]^{4+}$ system 78 (λ_{ex} = 374 nm) alongside the emission spectra of the dimetallic $[Ir–\phi_2–Ru]^{3+}$ complex 76 (λ_{ex} = 374 nm) and monometallic "building blocks" $[Ir(dpydmb)(mtbpy\text{-}\phi\text{-}ph)]^+$ 64 (λ_{ex} = 410 nm), $[Ru(bpy)_2(bpy–\phi)]^{2+}$ (λ_{ex} = 455 nm) and $[Ir(F_2ppy)_2(bpy–\phi)]^+$ (λ_{ex} = 400 nm) in degassed acetonitrile at 298 K, with the excitation spectrum (λ_{em} = 632 nm) of 78 overlaid and offset for clarity.

Excitation of **78**, at wavelengths between 275 and 500 nm, results in a single structureless emission band centred at 632 nm (Figure 5.20), with a luminescence lifetime of 1.2 μs and quantum yield of 0.077. This is characteristic of emission from a primarily MLCT excited state and closely resembles that observed from the dimetallic species **76** and its constituent "building block" $[Ru(bpy)_2(bpy–\phi)]^{2+}$. As for the dimetallic component $[Ir–\phi_2–Ru]^{3+}$ **76**, the emission is assigned to an excited state localised on the ruthenium terminus. Overlaying the excitation spectrum recorded at the emission maximum with the absorption profile of **78** (Figure 5.20) confirms that, in line with the energies of the individual "building blocks", the excitation of the trimetallic system $[^{F_4}Ir–\phi–Ir–\phi_2–Ru]^{4+}$ **78** is followed by rapid energy transfer from the high energy $[Ir(F_2ppy)_2(bpy\text{-}\phi)]^+$ end to the lower energy $[Ru(bpy)_2(bpy\text{-}\phi)]^{2+}$ terminus, from which emission occurs (Figure 5.8). This indicates that there is little or no communication between the "building blocks", $^{F_4}Ir(III)$ and $[Ir–\phi_2–Ru]^{3+}$ **76** (comprising of the monometallic units $[Ir(dpydmb)(mtbpy\text{-}\phi\text{-}ph)]^+$ **64** and $[Ru(bpy)_2(bpy\text{-}\phi)]^{2+}$) and that the phenylene bridges linking them do not affect the excited state properties of the trimetallic complex. De Cola *et al.*, similarly, reported rapid energy transfer from the $^{F_4}Ir(III)$ centre to the lower energy ruthenium terminus, with no involvement from the

phenylene bridge, in their related dinuclear $[(F_2ppy)_2Ir\text{-}\mu\text{-}(bpy\text{–}\phi_n\text{–}bpy)Ru(bpy)_2]^{3+}$ systems.[245]

5.6 Concluding remarks

The successful linear elaboration of the $[Ir(NCN)(NNC)]^+$ coordinated complex *via* Suzuki cross-coupling reactions with appropriately functionalised iridium and ruthenium complexes has been reported. Whilst the initial studies involved the coupling of monometallic complexes bearing appropriate functionality to form dinuclear complexes, the use of *in situ* bromination allows the further coupling of these dinuclear species to form trinuclear assemblies and beyond. This technique avoids the pre-synthesis of bridging ligands and provides a simple and reliable route to the controlled synthesis of multimetallic arrays.

The photophysical and electrochemical properties of the multinuclear complexes have been investigated. In the symmetrical ($[Ir\text{–}\phi_3\text{–}Ir]^{2+}$ **69** and $[Ir\text{–}\phi_4\text{–}Ir]^{2+}$ **70**) and asymmetrical homometallic complexes ($[^{A}Ir\text{–}\phi_2\text{–}^{B}Ir]^{4+}$ **74** and $[^{F_2}Ir\text{–}\phi\text{–}Ir]^{2+}$ **75**) the phenylene bridge appears to play a significant role in the excited state of the assembly. This results in long luminescence lifetimes characteristic of the $\pi\text{-}\pi^*$ excited states of phenylene bridge being observed for these systems at 77 K and both 298 and 77 K respectively. The heterometallic dinuclear ($[Ir\text{–}\phi_2\text{–}Ru]^{3+}$ **76**) and trinuclear systems ($[^{F_4}Ir\text{–}\phi\text{–}Ir\text{–}\phi_2\text{–}Ru]^{4+}$ **78**), however, behave as a true "supramolecular" assemblies in which the phenylene bridges play no role in the excited state and the properties of the individual "building blocks" are retained. Emission characteristic of the ruthenium centre is observed from both $[Ir\text{–}\phi_2\text{–}Ru]^{3+}$ **76** and the resulting trinuclear system, $[^{F_4}Ir\text{–}\phi\text{–}Ir\text{–}\phi_2\text{–}Ru]^{4+}$ **78**, where rapid energy transfer from the highest energy $^{F_4}Ir(III)$ centre to the lower energy ruthenium terminus is reported.

Multinuclear systems retain the photophysical properties displayed by the individual "building blocks", provided that the phenylene bridging units have little or no effect on the excited state energy of the overall system. The properties of such assemblies can thus be predicted based upon those of the individual units, allowing systems to be designed to channel energy to a specific part of the complex, an ideal concept in the design of assemblies for use as light harvesting agents.

CHAPTER 6

EXPERIMENTAL

6 Experimental

6.1 Synthetic procedures and characterisation

The solvents used throughout were of Analar® quality and used as supplied, except for acetonitrile which was HPLC grade. Water was purified using the Purite$_{STILL}$ Plus™ system having conductivity of ≤ 0.04 μS cm^{-1}. All reagents were used as supplied.

Thin layer chromatography was carried out using silica plates (Merck Art 5554) or neutral aluminium oxide plates (Merck Art 5550), both types being fluorescent upon irradiation at 254 nm. Preparative column chromatography was carried out using silica (Merck Silica Gel 60, 230-400 mesh), or neutral alumina (Merck Aluminium Oxide 90, Brockman activity 2-3).

NMR spectra were recorded on a Varian Mercury-200 spectrometer (200 MHz for ^{1}H, 50 MHz for ^{13}C and 188 MHz for ^{19}F), Varian Unity-300 spectrometer (300 MHz for ^{1}H), Varian Mercury-400 spectrometer (400 MHz for ^{1}H and 101 MHz for ^{13}C), Bruker Advance-400 spectrometer (400 MHz for ^{1}H), Varian Inova-500 spectrometer (500 MHz for ^{1}H, 126 MHz for ^{13}C and 470 MHz for ^{19}F) or Varian DD-700 spectrometer (700 MHz for ^{1}H, 176 MHz for ^{13}C and 658 MHz for ^{19}F), and were referenced to residual protiosolvent resonances. All NMR data is reported with chemical shifts (δ) quoted in ppm and coupling constants (J) in Hz. ^{1}H-NMR spectra were assigned with assistance from ^{1}H-^{1}H COSY (correlation spectroscopy, through-bond interactions) and ^{1}H-^{1}H NOESY (nuclear Overhauser effect spectroscopy, through-space interactions) spectra. ^{13}C-NMR spectra were recorded with proton decoupling and were assigned with assistance from ^{1}H-^{13}C HSQC (heteronuclear single quantum correlation) and ^{1}H-^{13}C HMBC (heteronuclear multiple bond correlation) spectra.

Electrospray ionisation mass spectra (ES^{+} MS and ES^{-} MS) were recorded with a Micromass LCT spectrometer or Thermo-Finnigan LTQ FT spectrometer with methanol or acetonitrile as the carrier solvent. MALDI mass spectra were recorded with a Voyager-DE STR BioSpectrometry Workstation or a Thermo-Finnigan LTQ FT

spectrometer. High resolution mass spectra were recorded with a Micromass LCT spectrometer at 5000 resolution using sodium iodide as the reference, or a Thermo Finnigan LTQ FT spectrometer at 100000 resolutions with external calibration. Electron ionisation, EI, mass spectra and the corresponding high resolution mass spectra were recorded by the EPSRC National Mass Spectrometry Service at the University of Wales, Swansea. Gas chromatography-mass spectra (GC-MS) were recorded using a Thermoquest Trace mass spectrometer.

C, H and N analysis was performed using an Exeter Analytical E-440 elemental analyser. Melting points were determined on a Gallenkamp 889339 capillary melting point apparatus and are quoted to the nearest 1°C.

6.2 Photochemical and photophysical measurements

UV-visible absorption spectra were measured using a Biotek Instruments XS spectrometer operating with LabPower software. All samples were contained in quartz cuvettes of 1 cm pathlength, and run against a reference of pure solvent contained within a matched cuvette. Extinction coefficients were determined by dilution technique and graphical application of the Beer-Lambert law.[6]

$$A(\lambda) = \varepsilon(\lambda)cl$$

$A(\lambda)$ is the absorbance at a specified wavelength, $\varepsilon(\lambda)$ is the extinction coefficient at that wavelength ($dm^3\ mol^{-1}\ cm^{-1}$), c is the concentration of the species that is absorbing ($mol\ dm^{-3}$) and l is the pathlength (cm).

Steady-state luminescence spectra were recorded using a Jobin Yvon FluoroMax-2 spectrofluorimeter, equipped with a red-sensitive Hamamatsu R928 photomultiplier tube (PMT), and operated with DataMax software. Samples for emission measurements were contained within quartz fluorescence cuvettes of 1 cm pathlength and the absorbance of each solution at the excitation wavelength was kept below 0.1 to minimise inner filter effects. Emission was detected at right angles to the emission source, with appropriate filters used where required to remove second order peaks. All emission spectra were corrected after data acquisition for the dark count and for the

wavelength dependent spectral response of the detector. All quoted emission maxima refer to the values after correction. Excitation spectra were automatically corrected for lamp output, through use of a beam splitter, which directs 8% of the excitation light to a reference photodiode.

Luminescence quantum yields were recorded with respect to a standard of ruthenium(II) tris(2,2'-bipyridine) chloride in aqueous solution, where $\Phi_{st} = 0.028$.[247] The luminescence quantum yield of the sample (Φ) is calculated relative to the standard using the following equation.[248]:-

$$\Phi = \Phi_{st}\left[\frac{I}{I_{st}}\right]\left[\frac{A_{st}}{A}\right]\left[\frac{n^2}{n_{st}^2}\right]$$

Where I is the integrated emission intensity at a given excitation wavelength, A is the absorbance at that wavelength and n is the refractive index of the solvent. The symbols with the subscript 'st' are the respective values for the standard.

The quartz cuvettes of 1 cm pathlength used for emission measurements were modified with appropriate glassware to allow connection to a high-vacuum line. The degassing of samples was achieved by a minimum of three freeze-pump-thaw cycles, whilst connected to the high-vacuum line. A final vapour pressure of $< 5 \times 10^{-2}$ mbar at 77 K was achieved, monitored using a Pirani gauge.

Low temperature (77 K) measurements of the samples were obtained as EPA glasses (EPA = diethyl ether-isopentane-ethanol, 2:2:1 by volume). The sample as a solution in EPA was placed in a 4 mm diameter glass tube; then lowered inside a glass Dewar of liquid nitrogen where it remained whilst the measurements were taken.

The excited state lifetime measurements were measured using time-correlated single-photon counting (TCSPC). The samples were excited in 1 cm pathlength quartz fluorescence cuvettes at 374.0 nm with an EPL-375 pulsed-diode laser. The emitted light passed through a monochromator and was detected at 90° using a Peltier-cooled R928 photomultiplier tube. The estimated uncertainty in these lifetimes is < 10%.

Longer lifetimes, > ~ 10 μs, were measured using multi-channel scaling following excitation by a pulsed xenon lamp.

6.3 Electrochemical measurements

Cyclic voltammetry was carried out in a background electrolyte of tetrabutylammonium tetrafluoroborate (0.1 or 0.02 M) in acetonitrile. A μAutolab type III potentiostat was used with computer control and data storage *via* GPES Manager. A three electrode assembly was employed, consisting of a platinum wire counter electrode, platinum flag reference electrode and a platinum working electrode. The measurements were carried out in a glass cell charged with 2 mg of complex in 2 mL of electrolyte and purged with nitrogen.

6.4 Density functional theory calculations

B3LYP density functional theory, DFT, calculations were performed using the Gaussian98[249] and Gaussian03[250] software packages. "Double-ζ" quality basis sets were employed for the ligands (6-31G) and the iridium and rhodium metal centres (LANL2DZ).[236] The inner core electrons of iridium were replaced with a relativistic effective core potential (ECP), leaving the outer core $[(5s)^2(5p)^6]$ electrons and the $(5d)^6$ valence electrons of iridium(III). Likewise for rhodium(III) the inner core electrons were replaced leaving the outer core $[(4s)^2(4p)^6]$ electrons and the $(4d)^6$ valence electrons. The geometries were fully optimised without symmetry constraints.

6.5 *Synthesis of ligands*

6-phenyl-2,2'-bipyridine [phbpyH][77, 205] 1

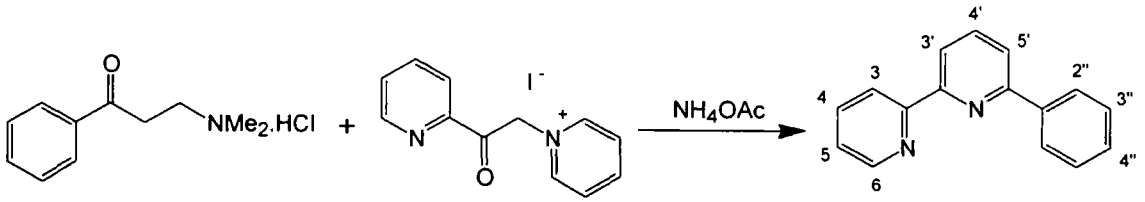

Step 1: 1-(2-oxo-2-pyridin-2-yl-ethyl)pyridinium iodide[203] 2

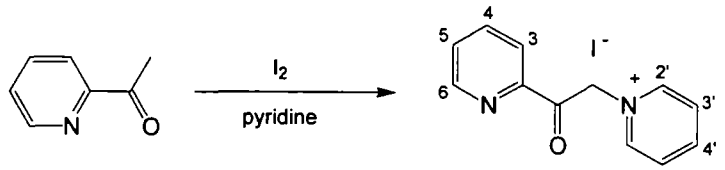

2-Acetylpyridine (4.87 g, 40.2 mmol) in pyridine (10 mL) was added to a solution of iodine (10.16 g, 40.0 mmol) in pyridine (30 mL) and synthesis carried out *via* the well established Kröhnke methodology. Following collection of the precipitate by filtration, it was washed with cold ethanol (3 x 5 mL) and dried under vacuum to give the desired product as a cream coloured crystalline solid (7.22 g, 55%).

^{1}H-NMR ($CDCl_3$, 500 MHz) δ = 9.21 (2H, d, ^3J = 6.0, $H^{2'}$), 8.75 (1H, d, ^3J = 5.0, H^6), 8.55 (1H, t, ^3J = 8.0, $H^{4'}$), 8.14 (2H, t, ^3J = 6.5, $H^{3'}$), 8.06 (1H, d, ^3J = 8.0, H^4), 7.91 (1H, td, ^3J = 7.5, ^4J = 1.5, H^3), 7.60 (1H, ddd, ^3J = 7.5, 5.0, ^4J = 1.5, H^5), 6.98 (2H, s, CH_2). ^{13}C-NMR ($CDCl_3$, 126 MHz) δ = 192.2 (C=O), 151.2 (C^2), 150.3 (C^6), 147.1 (C^2 or $C^{4'}$), 147.0 (C^2 or $C^{4'}$), 138.9 (C^4), 129.9 (C^5), 128.4 ($C^{3'}$), 122.8 (C^3), 67.4 (CH_2). MS (ES^+) m/z = 199.1 $[M - I]^+$. C, H & N analysis: 44.14% C, 3.39% H and 8.61% N measured; 44.19% C, 3.40% H and 8.59% N calculated for $[C_{12}H_{11}IN_2O]$. Mp = 204–206°C.

Step 2: Hydrochloride salt of *β*-dimethylaminopropiophenone[206] 3

Concentrated HCl (20 µL) was added to a mixture of acetophenone (1.23 g, 10.2 mmol), paraformaldehyde (0.40 g, 13.3 mmol) and dimethylamine hydrochloride (1.07 g, 13.1 mmol) in ethanol (5 mL). The suspension was heated under a N_2 atmosphere at reflux for 24 hours. After cooling to room temperature and subsequently

0°C in an ice bath, the precipitate was collected by filtration, washed with ethanol (4 x 5 mL) and dried under vacuum to give the product as a white solid (0.90 g, 50%). ^{1}H-NMR ($CDCl_3$, 500 MHz) δ = 7.93 (2H, dd, ^3J = 8.5, ^4J = 1.5, H^2), 7.55 (2H, tt, ^3J = 7.5, ^4J = 1.0, H^4), 7.42 (2H, td, ^3J = 6.5, ^4J = 2.0, H^3), 3.70 (2H, t, ^3J = 7.0, H^a), 3.50 (2H, m, H^b), 2.81 (6H, d, ^4J = 5.5, CH_3). ^{13}C-NMR ($CDCl_3$, 126 MHz) δ = 196.1 (C=O), 135.7 (C^1), 134.4 (C^4), 129.15 (C^3), 128.5 (C^2), 53.0 (CH_2^b), 43.6 (CH_3), 34.1 (CH_2^a). MS (ES^+) m/z = 178.1 $[M + H]^+$. C, H & N analysis: 57.60% C, 7.00% H and 5.93% N measured; 57.80% C, 6.82% H and 5.71% N calculated for $[C_{11}H_{15}NO].\{0.8(CH_2Cl_2)\}$. Mp = 138–141°C.

Step 3: 6-phenyl-2,2'-bipyridine [phbpyH][77, 205] 1

A mixture of **2** (1.31 g, 4.02 mmol), **3** (0.71 g, 4.01 mmol) and ammonium acetate (3.96 g, 51.4 mmol) in glacial acetic acid (13 mL) was refluxed at 125°C for two hours. After cooling the solution to room temperature water was added (200 mL) until a precipitate formed. The precipitate was collected by filtration and washed with cold ethanol (3 x 5 mL). The ethanol was found to partially dissolve the product, so it was fully dissolved in ethanol (100 mL), the solvent removed under reduced pressure and the crude product dried under vacuum. The resultant brown/grey solid was then purified by flash column chromatography (silica, hexane/diethyl ether, gradient elution from 100/0 to 60/40) to give the desired product as a cream solid (0.40 g, 43%). ^{1}H-NMR ($CDCl_3$, 400 MHz) δ = 8.68 (1H, ddd, ^3J = 4.8, ^4J = 2.0, ^5J = 0.8, H^6), 8.63 (1H, ddd, ^3J = 8.0, ^4J = 1.2, ^5J = 1.2, H^3), 8.37 (1H, dd, ^3J = 7.6, ^4J = 0.8, $H^{3'}$), 8.14 (2H, dd, ^3J = 8.8, ^4J = 1.6, $H^{2''}$), 7.86 (1H, t, ^3J = 7.6, $H^{4'}$), 7.80 (1H, td, ^3J = 8.0, ^4J = 1.6, H^4), 7.73 (1H, dd, ^3J = 8.0, ^4J = 0.8, $H^{5'}$), 7.49 (2H, td, ^3J = 7.6, ^4J = 1.6, $H^{3''}$), 7.42 (1H, tt, ^3J = 7.2, ^4J = 1.2, $H^{4''}$), 7.30 (1H, ddd, ^3J = 7.6, 4.8, ^4J = 1.2, H^5). ^{13}C-NMR ($CDCl_3$, 126 MHz) δ = 156.7 (C^q), 156.6 (C^q), 156.0 (C^q), 149.3 (C^6), 139.6 (C), 137.9 ($C^{4'}$), 137.1 (C^4), 129.2 ($C^{4''}$), 128.9 ($C^{3''}$), 127.2 ($C^{2''}$), 123.9 (C^5), 121.5 (C^3), 120.5 ($C^{5'}$), 119.5 ($C^{3'}$). MS (ES^+) m/z = 233.1 $[M + H]^+$ and 255.2 $[M + Na]^+$. HRMS (EI) m/z = 233.10735 $[M + H]^+$; 233.10732 calculated for $[C_{16}H_{13}N_2]^+$ and 255.08910 $[M + Na]^+$; 255.08927 calculated for $[C_{16}H_{12}N_2Na]^+$. C, H & N analysis: 82.44% C, 5.23% H and 12.05% N measured; 82.73% C, 5.21% H and 12.06% N calculated for $[C_{16}H_{12}N_2]$. TLC (silica) R_f = 0.46 in hexane/diethyl ether, 50/50. Mp = 78–80°C.

4'-(*p*-bromophenyl)-6'-(*m*-tolyl)-bipyridine [mtbpyH-ϕ-Br][a] [205] 4

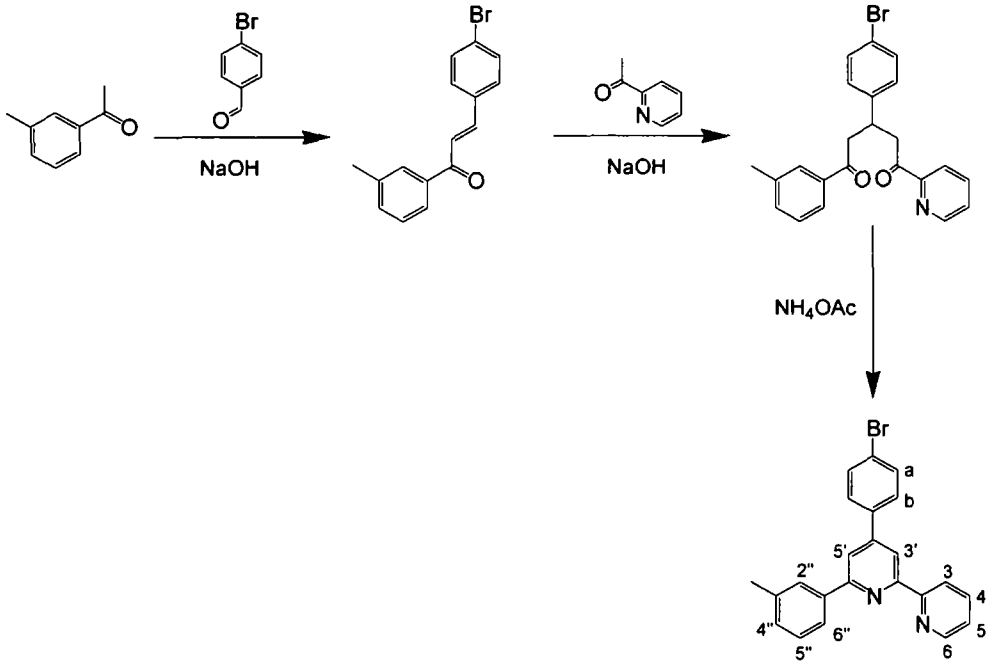

A mixture of 3-methylacetophenone (2.10 g, 15.65 mmol), *p*-bromobenzaldehyde (2.88 g, 15.65 mmol) and NaOH pellets (0.62 g, 15.50 mmol) were ground together with a pestle and mortar for 15 minutes, forming a pale yellow solid (5.12 g, 108%). This product (2.00 g, 6.64 mmol) was then ground together with 2-acetylpyridine (0.80 g, 6.64 mmol) and more NaOH pellets (0.27 g, 6.64 mmol) for 10 minutes, forming a paler yellow solid. The solid was dissolved in ethanol (60 mL) and excess ammonium acetate (2.05 g, 26.56 mmol) added. The reaction mixture was heated under reflux for 3 hours and after cooling to room temperature, the solvent was removed under reduced pressure. The resultant yellow solid was dissolved in DCM (150 mL), washed with aqueous sodium bicarbonate solution (5%, 2 x 100 mL) and dried over sodium carbonate. The solvent was removed under reduced pressure and the residue purified by flash column chromatography (silica, hexane/diethyl ether, gradient elution from 100/0 to 80/20) to give the desired product as a cream solid (0.40 g, 15%).

^{1}H-NMR ($CDCl_3$, 500 MHz) δ = 8.69 (1H, d, ^{3}J = 5.0, H^6), 8.66 (1H, d, ^{3}J = 8.0, H^3), 8.56 (1H, d, ^{4}J = 1.5, $H^{3'}$), 7.98 (1H, s, $H^{2''}$), 7.95 (1H, d, ^{3}J = 8.0, $H^{4''}$), 7.88 (1H, d, ^{4}J = 0.5, $H^{5'}$), 7.85 (1H, td, ^{3}J = 8.0, ^{4}J = 2.0, H^4), 7.66 (2H, d, ^{3}J = 8.5, H^a or H^b), 7.61 (2H, d, ^{3}J = 8.5, H^a or H^b), 7.39 (1H, t, ^{3}J = 7.5, $H^{5''}$), 7.32 (1H, ddd, ^{3}J = 7.5, 4.8, ^{4}J = 1.0, H^5), 7.26 (1H, d, ^{3}J = 8.0, $H^{6''}$), 2.47 (3H, s, Me). ^{13}C-NMR ($CDCl_3$, 126 MHz)

[a] This method was based upon work by Jameson *et al.*[204]

δ =157.8 (C^q), 156.6 (C^q), 156.4 (C^q), 149.3 (C^5), 149.2 (C^q),139.5 (C^q), 138.7 (C^q), 138.0 (C^q), 137.2 (C^4), 132.4 (C^a or C^b), 130.3 ($C^{6''}$), 129.1 (C^a or C^b), 129.0 ($C^{5''}$), 128.0 ($C^{2''}$), 124.5 ($C^{4''}$), 124.2 (C^q), 123.7 (C^3), 121.8 (C^6), 118.5 ($C^{5'}$), 117.3 ($C^{3'}$), 31.9 (CH_3). MS (ES^+) m/z = 401.2 $[M + H]^+$, 423.1 $[M + Na]^+$ and 824.7 $[2M + Na]^+$. HRMS (ES^+) m/z = 401.06501 $[M + H]^+$; 401.06479 calculated for $[C_{23}H_{18}{}^{79}BrN_2]^+$. C, H & N analysis: 68.82% C, 4.32% H and 6.95% N measured; 68.84% C, 4.27% H and 6.98% N calculated for $[C_{23}H_{17}N_2Br]$. TLC (silica) R_f = 0.44 in hexane/diethyl ether, 50/50. Mp = 103–106°C.

4'-*p*-tolyl-6-phenylpicolinic acid [tppicH_2][206] 5

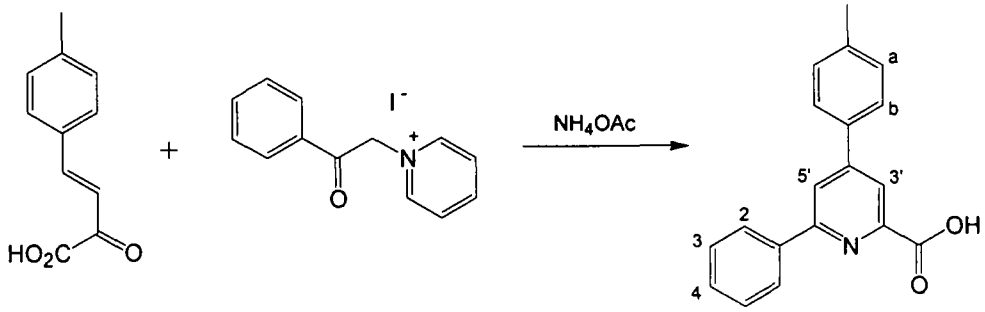

Step 1: 1-(2-oxo-2-phenylethyl)pyridinium iodide[203] 6

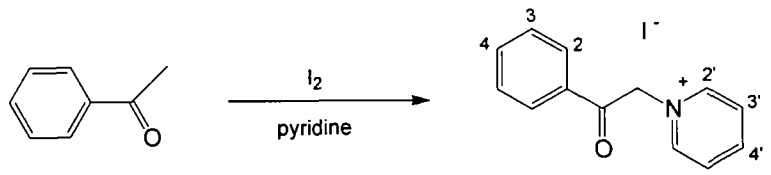

Acetophenone (4.7 mL, 40.0 mmol) was added to a solution of iodine (10.44 g, 41.1 mmol) in pyridine (40 mL) and synthesis carried out *via* the well established Kröhnke methodology. The desired product was isolated (as outlined for **2**) as a cream coloured crystalline solid (6.51 g, 50%).

^{1}H-NMR (d_6-DMSO, 400 MHz) δ = 8.98 (2H, dd, ^3J = 7.2, ^4J = 1.6, $H^{2'}$), 8.73 (1H, tt, ^3J = 8.0, ^4J = 1.2, $H^{4'}$), 8.27 (2H, t, ^3J = 6.8, $H^{3'}$), 8.06 (2H, dd, ^3J = 8.4, ^4J = 1.6, H^2), 7.80 (1H, tt, ^3J = 7.6, ^4J = 1.2, H^4), 7.67 (2H, t, ^3J = 6.8, H^3). MS (ES^+) m/z = 198.1 $[M - I]^+$. ^{13}C-NMR (d_6-DMSO, 126 MHz) δ = 191.4 (C=O), 147.1 ($C^{4'}$), 147.0 ($C^{2'}$), 135.5 (C^4), 134.2 (C^1), 129.9 (C^3), 129.0 (C^2), 128.6 ($C^{3'}$), 67.0 (CH_2). C, H & N analysis: 47.98% C, 3.72% H and 4.31% N measured; 48.02% C, 3.72% H and 4.31% N calculated for $[C_{13}H_{12}INO]$. Mp = 215–217°C.

Step 2: 4'-*p*-tolyl-6-phenylpicolinic acid [tppicH$_2$][206] 5

A mixture of 2-oxo-4'-*p*-toly-but-3-enoic acid (1.51 g, 7.9 mmol), **6** (3.71 g, 11.4 mmol) and ammonium acetate (5.64 g, 73.2 mmol) in water (50 mL) was heated under reflux at 100°C for 6 hours. After cooling to room temperature the resultant precipitate was collected by filtration, washed with acetone (3 x 20 mL) and dried under vacuum to give the product a white solid (1.87 g, 82%).

^{1}H-NMR (d$_6$-DMSO, 700 MHz) δ = 8.20 (1H, d, ^{3}J = 7.0, H^2), 8.12 (1H, d, ^{4}J = 2.1, H$^{3'}$ or H$^{5'}$), 8.05 (1H, d, ^{4}J = 1.4, H$^{3'}$ or H$^{5'}$), 7.79 (1H, d, ^{3}J = 7.7, H^b), 7.50 (1H, t, ^{3}J = 7.7, H^3), 7.43 (1H, d, ^{3}J = 7.0, H^4), 7.34 (1H, d, ^{3}J = 7.7, H^a), 3.31 (1H, br s, OH), 2.37 (6H, s, CH$_3$). ^{13}C-NMR (d$_6$-DMSO, 176 MHz) δ = 169.1 (C^q), 156.6 (C^1) 148.8 (C^q), 139.9 (C$^{2'}$ or C$^{6'}$) 139.8 (C$^{2'}$ or C$^{6'}$) 135.6 (C$^{4'}$), 130.4 (C^a), 129.5 (C^4) 129.2 (C^3), 127.7 (C^2), 127.5 (C^b), 119.9 (C$^{3'}$or C$^{5'}$), 118.1 (C$^{3'}$or C$^{5'}$), 21.5 (CH$_3$). MS (ES$^-$) m/z = 288.1 [M – H]$^-$. HRMS (ES$^-$) m/z = 288.10243 [M – H]$^-$; 288.10300 calculated for [C$_{19}$H$_{14}$NO$_2$]$^-$. C, H & N analysis: 73.85% C, 5.84% H and 4.94% N measured; 74.25% C, 5.58% H and 4.56% N calculated for [C$_{19}$H$_{15}$NO$_2$].(CH$_3$COCH$_3$). Mp = 205–208°C.

1,3-di(2-pyridyl)-4,6-dimethylbenzene [dpydmbH][76, 206] 7

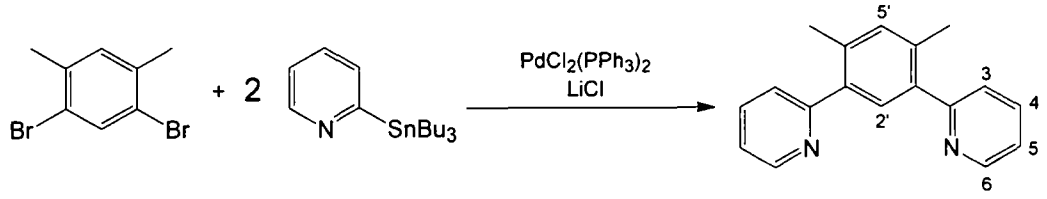

A mixture of 2-tri-n-butylstannylpyridine (6.00 g, 16.3 mmol, 90% pure by mass by ^{1}H-NMR assay), 1,3-dibromo-4,6-dimethylbenzene (1.61 g, 6.11 mmol), PdCl$_2$(PPh$_3$)$_2$ (0.17 g, 0.24 mmol) and lithium chloride (1.89 g, 44.6 mmol) in dry toluene (25 mL) was degassed by five freeze-pump-thaw cycles. The mixture was then heated under a N$_2$ atmosphere at reflux, 115°C, for 72 hours. The resultant brown/black solution was cooled to room temperature, saturated aqueous KF solution (15 mL) added and the solution stirred for 30 minutes. The precipitated tin residue was removed by filtration and washed with dry toluene (3 x 15 mL). The filtrate and washings were combined and the solvent removed under reduced pressure; the resultant brown solid was dissolved in DCM (150 mL) and washed with aqueous sodium bicarbonate solution (5%, 2 x 100 mL) to remove any aqueous impurities. The DCM layer was dried over magnesium sulfate, and the solvent removed under reduced pressure. The aliphatic impurities were removed from the product by flash column chromatography (silica,

hexane/diethyl ether, gradient elution from 100/0 to 0/100) and the desired product isolated as a cream coloured crystalline solid (1.23 g, 77%).

^{1}H-NMR ($CDCl_3$, 400 MHz) δ = 8.69 (2H, d, ^3J = 4.0, H^6), 7.75 (2H, td, ^3J = 7.2, ^4J = 2.0, H^4), 7.49 (1H, s, $H^{2'}$), 7.47 (2H, d, ^3J = 8.8, H^3), 7.26 (1H, s, $H^{5'}$), 7.25 (2H, ddd, ^3J = 9.6, 5.2, ^4J = 0.8, H^5), 2.41 (6H, s, CH_3). ^{13}C-NMR ($CDCl_3$, 126 MHz) δ = 159.8 (C^q), 149.3 (C^6), 138.2 (C^q), 136.2 (C^4), 135.9 (C^q), 133.4 ($C^{5'}$), 131.2 ($C^{2'}$), 124.3 (C^3), 121.6 (C^5), 20.1 (CH_3). MS (ES^+) m/z = 261.1 $[M + H]^+$, 283.1 $[M + Na]^+$. HRMS (ES^+) m/z = 283.11982 $[M + Na]^+$; 283.12114 calculated for $[C_{18}H_{16}N_2Na]^+$. C, H & N analysis: 82.54% C, 6.23% H and 10.57% N measured; 82.47% C, 6.23% H and 10.69% N calculated for $[C_{18}H_{16}N_2].\{0.1(H_2O)\}$. TLC (silica) R_f = 0.30 in hexane/diethyl ether, 10/90. Mp = 84–86°C

1,3,5-tribromo-4,6-dimethylbenzene 8

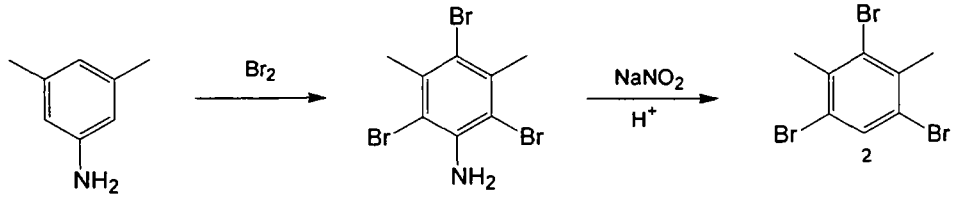

Step 1: 2,4,6-tribromo-3,5-dimethylaniline[251]

A solution of 3,5-dimethylaniline (3.05 g, 3.14 mL, 25.2 mmol) in acetic acid (15 mL) was stirred at room temperature for 15 minutes until homogeneous. After cooling to 0°C in an ice bath, bromine (12.47 g, 4 mL, 78.0 mmol) was added during continual stirring. After the exothermic reaction ceased, the reaction mixture was warmed to room temperature, water (10 mL) added and the suspension stirred for a further 15 minutes. The solid was collected by filtration, washed with water (3 x 20 mL) and dried under vacuum to give the product as an off-white solid (8.32 g, 92%).

^{1}H-NMR ($CDCl_3$, 400 MHz) δ = 4.58 (2H, br s, NH_2), 2.57 (6H, s, CH_3). TLC (silica) R_f = 0.70 in hexane/diethyl ether, 50/50.

Step 2: 1,3,5-tribromo-2,6-dimethylbenzene 8

Hot ethanol (100 mL) was added to 2,4,6-tribromo-3,5-dimethylaniline (7.44 g, 20.79 mmol) and heated under reflux for 30 minutes. Concentrated sulfuric acid (2.15 mL, 41.58 mmol) was then added, the heat source removed and sodium nitrite (2.65 g, 3.19 mmol) added. The suspension was stirred at room temperature for 15 minutes and then heated under reflux for a further 45 minutes until there was no

further gas evolution. The suspension was cooled to room temperature and subsequently to 0°C in an ice bath; the solid was collected by filtration and washed with cold ethanol (3 x 5 mL) and cold water (3 x 5 mL), then dried under vacuum to give the crude product as an orange solid (4.40 g). Further product was isolated, by adding more water to the filtrate (total yield: 5.74 g). Purification by flash column chromatography (silica, hexane) gave the desired product a white solid (4.96 g, 70%).

^{1}H-NMR ($CDCl_3$, 700 MHz) δ = 7.72 (1H, s, H^2), 2.53 (6H, s, CH_3). ^{13}C-NMR ($CDCl_3$, 176 MHz) δ = 137.4 (C^1 or C^4), 134.6 (C^2), 128.4 (C^5), 122.2 (C^1 or C^4), 24.9 (CH_3). C, H & N analysis: 28.34% C and 1.78% H measured; 28.03% C and 2.06% H calculated for [$C_8H_7Br_3$]. TLC (silica) R_f = 0.83 in hexane. Mp = 75–77°C.

1-bromo-3,5-di(2-pyridyl)-2,6-dimethylbenzene [dpydmbH-Br] 9

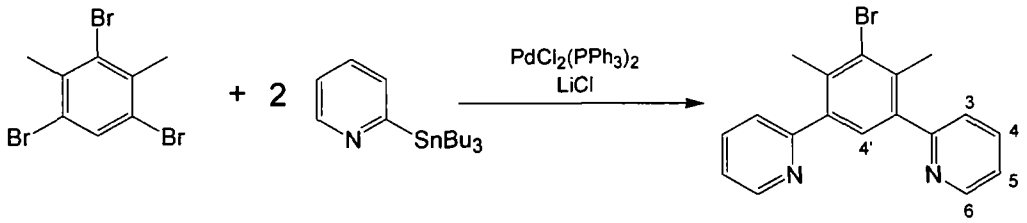

A mixture of 2-tri-n-butylstannylpyridine (3.57 g, 9.70 mmol, 95% pure by mass by ^{1}H-NMR assay), **8** (1.50 g, 4.38 mmol), $PdCl_2(PPh_3)_2$ (0.11 g, 0.16 mmol) and lithium chloride (1.30 g, 30.67 mmol) in dry toluene (35 mL) was degassed by five freeze-pump-thaw cycles. The same reaction methodology was then employed as for dpydmbH **7**, with the crude reaction mixture being purified by flash column chromatography (silica, hexane/diethyl ether, gradient elution from 100/0 to 20/80) to give the desired product as a pale brown solid (0.11 g, 7%).

^{1}H-NMR ($CDCl_3$, 400 MHz) δ = 8.65 (2H, m, H^6), 7.71 (2H, td, ^3J = 7.6, ^4J = 2.0, H^4), 7.38-7.33 (3H, m, H^3 and $H^{4'}$), 7.25-7.20 (2H, m, H^5), 2.43 (6H, s, CH_3). MS (ES^+) m/z = 339.1 $[M + H]^+$. TLC (silica) R_f = 0.34 in DCM/methanol, 90/10.

1,3-Dibromo-5-(2-pyridyl)-2,4-dimethylbenzene [pydmbH-Br_2] **10** was also isolated as an off-white solid (0.48 g, 32%) from flash column chromatography of the crude product (silica, hexane/diethyl ether, gradient elution from 100/0 to 80/20).

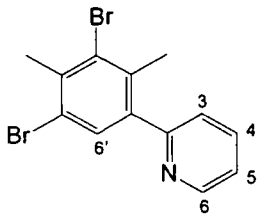

^{1}H-NMR ($CDCl_3$, 400 MHz) δ = 8.60 (1H, ddd, ^{3}J = 4.8, ^{4}J = 2.0, ^{5}J = 0.8, H^6), 7.66 (1H, td, ^{3}J = 7.6, ^{4}J = 1.6, H^4), 7.47 (1H, s, $H^{6'}$), 7.23 (1H, d, ^{3}J = 8.0, H^3), 7.18 (1H, ddd, ^{3}J = 7.6, 4.8, ^{4}J = 1.2, H^5), 2.57 (3H, s, $CH_3^{2'}$), 2.26 (3H, s, $CH_3^{4'}$). MS (ES^+) m/z = 342.0 $[M + H]^+$. TLC (silica) R_f = 0.84 in hexane/diethyl ether, 10/90.

1,3,5-tri(2-pyridyl)-2,4-dimethylbenzene [tpydmbH] 11

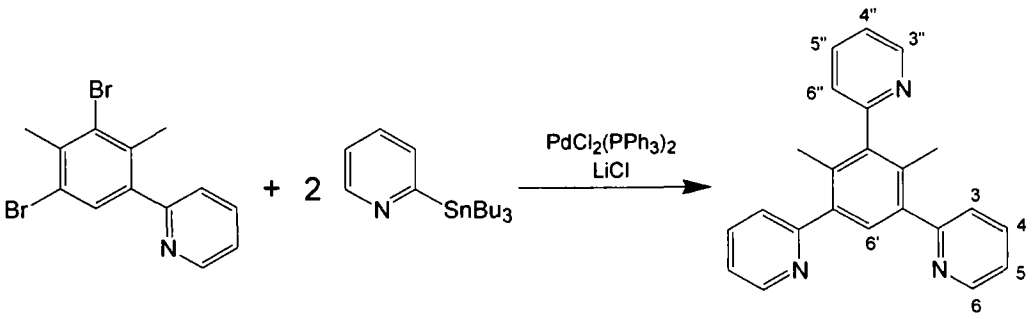

A mixture of 2-tri-n-butylstannylpyridine (0.76 g, 1.97 mmol, 95% pure by mass by ^{1}H-NMR assay), pydmbH-Br_2 **10** (0.48 g, 1.41 mmol), $PdCl_2(PPh_3)_2$ (0.033 g, 0.047 mmol) and lithium chloride (0.24 g, 5.66 mmol) in dry toluene (15 mL) was degassed by five freeze-pump-thaw cycles. The same reaction methodology was then employed as for dpydmbH **7**, with the crude reaction mixture being purified by flash column chromatography (silica, hexane/diethyl ether, gradient elution from 100/0 to 0/100) followed by (silica, ethyl acetate) to give the product as a white crystalline solid (0.17 g, 71%).

^{1}H-NMR ($CDCl_3$, 500 MHz) δ = 8.72 (1H, ddd, ^{3}J = 5.0, ^{4}J = 2.0, ^{5}J = 1.0, $H^{6''}$), 8.65 (2H, ddd, ^{3}J = 5.0, ^{4}J = 2.0, ^{5}J = 1.0, H^6), 7.77 (1H, td, ^{3}J = 7.0, ^{4}J = 2.0, $H^{4''}$), 7.69 (2H, td, ^{3}J = 8.0, ^{4}J = 2.0, H^4), 7.46 (1H, s, $H^{6'}$), 7.41 (2H, d, ^{3}J = 8.0, H^3), 7.30 (1H, d, ^{3}J = 7.5, $H^{3''}$) 7.26 (1H, ddd, ^{3}J = 7.5, 5.0, ^{4}J = 1.5, $H^{5''}$), 7.19 (2H, ddd, ^{3}J = 7.5, 5.5, ^{4}J = 1.0, H^5), 1.98 (6H, s, CH_3). ^{13}C-NMR δ = 160.7 (C^q), 160.2 (C^q), 130.1 ($C^{6''}$), 149.4 (C^6), 142.7 (C^q), 1439.0 (C^q), 136.8 ($C^{4''}$), 136.4 (C^4), 134.0 (C), 131.2 ($C^{6'}$), 125.0 ($C^{3''}$), 124.9 (C^3), 122.1 ($C^{5''}$), 121.9 (C^5), 18.3 (CH_3). MS (ES^+) m/z = 338.3 $[M + H]^+$. HRMS (ES^+) m/z = 338.16511 $[M + H]^+$; 338.16517 calculated for $[C_{23}H_{20}N_3]^+$. C, H & N analysis: 79.11% C, 5.82% H and 11.85% N measured; 79.41% C, 5.56% H

and 12.00% N calculated for $[C_{23}H_{19}N_3].\{0.15(CH_2Cl_2)\}$. TLC (silica) R_f = 0.12 in ethyl acetate. Mp = 189–192°C.

1,3-bis(3-fluorophenyl)pyridine [F_2dppyH_2] 12

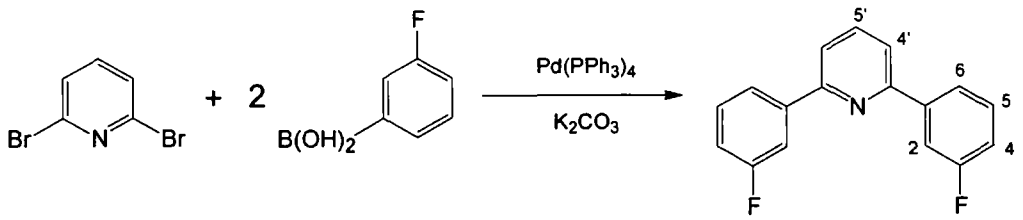

A mixture of 2,6-dibromopyridine (0.30 g, 1.25 mmol), 3-fluorophenyl boronic acid (0.52 g, 3.75 mmol) and K_2CO_3 (1.04 g, 7.50 mmol) in DME (10 mL) and water (3 mL) was degassed by 4 freeze-pump-thaw cycles. $Pd(PPh_3)_4$ (0.14 g, 0.13 mmol) was added under a flow of N_2 and the reaction mixture stirred at room temperature, under a N_2 atmosphere, for 1 hour before heating to 80°C for 72 hours. After cooling to room temperature the solvent was removed under reduced pressure, and the product dissolved in DCM (50ml). The DCM solution was washed with aqueous sodium bicarbonate solution (0.6 M, 3 x 50 mL), dried over magnesium sulfate and the solvent removed under reduced pressure. Purification was achieved by flash column chromatography (silica, hexane/diethyl ether, gradient elution from 100/0 to 98/2) to give the product as a white solid (0.32 g, 97 %).

^{1}H-NMR ($CDCl_3$, 500 MHz) δ = 7.89-7.85 (4H, m, H^2 and H^6), 7.79 (1H, t, ^3J = 8.5, $H^{5'}$), 7.66 (2H, d, ^3J = 8.0, $H^{4'}$), 7.46-7.40 (2H, m, H^5) and 7.11 (2H, td, ^3J = 8.5, ^4J = 2.0, H^4). ^{13}C-NMR ($CDCl_3$, 126 MHz) δ = 164.6 (C^q), 162.6 (C^q), 155.7 (C^q), 141.7 (C^q), 138.1 ($C^{5'}$), 130.4 (C^5), 122.7 (C^2 or C^6), 119.4 ($C^{4'}$), 116.1 (C^4), 114.2 (C^2 or C^6). ^{19}F-NMR ($CDCl_3$, 658 MHz) δ = –113.0 to –112.9 (2F, m, F^3). GC-MS (EI) retention time = 24.55 minutes, m/z = 267.2 $[M]^+$. C, H & N analysis: 76.24% C, 4.14% H and 5.27% N measured; 76.39% C, 4.15% H and 5.24% N calculated for $[C_{17}H_{11}F_2N]$. TLC (silica) R_f = 0.68 in hexane/diethyl ether, 50/50. Mp = 67–69°C.

1,3,5-tri(1-pyrazolyl)benzene [tpzbH][b] 13

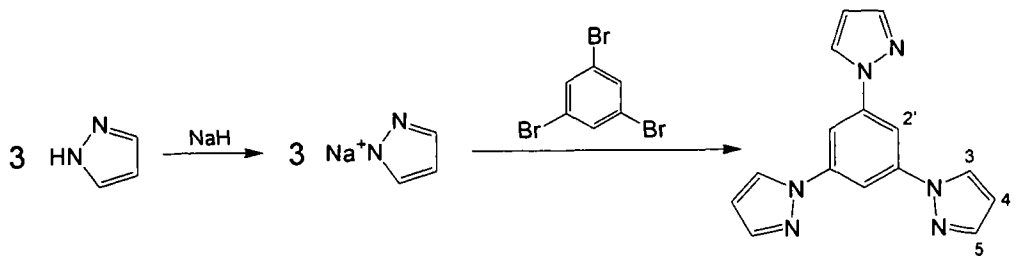

Pyrazole (1.32 g, 19.39 mmol) in DMF (15 mL) was degassed by three freeze-pump-thaw cycles and sodium hydride (0.54 g, 22.5 mmol) added under a flow of N_2. The reaction mixture was heated to 50°C for 1 hour, then 1,3,5-tribromobenzene (1.00 g, 3.18 mmol) was added under a flow of N_2 and the resultant suspension heated to 95°C for 96 hours. After cooling to room temperature, water (25 mL) was added and the off-white precipitate collected by filtration. The solid was dissolved in acetone, the solvent removed under reduced pressure and purification achieved by flash column chromatography (silica, hexane/diethyl ether, gradient elution from 100/0 to 55/45) to give the product as a white solid (0.014 g, 2%).

^{1}H-NMR ($CDCl_3$, 500 MHz) δ = 8.08 (3H, d, ^3J = 2.5, H^3), 8.01 (3H, s, $H^{2'}$), 7.74 (3H, d, ^3J = 1.5, H^5), 6.50 (3H, t, ^3J = 2.0, H^4). ^{13}C-NMR ($CDCl_3$, 126 MHz) δ = 142.1 ($C^{1'}$), 142.0 (C^5), 127.4 (C^3), 108.7 (C^4), 106.9 ($C^{2'}$). MS (ES^+) m/z = 277.2 $[M + H]^+$ and 299.2 $[M + Na]^+$. HRMS (ES^+) m/z = 277.11963 $[M + H]^+$; 277.11962 calculated for $[C_{15}H_{13}N_6]^+$ and 299.10157 $[M + Na]^+$; 299.10157 calculated for $[C_{15}H_{12}N_6Na]^+$. TLC (silica) R_f = 0.09 in hexane/diethyl ether, 50/50. Mp = 106–110°C.

1-Pyrazolyl-3,5-dibromobenzene [pzbH-Br_2] **14** was also isolated as a white solid (0.47 g, 49%) from flash column chromatography of the crude product (silica, hexane/diethyl ether, gradient elution from 100/0 to 90/10).

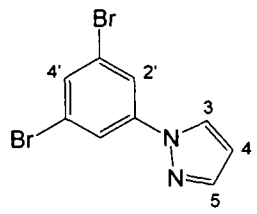

^{1}H-NMR ($CDCl_3$, 500 MHz) δ = 7.85 (1H, d, ^3J = 2.5, H^3), 7.80 (2H, d, ^3J = 1.5, $H^{2'}$), 7.70 (1H, d, ^3J = 1.5, H^5), 7.53 (1H, t, ^3J = 1.5, $H^{4'}$), 7.46 (1H, dd, ^3J = 2.5, 2.0, H^4).

---

[b] This methodology was based upon similar work by Hosseini *et al.*[215, 216]

^{13}C-NMR ($CDCl_3$, 126 MHz) δ = 142.3 (C^5), 142.0 ($C^{1'}$), 131.9 ($C^{4'}$), 127.1 (C^3), 123.8 ($C^{3'}$), 121.0 ($C^{2'}$), 108.9 (C^4). MS (ES^+) m/z = 303.0 $[M + H]^+$. HRMS (ES^+) m/z = 300.89705 $[M + H]^+$; 300.89705 calculated for $[C_9H_7{}^{79}Br_2N_2]^+$ and 302.89497 $[M + H]^+$; 302.89500 calculated for $[C_9H_7{}^{79}Br^{81}BrN_2]^+$. C, H & N analysis: 35.90% C, 2.06% H and 9.22% N measured; 35.80% C, 2.00% H and 9.28% N calculated for $[C_9H_6Br_2N_2]$. TLC (silica) R_f = 0.64 in hexane/diethyl ether, 50/50. Mp = 66–68°C.

Alongside 1,3-di(1-pyrazolyl)-5-bromobenzene [dpzbH-Br] **15**, which was also isolated as a white solid (0.31 g, 34%) from flash column chromatography of the crude product (silica, hexane/diethyl ether, gradient elution from 100/0 to 70/30).

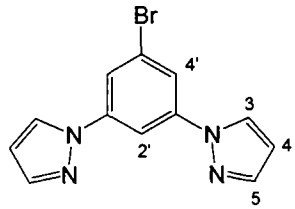

^{1}H-NMR ($CDCl_3$, 500 MHz) δ = 8.02 (1H, t, ^3J = 1.5, $H^{2'}$), 7.96 (2H, d, ^3J = 2.5, H^3), 7.77 (2H, d, ^4J = 2.0, $H^{4'}$), 7.72 (2H, d, ^3J = 1.5, H^5), 7.48 (2H, dd, ^3J = 2.5, 2.0, H^4). ^{13}C-NMR ($CDCl_3$, 126 MHz) δ = 142.1 (C^5), 142.0 ($C^{1'}$), 127.2 (C^3), 124.0 ($C^{3'}$), 119.7 ($C^{4'}$), 108.8 (C^4), 108.4 ($C^{2'}$). MS (ES^+) m/z = 289.1 $[M + H]^+$ and 311.0 $[M + Na]^+$. HRMS (ES^+) m/z = 289.00832 $[M + H]^+$; 289.00833 calculated for $[C_{12}H_{10}{}^{79}BrN_4]^+$ and 310.99025 for $[M + Na]^+$; 310.99028 calculated for $[C_{12}H_9{}^{79}Br\ N_4{}^{23}Na]^+$. C, H & N analysis: 49.64% C, 3.18% H and 19.39% N measured; 49.85% C, 3.14% H and 19.38% N calculated for $[C_{12}H_9BrN_4]$. TLC (silica) R_f = 0.32 in hexane/diethyl ether, 50/50. Mp = 130–132°C.

1,3-di(1-pyrazolyl)benzene [dpzbH][c] 16

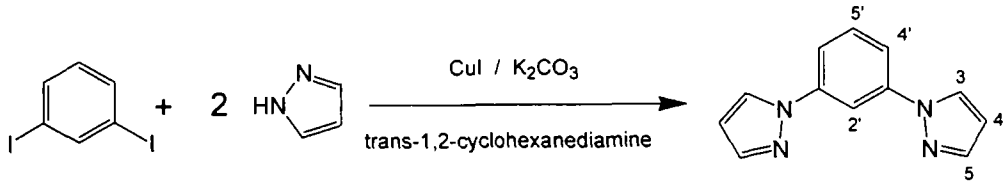

A mixture of 1,3-di-iodobenzene (1.01 g, 3.03 mmol), pyrazole (0.62 g, 9.11 mmol), copper iodide (0.014 g, 0.074 mmol), K_2CO_3 (1.62 g, 11.72 mmol) and trans-1,2-cyclohexanediamine (0.090 g, 0.79 mmol) in 1,4-dioxane (8 mL) was degassed by three

[c] This method was based upon an adaptation of that used by Lexy and Kauffmann for 3b.[214]

freeze-pump-thaw cycles. The resultant suspension was stirred at 110°C, under a N_2 atmosphere, for 24 hours. After cooling to room temperature the suspension was filtered through Celite® and the product washed through with hexane/diethyl ether (90/10, 1 L). The solvent was removed under reduced pressure and dried under vacuum giving a pale brown oil. Purification was achieved by flash column chromatography (silica, hexane/diethyl ether, gradient elution from 100/0 to 70/30) to give the product as a pale yellow oil. (0.41 g, 64%)

^{1}H-NMR ($CDCl_3$, 500 MHz) δ = 8.08 (1H, s, $H^{2'}$), 7.99 (2H, d, ^3J = 2.5, H^3), 7.72 (2H, d, ^3J = 1.5, H^5), 7.60 (2H, dd, ^3J = 8.5, ^4J = 2.0, $H^{4'}$), 7.50 (1H, t, ^3J = 8.0, $H^{5'}$), 6.47 (2H, t, ^3J = 2.0, H^4). ^{13}C-NMR ($CDCl_3$, 126 MHz) δ = 141.7 (C^5), 141.4 ($C^{3'}$), 130.7 ($C^{5'}$), 127.2 (C^3), 116.9 ($C^{4'}$), 110.2 ($C^{2'}$), 108.3 (C^4). MS (ES^+) m/z = 211.1 $[M + H]^+$ and 233.1 $[M + Na]^+$. HRMS (ES^+) m/z = 211.09779 $[M + H]^+$; 211.09782 calculated for $[C_{12}H_{11}N_4]^+$ and 233.07973 $[M + Na]^+$; 233.07977 calculated for $[C_{12}H_{10}N_4Na]^+$. TLC (silica) R_f = 0.34 in hexane/diethyl ether, 50/50.

1,3-di(1-pyrazolyl)-5-methylbenzene [dpzmbH] 17

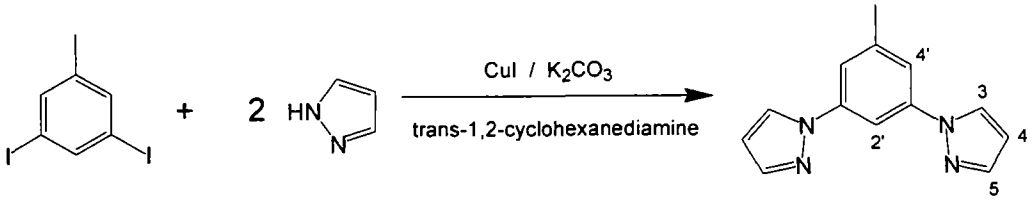

Step 1: 1,3-di-iodo-5-methylbenzene[d] 18a

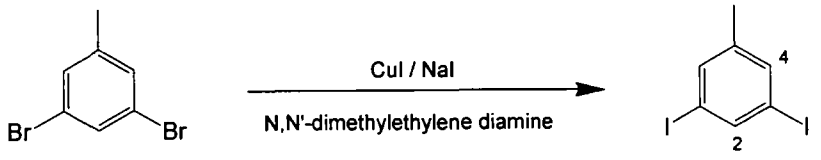

A mixture of copper iodide (0.46 g, 2.42 mmol), sodium iodide (3.60 g, 24.02 mmol), 1,3-dibromo-5–methylbenzene (1.00 g, 4.00 mmol) and N,N'-dimethylethylene diamine (0.43 g, 4.88 mmol) in toluene (20 mL) was degassed by three freeze-pump-thaw cycles. The resultant blue suspension was heated to 110°C under a N_2 atmosphere for 48 hours. After cooling to room temperature the solvent was removed under reduced pressure, the product dissolved in DCM (200 mL) and washed with water (3 x 100 mL). The DCM solution was dried over magnesium sulfate, the solvent removed under

[d] This procedure was based upon that used by Buchwald *et al.*[252]

reduced pressure and the solid dried under vacuum to give the product as a cream solid (1.22 g, 88%).

^{1}H-NMR ($CDCl_3$, 500 MHz) δ = 7.82 (1H, s, H^2), 7.47 (2H, s, H^4), 2.22 (3H, s, CH_3). ^{13}C-NMR ($CDCl_3$, 126 MHz) δ = 142.4 (C^2 and C^5), 137.7 (C^4), 94.9 (C^3), 20.8 (CH_3). TLC (silica) R_f = 0.84 in hexane/diethyl ether, 50/50.

Step 2: 1,3-di(1-pyrazolyl)-5-methylbenzene [dpzmbH][e] 17

A mixture of **18a** (1.10 g, 3.20 mmol), pyrazole (0.65 g, 9.55 mmol), copper iodide (0.016 g, 0.084 mmol), K_2CO_3 (1.55 g, 11.21 mmol) and trans-1,2-cyclohexanediamine (0.095 g, 0.83 mmol) in 1,4-dioxane (10 mL) was degassed by three freeze-pump-thaw cycles. The resultant suspension was stirred at 110°C, under a N_2 atmosphere, for 24 hours. After cooling to room temperature the suspension was filtered through Celite® and the product washed through with hexane/diethyl ether (90/10, 1 L). The solvent was removed under reduced pressure and dried under vacuum to give a yellow/brown oil. Purification was achieved by flash column chromatography (silica, hexane/diethyl ether, gradient elution from 100/0 to 70/30) to give the product as a pale yellow oil (0.54 g, 75%).

^{1}H-NMR ($CDCl_3$, 500 MHz) δ = 7.95 (2H, d, ^3J = 2.5, H^3), 7.82 (1H, s, $H^{2'}$) 7.70 (2H, d, ^3J = 1.0, H^5), 7.43 (2H, d, ^4J = 1.5, $H^{4'}$), 6.44 (2H, dd, ^3J = 2.0, 2.0, H^4), 2.43 (3H, s CH_3). ^{13}C-NMR ($CDCl_3$, 126 MHz) δ = 141.5 (C^5), 141.2 (C^q), 141.1 (C^q), 127.2 (C^3), 117.7 ($C^{4'}$), 108.1 (C^4), 107.4 ($C^{2'}$), 21.9 (CH_3). MS (ES^+) m/z = 225.2 $[M + H]^+$ and 241.1 $[M + Na]^+$. HRMS (ES^+) m/z = 225.11364 $[M + H]^+$; 225.11347 calculated for $[C_{13}H_{13}N_4]^+$. C, H & N analysis: 69.61% C, 5.51% H and 24.97% N measured; 69.62% C, 5.39% H and 24.96% N calculated for $[C_{13}H_{12}N_4]$. TLC (silica) R_f = 0.27 in hexane/diethyl ether, 50/50.

1,3-di(1-pyrazolyl)-4,6-dimethylbenzene [dpzdmbH] 19

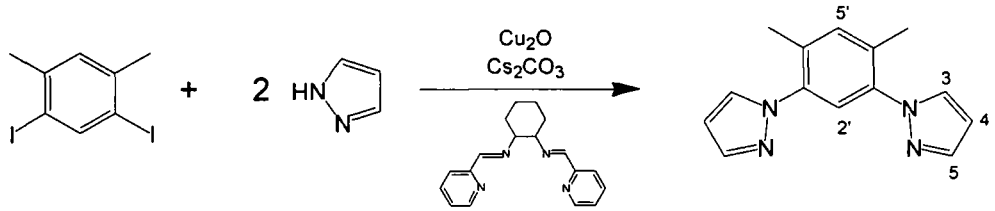

[e] This method was based upon an adaptation of that used by Buchwald *et al.*[218]

Step 1: 1,3-di-iodo-4,6-dimethylbenzene 18b

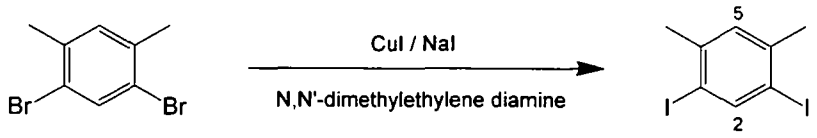

A mixture of copper iodide (0.52 g, 2.73 mmol), sodium iodide (4.10 g, 27.35 mmol), 1,3-dibromo-4,6–dimethylbenzene (1.20 g, 4.55 mmol) and N,N'-dimethylethylene diamine (0.56 g, 6.35 mmol) in toluene (20 mL) was degassed by three freeze-pump-thaw cycles. The same reaction methodology was then employed as for **16**, with product being isolated as a cream solid (1.55 g, 95%).

^{1}H-NMR ($CDCl_3$, 500 MHz) δ = 8.15 (1H, s, H^2), 7.08 (1H, s, H^5), 2.31 (6H, s, CH_3). ^{13}C-NMR ($CDCl_3$, 126 MHz) δ = 147.4 (C^2), 141.7 (C^q), 131.0 (C^5), 98.1 (C^q), 27.6 (CH_3). GC-MS (EI) retention time = 17.6 minutes, m/z= 357.8 for $[M]^+$. C, H & N analysis: 26.74% C and 2.50% H measured; 26.84% C and 2.25% H calculated for $[C_8H_8I_2]$. TLC (silica) R_f = 0.85 in hexane/diethyl ether, 95/5. Mp = 61–63°C.

Step 2: N,N-bis(pyridyl)-1,2-cyclohexanediamine[221] 20

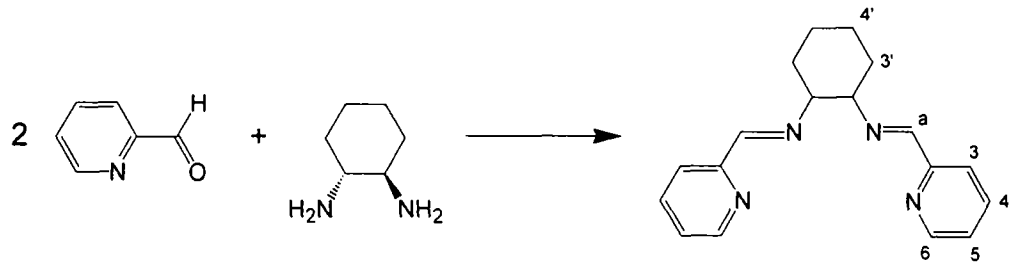

Trans-1,2-diaminocyclohexane (0.86 g, 7.5 mmol) in ethanol (2 mL) was added to 2-pyridine carboxaldehyde in ethanol (10 mL) and heated to 80°C for 1 hour. The reaction mixture was cooled to room temperature and subsequently to 0°C in an ice bath forming a white precipitate in an orange solution. The precipitate was collected by filtration, washed with cold ethanol (3 x 1 mL) and dried under vacuum to give the product as a white crystalline solid (0.51 g). The filtrate was concentrated twice to afford additional product (total yield: 1.38 g, 63%).

^{1}H-NMR ($CDCl_3$, 500 MHz) δ = 8.51 (2H, dd, ^3J = 5.0, ^4J = 0.5, H^6), 8.27 (2H, s, H^a), 7.84 (2H, d, ^3J = 8.0, H^3), 7.60 (2H, td, ^3J = 7.5, ^4J = 1.5, H^4), 7.18 (2H, ddd, ^3J = 7.5, 4.5, ^4J = 1.0, H^5), 3.50 (2H, d, ^3J = 5.0, $H^{2'}$), 1.87-1.73 (8H, m $H^{3'}$ and $H^{4'}$). ^{13}C-NMR ($CDCl_3$, 126 MHz) δ = 161.7 (C^2 or C^a), 154.8 (C^2 or C^a), 149.5 (C^6), 136.7 (C^4), 124.7 (C^5), 121.6 (C^3), 73.8 ($C^{2'}$), 33.0 ($C^{3'}$ or $C^{4'}$), 24.6 ($C^{3'}$ or $C^{4'}$). MS (ES^+) m/z = 293.2 $[M + H]^+$ and 315.2 $[M + Na]^+$. HRMS (ES^+) m/z = 293.17605 $[M + H]^+$; 293.17607

calculated for $[C_{18}H_{21}N_4]^+$ and 315.15792 $[M + Na]^+$; 315.15802 calculated for $[C_{18}H_{20}N_4Na]^+$. C, H & N analysis: 73.65% C, 6.85% H and 19.02% N measured; 73.94% C, 6.89% H and 19.16% N calculated for $[C_{18}H_{20}N_4]$. TLC (silica) $R_f = 0.23$ in hexane/diethyl ether, 50/50. Mp = 135–138°C.

Step 3: 1,3-di(1-pyrazolyl)-4,6-dimethylbenzene [dpzdmbH][f] 19

A Schlenk tube was charged with a mixture of **18b** (0.41 g, 1.15 mmol), pyrazole (0.16 g, 2.30 mmol), caesium carbonate (1.50 g, 4.60 mmol), copper(I) oxide (0.017 g, 0.12 mmol) and **20** (0.13 g, 0.46 mmol); then degassed and back-filled with N_2 three times. Acetonitrile (3 mL) was degassed separately by three freeze-pump-thaw cycles and added to the dry reagents under a flow of N_2; the reaction mixture was heated to 82°C for 72 hours. During this time solid accumulated on the walls of the Schlenk tube, this was scraped down into the reaction mixture, under a positive pressure of N_2, and reacted for a further 24 hours. After cooling to room temperature, the suspension was diluted with DCM (10 mL), filtered through Celite® and the product washed through with DCM (250 mL). The filtrate was concentrated to ~50 mL under reduced pressure, washed with water (2 x 50 mL), brine (2 x 50 mL) and dried over magnesium sulfate. The solvent was removed under reduced pressure and the crude product purified by flash column chromatography (silica, hexane/diethyl ether, gradient elution from 100/0 to 60/40) to give a white solid (0.049 g, 18%).

^{1}H-NMR ($CDCl_3$, 500 MHz) δ = 7.72 (2H, d, ^3J = 1.5, H^5), 7.62 (2H, d, ^3J = 2.0, H^3), 7.35 (1H, s, $H^{2'}$), 7.27 (1H, s, $H^{5'}$), 6.44 (2H, t, ^3J = 2.0, H^4), 2.29 (6H, s, CH_3). ^{13}C-NMR ($CDCl_3$, 126 MHz) δ = 140.8 (C^5), 138.3 ($C^{4'}$), 134.2 ($C^{5'}$), 133.9 ($C^{3'}$), 130.8 (C^3), 124.0 ($C^{2'}$), 106.7 (C^4), 18.0 (CH_3). MS (ES^+) m/z = 239.2 $[M + H]^+$ and 261.1 $[M + Na]^+$. HRMS (ES^+) m/z = 239.12929 $[M + H]^+$; 239.12912 calculated for $[C_{14}H_{15}N_4]^+$. C, H & N analysis: 70.24% C, 5.55% H and 23.14% N measured; 70.57% C, 5.92% H and 23.51% N calculated for $[C_{14}H_{14}N_4]$. TLC (silica) R_f = 0.25 in hexane/diethyl ether, 50/50. Mp = 75–77°C.

1-Iodo-3-pyrazolyl-4,6-dimethylbenzene [pzdmbH-I] **21** was also isolated as a white solid (0.12 g, 44%) from flash column chromatography of the crude product (silica, hexane/diethyl ether, gradient elution from 100/0 to 85/15).

---

[f] This method was based upon that used by Cristau *et al.* for 3q.[220]

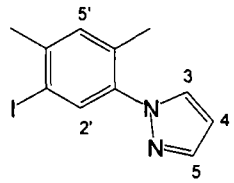

^{1}H-NMR ($CDCl_3$, 500 MHz) δ = 7.73 (1H, s, $H^{2'}$), 7.67 (1H, d, ^3J = 1.5, H^5), 7.53 (1H, d, ^3J = 2.5, H^3), 7.14 (1H, s, $H^{5'}$), 6.40 (1H, t, ^3J = 2.5, H^4), 2.41 (3H, s, $CH_3^{6'}$), 2.13 (3H, s, $CH_3^{4'}$). ^{13}C-NMR ($CDCl_3$, 126 MHz) δ = 141.8 (C^q), 140.8 (C^5), 138.8 (C^q), 136.2 ($C^{2'}$), 133.8 (C^q), 132.2 ($C^{5'}$), 130.8 (C^3), 106.7 (C^4), 96.8 (C^q), 27.0 (CH_3), 18.0 (CH_3). TLC (silica) R_f = 0.61 in hexane/diethyl ether, 50/50.

1,3,5-tri(2-pyridyl)benzene [tpybH][222] 22

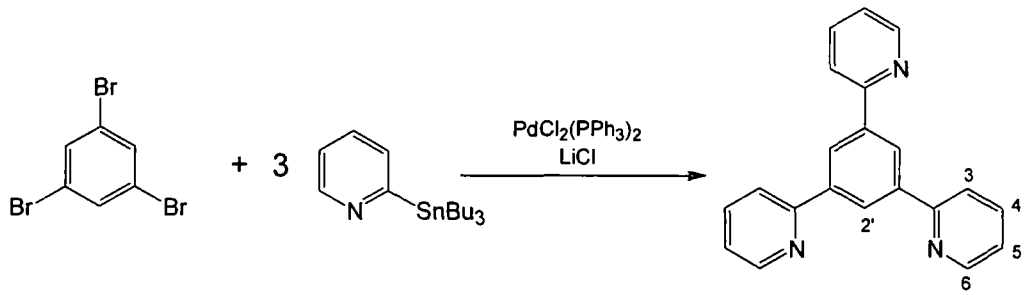

A mixture of 2-tri-n-butylstannylpyridine (4.80 g, 13.04 mmol, 90% pure by ^{1}H-NMR assay), 1,3,5-tribromobenzene (1.01 g, 3.21 mmol), $PdCl_2(PPh_3)_2$ (0.22 g, 0.31 mmol) and lithium chloride (1.36 g, 32.08 mmol) in dry toluene (35 mL) was degassed by five freeze-pump-thaw cycles. The same reaction methodology was then employed as for dpydmbH **7**, with the crude reaction mixture being purified by flash column chromatography (silica, hexane/diethyl ether, gradient elution from 100/0 to 0/100) to give the product as a cream coloured solid (0.19 g, 19%).

^{1}H-NMR ($CDCl_3$, 500 MHz) δ = 8.75 (3H, d, ^3J = 4.5, H^6), 8.74 (3H, s, $H^{2'}$), 7.97 (3H, d, ^3J = 8.0, H^3), 7.80 (3H, td, ^3J = 8.0, ^4J = 1.5, H^4), 7.28 (3H, dd, ^3J = 7.5, 5.0, H^5). ^{13}C-NMR ($CDCl_3$, 126 MHz) δ = 157.3 (C^q), 149.9 ($C^{2'}$), 140.7 (C^q), 137.0 (C^4), 126.3 (C^6), 122.7 (C^5), 121.2 (C^3). MS (ES^+) m/z = 332.0 $[M + Na]^+$ and 640.9 $[2M + Na]^+$. HRMS (ES^+) m/z = 310.13385 $[M + H]^+$; 310.13387 calculated for $[C_{21}H_{16}N_3]^+$. C, H & N analysis: 79.68% C, 4.98% H and 12.92% N measured; 79.73% C, 4.82% H and 13.22% N calculated for $[C_{21}H_{15}N_3].\{0.1(CH_2Cl_2)\}$. TLC (silica) R_f = 0.45 in diethyl ether. Mp = 213–216°C.

4'-(*p*-neopentylglycolatoboron)-phenyl-6'-(*m*-tolyl)-bipyridine [mtbpyH-ϕ-Bneo][g] 67

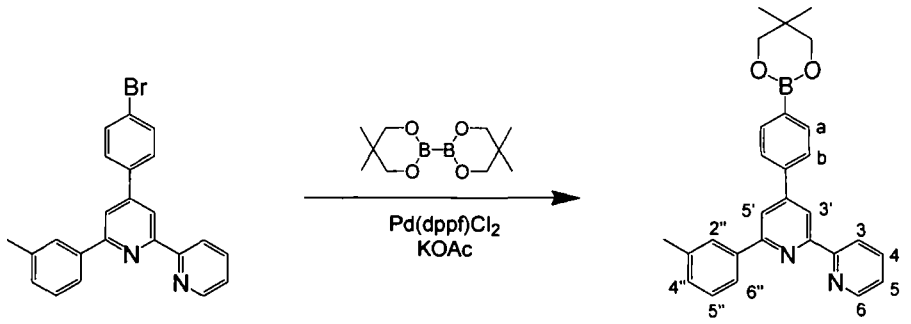

A mixture of 4'-(*p*-bromobenzene)-6'-(*m*-tolyl)-bipyridine (0.10 g, 0.25 mmol), $B_2(neo)_2$ (0.68 g, 0.30 mmol) and potassium acetate (0.068 g, 0.30 mmol) in DMSO (6 mL) was degassed by 4 freeze-pump-thaw cycles. $Pd(dppf)Cl_2$ (0.074 g, 0.075 mmol) was added under a positive pressure of N_2 and the reaction mixture heated at 80°C, under a N_2 atmosphere, for 16 hours. The resultant black solution was diluted with DCM (20 mL), washed with water (5 x 100 mL), dried over sodium sulfonate and filtered through Celite®. The solvent was removed from the filtrate under reduced pressure and the product dried under vacuum giving a brown/black solid (0.15 g). The product was used without further purification.

^{1}H-NMR ($CDCl_3$, 500 MHz) δ = 8.73-8.64 (2H, m, H^3 and H^6), 8.63 (1H, s, $H^{3'}$), 8.02-7.93 (3H, m, $H^{4''}$ and H^a), 7.91 (1H, d, ^3J = 8.0, $H^{5'}$), 7.85 (1H, t, ^3J = 8.0, H^4), 7.82-7.78 (3H, m, $H^{2''}$ and H^b), 7.38 (1H, t, ^3J = 7.5, $H^{5''}$), 7.32 (1H, t, ^3J = 5.0, H^5), 7.24 (1H, d, ^3J = 9.0, $H^{6''}$), 3.79 (4H, s, CH_2), 2.48 (3H, s, CH_3), 1.03 (6H, s, CH_3-Bneo). ^{13}C-NMR ($CDCl_3$, 126 MHz) δ = 207.3 (C), 157.6 (C), 156.6 (C), 150.5 (C), 149.2 (C^3), 140.9 (C), 139.7 (C), 138.7 (C), 138.6 (C), 137.2 (C^4), 134.8 (C^b), 130.2 (C), 130.1 ($C^{6''}$), 128.9 ($C^{5''}$), 128.0 ($C^{2''}$), 127.9 (C), 126.6 (C^a), 124.5 ($C^{4''}$), 124.0 (C^5), 121.9 (C^6), 118.9 (C), 117.7 ($C^{3'}$), 72.6 (CH_2), 21.9 (CH_3-Bneo), 21.8 (CH_3). MS (MALDI, DCTB matrix) m/z = 453.3 $[M + H]^+$. HRMS (ES^+) m/z = 434.22672 $[M + H]^+$; 434.22747 calculated for $[C_{28}H_{28}{}^{10}BN_2O_2]^+$.

[g] An adaptation of the method used by Aspley and Williams for L^6 was followed.[51]

6.6 *Synthesis of metal dimers*

Bis(μ-chloro)bis(1,3,5-tri(2-pyridyl)benzene-N,C$^{2'}$,N iridium chloride) [Ir(tpyb)Cl(μ-Cl)]$_2$ [h] 23

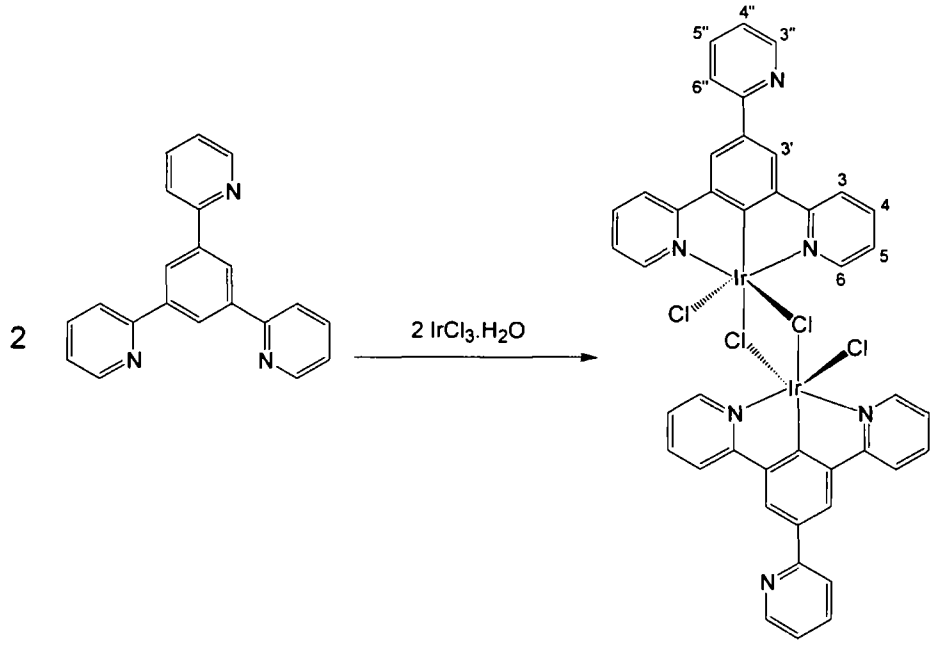

A suspension of tpybH **22** (0.18 g, 0.58 mmol) and iridium trichloride monohydrate (0.18 g, 0.58 mmol) in a mixture of 2-ethoxyethanol (14 mL) and water (6 mL) was stirred at 80°C under a N_2 atmosphere for 24 hours. After cooling to room temperature the precipitate was collected by centrifuge, washed with water (3 x 5 mL), ethanol (3 x 5 mL) and diethyl ether (3 x 5 mL) and dried under vacuum to give the product as an orange solid. Further product was obtained by repeating the procedure with the remaining solution (0.22 g, 67%).

Although insoluble in all common solvents, heating in d_6-DMSO results in a solution of monomeric, d_6-DMSO solvated, [Ir(tpyb)(d_6-DMSO)Cl_2]. ^{1}H-NMR (d_6-DMSO with heating, 400 MHz) δ = 9.05 (2H, dd, ^{3}J = 6.0, ^{4}J = 1.2, H^6), 8.78 (1H, d, ^{3}J = 6.0, $H^{3''}$), 8.70 (2H, s, $H^{3'}$), 8.45 (2H, d, ^{3}J = 8.4, H^3), 8.34 (1H, d, ^{3}J = 7.6, $H^{6''}$), 8.15 (2H, td, ^{3}J = 7.6, ^{4}J = 1.6, H^4), 8.04 (1H, td, ^{3}J = 7.6, ^{4}J = 1.2, $H^{5''}$), 7.62 (2H, ddd, ^{3}J = 7.6, 6.0, ^{4}J = 1.2, H^5), 7.55 (1H, t, ^{3}J = 5.6, $H^{4''}$). Mp > 250°C.

---

[h] This method was based upon an adaptation of that used by Wilkinson *et al.* for [Ir(dpydmb)Cl(μ-Cl)]$_2$.[78]

Bis(μ-chloro)bis(1,3-di(2-pyridyl)benzene-N,C$^{2'}$,N rhodium chloride) [Rh(dpyb)Cl(μ-Cl)]$_2$ **24**

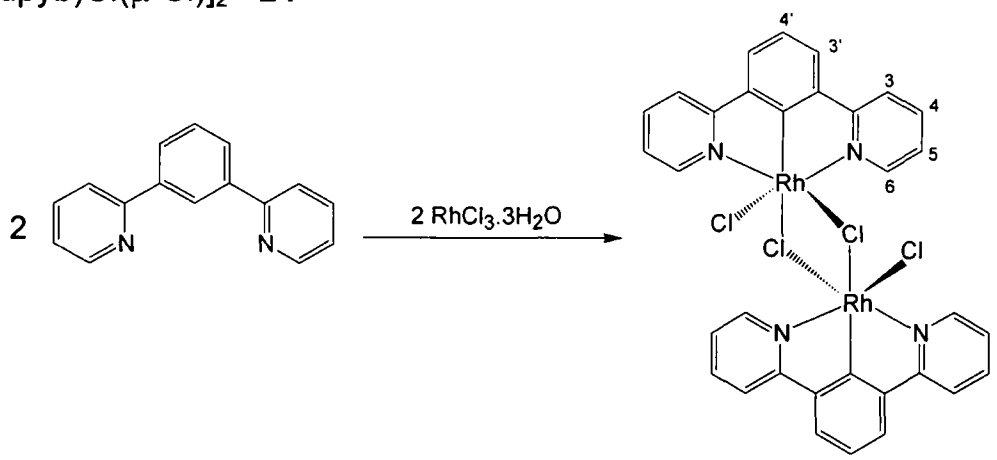

The same procedure was employed as for [Ir(tpyb)Cl(μ-Cl)]$_2$ **23**, but with an reduced reaction time of 6 hours. Reaction of 1,3-di(2-pyridyl)benzene (0.070 g, 0.30 mmol) and rhodium trichloride trihydrate (0.065 g, 0.31 mmol) in a mixture of 2-ethoxyethanol (7 mL) and water (3 mL) gave the product as an orange solid (0.066 g, 54%).

Although insoluble in all common solvents, heating in d_6-DMSO results in a solution of monomeric, d_6-DMSO solvated, [Rh(dpyb)(d_6-DMSO)Cl$_2$]. ^{1}H-NMR (d_6-DMSO with heating, 300 MHz) δ = 8.60 (4H, d, ^{3}J = 4.8, H^6), 8.43 (4H, m, H^3), 8.18 (4H, t, ^{3}J = 8.1, H^4), 7.61 (4H, t, ^{3}J = 6.6, H^5), 7.45 (4H, d, ^{3}J = 7.8, H$^{3'}$), 7.35 (2H, t, ^{3}J = 5.4, H$^{4'}$).

The product was not fully pure, due to the ligand binding in both the desired terdentate, and alternate bidentate manner. Low solubility in all common solvents made purification unfeasible, thus the product was used without further purification and full characterisation.

Bis(μ-chloro)bis(1,3-di(2-pyridyl)-4,6-dimethylbenzene-N,C$^{2'}$,N rhodium chloride) [Rh(dpydmb)Cl(μ-Cl)]$_2$ **25**

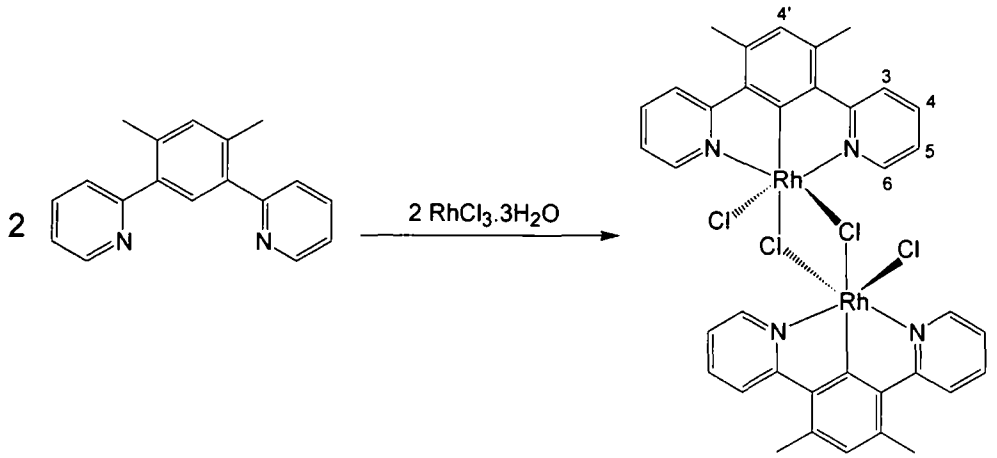

Procedure as for [Ir(tpyb)Cl(μ-Cl)]$_2$ **23**. Reaction of dpydmbH **7** (0.15 g, 0.58 mmol) and $RhCl_3.3H_2O$ (0.13 g, 0.62 mmol) in a mixture of 2-ethoxyethanol (14 mL) and water (6 mL) afforded the product as a yellow/orange solid (0.18 g, 72%).

Although insoluble in all common solvents, heating in d_6-DMSO results in a solution of monomeric, d_6-DMSO solvated, [Rh(dpydmb)(d_6-DMSO)Cl_2]. ^{1}H-NMR (d_6-DMSO with heating, 500 MHz) δ = 9.22 (2H, d, ^3J = 4.0, H^6), 8.17 (2H, d, ^3J = 8.0, H^3), 8.11 (2H, td, ^3J = 7.5, H^4), 7.54 (2H, ddd, ^3J = 7.0, 6.5, ^4J = 1.5, H^5), 7.04 (1H, s, $H^{4'}$), 2.76 (6H, s, CH_3). ^{13}C-NMR (d_6-DMSO with heating, 126 MHz) δ = 165.8 (C^q), 153.9 (C^6), 140.3 (C^4 and C^q), 138.1 (C^q), 138.0 (C^q), 125.4 ($C^{4'}$), 122.9 (C^3), 122.8 (C^5), 23.2 (CH_3). MS (EI) m/z = 432.0 [^{103}Rh(dpydmb)$^{35}Cl_2$]$^+$, 434.0 [^{103}Rh(dpydmb)^{35}Cl^{37}Cl]$^+$ and 436.0 [^{103}Rh(dpydmb)$^{37}Cl_2$]$^+$. HRMS (EI) m/z = 431.9662 [^{103}Rh(dpydmb)$^{35}Cl_2$]$^+$; 431.9665 calculated for [$C_{18}H_{15}{}^{35}Cl_2N_2{}^{103}Rh$]$^+$. C, H & N analysis: 49.63% C, 3.51% H and 6.99% N measured; 49.91% C, 3.49% H and 6.47% N calculated for [$C_{36}H_{30}Cl_4N_4Rh_2$]. Mp > 250°C.

Bis(μ-chloro)bis(1,3-di(2-pyridyl)-4,6-dimethylbenzene-N,C$^{2'}$,N iridium chloride) [Ir(dpydmb)Cl(μ-Cl)]$_2$ [76, 78] **29**

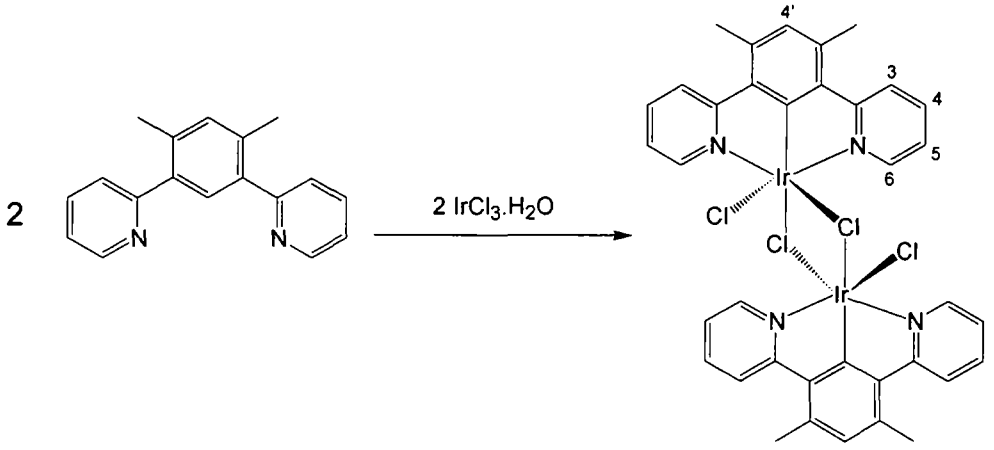

Procedure as for [Ir(tpyb)Cl(μ-Cl)]$_2$ **23**. Reaction of dpydmbH **7** (0.25 g, 0.96 mmol) and iridium trichloride monohydrate (0.30 g, 0.96 mmol) gave the desired product as a yellow solid (0.39 g, 78%).

Although insoluble in all common solvents, heating in d_6-DMSO results in a solution of monomeric, d_6-DMSO solvated, [Ir(dpydmb)(d_6-DMSO)Cl_2]. ^{1}H-NMR (d_6-DMSO with heating, 400 MHz) δ = 9.20 (2H, d, ^3J = 5.6, H^6), 8.16 (2H, d, ^3J = 8.4, H^3), 8.05 (2H, td, ^3J = 8.4, ^4J = 1.6, H^4), 7.53 (2H, dd, ^3J = 6.0, 6.0, H^5), 6.97 (1H, s, $H^{4'}$), 2.75 (6H, s, CH_3). MS (MALDI, DCTB matrix) m/z = 522.0 [^{193}Ir(dpydmb)$^{35}Cl_2$]$^+$.

C, H & N analysis: 41.75% C, 2.87% H and 5.28% N measured; 41.38% C, 2.89% H and 5.36% N calculated for $[C_{36}H_{30}Cl_4Ir_2N_4]$. Mp > 250°C.

Bis(μ-chloro)bis(1,3-di(1-pyrazolyl)benzene-N,C$^{2'}$,N iridium chloride) $[Ir(dpzb)Cl(\mu\text{-}Cl)]_2$ 44

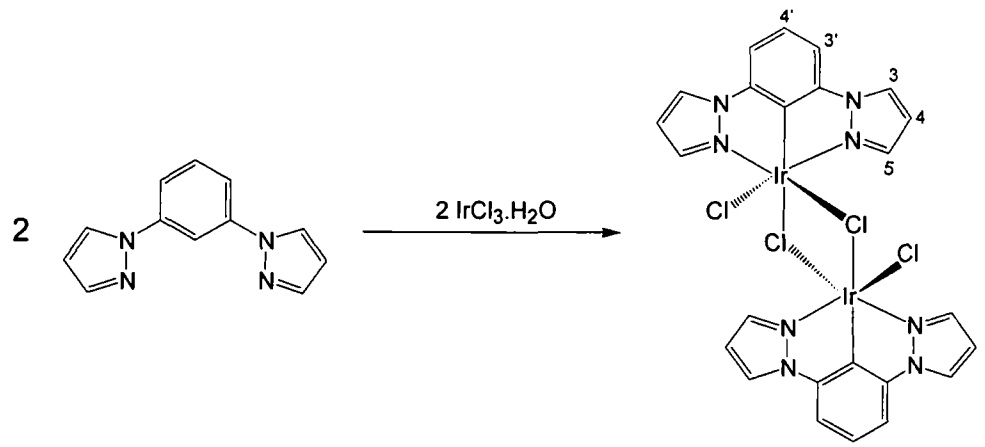

Procedure as for $[Ir(tpyb)Cl(\mu\text{-}Cl)]_2$ **23**. Reaction of dpzbH **16** (0.20 g, 0.95 mmol) and $IrCl_3.H_2O$ (0.30 g, 0.96 mmol) gave the product as a yellow/green solid (0.31 g, 67%).

The product was not fully pure, due to the ligand binding in both the desired terdentate, and alternate bidentate manner. Low solubility in all common solvents made purification unfeasible, thus the product was used without further purification and characterisation.

Bis(μ-chloro)bis(1,3-di(1-pyrazolyl)-5-methylbenzene-N,C$^{2'}$,N iridium chloride) $[Ir(dpzmb)Cl(\mu\text{-}Cl)]_2$ 45

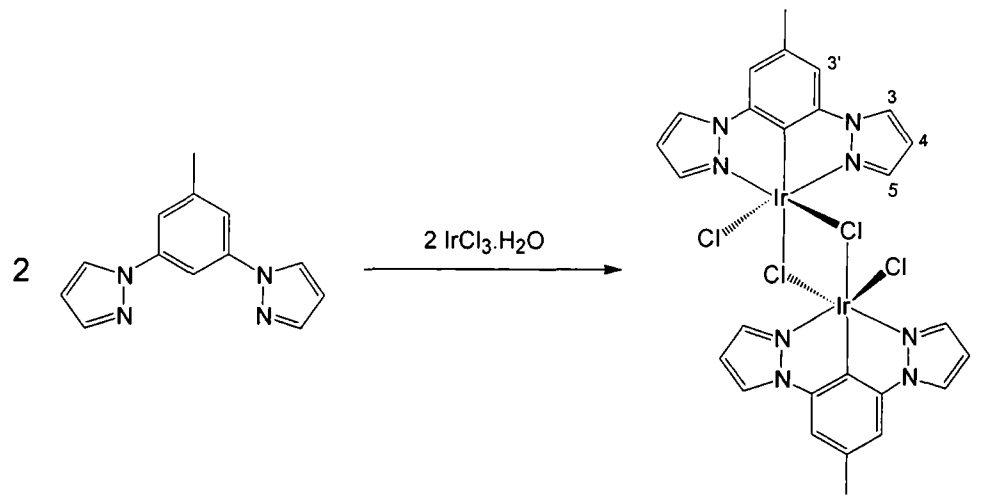

Procedure as for [Ir(tpyb)Cl(μ-Cl)]$_2$ **23**. Reaction of dpzmbH **17** (0.20 g, 0.89 mmol) and $IrCl_3.H_2O$ (0.27 g, 0.86 mmol) gave the product as a yellow/green solid (0.21 g, 50%).

Although insoluble in all common solvents, heating in d_6-DMSO results in a solution of monomeric, d_6-DMSO solvated, [Ir(dpzmb)(d_6-DMSO)Cl_2]. ^{1}H-NMR (d_6-DMSO with heating, 500 MHz) δ = 8.80 (2H, d, ^3J = 3.0, H^3), 8.10 (2H, d, ^3J = 2.5, H^5), 7.55 (2H, s, $H^{3'}$), 6.73 (2H, t, ^3J = 2.5, H^4), 2.58 (3H, s, CH_3).

The product was not fully pure, due to the ligand binding in both the desired terdentate, and alternate bidentate manner. Low solubility in all common solvents made purification unfeasible, thus the product was used without further purification and full characterisation.

Bis(μ-chloro)bis(1,3-di(1-pyrazolyl)-5-bromobenzene-N,C$^{2'}$,N iridium chloride) [Ir(dpzb-Br)Cl(μ-Cl)]$_2$ 46

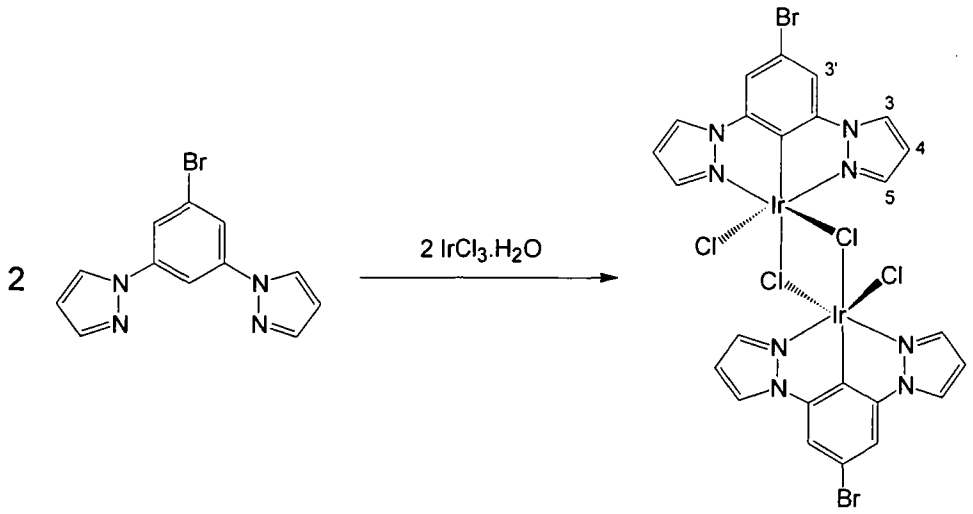

The same procedure was employed as for [Ir(tpyb)Cl(μ-Cl)]$_2$ **23**, but with an extended reaction time of 72 hours. Reaction of dpzbH-Br **15** (0.10 g, 0.35 mmol) and $IrCl_3.H_2O$ (0.11 g, 0.35 mmol) gave the product as a pale yellow solid (0.098 g, 49%).

Although insoluble in all common solvents, heating in d_6-DMSO results in a solution of monomeric, d_6-DMSO solvated, [Ir(dpzb-Br)(d_6-DMSO)Cl_2]. ^{1}H-NMR (d_6-DMSO with heating, 500 MHz) δ = 8.90 (2H, d, ^3J = 3.0, H^3), 8.15 (2H, d, ^3J = 2.5, H^5), 8.05 (2H, s, $H^{3'}$), 6.79 (2H, t, ^3J = 3.0, H^4).

The product was not fully pure, due to the ligand binding in both the desired terdentate, and alternate bidentate manner. Low solubility in all common solvents made

purification unfeasible, thus the product was used without further purification and full characterisation.

Bis(μ-chloro)bis(1,3-di(1-pyrazolyl)-4,6-dimethylbenzene-N,C$^{2'}$,N iridium chloride) [Ir(dpzdmb)Cl(μ-Cl)]$_2$ 47

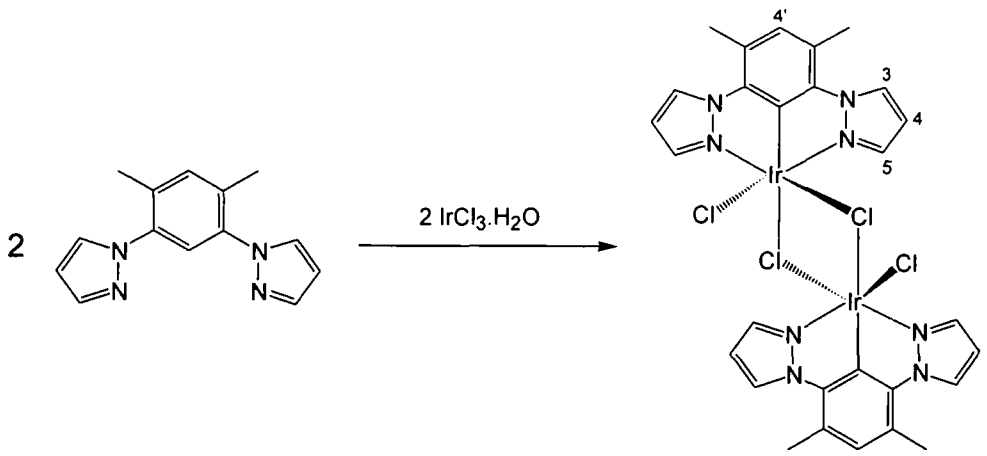

The same procedure was employed as for [Ir(tpyb)Cl(μ-Cl)]$_2$ **23**, but with an extended reaction time of 48 hours. Reaction of dpzdmbH **19** (0.15 g, 0.63 mmol) and $IrCl_3.H_2O$ (0.20 g, 0.64 mmol) gave the product as an orange solid (0.21 g, 66%).

Although insoluble in all common solvents, heating in d_6-DMSO results in a solution of monomeric, d_6-DMSO solvated, [Ir(dpzdmb)(d_6-DMSO)Cl_2]. ^{1}H-NMR (d_6-DMSO with heating, 500 MHz) δ = 8.58 (2H, d, ^{3}J = 3.0, H^3), 8.16 (2H, d, ^{3}J = 2.5, H^5), 6.97 (1H, s, $H^{4'}$), 6.75 (2H, t, ^{3}J = 2.5, H^4), 2.67 (6H, s, CH_3). ^{13}C-NMR (d_6-DMSO with heating, 126 MHz) δ = 142.4 (C^5), 140.3 ($C^{1'}$), 139.2 ($C^{3'}$), 133.6 (C^3), 131.9 ($C^{4'}$), 120.4 ($C^{2'}$), 107.1 (C^4), 19.6 (CH_3). MS (EI) m/z = 995.9 $[M]^+$. HRMS (EI) m/z = 996.0246 $[M]^+$; 996.0241 calculated for $[C_{28}H_{26}Cl_4{}^{191}Ir_2N_8]^+$. C, H & N analysis: 32.59% C, 2.89% H and 10.76% N measured; 32.44% C, 2.92% H and 10.81% N calculated for $[C_{28}H_{26}Cl_4Ir_2N_8].\{2(H_2O)\}$. Mp > 250°C.

6.7 *Synthesis of monometallic rhodium(III) complexes*

Rhodium (1,3-di(2-pyridyl)benzene-N,C$^{2'}$,N)(2,2':6',2"-terpyridine)$^{2+}$ [Rh(dpyb)(tpy)]$^{2+}$ [i] **26**

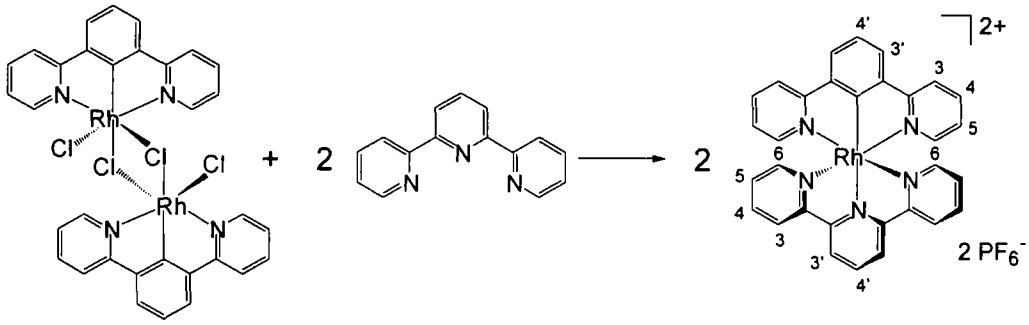

A suspension of [Rh(dpyb)Cl(μ-Cl)]$_2$ **24** (0.058 g, 0.072 mmol) and 2,2':6',2"-terpyridine (0.034 g, 0.15 mmol) in ethylene glycol (3 mL) was stirred at room temperature under a N_2 atmosphere for 1 hour, then heated to 196°C for a further hour. After cooling to room temperature, water (10 mL) was added to the reaction mixture and the water insoluble impurities removed by filtration. Saturated aqueous KPF_6 solution (20 mL) was added to the filtrate and the resulting orange precipitate collected by centrifuge, washed with water (4 x 5 mL) and dried under vacuum. Purification was achieved by flash column chromatography (silica, acetonitrile/water/$KNO_{3\,(aq)}$, gradient elution from 100/0/0 to 88.0/11.8/0.2). After evaporation of the solvent, the product was separated from the excess KNO_3 by selective dissolution into hot acetonitrile containing a drop of water. The solution was concentrated and filtered into saturated aqueous KPF_6 solution to precipitate the product as the PF_6^- salt. This was collected by centrifuge, washed with water (3 x 5 mL) and dried under vacuum to give the desired product as an orange solid (0.0085 g, 7%).

^{1}H-NMR (d_6-acetone, 500 MHz) δ = 9.92 (2H, d, ^{3}J = 8.0, H$^{3'}$-tpy), 9.01 (1H, t, ^{3}J = 8.5, H$^{4'}$-tpy), 8.90 (2H, d, ^{3}J = 8.0, H^3-tpy), 8.47 (2H, d, ^{3}J = 8.5, H^3). 8.46 (2H, d, ^{3}J = 7.5, H$^{3'}$), 8.29 (2H, t, ^{3}J = 8.0, H^4-tpy), 8.10 (2H, t, ^{3}J = 7.5, H^4), 7.87 (1H, t, ^{3}J = 8.0, H$^{4'}$), 7.83 (2H, d, ^{3}J = 5.5, H^6), 7.71 (2H, d, ^{3}J = 5.5, H^6-tpy), 7.52 (2H, t, ^{3}J = 6.5, H^5-tpy), 7.18 (2H, t, ^{3}J = 6.0, H^5). MS (ES$^+$) m/z = 283.5 [M]$^{2+}$/2 and 712.1 [M + PF_6^-]$^+$. HRMS (ES$^+$) m/z = 283.54600 [M]$^{2+}$/2; 283.54596 calculated for [$C_{31}H_{22}N_5{}^{103}Rh$]$^{2+}$/2 and 712.05686 [M + PF_6^-]$^+$; 712.05666 calculated for [$C_{31}H_{22}F_6N_5P_1{}^{103}Rh$]$^+$. TLC (silica) R_f = 0.21 in MeCN/H_2O/$KNO_{3\,(aq)}$, 90/9/1. Mp > 250°C.

---

[i] Based upon work by Wilkinson.[76, 206]

Rhodium (1,3-di(2-pyridyl)-4,6-dimethylbenzene-N,$C^{2'}$,N)(2,2':6',2''-terpyridine)$^{2+}$ $[Rh(dpydmb)(tpy)]^{2+}$ **27**

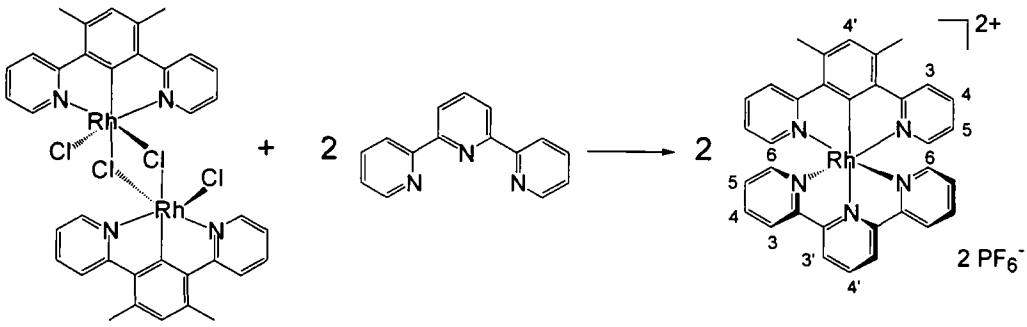

A suspension of $[Rh(dpydmb)Cl(\mu\text{-}Cl)]_2$ **25** (0.052 g, 0.060 mmol) and 2,2':6',2''-terpyridine (0.029 g, 0.12 mmol) in ethylene glycol (3 mL) underwent the same reaction procedure used in the synthesis of $[Rh(dpyb)(tpy)]^{2+}$ **26**. The resultant yellow/orange crude product was purified by flash column chromatography (silica, acetonitrile/water/$KNO_{3\ (aq)}$, gradient elution from 100/0/0 to 92.0/7.8/0.2). Following evaporation of the solvent, the product was ion exchanged back to the PF_6^- salt (as outlined for $[Rh(dpyb)(tpy)]^{2+}$ **26**) and isolated as a yellow/orange solid (0.064 g, 58%). ^{1}H-NMR (d_6-acetone, 500 MHz) δ = 9.22 (2H, d, ^3J = 8.5, $H^{3'}$-tpy), 9.02 (1H, t, ^3J = 8.0, $H^{4'}$-tpy), 8.90 (2H, d, ^3J = 7.5, H^3-tpy), 8.48 (2H, d, ^3J = 8.5, H^3), 8.30 (2H, td, ^3J = 7.5, ^4J = 1.5, H^4-tpy), 8.09 (2H, td, ^3J = 8.0, ^4J = 1.5, H^4), 7.82 (2H, d, ^3J = 6.0, H^6), 7.75 (2H, d, ^3J = 5.5, H^6-tpy), 7.53 (1H, s, $H^{4'}$), 7.52 (2H, td, ^3J = 6.5, ^4J = 1.0, H^5-tpy), 7.16 (2H, td, ^3J = 7.0, ^4J = 1.0, H^5), 3.06 (6H, s, CH_3). ^{13}C-NMR (d_6-acetone, 126 MHz) δ = 167.6 (C), 158.7 (C), 154.5 (C), 152.8 (C), 151.7 (C^6), 142.8 ($C^{4'}$-tpy), 141.6 (C), 141.5 (C), 140.8 (C), 140.2 (C), 138.1 (C), 134.3 (C^4), 129.4 (C^5-tpy), 126.8 (C^3-tpy), 126.2 (C), 125.3 (C^3), 124.5 (C) and 22.30 (CH_3). MS (ES^+) m/z = 297.5 $[M]^{2+}$. HRMS (ES^+) m/z = 297.56189 $[M]^{2+}/2$; 297.56161 calculated for $[C_{33}H_{26}N_5{}^{103}Rh]^{2+}/2$. C, H & N analysis: 44.94% C, 2.59% H and 7.83% N measured; 44.76% C, 2.96% H and 7.91% N calculated for $[C_{33}H_{26}F_{12}N_5P_2Rh]$. TLC (silica) R_f = 0.30 in $MeOH/H_2O/KNO_{3\ (aq)}$, 90/9/1. Mp > 250°C.

Rhodium (1,3-di(2-pyridyl)-4,6-dimethylbenzene-N,C$^{2'}$,N)(4-(4-bromo) phenyl)-2,2':6',2''-terpyridine)$^{2+}$ [Rh(dpydmb)(tpy-ϕ-Br)]$^{2+}$ **28**

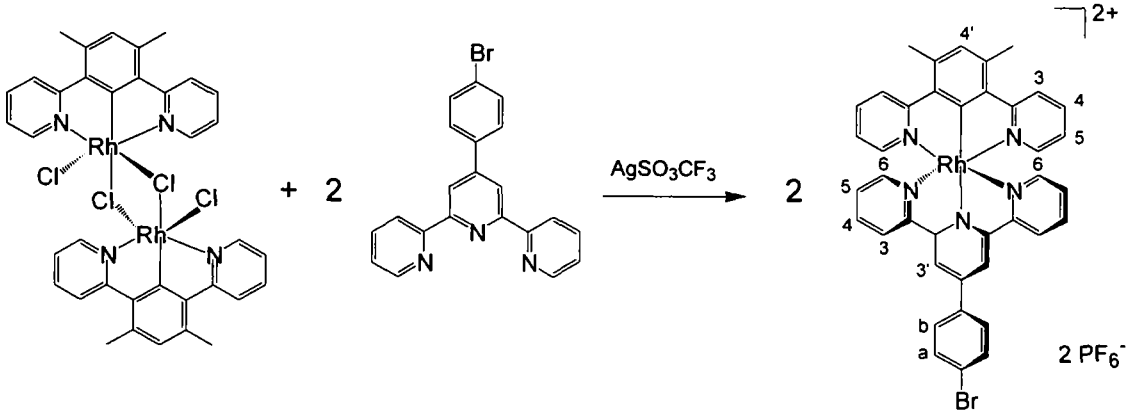

A suspension of [Rh(dpydmb)Cl(μ-Cl)]$_2$ **25** (0.039 g, 0.05 mmol), 4-(4-bromo)phenyl)-2,2':6',2''-terpyridine (0.039 g, 0.10 mmol) and silver triflate in ethylene glycol (3 mL) was stirred at room temperature under a N_2 atmosphere for 1 hour, then heated to 196°C for a further hour. After cooling to room temperature, the precipitated AgCl was removed by centrifuge and washed with acetonitrile (2 x 1mL). The acetonitrile washings and ethylene glycol solution were combined and added to saturated aqueous KPF_6 solution (25 mL) forming a pale yellow precipitate. This was collected by centrifuge, washed with water (5 x 3 mL) and purified by flash column chromatography (silica, acetonitrile/water/$KNO_{3\ (aq)}$, gradient elution from 100/0/0 to 89.0/10.2/0.8). Following evaporation of the solvent, the product was ion exchanged back to the PF_6^- salt (as outlined for [Rh(dpyb)(tpy)]$^{2+}$ **26**) affording a pale yellow solid (0.46 g, 46%). ^{1}H-NMR (CH_3CN, 500 MHz) δ = 9.09 (2H, s, H$^{3'}$-NNN), 8.68 (2H, d, ^{3}J = 8.0, H^3-NNN), 8.32 (2H, d, ^{3}J = 8.5, H^3-NCN), 8.13 (4H, m, H^b-NNN and H^4-NNN), 8.00 (2H, d, ^{3}J = 8.5, H^a-NNN), 7.95 (2H, t, ^{3}J = 8.0, H^4-NCN), 7.52 (2H, d, ^{3}J = 6.0, H^6-NCN), 7.48 (2H, d, ^{3}J = 5.5, H^6-NNN), 7.44 (1H, s, H$^{4'}$-NCN), 7.32 (2H, t, ^{3}J = 6.5, H^5-NNN), 7.04 (2H, t, ^{3}J = 6.5, H^5-NCN), 2.98 (6H, s, CH_3). MS (MALDI, DCTB matrix) m/z = 751.1 [M + e$^-$]$^+$. HRMS (ES$^+$) m/z = 749.06596 [M + e$^-$]$^+$; 749.06559 calculated for [$C_{39}H_{29}{}^{79}BrN_5{}^{103}Rh$]$^+$. C, H & N analysis: 44.80% C, 2.86% H and 6.95% N measured; 45.02% C, 2.81% H and 6.73% N. calculated for [$C_{33}H_{26}F_{12}N_5P_2Rh$]. TLC (silica) R_f = 0.20 in MeCN/H_2O/$KNO_{3\ (aq)}$, 90.0/9.8/0.2. Mp > 250°C.

Rhodium (1,3-di(2-pyridyl)-4,6-dimethylbenzene-N,$C^{2'}$,N)(2,2'-bipyridine) chloride$^+$ [Rh(dpydmb)(bpy)Cl]$^+$ **31**

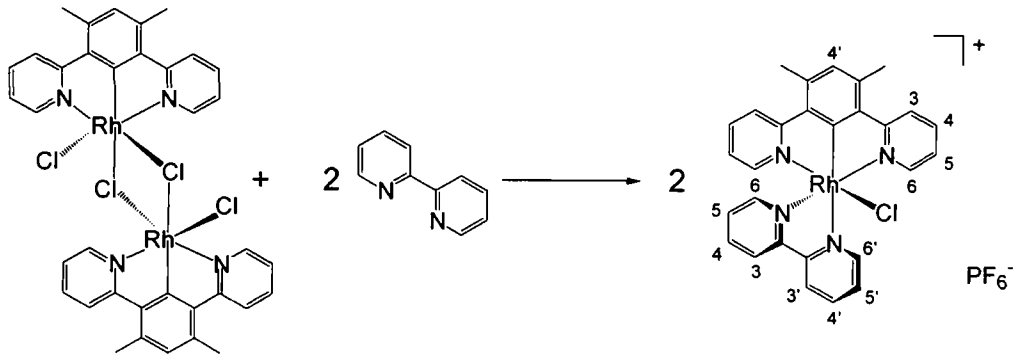

A suspension of [Rh(dpydmb)Cl(μ-Cl)]$_2$ **25** (0.053 g, 0.061 mmol) and 2,2'-bipyridine (0.019 g, 0.13 mmol) in ethylene glycol (3 mL) was stirred at room temperature under a N_2 atmosphere for 1 hour and then heated to 196°C for a further hour. A yellow/orange solution formed alongside a black insoluble solid. After cooling to room temperature, the ethylene glycol solution was diluted with acetonitrile (1 mL) and filtered into saturated aqueous KPF_6 solution (20 mL). The resultant precipitate was collected by centrifuge, washed with water (3 x 5 mL) and dried under vacuum, to give the product as a pale yellow solid (0.083 g, 99%).

^{1}H-NMR (CD_3CN, 500 MHz) δ = 9.89 (1H, d, ^3J = 5.0, $H^{6'}$), 8.64 (1H, d, ^3J = 8.5, $H^{3'}$), 8.51 (1H, td, ^3J = 8.0, ^4J = 1.5, $H^{4'}$), 8.36 (1H, d, ^3J = 7.5, H^3), 8.20 (2H, d, ^3J = 8.5, H^3-NCN), 8.17 (1H, ddd, ^3J = 8.0, 5.0, ^4J = 1.0, $H^{5'}$), 7.91-7.86 (3H, m, H^4 and H^4-NCN), 7.61 (2H, dd, ^3J = 5.0, ^4J = 0.5, H^6-NCN), 7.41 (1H, d, ^3J = 6.0, H^6), 7.21 (1H, s, $H^{4'}$-NCN), 7.13 (1H, ddd, ^3J = 8.0, 5.5, ^4J = 1.0, H^5), 7.05 (2H, ddd, ^3J = 7.5, 5.5, ^4J = 1.5, H^5-NCN), 2.87 (6H, s, CH_3). MS (ES^+) m/z = 553.4 $[M]^+$. HRMS (ES^+) m/z = 553.06623 $[M]^+$; 553.06608 calculated for $[C_{28}H_{23}{}^{35}ClN_4{}^{103}Rh]^+$. C, H & N analysis: 31.25% C, 2.24% H and 5.54% N measured; 31.52% C, 2.17% H and 5.25% N calculated for $[C_{28}H_{23}ClF_6N_4PRh].(KPF_6)$. TLC (silica) R_f = 0.43 in DCM/MeOH, 90/10. Mp > 250°C.

Rhodium (1,3-di(2-pyridyl)-4,6-dimethylbenzene-N,$C^{2'}$,N)(6-phenyl-2,2'-bipyridine)$^+$ [Rh(dpydmb)(phbpy)]$^+$ **34**

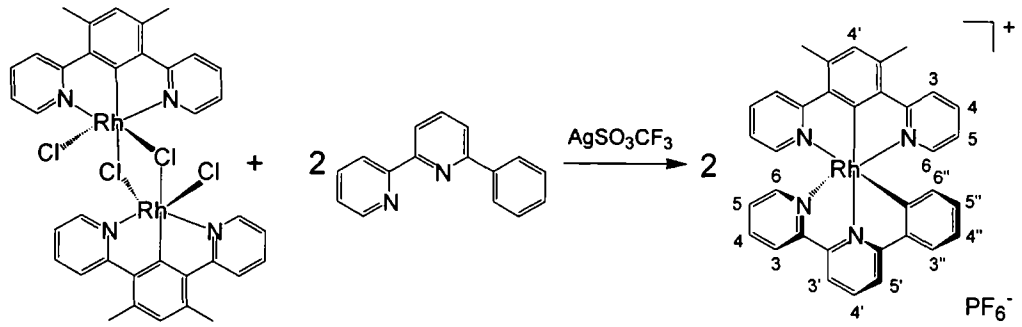

A suspension of [Rh(dpydmb)Cl(μ-Cl)]$_2$ **25** (0.043 g, 0.050 mmol), phbpyH **1** (0.027 g, 0.12 mmol) and silver triflate (0.057 g, 0.22 mmol) in ethylene glycol (4 mL) was stirred at room temperature under a N_2 atmosphere for 1 hour, then heated to 196°C for a further 3 hours. After cooling to room temperature, the precipitated AgCl was collected by centrifuge and washed with acetonitrile (2 x 2 mL). The acetonitrile washings and ethylene glycol solution were combined and added to saturated aqueous KPF_6 solution (20 mL), forming a pale yellow precipitate, which was collected by centrifuge and washed with water (3 x 5 mL). Purification was achieved by flash column chromatography (silica, acetonitrile/water/$KNO_{3\ (aq)}$, gradient elution from 100/0/0 to 90/9/1). Following evaporation of the solvent, the product was ion exchanged back to the PF_6^- salt (as outlined for [Rh(dpyb)(tpy)]$^{2+}$ **26**) and further purified by flash column chromatography (silica, DCM/methanol, gradient elution from 100/0 to 99/1) to give the desired product as a yellow solid (0.032 g, 43%).

^{1}H-NMR (d_6-acetone, 500 MHz) δ = 8.73 (1H, d, ^{3}J = 8.0, H^3), 8.70 (1H, d, ^{3}J = 7.0, $H^{3'}$), 8.55-8.50 (2H, m, $H^{4'}$ and $H^{5'}$), 8.27 (2H, d, ^{3}J = 8.5, H^3-NCN), 8.13 (1H, dd, ^{3}J = 8.5, 8.0, H^4), 7.94 (1H, d, ^{3}J = 8.0, $H^{3''}$), 7.86 (2H, dd, ^{3}J = 8.0, 7.5, H^4-NCN), 7.78 (1H, d, ^{3}J = 5.0, H^6), 7.59 (2H, d, ^{3}J = 5.5, H^6-NCN), 7.39 (1H, dd, ^{3}J = 6.5, 6.5, H^5), 7.22 (1H, s, $H^{4'}$-NCN), 6.97 (2H, dd, ^{3}J = 7.0, 6.5, H^5-NCN), 6.90 (1H, dd, ^{3}J = 7.5, 7.0, $H^{4''}$), 6.67 (1H, dd, ^{3}J = 7.5, 7.5, $H^{5''}$), 6.19 (1H, d, ^{3}J = 8.0, $H^{6''}$), 2.94 (6H, s, CH_3). MS (ES^+) m/z = 593.3 $[M]^+$. HRMS (ES^+) m/z = 593.12071 $[M]^+$; 593.12070 calculated for $[C_{34}H_{26}N_4{}^{103}Rh]^+$. TLC (silica) R_f = 0.89 in DCM/methanol, 80/20. Mp > 250°C

Rhodium (1,3-di(2-pyridyl)-4,6-dimethylbenzene-N,$C^{2'}$,N)(2,6-di-phenylpyridine-$C^{2'}$,N)$^+$ [Rh(dpydmb)(dppyH-*C,N*)]$^{+}$ [j] **35**

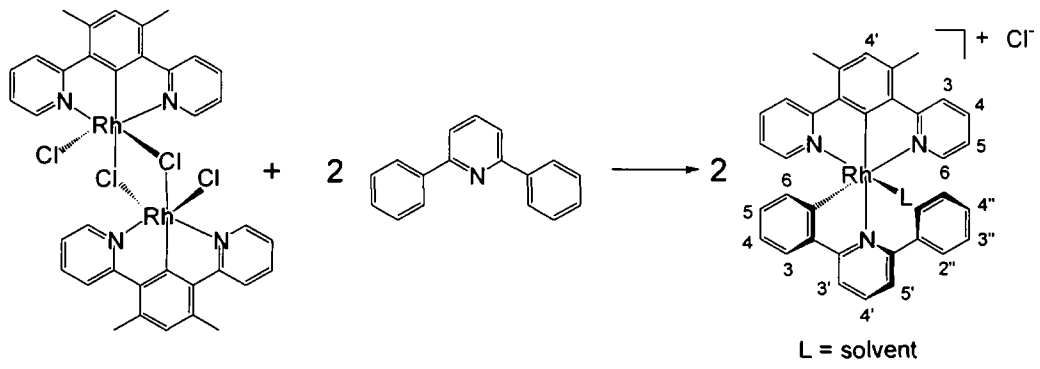

A mixture of [Rh(dpydmb)Cl(μ-Cl)]$_2$ **25** (0.044 g, 0.051 mmol), 2,6-diphenylpyridine (0.68 g, 2.94 mmol) and silver triflate (0.069 g, 0.27 mmol) were ground together in an agar mortar. The resultant fine powder was heated to 110°C and stirred under a N_2 atmosphere for 24 hours. After cooling to room temperature, the product was extracted into ethanol (20 mL) and the insoluble impurities removed by filtration. The solvent was removed from the filtrate under reduced pressure and the resultant yellow residue purified by flash column chromatography (silica, diethyl ether) followed by (silica, DCM/methanol, gradient elution from 100/0 to 96.5/3.5) to give the product as a yellow solid (0.035 g, 58%).

^{1}H-NMR ($CDCl_3$, 500 MHz) δ = 8.15 (2H, m, $H^{3'}$-CNC and $H^{5'}$-CNC), 7.95 (2H, d, ^3J = 8.0, H^3-NCN), 7.70 (2H, s, H^6-NCN), 7.67-7.63 (3H, m, H^4-NCN and H^6-CNC), 7.58 (3H, d, ^3J = 7.0, $H^{2"}$-CNC and $H^{4'}$-CNC), 7.40-7.39 (3H, m, $H^{3"}$-CNC and $H^{4"}$-CNC), 6.94-6.90 (3H, m, $H^{4'}$-NCN and H^5-NCN), 6.82 (1H, t, ^3J = 6.5, H^5-CNC), 6.59 (1H, td, ^3J = 7.0, ^4J = 1.5, H^4-CNC), 6.18 (1H, d, ^3J = 7.5, H^3-CNC), 2.73 (6H, s, CH_3). MS (ES^+) m/z = 592.1 $[M - L]^+$. HRMS (ES^+) m/z = 592.12513 $[M - L]^+$; 592.12545 calculated for $[C_{35}H_{27}N_3{}^{103}Rh]^+$. TLC (silica) R_f = 0.34 in DCM/methanol, 90/10. Mp > 250°C.

[j] Based upon the method employed by Wilkinson *et al.* for the synthesis of [Ir(dpydmb)(dppy)].[78]

Rhodium (1,3-di(2-pyridyl)-4,6-dimethylbenzene-N,C$^{2'}$,N)(2,6-di(2'-indolyl)pyridine-N,N,N) [Rh(dpydmb)(dinpy)][k] 37

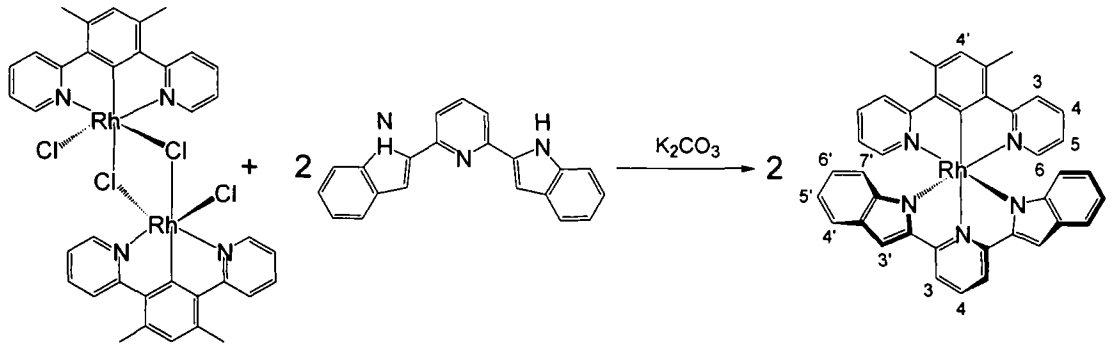

A suspension of [Rh(dpydmb)Cl(μ-Cl)]$_2$ **25** (0.044 g, 0.051 mmol), 2,6-di(2'-indolyl)pyridine (0.031 g, 0.10 mmol) and K_2CO_3 (0.070 g, 0.51 mmol) in ethylene glycol (3 mL) was heated to 196°C under a N_2 atmosphere for 24 hours. After cooling to room temperature, water (8 mL) was added, the resultant pale brown precipitate collected by centrifuge and washed with water (3 x 5 mL). The product was extracted into DCM (30 mL), dried over magnesium sulfate and filtered through Celite®. The solvent was removed under reduced pressure and the crude product purified by flash column chromatography (silica, hexane/ethyl acetate, gradient elution from 100/0 to 82/18) to give the desired product as a yellow solid (0.0067 g, 10%).

^{1}H-NMR ($CDCl_3$, 500 MHz) δ = 8.01 (1H, t, ^3J = 7.5, H^4), 7.90 (2H, d, ^3J = 8.5, H^3-NCN), 7.78 (2H, d, ^3J = 7.5, H^3), 7.44-7.40 (4H, m, H^4-NCN and H^6-NCN), 7.34 (2H, d, ^3J = 8.0, $H^{4'}$), 7.25 (1H, s, $H^{4'}$-NCN), 7.08 (2H, s, $H^{3'}$), 6.63-6.57 (4H, m, $H^{5'}$ and H^5-NCN), 6.50 (2H, dd, ^3J = 7.5, 7.5, $H^{6'}$), 5.78 (2H, d, ^3J = 8.0, $H^{7'}$), 2.92 (6H, s, CH_3). ^{13}C-NMR ($CDCl_3$, 126 MHz) δ = 168.5 (C^q), 154.2 (C^q), 150.5 (C^q), 147.6 (C^q), 146.6 (C^q), 140.2 (C^q), 138.5 (C^4), 137.2 and 137.1 (C^4-NCN and C^6-NCN), 131.6 ($C^{4'}$-NCN), 130.5 (C^q), 130.2 (C^q), 122.8 (C^3-NCN), 122.0 (C^5-NCN), 121.0 ($C^{6'}$), 120.8 ($C^{4'}$), 117.0 ($C^{5'}$), 115.0 (C^3), 114.5 ($C^{7'}$), 101.9 ($C^{3'}$), 23.2 (CH_3). MS (ES^+) m/z = 670.3 $[M + H]^+$. TLC (silica) R_f = 0.61 in hexane/ethyl acetate 50/50. Mp > 250°C.

[k] Methodology based upon that used by Wilkinson to synthesise the iridium analogue.[206]

Rhodium (1,3-di(2-pyridyl)-4,6-dimethylbenzene-N,C$^{2'}$,N)(4'-*p*-tolyl-6-phenylpicolinic acid-O,N)$^+$ [Rh(dpydmb)(tppicH-*ON*)L]$^{+}$[1] **38**

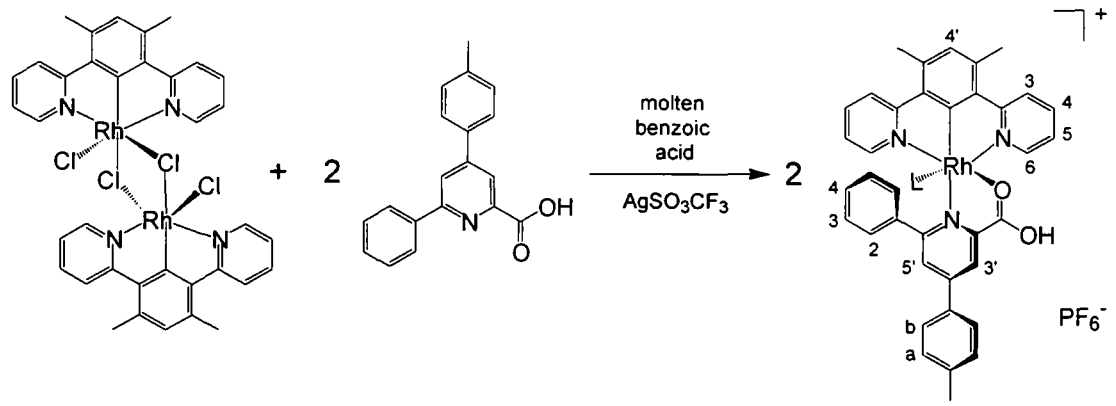

A mixture of [Rh(dpydmb)Cl(μ-Cl)]$_2$ **24** (0.043 g, 0.050 mmol), tppicH **5** (0.15 g, 0.52 mmol), silver triflate (0.089 g, 0.35 mmol) and benzoic acid (0.55 g, 4.50 mmol) were ground together in an agate mortar. The resultant fine powder was heated to 150°C with stirring under a N_2 atmosphere for 24 hours. After cooling to room temperature, the product was dissolved in DCM (15 mL), the insoluble impurities collected by centrifuge and washed with DCM (2 x 5 mL). The washings and filtrate were combined, washed with aqueous sodium bicarbonate solution (1 M, 3 x 25 mL), dried over sodium carbonate and filtered through Celite®. The solvent was removed from the filtrate under reduced pressure and the crude product purified by flash column chromatography (silica, DCM/methanol, gradient elution from 100/0 to 50/50) followed by (silica, acetonitrile/water/$KNO_{3\ (aq)}$, gradient elution from 100/0/0 to 76/20/4). Following evaporation of the solvent from the second column, the product was ion exchanged back to the PF_6^- salt (as outlined for [Rh(dpyb)(tpy)]$^{2+}$ **26**) to give the desired product as a yellow/red solid (0.011 g, 14%).

^{1}H-NMR ($CDCl_3$, 500 MHz) δ = 8.54 (2H, d, ^{3}J = 5.0, H^6-NCN), 8.45 (1H, s, H$^{3'}$), 7.99-7.93 (4H, m, H^3-NCN and H^4-NCN), 7.45 (2H, d, ^{3}J = 8.5, H^b), 7.34 (2H, t, ^{3}J = 5.5, H^5-NCN), 7.17 (2H, d, ^{3}J = 8.0, H^a), 7.06 (1H, t, ^{3}J = 7.5, H^4), 7.04 (1H, s, H$^{5'}$), 6.81 (2H, t, ^{3}J = 7.5, H^3), 6.65 (1H, s, H$^{4'}$-NCN), 6.01 (2H, d, ^{3}J = 7.0, H^2), 2.62 (6H, s, CH_3-NCN), 2.32 (3H, s, CH_3). ^{13}C-NMR ($CDCl_3$, 126 MHz) δ = 186.3 (C=O), 166.7 (C^q), 164.6 (C^q), 151.0 (C^q), 150.9 (C^q), 141.7 (C^q), 139.9 (C^3-NCN or C^4-NCN), 138.5 (C^q), 138.1 (C^q), 137.2 (C^q), 132.6 (C$^{4'}$-NCN), 131.9 (C^q), 130.4 (C^a), 129.1 (C^q),

[1] Based upon the related synthesis of [Ir(dpydmb)(tppic)]$^+$ by Wilkinson.[76]

127.4(C^q), 127.3(C^2 or C^b), 127.2(C^2 or C^b), 126.8(C^4), 125.0($C^{3'}$), 124.1 (C^3-NCN or C^4-NCN), 123.6 (C^5-NCN), 22.8(CH_3-NCN), 21.6 (CH_3). MS (ES^+) m/z = 668.1 $[M (L = H_2O)]^+$. HRMS (ES^+) m/z = 667.15710 $[M (L = H_2O)]^+$; 667.13367 calculated for $[C_{37}H_{31}N_3O_3{}^{103}Rh]^+$. TLC (silica) R_f = 0.60 in $MeCN/H_2O/KNO_{3\,(aq)}$, 80/18/2. Mp > 250°C.

Rhodium (1,3-di(2-pyridyl)-4,6-dimethylbenzene-N,$C^{2'}$,N)(2-phenylpyridine) chloride [Rh(dpydmb)(ppy)Cl] 40

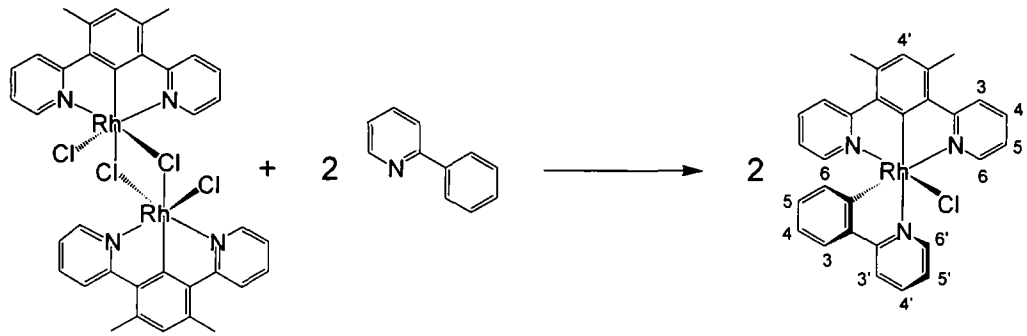

Reaction in ethylene glycol, using stoichiometric amounts of 2-phenylpyridine

$[Rh(dpydmb)Cl(\mu\text{-}Cl)]_2$ **25** (0.045 g, 0.052 mmol) and 2-phenylpyridine (15 µL, 0.16 g, 0.10 mmol) in ethylene glycol (3 mL) was stirred at room temperature under a N_2 atmosphere for 1 hour, then heated to 196°C for a further hour. After cooling to room temperature, the precipitate was collected by centrifuge, washed with water (3 x 5 mL) and dried under vacuum to give the product as a yellow solid (0.041 g, 75%).

^{1}H-NMR ($CDCl_3$, 500 MHz) δ = 10.12 (1H, d, ^3J = 4.4, $H^{6'}$-ppy), 8.06-7.97 (2H, m, $H^{3'}$-ppy and $H^{4'}$-ppy), 7.92 (2H, d, ^3J = 8.4, H^3), 7.50-7.62 (6H, m, H^3-ppy, H^4, $H^{5'}$-ppy and H^6), 6.88 (1H, s, $H^{4'}$), 6.71-6.79 (3H, m, H^4-ppy and H^5), 6.58 (1H, td, ^3J = 7.6, ^4J = 1.6, H^5-ppy), 6.16 (1H, d, ^3J = 8.0, H^6-ppy), 2.78 (6H, s, CH_3). MS (ES^+) m/z = 550.1 $[M + H]^+$; recorded after >72 hours in acetonitrile solution, m/z = 516.1 $[M - Cl]^+$. HRMS (ES^+) m/z = 516.09423 $[M - Cl]^+$; 516.09415 calculated for $[C_{29}H_{23}N_3{}^{103}Rh]^+$ and 550.05721 $[M + H]^+$; 550.05518 calculated for $[C_{29}H_{24}{}^{35}ClN_3{}^{101}Rh]^+$. C, H & N analysis: 62.11% C, 4.20% H and 7.61% N measured; 62.48% C, 4.20% H and 7.54% N calculated for $[C_{29}H_{23}ClN_3Rh]$. TLC (silica) R_f = 0.54 in DCM/MeOH, 90/10. Mp > 250°C.

Using 2-phenylpyridine as the solvent

This method afforded [Rh(dpydmb)(ppy)L] **39**, where the sixth coordination site was occupied by a labile solvent molecule rather than a chloride ion, alongside $[Rh(ppy)_3]$ as a significant side product.

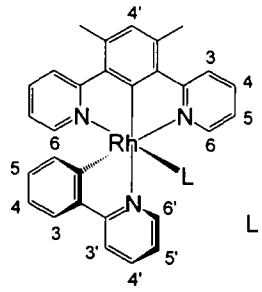

L = solvent

A mixture of $[Rh(dpydmb)Cl(\mu\text{-}Cl)]_2$ **25** (0.035 g, 0.040 mmol) and silver triflate (0.059 g, 0.23 mmol) in 2-phenylpyridine (290 μL, 0.31 g, 2.02 mmol) was stirred at 110°C under a N_2 atmosphere for 6 hours. After cooling to room temperature, the product was dissolved in DCM (40 mL); the insoluble impurities collected by centrifuge and washed with DCM (2 x 5 mL). The washings and filtrate were then combined, washed with HCl (1 M, 3 x 40 mL), and dried over magnesium sulfate. The solvent was removed under reduced pressure and the crude product purified by flash column chromatography (silica, DCM/methanol, gradient elution from 100/0 to 98.5/1.5) to give the product as a yellow solid (0.016 g, 16%).

^{1}H-NMR ($CDCl_3$, 500 MHz) δ = 10.12 (1H, d, ^3J = 4.5, $H^{6'}$-ppy), 8.06 (1H, d, ^3J=8.0, $H^{3'}$-ppy), 8.00 (1H, td, ^3J = 7.0, ^4J = 1.5, $H^{4'}$-ppy), 7.93 (2H, d, ^3J = 8.5, H^3),7.61 (1H, dd, ^3J = 8.0, ^4J = 1.0, H^3-ppy), 7.57-7.51 (5H, m, H^4, $H^{5'}$-ppy and H^6), 6.88 (1H, s $H^{4'}$), 6.78-6.73 (3H, m, H^4-ppy and H^5), 6.58 (1H, td, ^3J = 8.0, ^4J = 1.5, H^5-ppy), 6.16 (1H, d, ^3J = 8.0, H^6-ppy), 2.78 (6H, s, CH_3). MS (ES^+) m/z = 516.0 $[M - L]^+$. HRMS (ES^+) m/z = 516.09188 $[M - L]^+$; 516.09415 calculated for $[C_{29}H_{23}N_3{}^{103}Rh]^+$. TLC (silica) R_f = 0.54 in DCM/MeOH, 90/10. Mp > 250°C.

6.8 *Synthesis of monometallic iridium(III) complexes*

Iridium (1,3-di(2-pyridyl)-4,6-dimethylbenzene-N,$C^{2'}$,N)(2,2'-bipyridine) chloride$^+$ $[Ir(dpydmb)(bpy)Cl]^+$ 30

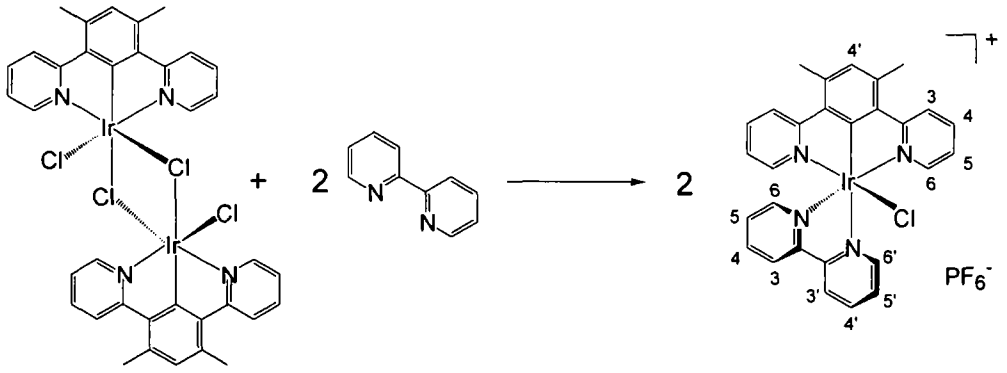

A suspension of $[Ir(dpydmb)Cl(\mu\text{-}Cl)]_2$ **29** (0.064 g, 0.061 mmol) and 2,2'-bipyridine (0.018 g, 0.12 mmol) in ethylene glycol (3 mL) was stirred at room temperature under a N_2 atmosphere for 1 hour, then heated to 196°C for a further hour. After cooling to room temperature the reaction mixture was added to saturated aqueous KPF_6 solution (20 mL). The resultant precipitate was collected by centrifuge, washed with water (3 x 5 mL) and dried under vacuum to give the desired product as a yellow solid (0.090 g, 95%).

^{1}H-NMR (CD_3CN, 500 MHz) δ = 9.83 (1H, d, ^3J = 4.5, $H^{6'}$), 8.59 (1H, d, ^3J = 8.5, $H^{3'}$), 8.43 (1H, td, ^3J = 8.0, ^4J = 1.0, $H^{4'}$), 8.31 (1H, d, ^3J = 8.0, H^3), 8.18 (2H, d, ^3J = 8.5, H^3-NCN), 8.13 (1H, dd, ^3J = 6.5, 6.5, $H^{5'}$), 7.79 (3H, m, H^4 and H^4-NCN), 7.58 (2H, d, ^3J = 5.0, H^6-NCN), 7.39 (1H, d, ^3J = 6.0, H^6), 7.08 (1H, s, $H^{4'}$-NCN), 7.06 (1H, td, ^3J = 7.0, ^4J = 1.0, H^5), 7.01 (2H, td, ^3J = 6.5, ^4J = 1.0, H^5-NCN), 2.82 (6H, s, CH_3). MS (ES^+) m/z = 643.5 $[M]^+$. HRMS (ES^+) m/z = 643.12352 $[M]^+$; 643.12411 calculated for $[C_{28}H_{23}{}^{35}Cl^{193}IrN_4]^+$. C, H & N analysis: 42.67% C, 2.87% H and 7.08% N measured; 42.67% C, 2.94% H and 7.11% N calculated for $[C_{28}H_{23}ClF_6IrN_4P]$. TLC (silica) R_f = 0.48 in DCM/methanol, 90/10. Mp > 250°C.

Iridium (1,3,5-tri(2-pyridyl)benzene-N,$C^{2'}$,N)(2,2'-bipyridine) chloride^{+} $[Ir(tpyb)(bpy)Cl]^{+}$ **32**

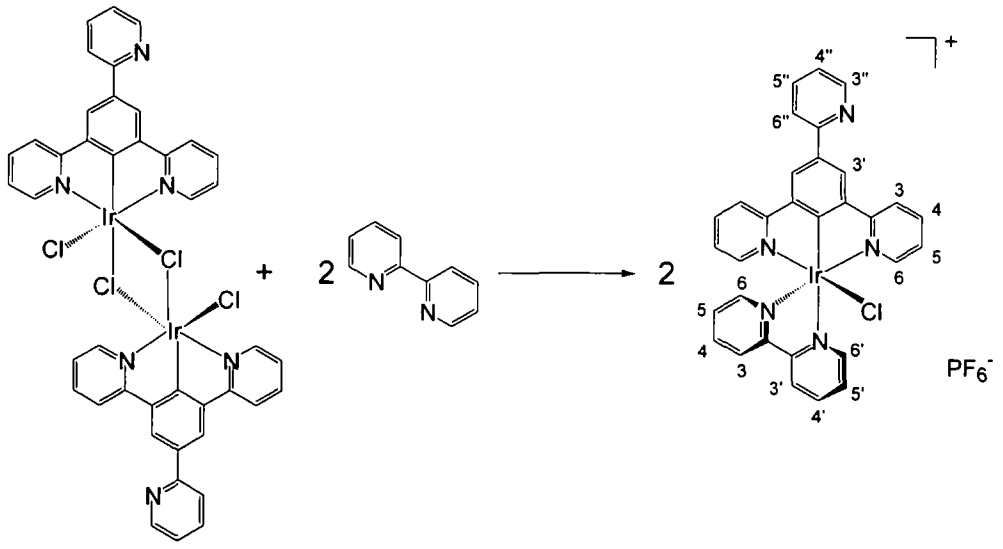

A suspension of $[Ir(tpyb)Cl(\mu\text{-}Cl)]_2$ **23** (0.050 g, 0.044 mmol) and 2,2'-bipyridine (0.016 g, 0.10 mmol) in ethylene glycol (3 mL) was stirred at room temperature under a N_2 atmosphere for 1 hour, then heated to 196°C for a further 3 hours. After cooling to room temperature the solution was added to saturated aqueous KPF_6 solution (25 mL) forming an orange/yellow precipitate. This was collected by centrifuge, washed with water (3 x 5 mL) and dried under vacuum, to give the product as a yellow/orange solid (0.062 g, 84%).

^{1}H-NMR (d_6-acetone, 500 MHz) δ = 10.02 (1H, d, ^{3}J = 5.0, $H^{6'}$-bpy), 8.97 (1H, d, ^{3}J = 8.5, $H^{3'}$-bpy), 8.88 (2H, s, $H^{3'}$), 8.79 (1H, d, ^{3}J = 5.0, H^{6}-bpy), 8.71 (1H, d, ^{3}J = 7.5, H^{3}-bpy), 8.64 (1H, td, ^{3}J = 8.0, ^{4}J = 1.5, $H^{4'}$-bpy), 8.48 (2H, d, ^{3}J = 8.0, H^{3}), 8.34 (1H, td, ^{3}J = 8.5, ^{4}J = 1.0, $H^{5'}$-bpy), 8.27 (1H, d, ^{3}J = 8.0, $H^{6''}$), 8.01-7.95 (4H, m, H^{4}, H^{4}-bpy and $H^{5''}$), 7.86 (2H, d, ^{3}J = 5.5, H^{6}), 7.74 (1H, d, ^{3}J = 6.0, $H^{3''}$), 7.42 (1H, ddd, ^{3}J = 7.0, 5.0, ^{4}J = 1.0, H^{5}-bpy), 7.33 (1H, td, ^{3}J = 8.0, ^{4}J = 1.0, $H^{4''}$), 7.23 (2H, td, ^{3}J = 7.5, ^{4}J = 1.5, H^{5}). MS (ES^{+}) m/z = 692.1 $[M]^{+}$. HRMS (ES^{+}) m/z = 348.08721 $[M - Cl + MeCN]^{2+}/2$; 348.08679 calculated for $[C_{33}H_{25}{}^{35}Cl^{191}IrN_6]^{2+}/2$. C, H & N analysis: 44.69% C, 3.08% H and 8.55% N measured; 44.47% C, 2.65% H and 8.37% N calculated for $[C_{31}H_{22}ClF_6IrN_5P]$. TLC (silica) R_f = 0.34 in DCM/methanol, 90/10. Mp > 250°C.

Iridium (1,3-di(2-pyridyl)-4,6-dimethylbenzene-N,C$^{2'}$,N)(6-phenyl-2,2'-bipyridine)$^+$ [Ir(dpydmb)(phbpy)]$^+$ [205] **33**

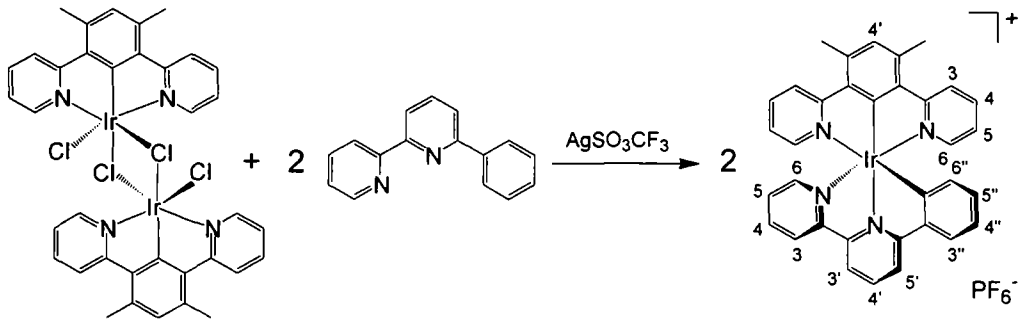

The same reaction procedure used in the synthesis of [Rh(dpydmb)(phbpy)]$^+$ **34** was applied to a suspension of [Ir(dpydmb)Cl(μ-Cl)]$_2$ **29** (0.050 g, 0.048 mmol), phbpyH **1** (0.025 g, 0.1 mmol) and silver triflate (0.058 g, 0.23 mmol) in ethylene glycol (4 mL). The resultant yellow/orange crude product was purified by flash column chromatography (silica, DCM/methanol, gradient elution from 100/0 to 99/1) followed by a second column (silica, DCM/methanol, gradient elution from 100/0 to 99.2/0.8) to give the desired product as a yellow/orange solid (0.061 g, 78%).

^{1}H-NMR (d$_6$-acetone, 500 MHz) δ = 8.72 (1H, d, ^{3}J = 8.0, H^3), 8.70 (1H, d, ^{3}J = 8.0, H$^{3'}$), 8.54 (1H, d, ^{3}J = 8.5, H$^{5'}$), 8.38 (1H, t, ^{3}J = 8.0, H$^{4'}$), 8.31 (2H, d, ^{3}J = 8.5, H^3-NCN), 8.10 (1H, td, ^{3}J = 8.0, ^{4}J = 1.5, H^4), 7.86 (1H, d, ^{3}J = 7.5, H$^{3''}$), 7.83 (2H, td, ^{3}J = 8.0, ^{4}J = 1.5, H^4-NCN), 7.68 (2H, d, ^{3}J = 5.5, H^6-NCN), 7.65 (1H, d, ^{3}J = 5.0, H^6), 7.39 (1H, t, ^{3}J = 7.0, H^5), 7.21 (1H, s, H$^{4'}$-NCN), 6.95 (2H, t, ^{3}J = 7.0, H^5-NCN), 6.85 (1H, t, ^{3}J = 7.5, H$^{4''}$), 6.62 (1H, td, ^{3}J = 7.5, ^{4}J = 1.0, H$^{5''}$), 5.94 (1H, d, ^{3}J = 7.5, H$^{6''}$), 2.97 (6H, s, CH$_3$). ^{13}C-NMR (d$_6$-acetone, 126 MHz) δ = 186.0 (C), 170.0 (C), 163.4 (C), 158.8 (C), 153.7 (C), 153.0 (C), 150.9 (C^6-NCN), 146.2 (C), 143.4 (C), 140.0 (C), 139.9 (C), 138.4 (C^4-NCN), 138.0 (C), 136.6 (C), 136.3 (C), 130.5 (C), 130.0 (C$^{4'}$-NCN), 128.0 (C), 126.2 (C), 125.1 (C), 123.7 (C^5-NCN), 123.0 (C), 122.6 (C^3-NCN), 120.4 (C), 120.3 (C$^{3'}$), 22.05 (CH$_3$). MS (ES$^+$) m/z = 681.3 [M]$^+$. HRMS (ES$^+$) m/z = 683.17801 [M]$^+$; 683.17812 calculated for [C$_{34}$H$_{26}$^{193}IrN$_4$]$^+$. C, H & N analysis: 49.87% C, 3.56% H and 6.02% N measured; 49.33% C, 3.17% H and 6.77% N calculated for [C$_{34}$H$_{26}$F$_6$IrN$_4$P]. TLC (silica) R$_f$ = 0.43 in DCM/methanol, 90/10. Mp > 250°C.

Iridium (1,3-di(2-pyridyl)-4,6-dimethylbenzene-N,C$^{2'}$,N)(1,3-bis(3-fluorophenyl)pyridine) [Ir(dpydmb)(F_2dppy)] **36**

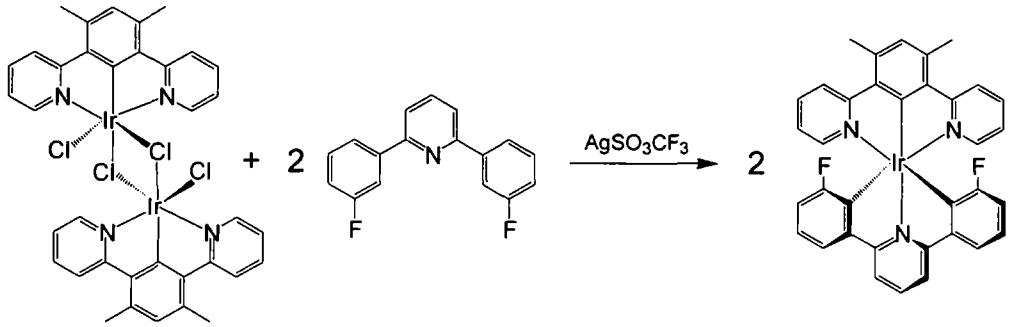

The same reaction procedure used in the synthesis of [Rh(dpydmb)(tpy-ϕ-Br)]$^{2+}$ **28** was applied to a suspension of [Ir(dpydmb)Cl(μ-Cl)]$_2$ **29** (0.050 g, 0.048 mmol), F_2dppy **12** (0.026 g, 0.096 mmol) and silver triflate (0.075 g, 0.29 mmol) in ethylene glycol (3 mL). The crude product was then purified by flash column chromatography (silica, DCM/methanol, gradient elution from 100/0 to 98.25/1.75) to give the desired product as a yellow solid (0.012 g, 17%).

MS (ES$^+$) m/z = 718.2 [M + H]$^+$; correct isotope pattern for [$C_{35}H_{25}F_2{}^{193}IrN_3$]$^+$.

TLC (silica) R_f = 0.46 in DCM/methanol, 90/10.

Iridium (1,3,5-tri(2-pyridyl)benzene-N,C$^{2'}$,N)(2-phenylpyridine) chloride [Ir(tpyb)(ppy)Cl] **41**

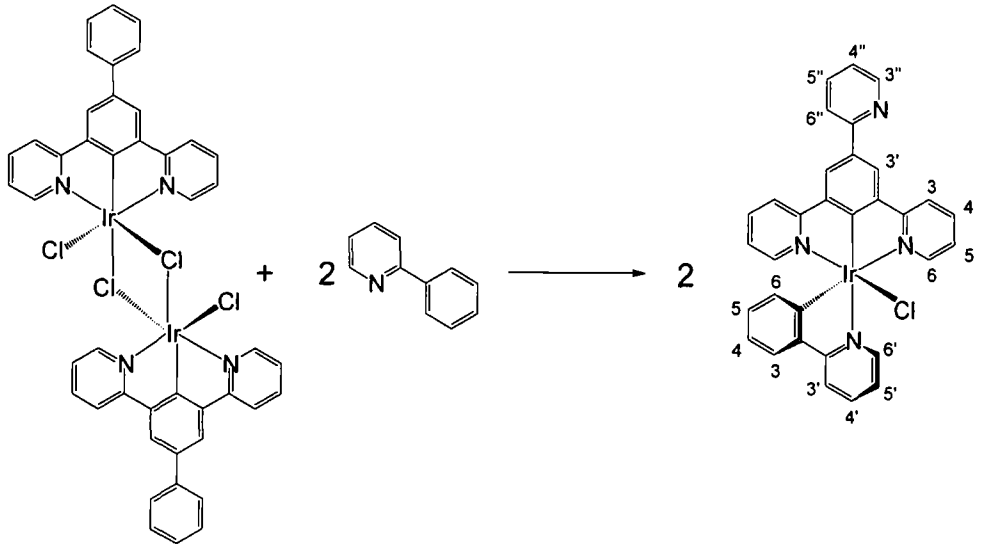

A suspension of [Ir(tpyb)Cl(μ-Cl)]$_2$ **23** (0.041 g, 0.044 mmol) and 2-phenylpyridine (0.012 g, 0.076 mmol) in ethylene glycol (3 mL) was stirred at room temperature under a N_2 atmosphere for 1 hour, then heated to 196°C for a further 18 hours. After cooling to room temperature, the precipitate was collected by centrifuge, washed with water

(3 x 5 mL) and dried under vacuum to give the desired product as an orange solid (0.026 g, 50%).

^{1}H-NMR (d_6-DMSO, 500 MHz) δ = 9.90 (1H, d, ^{3}J = 5.5, H$^{6'}$-ppy), 8.75 (2H, s, H$^{3'}$), 8.55 (1H, d, ^{3}J = 8.0, H$^{6''}$), 8.36 (2H, d, ^{3}J = 8.0, H^3), 8.30 (1H, d, ^{3}J = 8.0, H$^{3'}$-ppy), 8.16 (1H, td, ^{3}J = 7.5, ^{4}J = 2.0, H$^{4'}$-ppy), 8.05 (1H, td, ^{3}J = 7.5, ^{4}J = 1.5, H$^{5''}$), 7.97 (1H, td, ^{3}J = 7.5, ^{4}J = 2.0, H^3-ppy), 7.84 (2H, td, ^{3}J = 8.0, ^{4}J = 1.5, H^4), 7.77 (1H, t, ^{3}J = 7.5, H$^{5'}$-ppy), 7.57 (2H, d, ^{3}J = 6.0, H^6), 7.39 (1H, dd, ^{3}J = 8.0, ^{4}J = 4.0, H$^{3''}$), 7.27 (1H, t, ^{3}J = 6.0, H$^{4''}$), 7.09 (2H, td, ^{3}J = 6.5, ^{4}J = 1.0, H^5), 6.65 (1H, t, ^{3}J = 7.0, H^4-ppy), 6.43 (1H, td, ^{3}J = 8.0, ^{4}J = 1.5, H^5-ppy), 5.76 (1H, d, ^{3}J = 6.5, H^6-ppy). MS (MALDI, DCTB matrix) m/z = 655.3 [M – Cl]$^+$. HRMS (ES$^+$) m/z = 694.17110 [M – Cl + MeCN]$^+$; 694.17105 calculated for [$C_{34}H_{25}{}^{191}IrN_5$]$^+$. C, H & N analysis: 55.37% C, 3.15% H and 5.56% N measured; 55.68% C, 3.21% H and 5.14% N calculated for [$C_{32}H_{22}ClIrN_4$]. TLC (silica) R_f = 0.43 in DCM/methanol, 90/10. Mp > 250°C.

Iridium (1,3-di(2-pyridyl)-4,6-dimethylbenzene-N,C$^{2'}$,N)(1-phenyl pyrazole) chloride [Ir(dpydmb)(pzb)Cl] 42

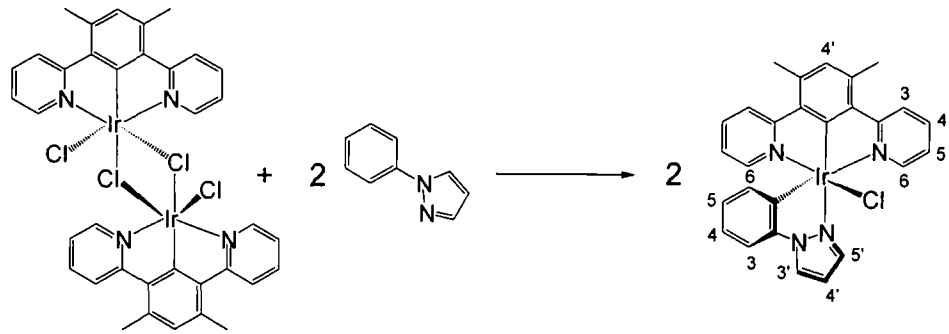

A suspension of [Ir(dpydmb)Cl(μ-Cl)]$_2$ **29** (0.065 g, 0.062 mmol) and 1-phenylpyrazole (0.018 g, 0.12 mmol) in ethylene glycol (4 mL) was stirred at room temperature under a N_2 atmosphere for 1 hour, then heated to 196°C for a further hour. After cooling to room temperature the precipitate was collected by centrifuge, washed with water (3 x 5mL) and dried under vacuum. Purification was achieved by flash column chromatography (silica, DCM/methanol, gradient elution from 100/0 to 95/5) to give the product as a yellow solid (0.041 g, 54%).

^{1}H-NMR (CD_3CN, 500 MHz) δ = 8.98 (1H, d, ^{3}J = 4.5, H$^{5'}$), 8.46 (2H, d, ^{3}J = 5.5, H^3-NCN), 8.12 (2H, d, ^{3}J = 8.0, H^6-NCN), 7.82 (1H, d, ^{3}J = 5.5, H$^{3'}$), 7.70 (2H, t, ^{3}J = 7.0, H^4-NCN), 7.34 (1H, t, ^{3}J = 6.0, H$^{4'}$), 7.29 (1H, d, ^{3}J = 8.0, H^3), 6.96 (3H, m, H$^{4'}$-NCN and H^5-NCN), 6.68 (1H, t, ^{3}J = 7.5, H^4), 6.38 (1H, t, ^{3}J = 8.0, H^5), 5.70 (1H, d, ^{3}J = 8.5, H^6), 2.77 (6H, s, CH_3-NCN). MS (ES$^+$) m/z = 636.0 [M – Cl + MeCN)]$^+$.

HRMS (ES^+) m/z = 636.17363 [M – Cl + MeCN]$^+$; 636.17339 calculated for [$C_{29}H_{25}{}^{193}IrN_5$]$^+$. C, H & N analysis: 51.39% C, 3.50% H and 8.56% N measured; 51.46% C, 3.52% H and 8.89% N calculated for [$C_{27}H_{22}ClIrN_4$]. TLC (silica) R_f = 0.53 in DCM/methanol, 90/10. Mp > 250°C.

Iridium (1,3-di(2-pyridyl)-4,6-dimethylbenzene-N,C$^{2'}$,N)(1-pyrazolyl-3,5-dibromobenzene) chloride [Ir(dpydmb)(pzb-Br_2)Cl] 43

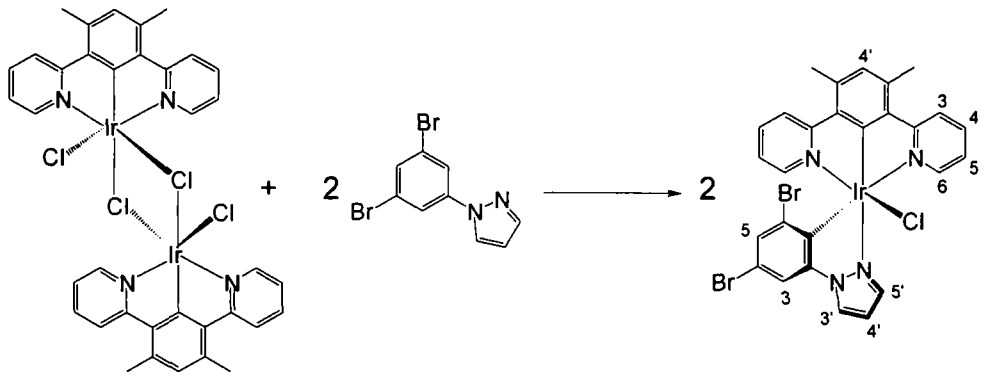

A suspension of [Ir(dpydmb)Cl(μ-Cl)]$_2$ **29** (0.049 g, 0.047 mmol) and pzb-Br_2 **14** (0.030 g, 0.10 mmol) in ethylene glycol (4 mL) was stirred at room temperature under a N_2 atmosphere for 1 hour, then heated to 196°C for a further 2 hours. After cooling to room temperature the resultant precipitate was collected by centrifuge, washed with water (3 x 5 mL) and dried under vacuum to give the product as a yellow/orange solid. This was then dissolved in acetonitrile (2 mL), combined with the ethylene glycol solution and added to saturated aqueous KPF_6 solution (25 mL) to isolate the product as the PF_6^- salt. The yellow/orange precipitate was collected by centrifuge, washed with water (3 x 5 mL) and dried under vacuum. Purification was achieved by flash column chromatography (silica, DCM/methanol, gradient elution from 100/0 to 99.4/0.6) to give the product as a yellow/orange solid (0.033 g, 45%).

^{1}H-NMR ($CDCl_3$, 500 MHz) δ = 8.78 (1H, d, ^3J = 2.0, $H^{5'}$), 8.21 (1H, d, ^3J = 2.5, $H^{3'}$), 8.00 (2H, d, ^3J = 8.5, H^3-NCN), 7.56 (2H, td, ^3J = 8.0, ^4J = 1.5, H^4-NCN), 7.52 (2H, d, ^3J = 5.0, H^6-NCN), 7.32 (1H, d, ^3J = 2.0, H^3), 6.91 (1H, d, ^3J = 2.0, H^5), 6.86 (1H, t, ^3J = 2.5, $H^{4'}$), 6.81 (1H, s, $H^{4'}$-NCN), 6.79 (2H, td, ^3J = 6.5, ^4J = 1.0, H^5-NCN), 2.76 (6H, s, CH_3). ^{13}C-NMR ($CDCl_3$, 126 MHz) δ = 183.1 (C), 170.6 (C), 151.0 (C^6-NCN), 146.4 (C), 145.6 (C), 138.5 (C), 137.1 (C^4-NCN), 136.6 (C), 135.3 (C), 133.3 (C^5) 129.8 ($C^{4'}$-NCN), 127.2 (C), 127.1 (C), 122.9 (C^3-NCN), 121.4 (C^5-NCN), 115.7 (C), 114.0 (C^3), 109.0 ($C^{4'}$), 22.8 (CH_3). MS (ES^+) m/z = 753.1 [M – Cl]$^+$. HRMS (ES^+) m/z = 748.96730 [M – Cl]$^+$; 748.96552 calculated for [$C_{27}H_{20}{}^{79}Br_2{}^{191}IrN_4$]$^+$ and

789.99338 [M – Cl + MeCN]$^+$; 789.99207 calculated for $[C_{29}H_{23}{}^{79}Br_2{}^{191}IrN_5]^+$. C, H & N analysis: 34.28% C, 2.31% H and 5.86% N measured; 34.23% C, 2.26% H and 5.70% N calculated for $[C_{28}H_{22}Br_2ClF_6IrN_4P]$. TLC (silica) R_f = 0.32 in DCM/methanol, 90/10. Mp > 250°C.

Iridium di(1,3-di(1-pyrazolyl)benzene-N,C$^{4'}$)(2,2'-bipyridine)$^+$ [Ir(dpzb-*N*,*C*$^{4'}$)$_2$(bpy)]$^+$ 48

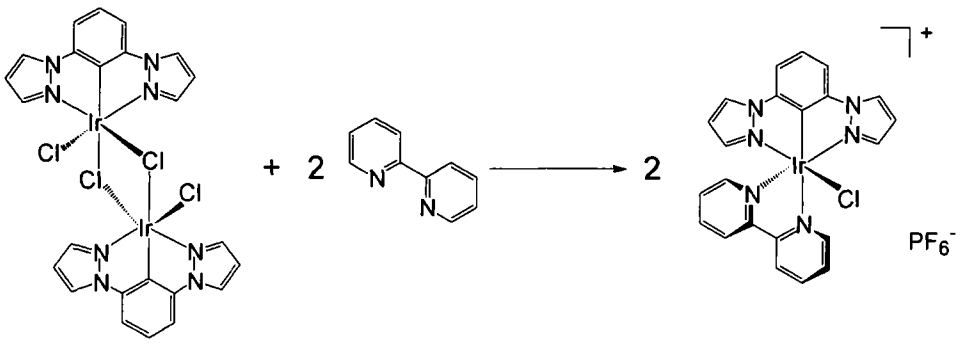

The same reaction procedure used to synthesise [Ir(dpydmb)(bpy)Cl]$^+$ **30** was applied to a suspension of [Ir(dpzb)Cl(μ-Cl)]$_2$ **44** (0.15 g, 0.16 mmol) and 2,2'-bipyridine (0.051 g, 0.33 mmol) in ethylene glycol (5 mL). The resultant yellow/orange crude product was purified by flash column chromatography (silica, DCM/methanol, gradient elution from 100/0 to 97.8/2.2) to give [Ir(dpzb-*N*,*C*$^{4'}$)$_2$(bpy)]$^+$ **48** as a yellow solid (0.010 g, 4%).

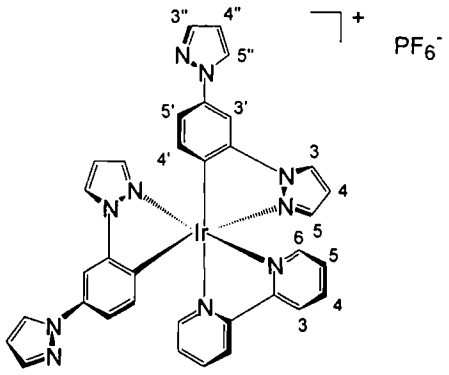

The bidentate binding of the dpzbH ligands to the metal centre results from cyclometalation occurring at the alternative C$^{4'}$-position. ^{1}H-NMR ($CDCl_3$, 500 MHz) δ = 8.63 (2H, d, ^{3}J = 8.5, H^6-bpy), 8.19 (2H, d, ^{3}J = 3.0, H^3), 8.15-8.13 (4H, m, H^3-bpy, H^5-bpy), 7.84 (2H, d, ^{3}J = 2.5, H$^{5''}$), 7.79 (2H, d, ^{4}J = 2.5, H$^{3'}$), 7.67 (2H, d, ^{3}J = 1.5, H$^{3''}$), 7.44 (2H, t, ^{3}J = 4.5, H^4-bpy), 7.08 (2H, dd, ^{3}J = 8.0, ^{4}J = 2.5, H$^{5'}$), 6.94 (2H, d, ^{3}J = 2.0, H^5), 6.58 (2H, t, ^{3}J = 2.5, H^4), 6.42 (2H, t, ^{3}J = 2.5, H$^{4''}$), 6.33 (2H, d, ^{3}J = 8.0, H$^{6'}$). MS (ES$^+$) m/z = 767.0 [M]$^+$. HRMS (ES$^+$) m/z = 767.19634 [M]$^+$; 767.19658

calculated for $[C_{34}H_{26}{}^{193}IrN_{10}]^+$. TLC (silica) $R_f = 0.64$ in DCM/methanol, 90/10. Mp > 250°C.

Iridium (1,3-di(1-pyrazolyl)-5-methylbenzene-N,C$^{2'}$,N)(2,2'-bipyridine) chloride$^+$ [Ir(dpzmb)(bpy)Cl]$^+$ 49

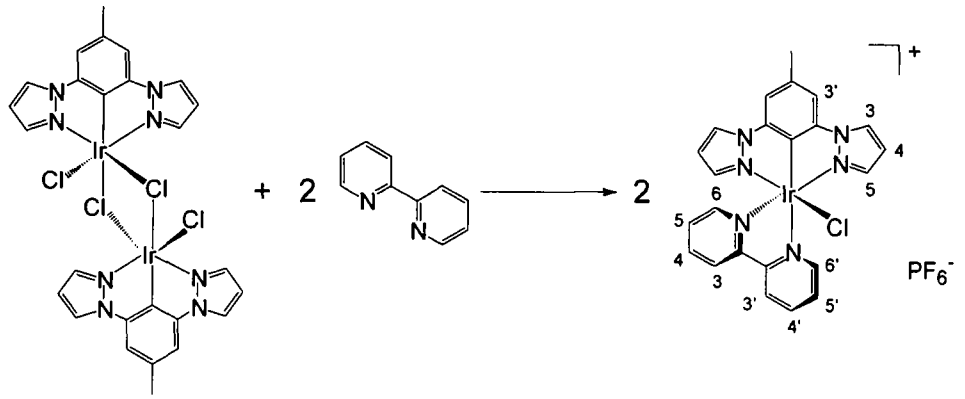

The same reaction procedure used to synthesise $[Ir(dpydmb)(bpy)Cl]^+$ **30** was applied to a suspension of $[Ir(dpzmb)Cl(\mu\text{-}Cl)]_2$ **45** (0.050 g, 0.054 mmol) and 2,2'-bipyridine (0.017 g, 0.11 mmol) in ethylene glycol (3 mL). The resultant orange solid was purified by flash column chromatography (silica, DCM/methanol, gradient elution from 100/0 to 98.1/1.9) to give the desired product as a yellow solid (0.013 g, 16%).

^{1}H-NMR (CD_3CN, 400 MHz) δ = 9.90 (1H, ddd, ^3J = 5.6, ^4J = 1.6, ^5J = 0.8, H$^{6'}$-bpy), 8.62 (1H, d, ^3J = 8.0, H$^{3'}$-bpy), 8.44 (1H, ddd, ^3J = 8.4, 8.0, ^4J = 1.6, H$^{4'}$-bpy), 8.39 (3H, m, H^3 and H^6-bpy), 8.10 (1H, ddd, ^3J = 7.6, 5.6, ^4J = 1.2, H$^{5'}$-bpy), 7.88 (1H, ddd, ^3J = 8.0, 7.6, ^4J = 1.6, H^5-bpy), 7.55 (2H, d, ^4J = 0.8, H$^{3'}$), 7.47 (1H, ddd, ^3J = 6.0, ^4J = 0.8, ^5J = 0.8, H^3-bpy), 7.15 (3H, m, H^4-bpy and H^5), 6.53 (2H, t, ^3J = 2.4, H^4), 2.71 (3H, s, CH_3). MS (ES$^+$) m/z = 607.2 $[M]^+$. HRMS (ES$^+$) m/z = 605.09662 $[M]^+$; 605.09603 calculated for $[C_{23}H_{19}{}^{35}Cl^{191}IrN_6]^+$. C, H & N analysis: 36.82% C, 2.67% H and 11.68% N measured; 36.73% C, 2.55% H and 11.17% N calculated for $[C_{23}H_{19}ClF_6IrN_6P]$. TLC (silica) $R_f = 0.28$ in DCM/methanol, 90/10. Mp > 250°C.

Iridium (1,3-di(1-pyrazolyl)-5-methylbenzene-N,$C^{2'}$,N)(2,2':6',2''-terpyridine)$^{2+}$ $[Ir(dpzmb)(tpy)]^{2+}$ **50**

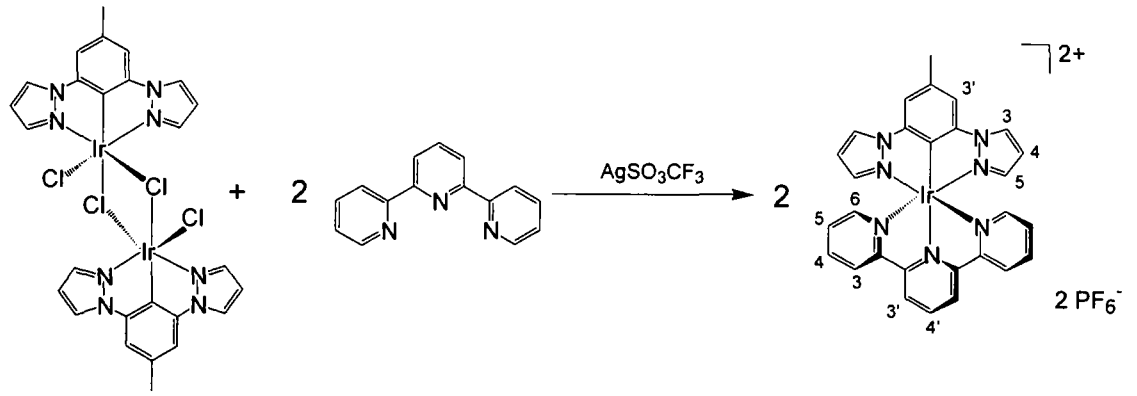

The same reaction procedure outlined for $[Rh(dpydmb)(tpy\text{-}\phi\text{-}Br)]^{2+}$ **28** was applied to a suspension of $[Ir(dpzmb)Cl(\mu\text{-}Cl)]_2$ **45** (0.073 g, 0.075 mmol), 2,2':6',2''-terpyridine (0.035 g, 0.15 mmol) and silver triflate (0.12 g, 0.45 mmol) in ethylene glycol (3 mL). The resultant product was purified by flash column chromatography (silica, acetonitrile/water/$KNO_{3\,(aq)}$, gradient elution from 100/0/0 to 89.0/10.6/0.4). Following evaporation of the solvent, the product was ion exchanged to the PF_6^- salt (as outlined for $[Rh(dpyb)(tpy)]^{2+}$ **26**) to give the desired product as an orange solid (0.032 g, 23%). ^{1}H-NMR (d_6-acetone, 500 MHz) δ = 9.10 (2H, d, ^3J = 8.5, $H^{3'}$-tpy), 8.87-8.78 (5H, m, H^3, $H^{4'}$-tpy and H^6-tpy), 8.26 (2H, td, ^3J = 8.0, ^4J = 1.5, H^5-tpy), 7.92 (2H, s, $H^{3'}$), 7.70 (2H, d, ^3J = 6.0, H^3-tpy), 7.57-7.53 (4H, m, H^4-tpy and H^5), 6.59 (2H, t, ^3J = 3.0, H^4), 2.76 (3H, s, CH_3). ^{13}C-NMR (d_6-acetone, 126 MHz) δ = 160.6 (C), 155.2 (C), 155.1 (C), 143.5 (C), 142.0 (C), 142.0 (C), 141.8 (C), 138.0 (C), 137.7 (C), 132.2 (C), 129.3 (C^5), 126.5 (C^3), 125.4 (C), 112.1 ($C^{3'}$), 108.2 (C^4), 21.7 (CH_3). MS (MALDI, DCTB matrix) m/z = 649.2 $[M + e^-]^+$ and 794.3 $[M + PF_6^-]^+$. HRMS (ES^+) m/z = 792.11909 $[M + PF_6^-]^+$; 792.11791 calculated for $[C_{28}H_{22}F_6{}^{191}IrN_7P]^+$. C, H & N analysis: 31.51% C, 2.18% H and 9.06% N measured; 35.83% C, 2.36% H and 10.45% N calculated for $[C_{28}H_{22}F_{12}IrN_7P_2]$. TLC (silica) R_f = 0.62 in $MeCN/H_2O/KNO_{3\,(aq)}$, 80/18/2. Mp > 250°C.

Iridium (1,3-di(1-pyrazolyl)-5-bromobenzene-N,$C^{2'}$,N)(2,2'-bipyridine) chloride$^+$ $[Ir(dpzb\text{-}Br)(bpy)Cl]^+$ **51**

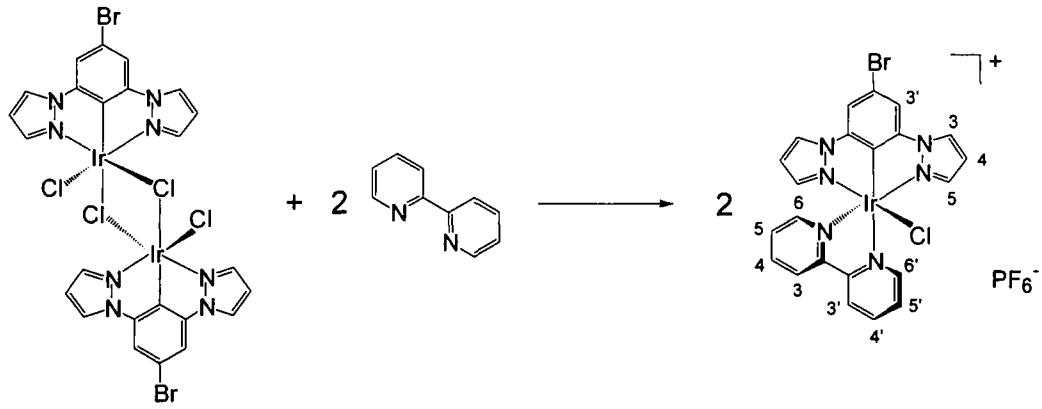

The same reaction procedure used in the synthesis of $[Ir(dpydmb)(bpy)Cl]^+$ **30** was applied to a suspension of $[Ir(dpzb\text{-}Br)Cl(\mu\text{-}Cl)]_2$ **46** (0.041 g, 0.037 mmol) and 2,2'-bipyridine (0.012 g, 0.077 mmol) in ethylene glycol (3 mL). The crude product was purified flash column chromatography (silica, DCM/methanol, gradient elution from 100/0 to 98.9/1.1) to give the product as a yellow solid (0.011 g, 19%).

^{1}H-NMR (CD_3CN, 500 MHz) δ = 9.85 (1H, d, ^3J = 5.5, $H^{6'}$-bpy), 8.59 (1H, d, ^3J = 8.5, $H^{3'}$-bpy), 8.44-8.35 (4H, m, H^3, $H^{4'}$-bpy and H^6-bpy), 8.07 (1H, dd, ^3J = 7.5, 5.5, $H^{5'}$-bpy), 7.89-7.85 (3H, m, $H^{3'}$ and H^5-bpy), 7.46 (1H, d, ^3J = 6.0, H^3-bpy), 7.16-7.12 (3H, m, H^4-bpy and H^5), 6.53 (2H, t, ^3J = 2.5, H^4). ^{13}C-NMR (CD_3CN, 126 MHz) δ = 158.6 (C), 156.4 (C), 153.4 (C^3-bpy), 150.3 (C), 143.2 (C), 143.0 (C), 140.4 (C), 140.0 (C), 137.4 (C), 131.7 (C), 128.5 (C), 128.0 ($C^{3'}$-bpy), 124.6 (C), 124.5 (C), 116.7 (C), 113.7 (C^5-bpy or $C^{3'}$), 108.3 (C). MS (ES^+) m/z = 671.0 $[M]^+$. HRMS (ES^+) m/z = 668.99118 $[M]^+$; 668.99089 calculated for $[C_{22}H_{16}{}^{79}Br^{35}Cl^{191}IrN_6]^+$. TLC (silica) R_f = 0.31 in DCM/methanol, 90/10. Mp > 250°C.

Flash column chromatography of the crude product mixture (silica, DCM/methanol, gradient elution from 100/0 to 98.1/1.9) also isolated iridium di(1,3-di(1-pyrazolyl)-5-bromobenzene-N,$C^{4'}$)(2,2'-bipyridine) $[Ir(dpzb\text{-}Br\text{-}N,C^{4'})_2(bpy)]^+$ **52** as a yellow solid (0.0090 g, 11%).

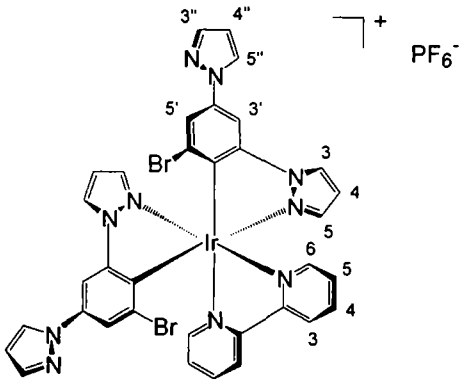

^{1}H-NMR (CD_3CN, 500 MHz) δ = 8.51 (2H, d, ^3J = 8.0, H^6-bpy), 8.45 (2H, d, ^3J = 3.0, H^3), 8.21-8.17 (6H, m, H^3-bpy, H^5-bpy and $H^{5''}$), 8.01 (2H, d, ^4J = 2.0, $H^{3'}$), 7.71 (2H, d, ^3J = 1.5, $H^{3''}$), 7.65 (2H, d, ^4J = 2.0, $H^{5'}$), 7.55 (2H, t, ^3J = 7.5, H^4-bpy), 6.78 (2H, d, ^3J = 2.5, H^5), 6.52 (2H, t, ^3J = 2.0, $H^{4''}$), 6.45 (2H, t, ^3J = 2.5, H^4). ^{13}C-NMR (CD_3CN, 126 MHz) δ = 156.3 (C), 151.9 (C), 146.7 (C), 141.4 (C), 140.7 (C), 139.8 (C), 138.5 (C), 132.2 (C), 129.1 (C), 129.0 (C^4-bpy), 127.7 (C), 125.3 (C^3), 124.8, 121.1 ($C^{5'}$) 109.1 (C^4), 108.1 ($C^{4''}$), 102.9 ($C^{3'}$). MS (ES^+) m/z = 925.1 $[M]^+$. HRMS (ES^+) m/z = 921.01395 $[M]^+$; 921.01527 calculated for $[C_{34}H_{24}{}^{79}Br_2{}^{191}IrN_{10}]^+$. TLC (silica) R_f = 0.36 in DCM/methanol, 90/10. Mp > 250°C.

Iridium (1,3-di(1-pyrazolyl)-5-bromobenzene-N,$C^{4'}$)(2,2':6',2''-terpyridine) chloride$^+$ $[Ir(dpzb\text{-}Br\text{-}NC^{4'})(tpy)Cl]^+$ **53**

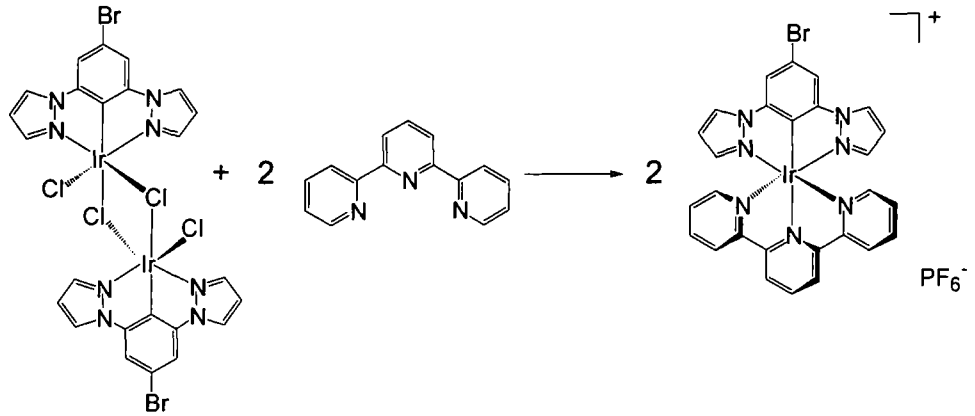

The same reaction procedure used in the synthesis of $[Ir(dpydmb)(bpy)Cl]^+$ **30** was applied to a suspension of $[Ir(dpzb\text{-}Br)Cl(\mu\text{-}Cl)]_2$ **46** (0.049 g, 0.044 mmol) and 2,2':6',2''-terpyridine (0.020 g, 0.086 mmol) in ethylene glycol (3 mL). The resultant product was purified by flash column chromatography (silica, DCM/methanol, gradient elution from 100/0 to 96.6/3.4) to give $[Ir(dpzb\text{-}Br\text{-}NC^{4'})(tpy)Cl]^+$ **53** as a yellow solid (0.016 g, 20%).

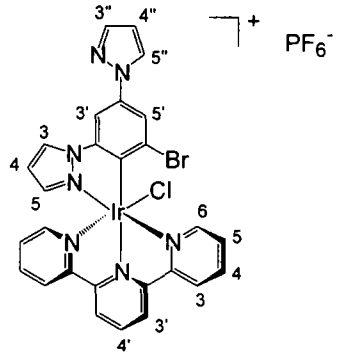

The bidentate, binding of the dpzb-Br ligand results from cyclometalation occurring at the alternate $C^{4'}$-position. ^{1}H-NMR (d_6-acetone, 500 MHz) δ = 9.18 (1H, d, ^3J = 3.0, $H^{5''}$), 8.66 (1H, d, ^3J = 2.0, $H^{3''}$), 8.61 (2H, d, ^3J = 8.0, H^3-tpy), 8.52 (2H, d, ^3J = 8.0, $H^{3'}$-tpy), 8.28-8.23 (3H, m, H^4-tpy, $H^{4'}$-tpy), 8.18 (1H, d, ^4J = 1.5, $H^{3'}$), 7.84 (2H, d, ^3J = 5.5, H^6-tpy), 7.63 (2H, ddd, ^3J = 12.0, 5.5, ^4J = 1.0, H^5-tpy), 7.23 (1H, t, ^3J = 2.0, $H^{4''}$), 6.98 (1H, d, ^3J = 2.0, H^3), 6.95 (1H, d, ^3J = 2.0, H^5), 6.67 (1H, d, ^3J = 2.0, $H^{5'}$), 5.89 (1H, t, ^3J = 2.0, H^4). MS (ES^+) m/z = 748.2 $[M]^+$. HRMS (ES^+) m/z = 746.01811 $[M]^+$; 746.01744 calculated for $[C_{27}H_{19}{}^{79}Br^{35}Cl^{191}IrN_7]^+$. C, H & N analysis: 36.11% C, 2.30% H and 10.94% N measured; 36.27% C, 2.14% H and 10.97% N calculated for $[C_{27}H_{19}BrClF_6IrN_7P]$. TLC (silica) R_f = 0.23 in DCM/methanol, 90/10. Mp > 250°C.

Iridium (1,3-di(1-pyrazolyl)-5-bromobenzene-N,$C^{2'}$,N)(2,2':6',2''-terpyridine)$^{2+}$ $[Ir(dpzb\text{-}Br)(tpy)]^{2+}$ 54

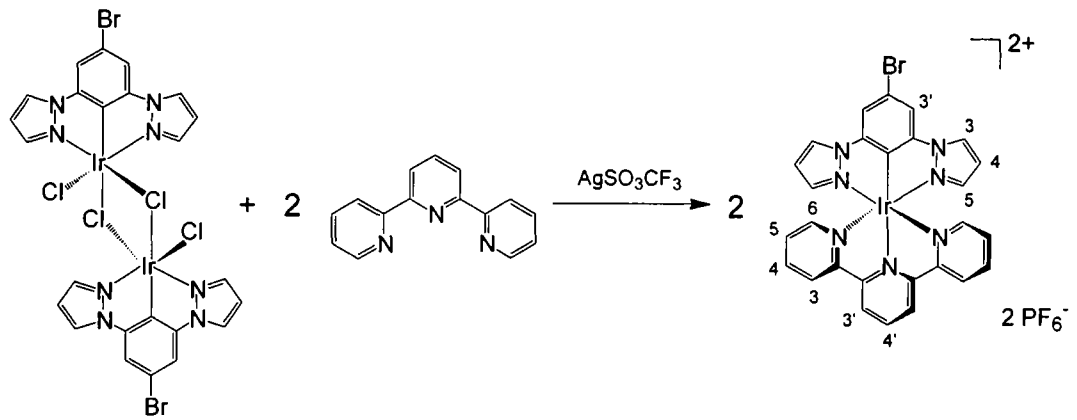

The same reaction procedure outlined for $[Rh(dpydmb)(tpy\text{-}\phi\text{-}Br)]^{2+}$ **28** was applied to a suspension of $[Ir(dpzb\text{-}Br)Cl(\mu\text{-}Cl)]_2$ **46** (0.055 g, 0.050 mmol), 2,2':6',2''-terpyridine (0.023 g, 0.10 mmol) and silver triflate (0.077 g, 0.30 mmol) in ethylene glycol (3 mL). The resultant product was purification by flash column chromatography (silica, acetonitrile/water/ $KNO_{3\,(aq)}$, gradient elution from 100/0/0 to 91.0/8.6/0.4). Following

evaporation of the solvent, the product was ion exchanged to the PF_6^- salt (as outlined for $[Rh(dpyb)(tpy)]^{2+}$ **26**) to give the desired product as a yellow solid (0.027 g, 27%). ^{1}H-NMR (d_6-acetone, 500 MHz) δ = 9.11 (2H, d, ^3J = 8.0, $H^{3'}$-tpy), 8.95 (2H, d, ^3J = 2.5, H^3), 8.86-8.80 (3H, m, H^3-tpy and $H^{4'}$-tpy), 8.28 (2H, s, $H^{3'}$), 8.27 (2H, td, ^3J = 8.0, ^4J = 1.5, H^4-tpy), 7.81 (2H, dd, ^3J = 6.0, ^4J = 1.0, H^6-tpy), 7.60 (2H, d, ^3J = 2.0, H^5), 7.54 (2H, ddd, ^3J = 7.5, 5.5, ^4J = 1.5, H^5-tpy), 6.64 (2H, t, ^3J = 2.5, H^4). ^{13}C-NMR (d_6-acetone, 126 MHz) δ = 160.4 (C), 155.5 (C), 155.1 (C^6-tpy), 144.2 (C), 143.0 (C), 142.2 (C), 141.9 (C), 140.1 (C), 132.9 (C), 129.3 (C^5-tpy), 126.6 (C^3-tpy or $C^{4'}$-tpy), 125.5 (C), 118.5 (C), 114.6 (C^4-tpy or $C^{3'}$), 108.6 (C). MS (MALDI, DCTB matrix) m/z = 713.0 $[M + e^-]^+$ and 860.0 $[M + PF_6^-]^+$. HRMS (ES^+) m/z = 856.01264 $[M + PF_6^-]^+$; 856.01277 calculated for $[C_{27}H_{19}{}^{79}BrF_6{}^{191}IrN_7P]^+$. C, H & N analysis: 32.55% C, 2.03% H and 9.51% N measured; 32.31% C, 1.91% H and 9.77% N calculated for $[C_{27}H_{19}BrF_{12}IrN_7P_2]$. TLC (silica) R_f = 0.48 in $MeCN/H_2O/KNO_{3\,(aq)}$, 80/18/2. Mp > 250°C.

Iridium (1,3-di(1-pyrazolyl)-4,6-dimethylbenzene-N,$C^{2'}$,N)(2,2'-bipyridine) chloride$^+$ $[Ir(dpzdmb)(bpy)Cl]^+$ 55

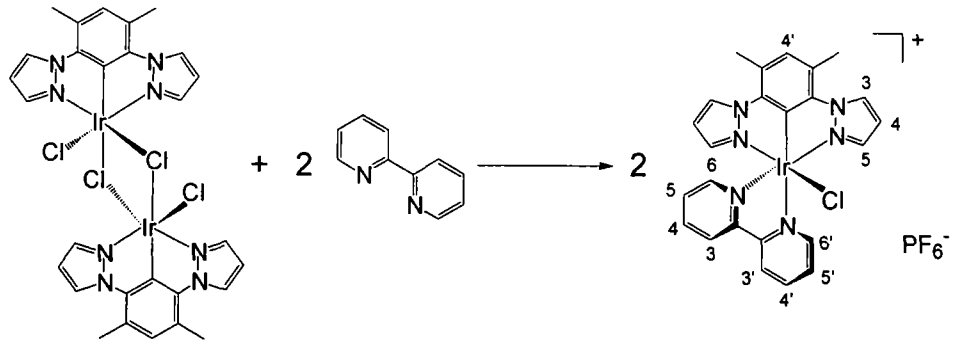

The same reaction procedure outlined for $[Ir(dpydmb)(bpy)Cl]^+$ **30** was applied to a suspension $[Ir(dpzdmb)Cl(\mu\text{-}Cl)]_2$ **47** (0.051 g, 0.051 mmol) and 2,2'-bipyridine (0.017 g, 0.11 mmol) in ethylene glycol (3 mL). The resultant yellow solid was purified by flash column chromatography (silica, DCM/methanol, gradient elution from 100/0 to 98.8/1.2) to give the desired product as a yellow solid (0.041 g, 49%).

^{1}H-NMR (CD_3CN, 500 MHz) δ = 9.91 (1H, d, ^3J = 5.0, $H^{6'}$-bpy), 8.62 (1H, d, ^3J = 8.0, $H^{3'}$-bpy), 8.46-8.43 (3H, m, H^3 and $H^{4'}$-bpy), 8.39 (1H, d, ^3J = 7.5, H^6-bpy), 8.11 (1H, ddd, ^3J = 8.0, 5.5, ^4J = 1.0, $H^{5'}$-bpy), 7.89 (1H, td, ^3J = 8.0, ^4J = 1.5, H^5-bpy), 7.48 (1H, dd, ^3J = 6.0, ^4J = 1.0, H^3-bpy), 7.18-7.15 (2H, m, H^4-bpy and $H^{4'}$), 7.12 (2H, d, ^3J = 2.5, H^5), 6.54 (2H, t, ^3J = 2.5, H^4), 2.79 (6H, s, CH_3). ^{13}C-NMR (CD_3CN, 126 MHz)

δ = 158.6 (C), 156.4 (C), 153.3 (C), 150.1 (C), 141.2 (C), 140.4 (C), 140.2 ($C^{3'}$-bpy), 139.8 (C), 139.5 (C^{5}-bpy), 133.7 (C^{3} or $C^{4'}$-bpy), 131.7 (C^{4}-bpy, $C^{4'}$), 128.5 ($C^{5'}$-bpy), 127.8 (C), 124.6 (C), 124.4 (C^{6}-bpy), 122.0 (C), 107.6 (C), 18.6 (CH_3). MS (ES^+) m/z = 621.3 $[M]^+$. HRMS (ES^+) m/z = 619.11268 $[M]^+$; 619.11168 calculated for $[C_{24}H_{21}{}^{35}Cl^{191}IrN_6]^+$. C, H & N analysis: 37.41% C, 2.85% H and 10.88% N measured; 37.63% C, 2.76% H and 10.97% N calculated for $[C_{24}H_{21}ClF_6IrN_6P]$. TLC (silica) R_f = 0.39 in DCM/methanol, 90/10. Mp > 250°C.

Iridium (1,3-di(1-pyrazolyl)-4,6-dimethylbenzene-N,$C^{2'}$,N)(2,2':6',2''-terpyridine-N,N) chloride$^+$ $[Ir(dpzdmb)(tpy\text{-}NN)Cl]^+$ 56

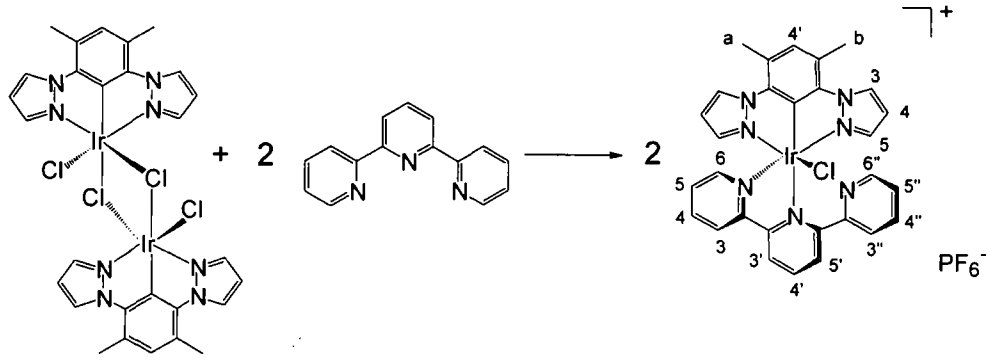

The same reaction procedure used in the synthesis of $[Ir(dpydmb)(bpy)Cl]^+$ **30** was applied to a suspension of $[Ir(dpzdmb)Cl(\mu\text{-}Cl)]_2$ **47** (0.051 g, 0.051 mmol) and 2,2':6',2''-terpyridine (0.023 g, 0.099 mmol) in ethylene glycol (3 mL). The resultant solid was purified by flash column chromatography (silica, acetonitrile/water/$KNO_{3\,(aq)}$, gradient elution from 100/0/0 to 94.0/5.9/0.1). Following evaporation of the solvent, the product was ion exchanged to the PF_6^- salt (as outlined for $[Rh(dpyb)(tpy)]^{2+}$ **26**) to give the desired product as a yellow solid (0.039 g, 41%).

^{1}H-NMR (CD_3CN, 500 MHz) δ = 8.86 (1H, d, ^3J = 3.0, $H^{3''}$), 8.68 (1H, d, ^3J = 2.0, $H^{5''}$), 8.33-8.29 (2H, m, $H^{3''}$-tpy and H^{4}-tpy), 8.22 (1H, d, ^3J = 7.0, $H^{3'}$-tpy), 8.17-8.09 (3H, m, H^{3}-tpy, $H^{4''}$-tpy and $H^{5'}$-tpy), 8.06 (1H, t, ^3J = 8.5, $H^{4'}$-tpy), 7.62 (1H, d, ^3J = 5.5, $H^{6''}$-tpy), 7.57 (1H, d, ^3J = 5.0, H^{6}-tpy) , 7.49 (1H, ddd, , ^3J = 7.5, 6.0, ^4J = 1.5, $H^{5''}$-tpy), 7.45 (1H, ddd, ^3J = 8.0, 6.0, ^4J = 1.5, H^{5}-tpy), 7.09 (1H, t, ^3J = 2.0, $H^{4''}$), 7.00 (1H, d, ^3J = 1.0, H^{3}), 6.87 (1H, s, $H^{4'}$), 6.56 (1H, d, ^3J = 2.5, H^{5}), 5.80 (1H, d, ^3J = 2.0, H^{4}), 2.79 (3H, s, $CH_3{}^a$), 2.16 (3H, s, $CH_3{}^b$). ^{13}C-NMR (CD_3CN, 126 MHz) δ = 160.0 (C), 159.3 (C), 157.2 (C), 156.2 (C), 152.2 (C), 151.9 (C), 145.2 (C), 141.9 (C), 140.8 (C^{3}), 140.7 (C), 140.5 (C), 140.4 ($C^{4''}$-tpy or $C^{5'}$-tpy), 139.3 (C), 135.0 (C), 134.2 (C), 131.5 (C), 131.4 ($C^{4'}$), 128.7 (C), 128.3 (C), 125.5 (C), 125.1 (C), 124.7 (C), 123.5 (C), 123.4 (C),

122.5 (C), 109.1 (C), 106.6 (C^4), 21.3 (CH_3^b), 15.3 (CH_3^a). MS (MALDI, DCTB matrix) m/z = 698.1 $[M]^+$. HRMS (ES^+) m/z = 696.13920 $[M]^+$; 696.13823 calculated for $[C_{29}H_{24}{}^{35}Cl^{191}IrN_7]^+$. C, H & N analysis: 39.21% C, 2.80% H and 11.32% N measured; 39.58% C, 2.75% H and 11.14% N calculated for $[C_{29}H_{24}ClF_6IrN_7P].\{0.2(H_2O)\}$. TLC (silica) R_f = 0.28 in $MeCN/H_2O/KNO_{3\,(aq)}$, 90.0/9.8/0.2. Mp > 250°C.

Iridium (1,3-di(1-pyrazolyl)-4,6-dimethylbenzene-N,$C^{2'}$,N)(2,2':6',2''-terpyridine)$^{2+}$ $[Ir(dpzdmb)(tpy)]^{2+}$ 57

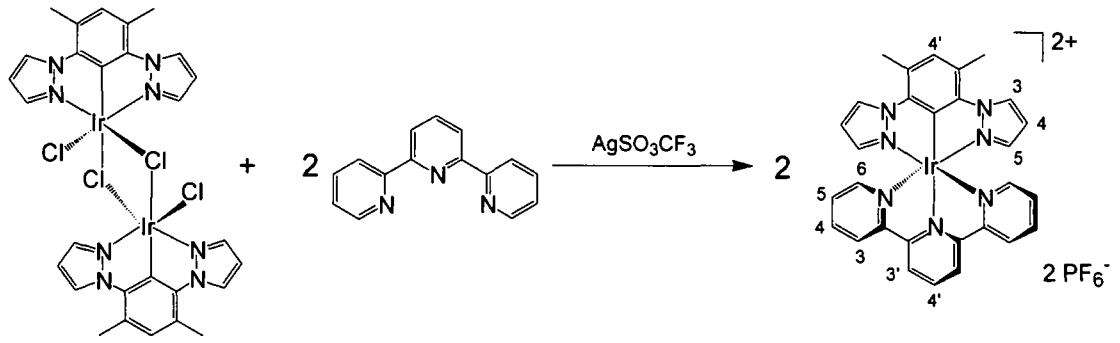

The same reaction procedure outlined for $[Rh(dpydmb)(tpy\text{-}\phi\text{-}Br)]^{2+}$ **28** was applied to a suspension of $[Ir(dpzdmb)Cl(\mu\text{-}Cl)]_2$ **47** (0.060 g, 0.060 mmol), 2,2':6',2''-terpyridine (0.028 g, 0.12 mmol) and silver triflate (0.092 g, 0.36 mmol) in ethylene glycol (3 mL). The resultant product was purified by flash column chromatography (silica, acetonitrile/water/$KNO_{3\,(aq)}$, gradient elution from 100/0/0 to 88.0/11.4/0.6). Following evaporation of the solvent, the product was ion exchanged to the PF_6^- salt (as outlined for $[Rh(dpyb)(tpy)]^{2+}$ **26**) to give the desired product as a yellow solid (0.069 g, 62%). ^{1}H-NMR (d_6-acetone, 500 MHz) δ = 9.10 (2H, d, ^3J = 8.5, $H^{3'}$-tpy), 8.85-8.79 (3H, m, H^6-tpy and $H^{4'}$-tpy), 8.77 (2H, d, ^3J = 3.0, H^3), 8.26 (2H, t, ^3J = 8.0, H^5-tpy), 7.73 (2H, d, ^3J = 5.0, H^3-tpy), 7.52 (2H, t, ^3J = 7.0, H^4-tpy), 7.49-7.45 (3H, m, $H^{4'}$ and H^5) , 6.58 (2H, t, ^3J = 2.5, H^4), 2.93 (6H, s, CH_3). ^{13}C-NMR (d_6-acetone, 126 MHz) δ = 160.4 (C), 155.3 (C), 155.0 (C), 143.3 (C), 142.2 (C), 142.0 (C), 141.7 ($C^{4'}$ or C^5), 139.2 (C), 134.9 (C), 133.4 ($C^{4'}$ or C^5), 129.2 (C), 126.5 ($C^{4'}$-tpy or C^6-tpy), 125.4 (C), 122.9 (C), 108.0 (C^4), 18.7 (CH_3). MS (MALDI, DCTB matrix) m/z = 663.2 $[M + e^-]^+$. HRMS (ES^+) m/z = 808.13510 $[M + PF_6^-]^+$; 808.13590 calculated for $[C_{29}H_{24}F_6{}^{193}IrN_7P]^+$. C, H & N analysis: 36.51% C, 2.53% H and 9.99% N measured; 36.56% C, 2.54% H and 10.29% N calculated for $[C_{29}H_{24}F_{12}IrN_7P_2]$. TLC (silica) R_f = 0.49 in $MeCN/H_2O/KNO_{3\,(aq)}$, 80/18/2. Mp > 250°C.

Iridium (1,3-di(1-pyrazolyl)-4,6-dimethylbenzene-N,C$^{2'}$,N)(2,phenylpyridine) chloride [Ir(dpzdmb)(ppy)Cl] **58**

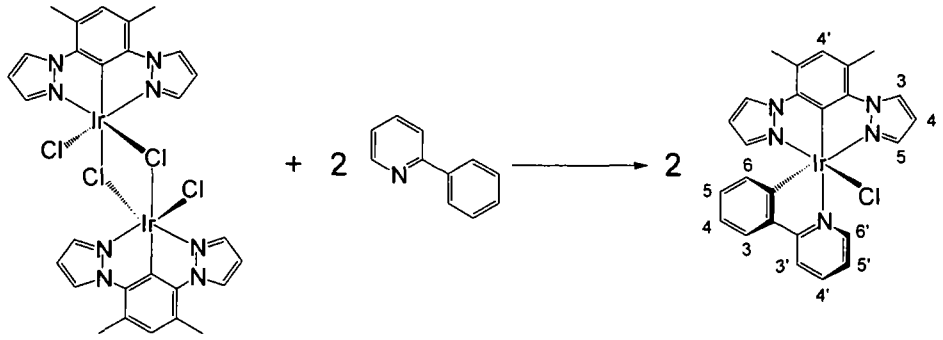

A suspension of [Ir(dpzdmb)Cl(μ-Cl)]$_2$ **47** (0.035 g, 0.035 mmol) and 2-phenylpyridine (0.011 g, 0.070 mmol) in ethylene glycol (3 mL) was stirred at room temperature under a N_2 atmosphere for 1 hour, then heated to 196°C for a further 3 hours. After cooling to room temperature the precipitated solid was collected by centrifuge, washed with water (3 x 5 mL) and dried under vacuum to give a yellow solid. Purification was achieved by flash column chromatography (silica, DCM/methanol, gradient elution from 100/0 to 98.7/1.3) to give the desired product as a yellow solid (0.012 g, 28%).

^{1}H-NMR (CD_3CN, 500 MHz) δ = 10.12 (1H, ddd, ^3J = 5.5, ^4J = 1.0, ^5J = 0.5, H$^{6'}$-ppy), 8.12 (2H, d, ^3J = 3.0, H^3), 7.98 (1H, d, ^3J = 8.0, H$^{3'}$-ppy), 7.88 (1H, td, ^3J = 7.5, ^4J = 1.5, H$^{4'}$-ppy), 7.56 (1H, dd, ^3J = 7.5, ^4J = 1.0, H^3-ppy), 7.42 (1H, ddd, ^3J = 7.5, 5.5, ^4J = 1.5, H$^{5'}$-ppy), 6.81 (1H, s, H$^{4'}$), 6.81 (2H, d, ^3J = 2.0, H^5), 6.73 (1H, td, ^3J = 7.0, ^4J = 1.0, H^4-ppy), 6.55 (1H, td, ^3J = 7.5, ^4J = 1.5, H^5-ppy), 6.25 (2H, t, ^3J = 2.0, H^4), 6.01 (1H, d, ^3J = 8.0, H^6-ppy), 2.69 (6H, s, CH_3). ^{13}C-NMR (CD_3CN, 126 MHz) δ = 165.6 (C), 150.7 (C), 149.3 (C), 144.5 (C), 143.7 (C), 139.6 (C), 139.3 (C), 137.5 (C$^{4'}$-ppy), 135.7 (C^6-ppy), 130.3 (C^3), 129.1 (C^5-ppy), 128.8 (C$^{4'}$ and C^5), 123.9 (C^3-ppy), 122.3 (C$^{5'}$-ppy), 121.7 (C^4-ppy), 119.6 (C$^{3'}$-ppy), 118.6 (C), 106.7 (C^4), 19.6 (CH_3). MS (MALDI, DCTB matrix) m/z = 584.1 [M – Cl]$^+$ and 618.0 [M + H]$^+$. HRMS (ES$^+$) m/z = 582.14041 [M – Cl]$^+$; 582.13975 calculated for [$C_{25}H_{21}{}^{191}IrN_5$]$^+$ and 623.16664 [M – Cl + MeCN]$^+$; 623.16630 calculated for [$C_{27}H_{24}{}^{191}IrN_6$]$^+$. C, H & N analysis: 47.23% C, 4.32% H and 9.05% N measured; 39.30% C, 2.77% H and 9.17% N calculated for [$C_{25}H_{21}ClF_6IrN_5P$]. TLC (silica) R_f = 0.53 in DCM/methanol, 90/10. Mp > 250°C.

6.9 *Chemistry on the complex: Synthesis of functionalised and elaborated monometallic iridium(III) complexes*

Iridium (5-bromo-1,3-di(2-pyridyl)-4,6-dimethylbenzene-N,$C^{2'}$,N)(4'-(*p*-toly)-2,2':6',2''-terpyridine)$^{2+}$ $[Ir(dpydmb\text{-}Br)(ttpy)]^{2+}$ **59**

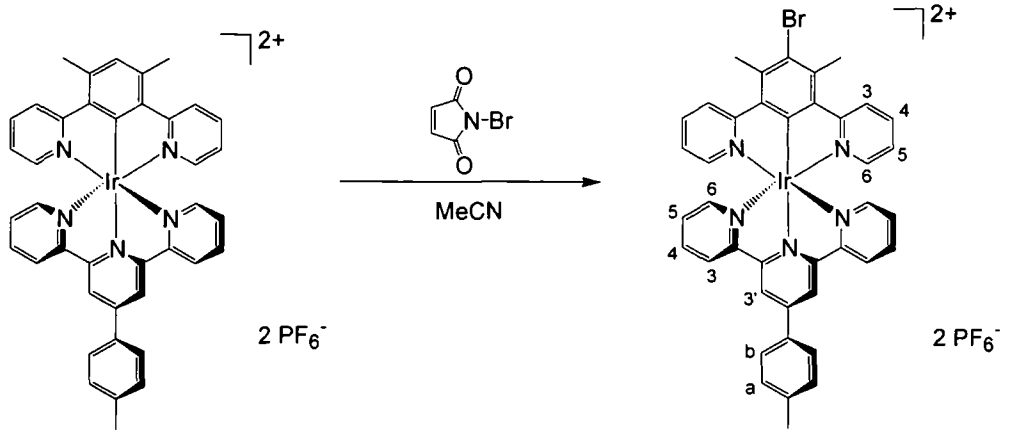

A mixture of $[Ir(dpydmb)(ttpy)]^{2+}$ (0.032 g, 0.030 mmol) and N-bromosuccinimide (0.0055 g, 0.031 mmol) was stirred in acetonitrile (1 mL) in a sealed vial for 20 hours. The solution was added to water (5 mL), the resultant precipitate collected by centrifuge, washed with water (3 x 5 mL) and dried under vacuum to give the product as a yellow/orange solid (0.024 g, 71%).

^{1}H-NMR (d_6-acetone, 500 MHz) δ = 9.51 (2H, s, $H^{3'}$-ttpy), 9.09 (2H, d, ^3J = 8.0, H^3-ttpy), 8.57 (2H, d, ^3J = 7.5, H^3-NCN), 8.24 (4H, m, H^4-ttpy and H^6-ttpy) 8.04 (2H, td, ^3J = 8.0, ^4J = 1.5, H^4-NCN), 7.97 (2H, d, ^3J = 5.0, H^6-NCN), 7.80 (2H, d, ^3J = 5.5, H^b-ttpy), 7.59 (2H, d, ^3J = 7.5, H^a-ttpy), 7.49 (2H, t, ^3J = 6.5, H^5-ttpy), 7.17 (2H, t, ^3J = 6.0, H^5-NCN), 3.23 (6H, s, CH_3-NCN), 2.53 (3H, s, CH_3-ttpy). ^{13}C-NMR (d_6-acetone, 126 MHz) δ = 174.6 (C), 169.6 (C), 160.0 (C), 155.8 (C), 154.2 (C), 154.0 (C), 152.4 (C), 142.2 (C), 141.4 (C^4-ttpy), 140.8 (C), 139.6 (C), 133.4 (C), 130.5 (C^a-ttpy), 129.5 (C^5-ttpy), 128.5 (C), 128.3 (C^3-ttpy), 127.1 (C^3-NCN), 125.9 (C), 124.6 (C), 123.2 ($C^{3'}$-ttpy), 23.3 (CH_3-NCN), 20.7 (CH_3-ttpy). TLC (silica) R_f = 0.29 in DCM/methanol, 90/10. Mp > 250°C.

Iridium (5-bromo-1,3-di(2-pyridyl)-4,6-dimethylbenzene-N,$C^{2'}$,N)(6-(3-bromophenyl)-2,2'-bipyridine)$^+$ $[Ir(dpydmb\text{-}Br)(phbpy\text{-}Br)]^+$ [m 205] **60**

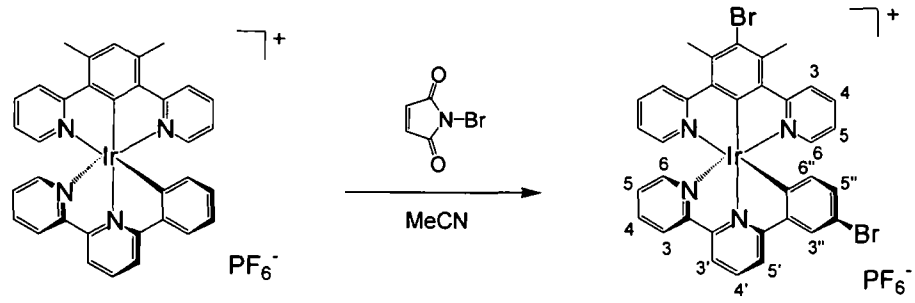

A mixture of $[Ir(dpydmb)(phbpy)]^+$ **33** (0.037 g, 0.045 mmol) and N-bromosuccinimide (0.0080 g, 0.045 mmol) in acetonitrile (1 mL) was stirred at room temperature for 24 hours. The solvent was then removed under reduced pressure and dried under vacuum to give a yellow/orange solid (0.033 g) which was analysed by ^{1}H-NMR. Following this the product was re-dissolved in acetonitrile (1 mL), additional NBS (0.0034 g, 0.019 mmol) added and the reaction mixture stirred at room temperature. Additional NBS was added after a further 24 hours (0.0044 g, 0.025 mmol) and 48 hours (0.0022 g, 0.012 mmol). Following a 24 hours reaction after the final addition of NBS, the reaction mixture was added drop-wise to saturated aqueous KPF_6 solution (5 mL) and the resultant precipitate collected by centrifuge, washed with water (3 x 5 mL) and dried under vacuum to give a yellow/orange solid (0.020 g, 45%).

The reaction was followed by ^{1}H-NMR at 24 hours intervals. At all intermediate stages the product was identified as being a mixture of $[Ir(dpydmb)(phbpy)]^+$ **33**, a complex brominated at the $C^{4'}$-position of dpydmb and $[Ir(dpydmb\text{-}Br)(phbpy\text{-}Br)]^+$ **60**.

^{1}H-NMR (d_6-acetone, 500 MHz) δ = 8.78 (2H, m, H^3 and $H^{3'}$), 8.68 (1H, d, ^3J = 7.5, $H^{5'}$), 8.45 (3H, m, H^3-NCN and $H^{4'}$), 8.14 (1H, td, ^3J = 7.5, ^4J = 1.5, H^4), 8.06 (1H, d, ^4J = 2.5, $H^{3''}$), 7.91 (2H, td, ^3J = 8.5, ^4J = 1.5, H^4-NCN), 7.74 (3H, m, H^6-NCN and H^6), 7.41 (1H, td, ^3J = 5.5, ^4J = 1.5, H^5), 7.03 (2H, td, ^3J = 6.5, ^4J = 1.0, H^5-NCN), 6.81 (1H, dd, ^3J = 7.5, ^4J = 2.0, $H^{5''}$), 5.91 (1H, d, ^3J = 8.5, $H^{6''}$), 3.20 (6H, s, CH_3). ^{13}C-NMR (d_6-acetone, 126 MHz) δ = 181.74 (C), 169.2 (C), 161.9 (C), 158.5 (C), 153.9 (C), 153.2 (C), 151.2 (C), 148.8 (C), 141.7 (C), 140.4 (C), 140.1 (C), 138.6 (C), 138.2 ($C^{6''}$), 138.1 (C), 137.8 (C), 133.0 (C), 128.8 ($C^{3''}$), 128.2 (C^5), 125.4 (C), 125.2 (C), 124.9 (C^3-NCN or $C^{4'}$), 123.5 (C^5-NCN), 121.2 (C), 121.1 (C), 116.7 (C), 23.2 (CH_3). MS (ES^+)

[m] Based upon work by Coudret.[228]

m/z = 841.0 $[M]^+$. HRMS (ES^+) m/z = 836.99869 $[M]^+$; 836.99682 calculated for $[C_{34}H_{24}{}^{79}Br^{191}IrN_4]^+$. TLC (silica) R_f = 0.42 in DCM/methanol, 90/10. Mp > 250°C.

Iridium (1,3-di(2-pyridyl)-4,6-dimethylbenzene-N,$C^{2'}$,N)(4'-(*p*-bromo-phenyl)-6'-(*m*-tolyl)-bipyridine)$^+$ $[Ir(dpydmb)(mtbpy\text{-}\phi\text{-}Br)]^+$ [205] **61**

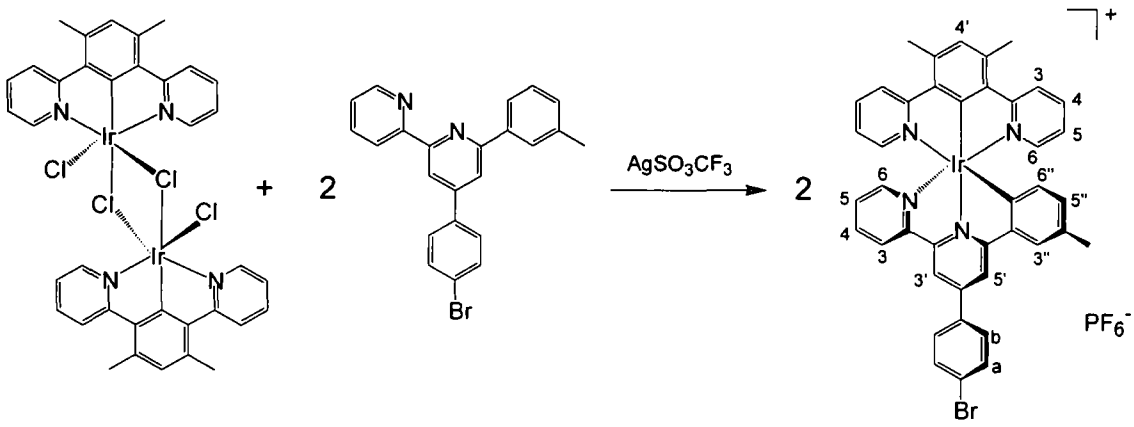

A suspension of $[Ir(dpydmb)Cl(\mu\text{-}Cl)]_2$ **29** (0.052 g, 0.050 mmol), mtbpyH-ϕ-Br **4** (0.041 g, 0.10 mmol) and silver triflate (0.080 g, 0.31 mmol) in ethylene glycol (3 mL) was stirred at room temperature under a N_2 atmosphere for 1 hour, then heated to 196°C for a further 2 hours. After cooling to room temperature, an orange precipitate formed. The solids were collected by centrifuge and the orange product dissolved in acetonitrile (5 mL) leaving behind a grey residue of AgCl. The acetonitrile washings and ethylene glycol solution were combined and reduced in volume, before being added drop-wise to saturated aqueous KPF_6 solution (25 mL). The resultant orange precipitate was collected by centrifuge, washed with water (3 x 5 mL) and dried under vacuum. Purification was achieved by flash column chromatography (silica, DCM/methanol, gradient elution from 100/0 to 98.75/1.25) affording an orange solid (0.084 g, 84%).

^{1}H-NMR (d_6-acetone, 500 MHz) δ = 9.05 (1H, d, ^4J = 2.0, $H^{3'}$-NNC), 8.95 (1H, d, ^3J = 8.0, H^3-NNC), 8.88 (1H, d, ^4J = 1.0, $H^{5'}$-NNC), 8.32 (2H, d, ^3J = 8.0, H^3-NCN) 8.21 (2H, d, ^3J = 8.5, H^b-NNC), 8.13 (1H, td, ^3J = 8.0, ^4J = 1.5, H^4-NNC), 7.90 (3H, m, $H^{3''}$-NNC and H^a-NNC), 7.83 (2H, td, ^3J = 8.0, ^4J = 1.5, H^4-NCN) , 7.76 (2H, dd, ^3J = 6.0, ^4J = 1.0, H^6-NCN), 7.68 (1H, d, ^3J = 5.0, H^6-NNC), 7.41 (1H, ddd, ^3J = 8.5, 7.0, ^4J = 1.0, H^5-NNC), 7.21 (1H, s, $H^{4'}$-NCN), 6.94 (2H, td, ^3J = 7.5, ^4J = 1.0, H^5-NCN), 6.49 (1H, d, ^3J = 7.5, $H^{5''}$-NNC), 5.83 (1H, d, ^3J = 8.0, $H^{6''}$-NNC), 2.97 (6H, s, CH_3-NCN), 2.16 (3H, s, CH_3-NNC). MS (MALDI, DCTB matrix) m/z = 851.3 $[M]^+$. HRMS (ES^+) m/z = 849.13533 $[M]^+$; 849.13326 calculated for $[C_{41}H_{31}{}^{79}Br^{191}IrN_4]^+$. C, H & N analysis: 49.38% C, 3.24% H and 5.57% N measured; 49.40% C, 3.13% H

and 5.62% N calculated for $[C_{41}H_{31}BrF_6IrN_4P]$. TLC (silica) R_f = 0.65 in DCM/methanol, 90/10. Mp > 250°C.

Iridium (5-(4-dimethylamino)phenyl)-1,3-di(2-pyridyl)-4,6-dimethyl-benzene-N,$C^{2'}$,N)(4'-(*p*-toly)-2,2':6',2''-terpyridine)$^{2+}$ $[Ir(dpydmb\text{-}\phi\text{-}NMe_2)(ttpy)]^{2+}$ **62**

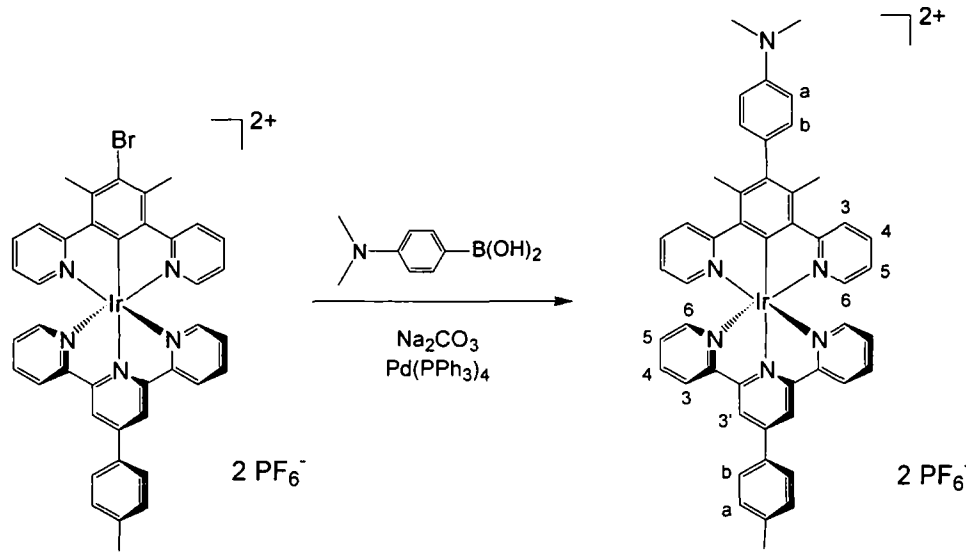

A mixture of $[Ir(dpydmb\text{-}Br)(ttpy)]^{2+}$ **59** (0.021 g, 0.018 mmol), 4-dimethylamino-phenyl boronic acid (0.0059 g, 0.036 mmol) and Na_2CO_3 (0.0057 g, 0.0054 mmol in 100 μL water) in DMSO (3 mL) was degassed by 3 freeze-pump-thaw cycles. $Pd(PPh_3)_4$ (0.0013 g, 0.0011 mmol) was added under a positive pressure of N_2 and the resultant suspension stirred at 80°C under a N_2 atmosphere for 18 hours. After cooling to room temperature the reaction mixture was diluted with acetonitrile (2 mL) and filtered into saturated aqueous KPF_6 solution (25 mL). The resultant orange precipitate was collected by centrifuge, washed with water (5 x 5 mL) and dried under vacuum, then purified by flash column chromatography (silica, DCM/methanol, gradient elution from 100/0 to 80/20) followed by (silica, acetonitrile/water/$KNO_{3\,(aq)}$, gradient elution from 100/0/0 to 90.0/9.5/0.5). Following evaporation of the solvent from the second column, the product was ion exchanged to the PF_6^- salt (as outlined for $[Rh(dpyb)(tpy)]^{2+}$ **26**) to give an orange solid (0.016 g, 65%).

^{1}H-NMR (d_6-acetone, 500 MHz) δ = 9.54 (2H, s, $H^{3'}$-ttpy), 9.11 (2H, d, ^3J = 8.0, H^3-ttpy), 8.53 (2H, d, ^3J = 8.5, H^3-NCN), 8.25 (4H, m, H^4-ttpy and H^6-ttpy) 7.99 (2H, t, ^3J = 7.5, H^4-NCN), 7.93 (2H, d, ^3J = 5.0, H^6-NCN), 7.81 (2H, d, ^3J = 5.0, H^b-ttpy), 7.61 (2H, d, ^3J = 8.0, H^a-ttpy), 7.55 (2H, t, ^3J = 6.5, H^5-ttpy), 7.24 (2H, t, ^3J = 8.5, H^b-NCN), 7.12 (2H, t, ^3J = 6.0, H^5-NCN), 7.01 (2H, d, ^3J = 7.5, H^a-NCN), 3.09 (6H, s, CH_3-NCN),

2.72 (6H, s, CH_3-NMe_2), 2.54 (3H, s, CH_3-ttpy). MS (MALDI, DCTB matrix) m/z = 447.5 $[M]^{2+}/2$, 895.4 $[M + e^-]^+$ and 1039.2 $[M + PF_6^-]^+$. HRMS (ES^+) m/z = 446.14902 $[M]^{2+}/2$; 446.14939 calculated for $[C_{48}H_{41}{}^{191}IrN_6]^+$ and 1037.26239 $[M + PF_6^-]^+$; 1037.26351 calculated for $[C_{48}H_{41}F_6{}^{191}IrN_6P]^+$. TLC (silica) R_f = 0.34 in DCM/methanol, 90/10. Mp > 250°C.

Iridium (1,3-di(2-pyridyl)-4,6-dimethylbenzene-N,$C^{2'}$,N)(4'-(*p*-dimethylamino)biphenyl)-6'-(*m*-tolyl)-bipyridine)$^+$ $[Ir(dpydmb)(mtbpy\text{-}\phi_2\text{-}NMe_2)]^{+\,n}$ **63**

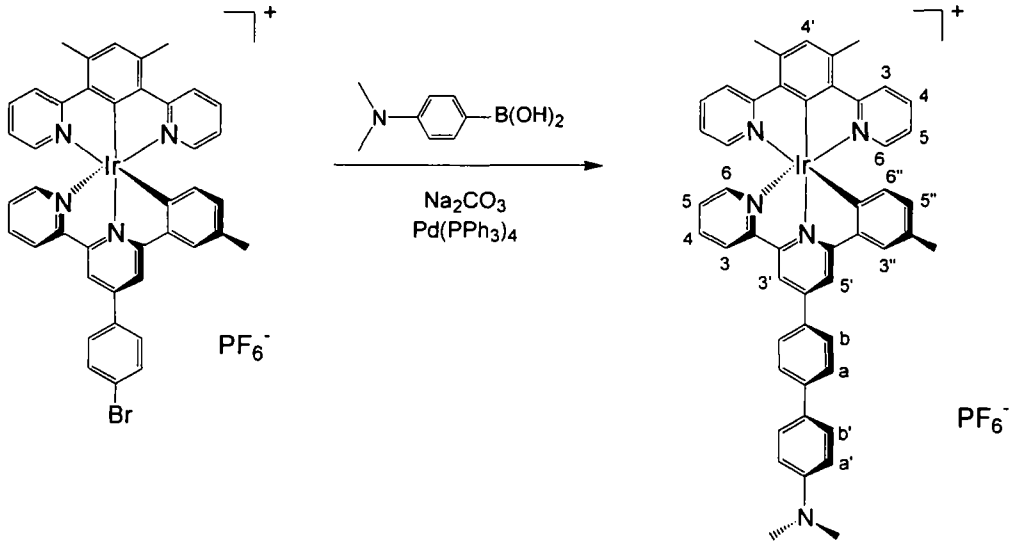

A mixture of $[Ir(dpydmb)(mtbpy\text{-}\phi\text{-}Br)]^+$ **61** (0.036 g, 0.036 mmol), 4-dimethylaminnophenylboronic acid (0.023 g, 0.14 mmol) and Na_2CO_3 (0.023 g, 0.23 mmol in 200 µL water) in DMSO (5 mL) was degassed by 3 freeze-pump-thaw cycles. $Pd(PPh_3)_4$ (0.0050 g, 0.0043 mmol) was added under a positive pressure of N_2 and the same reaction procedure employed as for $[Ir(dpydmb\text{-}\phi\text{-}NMe_2)(ttpy)]^{2+}$ **62**. The crude product was purified by flash column chromatography (silica, DCM/methanol, gradient elution from 100/0 to 98.5/1.5) to give the desired product as an orange solid (0.031 g, 84%).

^{1}H-NMR (d_6-acetone, 500 MHz) δ = 9.08 (1H, s, $H^{3'}$-NNC), 9.00 (1H, d, ^3J = 8.0, H^3-NNC), 8.90 (1H, s, $H^{5'}$-NNC), 8.34 (2H, d, ^3J = 8.0, H^3-NCN), 8.30 (2H, d, ^3J = 8.0, H^b-NNC), 8.15 (1H, td, ^3J = 7.5, ^4J = 1.0, H^4), 7.98-7.93 (3H, m, $H^{3''}$-NNC and H^a-NNC), 7.85 (2H, t, ^3J = 7.5, H^4-NCN) 7.80 (2H, d, ^3J = 5.5, H^6-NCN), 7.73 (2H, d, ^3J = 8.5, $H^{b'}$-NNC), 7.69 (1H, d, ^3J = 5.0, H^6-NNC), 7.42 (1H, t, ^3J = 7.0, H^5), 7.23 (1H,

[n] This is based upon previous work in the Williams' group by Aspley[51] and Leslie[54].

s, $H^{4'}$-NCN), 6.98 (2H, t, ^3J = 6.0, H^5-NCN) 6.92 (2H, d, ^3J = 8.5, $H^{a'}$-NNC), 6.51 (1H, d, ^3J = 8.0, $H^{5''}$-NNC), 5.84 (1H, d, ^3J = 8.0, $H^{6''}$-NNC), 3.05 (6H, s, CH_3-NMe_2), 2.99 (6H, s, CH_3-NCN), 2.09 (3H, s, CH_3-NNC). MS (MALDI, DCTB matrix) m/z = 892.1 $[M]^+$. HRMS (ES^+) m/z = 890.29635 $[M]^+$; 890.29625 calculated for $[C_{49}H_{41}{}^{191}IrN_5]^+$. TLC (silica) R_f = 0.44 in DCM/methanol, 90/10. Mp > 250°C.

Iridium (1,3-di(2-pyridyl)-4,6-dimethylbenzene-N,$C^{2'}$,N)(4'-(*p*-bi-phenyl)-6'-(*m*-tolyl)-bipyridine)$^+$ $[Ir(dpydmb)(mtbpy\text{-}\phi\text{-}ph)]^+$ [205] **64**

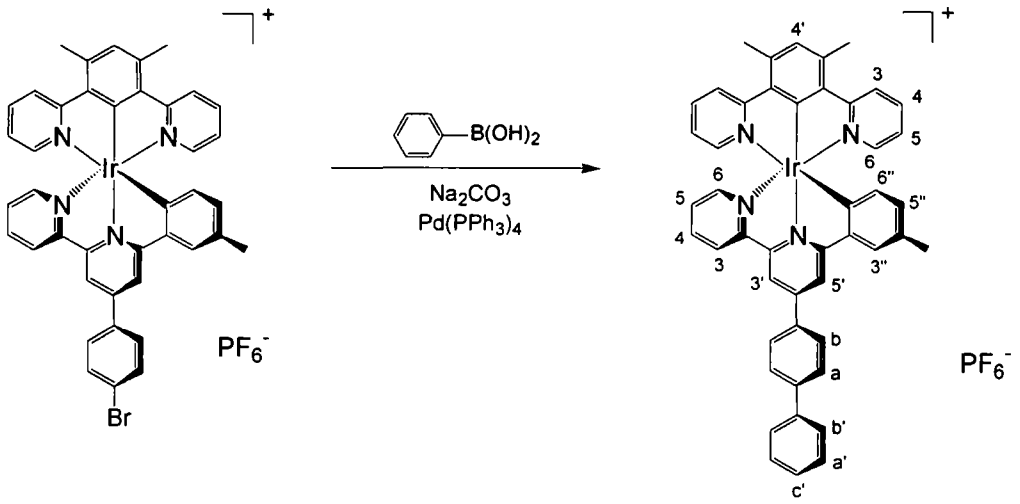

A mixture of iridium $[Ir(dpydmb)(mtbpy\text{-}\phi\text{-}Br)]^+$ **61** (0.042 g, 0.042 mmol), phenylboronic acid (0.010 g, 0.084 mmol) and Na_2CO_3 (0.014 g, 0.13 mmol in 100 µL water) in DMSO (5 mL) was degassed by three freeze-pump-thaw cycles. $Pd(PPh_3)_4$ (0.0058 g, 0.0050 mmol) was added under a positive pressure of N_2 and the same reaction procedure employed as for $[Ir(dpydmb)(mtbpy\text{-}\phi_2\text{-}NMe_2)]^+$ **63**. Purification of the crude product was achieved by flash column chromatography (silica, DCM/methanol, gradient elution from 100/0 to 99/1) to give the desired product as an orange solid (0.033 g, 79%).

^{1}H-NMR (d_6-acetone, 500 MHz) δ = 9.10 (1H, d, ^4J = 1.0, $H^{3'}$-NNC), 9.00 (1H, dd, ^3J = 13.5, 7.5, H^3-NNC), 8.93 (1H, d, ^4J = 1.0, $H^{5'}$-NNC), 8.35 (4H, m, H^3-NCN and H^b), 8.14 (1H, td, ^3J = 7.5, ^4J = 1.5, H^4-NNC), 8.02 (2H, d, ^3J = 8.0, H^a), 7.97 (1H, s, $H^{3''}$-NNC), 7.84 (4H, m, H^4-NCN, $H^{b'}$), 7.79 (2H, d, ^3J = 6.0, H^6-NCN), 7.68 (1H, d, ^3J = 4.5, H^6-NNC), 7.56 (2H, t, ^3J = 7.5, $H^{a'}$), 7.46 (1H, t, ^3J = 7.5, $H^{c'}$) 7.42 (1H, dd, ^3J = 7.0, 5.5, H^5-NNC), 7.22 (1H, s, $H^{4'}$-NCN), 6.96 (2H, td, ^3J = 6.5, ^4J = 1.0, H^5-NCN), 6.50 (1H, d, ^3J = 7.5, $H^{5''}$-NNC), 5.84 (1H, d, ^3J = 7.5, $H^{6''}$-NNC), 2.98 (6H, s, CH_3-NCN), 2.17 (3H, s, CH_3-NNC). MS (MALDI, DCTB matrix) m/z = 849.4 $[M]^+$.

HRMS (ES^+) m/z = 847.25409 $[M]^+$; 847.25405 calculated for $[C_{47}H_{36}{}^{191}IrN_4]^+$. C, H & N analysis: 56.39% C, 3.89% H and 5.21% N measured; 56.79% C, 3.65% H and 5.66% N calculated for $[C_{55}H_{44}F_6IrN_4P]$. TLC (silica) R_f = 0.49 in DCM/methanol, 90/10. Mp > 250°C.

Iridium (5-bromo-1,3-di(2-pyridyl)-4,6-dimethylbenzene-N,$C^{2'}$,N)(4'-(*p*-biphenyl)-6'-(*m*-tolyl)-bipyridine)$^+$ $[Ir(dpydmb\text{-}Br)(mtbpy\text{-}\phi\text{-}ph)]^+$ [205] **65**

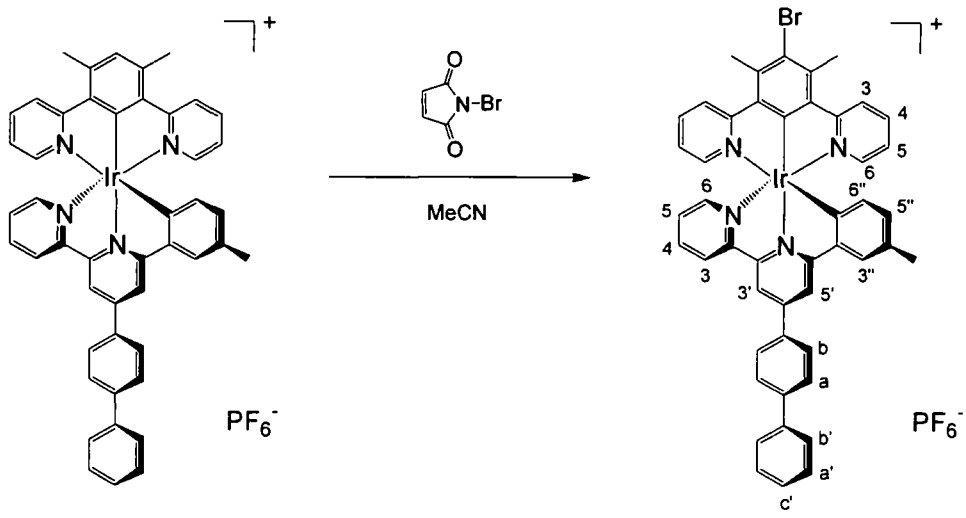

A mixture of $[Ir(dpydmb)(mtbpy\text{-}\phi\text{-}ph)]^+$ **64** (0.029 g, 0.029 mmol) and N-bromosuccinimide (0.0052 g, 0.029 mmol) was stirred in acetonitrile (2 mL) for 20 hours, during this time some precipitation of an orange solid was observed. Additional acetonitrile (2 mL) was added to fully dissolve the product, and then the reaction mixture added drop-wise to saturated aqueous KPF_6 solution (20 mL). The resultant precipitate was collected by centrifuge, washed with water (3 x 5mL) and dried under vacuum to give the product as an orange solid (0.031 g, 100%).

^{1}H-NMR (d_6-acetone, 500 MHz) δ = 9.13 (1H, s, $H^{3'}$-NNC), 9.04 (1H, t, ^3J = 8.5, H^3-NNC), 8.96 (1H, s, $H^{5'}$-NNC), 8.46 (2H, d, ^3J = 8.5, H^3-NCN) 8.38 (2H, d, ^3J = 8.5, H^b), 8.17 (1H, t, ^3J = 7.0, H^4-NNC), 8.05 (2H, d, ^3J = 8.0, H^a), 8.00 (1H, s, $H^{3''}$-NNC), 7.92 (2H, t, ^3J = 6.5, H^4-NCN), 7.87 (4H, m, H^6-NCN and $H^{b'}$), 7.77 (1H, d, ^3J = 5.5, H^6-NNC), 7.58 (2H, t, ^3J = 7.5, $H^{a'}$), 7.49 (1H, t, ^3J = 7.5, $H^{c'}$), 7.43 (1H, t, ^3J = 7.5, H^5-NNC), 7.05 (2H, t, ^3J = 7.5, H^5-NCN), 6.53 (1H, d, ^3J = 7.0, $H^{5''}$-NNC), 5.86 (1H, d, ^3J = 8.0, $H^{6''}$-NNC), 3.22 (6H, s, CH_3-NCN), 2.20 (3H, s, CH_3-NNC). MS (MALDI, DCTB matrix) m/z = 927.3 $[M]^+$. HRMS (ES^+) m/z = 925.16344 $[M]^+$; 925.16456 calculated for $[C_{47}H_{35}{}^{79}Br^{191}IrN_4]^+$. TLC (silica) R_f = 0.53 in DCM/methanol, 90/10. Mp > 250°C.

Iridium (5-(1,3-dimethylphenyl)-1,3-di(2-pyridyl)-4,6-dimethyl-benzene-N,$C^{2'}$,N)(4'-(*p*-biphenyl)-6'-(*m*-tolyl)-bipyridine)$^+$
$[Ir(dpydmb–C_6H_3Me_2)(mtbpy\text{-}\phi\text{-}ph)]^+$ [205] **66**

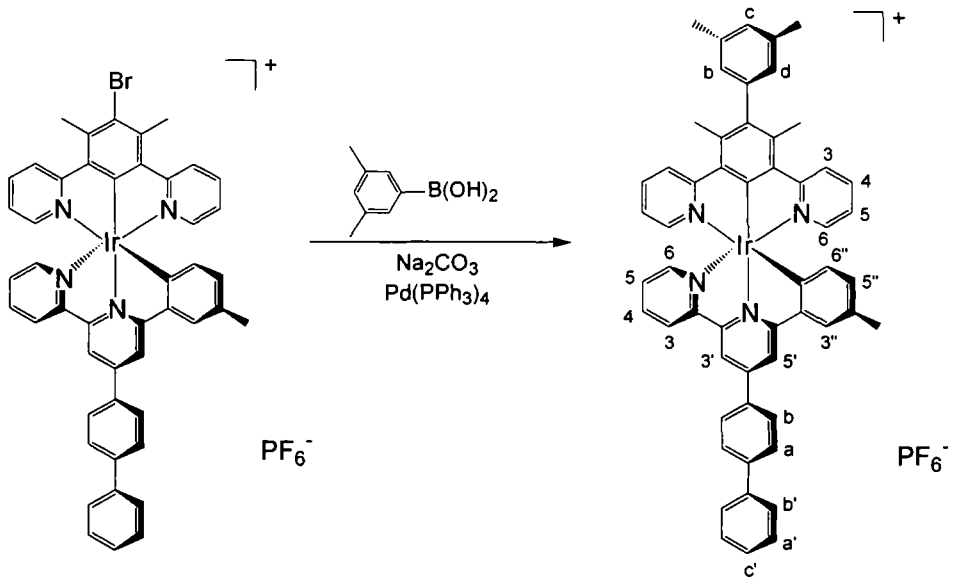

A mixture of $[Ir(dpydmb\text{-}Br)(mtbpy\text{-}\phi\text{-}ph)]^+$ **65** (0.035 g, 0.035 mmol), 3,5-dimethylphenyl boronic acid (0.010 g, 0.070 mmol) and Na_2CO_3 (0.012 g, 0.11 mmol in 100 μL water) in DMSO (5 mL) was degassed by 3 freeze-pump-thaw cycles. $Pd(PPh_3)_4$ (0.0049 g, 0.0042 mmol) was added under a positive pressure of N_2 and the same reaction procedure employed as for $[Ir(dpydmb)(mtbpy\text{-}\phi_2\text{-}NMe_2)]^+$ **63**. The crude product was purified by flash column chromatography (silica, DCM/methanol, gradient elution from 100/0 to 99.1/0.9) to give the desired product as an orange solid (0.020 g, 53%).

^{1}H-NMR (d_6-acetone, 500 MHz) δ = 9.12 (1H, d, ^4J = 1.0, $H^{3'}$-NNC), 9.02 (1H, d, ^3J = 8.5, H^3-NNC), 8.94 (1H, d, ^4J = 1.0, $H^{5'}$-NNC), 8.37 (4H, m, H^3-NCN and H^b-NNC), 8.16 (1H, td, ^3J = 8.0, ^4J = 1.5, H^4-NNC), 8.03 (2H, d, ^3J = 8.5, H^a-NNC), 7.99 (1H, s, $H^{3''}$-NNC), 7.83 (6H, m, H^4-NCN, H^6-NCN and $H^{b'}$-NNC), 7.76 (1H, d, ^3J = 5.0, H^6-NNC), 7.56 (2H, t, ^3J = 7.5, $H^{a'}$-NNC), 7.45 (2H, m, H^5-NNC and $H^{c'}$-NNC), 7.16 (1H, s, H^c-NCN), 7.07 (1H, s, H^b-NCN or H^d-NCN), 7.02 (1H, s, H^b-NCN or H^d-NCN), 6.97 (2H, td, ^3J = 6.0, ^4J = 1.5, H^5-NCN), 6.55 (1H, d, ^3J = 8.5, $H^{5''}$-NNC), 5.95 (1H, d, ^3J = 8.0, $H^{6''}$-NNC), 2.66 (6H, s, CH_3-NCN), 2.46 (2 x 3H, 2 x s, CH_3-NCN-pendant), 2.19 (3H, s, CH_3-NNC). MS (MALDI, DCTB matrix) m/z = 953.4 $[M]^+$. HRMS (ES^+) m/z = 951.31694 $[M]^+$; 951.31665 calculated for $[C_{55}H_{44}{}^{191}IrN_4]^+$. C, H & N analysis: 57.09% C, 4.10% H and 4.91% N measured; 57.33% C, 4.37% H

and 4.86% N calculated for $[C_{55}H_{44}F_6IrN_4P].\{3(H_2O)\}$. TLC (silica) R_f = 0.48 in DCM/methanol, 90/10. Mp > 250°C.

Iridium (1,3-di(2-pyridyl)-4,6-dimethylbenzene-N,C$^{2'}$,N)(4'-(*p*-phenyl-boronic acid)-6'-(*m*-tolyl)-2,2'-bipyridine)$^+$ [Ir(dpydmb){mtbpy-ϕ-B(OH)(OMe)}]$^{+\,o}$ **68**

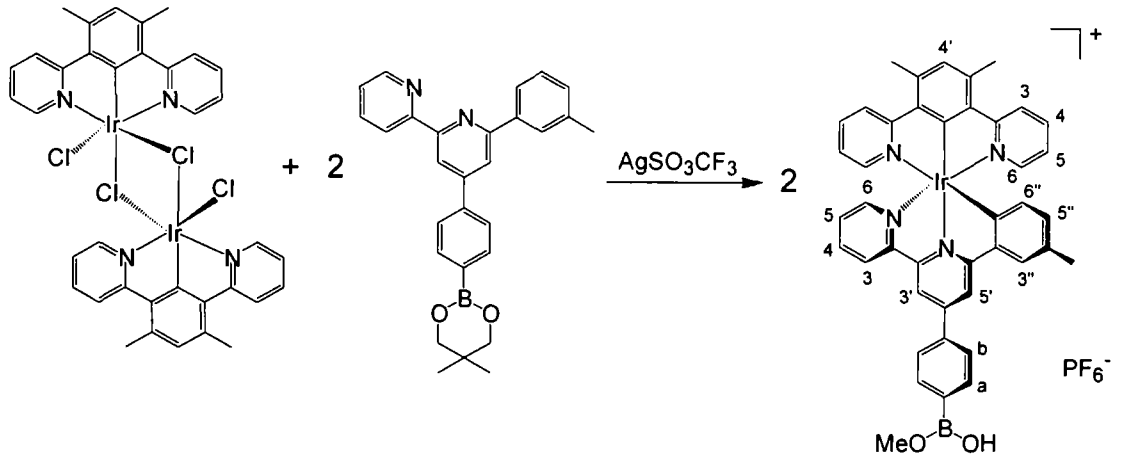

A suspension of [Ir(dpydmb)Cl(μ-Cl)]$_2$ **29** (0.052 g, 0.050 mmol), mtbpyH-ϕ-Bneo **67** (0.076 g, 0.18 mmol) and silver triflate (0.051 g, 0.20 mmol) in ethylene glycol (4 mL) was stirred at room temperature under a N_2 atmosphere for 1 hour, before being heated to 140°C for a further 3 hours. After cooling to room temperature, the precipitated AgCl was collected by centrifuge and washed with acetonitrile (2 x 1 mL). The washings and filtrate were combined, added to saturated aqueous KPF_6 solution (25 mL) and the resulting orange precipitate collected by centrifuge, washed with water (3 x 5 mL) and dried under vacuum. Purification was achieved by flash column chromatography (silica, DCM/methanol, gradient elution from 100/0 to 93/7) to give the desired product as an orange solid (0.087 g, 89%).

^{1}H-NMR (d_6-acetone, 400 MHz) δ = 9.07 (1H, d, ^{4}J = 1.6, H$^{3'}$-NNC), 8.99 (1H, d, ^{3}J = 8.0, H^3-NNC), 8.90 (1H, d, ^{4}J = 1.2, H$^{5'}$-NNC), 8.33 (2H, d, ^{3}J = 4.4, H^3-NCN) 8.28 (2H, d, ^{3}J = 8.0, H^b-NNC), 8.14 (1H, td, ^{3}J = 7.6, ^{4}J = 1.6, H^4-NNC), 8.07 (2H, d, ^{3}J = 8.4, H^a-NNC), 7.96 (1H, s, H$^{3"}$-NNC), 7.85 (2H, ddd, , ^{3}J = 8.4, 7.6, ^{4}J = 1.6, H^4-NCN), 7.79 (2H, dd, ^{3}J = 5.6, ^{4}J = 1.2, H$^{6"}$-NNC), 7.69 (1H, dd, ^{3}J = 5.6, ^{4}J = 1.6, H^6-NNC), 7.42 (1H, ddd, ^{3}J = 7.6, 5.6, ^{4}J = 1.2, H^5-NNC), 7.23 (1H, s, H$^{4'}$-NCN), 6.96 (2H, ddd, ^{3}J = 7.6, 5.6, ^{4}J = 1.2, H^5-NCN), 6.51 (1H, dd, ^{3}J = 8.4, ^{4}J = 1.2, H$^{5"}$-NNC), 5.84 (1H, d, ^{3}J = 7.2, H$^{6"}$-NNC), 4.49 (3H, s, OMe) 2.99 (6H, s, CH_3-NCN), 2.18 (3H, s,

---

° Adapted from the synthesis of related tris-bidentate complexes by Arm.[52]

CH_3-NNC). MS (MALDI, DCTB matrix) m/z = 817.3 [Ir(dpydmb){mtbpy-ϕ-$B(OH)_2$}]$^+$, 831.3 [Ir(dpydmb){mtbpy-ϕ-B(OH)(OMe)}]$^+$ and 847.3 [Ir(dpydmb){mtbpy-ϕ-$B(OMe)_2$}]$^+$. HRMS (ES^+) m/z = 830.25034 [Ir(dpydmb){mtbpy-ϕ-B(OH)(OMe)}]$^+$; 830.25133 calculated for $[C_{42}H_{35}{}^{10}B^{193}IrN_4O_2]^+$. TLC (silica) R_f = 0.26 in DCM/methanol, 90/10. Mp > 250°C.

2,2':6',2"-Terpyridine iridium(III) trichloride $[Ir(tpy)Cl_3]$[46] 73

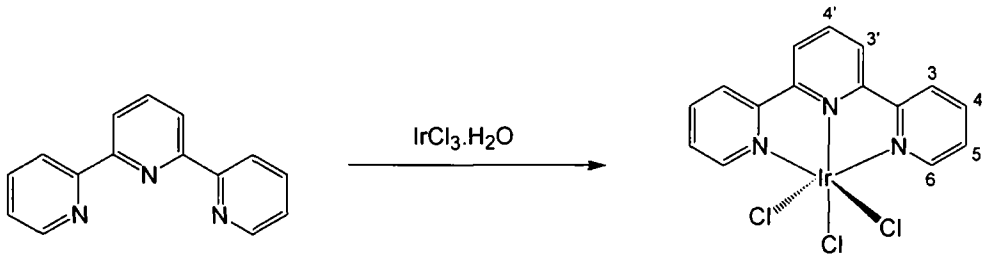

A mixture of 2,2':6',2"-terpyridine (0.093 g, 0.040 mmol) and $IrCl_3.H_2O$ (0.13 g, 0.40 mmol) in ethylene glycol (8 mL) was stirred at 160°C for 15 minutes. After cooling to room temperature the precipitate was collected by centrifuge. This was washed with ethanol (3 x 5mL), water (3 x 5 mL), ethanol (3 x 5 mL) and diethyl ether (3 x 5 mL), then dried under vacuum to give the product as a red solid (0.10 g, 48%). ^{1}H-NMR (d_6-DMSO, 500 MHz) δ = 9.20 (2H, dd, ^3J = 5.5, ^4J = 1.0, H^6), 8.74 (2H, d, ^3J = 8.5, $H^{3'}$), 8.70 (2H, d, ^3J = 7.5, H^3), 8.25 (2H, td, ^3J = 7.5, ^4J = 1.5, H^4), 8.21 (1H, t, ^3J = 8.5, $H^{4'}$), 7.96 (2H, ddd, ^3J = 7.5, 5.5, ^4J = 1.5, H^5). ^{13}C-NMR (d_6-DMSO, 126 MHz) δ = 159.7 (C^5), 157.9 ($C^{3'}$), 153.7 (C^3), 141.1 (C^q), 140.5 (C^q), 129.1 (C^4), 125.8 (C^6), 124.2 ($C^{4'}$). MS (MALDI, DCTB matrix) m/z = 532.9 $[M + H]^+$. TLC (silica) R_f = 0.50 in DCM/methanol, 90/10.

Iridium(2,2':6',2"-terpyridine)(4'-(*p*-bromo)phenyl)-2,2':6',2"-terpyridine)$^{3+}$ $[Ir(tpy)(tpy-ϕ-Br)]^{3+}$[54] 72

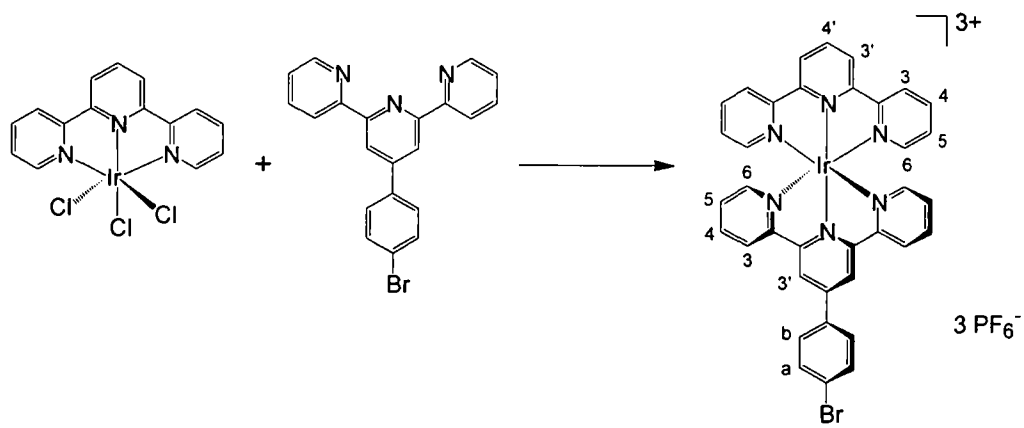

A mixture of [Ir(tpy)Cl_3] **73** (0.095 g, 0.18 mmol) and 4'-*p*-brompophenyl-2,2':6',2''-terpyridine (0.070 g, 0.18 mmol) in ethylene glycol (7 mL) was heated under a N_2 atmosphere at reflux (196°C) for 15 minutes. After cooling to room temperature, the solution was added to water (20 mL) and the resultant precipitate of unreacted [Ir(tpy)Cl_3] collected by centrifuge. The filtrate was added to saturated aqueous KPF_6 solution (40 mL), forming a pale orange precipitate, which was collected by centrifuge, washed with water (3 x 5 mL) and dried under vacuum. Purification was achieved by flash column chromatography (silica, acetonitrile/water/$KNO_{3\,(aq)}$, gradient elution from 100/0/0 to 55/42/3). Following evaporation of the solvent, the product was ion exchanged to the PF_6^- salt (as outlined for $[Rh(dpyb)(tpy)]^{2+}$ **26**) to give the desired product as an orange solid (0.082 g, 37%).

^{1}H-NMR (CD_3CN, 500 MHz) δ = 9.06 (2H, s, $H^{3'}$), 8.87 (2H, d, ^3J = 8.0, $H^{3'}$-tpy), 8.78 (1H, t, ^3J = 8.5, $H^{4'}$-tpy), 8.70 (2H, d, ^3J = 7.5, H^3) 8.59 (2H, d, ^3J = 7.5, H^3-tpy), 8.25-8.19 (4H, m, H^4 and H^4-tpy), 8.13 (2H, d, ^3J = 9.0, H^b), 7.99 (2H, d, ^3J = 8.5, H^a), 7.69 (2H, dd, ^3J = 5.5, ^4J = 1.0, H^6 or H^6-tpy), 7.60 (2H, dd, ^3J = 5.5, ^4J = 1.0, H^6 or H^6-tpy), 7.52- 7.47 (4H, m, H^5 and H^5-tpy). MS (MALDI, DCTB matrix) m/z = 1103.1 $[M + 2PF_6^-]^+$. HRMS (ES^+) m/z = 1101.02046 $[M + 2PF_6^-]^+$; 1101.02083 calculated for $[C_{36}H_{25}{}^{79}BrF_{12}{}^{191}IrN_6P_2]^+$. C, H & N analysis: 34.09% C, 2.18% H and 6.49% N measured; 34.14% C, 2.15% H and 6.63% N calculated for $[C_{36}H_{25}BrF_{18}IrN_6P_3].H_2O$. TLC (silica) R_f = 0.79 in MeCN/H_2O/$KNO_{3\,(aq)}$, 80/18/2. Mp > 250°C.

6.10 Synthesis of multimetallic complexes

[{Ir(dpydmb)}$_2$μ-(mtbpy-ϕ$_3$-mtbpy)]$^{2+}$ [p 205] 69

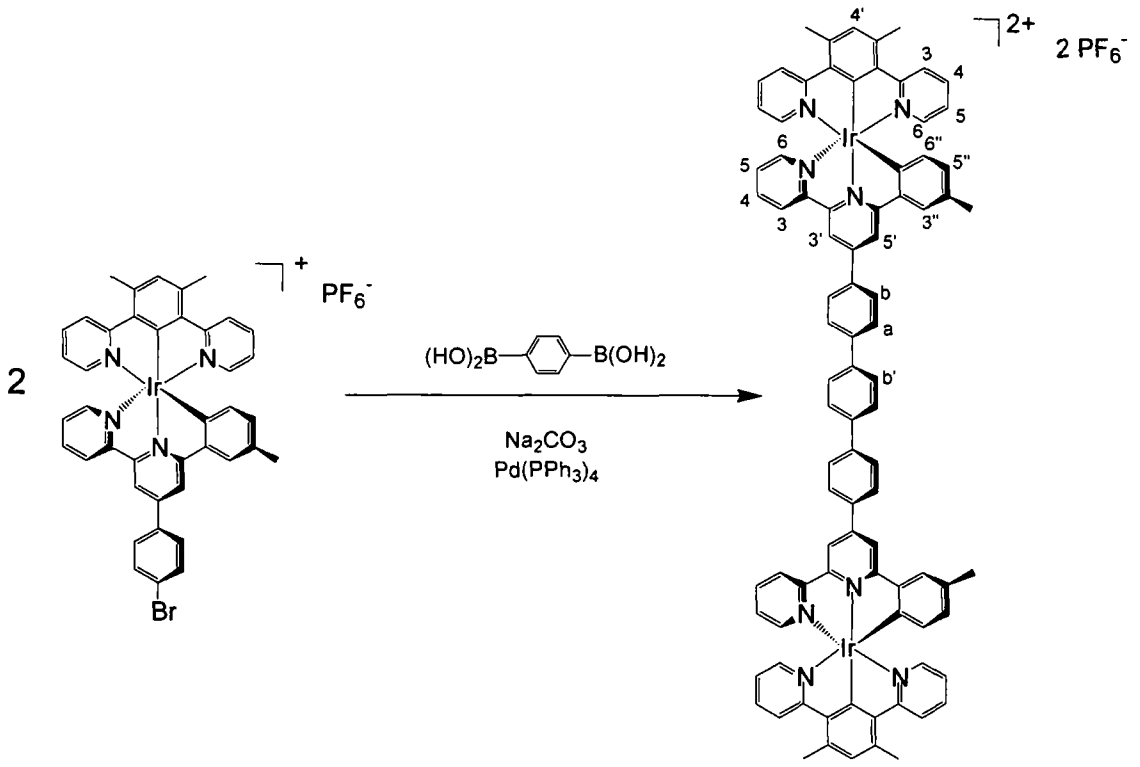

A mixture of [Ir(dpydmb)(mtbpy-ϕ-Br)]$^+$ **61** (0.060 g, 0.060 mmol), 1,4-benzene-diboronic acid (0.0060 g, 0.036 mmol) and Na_2CO_3 (0.0095 g, 0.090 mmol in 100 μL water) in DMSO (5 mL) was degassed by 3 freeze-pump-thaw cycles. $Pd(PPh_3)_4$ (0.0042 g, 0.0036 mmol) was added under a positive pressure of N_2 and the same reaction procedure employed as for [Ir(dpydmb)(mtbpy-ϕ$_2$-NMe_2)]$^+$ **63**. Purification of the crude product was achieved by flash column chromatography (silica, acetonitrile/water/KNO_3 $_{(aq)}$, gradient elution from 100/0/0 to 95.00/4.95/0.05). Following evaporation of the solvent, the product was ion exchanged to the PF_6^- salt (as outlined for [Rh(dpyb)(tpy)]$^{2+}$ **26**) to give the product as an orange solid (0.023 g, 30%). ^{1}H-NMR (CD_3CN, 500 MHz) δ = 8.79 (2H, s, H$^{3'}$-NNC), 8.71 (2H, s, H$^{5'}$-NNC), 8.67 (2H, d, ^{3}J = 8.0, H^3-NNC), 8.32 (4H, d, ^{3}J = 8.0, H^b), 8.26 (4H, d, ^{3}J = 8.0, H^3-NCN), 8.16 (4H, d, ^{3}J = 8.0, H^a), 8.07 (4H, s, H$^{b'}$), 8.03 (2H, t, ^{3}J = 7.0, H^4-NNC), 7.90 (2H, s, H$^{3''}$-NNC), 7.78 (4H, t, ^{3}J = 7.5, H^4-NCN), 7.61 (4H, d, ^{3}J = 6.0, H^6-NCN), 7.56 (2H, d, ^{3}J = 5.5, H^6-NNC), 7.28 (2H, t, ^{3}J = 6.5, H^5-NNC), 7.21 (2H, s, H$^{4'}$-NNC), 6.89 (4H, t, ^{3}J = 6.5, H^5-NCN), 6.57 (2H, d, ^{3}J = 9.0, H$^{5''}$-NNC), 5.82 (2H, d, ^{3}J = 7.5, H$^{6''}$-NNC),

[p] Procedure based upon work by De Cola *et al.*[128]

2.96 (12H, s, CH_3-NCN), 2.46 (6H, s, CH_3-NNC). MS (MALDI, DCTB matrix) m/z = 1765.4 $[M + PF_6^-]^+$ and 1620.4 $[M + e^-]^+$. HRMS (MALDI, DCTB matrix) m/z = 1761.41219 $[M + PF_6^-]^+$; 1761.42589 calculated for $[C_{88}H_{66}F_6{}^{191}Ir_2N_8P]^+$. C, H & N analysis: 46.40% C, 3.09% H and 4.57% N measured; 46.40% C, 2.92% H and 4.92% N calculated for $[C_{88}H_{66}F_{12}Ir_2N_8P_2].\{2(KPF_6)\}$. TLC (silica) R_f = 0.51 in $MeCN/H_2O/KNO_{3\,(aq)}$, 90.0/9.8/0.2. Mp > 250°C.

Flash column chromatography of the crude product mixture (silica, acetonitrile/water/$KNO_{3\,(aq)}$, gradient elution from 100/0/0 to 95.00/4.95/0.05) also isolated iridium (1,3-di(2-pyridyl)-4,6-dimethylbenzene-N,$C^{2'}$,N)(4'-(*p*-diphenylboronic acid)-6'-(*m*-tolyl)-bipyridine)$^+$ $[Ir(dpydmb)\{mtbpy\text{-}\phi_2\text{-}B(OH)_2\}]^+$ **71** as a orange solid (0.0011 g, 19%).

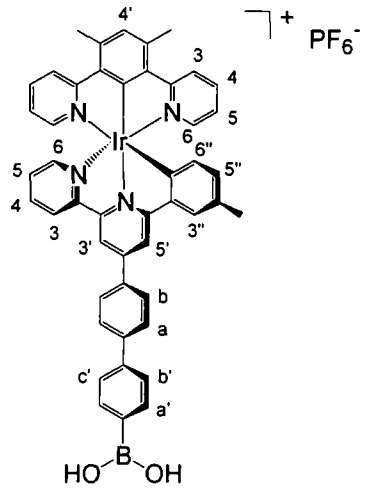

^{1}H-NMR (CD_3CN, 500 MHz) δ = 8.74 (1H, d, ^4J = 1.0, $H^{3'}$-NNC), 8.71-8.60 (2H, m, H^3-NNC and $H^{5'}$-NNC), 8.28-8.20 (4H, m, H^3-NCN and H^b-NNC), 8.16 (1H, d, ^3J = 7.0, $H^{b'}$-NNC), 8.05-7.94 (3H, m, H^4-NNC and H^a-NNC), 7.87 (1H, s, $H^{3''}$-NNC), 7.79-7.70 (4H, m, H^4-NCN and $H^{a'}$-NNC), 7.59 (2H, d, ^3J = 4.5, H^6-NCN), 7.54 (1H, d, ^3J = 4.0, H^6-NNC), 7.25 (1H, t, ^3J = 6.5, H^5-NNC), 7.20 (1H, s, $H^{4'}$-NCN), 7.02 (1H, d, ^3J = 8.5, $H^{c'}$-NNC), 6.87 (2H, ddd, ^3J = 7.5, 5.5, ^4J = 1.5, H^5-NCN), 6.55 (1H, d, ^3J = 8.0, $H^{5''}$-NNC), 5.80 (1H, d, ^3J = 8.0, $H^{6''}$-NNC), 2.96 (6H, s, CH_3-NCN), 2.23 (3H, s, CH_3-NNC). MS (MALDI, DCTB matrix) m/z = 893.3 $[M]^+$. TLC (silica) R_f = 0.60 in $MeCN/H_2O/KNO_{3\,(aq)}$, 90.0/9.8/0.2. Mp > 250°C.

[{Ir(dpydmb)}$_2$μ-(mtbpy-ϕ$_4$-mtbpy)]$^{2+}$ [205] **70**

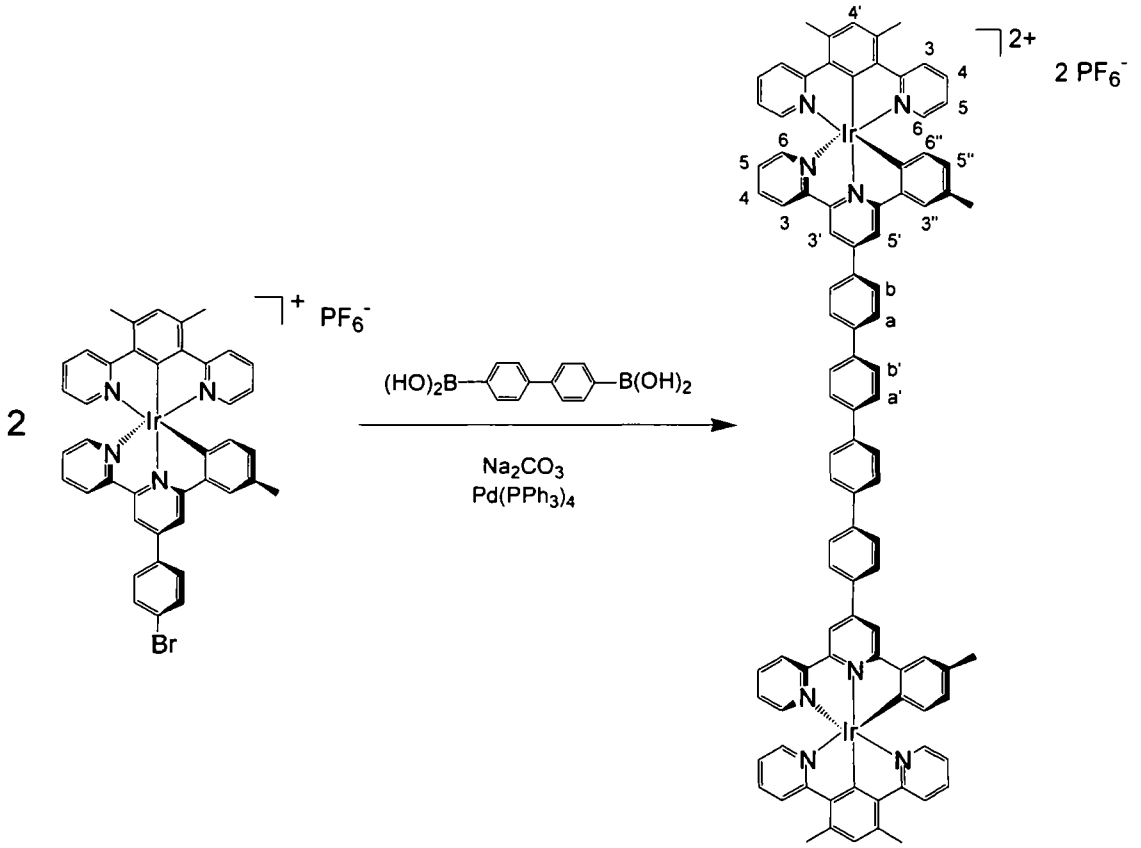

A mixture of [Ir(dpydmb)(mtbpy-ϕ-Br)]$^+$ **61** (0.060 g, 0.060 mmol), 4,4'-biphenyl-diboronic acid (0.0087 g, 0.036 mmol) and Na_2CO_3 (0.0095 g, 0.090 mmol in 100 μL water) in DMSO (5 mL) was degassed by 3 freeze-pump-thaw cycles. $Pd(PPh_3)_4$ (0.0042 g, 0.0036 mmol) was added under a positive pressure of N_2 and the same reaction procedure employed as for [Ir(dpydmb)(mtbpy-ϕ$_2$-NMe_2)]$^+$ **63**. Purification of the crude product was achieved by flash column chromatography (silica, acetonitrile/water/KNO_3 $_{(aq)}$, gradient elution from 100/0/0 to 95.00/4.95/0.05). Following evaporation of the solvent, the product was ion exchanged to the PF_6^- salt (as outlined for [Rh(dpyb)(tpy)]$^{2+}$ **26**) to give the desired product as an orange solid (0.021 g, 35%).

^{1}H-NMR (CD_3CN, 700 MHz) δ = 8.78 (2H, s, H$^{3'}$-NNC), 8.70 (2H, s, H$^{5'}$-NNC), 8.66 (2H, d, ^{3}J = 7.0, H^3-NNC), 8.30 (4H, d, ^{3}J = 7.7, H^b), 8.26 (4H, d, ^{3}J = 7.7, H^3-NCN), 8.14 (4H, d, ^{3}J = 7.7, H^a), 8.04-8.00 (10H, m, H^4-NNC, H$^{a'}$ and H$^{b'}$), 7.89 (2H, s, H$^{3''}$-NNC), 7.78 (4H, t, ^{3}J = 7.0, H^4-NCN), 7.61 (4H, d, ^{3}J = 6.3, H^6-NCN), 7.55 (2H, d, ^{3}J = 6.3, H^6-NNC), 7.27 (2H, t, ^{3}J = 7.0, H^5-NNC), 7.21 (2H, s, H$^{4'}$-NNC), 6.89 (4H, t, ^{3}J = 6.3, H^5-NCN), 6.57 (2H, d, ^{3}J = 8.4, H$^{5''}$-NNC), 5.82 (2H, d, ^{3}J = 8.4, H$^{6''}$-NNC), 2.96 (12H, s, CH_3-NCN), 2.25 (6H, s, CH_3-NNC). MS (MALDI, DCTB matrix)

m/z = 1841.4 $[M + PF_6^-]^+$. HRMS (MALDI, DCTB matrix) m/z = 1837.45778 $[M + PF_6^-]^+$; 1837.45719 $[C_{94}H_{70}F_6{}^{191}Ir_2N_8P]^+$. C, H & N analysis: 29.36% C, 1.85% H and 2.61% N measured; 29.50% C, 1.84% H and 2.93% N calculated for $[C_{94}H_{70}F_{12}Ir_2N_8P_2].\{10(KPF_6)\}$. TLC (silica) R_f = 0.57 in $MeCN/H_2O/KNO_{3\,(aq)}$, 90.0/9.8/0.2. Mp > 250°C.

[(dpydmb)Ir-μ-(mtbpy-ϕ_2-tpy)Ir(tpy)]$^{4+\,q}$ 74

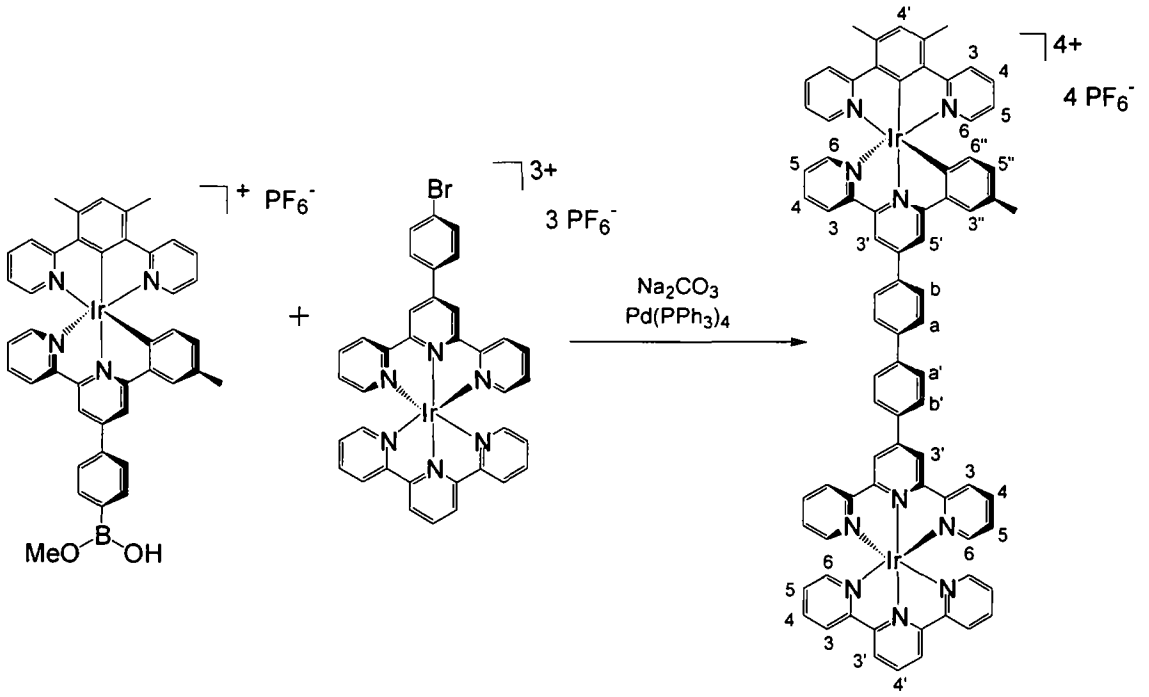

A mixture of $[Ir(dpydmb)\{mtbpy\text{-}\phi\text{-}B(OH)(OMe)\}]^+$ **68** (0.030 g, 0.031 mmol), $[Ir(tpy)(tpy\text{-}\phi\text{-}Br)]^{3+}$ **72** (0.039 g, 0.031 mmol) and Na_2CO_3 (0.0099 g, 0.093 mmol in 100 μL water) in DMSO (5 mL) was degassed by 3 freeze-pump-thaw cycles. $Pd(PPh_3)_4$ (0.0043 g, 0.0037 mmol) was added under a positive pressure of N_2 and the same reaction procedure employed as for $[Ir(dpydmb)(mtbpy\text{-}\phi_2\text{-}NMe_2)]^+$ **63**. Purification of the crude product was achieved by flash column chromatography (silica, acetonitrile/water/$KNO_{3\,(aq)}$, gradient elution from 100/0/0 to 78.0/20.7/1.3). Following evaporation of the solvent, the product was ion exchanged to the PF_6^- salt (as outlined for $[Rh(dpyb)(tpy)]^{2+}$ **26**) to give the product as an orange solid (0.011 g, 16%).

^{1}H-NMR (CD_3CN, 500 MHz) δ = 9.21 (2H, s, $H^{3'}$-tpy-ϕ), 8.91 (2H, d, ^3J = 8.0, $H^{3'}$-tpy), 8.84-8.79 (4H, m, H^3-tpy-ϕ, $H^{3'}$-NNC and $H^{4'}$-tpy), 8.73 (1H, s, $H^{5'}$-NNC), 8.68 (1H, d,

[q] This is based upon previous work within the Williams' group by Arm.[52, 130]

^3J = 8.0, H^3-NNC), 8.64 (2H, d, ^3J = 8.0, H^3-tpy), 8.45 (2H, d, ^3J = 8.5, H^a-NNC), 8.38 (2H, d, ^3J = 8.5, $H^{b'}$-tpy-ϕ), 8.33-8.24 (10H, m, H^3-NCN, H^4-tpy, H^4-tpy-ϕ, $H^{a'}$-tpy-ϕ and H^b-NNC), 8.04 (1H, t, ^3J = 8.0, H^4-NNC), 7.91 (1H, s, $H^{3''}$-NNC), 7.81-7.75 (4H, m, H^4-NCN, H^6-tpy and H^6-tpy-ϕ), 7.66-7.61 (4H, m, H^6-tpy, H^6-tpy-ϕ and H^6-NCN), 7.59-7.51 (5H, m, H^5-tpy, H^5-tpy-ϕ and H^6-NNC), 7.29 (1H, t, ^3J = 6.0, H^5-NNC), 7.22 (1H, s, $H^{4'}$-NCN), 6.90 (2H, t, ^3J = 6.0, H^5-NCN), 6.58 (1H, d, ^3J = 7.0, $H^{5''}$-NNC), 5.83 (1H, d, ^3J = 8.0, $H^{6''}$-NNC), 2.97 (6H, s, CH_3-NCN), 2.26 (3H, s, CH_3-NNC). MS (MALDI, DCTB matrix) m/z = 1939.4 $[M + 3PF_6^-]^+$. HRMS (ES^+) m/z = 375.59682 $[M]^{4+}/4$; 375.59699 calculated for $[C_{77}H_{56}{}^{191}Ir_2N_{10}]^{4+}/4$. TLC (silica) R_f = 0.15 in $MeCN/H_2O/KNO_{3\,(aq)}$, 80/18/2. Mp > 250°C.

$[(Fppy)_2Ir$-μ-(bpy-ϕ-dpydmb)$Ir(mtbpy$-ϕ-ph$)]^{2+}$ 75

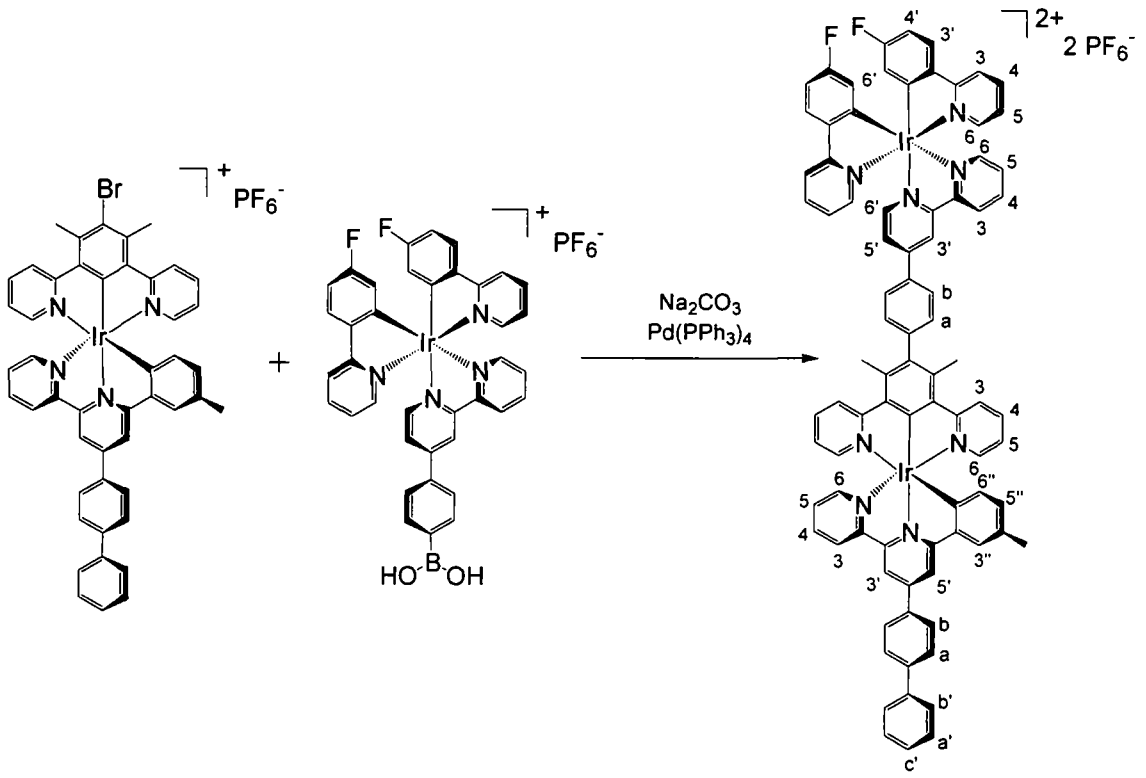

A mixture of $[Ir(dpydmb)(mtbpy$-ϕ-ph$)]^+$ **64** (0.025 g, 0.023 mmol), $[Ir(Fppy)_2\{bpy$-ϕ-$B(OH)_2\}]^+$ (0.022 g, 0.023 mmol) and Na_2CO_3 (0.0073 g, 0.069 mmol in 100 μL water) in DMSO (5 mL) was degassed by 3 freeze-pump-thaw cycles. $Pd(PPh_3)_4$ (0.0032 g, 0.0028 mmol) was added under a positive pressure of N_2 and the same reaction procedure employed as for $[Ir(dpydmb)(mtbpy$-ϕ_2-$NMe_2)]^+$ **63**. The crude product was purified by flash column chromatography (silica, acetonitrile/water/$KNO_{3\,(aq)}$, gradient elution from 100/0/0 to 95.00/4.95/0.05).

Following evaporation of the solvent, the product was ion exchanged to the PF_6^- salt (as outlined for $[Rh(dpyb)(tpy)]^{2+}$ **26**) to give the product as a yellow solid (0.015 g, 35%).

^{1}H-NMR (d_6-acetone, 500 MHz) δ = 9.36 (1H, s, $H^{3'}$-bpy-ϕ), 9.25 (1H, d, ^3J = 8.0, H^3-bpy-ϕ), 9.13 (1H, s, $H^{3'}$-NNC), 9.03 (1H, d, ^3J = 8.0, H^3-NNC), 8.96 (1H, s, $H^{5'}$-NNC), 8.42-8.37 (5H, m, H^3-NCN, H^4-bpy-ϕ and H^b-NNC), 8.33-8.23 (7H, m, H^3-ppy, $H^{5'}$-bpy-ϕ, H^6-bpy-ϕ, $H^{6'}$-bpy-ϕ and H^a-bpy-ϕ), 8.17 (1H, t, ^3J = 7.5, H^4-NNC), 8.09-7.92 (9H, m, $H^{3'}$-ppy, $H^{3''}$-NNC, H^4-ppy, H^6-ppy and H^a-NNC), 7.88-7.84 (6H, m, H^6-NNC, H^5-bpy-ϕ and H^b-bpy-ϕ), 7.57 (2H, t, ^3J = 8.0, $H^{a'}$-NNC), 7.50-7.44 (2H, m, H^5-NNC and $H^{c'}$-NNC), 7.25 (2H, dd, ^3J = 14.0, 6.0, H^5-ppy), 7.00 (2H, t, ^3J = 7.0, H^5-NCN), 6.92-6.85 (2H, m, $H^{4'}$-ppy) 6.56 (1H, d, ^3J = 8.5, $H^{5''}$-NNC), 6.09-6.03 (2H, m, $H^{6'}$-ppy), 5.96 (1H, d, ^3J = 7.5, $H^{6''}$-NNC), 2.72 (6H, s, CH_3-NCN), 2.21 (3H, s, CH_3-NNC). ^{19}F-NMR (CD_3CN, 470 MHz) δ = –73.0 (12F, d, $J_{F\text{-}P}$ = 707.7, PF_6^-), –111.2 to –111.1 (2F, m, $F^{5'}$). MS (MALDI, DCTB matrix) m/z = 1761.4 $[M + PF_6^-]^+$. HRMS (ES^+) m/z = 808.20926 $[M]^{2+}/2$; 808.20784 calculated for $[C_{85}H_{60}F_2{}^{193}Ir_2N_8]^+$. TLC (silica) R_f = 0.46 in $MeCN/H_2O/KNO_{3\,(aq)}$, 90.0/9.8/0.2. Mp > 250°C.

[(dpydmb)Ir-μ-(mtbpy-ϕ_2-bpy)Ru(bpy)$_2$]$^{3+}$ 76

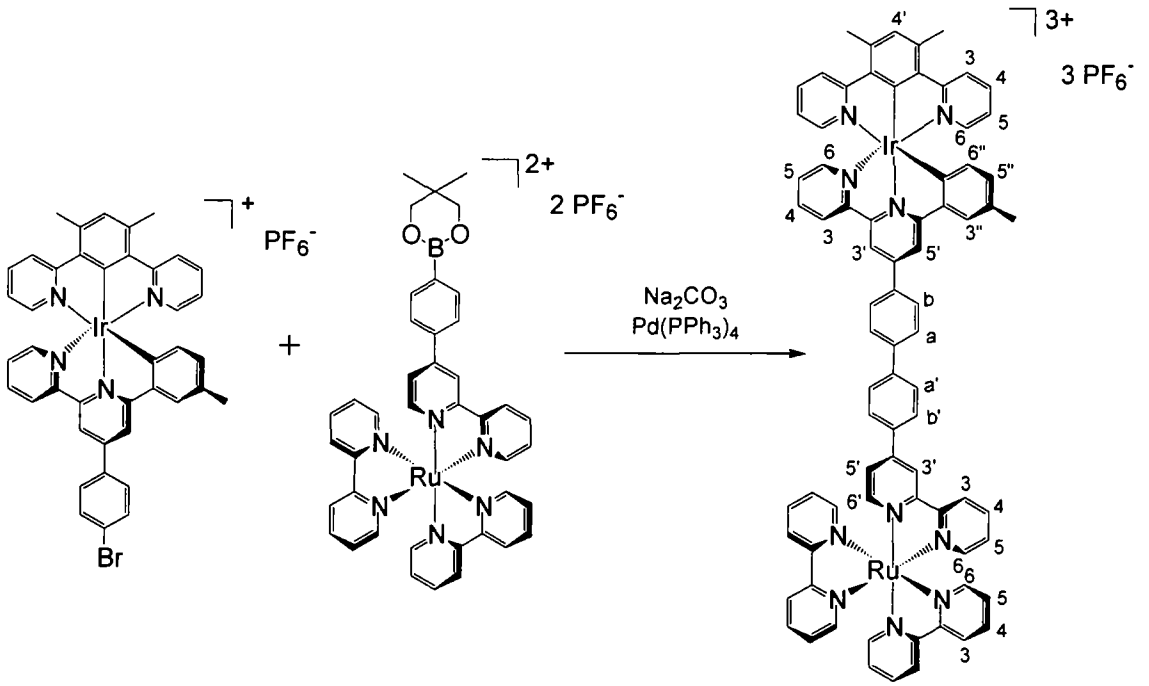

A mixture of $[Ir(dpydmb)(mtbpy\text{-}\phi\text{-}Br)]^+$ **61** (0.030 g, 0.030 mmol), $[Ru(bpy)_2(bpy\text{-}\phi\text{-}Bneo)]^{2+}$ (0.031 g, 0.030 mmol) and Na_2CO_3 (0.0095 g, 0.090 mmol in 100 μL water) in DMSO (5 mL) was degassed by 3 freeze-pump-thaw cycles. $Pd(PPh_3)_4$ (0.0042 g, 0.0035 mmol) was added under a positive pressure of N_2 and the same reaction procedure employed as for $[Ir(dpydmb)(mtbpy\text{-}\phi_2\text{-}NMe_2)]^+$ **63**. The crude product was purified by flash column chromatography (silica, acetonitrile/water/$KNO_{3\,(aq)}$, gradient elution from 100/0/0 to 89.0/10.8/0.4). Following evaporation of the solvent, the product was ion exchanged to the PF_6^- salt (as outlined for $[Rh(dpyb)(tpy)]^{2+}$ **26**) to give the product as an orange solid (0.024 g, 43%).

^{1}H-NMR (CD_3CN, 500 MHz) δ = 8.86 (1H, s, $H^{3'}$-bpy-ϕ), 8.77 (1H, d, ^3J = 9.0, H^3-bpy-ϕ), 8.76 (1H, s, $H^{3'}$-NNC), 8.68 (1H, s, $H^{5'}$-NNC), 8.65 (1H, d, ^3J = 8.0, H^3-NNC), 8.56 (4H, t, ^3J = 9.0, H^3-bpy) 8.31 (2H, d, ^3J = 8.5, $H^{b'}$-bpy-ϕ), 8.26 (2H, d, ^3J = 8.5, H^3-NCN), 8.15-8.07 (10H, m, H^4-bpy, H^4-bpy-ϕ, $H^{6'}$-bpy-ϕ, $H^{a'}$-bpy-ϕ and H^b-NNC), 8.02 (1H, t, ^3J = 7.0, H^4-NNC), 7.88 (1H, s, $H^{3''}$-NNC), 7.87 (1H, d, ^3J = 6.5, H^6-bpy-ϕ), 7.84-7.75 (9H, m, H^4-NCN, $H^{5'}$-bpy-ϕ, H^6-bpy and H^a-NNC), 7.59 (2H, d, ^3J = 5.0, H^6-NCN), 7.55 (1H, d, ^3J = 5.5, H^6-NNC), 7.49-7.44 (5H, m, H^5-bpy and H^5-bpy-ϕ), 7.27 (1H, t, ^3J = 7.0, H^5-NNC), 7.21 (1H, s, $H^{4'}$-NCN), 6.88 (2H, t, ^3J = 6.5, H^5-NCN), 6.56 (1H, d, ^3J = 8.5, $H^{5''}$-NNC), 5.81 (1H, d, ^3J = 8.0, $H^{6''}$-NNC), 2.96 (6H, s, CH_3-NCN), 2.24 (3H, s, CH_3-NNC). MS (MALDI, DCTB matrix) m/z = 1707.3 $[M + PF_6^-]^+$. HRMS (ES^+) m/z = 777.15976 $[M + PF_6^-]^{2+}/2$; 777.15794 calculated for $[C_{77}H_{58}F_6{}^{191}IrN_{10}P^{96}Ru]^{2+}/2$. TLC (silica) R_f = 0.59 in $MeCN/H_2O/KNO_{3\,(aq)}$, 80/18/2. Mp > 250°C.

[(dpydmb-Br)Ir-μ-(mtbpy-ϕ_2-bpy)Ru(bpy)$_2$]$^{3+}$ 77

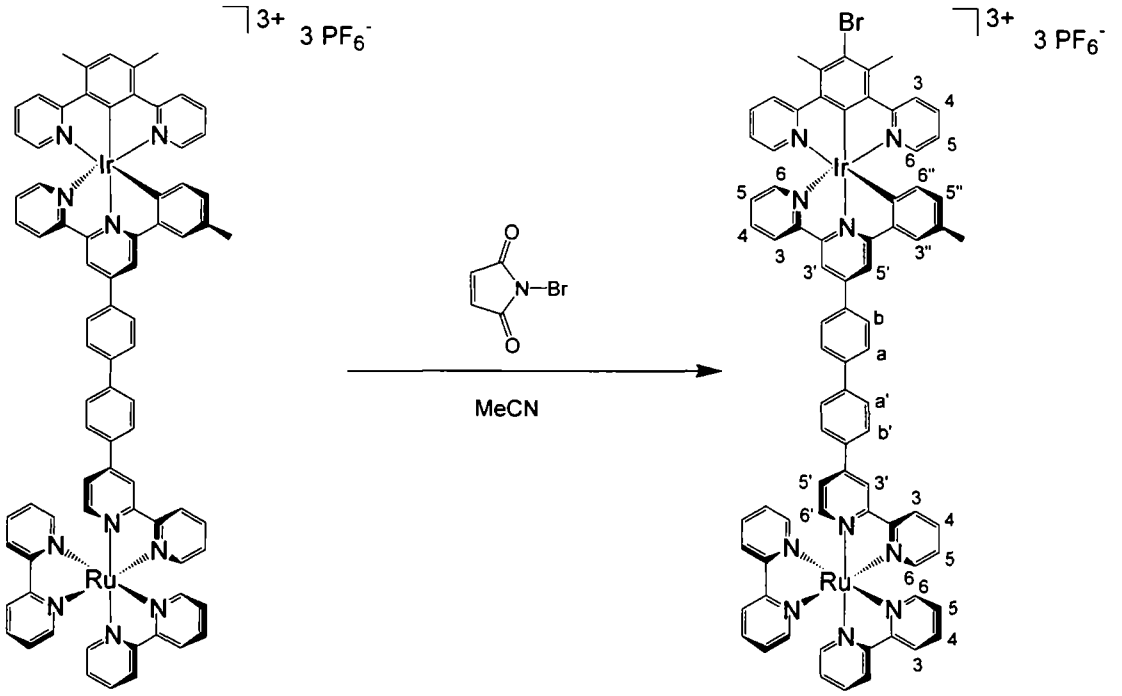

A mixture of iridium [(dpydmb)Ir-μ-(mtbpy-ϕ_2-bpy)Ru(bpy)$_2$]$^{3+}$ **76** (0.029 g, 0.029 mmol) and N-bromosuccinimide (0.0034 g, 0.019 mmol) was stirred in acetonitrile (5 mL) for 18 hours. The solution was then added to saturated aqueous KPF_6 solution (20 mL), forming a precipitate which was collected by centrifuge, washed with water (3 x 2mL) and dried under vacuum to give the product as a red solid (0.036 g, 97%).

^{1}H-NMR (CD_3CN, 400 MHz) δ = 8.86 (1H, s, H$^{3'}$-bpy-ϕ), 8.77 (1H, d, ^{3}J = 7.2, H^3-bpy-ϕ), 8.76 (1H, s, H$^{3'}$-NNC), 8.69 (1H, s, H$^{5'}$-NNC), 8.65 (1H, d, ^{3}J = 8.0, H^3-NNC), 8.56 (4H, t, ^{3}J = 8.0, H^3-bpy), 8.59-8.53 (4H, m, H$^{b'}$-bpy-ϕ and H^3-NCN), 8.17-8.06 (10H, m, H^4-bpy, H^4-bpy-ϕ, H$^{6'}$-bpy-ϕ, H$^{a'}$-bpy-ϕ and H^b-NNC), 8.02 (1H, td, ^{3}J = 6.8, 1.6, H^4-NNC), 7.89-7.86 (2H, m, H$^{3''}$-NNC and H^6-bpy-ϕ), 7.85-7.76 (9H, m, H^4-NCN, H$^{5'}$-bpy-ϕ, H^6-bpy and H^a-NNC), 7.65 (2H, d, ^{3}J = 6.0, H^6-NCN), 7.58 (1H, d, ^{3}J = 4.8, H^6-NNC), 7.50-7.43 (5H, m, H^5-bpy and H^5-bpy-ϕ), 7.27 (1H, t, ^{3}J = 6.4, H^5-NNC), 6.93 (2H, td, ^{3}J = 7.2, ^{4}J = 1.2, H^5-NCN), 6.57 (1H, d, ^{3}J = 8.0, H$^{5''}$-NNC), 5.83 (1H, d, ^{3}J = 7.6, H$^{6''}$-NNC), 3.18 (6H, s, CH_3-NCN), 2.24 (3H, s, CH_3-NNC). MS (MALDI, DCTB matrix) m/z = 1758.3 [M + 2PF_6^-]$^+$. HRMS (ES$^+$) m/z = 498.42015 [M]$^{3+}$/3; 498.42025 calculated for [$C_{77}H_{57}{}^{79}Br^{191}Ir^{193}IrN_{10}$]$^{3+}$/3. TLC (silica) R_f = 0.65 in MeCN/H_2O/$KNO_{3\,(aq)}$, 80/18/2. Mp > 250°C.

$[(F_2ppy)_2Ir\text{-}\mu\text{-}(bpy\text{-}\phi\text{-}dpydmb)Ir\text{-}\mu\text{-}(mtbpy\text{-}\phi_2\text{-}bpy)Ru(bpy)_2]^{4+}$ 78

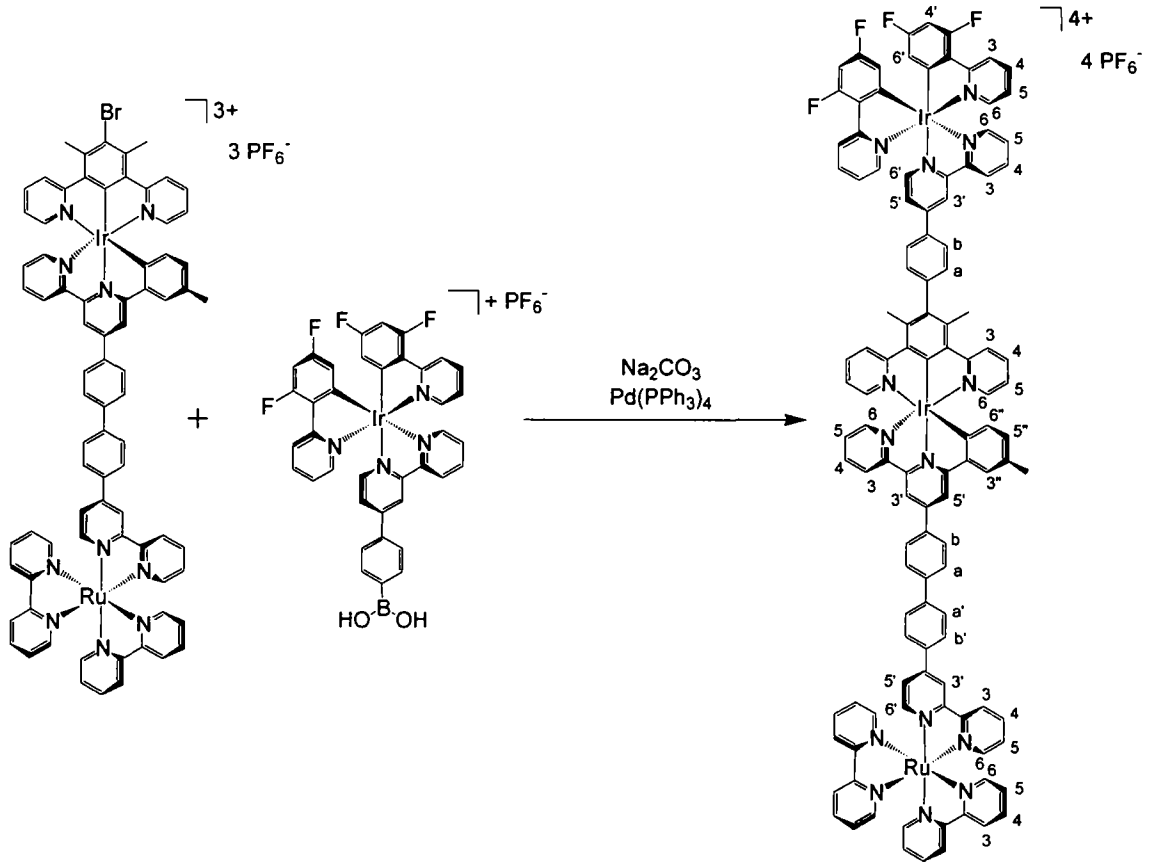

A mixture of $[(dpydmb\text{-}Br)Ir\text{-}\mu\text{-}(mtbpy\text{-}\phi_2\text{-}bpy)Ru(bpy)_2]^{3+}$ **78** (0.030 g, 0.016 mmol), $[Ir(F_2ppy)_2\{bpy\text{-}\phi\text{-}B(OH)_2\}]^+$ (0.016 g, 0.016 mmol) and Na_2CO_3 (0.0051 g, 0.048 mmol in 100 μL water) in DMSO (5 mL) was degassed by 3 freeze-pump-thaw cycles. $Pd(PPh_3)_4$ (0.0022 g, 0.0019 mmol) was added under a positive pressure of N_2 and the same reaction procedure employed as for $[Ir(dpydmb)(mtbpy\text{-}\phi_2\text{-}NMe_2)]^+$ **63**. The crude product was purified by flash column chromatography (silica, acetonitrile/water/$KNO_{3\,(aq)}$, gradient elution from 100/0/0 to 89.0/10.8/0.4). Following evaporation of the solvent, the product was ion exchanged to the PF_6^- salt (as outlined for $[Rh(dpyb)(tpy)]^{2+}$ **26**) to give the desired product as an orange/red solid (0.028 g, 62%).

^{1}H-NMR (CD_3CN, 500 MHz) δ = 8.95 (1H, s, $H^{3'}$-Ir-bpy-ϕ), 8.87 (1H, s, $H^{3'}$-Ru-bpy-ϕ), 8.84 (1H, d, ^3J = 8.0, H^3-Ir-bpy-ϕ), 8.79 (1H, s, $H^{3'}$-NNC), 8.78 (1H, d, ^3J = 10.0, H^3-Ru-bpy-ϕ), 8.71 (1H, s, $H^{5'}$-NNC), 8.68 (1H, d, ^3J = 8.5, H^3-NNC), 8.56 (4H, t, ^3J = 9.0, H^3-Ru-bpy), 8.40 (2H, t, ^3J = 9.5, $H^{b'}$-Ru-bpy-ϕ), 8.34-8.25 (4H, m, H^3-NCN, H^4-Ir-bpy-ϕ and H^5-Ir-bpy-ϕ), 8.19-8.07 (15H, m, H^4-Ru-bpy, H^4-Ru-bpy-ϕ, H^6-Ir-bpy-ϕ, $H^{6'}$-Ru-bpy-ϕ, H^a-Ir-bpy-ϕ, $H^{a'}$-Ru-bpy-ϕ, H^b-Ir-bpy-ϕ and H^b-NNC), 8.05

(1H, t, ^3J = 8.0, H^4-NNC), 8.02-7.96 (3H, m, H^3-Ir-ppy and $H^{5'}$-Ir-bpy-ϕ), 7.91 (1H, s, $H^{3'}$-NNC), 7.87 (1H, d, ^3J = 5.5, H^6-Ru-bpy-ϕ), 7.85-7.74 (11H, m, H^4-NCN, H^4-Ir-ppy, $H^{5'}$-Ru-bpy-ϕ, H^6-Ru-bpy and H^a-NNC), 7.70 (2H, d, ^3J = 9.0, H^6-Ir-ppy), 7.67-7.59 (4H, m, H^6-NCN, H^6-NNC and $H^{6'}$-Ir-bpy-ϕ), 7.50-7.44 (5H, m, H^5-Ru-bpy and H^5-Ru-bpy-ϕ), 7.33 (1H, t, ^3J = 6.5, H^5-NNC), 7.20-7.15 (2H, m, H^5-Ir-ppy), 6.91 (2H, t, ^3J = 6.5, H^5-NCN), 6.82-6.74 (2H, m, $H^{4'}$-Ir-ppy), 6.62 (1H, d, ^3J = 8.0, $H^{5''}$-NNC), 5.95 (1H, d, ^3J = 7.5, $H^{6''}$-NNC), 5.85-5.80 (2H, m, $H^{6'}$-Ir-ppy), 2.65 (6H, s, CH_3-NCN), 2.27 (3H, s, CH_3-NNC). ^{19}F-NMR (CD_3CN, 658 MHz) δ = –73.0 (24F, d, J_{F-P} = 707.1, PF_6^-, –108.3 to –108.2 (2F, m, $F^{5'}$), –110.1 (2F, t, J_{F-P} = 13.2, $F^{3'}$). MS (MALDI, DCTB matrix) m/z = 2655.5 $[M + 3PF_6^-]^+$. HRMS (ES^+) m/z = 553.12276 $[M]^{4+}/4$; 553.12290 calculated for $[C_{115}H_{80}F_4{}^{191}Ir^{193}IrN_{14}{}^{96}Ru]^{4+}/4$. TLC (silica) R_f = 0.62 in $MeCN/H_2O/KNO_{3\,(aq)}$, 80/18/2. Mp > 250°C.

CHAPTER 7

REFERENCES

7 References

1. A. P. de Silva, H. Q. N. Gunaratne, T. Gunnlaugsson, A. J. M. Huxley, C. P. McCoy, J. T. Rademacher, and T. E. Rice, *Chem. Rev.*, 1997, **97**, 1515.

2. K. S. Schanze and R. H. Schmehl, *J. Chem. Educ.*, 1997, **74**, 633.

3. F. H. Burstall, *J. Chem. Soc.*, 1930, 173.

4. J. Paris and W. W. Brandt, *J. Am. Chem. Soc.*, 1959, **81**, 5001.

5. M. Kasha, *Discuss. Faraday Soc.*, 1950, **9**, 14.

6. J. R. Lakowicz, '*Principles of Fluorescence Spectroscopy*', Plenum Press, 1999.

7. A. Gilbert and J. Baggott, '*Essentials of Molecular Photochemistry*', Blackwell Scientific Publications, 1991.

8. V. Balzani, A. Juris, M. Venturi, S. Campagna, and S. Serroni, *Chem. Rev.*, 1996, **96**, 759.

9. A. Juris, V. Balzani, F. Barigelletti, S. Campagna, P. Belser, and A. von Zelewsky, *Coord. Chem. Rev.*, 1988, **84**, 85.

10. F. E. Lytle and D. M. Hercules, *J. Am. Chem. Soc.*, 1969, **91**, 253.

11. D. M. Klassen and G. A. Crosby, *J. Chem. Phys.*, 1968, **48**, 1853.

12. G. A. Crosby, W. G. Perkins, and D. M. Klassen, *J. Chem. Phys.*, 1965, **43**, 1498.

13. J. N. Demas and G. A. Crosby, *J. Mol. Spectrosc.*, 1968, **26**, 72.

14. D. P. Rillema, D. S. Jones, and H. A. Levey, *J. Chem. Soc., Chem. Commun.*, 1979, 849.

15. N. H. Damrauer, T. R. Boussie, M. Devenney, and J. K. McCusker, *J. Am. Chem. Soc.*, 1997, **119**, 8268.

16. E. C. Constable, C. E. Housecroft, A. M. W. Cargill-Thompson, P. Passaniti, S. Silvi, M. Maestri, and A. Credi, *Inorg. Chim. Acta*, 2007, **360**, 1102.

17. M. Maestri, N. Armaroli, V. Balzani, E. C. Constable, and A. M. W. Cargill-Thompson, *Inorg. Chem.*, 1995, **34**, 2759.

18. R. T. Brown, N. C. Fletcher, M. Nieuwenhuyzen, and T. E. Keyes, *Inorg. Chim. Acta*, 2005, **358**, 1079.

19. E. A. P. Armstrong, R. T. Brown, M. S. Sekwale, N. C. Fletcher, X.-Q. Gong, and P. Hu, *Inorg. Chem.*, 2004, **43**, 1714.

20. J.-P. Sauvage, J.-P. Collin, J.-C. Chambron, S. Guillerez, C. Coudret, V. Balzani, F. Barigelletti, L. De Cola, and L. Flamigni, *Chem. Rev.*, 1994, **94**, 993.

21. J. R. Winkler, T.L.Netzel, C. Cruetz, and N. Sutin, *J. Am. Chem. Soc.*, 1987, **109**, 2381.

22. D. W. Fink and W. E. Ohnesorge, *J. Am. Chem. Soc.*, 1969, **91**, 4995.

23. F. E. Lytle, L. M. Petrosky, and L. R. Carlson, *Anal. Chim. Acta*, 1971, **57**, 239.

24. J. M. Calvert, J. V. Caspar, R. A. Binstead, T. D. Westmoreland, and T. J. Meyer, *J. Am. Chem. Soc.*, 1982, **104**, 6620.

25. E. C. Constable, A. M. W. Cargill-Thompson, N. Armaroli, V. Balzani, and M. Maestri, *Polyhedron*, 1992, **11**, 2707.

26. L. Flamigni, A. Barbieri, C. Sabatini, B. Ventura, and F. Barigelletti, *Top. Curr. Chem.*, 2007, **281**, 143.

27. F. Barigelletti, L. Flamigni, M. Guardighi, J.-P. Sauvage, J. P. Collin, and A. Sour, *Chem. Commun.*, 1996, 1329.

28. A. C. Benniston, V. Goulle, A. Harriman, J.-M. Lehn, and B. Marczinke, *J. Phys. Chem.*, 1994, **98**, 7798.

29. F. Barigelletti, L. Flamigni, M. Guardigli, A. Juris, M. Beley, S. Chodorowski-Kimmes, J.-P. Collin, and J.-P. Sauvage, *Inorg. Chem.*, 1996, **35**, 136.

30. M. Beley, J.-P. Collin, J.-P. Sauvage, H. Sugihara, F. Heisel, and A. Miehé, *J. Chem. Soc., Dalton Trans.*, 1991, 3157.

31. C. R. Hecker, A. K. I. Gushurst, and D. R. McMillin, *Inorg. Chem.*, 1991, **30**, 538.

32. J. R. Kirchhoff, D. R. McMillin, P. A. Marnot, and J.-P. Sauvage, *J. Am. Chem. Soc.*, 1985, **107**, 1138.

33. E. C. Constable and J. M. Holmes, *J. Organomet. Chem.*, 1986, **301**, 203.

34. E. C. Constable, R. P. G. Henney, T. A. Leese, and D. A. Tocher, *J. Chem. Soc., Dalton Trans.*, 1990, 443.

35. J.-P. Collin, M. Beley, and J.-P. Sauvage, *Inorg. Chim. Acta*, 1991, **186**, 91.

36. E. C. Constable, A. M. W. Cargill-Thompson, J. Cherryman, and T. Liddiment, *Inorg. Chim. Acta*, 1995, **235**, 165.

37. F. Barigelletti, B. Ventura, J.-P. Collin, R. Kayhanian, P. Gavina, and J.-P. Sauvage, *Eur. J. Inorg. Chem.*, 2000, 113.

38. I. M. Dixon, J.-P.Collin, J.-P. Sauvage, L. Flamigni, S. Encinas, and F. Barigellettti, *Chem. Soc. Rev.*, 2000, **29**, 385.

39. B. Martin and G. M. Waind, *J. Chem. Soc.*, 1958, 4284.

40. C. M. Flynn and J. N. Demas, *J. Am. Chem. Soc.*, 1974, **96**, 1959.

41. N. Yoshikawa, Y. Masuda, and T. Matsumura-Inoue, *Chem. Lett.*, 2000, **29**, 1206.

42. J. L. Kahl, K. W. Hanck, and K. DeArmond, *J. Am. Chem. Soc.*, 1991, **113**, 3984.

43. G. Morgan and F. H. Burstall, *J. Chem. Soc.*, 1937, 1649.

44. N. P. Ayala, C. M. Flynn, L. Sacksteder Jr., J. N. Demas, and B. A. DeGraff, *J. Am. Chem. Soc.*, 1990, **112**, 3837.

45. J. N. Demas, E. W. Harris, C. M. Flynn Jr., and D. Diemente, *J. Am. Chem. Soc.*, 1975, **97**, 3838.

46. J.-P. Collin, I. M. Dixon, J.-P. Sauvage, J. A. G. Williams, F. Barigelletti, and L. Flamigni, *J. Am. Chem. Soc.*, 1999, **121**, 5009.

47. J. A. G. Williams, A. J. Wilkinson, and V. L. Whittle, *Dalton Trans.*, 2008, 2081.

48. M. Licini and J. A. G. Williams, *Chem. Commun.*, 1999, 1943.

49. K. J. Arm, W. Leslie, and J. A. G. Williams, *Inorg. Chim. Acta*, 2006, **359**, 1222.

50. W. Goodall and J. A. G. Williams, *J. Chem. Soc., Dalton Trans.*, 2000, 2893.

51. C. J. Aspley and J. A. G. Williams, *New J. Chem.*, 2001, **25**, 1136.

52. K. J. Arm and J. A. G. Williams, *Chem. Commun.*, 2005, 230.

53. W. Goodall, K. Wild, K. J. Arm, and J. A. G. Williams, *J. Chem. Soc., Perkin Trans. 2*, 2002, 1669.

54. W. Leslie, A. Batsanov, J. A. K. Howard, and J. A. G. Williams, *Dalton Trans.*, 2004, 623.

55. R. J. Watts, S. J. Harrington, and J. Van Houten, *J. Am. Chem. Soc.*, 1977, **99**, 2179.

56. R. D. Gillard, R. J. Lancashire, and P. A. Williams, *J. Chem. Soc., Dalton Trans.*, 1979, 190.

57. W. A. Wickramasinghe, P. H. Bird, and N. Serpone, *Chem. Commun.*, 1981, 1284.

58. P. J. Spellane and R. J. Watts, *Inorg. Chem.*, 1983, **22**, 4060.

59. P. S. Braterman, G. A. Heath, A. J. MacKenzie, B. C. Noble, R. D. Peacock, and L. J. Yellowlees, *Inorg. Chem.*, 1984, **23**, 3425.

60. S. Sprouse, K. A. King, P. J. Spellane, and R. J. Watts, *J. Am. Chem. Soc.*, 1984, **106**, 6647.

61. K. A. King, P. J. Spellane, and R. J. Watts, *J. Am. Chem. Soc.*, 1985, **107**, 1431.

62. S. Lamansky, P. Djurovich, D. Murphy, F. Abdel-Razzaq, R. Kwong, I. Tsyba, M. Bortz, B. Mui, R. Bau, and M. E. Thompson, *Inorg. Chem.*, 2001, **40**, 1704.

63. M. G. Colombo, T. C. Brunold, T. Riedener, and H. U. Güdel, *Inorg. Chem.*, 1994, **33**, 545.

64. K. Dedeian, P. I. Djurovich, F. O. Garces, G. Carlson, and R. J. Watts, *Inorg. Chem.*, 1991, **30**, 1685.

65. M. A. Baldo, M. E. Thompson, and S. R. Forrest, *Nature*, 2000, **403**, 750.

66. A. B. Tamayo, B. D. Alleyne, P. I. Djurovich, S. Lamansky, I. Tsyba, N. N. Ho, R. Bau, and M. E. Thompson, *J. Am. Chem. Soc.*, 2003, **125**, 7377.

67. F. O. Garces, K. Dedeian, N. L. Keder, and R. J. Watts, *Acta Crystallogr., Sect. C: Cryst. Struc. Commun.*, 1993, **49**, 1117.

68. K. A. King and R. J. Watts, *J. Am. Chem. Soc.*, 1987, **109**, 1589.

69. Y. Ohsawa, S. Sprouse, K. A. King, M. K. DeArmond, K. W. Hank, and R. J. Watts, *J. Phys. Chem.*, 1987, **91**, 1047.

70. A. P. Wilde, K. A. King, and R. J. Watts, *J. Phys. Chem.*, 1991, **95**, 629.

71. K. Ichimura, T. Kobayashi, K. A. King, and R. J. Watts, *J. Phys. Chem.*, 1987, **91**, 6104.

72. A. P. Wilde and R. J. Watts, *J. Phys. Chem.*, 1995, **95**, 622.

73. P. Didier, I. Ortmans, A. Kirsch-De Mesmaeker, and R. J. Watts, *Inorg. Chem.*, 1993, **32**, 5239.

74. I. Ortmans, P. Didier, and A. Kirsch-De Mesmaeker, *Inorg. Chem.*, 1995, **34**, 3695.

75. A. Mamo, I. Stefio, M. F. Parisi, A. Credi, M. Venturi, C. Di Pietro, and S. Campagna, *Inorg. Chem.*, 1997, **36**, 5947.

76. A. J. Wilkinson, H. Puschmann, J. A. K. Howard, C. E. Foster, and J. A. G. Williams, *Inorg. Chem.*, 2006, **45**, 8685.

77. A. J. S. Bexon and J. A. G. Williams, *C. R. Chim.*, 2005, **8**, 1326.

78. A. J. Wilkinson, A. E. Goeta, C. E. Foster, and J. A. G. Williams, *Inorg. Chem.*, 2004, **43**, 6513.

79. F. Barigelletti, L. Flamigni, J.-P. Collin, and J.-P. Sauvage, *Chem. Commun.*, 1997, 333.

80. J. A. G. Williams, A. Beeby, E. S. Davies, J. A. Weinstein, and C. Wilson, *Inorg. Chem.*, 2003, **42**, 8609.

81. D. J. Cárdenas, A. M. Echavarren, and M. C. Ramirez de Arellano, *Organometallics*, 1999, **18**, 3337.

82. T. Yutaka, S. Obara, S. Ogawa, K. Nozaki, N. Ikeda, T. Ohno, Y. Ishii, K. Sakai, and M.-A. Haga, *Inorg. Chem.*, 2005, **44**, 4737.

83. M. Polson, S. Fracasso, V. Bertolasi, M. Ravaglia, and F. Scandola, *Inorg. Chem.*, 2004, **43**, 1950.

84. M. Polson, M. Ravaglia, S. Fracasso, M. Garavelli, and F. Scandola, *Inorg. Chem.*, 2005, **44**, 1282.

85. L. Ghizdavu, O. Lentzen, S. Schumm, A. Brodkorb, C. Moucheron, and A. Kirsch-De Mesmaeker, *Inorg. Chem.*, 2003, **42**, 1935.

86. H. M. Burke, J. F. Gallagher, M. T. Indelli, and J. G. Vos, *Inorg. Chim. Acta*, 2004, **357**, 2989.

87. M. Y. Kim, W. K. Seok, Y. Dong, and H. Yun, *Inorg. Chim. Acta*, 2001, **319**, 194.

88. M. T. Indelli, C. Chiorboli, and F. Scandola, *Top. Curr. Chem.*, 2007, **280**, 215.

89. M. Nishizawa, T. M. Suzuki, S. Sprouse, R. J. Watts, and P. C. Ford, *Inorg. Chem.*, 1984, **23**, 1837.

90. J. N. Demas and G. A. Crosby, *J. Am. Chem. Soc.*, 1970, **92**, 7262.

91. M. K. DeArmond and J. E. Hillis, *J. Chem. Phys.*, 1971, **54**, 2247.

92. M. T. Indelli, A. Carioli, and F. Scandola, *J. Phys. Chem.*, 1984, **88**, 2685.

93. D. H. W. Carstens and G. A. Crosby, *J. Mol. Spectrosc.*, 1970, **34**, 113.

94. G. A. Crosby and W. H. Elfring Jr., *J. Phys. Chem.*, 1976, **80**, 2206.

95. W. Humbs and H. Yersin, *Inorg. Chem.*, 1996, **35**, 2220.

96. Y. Komada, S. Yamauchi, and N. Hirota, *J. Phys. Chem.*, 1986, **90**, 6425.

97. W. Halper and M. K. DeArmond, *J. Lumin.*, 1972, **5**, 225.

98. M. E. Frink, S. D. Sprouse, H. A. Goodwin, R. J. Watts, and P. C. Ford, *Inorg. Chem.*, 1988, **27**, 1283.

99. J. Paul, S. Spey, H. Adams, and J. A. Thomas, *Inorg. Chim. Acta*, 2004, **357**, 2827.

100. J.-P. Collin, A. Harriman, V. Heitz, F. Odebel, and J.-P. Sauvage, *J. Am. Chem. Soc.*, 1994, **116**, 5679.

101. J. M. Duff and B. L. Shaw, *J. Chem. Soc., Dalton Trans.*, 1972, 2219.

102. E. C. Constable, T. A. Leese, and D. A. Tocher, *Polyhedron*, 1990, **9**, 1613.

103. M. Maestri, D. Sandrini, V. Balzani, U. Maeder, and A. von Zelewsky, *Inorg. Chem.*, 1987, **26**, 1323.

104. M. G. Colombo, A. Zilian, and H. U. Güdel, *J. Am. Chem. Soc.*, 1990, **112**, 4581.

105. A. Zilian and H. U. Güdel, *Coord. Chem. Rev.*, 1991, **111**, 33.

106. M. G. Colombo, A. Hauser, and H. U. Güdel, *Inorg. Chem.*, 1993, **32**, 3088.

107. F. Barigelletti, D. Sandrini, M. Maestri, V. Balzani, A. von Zelewsky, L. Chassot, P. Jolliet, and U. Maeder, *Inorg. Chem.*, 1988, **27**, 3644.

108. D. Sandrini, M. Maestri, V. Balzani, U. Maeder, and A. von Zelewsky, *Inorg. Chem.*, 1988, **27**, 2640.

109. V. Gayathri, E. G. Leelamani, N. M. N. Gowda, and G. K. N. Reddy, *Polyhedron*, 1999, **18**, 2351.

110. G. Denti, S. Campagna, S. Serroni, M. Ciano, and V. Balzani, *J. Am. Chem. Soc.*, 1992, **114**, 2944.

111. E. A. Plummer, J. W. Hafstraat, and L. De Cola, *Dalton Trans.*, 2003, 2080.

112. F. Neve, A. Crispini, S. Serroni, F. Loiseau, and S. Campagna, *Inorg. Chem.*, 2001, **40**, 1093.

113. J. H. Vandiemen, R. Hage, J. G. Haasnoot, H. E. B. Lempers, J. Reedijk, J. G. Vos, L. De Cola, F. Barigelletti, and V. Balzani, *Inorg. Chem.*, 1992, **31**, 3518.

114. A. Tsuboyama, T. Takiguchi, S. Okada, M. Osawa, M. Hoshino, and K. Ueno, *Dalton Trans.*, 2004, 1115.

115. L. M. Vogler, B. Scott, and K. J. Brewer, *Inorg. Chem.*, 1993, **32**, 898.

116. S. Serroni, A. Juris, S. Campagna, M. Venturi, G. Denti, and V. Balzani, *J. Am. Chem. Soc.*, 1994, **116**, 9086.

117. M. Cavazzini, P. Pastorelli, S. Quici, F. Loiseau, and S. Campagna, *Chem. Commun.*, 2005, 5266.

118. A. Börje, O. Köthe, and A. Juris, *J. Chem. Soc., Dalton Trans.*, 2002, 843.

119. E. C. Constable, *Chem. Commun.*, 1997, 1073.

120. K. O. Johansson, J. A. Lotoski, C. C. Tong, and G. S. Hanan, *Chem. Commun.*, 2000, 819.

121. Y.-Q. Fang, M. I. J. Polson, and G. S. Hanan, *Inorg. Chem.*, 2003, **42**.

122. P. M. Griffiths, F. Loiseau, F. Puntoriero, S. Serroni, and S. Campagna, *Chem. Commun.*, 2000, 2297.

123. Y. Tor, *C. R. Chim.*, 2003, **6**, 755.

124. D. Tzalis and Y. Tor, *Chem. Commun.*, 1996, 1043.

125. P. J. Connors Jr., D. Tzalis, A. L. Dunnick, and Y. Tor, *Inorg. Chem.*, 1998, **37**, 1121.

126. S. Chodorowski-Kimmes, M. Beley, J.-P. Collin, and J.-P. Sauvage, *Tetrahedron Lett.*, 1996, **37**, 2963.

127. C. Patoux, J.-P. Launay, M. Beley, S. Chodorowski-Kimmes, J.-P. Collin, S. James, and J.-P. Sauvage, *J. Am. Chem. Soc.*, 1998, **120**, 3717.

128. F. Lafolet, S. Welter, Z. Popovic, and L. De Cola, *J. Mater. Chem.*, 2005, **15**, 2820.

129. A. Barbieri, F. Barigelletti, C. Sabatini, K. J. Arm, and J. A. G. Williams, *Photochem. Photobiol. Sci.*, 2007, **6**, 397.

130. K. J. Arm and J. A. G. Williams, *Dalton Trans.*, 2006, 2172.

131. C. W. Tang and S. A. VanSlyke, *Appl. Phys. Lett.*, 1987, **51**, 913.

132. U. Mitschke and P. Bauerle, *J. Mater. Chem.*, 2000, **10**.

133. L. S. Hung and C. H. Chen, *Mater. Sci. Eng., R.*, 2002, **39**, 143.

134. L. Akcelrud, *Prog. Polym. Sci.*, 2003, **28**, 875.

135. N. Holonyak Jr. and S. F. Bevacqua, *Appl. Phys. Lett.*, 1962, **1**, 82.

136. M. Grell and D. D. C. Bradley, *Adv. Mater.*, 1999, **11**, 895.

137. G. Gu, Z. Shen, P. E. Burrows, and S. R. Forrest, *Adv. Mater.*, 1997, **9**, 725.

138. E. Holder, B. M. W. Langeveld, and U. S. Schubert, *Adv. Mater.*, 2005, **17**, 1109.

139. J. D. Slinker, D. Bernards, P. L. Houston, H. D. Abruna, S. Bernhard, and G. G. Malliaras, *Chem. Commun.*, 2003, 2392.

140. S. Lamansky, P. Djurovich, D. Murphy, F. Abdal-Razzaq, H.-E. Lee, C. Adachi, P. E. Burrows, S. R. Forrest, and M. E. Thompson, *J. Am. Chem. Soc.*, 2001, **123**, 4304.

141. T. R. Hebner, C. C. Wu, D. Marcy, M. H. Lu, and J. C. Sturm, *Appl. Phys. Lett.*, 1998, **72**, 519.

142. M. A. Baldo, S. Lamansky, P. E. Burrows, M. E. Thompson, and S. R. Forrest, *Appl. Phys. Lett.*, 1999, **75**, 4.

143. M. A. Baldo, D. F. O'Brian, Y. You, A. Shoustikov, S. Sibley, M. E. Thompson, and S. R. Forrest, *Nature*, 1998, **395**, 151.

144. S.-J. Yeh, M.-F. Wu, C.-T. Chen, Y.-H. Song, Y. Chi, M.-H. Ho, S. F. Hsu, and C. H. Chen, *Adv. Mater.*, 2005, **17**, 285.

145. M. E. Thompson, P. E. Burrows, and S. R. Forrest, *Curr. Opin. Solid State Mater. Sci.*, 1999, **4**, 369.

146. V. Cleave, G. Yahioglu, P. Le Barny, R. H. Friend, and N. Tessler, *Adv. Mater.*, 1999, **11**, 285.

147. E. Holder, V. Marin, A. Alexeev, and U. S. Schubert, *J. Polym. Sci., Part A, Polym. Chem.*, 2005, **43**, 2765.

148. C. L. Lee, K. B. Lee, and J. J. Kim, *Appl. Phys. Lett.*, 2000, **77**, 2280.

149. K. M. Vaeth and C. W. Tang, *J. Appl. Phys.*, 2002, **92**, 3447.

150. H. Z. Xie, M. W. Lui, O. Y. Wang, X. H. Zhang, C. S. Lee, L. S. Hung, S. T. Lee, P. F. Teng, H. L. Kwong, H. Zheng, and C. M. Che, *Adv. Mater.*, 2001, **13**, 1245.

151. Y. Wang, N. Herron, V. V. Grushin, D. D. LeCloux, and V. A. Petrov, *Appl. Phys. Lett.*, 2001, **79**, 449.

152. V. V. Grushin, N. Herron, D. D. LeCloux, W. J. Marshall, V. A. Petrov, and Y. Wang, *Chem. Commun.*, 2001, 1494.

153. X. Gong, J. C. Ostrowski, G. C. Bazan, D. Moses, and A. J. Heeger, *Adv. Funct. Mater.*, 2003, **13**, 439.

154. J. K. Lee, D. S. Yoo, E. S. Handy, and M. F. Rubner, *Appl. Phys. Lett.*, 1996, **69**, 1686.

155. K. M. Mannes, H. Masui, R. M. Wightman, and R. W. Murray, *J. Am. Chem. Soc.*, 1997, **119**, 3987.

156. J. D. Slinker, A. A. Gorodetsky, M. S. Lowry, J. Wang, S. Parker, R. Rohl, S. Bernhard, and G. G. Malliaras, *J. Chem. Soc.*, 2004, **126**, 2763.

157. M. S. Lowry and S. Bernhard, *Chem. Eur. J.*, 2006, **12**, 7970.

158. E. F. G. Dickson, A. Pollak, and E. P. Diamandis, *J. Photochem. Photobiol., B*, 1995, **27**, 3.

159. J. N. Demas and B. A. DeGraff, *Coord. Chem. Rev.*, 2001, **211**, 317.

160. K. K.-W. Lo, D. C.-M. Ng, and C.-K. Chung, *Organometallics*, 2001, **20**, 4999.

161. M. C. DeRosa, D. J. Hodgson, G. D. Enright, B. Dawson, C. E. B. Evans, and R. J. Crutchley, *J. Am. Chem. Soc.*, 2004, **126**, 7619.

162. A. Beeby, S. W. Botchway, I. M. Clarkson, S. Faulkner, A. W. Parker, D. Parker, and J. A. G. Williams, *J. Photochem. Photobiol., B*, 2000, **57**, 83.

163. K. Suhling, P. M. W. French, and D. Phillips, *Photochem. Photobiol. Sci.*, 2005, **4**, 13.

164. M. C. DeRosa, P. J. Mosher, C. E. B. Evans, and R. J. Crutchley, *Macromol. Symp.*, 2003, **196**, 235.

165. K. K.-W. Lo, D. C.-M. Ng, W.-K. Hui, and K.-K. Cheung, *J. Chem. Soc., Dalton Trans.*, 2001, 2634.

166. K. K.-W. Lo, W.-K. Hui, D. C.-M. Ng, and K.-K. Cheung, *Inorg. Chem.*, 2002, **41**, 40.

167. L. Wei, J. Babich, W. C. Eckelman, and J. Zubieta, *Inorg. Chem.*, 2005, **44**, 2198.

168. D. J. Hurley and Y. Tor, *J. Am. Chem. Soc.*, 2002, **124**, 13231.

169. I. Ortmans, S.Content, N. Boutonnet, A. Kirsch-De Mesmaeker, W. Banwarth, J. F. Constant, E. Defrancq, and J. Lhomme, *Chem. Eur. J.*, 1999, **5**, 2712.

170. D. J. Hurley and Y. Tor, *J. Am. Chem. Soc.*, 2002, **124**, 3749.

171. S. I. Khan, A. E. Beilstein, M. T. Tierney, M. Sykora, and M. W. Grinstaff, *Inorg. Chem.*, 1999, **38**, 5999.

172. J. J. Rack, E. S. Krinder, and T. J. Meade, *J. Am. Chem. Soc.*, 2000, **122**, 6287.

173. K. K.-W. Lo, C.-K. Chung, and N. Zhu, *Chem. Eur. J.*, 2003, **9**, 475.

174. K. K.-W. Lo, C.-K. Chung, and N. Zhu, *Chem. Eur. J.*, 2006, **12**, 1500.

175. D. Herebian and W. S. Sheldrick, *J. Chem. Soc., Dalton Trans.*, 2002, 966.

176. K. K.-W. Lo, C.-K. Li, K.-W. Lau, and N. Zhu, *Dalton Trans.*, 2003, 4682.

177. K. K.-W. Lo, K. H.-K. Tsang, K.-S. Sze, C.-K. Chung, T. K.-M. Lee, K. Y. Zhang, W.-K. Hui, C.-K. Li, J. S.-Y. Lau, D. C.-M. Ng, and N. Zhu, *Coord. Chem. Rev.*, 2007, **251**, 2292.

178. K. K.-W. Lo and T. K.-M. Lee, *Inorg. Chem.*, 2004, **43**, 5275.

179. G. Kada, H. Falk, and H. J. Gruber, *Biochim. Biophys. Acta*, 1999, **1427**, 33.

180. G. Kada, K. Kaiser, H. Falk, and H. J. Gruber, *Biochim. Biophys. Acta*, 1999, **1427**, 44.

181. X. Song and B. I. Swanson, *Anal. Chim. Acta*, 2001, **442**, 79.

182. R. M. Hartshorn and J. K. Barton, *J. Am. Chem. Soc.*, 1992, **114**, 5919.

183. C. J. Murphy, M. R. Arkin, Y. Jenkins, N. D. Ghathia, S. H. Bossman, R. E. Holmlin, and J. K. Barton, *Science*, 1993, **262**, 1025.

184. K. K.-W. Lo, C.-K. Chung, D. C.-M. Ng, and N. Zhu, *New J. Chem.*, 2002, **26**, 81.

185. J. M. Haider, R. M. Williams, L. De Cola, and Z. Pikramenou, *Angew. Chem. Int. Ed.*, 2003, **42**, 1830.

186. E. Baranoff, J.-P. Collin, L. Flamigni, and J.-P. Sauvage, *Chem. Soc. Rev.*, 2004, **33**, 147.

187. L. Flamigni, F. Barigelletti, N. Armaroli, J.-P. Collin, J.-P. Sauvage, and J. A. G. Williams, *Chem. Eur. J.*, 1998, **4**, 1744.

188. L. Flamigni, F. Barigelletti, N. Armaroli, B. Ventura, J.-P. Collin, J.-P. Sauvage, and J. A. G. Williams, *Inorg. Chem.*, 1999, **38**, 661.

189. L. Flamigni, G. Marconi, I. M. Dixon, J.-P. Collin, and J.-P. Sauvage, *J. Phys. Chem., B*, 2002, **106**, 6663.

190. I. M. Dixon, J.-P. Collin, J.-P. Sauvage, and L. Flamigni, *Inorg. Chem.*, 2001, **40**, 5507.

191. I. M. Dixon, J.-P. Collin, J.-P. Sauvage, F. Barigelletti, and L. Flamigni, *Angew. Chem. Int. Ed.*, 2000, **39**, 1292.

192. A. Kalyanasundaram and M. Grätzel, *Coord. Chem. Rev.*, 1998, **177**, 347.

193. M. Grätzel, *Nature*, 2001, **414**, 338.

194. L. Spiccia, G. B. Deacon, and C. M. Kepert, *Coord. Chem. Rev.*, 2004, **248**, 1329.

195. A. S. Polo, M. K. Itokazu, and N. Y. M. Iha, *Coord. Chem. Rev.*, 2004, **248**, 1343.

196. B. O'Regan and M. Grätzel, *Nature*, 1991, **353**, 737.

197. M. K. Nazeeruddin, A. Kay, I. Rodico, R. Humphry-Baker, E. Muller, P. Liska, N. Vlachopoulos, and M. Grätzel, *J. Am. Chem. Soc.*, 1993, **115**, 6382.

198. M. K. Nazeeruddin, P. Péchy, T. Renouard, S. M. Zakeerruddin, R. Humphry-Baker, P. Comte, P. Liska, L. Cevey, E. Costa, V. Shklover, L. Spiccia, B. B. Deacon, C. A. Bignozzi, and M. Grätzel, *J. Am. Chem. Soc.*, 2001, **231**, 1613.

199. M. K. Nazeeruddin, S. M. Zakeeruddin, J.-J. Lagref, P. Liska, P. Comte, C. Barolo, G. Viscardi, K. Schenk, and M. Graetzel, *Coord. Chem. Rev.*, 2004, **248**, 1317.

200. M. S. Lowry, J. I. Goldsmith, J. D. S. Rohl, R. A. Pascal Jr., G. G. Malliarsas, and S. Bernhard, *Chem. Mater.*, 2005, **17**, 5712.

201. F. H. Case and T. J. Kasper, *J. Am. Chem. Soc.*, 1956, **78**, 5642.

202. F. Krönke and W. Zecher, *Angew. Chem. Int. Ed.*, 1962, **1**, 626.

203. F. Kröhnke, *Synthesis*, 1976, 1.

204. D. L. Jameson and L. E. Guise, *Tet. Lett.*, 1991, **32**, 1999.

205. V. L. Whittle and J. A. G. Williams, *Inorg. Chem.*, 2008, **47**, 6596.

206. A. J. Wilkinson, '*PhD Thesis*', University of Durham, 2004.

207. M. Beley, J.-P. Collin, R. Louis, B. Metz, and J.-P. Sauvage, *J. Am. Chem. Soc.*, 1991, **113**, 8521.

208. M. Beley, J.-P. Collin, and J.-P. Sauvage, *Inorg. Chem.*, 1993, **32**, 4539.

209. H. Bönnemann, *Agnew. Chem., Int. Ed. Engl.*, 1978.

210. M. D. Sindkhedkar, H. R. Mulla, M. A. Wurth, and A. Cammers-Goodwin, *Tetrahedron*, 2001, **57**, 2991.

211. M. Chavarot and Z. Pikramenou, *Tetrahedron Lett.*, 1999, **40**, 6865.

212. E. J. Negishi, *J. Org. Chem.*, 1977, **42**, 1821.

213. N. Miyaura and A. Suzuki, *Chem. Rev.*, 1995, **95**, 2457.

214. H. Lexy and T. Kauffmann, *Chem. Ber.*, 1980, **113**, 2755.

215. M. Loï, M. W. Hosseini, A. Jouaiti, A. De Cian, and J. Fischer, *Eur. J. Inorg. Chem.*, 1999, 1981.

216. A. Jouaiti, M. Loï, M. W. Hosseini, and A. De Cian, *Chem. Commun.*, 2000, 2085.

217. F. Ullmann and J. Bierlecki, *Chem. Ber.*, 1901, **34**, 2174.

218. A. Klapars, J. C. Antilla, X. Huang, and S. L. Buchwald, *J. Am. Chem. Soc.*, 2001, **123**, 7727.

219. A. Klapars and S. L. Buchwald, *J. Am. Chem. Soc.*, 2002, **124**, 14844.

220. H.-J. Cristau, P. P. Cellier, J.-F. Spindler, and M. Taillefer, *Eur. J. Org. Chem.*, 2004, **4**, 695.

221. Y. N. Belokon, M. North, T. D. Churkina, N. S. Ikonnikov, and V. I. Maleev, *Tetrahedron*, 2001, **57**, 2491.

222. S. J. Farley, D. L. Rochester, A. L. Thompson, J. A. K. Howard, and J. A. G. Williams, *Inorg. Chem.*, 2005, **44**, 9690.

223. J. Vicente, A. Arcas, D. Bautista, and M. C. Ramirez de Arellano, *J. Organomet. Chem.*, 2002, **663**, 164.

224. S. Obara, M. Itabashi, F. Okuda, S. Tamaki, Y. Tanabe, Y. Ishii, K. Nozaki, and M. Haga, *Inorg. Chem.*, 2006, **45**, 8907.

225. S. A. Willison, J. A. Krause, and W. B. Connick, *Inorg. Chem.*, 2008, **47**, 1258.

226. L. Yang, F. Okuda, K. Kobayashi, K. Nozaki, Y. Tanabe, Y. Ishii, and M. Haga, *Inorg. Chem.*, 2008, **47**, 7154.

227. T. Ren, *Chem. Rev.*, 2008, **108**, 4185.

228. C. Coudret, S. Fraysse, and J.-P. Launay, *Chem. Commun.*, 1998, 663.

229. T. Watanabe, N. Miyaura, and A. Suzuki, *Synlett.*, 1992, 207.

230. A. J. Grumadas, D. P. Poshkus, and A. V. Kiselev, *J. Chem. Soc., Faraday Trans.*, 1982, **78**, 2013.

231. *Metal complexes*, B. P. Hay and O. Clement, in *Encyclopedia of Computational Chemistry*, ed. P. R. Schleyer, John Wiley & Sons Ltd., Chichester, 1998, 1580

232. *Semiempirical methods: Transition metals*, A. J. Holder, in *Encyclopedia of Computational Chemistry*, ed. P. R. Schleyer, John Wiley & Sons Ltd., Chichester, 1998, 2578

233. *Transition metal chemistry*, G. Frenking and T. Wagener, in *Encyclopedia of Computational Chemistry*, ed. P. R. Schleyer, John Wiley & Sons Ltd., Chichester, 1998, 3073

234. *Density functional theory applications to transition metal problems*, W. Koch and R. H. Hertwig, in *Encyclopedia of Computational Chemistry*, ed. P. R. Schleyer, John Wiley & Sons Ltd., Chichester, 1998, 689

235. P. J. Hay, *J. Phys. Chem. A*, 2002, **106**, 1634.

236. P. J. Hay and W. R. Wadt, *J. Chem. Phys.*, 1985, **82**, 270.

237. K. J. Arm, '*PhD Thesis*', University of Durham, 2006.

238. K. D. Glusac, S. Jiang, and K. S. Schanze, *Chem. Commun.*, 2002, 2504.

239. P. Brulatti, A. J. Wilkinson, and J. A. G. Williams, Unpublished Results, 2008,

240. K. K.-W. Lo, C.-K. Li, K.-W. Lau, and N. Zhu, *Dalton Trans.*, 2003, **24**, 4682.

241. A. Auffrant, A. Barbieri, F. Barigelletti, J.-P. Collin, L. Flamigni, C. Sabatini, and J.-P. Sauvage, *Inorg. Chem.*, 2006, **45**, 10990.

242. A. Harriman, A. Mayeux, C. Stroh, and R. Ziessel, *Dalton Trans.*, 2005, 2925.

243. S. Encinas, L. Flamigni, F. Barigelletti, E. C. Constable, C. E. Housecroft, E. R. Schofield, E. Figgemeirer, D. Fenske, M. Neuburger, J. G. Vos, and M. Zehnder, *Chem. Eur. J.*, 2002, **8**, 137.

244. D. G. Whitten, *Angew. Chem.*, 1979, **91**, 472.

245. S. Welter, F. Lafolet, E. Cecchetto, F. Vergeer, and L. De Cola, *ChemPhysChem*, 2005, **6**, 2417.

246. J. Grimme, M. Kreyenschmidt, F. Uckert, K. Mullen, and U. Scherf, *Adv. Mater.*, 1995, **7**, 292.

247. K. Nakamaru, *Bull. Chem. Soc. Jpn.*, 1982, **55**, 2697.

248. J. N. Demas and G. A. Crosby, *J. Phys. Chem.*, 1971, **75**, 991.

249. M. J. Frisch, G. W. Trucks, H. B. Schlegel, G. E. Scuseria, M. A. Robb, J. R. Cheeseman, V. G. Zakrzewski, J. A. Montgomery Jr., R. E. Stratmann, J. C. Burant, S. Dapprich, J. M. Millam, A. D. Daniels, K. N. Kudin, M. C. Strain, O. Farkas, J. Tomasi, V. Barone, M. Cossi, R. Cammi, B. Mennucci, C. Pomelli, C. Adamo, S. Clifford, J. Ochterski, G. A. Petersson, P. Y. Ayala, Q. Cui, K. Morokuma, D. K. Malick, A. D. Rabuck, K. Raghavachari, J. B. Foresman, J. Cioslowski, J. V. Ortiz, A. G. Baboul, B. B. Stefanov, G. Liu, A. Liashenko, P. Piskorz, I. Komaromi, R. Gomperts, R. L. Martin, D. J. Fox, T. Keith, M. A. Al-

Laham, C. Y. Peng, A. Nanayakkara, M. Challacombe, P. M. W. Gill, B. Johnson, W. Chen, M. N. Wong, J. L. Andres, C. Gonzalez, M. Head-Gordon, E. S. Replogle, and J. A. Pople, in 'Gaussian 98, Revision A.9', Gaussian Inc., Pittsburgh PA, 1998.

250. M. J. Frisch, G. W. Trucks, H. B. Schlegel, G. E. Scuseria, M. A. Robb, J. R. Cheeseman, J. A. Montgomery Jr., T. Vreven, K. N. Kudin, J. C. Burant, J. M. Millam, S. S. Iyengar, J. Tomasi, V. Barone, B. Mennucci, M. Cossi, G. Scalmani, N. Rega, G. A. Petersson, H. Nakatsuji, M. Hada, M. Ehara, K. Toyota, R. Fukuda, J. Hasegawa, M. Ishida, T. Nakajima, Y. Honda, O. Kitao, H. Nakai, M. Klene, X. Li, J. E. Knox, H. P. Hratchian, J. B. Cross, V. Bakken, C. Adamo, J. Jaramillo, R. Gomperts, R. E. Stratmann, O. Yazyev, A. J. Austin, R. Cammi, C. Pomelli, J. W. Ochterski, P. Y. Ayala, K. Morokuma, G. A. Voth, P. Salvador, J. J. Dannenberg, V. G. Zakrzewski, S. Dapprich, A. D. Daniels, M. C. Strain, O. Farkas, D. K. Malick, A. D. Rabuck, K. Raghavachari, J. B. Foresman, J. V. Ortiz, Q. Cui, A. G. Baboul, S. Clifford, J. Cioslowski, B. B. Stefanov, G. Liu, A. Liashenko, P. Piskorz, I. Komaromi, R. L. Martin, D. J. Fox, T. Keith, M. A. Al-Laham, C. Y. Peng, A. Nanayakkara, M. Challacombe, P. M. W. Gill, B. Johnson, W. Chen, M. W. Wong, C. Gonzalez, and J. A. Pople, in 'Gaussian 03, Revision C.02', Gaussian Inc., Wallingford CT, 2003.

251. C. Patoux, C. Coudret, J.-P. Launay, C. Joachim, and A. Gourdon, *Inorg. Chem.*, 1997, **36**, 5037.

252. J. C. Antilla, J. M. Baskin, T. E. Barder, and S. L. Buchwald, *J. Org. Chem.*, 2004, **69**, 5578.

APPENDICES

Appendix A : Conferences Attended and Publications

Conferences Attended

- UK Macrocycles and Supramolecular Chemistry Meeting, University of Manchester, 19-20th December 2007. Poster presentation: *'New Luminescent Iridium(III) Complexes Containing Cyclometalating Terdentate Ligands.'*

- COST Meeting, University of Durham, 5th July 2006. Oral presentation: *'Luminescent Rhodium and Iridium Complexes.'*

- UK Macrocycles and Supramolecular Chemistry Meeting, University of Newcastle, 5-6th January 2005.

- RSC Photochemistry Group Young Researchers Meeting, Rutherford-Appleton Laboratories, Oxfordshire, 15th December 2004.

Publications

- Perspective article: 'Light-emitting iridium complexes with tridentate ligands.' J. A. Gareth Williams, Andrew J. Wilkinson and Victoria L. Whittle, *Dalton Trans.*, 2008, 2081.

- 'A new class of iridium complexes suitable for stepwise incorporation into linear assemblies: synthesis, electrochemistry and luminescence.' Victoria L. Whittle and J. A. Gareth Williams, *Inorg. Chem.*, 2008, **47**, 6596. This article features on the cover of this issue.

Work Outside of the Department

- 22nd-26th November 2004, Laser Microscopy Laboratory, Rutherford-Appleton Laboratories, Oxfordshire. Two-photon excitation measurements on a range of platinum complexes.